R-08-38

Safety assessment for a KBS-3H spent nuclear fuel repository at Olkiluoto

Radionuclide transport report

P Smith, SAM Ltd

H Nordman, VTT

B Pastina, M Snellman, T Hjerpe
Saanio & Riekkola Oy

L Johnson, Nagra

December 2008

Svensk Kärnbränslehantering AB
Swedish Nuclear Fuel
and Waste Management Co

Box 250, SE-101 24 Stockholm
Phone +46 8 459 84 00

ISSN 1402-3091
SKB Rapport R-08-38

Safety assessment for a KBS-3H spent nuclear fuel repository at Olkiluoto

Radionuclide transport report

P Smith, SAM Ltd

H Nordman, VTT

B Pastina, M Snellman, T Hjerpe
Saanio & Riekkola Oy

L Johnson, Nagra

December 2008

This report is a result of a joint project between SKB and Posiva.
This report is also printed as a Posiva report, Posiva 2007-07.

A pdf version of this document can be downloaded from www.skb.se.

Abstract

Posiva and SKB are carrying out safety studies of the KBS-3H design alternative, including a safety assessment of KBS-3H repository for spent nuclear fuel located about 400 m underground at the Olkiluoto site. As in the case of KBS-3V – the current reference concept for both organisations – the possibility of one or more canister failures cannot currently be excluded over a million year time frame, even though the majority of canisters are expected to provide complete containment of radionuclides over a prolonged period in all evolution scenarios. The consequences of canister failure are thus considered in the present Radionuclide Transport Report, taking into account uncertainties in the mode of failure and subsequent radionuclide release and transport processes. A range of assessment cases – i.e. specific model realisations of different possibilities or illustrations of how a system might evolve and perform in the event of canister failure – is defined and analysed. The assessment cases address each identified canister failure mode: (i), an initial penetrating defect, (ii), canister failure due to corrosion and (iii), canister failure due to rock shear. For each canister failure mode, a Base Case is defined against which to compare the results of variant assessment cases that illustrate the impact of specific uncertainties on the radiological consequences of canister failure.

In evaluating the assessment cases, extensive use has been made of SR-Can parameter values and model assumptions, except where these are affected by differences in the materials to be disposed of in Finnish and Swedish repositories, and differences between conditions at Olkiluoto and those at the Swedish sites considered in SR-Can. Where differences arise, the selection of parameter values and model assumptions has been made largely according to "expert judgement", based on considerations such as use in previous assessments, additional data gathering and laboratory studies. In the case of geosphere transport modelling, the modelling approach and parameter values used are based largely on TILA-99, although more recent developments in the understanding of the Olkiluoto site are used to provide additional support for the parameter values selected (for example, in terms of their conservatism).

The primary assessment endpoints in the present safety assessment are:

- annual effective dose to most exposed individual considering multiple exposure pathways in the biosphere, which is used for comparison with the Finnish regulatory dose constraints for the "environmentally predictable future"; and
- activity fluxes to the biosphere (geo-bio fluxes) which are used for comparison with Finnish regulatory geo-bio flux constraints.

In addition, a safety indicator based on an indicative stylised well scenario that considers only the drinking water pathway – WELL-2007 dose – has been calculated for all assessment cases. Calculation of WELL-2007 dose further facilitates comparison with regulatory guidelines for the "environmentally predictable future", as well as the results from other safety assessments and safety cases, without the need to justify a wide range of biosphere modelling assumptions.

In all cases, the calculational results comply with Finnish regulatory criteria.

Sammanfattning

Posiva och SKB har utfört säkerhetsstudier för den alternativa KBS-3H-utformningen i ett gemensamt forsknings-, utvecklings- och demonstrationsprogram (Fud) under åren 2002–2007. Säkerhetsstudierna, som utförts som en del av detta program, omfattar en säkerhetsanalys av en preliminär utformning av KBS-3H för ett slutförvar för använt kärnbränsle lokaliserat på 400 m djup i Olkiluoto, som är den föreslagna platsen för ett slutförvar för använt kärnbränsle i Finland. Liksom för KBS-3V – referensalternativet för ett slutförvar – kan möjligheten för ett eller flera kapselbrott inte uteslutas för en tidsperiod på en miljon år, fastän majoriteten av kapslarna förväntas ge fullständig integritet för en lång tidsperiod i alla utvecklingsscenarier. Konsekvensen av ett kapselbrott har analyserats i denna rapport över radionuklidtransport, genom att beakta osäkerheter i hur kapselbrottet sker och därpå följande utsläpp och transport av radionuklider. De analyserade fallen – dvs specifika modellrealiseringar av olika möjligheter eller illustrationer av hur systemet kan utvecklas och fungera i fall av kapselskada – har definierats och analyserats. De analyserade fallen omfattar varje identifierad process som kan leda till ett kapselbrott; (i) en initial genomträngande kapselskada, (ii) kapselbrott på grund av korrosion och (iii) kapselbrott orsakad av skjuvning i berget.

Dessa beräkningsfall har till stor del baserats på SR-Can parametervärden och modellantaganden, förutom i de fall där dessa påverkas av olikheter i material som deponeras i ett slutförvar i Finland och Sverige, och där det finns skillnader i förhållanden i Olkiluoto och på en svensk plats. När det förekommer skiljaktigheter har valet av parametrar och modellantaganden till stor del baserats på expertbedömningar, och baserats på överväganden som hur dessa använts i tidigare säkerhetsanalyser, ny datainsamling och laboratoriestudier. För transport i geosfären har modelleringen och parametervärden till stor del baserats på TILA-99, men även nyvunnen platskunskap om Olkiluoto har använts för att ge bättre stöd för parametervalet (t ex utvärdering av hur konservativ använd data är).

De primära slutresultaten i analysen är:

- Den årliga effektiva dosen för den mest exponerade individen via multipla exponeringsvägar i biosfären. Denna används för att jämföras med finska säkerhetsföreskrifter för den förutsägbara framtiden.
- Aktivitetsflöden till biosfären (geo-bio flöden) vilka används för jämförelser med de finska föreskrifterna för geo-bio flöden.

Ytterligare har en säkerhetsindikator, Well-2007-dosen, beräknats baserat på ett indikativt stiliserat brunnsscenario som enbart räknar med exponering via dricksvatten. Beräkningen av Well-2007-dosen förenklar ytterligare jämförandet med myndigheternas säkerhetsföreskrifter för den förutsägbara framtiden. Den underlättar också jämförandet med andra säkerhetsanalyser utan att ställa krav på en motivering av en omfattande bredd av modelleringsantaganden.

I alla beräkningsfall är de beräknade utsläppen begränsade i omfattning och ligger inom ramen för finska säkerhetskriterier.

Denna rapport finns även tryckt i Posivas rapportserie POSIVA 2007-07.

Contents

Foreword

This study was coordinated by Margit Snellman from Saanio & Riekkola Oy on behalf of Posiva Oy. The progress of the study was supervised by a KBS-3H Review Group consisting of Aimo Hautojärvi (Posiva), Jukka-Pekka Salo (Posiva), Marjut Vähänen (Posiva), Barbara Pastina (Saanio & Riekkola Oy), Margit Snellman (Saanio & Riekkola Oy), Jorma Autio (Saanio & Riekkola Oy), Stig Pettersson (SKB), Erik Thurner (SKB), Börje Torstenfelt (Swedpower), Lennart Börgesson (Clay Technology) and Lawrence Johnson (Nagra). The present Radionuclide Transport Report was largely written by Paul Smith (Safety Assessment Management Ltd.), with contributions from Margit Snellman (Saanio & Riekkola Oy), Barbara Pastina (Saanio & Riekkola Oy), Henrik Nordman (VTT), Lawrence Johnson (Nagra) and Thomas Hjerpe (Saanio & Riekkola Oy).

Most radionuclide transport calculations were carried out at VTT by Henrik Nordman. Calculations using the Nagra SPENT code reported in Appendix B were carried out by Paul Smith.

Christine Bircher (Nagra), Aline Playfair (Nagra), Heini Laine (Saanio & Riekkola Oy) and Päivikki Mäntylä (Saanio & Riekkola Oy) provided editorial support.

The report was reviewed in draft form by members of the KBS-3H Review Group and by the following individuals: Jordi Bruno (Enviros Spain LS, Spain), Ivars Neretnieks KTH (Royal Institute of Technology, Sweden), Mike Thorne ((Mike Thorne and Associates Limited, UK), Johan Andersson (Streamflow AB, Sweden), Jan-Olof Selroos (SKB, Sweden), Ari Ikonen (Posiva, Finland) and Nuria Marcos (Saanio & Riekkola Oy, Finland).

1 Introduction

1.1 KBS-3H long-term safety studies

The KBS-3 method, based on multiple barriers, is the selected spent fuel disposal method in both Sweden and Finland. There are two design alternatives for the KBS-3 method: KBS-3V in which the canisters are emplaced in individual vertical deposition holes and KBS-3H in which several canisters are emplaced in horizontal deposition drifts (see Figure 1-1). The reference alternative for the implementing organisations, SKB in Sweden and Posiva in Finland, is KBS-3V.

SKB and Posiva have conducted a Research, Development and Demonstration (RD&D) programme over the period 2002–2007 with the overall aim of establishing whether KBS-3H for the geological disposal of spent nuclear fuel represents a feasible alternative to KBS-3V.

The RD&D programme has included studies of long-term or post-emplacement safety, i.e. safety from the time of emplacement of the first canisters in the repository. Construction and operation of the repository drifts will continue over several decades following emplacement of the first canisters, and long-term safety studies consider evolution and performance in this period, as well as in the period subsequent to repository closure. The safety of the workforce and the public during construction, operation and closure of the repository (operational safety) is, however, considered separately from the long-term safety studies and will be addressed in the upcoming Design Description 2007. Throughout this report, the terms "safety studies" and "KBS-3H safety studies" refer to the KBS-3H long-term safety studies described here.

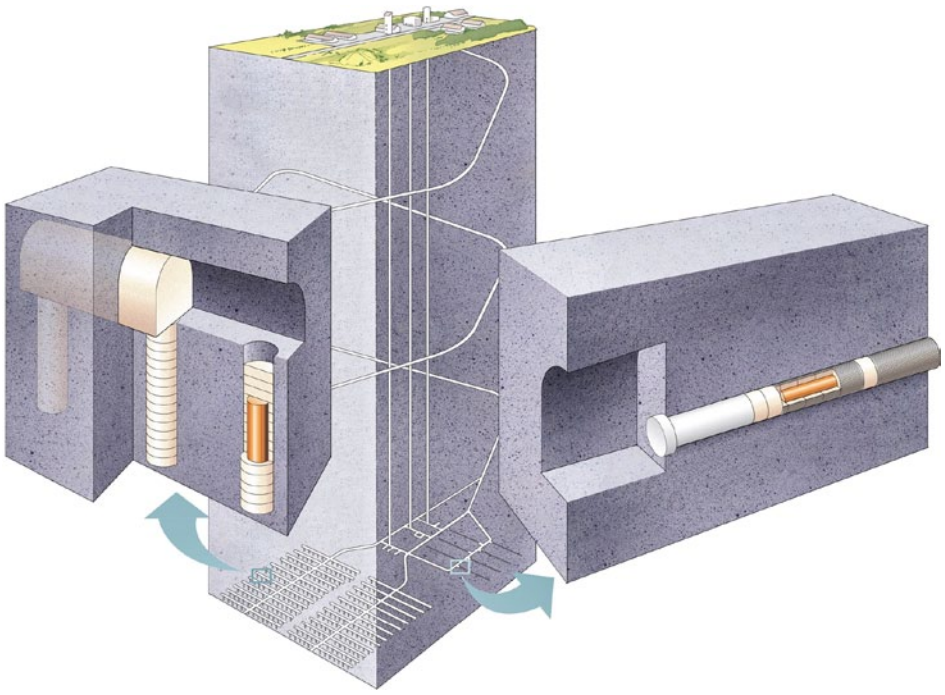

Figure 1-1. *The KBS-3V (left) and KBS-3H (right) alternatives of the KBS-3 spent fuel disposal method.*

Safety studies have been complemented by detailed studies of:

- the function of the bentonite buffer;
- repository design and layout adaptation to the Olkiluoto site in Finland;
- deposition equipment;
- the retrievability of the canister in the KBS-3H; and
- the comparative costs of the KBS-3H and KBS-3V alternatives.

These are intended to be sufficiently comprehensive that they can be used, along with other technical demonstration, environmental and cost studies, as a technical basis for a decision at the beginning of 2008 on whether or not to continue the development of the KBS-3H.

There are currently a number of design variants under consideration for a KBS-3H repository, as well as differences between the fuel types, between the characteristics and inventories of the canisters, and between the designated repository site for a spent fuel repository in Finland and the sites under consideration in Sweden. In order to focus the KBS-3H safety studies, however, they are applied to the Olkiluoto site, in the municipality of Eurajoki, which has been selected as the site for a spent fuel repository in Finland. The three fuel types are considered: VVER-440 PWR fuel from the Loviisa 1 and 2 reactors, BWR from the Olkiluoto 1 and 2 reactors and EPR fuel from Olkiluoto 3 (the reference fuel type for the majority of safety assessment calculations is the BWR fuel from Olkiluoto 1-2). The current basis for safety assessment is that disposal of 5,500 tU fuel will be required, encapsulated in approximately 3,000 canisters. The reference KBS-3H repository design for safety assessment is the Basic Design as described in the Design Description 2006 /Autio et al. 2007/. Other design variants, also based on the KBS-3H alternative, are also presented in the Design Description 2006. At the time of selection of the reference KBS-3H design for the long-term safety studies, no major differences between the Basic Design and the design alternative, termed DAWE (Drainage Artificial Watering and air Evacuation), had been identified that were relevant to long-term safety. The Basic Design is the outcome of several years of studies of different design options for the drift. DAWE was introduced at a later stage in the programme to address some uncertainties regarding the feasibility of implementing the Basic Design in less favourable locations along the drifts. At the time of selection, however, both designs were judged to be potentially feasible, and the Basic Design was selected for the safety assessment.

Specific high-level questions addressed by the KBS-3H safety studies are:

- are there safety issues specific to KBS-3H with the potential to lead to unacceptable radiological consequences?
- is KBS-3H promising at a site with the broad characteristics of Olkiluoto from the long-term safety point of view?

The safety studies are, however, limited in scope and do not currently address the questions:

- is KBS-3H more or less favourable than KBS-3V from a long-term safety point of view?
- does the specific realisation of the KBS-3H design considered in the safety studies satisfy all relevant regulatory guidelines?

Regarding the first question, a comparative study of favourable and less favourable features of KBS-3H and KBS-3V is beyond the scope of the safety studies carried out so far, although each concept has features that are favourable and less favourable to long-term safety and to its assessment. Regarding the second question, although the performance of a KBS-3H repository has been analysed for number of variant cases illustrating the impact of different uncertainties and the results compared with Finnish regulatory guidelines[1], the analyses are not comprehensive in

[1] The focus of the present report is on the comparison of releases with Finnish regulatory guidelines, with only brief comments about the Swedish regulatory context.

their consideration of uncertainty, and leave a number of issues unresolved. Limitations of the analyses are discussed in Section 1.5. These limitations would have to be addressed before it could be judged whether all relevant regulatory guidelines are satisfied.

In order to judge feasibility of implementing the KBS-3H alternative from a long-term safety point of view, relevant safety issues must be understood as well for KBS-3H as they are for KBS-3V. There is a broad scientific and technical foundation that is common to both alternatives, and much of the work carried out by both Posiva and SKB in the context of KBS-3V is also directly applicable to KBS-3H. Site properties and aspects of system evolution common to the two concepts are, for example, described in detail in the evolution report for a KBS-3V at Olkiluoto /Pastina and Hellä 2006 and references therein/. Much of the information and analysis conducted by SKB in SR-Can /SKB 2006abcde/ for a KBS-3V repository in Sweden is also relevant, and drawn upon extensively in KBS-3H safety studies and their documentation. Thus, comparatively little documentation is required that is specific to KBS-3H. The documentation that has been developed focuses primarily on the differences identified between the two alternatives in a systematic "difference analysis" reported in the KBS-3H Process Report[2] /Gribi et al. 2007/.

Consistent with the "difference analysis" approach, at the start of the KBS-3H safety studies a decision was taken to follow the SR-Can approach for process selection and to accept the understanding and modelling basis presented in SR-Can in areas where KBS-3H and KBS-3V are very similar, in particular in modelling canister processes and fuel processes. The reason for this is that major efforts would have to be made to advance the models beyond what was presented in SR-Can, and such advances were not part of the KBS-3H programme mandate. Such developments may, however, be considered in future project stages for both KBS-3H and 3V.

Differences between the fuel, canisters and repository sites under consideration in Sweden and Finland will have to be considered in transferring the detailed findings of the current safety studies to a Swedish context. However, the difference analysis shows that the key differences in the evolution and performance of the two design alternatives relate mainly to the engineered barrier system. With the exception of overall inventory, these are broadly similar in the Swedish and Finnish contexts. Thus, many of the broad findings on the engineered barrier system are expected to be applicable in a Swedish context.

1.2 Purpose and scope of this report

The purpose of the present report is to describe the radionuclide transport calculations carried out as part of the KBS-3H safety studies. The report is one of several that will document and support the safety studies of a KBS-3H repository at Olkiluoto, as shown in Figure 1-2 (although some are common to the KBS-3H and KBS-3V and will be developed in the context of Posiva's KBS-3V programme). The reporting structure of the KBS-3H safety studies is based on Posiva's safety case plan /Vieno and Ikonen 2005/.

The overall outcome of the KBS-3H safety studies is documented in the "Safety assessment for a KBS-3H spent nuclear fuel repository at Olkiluoto – summary report" report (referred to simply as **summary report** in Figure 1-2) /Smith et al. 2007b/. The summary report is supported by a number of further high-level reports (those shown in Figure 1-2), one of which is the present **Radionuclide Transport Report**.

The geoscientific basis of the safety case is provided in Olkiluoto **site reports** /Posiva 2003, 2005, Andersson et al. 2007/, including the present situation at, and past evolution of, the Olkiluoto site, and disturbances caused by ONKALO, which is an Underground Rock Characterisation Facility for site-specific underground investigations at Olkiluoto that will also

[2] Unless stated otherwise, the term Process Report refers to the KBS-3H Process Report /Gribi et al. 2007/ and the term Evolution Report refers to the KBS-3H Evolution Report /Smith et al. 2007a/.

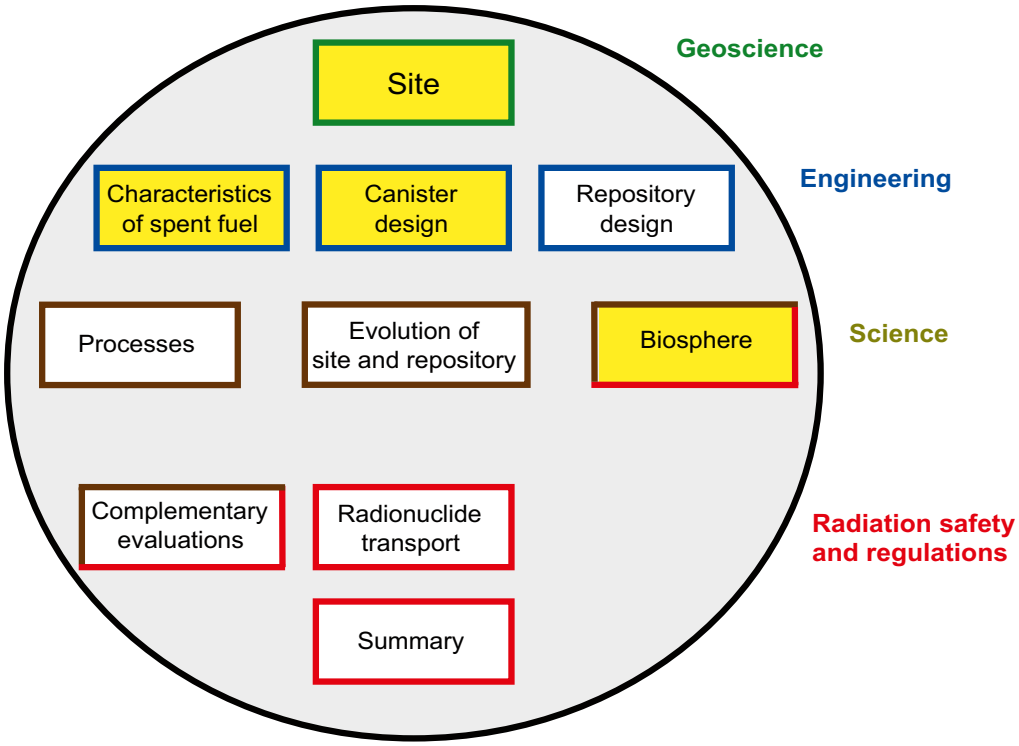

Figure 1-2. *The reporting structure for KBS-3H long-term safety studies. The colours of the boxes indicate the areas covered by the reports (as listed on the right-hand side of the figure). Yellow filling indicates reports common to the KBS-3H and -3V safety studies. All the other boxes represent reports produced within the KBS-3H safety studies or design studies. The safety assessment for a KBS-3H spent nuclear fuel repository at Olkiluoto is presented in the Summary report. For details see the main text.*

serve as an access route to the repository. Data from the most recent Olkiluoto Site Description 2006 /Andersson et al. 2007/ are used whenever possible in this report, although further work is required to incorporate these data fully in future safety assessments. The engineering basis is provided by the reports on the **characteristics of spent fuel** /Anttila 2005/, **canister design** /Raiko 2005/, and **repository design** /Autio 2007, Autio et al. 2007/. The preliminary "reference design" analysed in the present safety assessment is presented in the repository design report entitled "Design Description 2006" /Autio et al. 2007/. The reference design for the KBS-3H safety studies (termed Basic Design) was frozen at the beginning of 2007. KBS-3H repository design development is still ongoing. Recent progress is presented in the Design Description 2007 report /Autio et al. 2008/. The repository design report also discusses long-term safety features, together with manufacturing and installation aspects of the buffer and backfill for KBS-3H.

The scientific understanding supporting the safety studies is described in a **Process Report** /Gribi et al. 2007/ and in the **Evolution Report** /Smith et al. 2007a/. The Process Report, as its name indicates, describes the individual processes and discusses the relevance of selected processes (e.g. gas generation) through scoping calculations. The Evolution Report describes the same processes, but in broadly chronological order, highlighting the interactions between the processes and their coupling whenever possible, starting from repository construction and continuing up to one million years from the beginning of repository operations.[3] A **Complementary Evaluations of Safety Report** /Neall et al. 2007/ provides additional arguments, mostly non

[3] A certain degree of overlap between the Process and the Evolution Reports is unavoidable and deemed beneficial if the reports are read separately. However, the authors recognise that it is preferable to read both the Evolution and Process Reports together to fully grasp the couplings and relative importance of processes in such a complex system.

quantitative, on the long-term safety aspects of a KBS-3H repository located at the Olkiluoto site. A **Biosphere Analysis Report** /Broed et al. 2007/ was produced in parallel with the above-mentioned reports using input from the present Radionuclide Transport Report and the main conclusions on the ensuing releases to the biosphere are summarised in the Summary report /Smith et al. 2007b/. The Process and Evolution Reports provide the basis for the selection of the assessment cases described and analysed in the present Radionuclide Transport Report.

These high-level reports are further supported by more detailed technical reports compiled in support of KBS-3H safety studies, including reports on thermal analyses /Ikonen 2003, 2005/, thermo-mechanical analyses /Lönnqvist and Hökmark 2007/, analyses of geohydrological data from the Olkiluoto site and associated layout studies /Hellä et al. 2006/, discrete fracture network modelling of the site /Lanyon and Marschall 2006/, analyses of HMCGB (hydro-mechanical-thermal-gaseous-microbiological) processes related to the steel components /Johnson et al. 2005/, experimental and modelling studies on the interaction of iron and bentonite /Carlson et al. 2006, Wersin et al. 2007/, and solubility estimation in support of radionuclide release and transport calculations /Grivé et al. 2007/.

1.3 The regulatory context

The present safety assessment addresses the long-term safety of a KBS-3H repository for Finnish spent fuel located at the Olkiluoto site in Finland. It is therefore appropriate to base the assessment on Finnish regulatory requirements[4].

The regulatory requirements for a spent fuel repository at Olkiluoto are set out in the Government Decision on the safety of the disposal of spent nuclear fuel /STUK 1999/ and, in more detail, in Guide YVL 8.4 issued by the Finnish regulator /STUK 2001/. These requirements are, however, currently under revision. A detailed discussion of regulatory requirements related to the safety case, including dose and radionuclide release constraints in different time frames, is given in Posiva's TKS-2006 report on its programme for research, development and technical design /Posiva 2006/. Some key points relevant to the present report are summarised below.

Guide YVL 8.4 distinguishes between the "environmentally predictable future" (also referred to by the regulator as "several thousand years"), during which conservative estimates of dose must be made (i.e. estimates that tend to over-estimate dose where there is uncertainty), and the "era of large-scale climate changes" when periods of permafrost and glaciations are expected, and radiation protection criteria are based on constraints on nuclide-specific activity fluxes from the geosphere, termed "geo-bio flux constraints".

Posiva's interpretation of the duration of the "environmentally predictable future" is typically 10,000 years, which is consistent also with SKB's duration of the quantitative assessment period, although Swedish regulations also requires a more detailed assessment for the first 1,000 years following repository closure /SSI 2005/. The annual effective dose constraint for the most exposed members of the public applicable to the environmentally predictable future is 10^{-4} Sv per year, while the average annual effective doses to other members of the public should, according to the regulations, remain insignificantly low. It is also stated in YVL 8.4 that the radiation exposure of flora and fauna shall remain clearly below the levels that would cause decline in biodiversity or other significant detriment to any living population on the basis of the best available scientific knowledge. Moreover, rare animals and plants as well as domestic animals shall not be exposed detrimentally as individuals. Compliance with these requirements is not discussed in the present report, but is considered in the Biosphere Analysis Report /Broed et al. 2007/.

[4] The differences between the Swedish and Finnish regulatory systems are discussed in Appendix C of the Complementary Evaluations of Safety Report /Neall et al. 2007/.

YVL 8.4 also gives a qualitative requirement that:

"The barriers shall effectively hinder the release of disposed radioactive substances into the host rock for several thousands of years."

In the era of large-scale climate changes, Guide YVL 8.4 states that the sum of the ratios of nuclide-specific activity releases to their respective geo-bio flux constraints shall be less than one in order to satisfy regulatory requirements.

Geo-bio flux constraints, as set out in Guide YVL 8.4, are shown in Table 1-1. Guide YVL 8.4 covers all the safety relevant radionuclides considered in the present report, with the exception of Mo-93. For the purposes of this report, a geo-bio flux constraint of 3 GBq per year is assigned to this radionuclide. This is based on the activity of Mo-93 needed to give an annual dose of 10^{-4} Sv in the indicative stylised drinking water well scenario described in Section 4.3 of this report.

According to Guide YVL 8.4, when comparing calculated activity releases with the constraints, the calculated values can be averaged over 1,000 years at most. However, no averaging of calculated values has been performed for any of the assessment cases considered in the present safety assessment, with the exception of cases PD-VOL-1 and PD-VOL-2 (see Section 5.9), although there is some implicit averaging by the nature of the numerical models used in the safety assessment. The sum of the ratios of nuclide-specific activity releases to their respective constraints must be less than one in order to satisfy regulatory requirements.

Guide YVL 8.4 gives some indication as to the types of evolution scenarios[5] to be considered when evaluating doses and geo-bio fluxes. It states that:

"*A scenario analysis shall cover both the expected evolutions of the disposal system and unlikely disruptive events affecting long-term safety. The scenarios shall be composed systematically from features, events and processes, which are potentially significant to long-term safety and may arise from:*

- mechanical, thermal, hydrological and chemical processes and interactions occurring inside the disposal system;
- external events and processes, such as climate changes, geological processes and human actions."

Table 1-1. Geo-bio flux constraints, as set out in Guide YVL 8.4 issued by the Finnish regulator.

Radionuclides	Geo-bio flux constraints [GBq a^{-1}]
Long-lived alpha-emitting Ra, Th, Pa, Pu, Am and Cm isotopes	0.03
Se-79; I-129; Np-237	0.1
C-14; Cl-36; Cs-135; long-lived uranium isotopes	0.3
Nb-94; Sn-126	1
Tc-99; (*Mo-93 – see main text*)	3
Zr-93	10
Ni-59	30
Pd-107; Sm-151	100

[5] According to the IAEA definition, a scenario is a postulated or assumed sequence of states defined by the safety functions that are provided by the system components /IAEA 2003/.

The Guide goes on to state:

"*The base scenario shall assume the performance targets defined for each barrier, taking account of the incidental deviations from the target values. The influence of the declined overall performance of a single barrier or, in case of coupling between barriers, the combined effect of the declined performance of more than one barrier, shall be analysed by means of variant scenarios. Disturbance scenarios shall be defined for the analysis of unlikely disruptive events affecting long-term safety*".

The importance to long-term safety of unlikely disruptive events shall, according to the Guide, be assessed. According to STUK, these events are to include at least:

- boring a deep water well at the disposal site;
- core drilling hitting a spent fuel canister; and
- a substantial rock movement occurring in the environs of the repository.

Section 2.4 of Guide YVL 8.4 states that, whenever practicable, estimates of the probabilities of activity releases and radiation doses arising from unlikely disruptive events impairing long-term safety should be made. These probabilities should be multiplied by the calculated annual radiation dose or activity in order to evaluate the importance to safety of an event. In order to satisfy regulatory requirements, the expectation value should remain below the radiation dose or activity release constraints referred to above. If, however, the resulting individual dose implies deterministic radiation impacts (dose above 0.5 Sv), the order of magnitude estimate for its annual probability of occurrence should be 10^{-6} at the most.

In the present safety studies, the likelihood and consequence of the first two events is judged not to differ significantly between KBS-3V and KBS-3H repositories (although there will be some small difference in the probability of a vertical borehole intersecting vertically emplaced canisters compared with horizontally emplaced canisters) and these are not discussed in the present report. It should be noted that human intrusion is addressed in the main report of SR-Can by considering a borehole hitting a canister and then subsequently being used for drinking water abstraction. Drilling occurs 300 years after the sealing of the repository and the calculated doses are in the range of 10^{-4} to 10^{-3} Sv per year, assuming a fuel degradation rate of 10^{-7} per year and water flow through the affected canister of 1,000 litres per year /SKB 2006a/. The impact of substantial rock movement occurring in the environs of the repository is discussed in the present report in the context of the canister failure mode *rupture due to rock shear* – see Chapter 7.

In the very long term, after at least several hundred thousand years, Guide YVL 8.4 states that no rigorous quantitative safety assessment is required, but the judgement of safety can be based on more qualitative considerations. The types of considerations relevant to safety in the very long term are discussed further in /Ruokola 2002/. In the present safety studies, safety in the very long term is addressed mainly in the Complementary Evaluations of Safety Report /Neall et al. 2007/.

The present report focuses on the comparison of calculated doses and geo-bio fluxes with Finnish regulatory guidelines. The Swedish regulatory context differs from the Finnish one mainly in that the Swedish regulation SSI FS 1998 imposes a post-closure annual constraint on the risk of harmful effects (i.e. cancer and hereditary effects) of 10^{-6} for a representative individual in the group exposed to the greatest risk. This corresponds to a dose constraint of about 1.4×10^{-5} Sv per year, about one percent of the natural background radiation in Sweden /SKB 2006a/. The Swedish regulatory context is summarised in Appendix A of the main report of SR-Can /SKB 2006a/.

1.4 The current reference design

1.4.1 General description

In the KBS-3H repository design that is currently under consideration, spent fuel is disposed of deep underground, encapsulated in copper canisters with iron inserts. Each canister, with a surrounding partly saturated bentonite buffer, is placed in a perforated steel cylinder prior to emplacement. The entire assembly is called the supercontainer (Figure 1-3).

There are about 17–18 supercontainers per drift in the case of the reference BWR fuel from Olkiluoto 1 and 2. The supercontainers are positioned along parallel approximately horizontal deposition drifts, with an inclination of 1.5–2° to facilitate muck flushing. The supercontainers are supported by steel feet to leave an annular gap to the drift wall (about 4 cm in the current reference design) that will fill with bentonite as the buffer saturates and swells. Bentonite distance blocks separate the supercontainers, one from another, along the drift. These are also considered to form part of the buffer.

A KBS-3H drift and its components are shown in Figure 1-4. A section of drift with two supercontainers and one distance block is shown in Figure 1-5; the main dimensions are also indicated.

From a central tunnel (indicated in pale blue in Figure 1-4), the initial section of each deposition drift, before the drift end plug, is a 15-metre long, wider section of the drift with a 50 m^2 cross section that hosts the deposition equipment for supercontainers and distance blocks during the operational period. This section is called the "deposition niche".

The maximum length of the drift is 300 m, the estimated minimum length is 100 m and the average length is about 272 m, based on site-specific features /Autio et al. 2007/. In the current reference design, the drifts are dead-ended, i.e. there is no access tunnel on the other end.

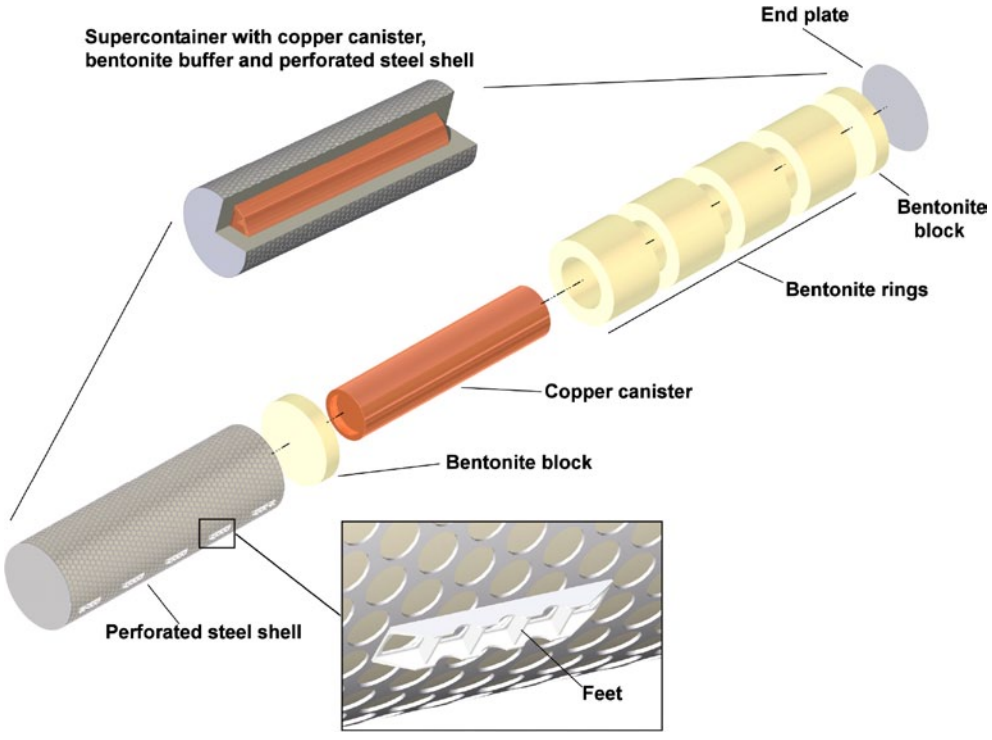

Figure 1-3. *The supercontainer with buffer and copper canister.*

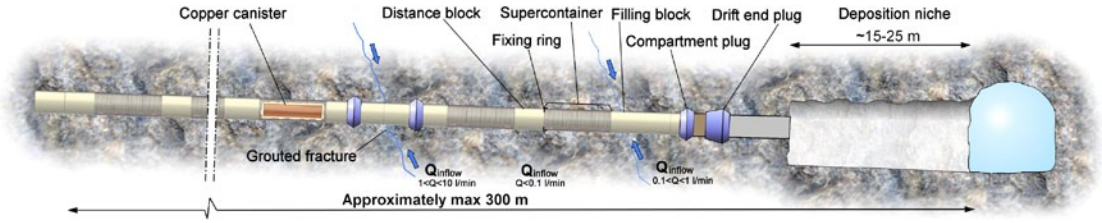

Figure 1-4. *Illustration of a generic KBS-3H drift showing one canister in copper colour for better visualisation. At one end of the drift, a wider area (deposition niche) hosts the deposition equipment while the other end of the drift is closed off.*

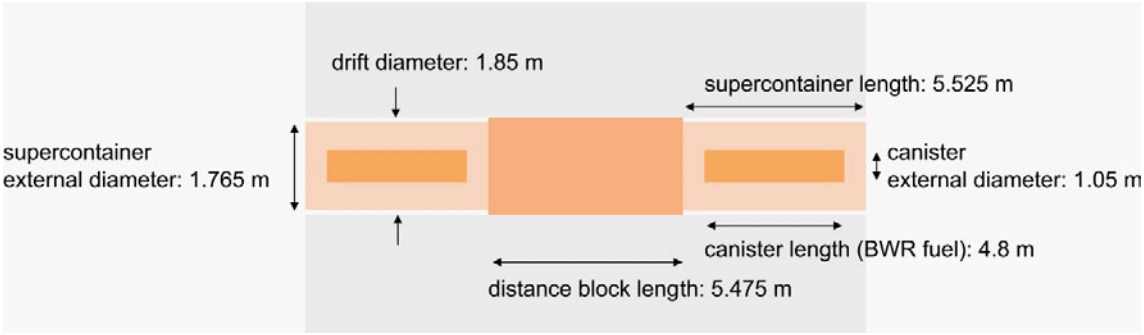

Figure 1-5. *Illustration of a section of a KBS-3H deposition drift with two supercontainers separated by a distance block. The 5.475 m distance block length is for the reference fuel for the present safety studies (BWR spent fuel from the Olkiluoto 1 and 2 reactors).*

Two broad realisations of KBS-3H design variants are currently being developed in parallel – the Basic Design, which is the current reference design option, and the Drainage, Artificial Watering and air Evacuation (DAWE) design variant /Autio 2007, Autio et al. 2007/. The final saturated state of the repository is essentially the same whichever option is implemented. Differences between the design options regarding the evolution of the repository principally affect the early evolution phase, prior to any possible release of any radionuclides (see Evolution Report by /Smith et al. 2007a, Appendix A/). Thus, the calculations reported here are applicable to either design option.

1.4.2 Safety concept, safety functions and the Base Scenario

Many aspects of evolution of KBS-3V and -3H repositories are expected to be the same or very similar. Furthermore, the essential elements of the KBS-3H safety concept – i.e. the conceptualisation of how the proposed system provides safety – are shared with KBS-3V. This common safety concept is illustrated in Figure 1-6, which shows the primary roles and relationships between the different technical components of the disposal systems.

The canister, the buffer (i.e. the bentonite material originally inside the supercontainers, together with the distance blocks) and the host rock are the main KBS-3H system components that together ensure isolation of the spent fuel and containment of radionuclides according to the KBS-3 safety concept shown in Figure 1-6. Each of these components performs a number of safety functions. Following SR-Can /SKB 2006a/, a safety function is defined as a qualitative role through which a repository component contributes to safety. Other KBS-3H system components, including the steel supercontainers, fixing rings and other structural materials, have not been assigned safety functions. They are, however, designed to be compatible with, and support the safety functions of the canister, the buffer and the host rock.

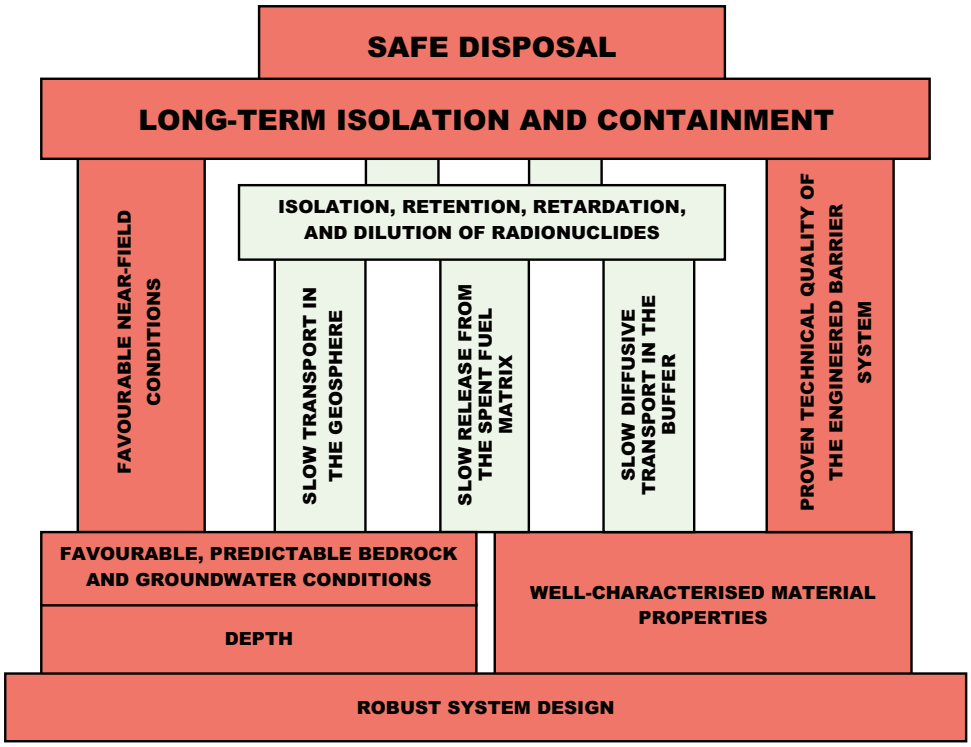

Figure 1-6. *Outline of the safety concept for a KBS-3 type repository for spent fuel in crystalline bedrock. Red pillars link characteristics of the disposal system to other characteristics on which they primarily depend. Green boxes and pillars indicate secondary characteristics and dependencies. /Posiva 2006/.*

The KBS-3H safety concept, like that of KBS-3V, rests first and foremost on the mechanical strength of the canister insert and the corrosion resistance of the copper surrounding it. The main safety function of the canisters is to ensure a prolonged period of complete containment of the spent fuel. As long as its copper shell is not breached, a canister will provide complete containment of radionuclides, and the spent fuel will interact with the environment only by means of heat generation and low level gamma and neutron radiation penetrating through the canister walls.

Safety functions of the buffer are (a), protection of the canisters, and (b), limitation and retardation of radionuclide releases in the event of canister failure. These safety functions are the same in KBS-3V and KBS-3H. The current KBS-3H design includes the use of steel components external to the canister, which will corrode over time and give rise to potentially[6] porous or fractured corrosion products. These may interact chemically with adjacent bentonite and the slow formation of an altered zone with perturbed mass-transport properties at the bentonite/rock interface at supercontainer locations cannot be excluded. A final safety function of the KBS-3H buffer (or, more specifically, the distance blocks) is, therefore, (c), to separate the supercontainers hydraulically one from another, thus preventing the possibility of preferential pathways for flow and advective transport within the drifts through the corrosion products or altered buffer.

[6] Magnetite, the most likely corrosion product, can form a thin but protective layer against corrosion with little or no connected porosity when produced under high pressure and temperature. In the repository, steel components external to the canister will be converted to magnetite under a high buffer swelling pressure, although the temperature will not be high. The porosity and hydraulic conductivity of the magnetite formed under these conditions are uncertain. Furthermore, it may also be fractured and the possibility of it forming a hydraulically conductive layer at the buffer-rock interface cannot currently be excluded. In addition, other corrosion products may also be formed.

The safety functions of the host rock are the same in KBS-3V and KBS-3H. These are (a), to isolate the spent fuel from the biosphere, (b), to provide favourable and predictable mechanical, geochemical and hydrogeological conditions for the engineered barriers, protecting them from potentially detrimental processes taking place above and near the ground surface, and (c), to limit and retard both the inflow of harmful substances[7] to the engineered barrier system and radionuclide releases to the biosphere.

Following the requirements given in regulatory Guide YVL 8.4 /STUK 2001/, a Base Scenario for the evolution of a KBS-3H repository at Olkiluoto assumes that the performance targets defined for each barrier are met. This is interpreted as meaning that each barrier fulfils the safety functions assigned to it in the safety concept for a period extending to a million years or more. If the engineered barrier system performs as designed, the expected minimum lifetime of the canister is in the order of tens of millions of years, as discussed in the KBS-3H Evolution Report /Smith et al. 2007a/ and in the KBS-3V Evolution Report /Pastina and Hellä 2006/. Thus, in the Base Scenario, there are no canister failures within a million year time frame. This does not imply that the system does not evolve over time in this scenario. Corrosion of the copper canisters initially due to oxygen entrapped at the time of emplacement, and, in the longer-term, due principally to sulphide present in the buffer and in the groundwater will inevitably occur and eventually lead to failure[8]. However, provided the other components of the system fulfil their safety functions, rates will be low – in the order of a few tens of nanometres per year /Pastina and Hellä 2006/ – and canister integrity should be preserved for at least a million years.

1.5 The purpose, scope and limitations of radionuclide release and transport analyses

The discussions in the Process Report /Gribi et al. 2007/ and Evolution Report /Smith et al. 2007a/ indicate that, while a prolonged period of isolation of the spent fuel and containment of radionuclides in the copper canisters, as in the Base Scenario, is the expected course of evolution for a KBS-3H repository, there are evolutionary paths or scenarios that cannot currently be excluded in which one or more canisters fail, giving rise to some radionuclide releases. According to the safety concept (Figure 1-6), safety in these scenarios rests principally on complete containment of radionuclides by the remaining canisters and, for the failed canisters, slow release from the spent fuel, slow diffusive transport in the buffer, and slow transport in the geosphere to the biosphere. Each of these is, however, subject to uncertainties. A key purpose of radionuclide release and transport calculations is to assess the robustness of the safety concept in view of these uncertainties.

Some uncertainties are treated using models, computer codes and parameter values that are conservative, meaning that they tend to over-estimate radiological consequences. Identifying what is a conservative model approach, assumption or parameter value is not, however, always straightforward – what is conservative with respect to one process may not be conservative with respect to another competing process. Furthermore, a purely conservative approach does not give a basis for deciding which uncertainties are the most important in terms of system performance. Thus, many uncertainties are treated by defining a range of assessment cases – i.e. specific model realisations of different possibilities or illustrations of how a system might evolve and perform in the event of canister failure – and analysing these cases in terms of hazard to humans

[7] Including the chemically toxic components of spent fuel, as discussed in the Complementary Evaluations of Safety Report /Neall et al. 2007/.

[8] As discussed in the Evolution Report, corrosion due to the migration of oxygen to repository depth in association with glacial retreat is considered highly unlikely (see Section 7.3.5 of /Smith et al. 2007a/). Furthermore, even if this were to occur, scoping calculations by /Ahonen and Vieno 1994/ indicate that canister failure by corrosion due to the presence of oxygen would hypothetically require exposure to oxygenated water to be maintained for at least 100,000 years, which is an unrealistically long period.

and the environment, quantified in terms of dose or nuclide-specific fluxes across the geosphere/biosphere interface (in order to compare with Finnish regulatory guidelines).

Given that a key question addressed by the KBS-3H safety studies is whether or not there are safety issues identified in the KBS-3V/KBS-3H difference analysis with the potential to lead to unacceptable radiological consequences, a number of specific assessment cases are defined addressing uncertainties related to features and processes that have a different significance for, or potential impact on, KBS-3H compared with KBS-3V. Additional cases are also analysed to illustrate the impact of other uncertainties in key features of the safety concept. Nevertheless, the range of cases analysed is significantly more limited than that considered, for example, in either TILA-99 /Vieno and Nordman 1999/ or SR-Can /SKB 2006a/, and not all conceivable uncertainties and combinations of uncertainties are covered. For example, uncertainties in the transport barrier provided by the geosphere, biosphere uncertainties and uncertainties related to future human actions are either not addressed or are analysed in less detail than others.

While use has been made, as far as possible, of well-tested and thoroughly reviewed models, computer codes and databases in analysing the assessment cases, these models, computer codes and databases involve significant simplification of the real system. Furthermore, data for analysing assessment cases are based on the preliminary design and data available at the time of writing the present report (see Section 2.3.3). The motivation for and plausibility (or conservatism) of selected parameter values and model assumptions used have been reported as much as possible in this text (or in the appendices) given the time constraints. This discussion is, however, often limited and largely qualitative. In the case of geosphere transport modelling, the modelling approach and parameter values used are based largely on TILA-99, and more recent developments in the understanding of the Olkiluoto site are used only to provide additional support for the parameter values selected (e.g. in terms of their conservatism). A comprehensive data report along the lines of that prepared for SR-Can /SKB 2006b/, with structured procedures for handling input data to radionuclide release and transport calculations, will be considered in any future safety studies of a KBS-3H repository, and is likely to be required in support of a future safety case.

Consistent with Finnish regulations, assessment cases address radionuclide release and transport over a million year time frame. While different possible canister failure modes leading to the release of radionuclides in this time frame are considered, there is only limited discussion of the likelihood of occurrence of these different modes. The consequences of the ultimate failure of the repository multi-barrier system in the farthest future (beyond a million years), including the possible exhumation of the repository, are discussed in the Complementary Evaluations of Safety Report /Neall et al. 2007/.

Groundwater flow and composition will vary significantly over a million year time frame, particularly following major climate change. For example, following a change to a colder climate, the development of permafrost would be likely to lead to a more stagnant flow pattern at repository depth, whereas the high pressure exerted by an overlying warm-based ice on the liquid water between the ice and the rock could conceivably force large volumes of dilute meltwater into deeper parts of the bedrock. The impact of major climate change on groundwater flow and composition is described in detail in Section 8.3.3 of /Pastina and Hellä 2006/. A significant limitation of the present safety assessment is the assumption of steady groundwater flow and (with the exception of one assessment case – PD-GMWV, see Section 5.11) composition, although the impact of assuming different (though steady) flow rates and compositions is assessed.

Given the above-mentioned limitations, the present analysis of a limited range of assessment cases in not considered sufficient to determine whether or not the current realisation of KBS-3H satisfies all relevant regulatory guidelines. A full safety assessment of the KBS-3H that answers this question is not likely to be made until such time as an updated KBS-3V assessment of the Olkiluoto Site is available (i.e. in late 2012).

1.6 Contents and structure of this report

In documenting radionuclide release and transport calculations in the present report, efforts have been made to ensure transparency in scenario and case selection, and in the selection of models and parameter values to analyse the cases. Efforts have also been made to ensure that the descriptions of model assumptions and parameters allow traceability – i.e. that they are sufficiently comprehensive to allow the analyses to be reproduced in all their important details either by Posiva or by an external party, if required.

The structure of the remaining chapters of the report is as follows.

Chapter 2 of this report deals with the selection of assessment cases for quantitative analysis.

Chapter 3 describes the general modelling approach, the computer codes used to calculate the resulting doses and discusses the comparisons of calculated releases with regulatory guidelines, including the indicative stylised drinking water well used to evaluate doses.

Chapter 4 describes radionuclide release and transport processes in the near field and in the geosphere.

Chapters 5, 6 and 7 present the calculated releases from the geosphere into the biosphere. Chapter 5 addresses the cases of an initial penetrating defect in a canister; Chapter 6 addresses the cases of canister failure due to copper corrosion; Chapter 7 addresses the cases of canister failure due to a rock shear movement. For each canister failure mode, a Base Case and one or more variants are described in terms of the near-field model and geosphere model employed and the results obtained.

Chapter 8 provides an overview of the results and discusses the compliance with regulatory guidelines.

Finally, Chapter 9 summarises the main issues requiring further work.

The verification of computer codes is described in Appendices A and B. A quality check of the correctness of the application of the main near-field release and transport code used in this report against an alternative code used in Switzerland in recent Nagra safety assessments has been carried out, which also illustrates the consequences of some model differences incorporated in the codes (Appendix B). Appendix C presents some sensitivity analyses illustrating the impact of variations in the rock matrix penetration depth on geosphere performance. The compositions of the groundwaters and bentonite porewaters used in the modelling of solubilities are presented in Appendix D. The solubility data, assumptions and uncertainties associated with the results are presented in Appendix E. The biosphere and the evaluation of dose are discussed in Appendix F. Appendix G presents a comprehensive set of results for all assessment cases and all calculated radionuclides in the form of near-field and geosphere releases as functions of time.

2 Selection of assessment cases

2.1 General approach

The approach adopted to assessment case selection in the present study involves the following main steps:

- identify plausible sequences of events or processes (scenarios) potentially leading to canister failure within a million year time frame, and the canister failure modes to which these scenarios give rise (Section 2.2);
- for each canister failure mode, define a Base Case against which to compare the results of variant cases (Section 2.3); and
- define a number of variant cases that illustrate the impact of specific uncertainties on the radiological consequences of canister failure (also Section 2.3).

The definition of an assessment case includes (i), the canister failure mode that is presumed to lead to the formation of transport pathways between the canister interior and its surroundings, and (ii), the models and data that describe subsequent radionuclide release and transport.

The discussions in the Process Report /Gribi et al. 2007/ and Evolution Report /Smith et al. 2007a/ indicate that, for a period extending to 1,000,000 years or more, the repository is expected to isolate the spent fuel from the surface environment, and the canisters are expected to provide complete containment of radionuclides, given the expected favourable near-field conditions and the proven technical quality of the engineered barrier system. However, these reports also identify three[9] plausible modes by which one or more canisters could fail within this time frame, namely:

- the presence of an initial, penetrating defect;
- failure due to corrosion of the copper canister shell; and
- rupture due to rock shear and the transfer of shear stresses from the rock via the buffer to the canister (in particular, in the event of post-glacial earthquake).

These failure modes are referred to, respectively, as PD, CC and RS in the nomenclature used to identify the assessment cases. The grouping of assessment cases according to the canister failure mode postulated is illustrated in Figure 2-1.

For each failure mode, a Base Case is defined, along with a number of variant assessment cases that address specific uncertainties. As noted in Chapter 1, the assessment cases address uncertainties that relate to features and processes that have a different significance for, or potential impact on, KBS-3H compared with KBS-3V, although additional cases are also identified to illustrate the impact of other key uncertainties.

Some additional cases not associated with any specific canister failure mode are also defined and analysed in order to enhance understanding of the geosphere as a transport barrier. These are sensitivity analyses illustrating the impact of variations in the thickness of the diffusion-accessible rock matrix on geosphere performance, and are presented in Appendix C.

[9] A fourth mode – collapse due to isostatic loading – is excluded on the basis that the stability of the canister under isostatic loading is ensured with a large safety margin. This failure mode is, therefore, not addressed in analyses of radionuclide release and transport (except as a secondary failure mode in the case of canisters with initial penetrating defects that have been weakened by corrosion of the insert); see Sections 5.4.3 and 7.4.4 of /Smith et al. 2007a/.

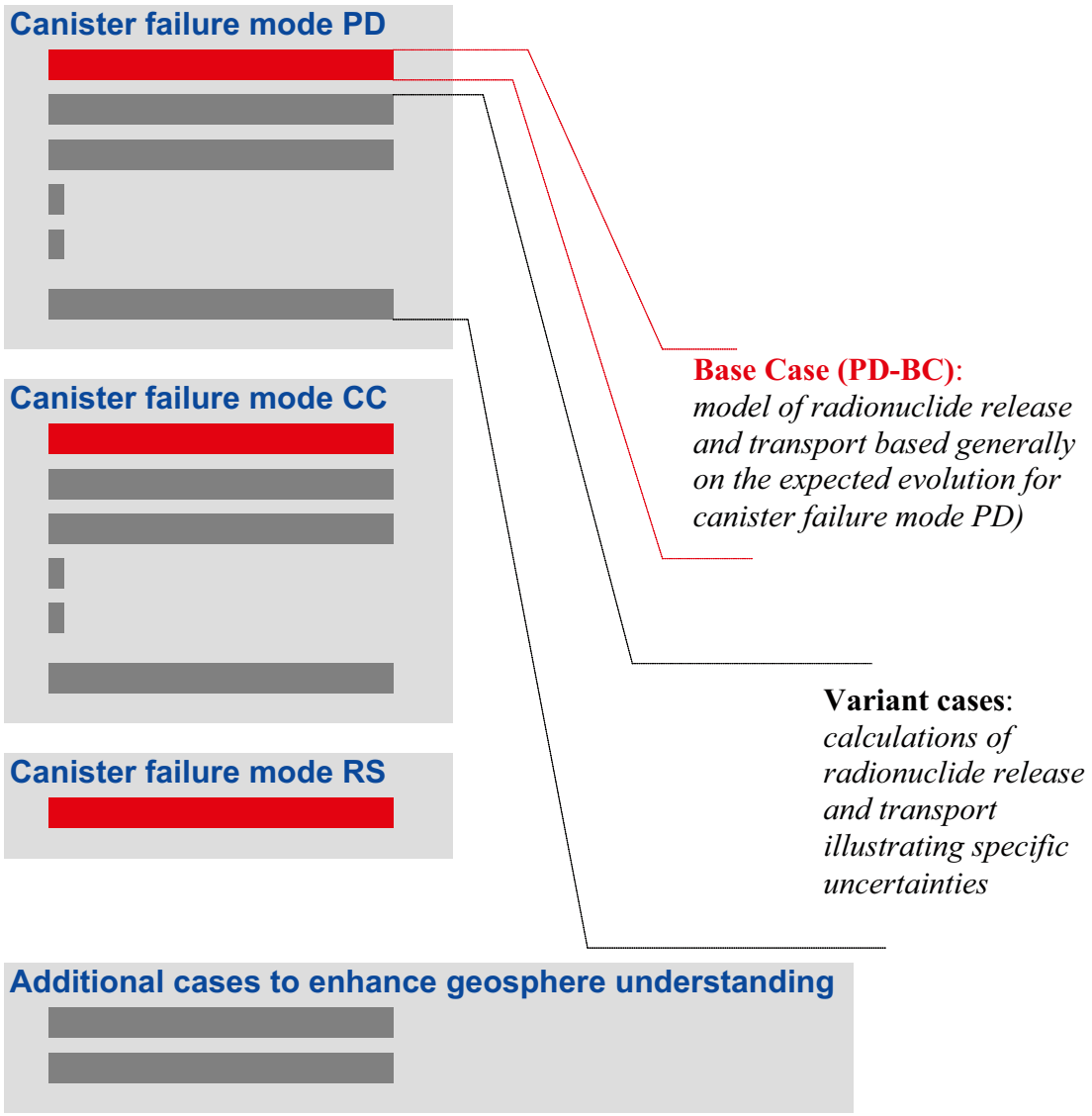

Figure 2-1. *Grouping of assessment cases according to the canister failure mode postulated.*

The models and data that define each case are individually specified, based on experience from, and practice in, earlier safety assessments, primarily TILA-99 /Vieno and Nordman 1999/ and SR-Can /SKB 2006abcde/, but modified where necessary to take account of the specific features of the reference KBS-3H design. This "deterministic" approach has been adopted, rather than a "probabilistic" approach in which parameter values are sampled randomly from probability density functions (PDFs). A deterministic approach can give a clear illustration of the impact of specific uncertainties. Furthermore, it avoids the need to define PDFs that quantify in single distributions widely different types of uncertainty (e.g. "aleatory" uncertainties related to variability or randomness and "epistemic" uncertainties arising, for example, where there is a range of plausible alternative models consistent with current scientific knowledge). Furthermore, in the present safety assessment, the treatment of some uncertainties involves model assumptions that are hypothetical and highly conservative (e.g. the treatment of a perturbed buffer/rock interface as a highly conductive "mixing tank"), and it is unclear whether or not it is meaningful to assign a probability attached to such assumptions. However, both deterministic and probabilistic approaches, however, have advantages and disadvantages, as discussed in Section 5.7.2 of the Complementary Evaluations of Safety Report /Neall et al. 2007/, and, in some recent safety assessments, a combination of the two approaches has been employed. Examples of combined approaches are SR-Can /SKB 2006a/ and the Swiss Project Opalinus Clay /Nagra 2002/.

2.2 Scenarios leading to canister failure and radionuclide release in a million year time frame

2.2.1 Methodology to identify scenarios

The methodology used to identify scenarios leading to canister failure and radionuclide release from a KBS-3H repository is taken directly from SR-Can. It can be described in terms of the following steps:

1. Consider the safety functions of each of the main components of the disposal system.
2. For each safety function, identify one or more safety function indicators.
3. For each safety function indicator, derive safety function indicator criteria.
4. Develop understanding of the system and its evolution – with a focus on the safety functions.
5. Identify the failure modes (loss of safety functions) that could occur in the course of system evolution.
6. Consider if and when the occurrence of such failure modes is plausible.
7. Consider the implications of loss of one safety function on the others.
8. Identify plausible descriptions of the evolution of safety functions over time.

The products of this methodology – plausible descriptions of the evolution of safety functions over time – are described in the following as "scenarios", although, in SR-Can, because of the way in which Swedish regulatory guidance is formulated, all those that are considered "probable" fall within the scope of one or or both of the two variants of a single scenario (termed the "main" scenario in SR-Can) describing the reference evolution of the disposal system. Other scenarios considered in SR-Can address situations that are considered less likely to occur (see Section 11.3 of the main report of SR-Can, /SKB 2006a/).

The application of the methodology is also described in the Evolution Report /Smith et al. 2007a/. It draws extensively on system understanding developed in the course of SR-Can, /SKB 2006a/ as well as that described in the Evolution Report for a KBS-3V repository at Olkiluoto /Pastina and Hellä 2006/, but also involves consideration of features and processes of specific relevance to KBS-3H which have the potential to lead to significant perturbations to the safety functions. These features and processes, which may affect not only the canister failure mode and the timing of canister failure but also, in some cases, radionuclide transport subsequent to canister failure, are described in the following section.

2.2.2 Consideration of features and processes in the evolution of a KBS-3H repository

Most of the identified features and processes with aspects that have a different significance for, or potential impact on, KBS-3H compared with KBS-3V.have the potential to affect, in the first place, the mass transport properties of the buffer and the buffer/rock interface. As a consequence, however, they may affect canister lifetime by increasing the rate at which sulphide from the groundwater migrates to, and corrodes, the canister surface, as well as the rate at which released radionuclides are transferred across the interface. These features and processes, associated uncertainties and the evaluation of impact of these on the mode and timing of canister failure and on subsequent radionuclide release and transport, are shown in Table 2-1, and described further, below.

Some limited piping and erosion may occur during the saturation of the KBS-3H buffer, but it is not expected to be sufficiently extensive to result in loss or significant degradation of the buffer safety functions (see Process Report Section 4.5.2 and scoping calculations in Evolution Report Appendix B.4). In particular, although it may result in some local changes in the diffusion coefficient of the buffer, transport within the buffer is expected to remain diffusion dominated.

Table 2-1. Features and processes with different significance for, or potential impact on, KBS-3H compared with KBS-3V, their relevance to radionuclide release and transport and major uncertainties, including an evaluation of the impact of uncertainties on canister failure mode and timing and on radionuclide transport. PR: Process Report /Gribi et al. 2007/, ER: Evolution Report /Smith et al. 2007a/.

Feature/process	Relevance to system evolution	Major uncertainties	Evaluation of impact	
			Impact on canister failure mode/timing	Impact on radionuclide transport (see Section 2.3)
Piping and erosion during the operational phase and during saturation (cf. PR Section 4.5.2; ER Section 5.5.6)	May locally perturb buffer density and increase rate of diffusion of corrosive agents to canister surface and rate of radionuclide diffusion from failed canister	Likelihood of occurrence; amount of bentonite conveyed by piped water; degree of homogenisation after piping/ erosion ceases	Scoping calculations in ER Appendix B.7	Illustration of impact of increased radionuclide diffusion rates in buffer in assessment case **PD-HIDIFF**
Processes due to the presence of steel components (external to canister) and their corrosion products (cf. PR Section 4.7.1; ER Sections 5.4.2; 5.6.4; 6.5.3)	May result in chemical alteration of buffer and consequent changes to physical properties; may perturb mass transfer at buffer/rock interface	Degree and spatial extent of perturbation	Scoping calculations in ER Appendix B.7 (impact on capacity of buffer to protect canister in the event of rock shear movements < 10 cm assumed to be negligible)	Illustration of impact of increased radionuclide mass transfer at buffer/ rock interface and mixing in outer part of buffer in assessment cases **PD-FEBENT1**; **PD-FEBENT2**; **PD-FEBENT3**
	May provide sorbing surfaces for radionuclides (which could be released following a change in groundwater chemistry); Fe(II) may compete for sorption sites on buffer; it may also act as a sink for dissolved sulphide, reducing the flux of sulphide to the canister surface.	Quantitative understanding of impact; possibility of release of sorbed radionuclides in the event of change in groundwater chemistry	Favourable effect of iron acting as sink for sulphides not evaluated quantitatively.	Impact on sorption not assessed (remaining issue for further study); impact on buffer as a whole of change in groundwater chemistry at 70,000 years due to influx of glacial meltwater illustrated in **PD-GWMC**
H_2 from corrosion of steel components (external to canister) (cf. ER Sections 5.3.1; 5.6.4; 5.7.4)	May delay saturation in tight drift sections	Quantitative understanding of impact	None expected	None expected
	May participate in microbial reduction of sulphate to sulphide, which may subsequently corrode canister surface	Quantitative understanding of impact	Scoping calculations in ER Appendix B.7 (minor impact)	None expected
	May perturb groundwater flow and radionuclide transport in the geosphere for the first few thousand years	Quantitative understanding of impact	Minor impact on mass transfer of corrosive agents between geosphere and buffer (not quantitatively evaluated)	Impact on radionuclide transport for an initially defective canister not assessed (remaining issue for further study)

High-pH leachates from cementitious components (cf. ER Section 5.6.5)	May result in chemical alteration of buffer and consequent changes to physical properties; may perturb mass transfer at buffer/rock interface	Degree and spatial extent of perturbation	Scoping calculations in ER Appendix B.7	Illustration of impact of increased radionuclide mass transfer at buffer/ rock interface and mixing in outer part of buffer in assessment cases **PD-FEBENT1**; **PD-FEBENT2**; **PD-FEBENT3**
KBS-3H drift and surrounding EDZ/rock spalling (cf. ER Sections 4.1.2; 5.4.5)	May perturb mass transfer at buffer/rock interface	EDZ hydraulic properties; impact of buffer swelling on rock spalling; transport characteristics of spalled zone	Scoping calculations in ER Appendix B.7.	Illustration of impact of rock spalling in assessment case **PD-SPALL**
Expulsion of water from a defective canister interior by gas (cf. PR Section 2.5; ER Section 8.10.3)	Expelled water may convey dissolved radionuclides	Location of canister defect; rate of gas pressure build-up inside canister	No major effects (minor impact on likelihood of canister failure by rock shear; ER Appendix B.5)	Impact of expulsion of contaminated water by gas illustrated in assessment case **PD-EXPELL**

The impact of a higher buffer diffusion coefficient on sulphide transport and canister lifetime has been evaluated in scoping calculations in Appendix B.7 of the Evolution Report, and shown to be minor. Piping and erosion does not, therefore, give rise to any specific canister failure scenarios, although an assessment case in which an increased buffer diffusion coefficient is used to model radionuclide transport through the buffer in the event of radionuclide release from a canister with an initial penetrating defect is defined in this report (case PD-HIDIFF; see Section 2.3).

Thermally-induced rock spalling[10] and the presence of an excavation disturbed or damaged zone (EdZ/EDZ) around the deposition drift (Process Report Section 7.6.3), the presence of porous or fractured supercontainer shell corrosion products[11] at the drift wall (Process Report Section 4.7.1), iron/bentonite interaction (Process Report Section 4.7.1) and cement/bentonite interaction (Process Report Section 4.7.2) may all affect mass transport at the buffer/rock interface. The affected region may be fractured or porous, and allow mass transport by advection as well as diffusion. In addition to the impact of steel and its corrosion products on mass transport at the buffer/rock interface, corrosion of the supercontainer shells and the other steel components a KBS-3H repository may lead to high hydrogen partial pressures, which could have an effect on the bentonite porewater chemistry. The impact of hydrogen gas on the bentonite porewater chemistry has not yet been fully evaluated. Various factors need to be considered, including acid-base equilibria and the pH buffering capacity of bentonite, as well as the limited timeframe of hydrogen production of several thousand years. The overall impacts, in particular any effects on the buffer, should be taken into account in future studies.

The impact of these processes on sulphide transport and canister lifetime has also been evaluated in scoping calculations in Appendix B.7 of the Evolution Report, in which the interface is treated as a mixing tank. Assuming a sulphide concentration in the groundwater of 12 mg per litre, which is the currently observed maximum value at Olkiluoto, the result is a minimum canister lifetime of about a million years. There is some uncertainty associated with the variability of sulphide concentration with time, and with the conservatism of the value assumed for the flow through fractures intersecting the drift. Nevertheless, a canister lifetime in excess of 100,000 years is expected, even in the event of a significantly perturbed buffer/rock interface. Perturbation to the buffer/rock interface will also affect radionuclide transport across the interface, and assessment cases involving transport across a perturbed interface in the event of radionuclide release from a canister with an initial penetrating defect are defined in this report (Cases PD-SPALL, PD-FEBENT1, PD-FEBENT2 and PD-FEBENT3; see Section 2.3). The impact of iron-bentonite interaction on radionuclide sorption in the buffer is not evaluated, and is noted as an issue requiring further study.

Mineral transformation in the buffer due to its interaction with supercontainer steel shell corrosion products could lead to a loss of buffer plasticity. If sufficiently extensive, transformation of the buffer could therefore make the canister more vulnerable to failure by rock shear in the event of a large earthquake. According to /Börgesson et al. 2004/, the unperturbed buffer is expected to protect the canister against rock shear movements of the order of 10 cm and smaller with a significant safety margin. Since, in reality, somewhat larger shear movements are also unlikely to result in canister damage in the case of an unperturbed buffer, and since mineral transformation is only expected to affect a small part of the buffer near to its interface with

[10] Although rock spalling is also relevant to KBS-3V, its impact on radionuclide release and transfer may differ because, in KBS-3V, the rock affected by spalling can be hydraulically connected to the relatively conductive deposition tunnel and its associated excavation disturbed/damaged zone (EdZ/EDZ).

[11] Magnetite, the most likely corrosion product, can be made to form a thin but protective layer against corrosion with little or no connected porosity when produced under high pressure and temperature. In the repository, steel components external to the canister will be converted to magnetite under a high buffer swelling pressure, although the temperature will not be high. The porosity and hydraulic conductivity of the magnetite formed under these conditions is uncertain, and may be very low, although it may also be fractured and the possibility of it forming a hydraulically conductive layer at the buffer/rock interface cannot currently be excluded.

the rock /Wersin et al. 2007/, the capacity of the buffer to protect the canisters from rock shear movements smaller than 10 cm is expected to be maintained in the event of such transformation.

Methane and hydrogen are present naturally in the groundwater and hydrogen will also be generated by the corrosion of the steel repository components, principally the supercontainer shell. These gases could participate in the reduction of groundwater sulphate to sulphide in the presence of sulphate reducing bacteria, increasing the sulphide concentration and the rate of canister corrosion. It is argued in Appendix B.7 of the Evolution Report /Smith et al. 2007a/ that the impact of repository-generated hydrogen on canister lifetime is small, although the impact of methane in the groundwater remains an issue for further study.

Repository-generated gas, principally hydrogen from the corrosion of steel components, may also form bubbles, which could affect groundwater flow to a degree not currently fully understood. However, since bubble formation is associated with the transient phase, any perturbation to groundwater flow is likely to have largely ceased by the time most radionuclides are released from failed canisters (in the case of a canister with an initial penetrating defect through the copper shell, it may take around a thousand years for a transport pathway to be established between the canister interior and exterior and releases are initially expected to be relatively small due the large transport resistance of the defect – it is likely to take several thousands of years more for the transport resistance of the defect to be lost – see Chapter 5).

If a canister has a penetrating defect, water ingress through the defect and subsequent expulsion of water and dissolved radionuclides by gas generated and trapped inside the canister is a possibility for both KBS-3H and KBS-3V. It is, however, more likely to occur in the case of KBS-3H compared with KBS-3V if it can be assumed that penetrating defects are a possibility primarily in the welding region, which is located at the top of the canister. If this is the case then, in KBS-3V, gas can escape from a vertically orientated defective canister without the development of pressures that could expel water and radionuclides. In KBS-3H, on the other hand, the defect could be located on the lower side of the horizontally orientated canister, which would allow gas to become trapped. The gas pressure inside the canister will then rise until it exceeds the gas breakthrough pressure of the bentonite. Gas pathways will form that may transport radionuclides present as volatile species (mainly C-14). This situation is considered in assessment case PD-EXPELL.

2.2.3 Overview of scenarios

The various scenarios shown in Figure 2-2 have been identified by applying the methodology outlined in Section 2.2.1. The scenarios are shown as combinations of barrier states (a “no fail” state indicates that all safety functions are assumed to be fulfilled), and are grouped according to the initial canister failure mode that they involve.

As indicated by arrows in Figure 2-2, scenarios involving canister failure and radionuclide release are initiated, in the first place, by:

- the presence of an initial, penetrating defect in one or more of the canisters;
- perturbations to the buffer and buffer/rock interface[12], giving rise to an increased rate of transport of sulphide from the geosphere to the canister surface and an increased canister corrosion rate;
- penetration of dilute glacial meltwater to repository depth, giving rise to chemical erosion of the buffer an increased rate of transport of sulphide from the geosphere to the canister surface and an increased canister corrosion rate; and
- rock shear movements of sufficient magnitude to give rise to shear failure of the canisters.

[12] The buffer state “low density/alteration (outer buffer)” includes perturbations to the buffer/rock interface that primarily affect the rock, i.e. rock spalling and the presence of a conductive EdZ/EDZ.

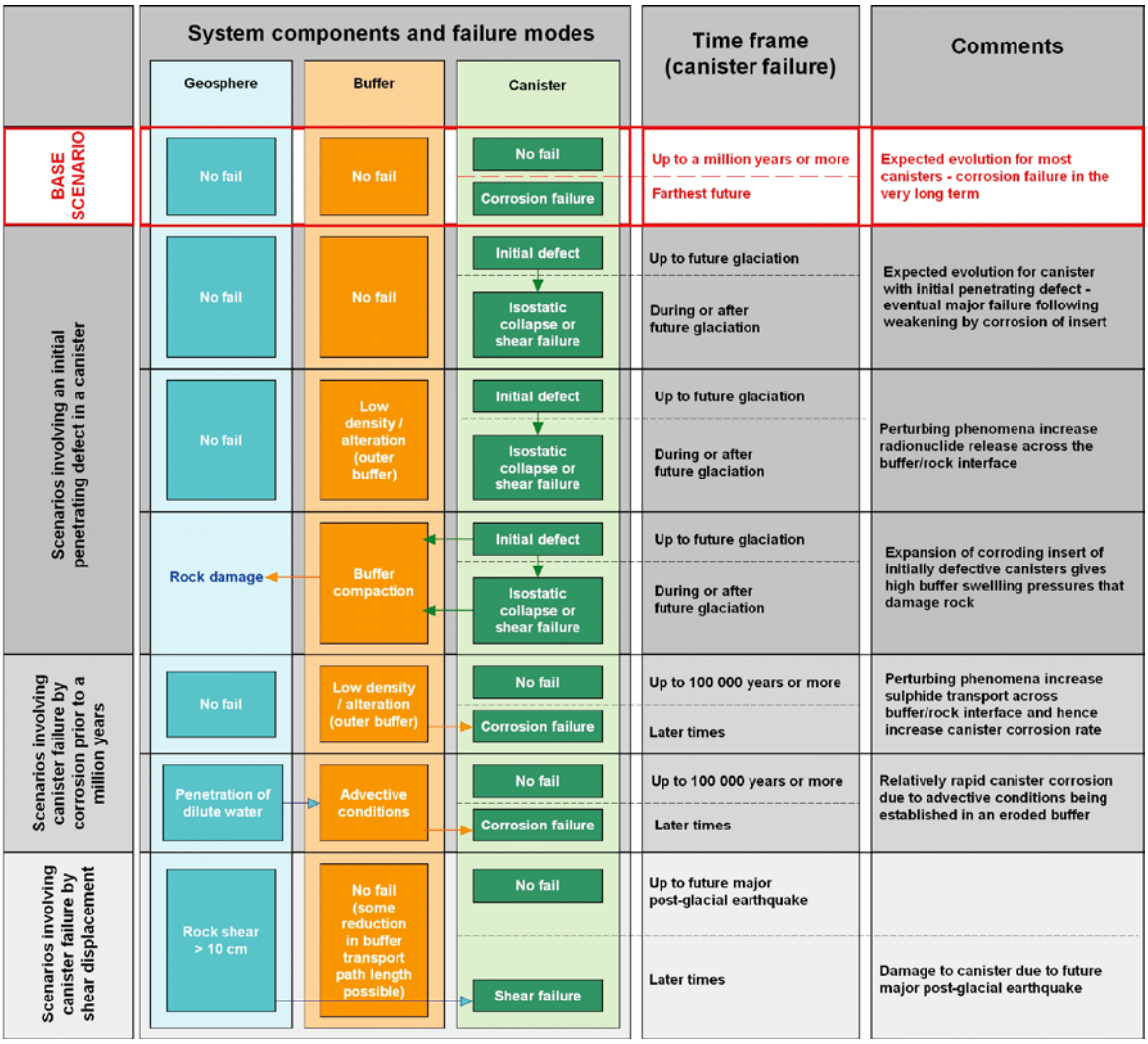

Figure 2-2. *Potential system states in different time frames analysed in the present safety case – the Base Scenario is shown in red.*

The Base Scenario in which there is no radionuclide release in a million year time frame has already been discussed in Section 1.4.2. Other scenarios, which involve canister failure and radionuclide release within this million-year time frame, are described in the following sections.

2.2.4 Scenarios involving the presence of initial penetrating defects

(i) General description

The evolution of a canister with a postulated initial penetrating defect is described in Chapter 8 of the Evolution Report /Smith et al. 2007a/. The defective canister will initially provide some transport resistance, limiting the rate of water ingress and radionuclide release. Corrosion and volume expansion of the insert are, however, expected to lead to a reduction of this transport resistance over time. They will also lead to a gradual weakening of the canister and eventual isostatic collapse or shear failure, possibly in association with a future glaciation.

Figure 2-2 depicts three scenarios involving the presence of one or more initial, penetrating defects. In all three scenarios, the canister is assumed to undergo eventual isostatic collapse or shear failure during or after a future glaciation.

- In the first scenario, the buffer and geosphere are assumed to fulfil all their safety functions for at least a million years.
- In the second scenario, the buffer/rock interface is perturbed, leading to enhanced release of radionuclides from the failed canisters across the interface. Features and processes that may lead to perturbations of the buffer/rock interface, and that have a different significance for, or potential impact on, KBS-3H compared with KBS-3V, have been described in Section 2.2.2. It should be noted that, while perturbations to the buffer/rock interface may also affect the rate of corrosion of the copper canister (Section 2.2.5), the corrosion rate of the copper canister will still remain low (isostatic collapse or shear failure will eventually occur, as in the other scenarios involving an initial penetrating defect).
- In the third scenario, corrosion and volume expansion of the cast iron insert is assumed to lead to compaction of the buffer around the canister, and an increase in swelling pressure that damages the rock. A conservative scoping calculation in Appendix B of the Evolution Report indicates that corrosion of the insert could lead to an increase in buffer density around the canister to about 2,160 kg m^{-3}, which could give swelling pressures of around 10 MPa or greater, depending on the salinity of the groundwater (see Figure 4-7 in /SKB 2006a/). A modelling study by /Lönnqvist and Hökmark 2007/ found that, for a KBS-3H repository at Olkiluoto, a pressure on the drift wall of 10 MPa or more might open pre-existing horizontal fractures intersecting the drift at mid-height, although the effects are expected to be small in terms of increase in fracture aperture and distance from the drift wall to which such effects extend. This is the case even at pressures as high as 20 to 25 MPa.

The first scenario is considered in the Base Case for an initial penetrating defect (case PD-BC). The second scenario is considered in variant assessment cases PD-SPALL, PD-FEBENT1, PD-FEBENT2 and PD-FEBENT3 (see Section 2.3). The third scenario is addressed implicitly in the safety assessment by defining assessment cases in which the transport resistance of the geosphere is reduced (e.g. case PD-LOGEOR).

(ii) Likelihood of occurrence of initial penetrating defects

Given the central role of the canisters in the KBS-3H and KBS-3V safety concepts, the possibility of initial defects that penetrate the copper shell is of crucial importance. In principle, such defects could occur anywhere in the copper shell, but they are most likely to occur along welds and, in particular, at the seal of the canister top lid, which is less amenable to inspection than other welds.

SKB has made a first evaluation of the reliability of the friction stir welding process for canister sealing, which is the reference method assumed in SR-Can, and concluded that "the welding process produces reproducible results which satisfy stipulated requirements on minimum copper thickness with very good margins" /Ronneteg et al. 2006/. According to SR-Can, there are expected to be no canisters with initial penetrating defects in their copper shells /SKB 2006b/. Furthermore, out of the entire canister inventory considered in the SR-Can assessment (4,500 canisters), it has been estimated that 99% have no defect deeper than 10 mm and 1% have no defect deeper than 15 mm. SKB also studied the reliability of non-destructive testing (NDT) of the copper seal welds and concluded that the proposed NDT methods are well suited to checking the weld quality /Müller et al. 2006/.

Posiva plans to seal the lid of the copper overpack with electron beam welding, but currently retains friction stir welding as an alternative option. Although there are differences in Posiva's and SKB's canister designs, including the chosen reference welding techniques, the probability of initial penetrating defects in Finnish canisters is also expected to be low. On the other hand, in Finland, the quality assurance program for non-destructive testing techniques is still in an early phase of development. A non-destructive examination method for canister component manufacture and sealing will be selected by the end of 2008. A qualification programme for the applicable examination procedures will be made by the end of 2009 and executed by the end of 2012, before the application of the encapsulation plant construction license is submitted. Thus, Posiva is not yet taking any position on the likelihood of occurrence of canisters with initial penetrating defects.

In both methods, the seal location is on, or within a few centimetres of, the end-face of the canister, so that no differences can be identified between electron beam welding and friction stir welding from the long-term safety point of view if an initial penetrating defect is assumed to be present.

2.2.5 Scenarios involving canister failure by corrosion

(i) General description

There are two scenarios depicted in Figure 2-2 in which canister failure by corrosion occurs before a million years. These are scenarios in which:

1. the buffer/rock interface is perturbed by one or more of the processes described in Section 2.2.2, leading to enhanced mass transfer at the interface; and
2. dilute glacial meltwater penetrates to repository depth, leading to chemical erosion of the buffer and to advective conditions becoming established in the buffer.

These scenarios lead to canister failure times earlier than in the Base Scenario, due to their effects on the transport of sulphide from the groundwater to the buffer and across the buffer, and hence on sulphide concentrations at the canister surface. Features and processes that may lead to perturbations of the buffer/rock interface, and which have a different significance for, or potential impact on, KBS-3H compared with KBS-3V, have been described in Section 2.2.2. The impact of these and other processes potentially altering the buffer transport properties and canister lifetime is assessed in the scoping calculations in Appendix B.7 of the Evolution Report /Smith et al. 2007a/. Penetration of dilute water to repository depth in association with glacial retreat cannot be ruled out during future glacial cycles. Flowing groundwater with a reduced salinity at repository depth could potentially lead to the erosion of buffer material intruded into fractures intersecting the repository drifts if the ionic concentration in the water (proportional to the ionic strength) is less than the Critical Coagulation Concentration (CCC), as discussed in some detail in Section 2.5.10 of /SKB 2006c/. If, during repeated glacial cycles, the density of the buffer were to be reduced by erosion to such a degree that advective transport takes place within the buffer region, this could increase the rate at which sulphide migrates to the copper surface, and hence increase the copper corrosion rate and reduce canister lifetime.

Following canister failure, radionuclide transport across the buffer will be perturbed by the same features and processes that lead to enhanced sulphide transport to the canister surface. In all assessment cases addressing canister failure by corrosion, it is assumed that transport across the buffer is instantaneous irrespective of the scenario by which corrosion failure occurs (the buffer is treated as a "mixing tank"). This represents a highly conservative representation of a scenario in which only the buffer/rock interface is perturbed. It should be noted, however, that radionuclide transport in assessment cases in which only the outer part of the buffer is treated as perturbed are considered in the context of an initial penetrating defect (Cases PD-SPALL, PD-FEBENT1, PD-FEBENT2 and PD-FEBENT3).

(ii) Timing and likelihood of occurrence of canister failure by corrosion

The scoping calculations presented in Appendix B.7 of the Evolution Report /Smith et al. 2007a/ indicate that corrosion is unlikely to result in a canister lifetime of less than several hundred thousand years, even in cases where mass transport in the buffer is severely perturbed. It is acknowledged that there are several simplifying assumptions in scoping calculations that could result in somewhat higher or lower canister lifetimes than those calculated. Nevertheless, as noted in Section 2.2.2, a canister lifetime in excess of 100,000 years is expected, even in the event of a significantly perturbed buffer/rock interface.

In the case of chemical erosion by glacial meltwater, assuming a repetition of the last glacial cycle (from the Eemian interglacial to the end of the Weichselian glaciation), the next glacial retreat and hence the next possibility for penetration of glacial meltwater to repository depth is in about 70,000 years time (see, e.g. Figure 7-1 in the Evolution Report, /Smith et al. 2007a/). There is, however, significant uncertainty associated with anthropogenic emissions, especially greenhouse gases, which could significantly delay the formation of permafrost and ice sheets (Section 6.1 of the Evolution Report, /Smith et al. 2007a/). Even following partial erosion of the buffer, the rate of corrosion is expected to remain low due to the limited supply of sulphide from the groundwater. The scoping calculations given in Appendix B.7 of the Evolution Report indicate that a period in the order of about one million years would be required for failure by corrosion even if the entire buffer is treated as a mixing tank, based on the currently observed maximum sulphide concentration in the groundwater at Olkiluoto, and the current hydraulic gradient, although higher flows are expected in association with glacial retreat.

For the above reasons, assessment cases addressing canister failure due to rock shear also assume that failure occurs 100,000 years in the future. However, in neither scenario can an estimate currently be made of the likelihood or rate of canister failure by corrosion in a million year time frame, given the limited quantitative understanding of relevant processes, such as chemical erosion of the buffer and the impact of methane and hydrogen on the microbial reduction of groundwater sulphate to sulphide.

The canister positions most vulnerable to failure will be those associated with the highest groundwater flows at the buffer/rock interface. Where the rock adjacent to the drift is relatively tight, it may, for example, take many glacial cycles before sufficient buffer erosion occurs for advective conditions to become established in the buffer. /Lanyon and Marschall 2006/ have estimated the distribution of the mean flow around different supercontainers using a discrete fracture network model of the Olkiluoto site, although there are significant uncertainties in this model, as acknowledged by the authors. Figure 2-3 shows the calculated cumulative distribution of the flows past supercontainers, calculated using two versions of the discrete fracture network model, one with a fracture transmissivity cut-off of 10^{-10} m^2 s^{-1}, and one with a cut off of 10^{-11} m^2 s^{-1}. Irrespective of the version used, the highest flow around any 5.5 m drift section used for canister emplacement (5.5 m being the length of the supercontainer) is about 1.5×10^{-10} m^3 s^{-1}. About 15% of canister positions have flows between 1.5×10^{-11} m^3 s^{-1} and 1.5×10^{-10} m^3 s^{-1}. Thus, for example, if canisters in positions with flows within an order of magnitude of the maximum flow were to fail by corrosion in a million year time frame, this would correspond to 15% of all canisters. The actual flows that would lead to canister failure due to buffer erosion and advective conditions enhancing the rate of supply of sulphide for copper corrosion within this time frame remain, however, an issue for further study.

2.2.6 Scenarios involving canister rupture due to rock shear

(i) General description

Significant shear movements on fractures intersecting the repository drifts are most likely to occur in association with large earthquakes. The buffer is expected to protect the canister against rock shear movements of the order of 0.1 m and smaller with a significant safety margin

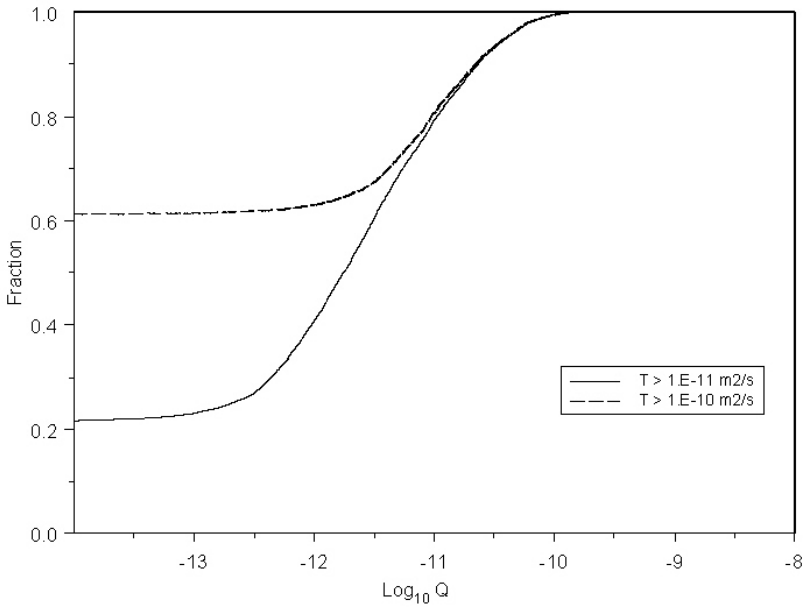

Figure 2-3. *Cumulative distribution of flows past supercontainers as calculated using discrete-facture network models with transmissivity cut-offs at 10^{-10} and 10^{-11} m^2/s (after Figure B-4 of /Lanyon and Marschall 2006/, curves for "Method 1").*

/Börgesson et al. 2004/. The maximum amount of movement is related to fracture size. There is, however, uncertainty in the degree to which large fractures with the potential to slip by more than 0.1 m can be identified and avoided when emplacing canisters along the drift, and so the potential consequences of shear movements greater than 0.1 m at canister emplacement locations need to be assessed.

A single scenario is depicted in Figure 2-2 involving, as the first mode of canister failure, rupture due to rock shear, where the shear movement is in excess of 0.1 m. In this scenario, following failure, the canister is assumed to cease to provide a barrier to water ingress and radionuclide release. There will be deformation and possibly some limited erosion of the buffer in this scenario, as well as some increase in the transmissivity of fractures intersecting the drifts, although the safety functions of the buffer and the geosphere (including protection of the remaining non-failed canisters) are assumed to be maintained.

(ii) Timing and likelihood of canister rupture due to rock shear

Any future large earthquakes occurring at the Olkiluoto site are not expected to be uniformly distributed in time. Studies of palaeoseismicity support the suggestion that major seismic activity was, in the past, limited to a short period after the last deglaciation, and it may be inferred that this will also be the case in the future (Section 2.2.2 of the Evolution Report, /Smith et al. 2007a/). Given that, based on a repetition of the last glacial cycle, the next glacial retreat will be in 70,000 years time (see the discussion of canister failure by corrosion in Section 2.2.5), assessment cases addressing canister failure due to rock shear also assume that failure occurs 70,000 years in the future.

Scoping calculations reported in Appendix B.5 of the Evolution Report give the expectation value of the number of canisters in the repository that could potentially be damaged by rock shear in the event of a large earthquake as 16 out of the total number of 3,000 canisters, although there are some significant uncertainties associated with these values that could lead to them giving either an underestimate or an overestimate of the actual likelihood of damage (see Section 7.4.5 in the Evolution Report, /Smith et al. 2007a/). The probability of an earthquake occurring that is sufficiently large to cause such damage in a 100,000 year time frame has been estimated as 0.02 (Table 5-8 in /La Pointe and Hermanson 2002/). A criterion for canister

positioning that reduces the number of potentially affected canisters – the Expanded Full Perimeter Criterion (EFPC) – has been developed and applied to the KBS-3V deposition tunnels in SR-Can /SKB 2006a/. However, a corresponding criterion has not so far been developed or tested for KBS-3H.

2.3 Selection of assessment cases for each canister failure mode

2.3.1 Methodology for case selection

The selection and detailed definition of assessment cases to evaluate radionuclide release and transport is in general a more subjective process than scenario identification.

As a first step, the Base Cases are selected, one for each of the canister failure modes. Parameters in the Base Cases are, in most instances, selected to be either realistic or moderately conservative in the sense that they are expected to lead to an overestimate of radiological consequences (see Section 2.3.3). Furthermore, perturbations to radionuclide release and transport caused, for example, by the steel and cementitious components of the KBS-3H repository external to the canisters are assumed to be negligible in the Base Cases (even though this may be non-conservative), but are considered in variant cases.

Variant cases are then selected, the results of which can be compared with those of the Base Cases to illustrate the impact of selected uncertainties. The variant cases for the most part take a more pessimistic view of uncertainties than the Base Cases.

Cases are identified to cover uncertainties that either:

- have different significance for, or potential impact on, KBS-3H compared with KBS-3V; or
- relate to key system features that are common to the KBS-3H and KBS-3V concepts.

In defining the various cases, it is ensured that the chosen models and parameter values are consistent with the scenarios that have been identified as leading to a given canister failure mode (e.g. a reduced geosphere transport resistance is assumed in cases dealing with canister failure due to rock shear, since rock shear may also have a detrimental impact on the geosphere as a transport barrier).

The uncertainties addressed by the assessment cases are shown in Table 2-2, with uncertainties with aspects specific to KBS-3H shown in italics and with a white background. Each uncertainty is assigned an identifier (shown in the third column in Table 2-2) in order to link it to one or more specific assessment cases.

The majority of variant cases are defined for the initial penetrating defect canister failure mode. Using the initial penetrating defect as a reference failure mode for exploring uncertainties provides a common basis for comparison with the earlier Finnish TILA-99 safety assessment /Vieno and Nordman 1999/, and is also the approach used in SR-Can. It should also be noted that many of these uncertainties are not specific to any particular canister failure mode. The assumption of an initial penetrating defect results in the earliest possible radiological impact, although not necessarily the largest impact, for each uncertainty considered.

Process tables that summarise the handling of internal processes in the safety assessment are used as check lists to ensure that no important processes and associated uncertainties have been overlooked in the identification of scenarios and assessment cases. Process tables for a KBS-3H repository at Olkiluoto are given in the Process Report /Gribi et al. 2007/. Furthermore, a detailed comparison of the calculational cases with those of TILA-99 and SR-Can has confirmed that there are no significant omissions or gaps in the KBS-3H assessment. The only exceptions are where limitations related to the scope of the assessment mean that the treatment of some uncertainties is put aside at this stage (see Complementary Evaluations of Safety Report, /Neall et al. 2007/).

Table 2-2. Uncertainties addressed by the assessment cases. Uncertainties that have a different significance for, or potential impact on, KBS-3H compared with KBS-3V are shown in italics and with a white background. PR: Process Report /Gribi et al. 2007/; ER: Evolution Report /Smith et al. 2007a/.

Feature	Uncertainty and identifier [used in Table 2-3]	
Canister/canister failure mode	Canister failure mode	Addressed in all cases
	Canister/fuel type in failed canister (BWR, VVER-440, EPR)	[C1]
	Size of initial penetrating defect	[C2]
	Delay until loss of transport resistance of defect	[C3]
Fuel characteristics	Fuel dissolution rate	[F1]
	Size of instantaneous release fraction (IRF)	[F2]
Canister insert/corrosion and gas generation/ expulsion (see PR Section 2.5; ER Section 8.10.3)	Gas generation rate	[G1]
	Potential for expulsion of contaminated water by repository-generated gas	[G2]
	Potential for repository-generated gas to convey radionuclides as volatile species	[G3]
Chemical speciation and solubility limitation	Near-field redox conditions	[R1]
	Chemical speciation of carbon and niobium	[R2]
Piping and erosion during buffer saturation (see PR section 4.5.2 and scoping calculations in ER Appendix B.4)	Occurrence/extent	[PE]
Buffer transport resistance	Impact of chemical erosion due to influx of glacial meltwater on mass transfer	[B1]
	Impact of rock shear	[B2]
Potential for perturbed mass transfer at buffer/rock interface due to: – Rock spalling (PR Section 7.6.3) – Supercontainer shell corrosion products at drift wall (PR Section 4.7.1) – Fe/bentonite interaction (PR Section 4.7.1 and scoping calculations in ER Appendix B.7) – Cement/bentonite interaction (PR Section 4.7.2 and scoping calculations in ER Appendix B.7)	Occurrence of perturbed interface	[MT]
	Physical extent of perturbed interface region (into buffer)	[MTX]
	Flow through perturbed region	[MTF]
Impact of hydrogen from corrosion of steel components external to canister on microbial reduction of sulphate to sulphide and on canister corrosion rate (ER Scoping calculations in Appendix B.7)	Occurrence/extent	[HCC]
Groundwater/buffer porewater salinity	General variability in space and time	[S1]
	Influx of glacial meltwater	[S2]
	Composition of glacial meltwater	[S3]
Groundwater flow/geosphere transport resistance	Groundwater flow at buffer/rock interface at location of failed canister – general variability	[G1]
	Geosphere transport resistance – general variability	[G2]
	Impact of rock shear/impact of corrosion of insert and buffer compaction	[G3]
Rock matrix diffusion	Matrix diffusion depth	[G4]

2.3.2 Overview of assessment cases

An overview of the assessment cases analysed in the present assessment is given in Table 2-3. The cases are grouped according to the canister failure mode that is assumed, each group having a Base Case and a number of variants. The uncertainties that are considered in each variant case are also indicated in the table, using the identifiers assigned in Table 2-2.

Each case is assigned a unique name by which it is identified in the following chapters. A name comprises two parts separated by a hyphen. The first part of the name indicates the canister failure mode that the case addresses:

PD: canister with an initial penetrating defect;

CC: canister failure due to copper corrosion; and

RS: canister failure due to rock shear.

The second part of the name identifies the case either as a Base Case (BC) for a given canister failure mode, or a variant case illustrating the impact of one or more uncertainties.

Cases MD-1, MD-2 and MD-3 illustrate the impact of rock matrix diffusion depth for a hypothetical pulse release to the geosphere, and therefore are not associated with a specific canister failure mode (these cases are discussed in Appendix C).

For practical reasons, in deterministic safety assessments, the number of cases defined and analysed is limited, generally to a few tens, and this is also true of the present assessment. All possible combinations of model assumptions and parameter values cannot be explored. Rather, the cases that are selected are chosen to illustrate the impact of some specific uncertainties with the potential to affect radionuclide release and transport, with an emphasis on uncertainties that have a different significance for, or potential impact on, KBS-3H compared with KBS-3V, although other important uncertainties are also addressed. Combinations of uncertainties (i.e. cases that address the question "*what if ... and if ...and ...*") are generally not considered, unless the uncertainties are clearly related to each other. For example, uncertainty in the size of an initial penetration is linked to uncertainty in the time at which the transport resistance of the hole will be lost (due to corrosion and volume expansion of the insert). These particular coupled uncertainties are addressed in case PD-BHLD.

Not all issues and uncertainties are covered by the assessment cases. Some, such as the impact of gas bubbles on groundwater flow and radionuclide transport, are left open (although, as noted in Section 2.2.2, any perturbation to groundwater flow is likely to have largely ceased by the time most radionuclides are released from failed canisters). Furthermore, some specific issues are considered implicitly in cases addressing more general uncertainties. For example, the impact on the geosphere transport barrier of high buffer swelling pressures resulting from corrosion of the cast iron insert of a failed canister is considered implicitly in variant cases dealing with reduced geosphere transport resistance. The cases are defined in detail, and the rationale for case selection discussed further, in Chapters 5, 6 and 7.

2.3.3 Models and datasets

For modelling near-field release and transport in the Base Cases and the variant cases, extensive use is made of SR-Can parameter values and model assumptions, except where these are affected by differences in the materials to be disposed of in Finnish and Swedish repositories, and differences between conditions at Olkiluoto and those at the Swedish sites considered in SR-Can. Where differences arise, the selection of parameter values and model assumptions is made largely according to "expert judgement" (see, for example, Appendix E) based on considerations such as use in previous assessments (e.g. TILA-99, SR-Can), additional data gathering and laboratory studies. In the case of geosphere transport modelling, the modelling approach and parameter values used are based largely on TILA-99, although more recent developments in the understanding of the Olkiluoto site, and, in particular, discrete fracture network modelling carried out in support of the KBS-3H safety studies /Lanyon and Marschall 2006/, are used to provide additional support for the parameter values selected (for example, in terms of their conservatism).

Table 2-3. Overview of assessment cases.

Cases assuming a single canister with an initial penetrating defect (PD-)			
Case	**Description**	**Uncertainties or FEPs addressed [see Table 2-2]**	**Presentation in report**
PD-BC	Base Case for initial penetrating defect in BWR-type canister	–	Section 5.2
PD-VVER	Initial penetrating defect in VVER-440 PWR type canister	[C1]	Section 5.3: other fuel types
PD-EPR	Initial penetrating defect in EPR type canister		
PD-HIFDR	Increased fuel dissolution rate	[F1]	Section 5.4: uncertainties in evolution of fuel and release of radionuclides from fuel and metallic components
PD-LOFDR	Reduced fuel dissolution rate		
PD-IRF	Evaluates transport only of radionuclides present in instant release fraction [1]	[F2]	
PD-BIGHOLE	Increased defect size	[C2]	Section 5.5: uncertainties in the characteristics and evolution of the defect
PD-HIDELAY	Increased delay until loss of defect transport resistance	[C3]	
PD-LODELAY	Decreased delay until loss of defect transport resistance		
PD-BHLD	Increased defect size plus decreased delay until loss of defect transport resistance	[C2], [C3]	
PD-HIDIFF	Increased diffusion rate in buffer	[PE]	Section 5.6: potential loss or redistribution of buffer mass during operation phase and in course of buffer saturation
PD-FEBENT1	Perturbed buffer/rock interface – high conductivity, narrow perturbed zone	[MT]	Section 5.7: processes originating at the buffer/rock interface
PD-FEBENT2	Perturbed buffer/rock interface – more extensive perturbed zone (2 different thicknesses)	[MT], [MTX]	
PD-FEBENT3			
PD-SPALL	Perturbed buffer/rock interface – high conductivity, narrow perturbed zone, lower flow through intersecting fractures than that assumed in cases PD-FEBENT1, 2 and 3.	[MT], [MTF]	
PD-EXPELL	Dissolved radionuclides expelled by gas from canister interior and across buffer to geosphere	[G2]	Section 5.8: expulsion of contaminated water by gas
PD-VOL-1	C-14 transported in volatile form by gas generated by corrosion (2 rates of gas generation)	[G1], [G3]	Section 5.9: transport of radionuclides as volatile species by gas
PD-VOL-2			
PD-BCN	Initial penetrating defect in BWR-type canister; Nb present in near field and geosphere in anionic form	[R2]	Section 5.10: chemical speciation, redox conditions and solubilities
PD-BCC	Initial penetrating defect in BWR-type canister; C-14 present in geosphere in anionic form (carbonate)	[R2]	
PD-VVERC	Initial penetrating defect in VVER-440 PWR type canister; C-14 present in geosphere in anionic form (carbonate)	[C2], [R2]	
PD-EPRC	Initial penetrating defect in EPR type canister; C-14 present in geosphere in anionic form (carbonate)	[C2], [R2]	
PD-NFSLV	Near-field solubilities varied according to redox uncertainties	[R1]	

Cases assuming a single canister with an initial penetrating defect (PD-)			
Case	**Description**	**Uncertainties or FEPs addressed [see Table 2-2]**	**Presentation in report**
PD-SAL	Brackish/saline water present at repository depth (all time)	[S1]	Section 5.11: variability in groundwater salinity
PD-HISAL [2]	Saline water present at repository depth (all time)	[S1]	
PD-GMW [2] PD-GMWV	Change from reference (dilute/brackish) water to glacial meltwater at 70,000 years (release also starts at 70,000 years – two alternative meltwater compositions)	[S2], [S3]	
PD-GMWC	Change from reference (dilutee/brackish) water to glacial meltwater at 70,000 years (release starts at 1,000 years, as in the reference case)		
PD-HIFLOW	Increased flow at buffer/rock interface	[G1]	Section 5.12: groundwater flow and geosphere transport resistance
PD-LOGEOR	Reduced geosphere transport resistance	[G2]	
PD-HIGEOR	Increased geosphere transport resistance		
PD-HIFLOWR	Increased flow at buffer/rock interface and reduced geosphere transport resistance	[G1], [G2], [G3]	
Cases assuming a single canister failing due to copper corrosion (CC-)			
CC-BC	Base Case for failure due to copper corrosion; buffer treated as mixing tank	[B1] (implicitly [MT] and [HCC]) [3]	Section 6.2: Base Case
CC-HIFDR	Increased fuel dissolution rate	[B1], [F1]	Section 6.3: fuel dissolution rate
CC-LOFDR	Reduced fuel dissolution rate		
CC-GMW	Glacial meltwater present at repository depth (impact on near-field solubilities and geosphere retention parameters)	[B1], [S2]	Section 6.4: geosphere transport resistance and groundwater composition
CC-LOGEOR	Reduced geosphere transport resistance	[B1], [G1]	
CC-LOGEORG	Reduced geosphere transport resistance, glacial meltwater	[B1], [G1], [S2]	
CC-LOGEORS	Reduced geosphere transport resistance, saline groundwater	[B1], [G1], [S1]	
Cases assuming a single canister failing due to rock shear (RS-)			
RS-BC	Base case for failure due to rock shear	[B2], [G3]	Section 7.2: Base Case
RS-GMW	Glacial meltwater present at repository depth (impact on near-field solubilities and geosphere retention parameters)	[B2], [S2]	Section 7.3: groundwater composition
Additional cases (hypothetical pulse release to geosphere)			
MD-1 MD-2 MD-3	Variations in matrix diffusion depth (3 cases)	[G4]	Appendix C

[1] Certain radionuclides are enriched at grain boundaries in the fuel, at pellet cracks and in the fuel/sheath gap as a result of thermally driven segregation during irradiation of the fuel in the reactor. These are assumed to enter solution rapidly once water contacts the fuel pellet surfaces, and are termed the instant release fraction (IRF). See section 5.2.2.

[2] Glacial meltwater is a very dilute ice-melting water. Saline groundwater represents a water with a TDS (Total Dissolved Solids) of about 20 g/l. For detailed composition of the waters used in the assessment, see Appendix D.

[3] Since these could, in combination, lead to canister failure by corrosion in a million year time frame.

In defining the Base Cases, combinations of multiple, highly conservative assumptions are avoided, since such combinations would be implausible and lead to unrealistically high radiological consequences. Thus, either realistic or moderately conservative parameter values are generally selected in the Base Cases, with variant cases assigned either more optimistic or (more often) more conservative values, within the identified ranges of uncertainty. In some cases, whether one alternative parameter value is more optimistic or conservative than another is well known from experience in past assessments or is clear from the nature of the release and transport processes involved. For example, a high geosphere transport resistance is clearly a more optimistic assumption than a low transport resistance. On the other hand, in other cases, a sensitivity analysis would, in principle be necessary to explore the impact of variations in one or more parameters on radionuclide releases, before it could be stated what is an optimistic parameter value, and what is conservative. Such sensitivity analyses have not, however, been performed in the present assessment (with the exception of sensitivity analyses of matrix diffusion depth in Appendix C). As noted earlier, a comprehensive data report, which would include such sensitivity analyses, will be considered in any future safety studies of the KBS-3H repository, and is likely to be required in support of a future safety case.

Models and datasets for the Base Cases and the variant cases are described in Chapters 5, 6 and 7. The Base Case assuming a canister with an initial penetrating defect (case PD-BC) is described in most detail. The main nuclide-independent parameter values for the near field in case PD-BC are given in Tables 5-4 and 5-5. Nuclide-independent geosphere values for case PD-BC are given in Table 5-8. Nuclide-dependent parameter values are given in other tables in Section 5.2. Models and datasets for other cases are described mainly in terms of the differences with respect to case PD-BC.

3 General modelling approach and computer codes

3.1 Near-field, geosphere and biosphere modelling

The general approach to analysing the assessment cases in the present safety assessment, in agreement with most safety assessments carried out internationally, is to separate near-field, geosphere and biosphere modelling. Advective transport in fractures is assumed to dominate in the geosphere (retarded by matrix diffusion and sorption), whereas diffusion is the dominant transport mechanism in the near field, taken here to comprise the canister, including the canister interior, the buffer and the buffer/rock interface. Conservatively, it is assumed that radionuclides may migrate from the near field to the geosphere, but not vice-versa. Biosphere modelling converts radionuclides fluxes from the geosphere to appropriate assessment endpoints, as discussed below.

Finnish regulations, as summarised in Section 1.4, distinguish between the "environmentally predictable future" (assumed to last about ten thousand years), during which conservative estimates of doses must be made, and the era of "large-scale climate changes" (beyond about ten thousand years) when periods of permafrost and glaciations are expected, and radiation protection criteria are based on constraints on nuclide-specific activity fluxes from the geosphere ("geo-bio flux constraints").

The primary endpoints used in the present safety assessment are:

- annual landscape dose, calculated over the "environmentally predictable future" using the biosphere modelling approach summarised in Section 3.4 and described in more detail in Appendix F; and
- geo-bio fluxes, which are calculated up to a million years, and are used for comparison with Finnish regulatory geo-bio flux constraints (Table 1-1) at times beyond the "environmentally predictable future".

In addition, a quantity (safety indicator) giving an indication of the possible magnitude of doses – the WELL-2007 – has been defined. Ingestion of contaminated water by humans is the only exposure pathway considered in this stylised well scenario[13]. WELL-2007 dose refers to committed effective[14] doses due to ingestion of water over one year, where the effects of ingestion are integrated over the adult life of an individual human /ICRP 1991/. Calculation of WELL-2007 dose, which is described in Section 3.5, further facilitates comparison with regulatory guidelines for the "environmentally predictable future", as well as the results from other safety assessments and safety cases, without the need to justify a wide range of biosphere modelling assumptions. Given the simplified nature of WELL-2007, however, comparison of WELL-2007 dose with regulatory constraints is not regarded by itself as an adequate test of compliance with the regulatory guidelines, which is why the annual landscape dose is also calculated.

Exposure of other (non-human) biota is not explicitly addressed in the present safety assessment, but is considered in the Biosphere Analysis Report /Broed et al. 2007/.

[13] A second stylised well scenario that includes additional exposure pathways, AgriWELL-2007, has also been used in calculations described in the Biosphere Analysis Report /Broed et al. 2007/.

[14] Effective dose is used in radiological protection to relate exposure, internal or external, to ionising radiation to stochastic effects, such as the induction of cancer and hereditary effects.

Geo-bio fluxes and WELL-2007 doses have been calculated for all assessment cases. Results are presented in Chapters 5–7 for the three identified canister failure modes. Annual landscape dose – the primary quantity used to assess compliance with Finnish regulations in the environmentally predictable future – has been calculated for a more limited, representative set of cases, chosen from those in which calculated radionuclide release to the biosphere begins within the first ten thousand years (see Section 3.4).

3.2 Evaluation of near-field release and transport using the REPCOM code

Modelling of near-field release and transport has been performed with the REPCOM code. REPCOM has been developed by the Technical Research Centre of Finland (VTT) for radionuclide transport analyses in the near field of repositories for low- and intermediate-level waste and spent fuel. The phenomena that can be modelled using REPCOM are:

- release from the waste – several waste types, each with different release functions, can be included;
- advective and/or diffusive transport within a system of engineered barriers;
- sorption on solid surfaces;
- solubility limitation of concentrations; and
- radionuclide decay and ingrowth.

The REPCOM code is described further in Appendix A, including verification aspects. In addition, a comparison has been made with results obtained using an alternative near-field code: the SPENT code used by Nagra in recent safety assessments in Switzerland (see Appendix B).

3.3 Evaluation of geosphere transport using the FTRANS code

Modelling of geosphere (far-field) transport has been performed with the FTRANS code /FTRANS 1983, Nordman and Vieno 1994/. FTRANS models transport and retardation processes in fractures and in the adjacent rock matrix. A single, representative geosphere fracture is considered, in which the phenomena that can be modelled with FTRANS are:

- groundwater flow;
- advective radionuclide transport; and
- longitudinal dispersion.

In the rock matrix domain (the wallrock adjacent to the fracture), phenomena that can be modelled are:

- diffusion; and
- sorption on solid surfaces.

Radioactive decay and ingrowth are represented in both domains, and transfer of radionuclides across the boundary between the domains takes place by diffusion.

The FTRANS code is also described further in Appendix A, again including verification aspects.

3.4 Evaluation of annual landscape dose

As described in more detail in Appendix F, biosphere modelling for the evaluation of annual landscape dose is divided into (i), predictions of the physical terrain and the ecosystems possibly receiving contaminant releases from the repository (referred to as "forecasts", below), and (ii), modelling the transport of radionuclides in the biosphere. The forecasts are produced by the terrain and ecosystems development model (TESM; /Ikonen et al. 2007/). Spatial distributions of radionuclide concentrations in the biosphere are the output from the landscape model (LSM; /Broed 2007/).

The climatic variations assumed by the TESM in making the forecasts are based on a repetition of the last glacial cycle (from the Eemian interglacial to the end of the Weichselian glaciation). Lakes, rivers and their catchment areas are identified using standard GIS (geographical information system) processing tools, specifically the approach found suitable for the site by /Ojala et al. 2006/ and further adjusted in /Ikonen et al. 2007/. The model of /Brydsten 2004/ was applied for simulating the accumulation of sediments and reed growth in the lakes and coastal areas, with rate functions updated for the site (for details, see /Ikonen et al. 2007/). On the basis of the TESM, biosphere objects (forests, wetlands, lakes, rivers and coastal areas possibly receiving even indirectly any contamination from the repository) were identified at each time step of the forecast and their properties calculated. See /Broed 2007/ for mathematical descriptions of the underlying ecosystem compartment models in the biosphere objects.

The LSM is a time-dependent linked transport model containing the above-mentioned biosphere objects. The connections between the objects were derived from the terrain forecasts for the period from the present to 8,000 years in the future with 500-year intervals. The LSM is implemented in Pandora /Åstrand et al. 2005/, which is a tool developed by Facilia AB and used by SKB and Posiva for biosphere modelling. Pandora is based on the Matlab/Simulink© environment (www.mathworks.com).

The LSM cannot currently be applied to releases of gaseous C-14 from the repository. Instead, a set of simplified models, based on a specific activity approach, has been developed for assessment of human exposures resulting from potential underground releases of C-14 /Avila and Pröhl 2007/.

In the safety assessment, the annual effective does to the most exposed individual calculated using the above models is termed the annual landscape dose. It is the primary assessment endpoint for the "environmentally predictable future" (se below). In order to calculate this dose, the most exposed individual is assumed to spend all his or her time within the single biosphere object producing the highest dose, including external exposure as well as internal exposure from eating and drinking food produced in and water available from that same biosphere object /Avila and Bergström 2006, Broed 2007, Broed et al. 2007/.

The results of the analysis of assessment cases show that there is a calculated release to the biosphere within the time frame from emplacement up to several thousand years in the future only in the assessment cases assuming an initial penetrating defect (and excluding cases PD-HIDELAY and PD-VOL-2). It is in these cases that dose assessments are explicitly required by regulations, and annual landscape doses have therefore been estimated. Results from seven representative assessment cases are included in Chapter 5: cases PD-BC (Section 5.2), PD-LODELAY (Section 5.5), PD-FEBENT3 (Section 5.7), PD-EXPELL (Section 5.8), PD-VOL-1 (Section 5.9), PD-HISAL (Section 5.11) and PD-LOGEOR (Section 5.12). Other cases assuming an initial penetrating defect have been treated by scaling approaches or qualitative arguments, as described in the Biosphere Analysis Report /Broed et al. 2007/. Other canister failure modes occur after the "environmentally predictable future" and so no evaluation of annual landscape dose is required.

3.5 Evaluation of WELL-2007 dose

In all assessment cases, activity release rates are converted to indicative doses using the set of dose conversion factors given in Table 3-1, derived using a simple and robust model of an indicative stylised drinking water well (WELL-2007), where ingestion of water is the only pathway considered[15].

Table 3-1. Dose conversion factors in WELL-2007, based on the assumptions that the annual releases from the repository into the biosphere are diluted in 100,000 m³ of water, and that an individual drinks 500 litres of contaminated water per year. Where decay chains are given, the dose conversion factors are for the parent radionuclide and the decay products, assumed to be in secular equilibrium.

Radionuclide/decay products	WELL-2007 dose conv. factor [Sv/Bq]
C-14	2.90E–15
Cl-36	4.65E–15
Ni-59	3.15E–16
Se-79	1.45E–14
Mo-93	1.55E–14
Zr-93 → Nb-93m	1.30E–14
Nb-94	8.50E–15
Tc-99	3.20E–15
Pd-107	1.85E–16
Sn-126 → Sb-126	3.55E–14
I-129	5.50E–13
Cs-135	1.00E–14
Ra-226 → Rn-222 → Pb-210 → Bi-210 → Po-210	1.09E–11
Th-229 → Ra-225 → Ac-225	3.07E–12
Th-230	1.05E–12
Pa-231 → Ac-227 → Th-227 → Ra-223	9.59E–12
U-233	2.55E–13
U-234	2.45E–13
U-235 → Th-231	2.37E–13
U-236	2.35E–13
Np-237 → Pa-233	5.54E–13
U-238 → Th-234	2.42E–13
Pu-239	1.25E–12
Am-241	1.00E–12
Pu-240	1.25E–12
Pu-242	1.20E–12
Am-243 → Np-239	1.00E–12
Cm-245 → Pu-241	1.07E–12
Cm-246	1.05E–12

[15] A second stylised well scenario that includes additional exposure pathways, AgriWELL-2007, has also been used in calculations described in the Biosphere Analysis Report /Broed et al. 2007/.

Multiplying the WELL-2007 dose conversion factors with the annual release rates from the geosphere to the biosphere results in an estimate of the committed effective[16] dose to an adult resulting from ingestion of the well during one year, i.e. the WELL-2007 dose, where the effects of ingestion are integrated over the adult life of an individual human /ICRP 1991/. Adult life is deemed to be from age 20 years to age 70 years, except for Ra, Pb, Th, U, Np, Pu, Am and Cm, where adulthood is taken to commence at age 25 years /ICRP 1996/. Dilution factors and annual water intake values are the same as in the WELL-97 model used in TILA-99 /Vieno and Nordman 1999/. Thus, WELL-2007 is based on the assumptions that the annual releases from the repository into the biosphere are diluted in 100,000 m^3 of water, and that an individual drinks 500 litres of contaminated water in one year. The only difference between WELL-2007 and WELL-97 is that the ingestion dose coefficient for Rn-222 has been updated. In WELL-2007, the dose coefficient for Rn-222 is taken from /NRC 1999/, and the ingestion dose coefficients for adults for all other nuclides from /ICRP 1996/.

The Finnish regulatory dose guideline is expressed in terms of a constraint to annual effective dose. /IAEA 2007/ defines the concept of an annual dose as "*the dose due to external exposure in a year plus the committed dose from intakes of radionuclides in that year*". The WELL-2007 dose is equivalent to the IAEA annual dose for the stylised system considered, in which there is no external exposure. The WELL-2007 dose is thus an appropriate safety indicator for comparison with the regulatory guideline.

[16] Effective dose is used in radiological protection to relate exposure, internal or external, to ionising radiation to stochastic effects, such as the induction of cancer and hereditary effects.

4 Radionuclide release and transport processes

4.1 The near field

4.1.1 Release processes

Once a canister has failed by one of the broad failure modes outlined in Chapter 2 and water enters its interior, three broad radionuclide release mechanisms may occur, as described in detail in Chapter 8 of the Evolution Report /Smith et al. 2007a/:

1. the cladding will slowly corrode on contact with water, resulting in the dissolution of activation products embedded within it;
2. radionuclides that have been segregated to grain boundaries in the fuel, to pellet cracks and to the fuel/sheath gap will rapidly dissolve in water (although some may also form volatile products such as methane or carbon dioxide that mix with hydrogen gas produced principally by corrosion of the insert); and
3. water will start to interact with the surfaces of the fuel matrix, resulting in the release of radionuclides embedded within it, and of radioactive gases present in fission gas bubbles.

Depending on the failure mode, there may be some delay between the failure of the copper shell on the one hand, and, on the other hand, ingress of water leading to radionuclide release and the establishment of radionuclide transport pathways from the canister interior to the buffer. This delay is described in the context of individual failure modes in Chapters 5–7.

4.1.2 Transport pathways

The near-field transport model used in the present safety assessment is described in detail in Section 5.2.3. Released radionuclides will be transported, primarily by aqueous diffusion, along continuous water pathways from the canister interior through the buffer and to the host rock. Transport will be retarded by sorption on solid surfaces and aqueous concentrations will be limited by solubility constraints. Potential radionuclide transport paths from a failed canister to the host rock are illustrated in Figure 4-1. In most of the assessment cases described in Chapters 5–7, paths R1 (transport in buffer) and R2 (transport in closest fracture) are assumed to be the most important, since the contact between the buffer and the host rock is expected to be tight by the time of any radionuclide releases[17].

4.1.3 The impact of repository-generated gas

Gas generated inside a canister, principally hydrogen from the corrosion of the insert subsequent to canister failure, may affect radionuclide release and transport in two broad ways. Firstly, there may be mixing of radionuclides present as volatile species (principally C-14) with repository-generated gas and subsequent migration of this gas along pathways from the canister interior through the buffer to the host rock. Secondly, the build-up of high gas pressure inside the canister following water ingress may lead to the expulsion of water from inside the canister into the buffer. This gas-induced displacement of water may convey dissolved radionuclides.

[17] This is expected even in the case of an initial penetrating defect, since in may take in the order of 1,000 years for contact of water with the fuel/metallic parts to take place and for transport paths from the canister interior to be established (see the discussion of water ingress in Section 11.5.2 of the Evolution Report, /Smith et al. 2007a/).

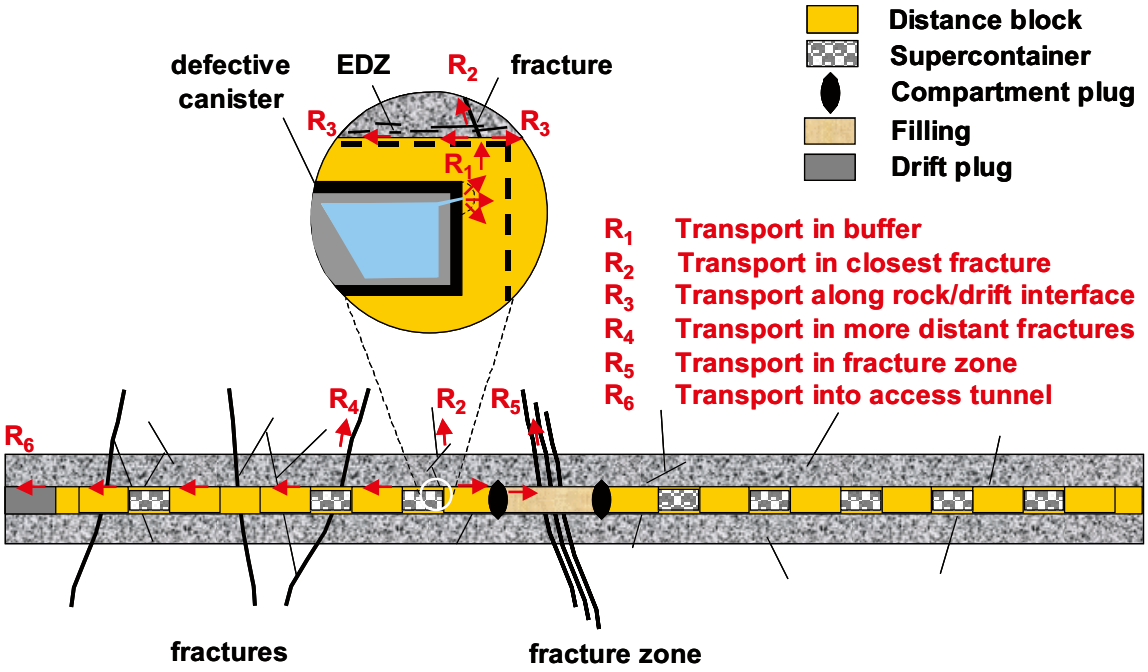

Figure 4-1. Radionuclide transport paths from a failed canister to the host rock.

Assessment cases to evaluate these effects are considered in Chapter 5 in the context of a canister with an initial penetrating defect. Similar effects may, however, also arise in the case of other canister failure modes[18].

4.2 The geosphere

Radionuclides will be transferred by diffusion from the buffer to flowing water in transmissive fractures intersecting the repository drift. Radionuclides will diffuse away from the buffer/rock interface and will be transported downstream by the flowing water.

The geosphere transport model used in the present safety assessment is described in detail in Section 5.2.4. Radionuclide transport in the geosphere will predominantly be by advection in channels within transmissive fractures. Diffusion will take place throughout the connected pore and fracture space in the geosphere; diffusion into stagnant pore water and sorption on fracture and rock matrix pore surfaces retards advection in fractures.

In the present safety assessment, gas and colloids, both naturally present in the groundwater and arising from the presence of the repository, are assumed not to affect geosphere transport, although these remain issues for further study (Chapter 9).

4.3 The biosphere

Radionuclides will be released from the geosphere to the biosphere either in solution in groundwater or in gaseous form. Radionuclides that are dissolved in groundwater will be transferred to surface water bodies (brooks, rivers and lakes) either directly, or indirectly through the porous

[18] Early canister failure (i.e. on a timescale of around 50,000–100,000 years) by general corrosion is only considered possible in cases where advective conditions prevail in the buffer (Section 11.6 of the Evolution Report /Smith et al. 2007a/). In these cases, the gas entry pressure of the buffer is also likely to be reduced and a build-up of high gas pressure inside the canister will not occur.

overburden. Any radioactive gases not dissolved in groundwater are expected to be ventilated relatively quickly to the atmosphere. Some, however, may be assimilated by biological organisms by inhalation and by plant gas exchange, and some may be captured and retained in pore spaces in the overburden.

Dissolved radionuclides entering the overburden will be transported by advection and diffusion, with retardation by sorption. In biosphere modelling for the present safety assessment, instantaneous transfer of radionuclides through the overburden to surface water bodies is, however, generally assumed in order to simplify the analysis. This simplification is conservative, since it will lead to overestimates of doses to humans. The impact of this simplification is explored in a number of variant cases in the Biosphere Analysis Report /Broed et al. 2007/. Some radionuclides will become associated with geological materials and soils, erosion of which provides a further transport mechanism, especially in agricultural lands. Furthermore, changes in the groundwater table and capillary rise may result in some radionuclides becoming available for the root uptake by plants, and subsequent further transfer in the food webs.

In the surface water bodies, the radionuclide concentration is affected by sedimentation, resuspension and erosion processes, in addition to the biological turnover. Some radionuclides will be transferred by flowing water to the Baltic Sea and further to the oceans, while others will remain in the Olkiluoto area.

Microbial processes are common in all parts of the biosphere. In biosphere modelling, they are usually included either in the sorption or the biological parameters, depending on the specific process under consideration and on the availability of data.

5 Cases assuming an initial penetrating defect

5.1 General considerations

The discussion in Chapter 8 of the KBS-3H Evolution Report /Smith et al. 2007a/ illustrates that there are considerable uncertainties regarding the internal evolution of a canister with an initial penetrating defect. The defect will have a relatively minor impact on the containment function of the canister as long as it remains small or becomes rapidly plugged with bentonite and iron corrosion products, limiting the supply of water to the surface of the insert and hence its rate of corrosion. On the other hand, the possibility that the corrosion products will lead to an expansion of the defect cannot currently be excluded. This could in turn lead to further corrosion, weakening and eventual failure of the insert, which would allow the water to contact the fuel and cladding and radionuclides to dissolve and migrate out of the canister. It is this possibility that is pessimistically assumed in the following analyses of radionuclide release and transport.

Radionuclide release and transport calculations are carried out for a Base Case and a set of variant cases, all of which are based on the assumption of an initial penetrating defect affecting a single canister. The cases, each of which is assigned a unique identifier, are summarised in Table 5-1. Detailed case definitions are given in the following sections.

5.2 Base Case

5.2.1 General assumptions of the Base Case

In the Base Case (case **PD-BC**), the initial penetrating defect is assumed to affect a single canister of BWR fuel from the Olkiluoto 1-2 reactors. The reference spent fuel is assumed to have a burnup of 40 MWd/kgU and an enrichment of 4.2%, which are at the high ends of the expected ranges. At the planned closure time of the repository (approximately the year 2100), the average cooling time of the fuel will be well over 30 years, but, for the release and transport analyses, a conservative cooling time of 30 years has been assumed. The impact of future likely increases in burnup have not been directly taken into account, but can be estimated by considering the results of case **PD-IRF**, in which only the instant release fractions (IRFs) of each radionuclide are calculated (Section 5.4.5). The IRFs are directly proportional to the fuel burnup.

Groundwater conditions are assumed to be reducing and dilute/brackish. Of the various groundwaters studied (Appendix D), dilute/brackish groundwater is closest in terms of total dissolved solids (TDS) to the expected undisturbed conditions at repository depth in the period up to 10,000 years in the future /Pastina and Hellä 2006/.

5.2.2 Radionuclide inventories, half-lives and partitioning

Radionuclide activity inventories (per tonne of uranium) after 30 years of cooling, together with their half-lives and partitioning between fuel matrix, instant release fraction (IRF), Zircaloy and other metallic parts, are given in Table 5-2. Each BWR-fuel element contains on average 180 kg of uranium metal. Therefore, a reference BWR-canister including 12 fuel elements contains 2.14 tU /Raiko 2005/. Radionuclide inventories usually are expressed per unit mass of uranium metal (or element) although it is generally in oxide form (UO_2) in the fuel. One tonne of uranium metal needs an additional 133 kg of oxygen to form UO_2. In fresh fuel, uranium is mainly U-238 and typically some 3.8% is U-235.

Table 5-1. Identifiers and summary descriptions of each of the assessment cases that assume an initial penetrating defect in a canister, with references to report sections where detailed case definitions are provided. Groundwater chemistry and its impact on buffer porewater (bentonite water) chemistry are discussed in Appendix D. The concepts of equivalent flow rate (Q_F) and geosphere transport resistance (WL/Q) are discussed in Section 5.2.3 in the context of the Base Case. In all cases, BC means the same as the Base Case.

Identifier	Summary description	Groundwater chemistry	Q_F [$m^3\ a^{-1}$]	WL/Q [$a\ m^{-1}$]	Full definition (report section)
PD-BC	Base Case (BC) for Initial Penetrating Defect (PD) canister failure mode	Dilute/brackish	2×10^{-4}	5×10^{4}	Section 5.2
Cases addressing different fuel types					
PD-VVER	Initial penetrating defect in VVER-440-type canister	BC	BC	BC	Section 5.3
PD-EPR	Initial penetrating defect in EPR-type canister	BC	BC	BC	
Cases addressing uncertainties in the evolution of the fuel and the release of radionuclides from the fuel and metallic components					
PD-HIFDR	Increased fuel dissolution rate	BC	BC	BC	Section 5.4
PD-LOFDR	Reduced fuel dissolution rate	BC	BC	BC	
PD-IRF	Instant release fraction only calculated	BC	BC	BC	
Cases addressing uncertainties in the characteristics and evolution of the defect					
PD-BIGHOLE	Increased defect size	BC	BC	BC	Section 5.5
PD-HIDELAY	Increased delay until loss of transport resistance	BC	BC	BC	
PD-LODELAY	Reduced delay until loss of transport resistance	BC	BC	BC	
PD-BHLD	Increased defect size and reduced delay until loss of transport resistance	BC	BC	BC	
Cases addressing potential loss or redistribution of buffer mass during the operational phase and in the course of buffer saturation					
PD-HIDIFF	Increased buffer diffusion coefficient	BC	BC	BC	Section 5.6
Cases addressing processes originating at the buffer/rock interface					
PD-SPALL	Thermally induced rock spalling	BC	1×10^{-4}	BC	Section 5.7
PD-FEBENT1	Iron-bentonite/cement-bentonite interaction, confined to a narrow zone at the interface	BC	3.1×10^{-4}	BC	
PD-FEBENT2	Iron-bentonite/cement-bentonite interaction, extending across 10% of the buffer thickness	BC	3.1×10^{-4}	BC	
PD-FEBENT3	Iron-bentonite/cement-bentonite interaction, extending across the half the buffer thickness	BC	3.1×10^{-4}	BC	

Identifier	Summary description	Groundwater chemistry	Q_F [$m^3\ a^{-1}$]	WL/Q [$a\ m^{-1}$]	Full definition (report section)
Cases addressing expulsion of contaminated water by gas					
PD-EXPELL	Expulsion of contaminated water by gas	BC	BC	BC	Section 5.8
Cases addressing transport of radionuclides as volatile species by gas					
PD-VOL-1	Transport of radionuclides as volatile species by gas – high gas generation rate	BC	BC	BC	Section 5.9
PD-VOL-2	Transport of radionuclides as volatile species by gas – low gas generation rate	BC	BC	BC	
Cases addressing uncertainties in chemical speciation, solubilities and redox conditions					
PD-BCN	Initial penetrating defect in BWR-type canister; Nb present in the near field and geosphere in anionic form	BC	BC	BC	Section 5.10
PD-BCC	Initial penetrating defect in BWR-type canister; C-14 present in geosphere in anionic form (carbonate)	BC	BC	BC	
PD-VVERC	Initial penetrating defect in VVER-440 PWR type canister; C-14 present in geosphere in anionic form (carbonate)	BC	BC	BC	
PD-EPRC	Initial penetrating defect in EPR type canister; C-14 present in geosphere in anionic form (carbonate)	BC	BC	BC	
PD-NFSLV	Near-field solubilities varied according to uncertainties in redox conditions	BC	BC	BC	
Cases addressing variability in groundwater salinity					
PD-SAL	Brackish/saline conditions	Brackish/saline	BC	BC	Section 5.11
PD-HISAL	Saline conditions	Saline	BC	BC	
PD-GMW	Glacial meltwater conditions	Dilute glacial meltwater type GMW	BC	BC	
PD-GMWV	Alternative glacial meltwater conditions	Dilute glacial meltwater type GWMV	BC	BC	
PD-GMWC	Change from reference (dilute/brackish) water to glacial meltwater at 70,000 years (release starts at 1,000 years, as in the reference case)	Dilute/brackish up to 70,000 years, dilute glacial meltwater type GMW later	BC	BC	
Cases addressing uncertainty in groundwater flow and geosphere transport resistance					
PD-HIFLOW	Increased flow at buffer/rock interface	BC	6.3×10^{-4}	BC	Section 5.12
PD-LOGEOR	Reduced transport resistance in geosphere	BC	BC	5×10^{3}	
PD-HIGEOR	Increased transport resistance in geosphere	BC	BC	5×10^{5}	
PD-HIFLOWR	Increased flow at buffer/rock interface and reduced geosphere transport resistance	BC	2×10^{-4}	5×10^{3}	

Table 5-2. Radionuclide inventories for a single canister of BWR fuel from the Olkiluoto 1-2 reactors after 30 years of cooling; burnup 40 MWd/kgU, enrichment 4.2%, together with their half-lives and partitioning between fuel matrix, instant release fraction (IRF), Zircaloy and other metallic parts. The activity inventory is from /Anttila 2005/.

Radionuclide	Half-life [a]	Activity inventory after 30 years of cooling [GBq/tU]	Partitioning [%]			
			Fuel matrix	IRF	Zircaloy	Other metal parts
Trace elements						
C-14	5.7×10^{3}	2.78×10^{1}	30	3	33	33
Cl-36	3.0×10^{5}	1.04×10^{0}	45	5	50	0
Mo-93	4.0×10^{3}	1.13×10^{1}	0	0	0	100
Actinides and fission products						
Se-79	2.95×10^{5}	3.30×10^{0}	99.9	0.1	0	0
Sr-90	2.9×10^{1}	1.70×10^{6}	99	1	0	0
Zr-93*	1.5×10^{6}	8.26×10^{1}	100	0	0	0
Tc-99	2.1×10^{5}	6.12×10^{2}	99	1	0	0
Pd-107	6.5×10^{6}	4.29×10^{0}	99	1	0	0
Sn-126	1.0×10^{5}	2.18×10^{1}	99.99	0.01	0	0
I-129	1.6×10^{7}	1.14×10^{0}	95	5	0	0
Cs-135	2.3×10^{6}	2.15×10^{1}	95	5	0	0
Cs-137	3.0×10^{1}	2.36×10^{6}	95	5	0	0
Sm-151	9.0×10^{1}	1.10×10^{4}	100	0	0	0
Ra-226	1.6×10^{3}	–	–	–	–	–
Th-229	7.3×10^{3}	–	–	–	–	–
Th-230	7.7×10^{4}	–	–	–	–	–
Pa-231	3.2×10^{4}	–	–	–	–	–
U-233	1.6×10^{5}	2.41×10^{-3}	100	0	0	0
U-234	2.4×10^{5}	5.59×10^{1}	100	0	0	0
U-235	7.0×10^{8}	7.45×10^{-1}	100	0	0	0
U-236	2.3×10^{7}	1.30×10^{1}	100	0	0	0
U-238	4.5×10^{9}	1.16×10^{1}	100	0	0	0
Np-237	2.1×10^{6}	1.30×10^{1}	100	0	0	0
Pu-238	8.8×10^{1}	8.71×10^{4}	100	0	0	0
Pu-239	2.4×10^{4}	1.05×10^{4}	100	0	0	0
Pu-240	6.5×10^{3}	1.98×10^{4}	100	0	0	0
Pu-241	1.4×10^{1}	9.84×10^{5}	100	0	0	0
Pu-242	3.8×10^{5}	7.61×10^{1}	100	0	0	0
Am-241	4.3×10^{2}	1.08×10^{5}	100	0	0	0
Am-243	7.4×10^{3}	7.62×10^{2}	100	0	0	0
Cm-245	8.5×10^{3}	6.16×10^{0}	100	0	0	0
Cm-246	4.7×10^{3}	1.19×10^{0}	100	0	0	0
Zircaloy and other metal parts						
Ni-59	8.0×10^{4}	1.32×10^{2}	0	0	0	100
Ni-63	9.6×10^{1}	1.41×10^{4}	0	0	0	100
Zr-93	1.5×10^{6}	8.16×10^{0}	0	0	100	0
Nb-94	2.0×10^{4}	3.00×10^{1}	0	0	0	100

* Originating from fuel; Zr-93 in Zircaloy listed separately under “Zircaloy and other metal parts”.

The radionuclide activity inventories are based on calculations described in /Anttila 2005/. For the purposes of release and transport calculations, the inventories of some shorter-lived parent radionuclides, in terms of moles, are added to those of their daughters, since transport times greatly exceed the half-lives of the parents. This applies to the parent radionuclides of Np-237, U-238, U-235 and U-236. Thus, for example, the inventories of Cm-245 and Am-241 are added to the inventory of Np-237.

In the present safety assessment, as in TILA-99, the activation products in the Zircaloy and in other metal parts are assumed to undergo delayed release upon the creation of a transport pathway from the canister interior to the buffer[19]. The inventory fractions contained in these components are uncertain; the values given in Table 5-2 are based on expert judgement, guided by considerations described in /Anttila 2005/ and /Werme et al. 2004/. Thus, for example, C-14 is divided equally between the Zircaloy (33%), other metal parts (33%) and the fuel matrix/IRF (33%).

Partitioning between the fuel matrix and the IRF is based on Table A-4 of the SR-Can data report /SKB 2006b/. The SR-Can data report gives distributions of values and pessimistic upper limit based on expert judgement and various measurements, as outlined in /Werme at al 2004/. The pessimistic, upper limits are the values used in the present safety assessment.

The use of SR-Can data is justified by the similarity in the fuels and burnups in the Swedish and Finnish cases, also given the likely future increases in fuel burnup expected in Finland. The pessimistic values given in the SR-Can Data Report are, according to the Data Report, interpreted to be related to high burn-ups. The reference fuel used in KBS-3H safety studies is the BWR fuel from the Olkiluoto 1 and 2 reactors. Fuel from these reactors has an average burn-up of 37–39 MWd/kgU and a maximum burnup of 50 MWd/kg U. As noted in Section 5.2.1, the reference spent fuel is assumed to have a burnup of 40 MWd/kg U. These values are already quite high, and there is a trend towards still higher burn-ups, which supports the use of the SR-Can pessimistic values. It should be noted that 45–50 MWd/kgU is the range where the fission gas release and instant release fraction of BWR fuel starts to increase /Johnson and McGinnes 2002/.

In future, although it will be difficult to improve the knowledge of the distribution of radionuclides between the IRF and within the fuel rods (which depends e.g. on reactor types, fuel manufacturer, spatial configuration in the reactor), confidence may be improved by studying fuel types at high burnups for which there are few data available.

The inventories of stable nuclides, which are required in order to evaluate whether solubility limits are exceeded (Section 5.2.3), are given in Table 5-3.

Table 5-3. Stable nuclides taken into account in estimating whether solubility limits are exceeded.

Element	Amount [mol/tU]
Mo	1.77×10^{1}
Nb	4.91
Ni	1.20×10^{2}
Pd	1.20×10^{1}
Se	7.70×10^{-1}
Sn	2.90×10^{-1}
Zr (cladding)	4.93×10^{3}
Zr (fuel matrix)	5.30×10^{1}

[19] In SR-Can, on the other hand, it is assumed that not only the IRF but also the inventories in Zircaloy and in other metal parts are released instantaneously upon the creation of a transport pathway from the canister interior to the buffer.

5.2.3 Near field model

(i) Geometry

The geometry of the domain represented by the Base Case near-field model is illustrated in Figure 5-1.

A drift section containing a canister with an initial penetrating defect is assumed to be intersected by a single transmissive fracture. Conservatively, it is assumed that the canister is located at a position that minimises the transport distance across the buffer between the defect and the fracture mouth (i.e. the centre plane of the fracture is assumed to pass through the centre of the defect, as illustrated in Figure 5-1).

In applying the code REPCOM to this system, two-dimensional diffusion in the buffer is modelled, including radial diffusion from the canister surface towards the rock, and diffusion parallel to the drift axis. Mass transfer from the defect to the buffer and from the buffer to the rock is modelled by means of mass transfer coefficients (see below). The modelling of diffusion in two dimensions is one of the main differences compared with the version of REPCOM used in TILA-99, where one-dimensional diffusion was considered. The details of how two-dimensional diffusion modelling of a KBS-3H repository is implemented in REPCOM are described in /Nordman and Vieno 2003/.

Geometrical parameter values are given in Table 5-4.

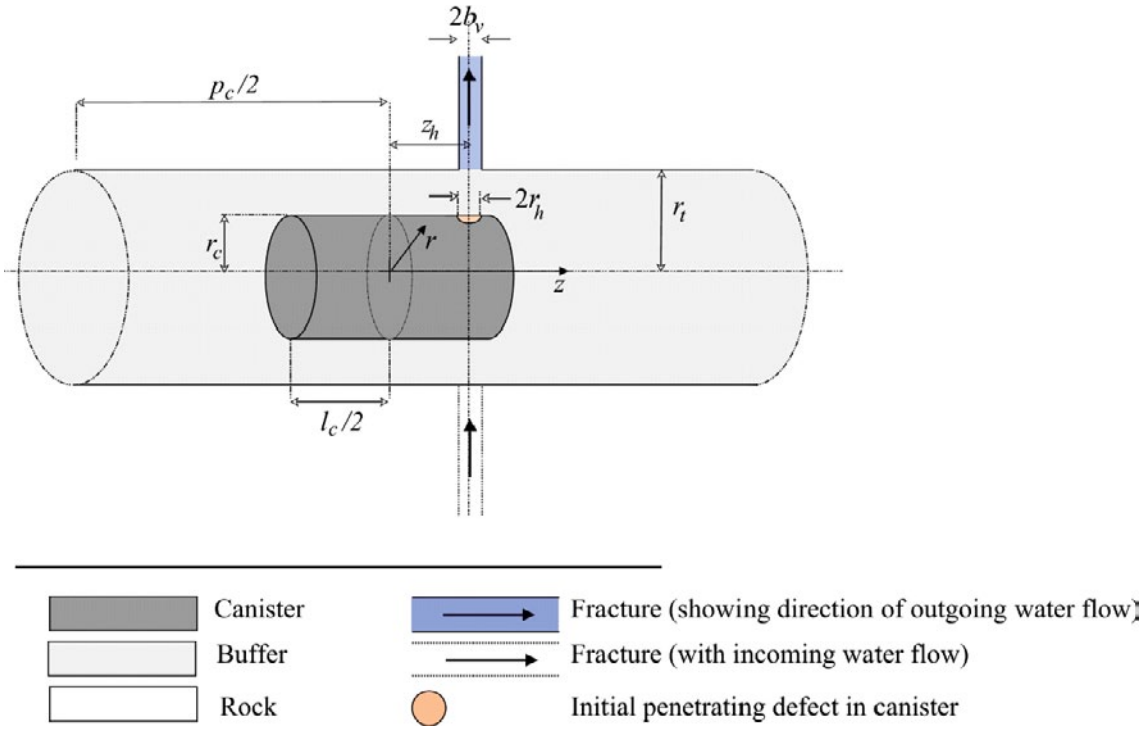

Figure 5-1. *Geometrical domain of the near field model in the Base Case for an initial penetrating defect. The canister has a length (l_c) of 4.835 m and an outer diameter ($2r_c$) of 1.05 m. The drift diameter ($2r_t$) is 1.85 m. The canister pitch (p_c) is 11 m. The defect diameter ($2r_h$) is 1 mm.*

Table 5-4. Geometrical parameter values for the near field model in the Base Case for an initial penetrating defect – symbols are those defined in Figure 5-1.

Parameter	Unit	Symbol	Value	Source
Canister outer diameter	m	$2r_c$	1.05	/Raiko 2005/
Canister length	m	l_c	4.835	/Raiko 2005/
Canister pitch	m	p_c	11.0	Value for 1,700 W BWR fuel /Autio et al. 2007/
Drift diameter	m	$2r_t$	1.850	/Börgesson et al. 2005/
Hole diameter	m	$2r_h$	10^{-3}	See main text
Hole length	m	d_h	0.05	Copper shell thickness
Hole position (axial distance of hole centre from canister centre)	m	z_h	2.417	Hole taken to coincide with canister end (distance of weld from end assumed negligible)
Fracture aperture	m	$2b_v$	3×10^{-5}	See main text

The diameter of the initial penetrating defect is taken to be 1 mm. This corresponds roughly to the maximum defect size that might escape detection using current non-destructive testing (NDT) quality control techniques. The thickness of the buffer around the canister is taken to be 0.4 m, i.e. the drift radius, r_t [m], minus the canister radius, r_c [m]. In the Base Case, the presence of the supercontainer, its corrosion products and potentially lower-density bentonite between the supercontainer and the drift wall is assumed to have a negligible impact on radionuclide transport through the buffer and across the buffer/rock interface. The buffer thickness inside the supercontainer is 0.35 m (the inner radius of the supercontainer is 0.875 m, which is 5 cm less than the drift radius). Scoping calculations show that radionuclide release rates from the near field are insensitive to the assumed buffer thickness within the range 0.35 m to 0.4 m, provided mass transport across the buffer/rock interface is unperturbed, and remains dominated by diffusion. Perturbations to radionuclide release and transport caused, for example, by rock spalling, the physical presence of the supercontainer and its corrosion products at or near the drift wall or iron-bentonite or cement-bentonite interactions are assumed to be negligible in the Base Cases (even though this may be non-conservative), but are considered in the variant cases PD-SPALL, PD-FEBENT1, PD-FEBENT2 and PD-FEBENT3 (Section 5.7).

The fracture aperture is assigned a value of 3×10^{-5} m, and is used to evaluate geosphere transport resistance at the buffer/rock interface (See Eq. 5-9). It is also used in modelling radionuclide transport in the geosphere, although experience in earlier safety assessments has shown that geosphere transport is highly insensitive to fracture aperture. The aperture value is determined using the relationship:

$$b_v = \frac{\sqrt{T}}{2c} \qquad \text{(Eq. 5-1)}$$

The same relationship was also used in the fracture network modelling carried out for a KBS-3H repository at Olkiluoto (in Appendix B of /Lanyon and Marschall 2006/). b_v [m] is the half aperture, T [$m^2\ s^{-1}$] is transmissivity ($3 \times 10^{-9}\ m^2\ s^{-1}$, see below) and c is a constant, given (in units of $seconds^{-1/2}$) as 2 in /Lanyon and Marschall 2006/. The relationship between aperture and transmissivity is, however, subject to significant uncertainty. For example, transmissivity is a property that is generally evaluated for a fracture as a whole. Aperture may, however, vary substantially, giving rise locally to flow channels and to constrictions that tend largely to determine the overall transmissivity. There was only limited information available on channel properties for the repository volume at the time of the present study, and so the impact of the uncertainty in the relationship between aperture and transmissivity has not so far been assessed.

(ii) Processes and material properties

Near-field parameter values that apply to all migrating species in the Base Case for an initial penetrating defect are summarised in Table 5-5. These and other parameter values related to the rates of processes and relevant material properties of the near field are discussed below.

a. Water ingress

Following SR-Can, it is assumed to take 1,000 years for water to contact the fuel, the Zircaloy and other metal parts and for a transport pathway to be established between the canister interior and exterior; this value is regarded as pessimistic. This assumption is based on the slow initial water ingress rate, which will be further decreased over time by the gradual build-up of an internal counter pressure due to hydrogen gas formation, as well as on the barriers provided by the cast iron insert and the fuel cladding. According to Section 10.5.2 of /SKB 2006a/, 1,000 years can be regarded as a pessimistic contact time, since any one of these factors is likely to provide more than 1,000 years of delay At later times, the supply of water to the canister interior is conservatively assumed to be unlimited, but the defect provides a continuing transport resistance for released radionuclides.

b. Radionuclide release

Following the SR-Can approach, after the ingress of water, fuel dissolution is assumed to take place at a constant fractional rate of 10^{-7} per year, with congruent release of radionuclides. This represents the peak of a triangular distribution recommended for use in SR-Can by /Werme et al. 2004/. Consistent with the difference analysis approach explained in Section 1.1, the SR-Can dissolution rate has been used without further evaluation, although there remains considerable uncertainty regarding the validity of this and other proposed models of fuel dissolution, and this remains an important area for further studies (Chapter 9).

Table 5-5. Near-field parameter values that apply to all migrating species in the Base Case for an initial penetrating defect.

Parameter	Unit	Value	Source/comments
Delay between canister emplacement and establishment of transport pathway	a	1,000	SR-Can – see main text (part a)
Fuel matrix fractional dissolution rate	a^{-1}	10^{-7}	SR-Can – see main text (part b)
Zircaloy fractional corrosion rate	a^{-1}	10^{-4}	TILA-99 – see main text (part b)
Fractional corrosion rate for other metal parts	a^{-1}	10^{-3}	TILA-99 – see main text (part b)
Solubility limits	mol dm^{-3}	–	See Tables 5-6 and E-2
Water volume for dissolution	m^3	0.7	TILA-99, Table 11-7 – see main text (part c)
Delay between establishment of transport pathway and loss of transport resistance of defect	a	9,000	See main text (part d)
Diffusion coefficient within defect (D_h)	$m^2\ s^{-1}$	2×10^{-9}	TILA-99 – hole assumed to be water filled – see main text (part d)
Buffer porosities	–	–	SR-Can – see main text (part e)
Effective diffusion coefficients in the buffer	$m^2\ s^{-1}$	–	SR-Can – see main text (part e)
Buffer sorption coefficients	$m^3\ kg^{-1}$	–	See Table 5-7
Buffer grain density	kg m^{-3}	2,700	TILA-99 – p. 105 of /Vieno and Nordman 1999/
Transmissivity of intersecting fracture	$m^2\ s^{-1}$	3×10^{-9}	/Lanyon and Marschall 2006/ – see main text (part f)
Equivalent flow rate	$m^3\ a^{-1}$	2×10^{-4}	See Eqs. 5-9 and 5-10
Regional hydraulic gradient	–	0.01	TILA-99 – see main text (part f)

It is assumed that the inventory of activation products in Zircaloy and other metal parts is released congruently with the corrosion of the metal (a more pessimistic approach is taken in SR-Can, where no credit is taken for the delay due to the limited rate of metal corrosion). The assumed fractional corrosion rate of Zircaloy of 10^{-4} per year, taken from TILA-99 (p. 101 of /Vieno and Nordman 1999/), is somewhat higher than the expected rate of corrosion /see Johnson and McGinnes 2002/, and is conservative, since it will lead to higher than expected radionuclide release rates. This high corrosion rate leads to an inconsistency, in that sustaining it would require more water than will enter through a defect of the postulated size. According to the Process Report (Section 2.5.1 of /Gribi et al. 2007/) the corrosion of the approximately 5,000 moles of Zircaloy in a canister at a rate of 10^{-4} per year will produce ~1 mole of H_2 per year (one mole of Zircaloy produces two moles of H_2), consuming 1 mole of water. However, it is also shown in the Process Report that the water flow rate into a canister with a one millimetre diameter defect is only in the order of 0.004 and 0.04 litres per year, or 0.2 to 2 moles per year, based on a hydraulic conductivity of the bentonite at the mouth of the hole of 10^{-13} to 10^{-12} m s^{-1} and a pressure difference across the buffer is 4.2 MPa (corresponding to the hydrostatic pressure at the depth of 420 m, the lower end of the inclined drift). Furthermore, plugging of the hole with bentonite or corrosion products and the decrease of the hydraulic gradient over time due to gas pressure build-up will reduce the rate of water inflow into the canister. In spite of this inconsistency, the decision has been taken to use the conservative Zircaloy corrosion rate from TILA-99 in the present safety assessment, although the possibility of using a more realistic corrosion rate may be considered in future studies.

The gap inventory is conservatively assumed to be instantaneously released and mixed with water. Instant release fractions are given in Table 5-2.

c. Solubility limitation and radionuclide transport inside the canister

Released radionuclides may be dissolved, or precipitated if relevant solubility limits are exceeded. In calculating whether the solubility limit for a given element is exceeded, the concentration of that element is evaluated taking into account all radionuclides and stable nuclides that are isotopes of that element. Solubility limits for the near field have been estimated by /Grivé et al. 2007/ for the range of groundwater types described in Appendix D. The process of selection of solubility limits and associated uncertainties are discussed in Appendix E. Base Case solubility limits are given in Table 5-6, assuming dilute brackish groundwater in equilibrium with bentonite. Additional solubility limits for other water types are given in Appendix E.

As was the case in TILA-99, the solubility limits are applied in the near field model only inside the canister and at the buffer/rock interface, but not throughout the buffer. The effects of this model simplification are evaluated in additional calculations using the Nagra near-field code SPENT (Appendix B).

The solubilities of some elements (i.e. Se, Mo, Tc, Pd, Sn, U, Np and Pu) are redox sensitive. To obtain values for these solubilities, redox conditions are assumed to be determined by a long-term dynamic equilibrium between magnetite and hematite formed in the system around the corroding iron insert, with a pH_2 of 10^{-7} atm. The system has an Eh of –230 mV (vs. SHE) in the case of a buffer porewater with a pH of 7.4 (/Grivé et al. 2007/ and Appendix E). All the other elements presented in Table 5-6 have about the same solubility values and solubility controlling solids irrespective of the defined redox conditions, although slight variations with pH values and speciation are observed for some elements.

Solubility limits that vary markedly between TILA-99 and the KBS-3H safety assessment are identified using coloured background shading in Table 5-6. The solubility limits used in TILA-99 were conservative values for non-saline (TDS < 1g/L) reducing conditions (Table 11-2 in /Vieno and Nordman 1999/). In the present Base Case, however, the solubility limits have been selected to be realistic, and so some differences compared with TILA-99 are to be expected, although, in some cases, the present Base Case solubility limits are higher (less favourable to safety) than the solubility limits in TILA-99. The significantly higher solubility limit applied to Ni compared with TILA-99, as well as other significant differences

Table 5-6. Base Case solubility limits. Blue shading indicates a solubility limit > 10 × higher than in TILA-99 (conservative solubility values for non-saline reducing conditions, Table 11-2 in /Vieno and Nordman 1999/, yellow shading indicates a solubility limit > 10 × lower than TILA-99. Further details on uncertainties are presented in Table E-2.

Element	Solubility (mol dm^{-3})	Solubility limiting phase
Am	4.0×10^{-7}	$Am(CO_3)_2Na \times 5H_2O$
C	High [1]	–
Cl	High	–
Cm	4.0×10^{-7}	Solubility based on analogy with Am
Cs	High	–
I	High	–
Nb	3.8×10^{-5}	Nb_2O_5
Mo [3]	2.6×10^{-8}	MoO_2
Ni	4.3×10^{-3}	$Ni(OH)_2$
Np	1.1×10^{-9}	$NpO_2 \times 2H_2O$(am)
Pa	3.0×10^{-7}	Pa_2O_5
Pd	2.5×10^{-6}	$Pd(OH)_2$
Pu	1.1×10^{-6}	$Pu(OH)_4$(am)
Ra	2.2×10^{-8}	$RaSO_4$
Se	3.1×10^{-10}	$FeSe_2$
Sm [2]	7.5×10^{-8}	$SmOHCO_3$
Sn	1.2×10^{-7}	SnO_2 (am)
Sr [2]	9.1×10^{-5}	Celestite $SrSO_4$
Tc	4.2×10^{-9}	$TcO_2 \times 1{,}6H_2O$
Th	6.3×10^{-9}	$ThO_2 \times 2H_2O$
U	9.5×10^{-10}	$UO_2 \times 2H_2O$
Zr	1.7×10^{-8}	$Zr(OH)_4$ (aged)

[1] High" indicates that no solubility limit is applied in radionuclide release and transport calculations.

[2] Not included in release calculations due to short half-lives and no ingrowth.

[3] Not included in CC and RS cases due to short half-life.

in the solubility limits applied for different elements in the two assessments, are discussed in Appendix E and in the Complementary Evaluations of Safety Report /Neall et al. 2007/. The Complementary Evaluations of Safety Report also includes a broader discussion of solubility limits and associated uncertainties. The solubility limits of uranium are particularly uncertain. For example, reported uranium concentrations at the cores of ore deposit such as in Cigar Lake are in the range 3×10^{-8} to 1×10^{-7} mol per litre, with a measured H_2(g) concentration 0.04 cm^3 per litre, indicating reducing conditions /Cramer and Smellie 1994/. This implies that the solubility of a massive crystalline UO_2 ore could be more than two orders of magnitude higher than the solubility proposed in the present Base Case for amorphous UO_2 under reducing conditions. However, according to the spent fuel model in SR-Can fuel and canister report /SKB 2006e/, the solubility of UO_2(s) under reducing conditions in presence of Fe and H_2 is 6.3×10^{-10} mol per litre. This apparent discrepancy in UO_2 solubilities is explained by considering that the Cigar Lake ore deposit comprises uraninite ($UO_{2.2}$) which is crystallographically the same as crystalline UO_2, but includes U(VI) atoms in its lattice. Because of the presence of U(VI) in the lattice, the solubility of uraninite is somewhat higher than that of UO_2 in spent fuel.

Once a radionuclide transport pathway is established, the transport of dissolved radionuclides from the canister interior to the defect is conservatively assumed to be instantaneous. Transport resistances of the inner structural parts of the canister, the fuel and the fuel cladding are disregarded, being subject to poorly quantifiable uncertainties.

Any colloids formed when solubility limits are exceeded are assumed to remain in the canister interior, because the microporous structure of the surrounding buffer provides an effective colloid filter. As discussed in the Evolution Report /Smith et al. 2007a/, this structure may be perturbed by processes affecting the evolution of the buffer, including drying/wetting, impact of iron saturation, silica precipitation and strain caused by deformation of the supercontainers, and these potential perturbations require more thorough investigation. Nevertheless, according to current understanding, none of these processes are likely to reduce the average buffer density between the canister and the rock below that required to filter colloids, lead to embrittlement and fracturing of the buffer across its entire thickness, or lead to canister sinking to the extent that the colloid filter provided by the buffer becomes ineffective.

Dissolved radionuclides are assumed to be uniformly mixed in the water present in the canister interior. The initial void space inside the canister is 0.95 m^3 for BWR spent fuel from the Olkiluoto 1-2 reactors (i.e. the reference spent fuel for the present safety assessment). The corresponding volumes are 0.61 m^3 for EPR spent fuel from Olkiluoto 3 and 0.65 m^3 for PWR (VVER-440) spent fuel from Loviisa 1-2 /Raiko 2005/. These volumes will, however, vary with time, as will the degree to which it is water filled, and the rates of these variations are uncertain. For example, the conversion of the iron in the insert to higher volume corrosion products will reduce the void volume available (see Chapter 8 in the Evolution Report /Smith et al. 2007a/).

In the Base Case, the assumed volume of water inside the canister interior is 0.7 m^3 at all times subsequent to water ingress, which is the same as the value used in TILA-99 /Vieno and Nordman 1999/. The volume significantly affects radionuclide release rates only at relatively early times following establishment of a transport pathway from the canister interior (a few thousand years), when releases are dominated by the radionuclide IRFs. In this time frame, a volume erring on the low side is conservative, since it gives radionuclide concentrations that err on the high side. The time to reduce the void space in the canister interior from 0.95 m^3 to 0.7 m^3 by corrosion of the insert at a rate, R, of 10^{-6} m a^{-1}, is given by:

$$\Delta t = \frac{\Delta V}{RF_0(\delta - 1)} = \text{ 7,400 years,} \qquad \text{(Eq. 5-2)}$$

where ΔV = 0.95 m^3–0.7 m^3, F_0 is the total inner surface area of the insert (about 34 m^2; see Section 2.5.1 of the Process Report, /Gribi et al. 2007/), and δ is the volume increase factor relative to iron, which takes value of about 2 assuming that iron is converted to magnetite. Thus, an assumption of an available void space of 0.7 m^3 is conservative at times when it is most relevant to radionuclide release, assuming that this void space is water filled.

The assumption that the void space is entirely water filled may not, however, be conservative. In particular, the build-up of hydrogen gas due to corrosion of the insert could hinder the ingress of water, and could conceivably lead to water expulsion. This latter situation is considered in case PD-EXPELL (Section 5.8).

d. Radionuclide transfer to the buffer/evolution of the defect

The penetrating defect provides a resistance to the release of radionuclides to the buffer that will evolve over time due to internal processes within the canister. This transfer resistance and its evolution is uncertain (see e.g. Figure 8-1 of the Evolution Report; /Smith et al. 2007a/). For example, corrosion products from the insert, as well as bentonite from the buffer, may plug the defect, increasing its mass transport resistance. Alternatively, corrosion products may expand the original defect, resulting in a decrease in mass transport resistance. Following the stylised analysis of the "growing pinhole failure mode" in SR-Can (Section 10.5 in /SKB 2006a/), it is assumed in the Base Case that the defect ceases to provide transport resistance at 10,000 years after canister emplacement (9,000 years after radionuclide transport pathways from the canister interior are established). It should be noted, however, that the SR-Can Data Report (Section 4.4.7 of /SKB 2006b/) suggests that loss of transport resistance could occur at any time between 1,000 and 100,000 years after radionuclide transport pathways from the canister interior are established, and the choice of 10,000 years as the Base Case parameter

value is somewhat arbitrary. Furthermore, loss of transport resistance may be a process that occurs gradually over time, rather than as a discrete event. An instantaneous loss of transport resistance is, however, a conservative assumption, since a gradual loss of transport resistance would spread the peak release over a longer period of time, reducing its magnitude.

Prior to 10,000 years, the mass transport resistance of the defect is calculated based on the assumption that it is filled with water, with a diffusion coefficient of 2×10^{-9} m^2 s^{-1} for all migrating species. In TILA-99, a higher diffusion coefficient was assumed in the case of cations and non-saline water. This was to account, for example, for the possibility of "surface diffusion" of cations in the case of the defect becoming bentonite filled, which could lower the mass transport resistance of the defect for cations; see Table 11-8 of /Vieno and Nordman 1999/. In the present assessment, the same diffusion coefficient in the defect is applied to all migrating species because of the uncertainty in the nature of any filling in the defect and the difficulty in reliably quantifying effects such as surface diffusion.

e. Radionuclide transport in the buffer

Radionuclides are transported through the buffer predominantly by diffusion, retarded by sorption. The governing equation for two-dimensional diffusive transport of a radionuclide in the r and z directions, as defined in Figure 5-1, (not including any radionuclide ingrowth from any parent radionuclide) is:

$$\frac{\partial C}{\partial t} = D_a\left(\frac{1}{r}\frac{\partial}{\partial r}\left(r\frac{\partial C}{\partial r}\right)+\frac{\partial^2 C}{\partial z^2}\right)-\lambda C \qquad \text{(Eq. 5-3)}$$

where C [mol m^{-3}] is concentration, λ [s^{-1}] is the radioactive decay rate and D_a [m^2 s^{-1} is an apparent diffusion coefficient, which takes into account the retarding effect of sorption on diffusive transport (see below).

The amount of any element sorbed on buffer pore surfaces is assumed to adjust rapidly to changes in aqueous concentration, and to be proportional to this aqueous concentration at any time, i.e. for transport modelling, equilibrium, linear sorption is assumed, quantified by an element-dependent sorption constant (K_d). The assumption of equilibrium linear sorption entails a simplification of relatively complex sorption processes. The assumption of linearity is, however, usually met at the low concentrations that are of interest, and the assumption of equilibrium is met if the sorption has a timescale that is much shorter than the timescale for slow diffusive transport across the buffer.

K_d values, which are mostly based conservatively on the lower limit values given in Table A-12 of the SR-Can Data Report /SKB 2006b/ for saline and non-saline groundwaters, are given in Table 5-7.

Table 5-7. Buffer sorption coefficients (K_d values).

Element	K_d [m^3 kg^{-1}]	Element	K_d [m^3 kg^{-1}]
Am	10	Pd	0.3
C	0	Pu	4
Cl	0	Ra	0.001
Cm	10	Th	6
Cs	0.018	Se	0
I	0	Sm	0.8
Mo	0	Sn	2.3
Ni	0.03	Sr	0.0009
Nb	0.2	Tc	2.3
Np	4	U	0.5
Pa	0.2	Zr	0.1

Diffusive transport through the buffer and retardation by sorption can vary significantly with the chemical form of the migrating species. Calculations of the speciation of certain elements in bentonite porewater indicate the main complexes expected to be formed in solution (Appendix E and /Grivé et al. 2007/). The calculations show that U, Pu and Np, in particular, may be present in the buffer in more than one oxidation state. Np(IV) dominates for this elements, and is the assumed species for the present calculations (the impact of less abundant but also less retarded species is an issue for future studies). In the case of Pu, Pu(III) dominates in the dilute/brackish water considered in the Base Case, although Pu(IV) is also present. According to Table A-12 of the SR-Can Data Report /SKB 2006b/, Pu(IV), with a lower limit K_d of 4 m^3 kg^1, is less sorbing than Pu(III), which has a lower limit K_d of 10 m^3 kg^1. A K_d of 4 m^3 kg^1 is conservatively assumed for Pu in the present calculations[20]. This is also in accordance with SR-Can. In the case of U, both U(IV) and U(VI) may be present in significant proportions. U(VI) is kept stable in solution by carbonate complexes, which dominate in the expected near-field redox and pCO_2 conditions. According to Table A-12 of the SR-Can Data Report /SKB 2006b/, U(VI), with a lower limit K_d of 0.5 m^3 kg^1, is less sorbing than U(IV), which has a lower limit K_d of 3.6 m^3 kg^1. A K_d of 0.5 m^3 kg^1 is conservatively assumed for U in the present calculations. An exception to the use of SR-Can sorption data is Mo. No data for Mo are given in SR-Can and, in Table 5-7, the K_d value for Mo, which is assumed to be present predominantly in anionic form (see below), is conservatively set to zero.

Buffer pore surfaces, being negatively charged, repel anions. Anion concentrations in narrow pores and near to pore surfaces in larger pores are therefore less than in the case of neutral and cationic species, for given concentrations at the boundaries. This "anion exclusion" effect is treated in transport modelling by assigning the matrix a lower porosity and a lower effective diffusion coefficient when modelling anion transport compared with the values for neutral and cationic species, the porosity assumed for neutral and cationic species being equal to the actual porosity of the buffer[21]. Based on Table A-11 of the SR-Can Data Report, buffer porosities and effective diffusion coefficients for the present Base Case are taken to be:

- 0.43 and 1.2×10^{-10} m^2 s^{-1} for neutral and cationic species;
- 0.17 and 1.0×10^{-11} m^2 s^{-1} for anions; and
- 0.43 and 3.0×10^{-10} m^2 s^{-1} for the particular case of Cs.

The apparent diffusion coefficient, which appears in the diffusion equation – Eq. 5-3, is related to the effective diffusion coefficient D_e [m^2 s^{-1}], porosity ε and the sorption constant K_d [m^3 kg^{-1}] using:

$$D_a = \frac{D_e}{\varepsilon + (1-\varepsilon)\rho_s K_d} \qquad \text{(Eq. 5-4)}$$

where ρ_s is the mineral density of the bentonite buffer, taken to be 2,700 kg m^{-3}.

[20] Pu(III) also dominates in the more saline groundwaters also considered in some variant assessment cases (assessment cases PD-SAL and PD- HISAL). On the other hand, in the glacial meltwater assessment cases (e.g. assessment cases PD-GMW and PD-GMWV), where the pH is assigned a higher value, Pu(IV) dominates. The assumption of K_d value based on Pu(IV) is, however, conservative in all cases, because it is lower than the value for Pu(III).

[21] In the various scoping calculations presented in the Process and Evolution Reports /Gribi et al. 2007, Smith et al. 2007a/, the porosity of the saturated buffer is taken to by 0.44, which is also the value given in the Design Description 2006 /Autio et al. 2007/. For the purposes of radionuclide transport calculations, the decision was taken to use near-field data from the SR-Can safety assessment, where this is not affected by the specific characteristics of the Olkiluoto site and the KBS-3H design. These near-field data include a slightly lower saturated buffer porosity of 0.43.

In the Base Case, on the basis of speciation calculations, I, Cl, Se and Mo are treated as anionic when assigning porosities and effective diffusion coefficients in the buffer, with remaining elements being treated as neutral and cationic complexes. Speciation calculations indicate that Th and Nb will also be present as anionic complexes, although Th and Nb speciation is particularly uncertain, because of limited thermodynamic data for Nb and limited data for the dominating anionic hydroxyl carbonate Th complexes. Both Th and Nb are reported to sorb on clays and thus should be present in non-anionic form; see the further discussions in Appendix E. Speciation calculations also indicate that Pu will be present in anionic and non-anionic forms in roughly equal amounts, and that U will be present, at least in part, in anionic form as U(VI) (buffer sorption is based on the assumption that U is present as U(VI), see above). Furthermore, some C may be present in anionic form as carbonate complexes, as well as in the form of neutrally charged methane and organic acids, although methanic carbon was omitted in the speciation calculations (Appendix E). For consistency with SR-Can, however, Nb, Th, Pu, U and C are treated as being entirely neutral or cationic in the near field in the present Base Case. The assumption of neutral or cationic form is clearly conservative in cases where there is either no difference in sorption or sorption of the anionic form is lower than that of the neutral or cationic forms. This is the case for C, since all C species are non-sorbing in the buffer according to SR-Can (Table A-13 of /SKB 2006b/). It is also the case for U, since U(VI) has a lower buffer sorption coefficient than U(IV), according to Table A-13 of /SKB 2006b/. For other elements assumed to be present in neutral or cationic form, the conservatism or otherwise of this assumption is not immediately apparent from the data, and, in the case of Nb, anionic speciation of Nb in the near field and in the geosphere is considered in the variant case PD-BCN (Section 5.10).

In the Base Case, all transport properties are assumed to be homogeneous throughout the buffer. However, as discussed in Section 2.2.2, processes may occur that perturb these properties, particularly near the buffer/rock interface. For example, Fe(II) generated by the corrosion of iron or steel components (principally the supercontainer steel shell and the canister insert) sorbs strongly to the pore surfaces of the buffer. This Fe(II) sorption may locally compete with that of some radionuclides, and thus weaken the barrier function of the buffer for these radionuclides, which include, for example, Ni. Competitive sorption of Fe(II) is currently not well understood and there is a lack of experimental data. However, a reduction in sorption has only a minor effect on the release of radionuclides that are solubility limited (except where the half-lives are relatively short). For example, a reduction in the Ni sorption coefficient by a factor 10 increases the Base Case maximum release rate of Ni-59 from the near field by a factor of 2.2. An assumption of no sorption leads to an increase by a factor of 2.4. Nevertheless, competitive sorption of Fe(II) is an issue that would benefit from further work (see Chapter 9).

Processes such as co-precipitation or sorption of radionuclides on iron corrosion products or other solids at or near the buffer/rock interface have not been considered. Although the supercontainer steel shell and its corrosion products are expected to display good sorption properties for some radionuclides (which may offset to some extent any detrimental effects of competitive sorption), no additional sorption capacity has been assigned to the buffer, since it is assumed that the sorption capacity of the buffer as a whole is large compared with the scavenging effects of iron. The partial release of sorbed or precipitated radionuclides following a change in groundwater composition from dilute/brackish to that of glacial meltwater is considered in case PD-GMWC (Section 5.11).

f. Radionuclide transfer to the geosphere

Radionuclides are transferred by diffusion from the buffer to the nearest fracture intersecting the drift, and migrate downstream by advection in flowing water (Figure 5-1). The rate of transfer of radionuclides to the fracture is determined by the rate of groundwater flow through the fracture – see the discussion of transfer coefficients in part (iv). It is also affected by possible perturbations to the mass transfer properties of the buffer/rock interface, as considered in cases PD-SPALL, PD-FEBENT1, PD-FEBENT2 and PD-FEBENT3 (Section 5.7).

Provided the elemental concentrations at the outer boundary of the buffer are less than the corresponding solubilities at the buffer/rock interface, then concentrations across the boundary are assumed to be continuous. Radionuclides are released to the geosphere at a rate $C.Q_{bl}$, where C is the radionuclide concentration at the boundary, and Q_{bl} is a transfer coefficient, as defined in part (iv) (Eq. 5-10). If, on the other hand, the solubility of a given element is exceeded, the combined rate of release of all isotopes of a given element is limited to $C_s.Q_{bl}$, where C_s is the elemental solubility.

Q_{bl} is a function of the transmissivity and aperture of the fracture intersecting the drift and the hydraulic gradient driving fracture flow. In the Base Case, it is conservatively assumed that the fracture is aligned with the regional hydraulic gradient. This gradient is assigned a value of 0.01, which is a conservative value given the range of gradients expected in the repository area (0.01 to 1%) according to /Löfman 1999/. The fracture is also assigned a transmissivity of 3×10^{-9} m^2 s^{-1}, based on a consideration of the 0.1 litre per minute criterion set for the maximum initial inflow to a ~ 10 m long drift section containing one supercontainer and one distance block (see Appendix B.2 of the Evolution Report, /Smith et al. 2007a/). The relationship between initial inflow and longer-term flow is, in reality, complicated by a number of factors not taken into account in deriving the Base Case transmissivity value (see Section 2.2.7 of the Evolution Report). Firstly, it may be possible to reduce the initial inflow through some larger aperture fractures intersecting the deposition drift by grouting, such that significant piping and erosion do not occur during the operational period and subsequent buffer saturation, but this grout is likely to become degraded and ineffective in reducing flow in the longer term (in view of current uncertainties in the performance of any grout, an inflow of less than 0.1 litres per minute *prior* to grouting[22] is currently assumed as a criterion for a drift section to be suitable for the emplacement of a supercontainer and distance block unit). Furthermore, initial inflows may also be reduced by drawdown of the water table, which will give a reduction in the hydrostatic pressure at repository depth, by the impact of other open repository tunnels and drifts, and potentially by mineral precipitation and degassing in the fracture. These are generally transient effects which do not affect flow in the longer term, once the drifts are saturated. Finally, inflow is determined not only by the hydraulic properties of fractures intersecting the drift, but also by those of other connected fractures in the wider fracture network. In view of these factors, some fractures intersecting the drift that have transmissivities higher than 3×10^{-9} m^2 s^{-1} cannot currently be excluded (assessment cases are defined and analysed that address the possibility of a higher transmissivity fracture intersecting the drift at the location of a failed canister, e.g. in variant cases PD-LOGEOR and PD-HIFLOW). The Base Case transmissivity of 3×10^{-9} m^2 s^{-1} at a supercontainer and distance block emplacement location is nevertheless considered to be towards the high end of the expected distribution, given that most supercontainer and distance block emplacement locations will have initial inflows significantly less than 0.1 litres per minute (according to /Hellä et al. 2006/, the initial inflow into 10 m drift intervals is less than 0.1 litres per minute over about 85% of the drift length).

The solubilities applied at the buffer/rock interface are the near-field solubilities given in Table 5-6, which are derived for bentonite porewater. In reality, the water at the interface is likely to have an uncertain transitional composition between that of bentonite porewater and the groundwater. Applying near-field solubilities at the interface rather than geosphere solubilities is, however, expected to have negligible impact, or to be conservative. In cases where the geosphere solubility of an element is higher than the near-field solubility, near-field releases are unlikely to be significantly affected by applying the near-field solubility at the interface, since near-field solubilities in any case apply inside the inner boundary of the buffer (due to a limitation in the REPCOM code, solubility limits are, in practice, applied at the inner and outer boundaries of the buffer, rather than throughout the buffer). In cases where the geosphere solubility of an element is lower than the near-field solubility, near-field releases will tend to be higher if near-field rather than the geosphere solubilities are applied at the interface – i.e.

[22] As a design boundary conditions, grouting is in any case ruled out in any drift sections where supercontainers or distance blocks are emplaced.

the assumption is conservative. Furthermore, applying (a lower) geosphere solubility at the interface could be non-conservative, since it implies that any precipitates formed at the interface because geosphere solubilities are exceeded would be immobile, whereas, in reality, they could form mobile colloids. Applying the near-field solubility at the interface is equivalent to assuming conservatively that any such precipitates are mobilised as colloids, but redissolve a short distance into the geosphere as a result of dilution.

Bentonite colloids might also form due to erosion of bentonite at the boundary between the buffer and rock e.g., in case of chemical buffer erosion following the influx of glacial meltwater to repository depth. Radionuclides may attach to these colloids and be transported through the geosphere more rapidly than radionuclides in solution, especially if the colloids are excluded from rock matrix pores due to their size and charge. Colloid formation at the buffer/rock interface and transport in the geosphere is not, however, considered in the present safety assessment. This is partly because of the poorly quantified uncertainties in transport parameters and limited mechanistic understanding, and also because the focus of the present safety assessment is mainly on the near field. Colloid facilitated radionuclide transport in the geosphere remains an issue to be addressed in future studies (Chapter 9).

(iii) Boundary conditions

Boundary conditions for radionuclide concentration C within the buffer can be specified in terms of the cylindrical polar coordinate system (r, z) shown in Figure 5-1, with its origin at the canister centre.

At the canister surface (except at the defect, where radionuclide flux is treated by means of a transfer coefficient, as defined in (iv), below), radionuclide flux is zero in the direction normal to the surface. Since transport in the buffer is assumed to take place by diffusion only, this implies zero normal concentration gradient:

$$\left.\frac{\partial C}{\partial r}\right|_{r=r_c} = 0; \quad -\frac{l_c}{2} \le z \le \frac{l_c}{2}; \qquad \text{(Eq. 5-5)}$$

$$\left.\frac{\partial C}{\partial z}\right|_{z=\pm\frac{l_c}{2}} = 0; \quad 0 \le r \le r_c\,. \qquad \text{(Eq. 5-6)}$$

Similarly at the buffer/rock interface (except where this is intersected by a fracture, in which case radionuclide flux is again treated by means of a transfer coefficient, as defined in (iv), below), radionuclide flux is also zero in the direction normal to the surface, implying:

$$\left.\frac{\partial C}{\partial r}\right|_{r=r_t} = 0; \quad -\frac{p_c}{2} \le z \le \frac{p_c}{2}\,. \qquad \text{(Eq. 5-7)}$$

Finally, over the two horizontal planes passing through the buffer midway between the defective canister and its immediate neighbours, it is assumed that radionuclide flux is zero:

$$\left.\frac{\partial C}{\partial z}\right|_{z=\pm\frac{p_c}{2}} = 0; \quad 0 \le r \le r_t\,. \qquad \text{(Eq. 5-8)}$$

This boundary condition is conservative, since dispersion and retention of released radionuclides in the buffer surrounding the canisters on either side of the failed canister is not included. These processes tend to reduce calculated releases.

(iv) Transfer coefficients

The code REPCOM makes use of analytically derived transfer coefficients to evaluate the transfer of radionuclides between system components where concentration gradients are high, and thus avoids the use of a large number of compartments to resolve these gradients. Transfer coefficients are effective flow rates that quantify transport rates of non-decaying species (transfer resistances are the inverses of the transfer coefficients). The transfer coefficients used by REPCOM are related to diffusive processes occurring:

- in the hole through the copper shell (assumed to be water filled[23]);
- at the mouth of the hole (within bentonite); and
- from the buffer to the rock.

Transfer coefficients for transport through the hole through the copper shell and at the mouth of the hole are calculated internally by REPCOM, using the equations given, for example, in Section 11.6 of TILA-99 /Vieno and Nordman 1999/.

The transfer coefficient from the buffer into the rock is provided as input into REPCOM in the form of a user-defined equivalent flow rate, Q_F [$m^3\ a^{-1}$]. In TILA-99, two mass transfer resistances were considered to contribute to Q_F:

- the mass transport resistance provided by the buffer between the canister and the fracture wall; and
- the boundary layer (film) resistance between stagnant water in the buffer and the water flowing in the fracture, quantified in terms of an equivalent flow rate Q_{bl} [$m^3\ a^{-1}$].

In the present modelling approach, the mass transport resistance provided by the buffer between the canister and the fracture wall is modelled explicitly by REPCOM, and thus:

$$Q_F = Q_{bl} \qquad \text{(Eq. 5-9)}$$

Q_{bl}, which may be thought of as the flow rate in a thin layer of flowing water in the fracture adjacent to the buffer/rock interface into which mass transfer from the buffer occurs, is given by

$$Q_{bl} = 4\sqrt{2b_v r_t D_w T \cdot i} \qquad \text{(Eq. 5-10)}$$

D_w is the diffusion coefficient within the fracture intersecting the deposition drift, which is taken to be 2×10^{-9} $m^2\ s^{-1}$. Diffusion coefficients of many ions in free groundwater are in the range 1×10^{-9} to 2×10^{-9} $m^2\ s^{-1}$, with some dependency on temperature and ionic strength. In a narrow fracture, the rate of diffusion of ions may be reduced, for example, by the tortuosity of transport paths (see, e.g. Section 3.4 in /Freeze and Cherry 1979/. In Eq. 5-10, the use of a diffusion coefficient representative of those for ions in free water is, however, conservative, since a lower (more realistic) diffusion coefficient would reduce mass transfer from the buffer to the rock.

Based on a fracture transmissivity T of 3×10^{-9} $m^2\ s^{-1}$, a regional hydraulic gradient i of 0.01, a diffusion coefficient D_w of 2×10^{-9} $m^2\ s^{-1}$, a fracture aperture $2b_v$ of 3×10^{-5} m (derived from transmissivity using Eq. 5-1) and a drift radius r_t of 1.85 m (Table 5-4), the value of Q_F in the Base Case is set to an upwardly rounded value of 2×10^{-4} $m^3\ a^{-1}$ (upward rounding of the transfer coefficient is conservative, since it tends to increase the rates of release of radionuclides from the buffer to the rock) This is the same as the equivalent flow rate used in TILA-99 /Vieno and Nordman 1999/.

[23] The assumption of a water-filled hole is judged to be conservative. A hole filled, for example, with bentonite or corrosion products from the insert will have a lower apparent diffusion coefficient, due to the small sizes of pores within these materials, and due to sorption on pore surfaces. It will therefore provide more resistance to radionuclide transport.

5.2.4 Geosphere model

The treatment of the geosphere is largely the same as in TILA-99, as described in /Vieno and Nordman 1999/. Parameter values that apply to all migrating species are given in Table 5-8. Element-dependent parameters are given in Tables 5-9 and 5-10.

Transport of dissolved radionuclides through the geosphere occurs along multiple transport paths, which are represented in the geosphere model as a single fracture, characterised by a transport resistance. Transport is retarded by matrix diffusion and, for many dissolved species, sorption on matrix pore surfaces. In reality, there will be variability in the transport properties of different paths but, for transport modelling purposes, this variability is omitted. This simplification means that, although there are multiple transport paths, the paths are treated as identical, and only transport along a single, representative path (or fracture) needs to be calculated.

Gas and colloids, both naturally present in the groundwater and arising from the presence of the repository, are assumed not to affect geosphere transport, although these remain issues to be considered in future studies (Chapter 9).

Values are taken for the most part from TILA-99, using data for reducing and, where relevant, non-saline conditions. The TILA-99 value of 50,000 years per metre assigned to the geosphere transport resistance parameter WL/Q is based, in the first place, on statistical data for hydraulic conditions at the Olkiluoto site /Löfman 1996/. The conservatism of this choice is, however, supported by the more recent discrete fracture network modelling of the Olkiluoto site carried out by /Lanyon and Marschall 2006/. Lanyon and Marschall evaluated transport resistances from various supercontainer deposition locations to the outer boundary of their model, 50 m from the modelled deposition drift. Histograms of the results for model drift W01T01, which were obtained using particle tracking, are given in Figure 5-2. Particles were released at the intersection of fracture sub-planes with the 1-D supercontainer drift elements and were then tracked within the detailed flow field obtained from a steady-state pressure distribution. The advective travel time and the F-quotient[24] are calculated for each particle. The results show that none of the particle tracks give transport resistances less than about 50,000 years per metre, the highest value being obtained for supercontainer location W01T01:CO16. The results for other modelled drifts show still higher minimum transport resistances (see Figure B-3 parts b–d in /Lanyon and Marschall 2006/. A transport resistance of 50,000 years per metre is therefore considered a reasonably conservative choice, although the possibility of lower as well as higher transport resistances is considered in variant cases (see Section 5.12).

Table 5-8. Geosphere parameter values that apply to all migrating species in the Base Case for an initial penetrating defect.

Parameter	Unit	Value	Source
Transport resistance of geosphere (WL/Q[1])	a m^{-1}	50,000	Median value for both saline and non-saline conditions at Olkiluoto; Table 11–19 in /Vieno and Nordman 1999/
Rock matrix grain density	kg m^{-3}	2,700	p. 119 in /Vieno and Nordman 1999/
Maximum rock matrix penetration depth	m	0.1	p. 119 in /Vieno and Nordman 1999/
Fracture aperture	m	3×10^{-5}	Eq. 5-1

[1] W [m] is the width of the flow channel, L [m] is the transport distance and Q [m^3 a^{-1}] is the flow rate in the channel.

[24] In numerical codes where transport calculations are based on particle tracking, like e.g. ConnectFlow, F is calculated as the sum of advective travel time, t, divided by half-aperture, b, in individual transport segments along the path (in the most general sense an integral). This definition and concept used by SKB is described in /Andersson et al. 1998/ and used in /Hartley et al. 2006ab/. Regarding flow rates the F-quotient (or F-factor) for a single planar fracture can be defined as $F=2WL/Q$ (= t/b), where W [m] is the channel width over which Q has been determined.

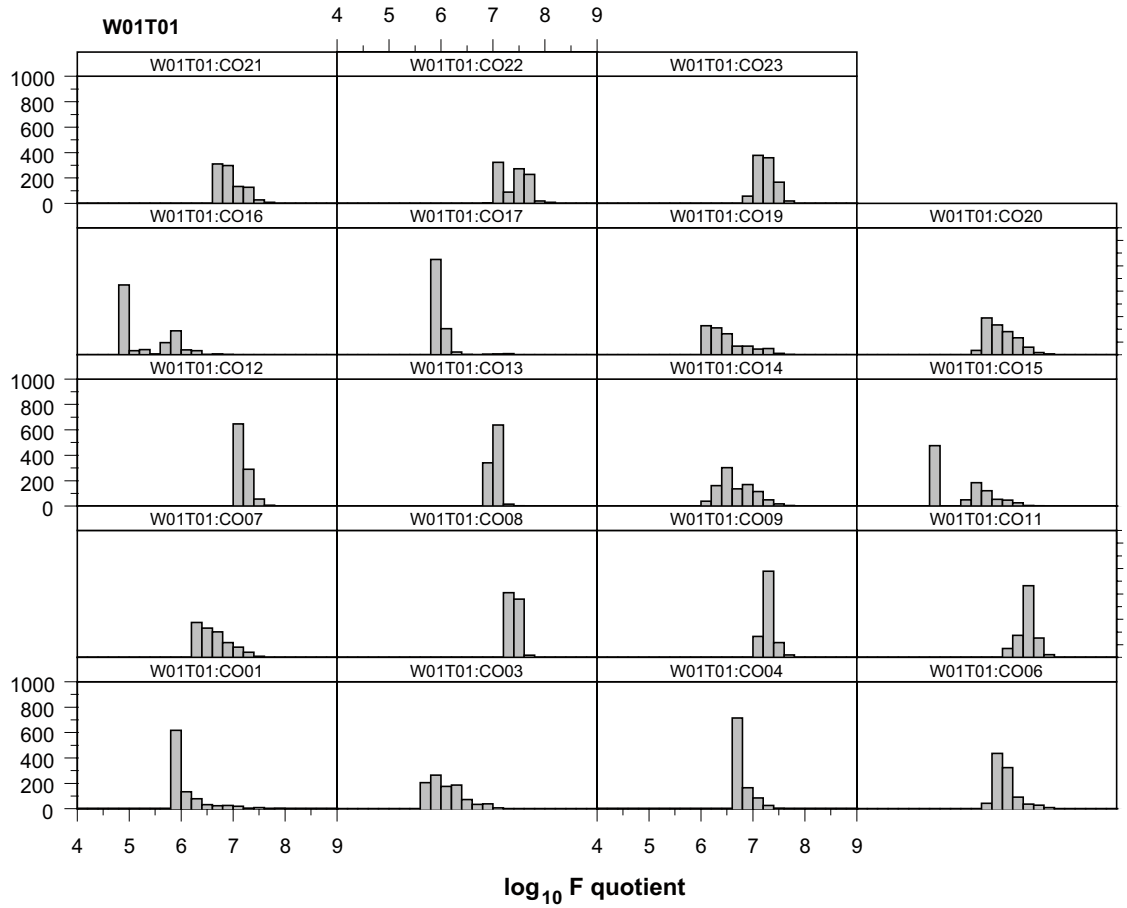

Figure 5-2. *Histograms of log of the transport resistances (termed here F quotient, in log units of years per metre) evaluated for particles released at different supercontainer locations in a DFN model of the Olkiluoto site (after Figure B-3 of /Lanyon and Marschall 2006/).*

The geosphere transport resistance can also be written in terms of transmissivity and gradient:

$$\frac{L}{Ti} = \frac{WL}{Q} \qquad \text{(Eq. 5-11)}$$

From this equation, a transport resistance of 50,000 years per metre is provided by fracture about 50 m long with a transmissivity of 3×10^{-9} m^2 s^{-1} with flow driven by a hydraulic gradient i of 0.01. Thus, the model can be interpreted in terms of transport from the drift wall through about 50 m of relatively tight rock via the Base Case 3×10^{-9} m^2 s^{-1} transmissivity fracture to the nearest more highly transmissive shear zone, assuming that this relatively tight rock dominates the overall transport resistance.

In the case of parameters describing retardation in the geosphere by matrix diffusion and sorption, TILA-99 conservative values, rather than realistic values, are used, since the conservative values were used to evaluate the TILA-99 reference scenarios (Chapter 11 in /Vieno and Nordman 1999/). There are, however, exceptions to the use of TILA-99 data related to the selection of radionuclides present as anionic neutral and cationic species, as described below.

The rock matrix between fractures contains connected porosity into which migrating solutes can diffuse ("matrix diffusion"). Matrix diffusion, coupled to sorption on matrix pore surfaces, is an important retardation mechanism for many radionuclides. The rock matrix immediately adjacent to the fractures may be mineralogically altered, as reflected in Table 5-9 by the relatively high porosities and higher effective diffusion coefficients in the first centimetre adjacent to the fracture wall. In the present study, as in TILA-99, lower porosities and lower effective diffusion coefficients are applied from one to ten centimetres from the wall compared with this inner, altered zone.

Table 5-9. Geosphere matrix porosity and effective diffusion coefficients (from Table 11-10 in /Vieno and Nordman 1999/, assuming non-saline groundwater). In the present study Cl, Se, Mo and I are assumed to be present as anions (see main text).

Parameter	Distance from fracture	Species	Value
Porosity	0–1 cm	Anions	0.1%
		Neutral and cationic species	0.5%
	1–10 cm	Anions	0.02%
		Neutral and cationic species	0.1%
Effective diffusion coefficient	0–1 cm	Anions	10^{-14} m^2 s^{-1}
		Neutral and cationic species	10^{-13} m^2 s^{-1}
	1–10 cm	Anions	10^{-15} m^2 s^{-1}
		Neutral and cationic species	10^{-14} m^2 s^{-1}

It is also conservatively assumed that the rock matrix further than ten centimetres from the fracture wall is inaccessible to migrating radionuclides. There is evidence from, for example, formation factor logging by electrical methods /Löfgren and Neretnieks 2003, Liu et al. 2006/, that greater matrix depths may, in reality, be accessible. The assumption of a limited matrix diffusion depth is, however, conservative, since a greater depth could potentially further retard and spread releases to the biosphere. A sensitivity analysis is described in Appendix C illustrating the limited impact of varying the matrix diffusion depth over a wide range in the hypothetical case of a pulse release of a non-decaying nuclide from the near field.

Matrix pore surfaces, being negatively charged, repel anions. Anion concentrations in narrow pores and near to pore surfaces in larger pores are therefore less than in the case of neutral or cationic species, for a given concentration in the fracture. This "anion exclusion" effect is treated in transport modelling by assigning the matrix a lower porosity and a lower effective diffusion coefficient when modelling anion transport compared with the values assigned to neutral and cationic species. In TILA-99, C, Cl, Se, Pd, Sn and I were assumed to exist as anions in all cases. According to the speciation calculations by /Grivé et al. 2007/, however, Sn will predominantly take the form of neutral hydroxide complexes. Mo, which was not among the safety-relevant elements considered in TILA-99, is also assumed to exist in anionic form in the present Base Case. Carbon, on the other hand, is assumed to be predominantly in methanic form and Pd is assumed to be dominated by neutral complexes /Grivé et al. 2007/. Thus, in the present study, Cl, Se, Mo and I are assumed to be present as anions in the geosphere.

The impact of anion exclusion may, in reality, be less than that implied by the parameter values in Table 5-9. /Liu et al. 2006/ note that anion exclusion is difficult to quantify because, at present, there is a lack of understanding of the mechanisms of the electrostatic interaction between the ions and the diffuse double layer within rock matrix pore water. The effect is, however, reduced as ionic strength increases, and is likely to be quite small in groundwater of the type found at repository depth at Olkiluoto. Nevertheless, the assumption of a high degree of anion exclusion, and hence reduced matrix diffusion, is conservative, since matrix diffusion in the geosphere has the favourable effect of retarding and spreading releases to the biosphere.

The sorption data for the geosphere (Table 5-10) are taken, for the most part, from the conservative data for non-saline reducing conditions in TILA-99 (Table 11-9 in /Vieno and Nordman 1999/). The TILA-99 K_d-values cover the rock and groundwater types encountered at the five investigation sites studied in the Finnish programme at that time, including Olkiluoto. The range of groundwater composition varied from fresh to brackish and saline groundwater, representing fairly well the reference groundwater composition for the present safety assessment. Uncertainties in sorption associated with redox conditions and the salinity of the groundwater were reported to be more significant than the differences due to rock type /Hakanen and Hölttä 1992/. It was noted that there are particular uncertainties in the K_d-value for Pa, and it was considered likely that higher K_d-values for this element would be used in the future.

Table 5-10. Geosphere sorption coefficients (K_d values).

Element	K_d [m^3 kg^{-1}]	Element	K_d [m^3 kg^{-1}]
Am	0.04	Pd	0.001
C	0	Pu	0.5
Cl	0	Ra	0.2
Cm	0.04	Th	0.2
Cs	0.05	Se	0.0005
I	0	Sm	0.02
Mo	0.0005	Sn	0.001
Ni	0.1	Sr	0.005
Nb	0.02	Tc	0.05
Np	0.2	U	0.1
Pa	0.05	Zr	0.2

Exceptions to the use of TILA-99 values are the K_d-values for C and Mo. C, which, as noted above, is assumed to be predominantly in methanic form, is assumed not to sorb. It is possible that microbial oxidation of methane could take place along with sulphate reduction if brackish, sulphate-rich water reaches repository depth during future evolution of the Olkiluoto site, leading to the formation of carbonate, which would be expected to sorb weakly (with a K_d of 0.0001 according to TILA-99). This possibility is considered in the present safety assessment in variant cases PD-BCC, PD-VVERC and PD-EPRC described in Section 5.10. There are no data available in the literature on which to base a K_d value for Mo in crystalline rocks. The value given in Table 5-10 has been chosen by expert judgement, based on a study of sorption on illite by /Motta and Miranda 1989/, a comparison of the cation exchange capacities (CECs) of illite and rock, and the known pH-dependency of K_d values for sorption on kaolinite.

5.2.5 Results

Table 5-11 gives calculated maximum near-field and geosphere release rates in Bq per year for each radionuclide in the Base Case for an initial penetrating defect (case PD-BC). It also gives the times at which these maxima occur (t_{max}). In many cases, t_{max} occurs shortly after 10,000 years, and is a result of the parameter selection whereby loss of transport resistance of the defect is assumed to occur at this time. As noted in Section 5.2.3, this choice is somewhat arbitrary; according to SR-Can, loss of transport resistance could, in reality, occur at any time between 1,000 and 100,000 years after radionuclide transport pathways from the canister interior are established. Furthermore, loss of transport resistance may be a process that occurs gradually over time, rather than as a discrete event. An instantaneous loss of transport resistance is, however, a conservative assumption, since a gradual loss of transport resistance would spread the peak release over a longer period of time, reducing its magnitude.

Figures. 5-3 and 5-4 show the near-field and geosphere release rates as functions of time for all radionuclides for which calculations were made. To place the timescales covered by these and subsequent figures in perspective, background shading is used to distinguish three successive time frames:

- 0 to 10,000 years.

This is Posiva's interpretation of the "environmentally predictable future". The Finnish regulatory dose constraint applies over this time frame (Section 1.3).

- 10,000 to 50,000 years.

Assuming a repetition of the last glacial cycle (from the Eemian interglacial to the end of the Weichselian glaciation), this period will be characterised by alternating permafrost and temperate climate phases /Pastina and Hellä 2006/.

- 50,000 to 1,000 000 years.

Table 5-11. Calculated maximum near-field and geosphere release rates for each radionuclide in the Base Case for an initial penetrating defect (case PD-BC) and the times at which these maxima occur.

Radionuclide			Near – field t_{max} [a]	Bq/a	Geosphere t_{max} [a]	Bq/a
Activation/fission products		C-14	1.01E+04	6.77E+05	1.04E+04	3.35E+05
		Cl-36	1.03E+04	1.10E+05	1.04E+04	1.05E+05
		Ni-59	1.23E+04	3.44E+05	3.80E+05	2.98E+02
		Se-79	2.15E+04	2.08E–01	3.42E+04	1.82E–01
		Mo-93	1.08E+04	3.67E–01	1.23E+04	1.52E–01
		Zr-93	2.20E+05	5.03E–02	1.00E+06	6.68E–03
		Zr-93p*	2.35E+05	3.68E+00	1.00E+06	4.89E–01
		Nb-94	1.99E+04	7.70E+03	9.73E+04	3.77E+01
		Tc-99	8.85E+05	2.25E+01	1.00E+06	4.56E+00
		Pd-107	8.90E+05	3.02E+01	1.00E+06	3.15E+01
		Sn-126	1.15E+05	4.84E+00	1.46E+05	3.92E+00
		I-129	1.03E+04	1.27E+04	1.04E+04	1.19E+04
		Cs-135	1.01E+04	7.78E+03	1.00E+06	7.97E+02
Actinide chains	4N	Pu-240	3.44E+04	1.65E+01	2.92E+04	3.01E–17
		U-236	1.00E+06	5.79E–04	1.00E+06	2.25E–04
	4N + 1	Cm-245	5.38E+04	6.05E–04	1.56E+05	3.04E–09
		Am-241	5.38E+04	6.38E–04	1.56E+05	3.20E–09
		Np-237	1.00E+06	8.21E–01	1.00E+06	6.79E–02
		U-233	1.00E+06	1.30E+00	1.00E+06	2.38E–01
		Th-229	1.00E+06	7.65E–01	1.00E+06	1.19E–01
	4N + 2	Cm-246	3.88E+04	6.19E–06	1.20E+05	6.85E–14
		Pu-242	3.94E+05	3.01E+01	1.00E+06	1.48E–03
		U-238	1.00E+06	4.95E–04	1.00E+06	1.95E–04
		U-234	1.29E+05	2.02E–03	1.00E+06	2.68E–04
		Th-230	5.64E+05	2.77E+01	1.00E+06	1.17E–02
		Ra-226	5.64E+05	3.59E+04	1.00E+06	1.19E–02
	4N + 3	Am-243	4.88E+04	4.05E–02	1.46E+05	6.03E–08
		Pu-239	5.88E+04	2.21E+02	8.36E+05	6.93E–13
		U-235	1.00E+06	3.60E–05	1.00E+06	1.42E–05
		Pa-231	1.00E+06	3.27E+01	1.00E+06	1.26E–01

* Zirconium originating from the fuel matrix only.

Again assuming a repetition of the last glacial cycle, after 50,000 years the Olkiluoto area will, for the first time in the future, be covered with ice and snow. This and subsequent glacial cycles are discussed in Chapter 7 of the Evolution Report /Smith et al. 2007a/. 1,000 000 years is the time at which calculations of radionuclide release and transport are terminated in the present safety assessment.

The figures show that releases from both the near field and from the geosphere at early times following the establishment of a transport pathway from the canister interior at 1,000 years are dominated by C-14, and that the release rates gradually increase from 1,000 years to 10,000 years. At 10,000 years, there is a marked spike in the C-14 near-field release rate, due to the assumed loss of transport resistance of the initially small penetrating defect. There are

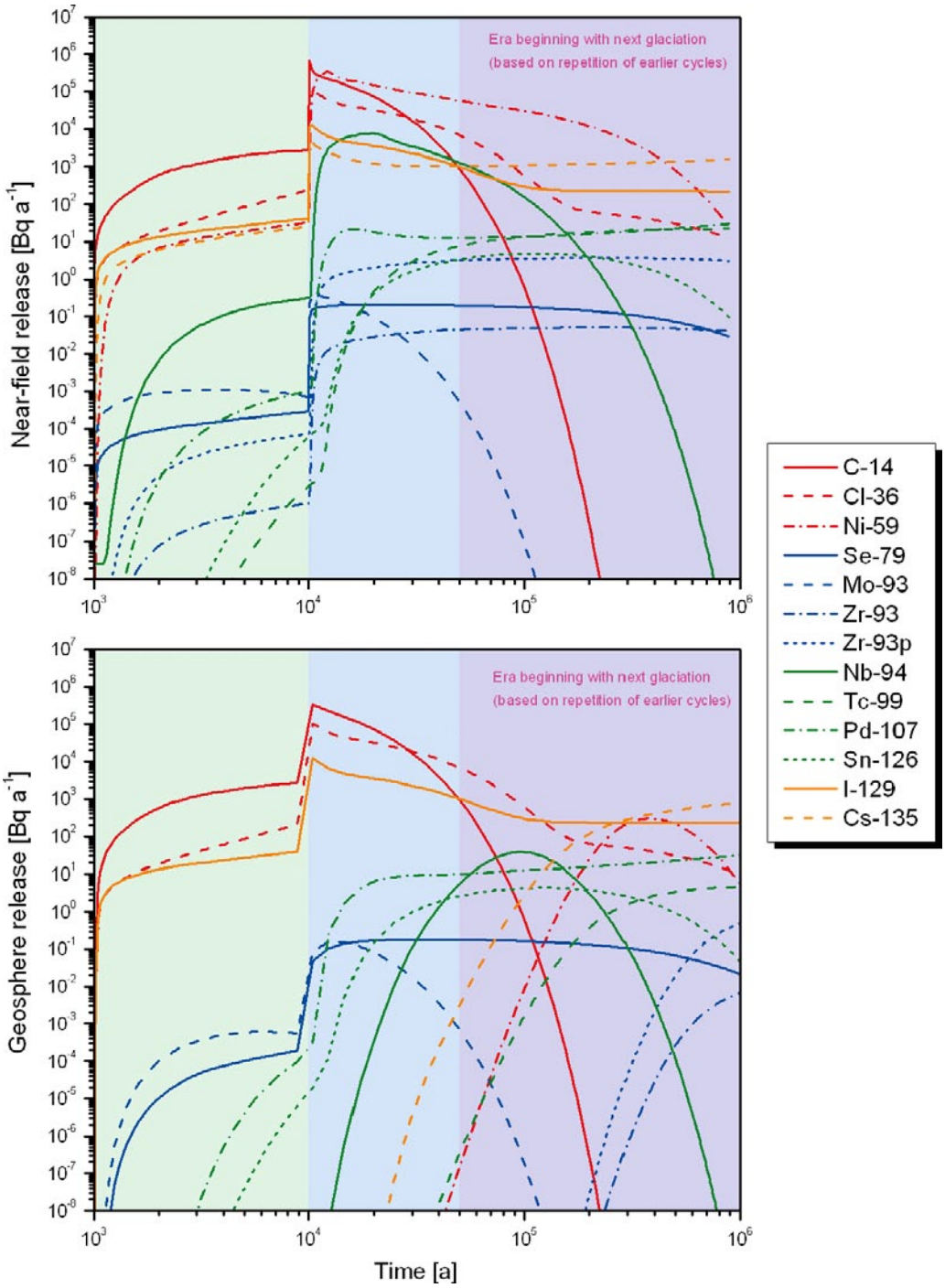

Figure 5-3. *Release rates of activation and fission products from the near field (upper figure) and geosphere (lower figure) as functions of time.*

also significant contributions to the total near-field release at 10,000 years from Ni-59, Cl-36, Nb-94, Cs-135, I-129 and others. The releases of Ni-59 and Cs-135 are, however, significantly delayed during geosphere transport and, in the case of Ni-59, there is significant attenuation of the release maximum by decay. The geosphere transport barrier also causes some spreading in time of the releases of C-14, Cl-36, Nb-94 and I-129, but gives far less attenuation of the peak release rate than in the case of Ni-59. At later times (beyond about 200,000 years) near-field releases are dominated by Ra-226, whereas geosphere releases become increasingly dominated by Cs-135 and I-129.

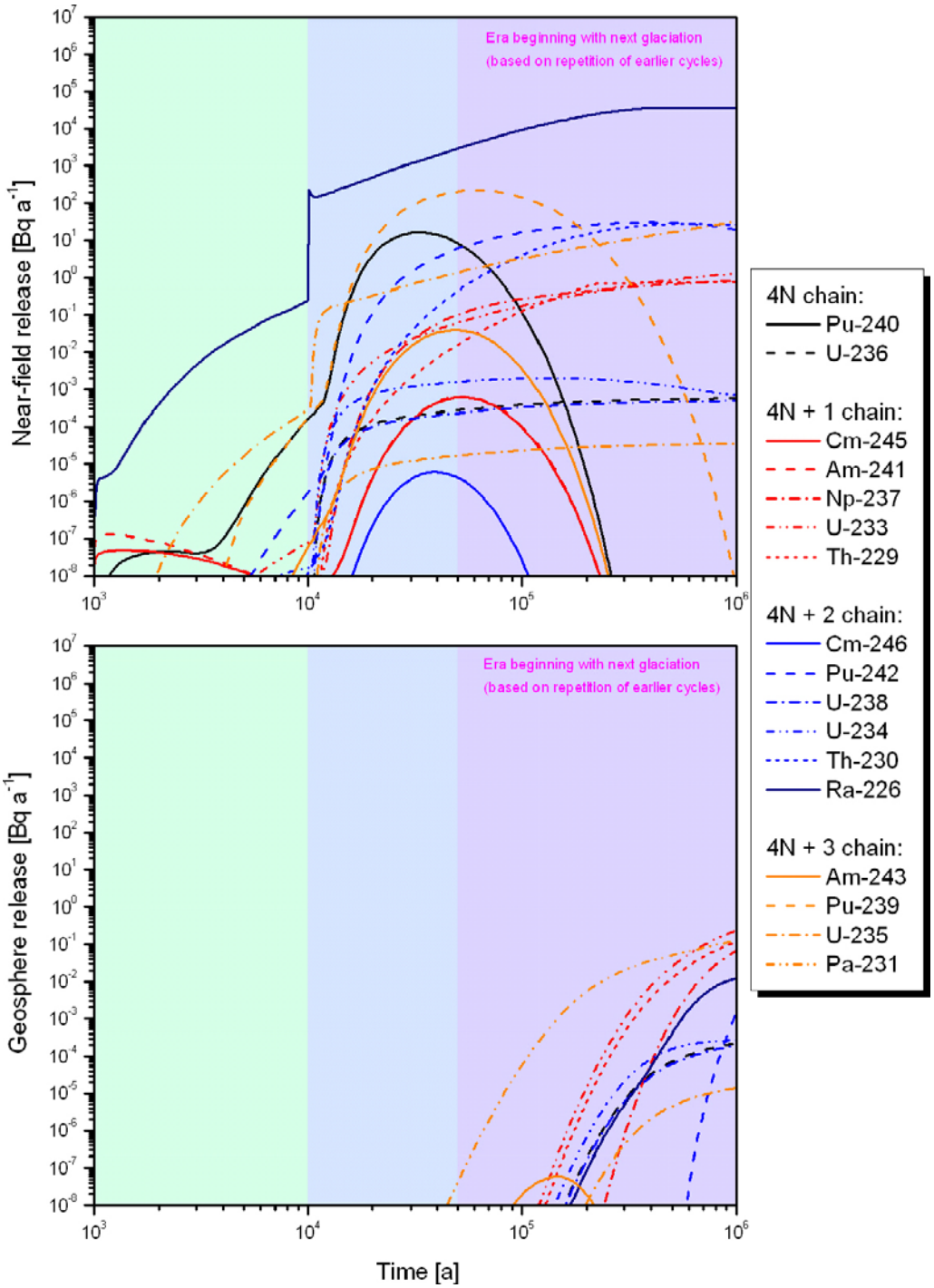

Figure 5-4. *Release rates of actinide chain members from the near field (upper figure) and geosphere (lower figure) as functions of time.*

Figure 5-5 shows the WELL-2007 dose (committed effective doses due to ingestion of water from a stylised well over one year, integrated over the adult life of an individual human, as described in Section 4.3) as a function of time based on the dose conversion factors given in Table 3-1. The figure shows total dose and the contribution to dose from individual radionuclides. The Finnish regulatory dose guideline of 10^{-4} Sv per year is shown during the "environmentally predictable future", which is the time frame over which it applies. Beyond this time frame (and especially after 50,000 years), the major climate changes that may occur are not necessarily consistent with the assumptions of WELL-2007 used to calculate the dose conversion factors, but doses are nonetheless calculated in order, for example, to facilitate comparison with other safety assessments /Neall et al. 2007/.

The results of this and other assessment cases show that, for some radionuclides, activity releases to the biosphere and the corresponding WELL-2007 doses are still increasing at the end of the million year assessment period, although in most cases[25], the magnitude of these releases, divided by the relevant geo-bio flux constraints, and doses are well below the maxima.

The dose maximum occurs shortly after loss of transport resistance of the defect at 10,000 years, and is about four orders of magnitude below the regulatory dose guideline of 10^{-4} Sv per year for this case where a single canister failure is assumed. Calculated dose is at all times dominated by I-129, with other significant contributions from C-14 (up to a few tens of thousands of years, after which this radionuclide substantially decays), Cl-36 (up to about 100,000 years), and, at later times, Cs-135.

Figure 5-6 shows the calculated annual landscape dose to the most exposed individual, together with the WELL-2007 dose. The highest annual landscape dose occurs at the end of the 10,000 period over which biosphere modelling was carried out, and is less than 10^{-6} Sv, compared with about 10^{-8} Sv in the case of WELL-2007 dose. Note that the apparent sudden increase in both doses at 9,000 years is an artefact of the finite time step size in geosphere transport modelling – the increase is associated with the loss of transport resistance of the defect, which occurs at 10,000 year. Although biosphere modelling has not been carried out beyond 10,000 years, annual landscape dose is expected to follow the same trend as WELL-2007 dose, since both are strongly correlated to radionuclide fluxes across the geosphere-biosphere interface. Thus, it is expected to have a maximum shortly after 10,000 years, with a decrease in dose thereafter.

Figure 5-7 shows release rate maxima from the near-field and geosphere, again expressed in terms of WELL-2007 dose, for all the radionuclides considered in the PD-BC calculation. The figure shows the substantial attenuation of some radionuclides during transport through the geosphere, including Ra-226, formed by the decay of U-238 and its daughters. It also shows the much lower attenuation of long-lived and poorly sorbing radionuclides, such as I-129.

Figure 5-8 shows time-dependent releases from the geosphere to the biosphere divided by the geo-bio flux constraints specified by the Finnish regulator and given in Table 1-1. Radionuclide-specific curves are shown, as well as a curve corresponding to the sum over all calculated radionuclides.

According to the Finnish regulator STUK, the sum of the ratios of nuclide-specific activity releases to their respective constraints shall be less than one in order to satisfy the corresponding regulatory requirement (Section 1.2). From Figure 5-8, the sum of these ratios, which has its maximum shortly after 10,000 years, is almost three orders of magnitude below this limit for this case where a single canister failure is assumed.

The results of this and other assessment cases show that, for some radionuclides, activity releases to the biosphere and the corresponding WELL-2007 doses are still increasing at the end of the million year assessment period, although in most cases, the magnitude of these releases, divided by the relevant geo-bio flux constraints, and doses are well below the maxima.

[25] See, however, Figures 9-8 and 9-9 and the discussion thereof.

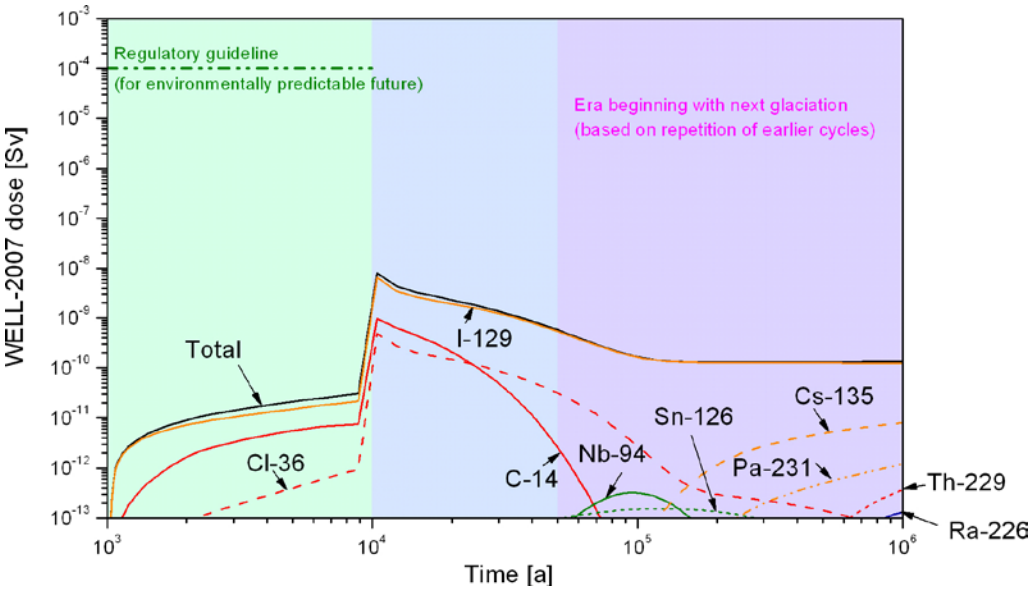

Figure 5-5. *WELL-2007 dose as a function of time in case PD-BC.*

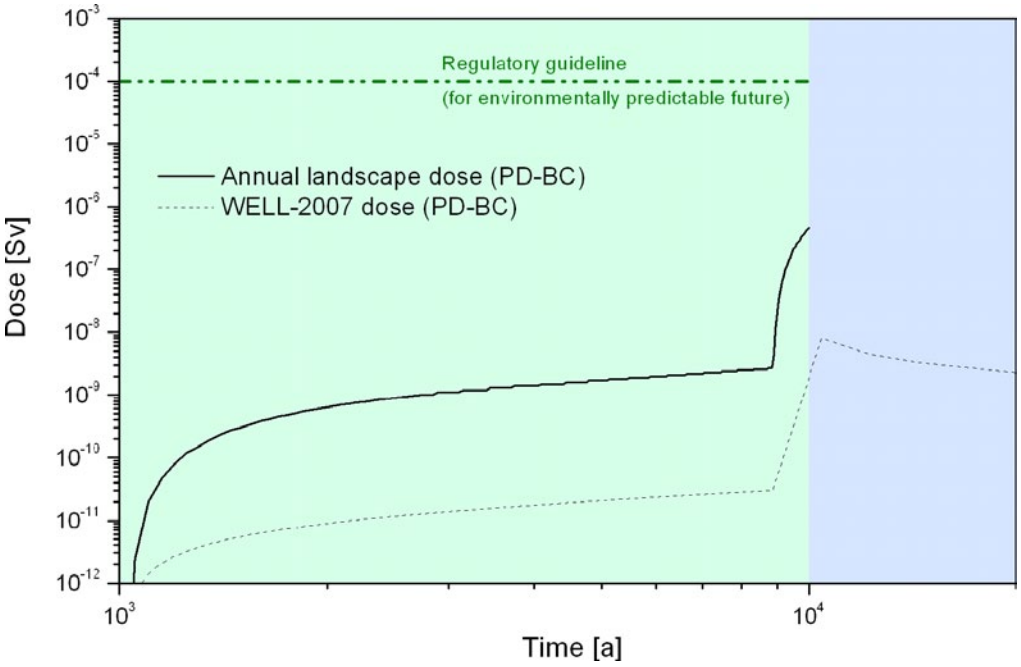

Figure 5-6. *Annual landscape dose and WELL-2007 dose as functions of time in case PD-BC.*

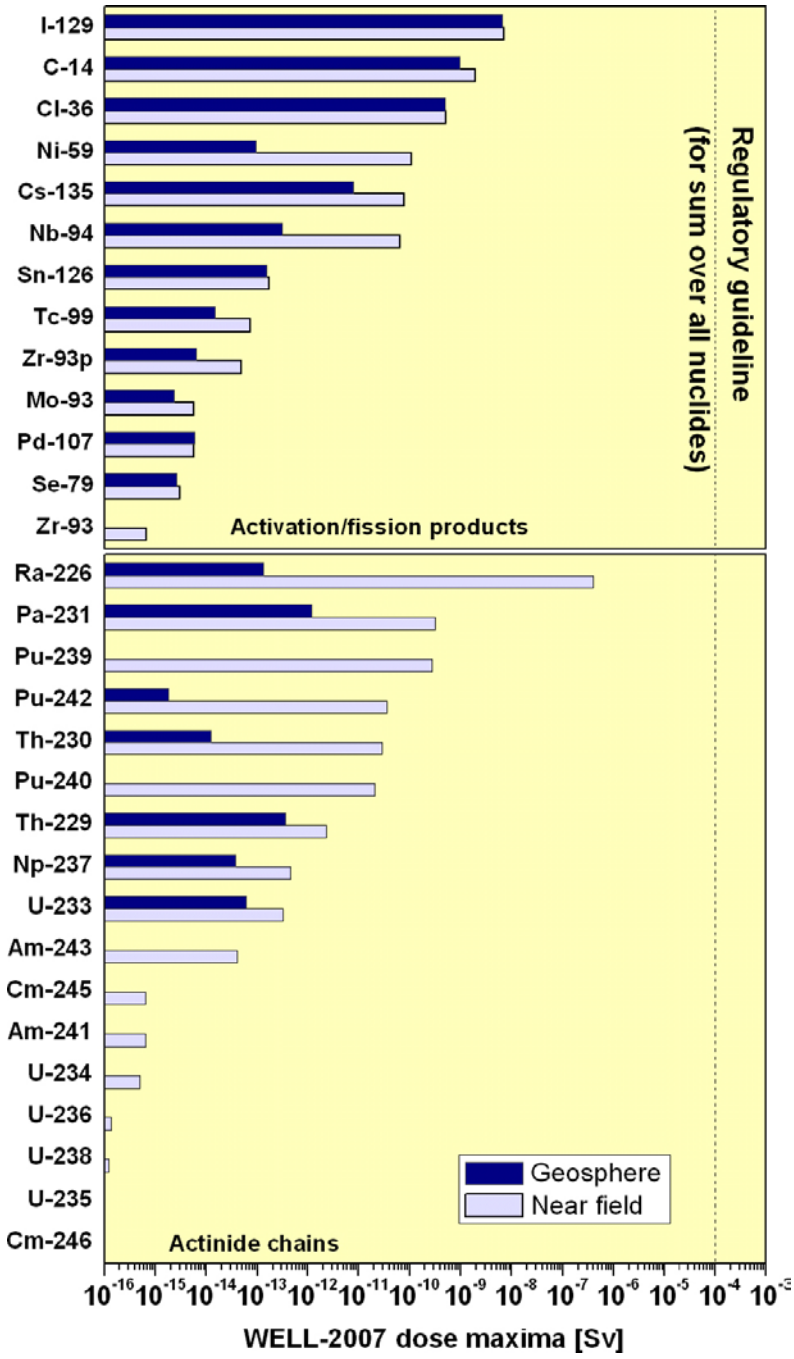

Figure 5-7. *Release rate maxima from the near field and geosphere, expressed as WELL-2007 dose, for all the radionuclides considered in the PD-BC calculation.*

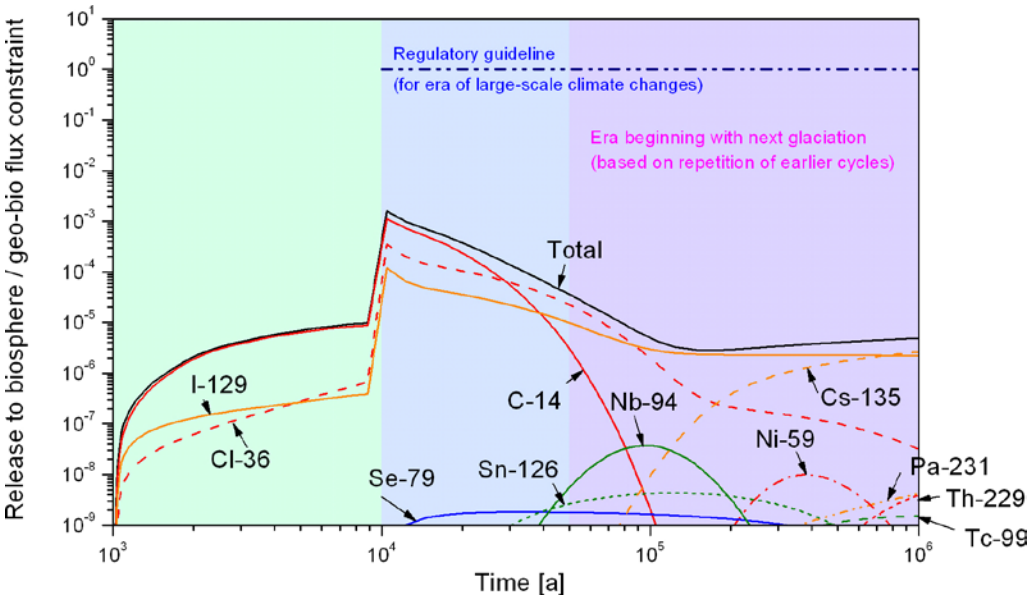

Figure 5-8. *Ratios of nuclide-specific activity releases to their respective geo-bio flux constraints in case PD-BC.*

This is the case, for example, for Cs 135 in Figures 5-5 and 5-8. The late break-through of this and other sorbing radionuclides illustrates their slowness of transport through the multi-barrier system. It is radionuclides such as I-129, Cl-36 and C-14, which are assumed to undergo little or no sorption in the buffer and geosphere that generally dominate calculated releases and doses until near the end of the assessment period. Although not calculated, Cs-135 release to the biosphere would be expected to fall shortly after a million years as its inventory becomes depleted by radionuclide decay, its half life being 2.3×10^6 years.

Finally, Figure 5-9 shows near-field and geosphere release rate maxima for the same radionuclides divided by the geo-bio flux constraints. Figures 5-8 and 5-9 show that C-14 gives the highest contribution to the maximum release rate summed over all radionuclides, but this maximum is nevertheless about three orders of magnitude below the regulatory guideline.

5.3 Cases addressing other fuel types

5.3.1 Differences compared with the Base Case

The repository will house canisters for three different spent fuel types:

- VVER-440 (Loviisa 1-2): 700 canisters containing 1,020 tU of spent fuel;
- BWR (Olkiluoto 1-2): 1,260 canisters containing 2,620 tU of spent fuel; and
- EPR (Olkiluoto 3): 1,040 canisters containing 2,190 tU of spent fuel.

The radionuclide inventories vary between fuel types, as described in /Anttila 2005/. In the Base Case, the initial penetrating defect is assumed to affect a single BWR-type canister. Alternative cases are, however, considered in which the initial penetrating defect is assumed to affect either a VVER-440-type canister (case **PD-VVER**) or an EPR-type canister (case **PD-EPR**). The VVER-400 (PWR) fuel in a canister in case PD-VVER contains 1.44 tonnes of U metal. The corresponding figure for EPR fuel in case PD-EPR is 2.13 tonnes.

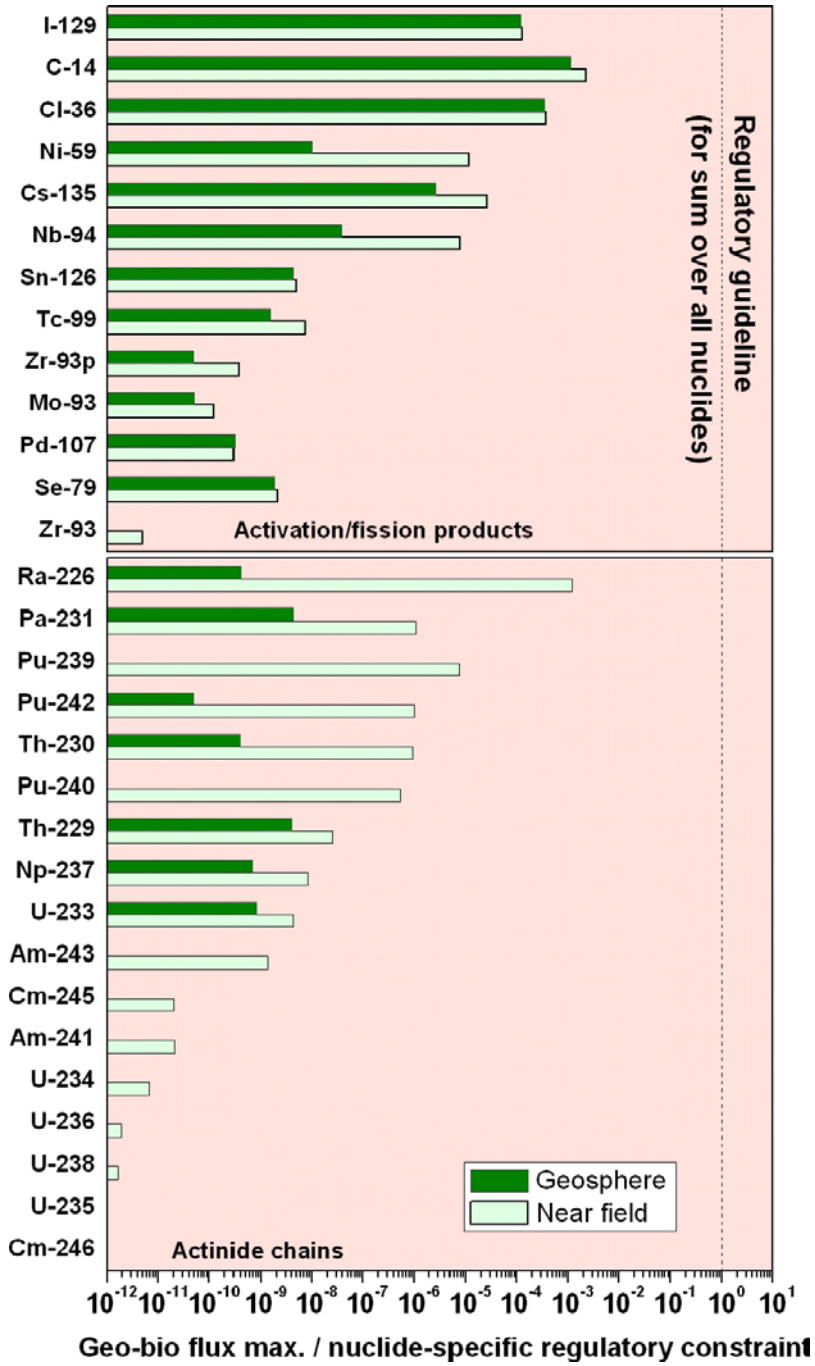

Figure 5-9. *Release rate maxima from the near field and geosphere divided by the geo-bio flux constraints specified by the Finnish regulator for all the radionuclides considered in the PD-BC calculation.*

5.3.2 Radionuclide inventories, half-lives and partitioning

Radionuclide activity inventories (per tonne of uranium), together with their half-lives and partitioning between fuel matrix, instant release fraction (IRF), Zircaloy and other metallic parts, are given in Tables 5-12 and 5-13 for cases PD-VVER and PD-EPR, respectively.

As in the case of BWR fuel, partitioning between the fuel matrix and the IRF is based on Table A-4 of the SR-Can data report (/SKB 2006b/ – realistic, central values). The inventory fractions contained in Zircaloy and other metal parts are again uncertain and the values given in the tables are based on expert judgement, guided by considerations in /Anttila 2005/.

Table 5-12. Radionuclide inventories for a single canister for VVER-440 (PWR) fuel (case PD-VVER), together with their half-lives and partitioning between fuel matrix, instant release fraction (IRF), Zircaloy and other metallic parts.

Radionuclide	Half-life [a]	Activity inventory [GBq/tU]	Partitioning [%]			
			Fuel matrix	IRF	Zircaloy	Other metal parts
Trace elements						
C-14	5.7×10^{3}	3.83×10^{1}	45	5	0	50
Cl-36	3.0×10^{5}	3.88×10^{-1}	72	8	20	0
Mo-93	4.0×10^{3}	1.80×10^{0}	0	0	0	100
Actinides and fission products						
Se-79	2.95×10^{5}	3.24×10^{1}	99.9	0.1	0	0
Sr-90	2.9×10^{1}	1.62×10^{6}	99	1	0	0
Zr-93*	1.5×10^{6}	7.93×10^{1}	100	0	0	0
Tc-99	2.1×10^{5}	5.96×10^{2}	99	1	0	0
Pd-107	6.5×10^{6}	4.92×10^{0}	99	1	0	0
Sn-126	1.0×10^{5}	2.32×10^{1}	99.99	0.01	0	0
I-129	1.6×10^{7}	1.19×10^{0}	95	5	0	0
Cs-135	2.3×10^{6}	2.06×10^{1}	95	5	0	0
Cs-137	3.0×10^{1}	2.37×10^{6}	95	5	0	0
Sm-151	9.0×10^{1}	1.53×10^{4}	100	0	0	0
Ra-226	1.6×10^{3}	–	–	–	–	–
Th-229	7.3×10^{3}	–	–	–	–	–
Th-230	7.7×10^{4}	–	–	–	–	–
Pa-231	3.2×10^{4}	–	–	–	–	–
U-233	1.6×10^{5}	2.88×10^{-3}	100	0	0	0
U-234	2.4×10^{5}	5.32×10^{1}	100	0	0	0
U-235	7.0×10^{8}	8.36×10^{-1}	100	0	0	0
U-236	2.3×10^{7}	1.21×10^{1}	100	0	0	0
U-238	4.5×10^{9}	1.16×10^{1}	100	0	0	0
Np-237	2.1×10^{6}	1.59×10^{1}	100	0	0	0
Pu-238	8.8×10^{1}	1.09×10^{5}	100	0	0	0
Pu-239	2.4×10^{4}	1.51×10^{4}	100	0	0	0
Pu-240	6.5×10^{3}	2.13×10^{4}	100	0	0	0
Pu-241	1.4×10^{1}	1.44×10^{6}	100	0	0	0
Pu-242	3.8×10^{5}	8.71×10^{1}	100	0	0	0
Am-241	4.3×10^{2}	1.57×10^{5}	100	0	0	0
Am-243	7.4×10^{3}	1.03×10^{3}	100	0	0	0
Cm-245	8.5×10^{3}	1.32×10^{1}	100	0	0	0
Cm-246	4.7×10^{3}	2.03×10^{0}	100	0	0	0
Zircaloy and other metal parts						
Ni-59	8.0×10^{4}	3.28×10^{2}	0	0	0	100
Ni-63	9.6×10^{1}	3.48×10^{4}	0	0	0	100
Zr-93	1.5×10^{6}	8.78×10^{0}	0	0	100	0
Nb-94	2.0×10^{4}	5.03×10^{2}	0	0	100	0

* Originating from fuel; Zr-93 in Zircaloy listed separately under “Zircaloy and other metal parts”.

Table 5-13. Radionuclide inventories for a single canister for EPR fuel (case PD-EPR), together with their half-lives and partitioning between fuel matrix, instant release fraction (IRF), Zircaloy and other metallic parts.

Radionuclide	Half-life [a]	Activity inventory [GBq/tU]	Partitioning [%]			
			Fuel matrix	IRF	Zircaloy	Other metal parts
Trace elements						
C-14	5.7×10^{3}	1.90×10^{1}	45	5	0	50
Cl-36	3.0×10^{5}	7.49×10^{-1}	72	8	20	0
Mo-93	4.0×10^{3}	1.34×10^{1}	0	0	0	100
Actinides and fission products						
Se-79	2.95×10^{5}	3.25×10^{0}	99.9	0.1	0	0
Sr-90	2.9×10^{1}	1.62×10^{6}	99	1	0	0
Zr-93*	1.5×10^{6}	7.98×10^{1}	100	0	0	0
Tc-99	2.1×10^{5}	5.98×10^{2}	99	1	0	0
Pd-107	6.5×10^{6}	4.89×10^{0}	99	1	0	0
Sn-126	1.0×10^{5}	2.31×10^{1}	99.99	0.01	0	0
I-129	1.6×10^{7}	1.19×10^{0}	95	5	0	0
Cs-135	2.3×10^{6}	2.22×10^{1}	95	5	0	0
Cs-137	3.0×10^{1}	2.37×10^{6}	95	5	0	0
Sm-151	9.0×10^{1}	1.50×10^{4}	100	0	0	0
Ra-226	1.6×10^{3}	–	–	–	–	–
Th-229	7.3×10^{3}	–	–	–	–	–
Th-230	7.7×10^{4}	–	–	–	–	–
Pa-231	3.2×10^{4}	–	–	–	–	–
U-233	1.6×10^{5}	2.90×10^{-3}	100	0	0	0
U-234	2.4×10^{5}	5.36×10^{1}	100	0	0	0
U-235	7.0×10^{8}	8.15×10^{-1}	100	0	0	0
U-236	2.3×10^{7}	1.22×10^{1}	100	0	0	0
U-238	4.5×10^{9}	1.16×10^{1}	100	0	0	0
Np-237	2.1×10^{6}	1.58×10^{1}	100	0	0	0
Pu-238	8.8×10^{1}	1.13×10^{5}	100	0	0	0
Pu-239	2.4×10^{4}	1.41×10^{4}	100	0	0	0
Pu-240	6.5×10^{3}	2.13×10^{4}	100	0	0	0
Pu-241	1.4×10^{1}	1.38×10^{6}	100	0	0	0
Pu-242	3.8×10^{5}	8.78×10^{1}	100	0	0	0
Am-241	4.3×10^{2}	1.51×10^{5}	100	0	0	0
Am-243	7.4×10^{3}	1.03×10^{3}	100	0	0	0
Cm-245	8.5×10^{3}	1.30×10^{1}	100	0	0	0
Cm-246	4.7×10^{3}	2.08×10^{0}	100	0	0	0
Zircaloy and other metal parts						
Ni-59	8.0×10^{4}	1.27×10^{2}	0	0	0	100
Ni-63	9.6×10^{1}	1.36×10^{4}	0	0	0	100
Zr-93	1.5×10^{6}	5.45×10^{0}	0	0	100	0
Nb-94	2.0×10^{4}	2.64×10^{2}	0	0	0	100

* Originating from fuel; Zr-93 in Zircaloy listed separately under “Zircaloy and other metal parts”.

The inventories of stable nuclides, which are required in order to evaluate whether solubility limits are exceeded, are given in Table 5-14.

5.3.3 Near-field model

The geometry of near-field model domain is as in the Base Case (as defined in Figure 5-1 and Table 5-4), except for modifications to the values for canister pitch, and different water volumes for fuel dissolution inside the canister, as shown in Table 5-15.

Parameter values related to:

- water ingress;
- radionuclide release;
- solubility limitation and radionuclide transport inside the canister;
- radionuclide transfer to the buffer/evolution of the defect;
- radionuclide transport in the buffer; and
- radionuclide transfer to the geosphere;

are as in the Base Case, and are given in Tables 5-5 to 5-7. Near-field model boundary conditions and transfer coefficients are also unchanged with respect to the Base Case.

Table 5-14. Stable nuclides taken into account in estimating whether solubility limits are exceeded.

Element	Amount [mol/tU]	
	VVER-440	EPR
Ni	3.45×10^{2}	1.31×10^{2}
Se	7.50×10^{-1}	7.56×10^{-1}
Zr (cladding)	5.37×10^{3}	3.11×10^{3}
Zr (fuel matrix)	5.00×10^{1}	5.10×10^{1}
Nb	6.80×10^{1}	3.50×10^{1}
Pd	1.50×10^{1}	1.50×10^{1}
Sn	3.08×10^{-1}	3.08×10^{-1}
Mo	3.60	1.70×10^{1}

Table 5-15. Near field model parameters that differ from the Base Case (PD-BC) in cases PD-VVER and PD-EPR.

Parameter	Unit	Case	Value	Source/comments
Canister pitch	m	PD-VVER	9.1	/Autio et al. 2007/
		PD-EPR	10.6	
Water volume for dissolution	m^3	PD-VVER	0.45	Scaled from /Raiko 2005/*
		PD-EPR	0.50	

* /Raiko 2005/ gives void volumes of 0.61 m^3 for VVER and 0.68 m^3 for EPR. These volumes are slightly higher than the volumes for dissolution used in the present safety assessment, because available space for dissolution is assumed to be reduced by the presence of corrosion products. The fractional reduction in volume is as in the Base Case (Section 5.2.2, part *c*).

5.3.4 Geosphere model

The geosphere model is as in the Base Case. Parameter values that apply to all migrating species are given in Table 5-8. Element-dependent parameters are given in Table 5-9 and 5-10.

5.3.5 Results

Table 5-16 gives calculated maximum near-field release rates in Bq per year for each radionuclide in the Base Case for an initial penetrating defect (case PD-BC) and in cases PD-VVER and PD-EPR. It also gives the times at which these maxima occur (t_{max}).

Table 5-16. Calculated maximum near-field release rates for each radionuclide in the Base Case for an initial penetrating defect (case PD-BC) and in cases PD-VVER and PD-EPR, and the times at which these maxima occur. Full results are presented in Appendix G.

Radionuclide			Base Case (PD-BC)		PD-VVER		PD-EPR	
			t_{max} [a]	Bq/a	t_{max} [a]	Bq/a	t_{max} [a]	Bq/a
Activation/fission products		C-14	1.01E+04	6.77E+05	1.01E+04	5.41E+05	1.01E+04	3.93E+05
		Cl-36	1.03E+04	1.10E+05	1.02E+04	1.88E+04	1.02E+04	5.13E+04
		Ni-59	1.23E+04	3.44E+05	1.62E+04	4.33E+05	1.26E+04	3.22E+05
		Se-79	2.15E+04	2.08E–01	2.15E+04	2.09E–01	2.15E+04	2.08E–01
		Mo-93	1.08E+04	3.67E–01	1.08E+04	2.89E–01	1.08E+04	6.12E–02
		Zr-93	2.20E+05	5.03E–02	2.10E+05	4.48E–02	2.15E+05	7.48E–02
		Zr-93p*	2.35E+05	3.68E+00	2.40E+05	3.73E+00	2.40E+05	3.69E+00
		Nb-94	1.99E+04	7.70E+03	2.35E+04	9.59E+03	2.35E+04	9.78E+03
		Tc-99	8.85E+05	2.25E+01	8.85E+05	2.25E+01	8.85E+05	2.25E+01
		Pd-107	8.90E+05	3.02E+01	8.90E+05	2.33E+01	8.90E+05	3.42E+01
		Sn-126	1.15E+05	4.84E+00	1.15E+05	3.46E+00	1.15E+05	5.12E+00
		I-129	1.03E+04	1.27E+04	1.02E+04	1.15E+04	1.02E+04	1.61E+04
		Cs-135	1.01E+04	7.78E+03	1.01E+04	5.09E+03	1.01E+04	8.09E+03
Actinide chains	4N	Pu-240	3.44E+04	1.65E+01	3.44E+04	1.19E+01	3.44E+04	1.76E+01
		U-236	1.00E+06	5.79E–04	1.00E+06	5.79E–04	1.00E+06	5.50E–04
	4N + 1	Cm-245	5.38E+04	6.05E–04	5.38E+04	8.74E–04	5.38E+04	1.29E–03
		Am-241	5.38E+04	6.38E–04	5.38E+04	9.20E–04	5.38E+04	1.36E–03
		Np-237	1.00E+06	8.21E–01	1.00E+06	8.21E–01	1.00E+06	8.21E–01
		U-233	1.00E+06	1.30E+00	1.00E+06	1.30E+00	1.00E+06	1.30E+00
		Th-229	1.00E+06	7.65E–01	1.00E+06	7.65E–01	1.00E+06	7.65E–01
	4N + 2	Cm-246	3.88E+04	6.19E–06	3.88E+04	7.10E–06	3.88E+04	1.07E–05
		Pu-242	3.94E+05	3.01E+01	3.94E+05	2.32E+01	3.94E+05	3.46E+01
		U-238	1.00E+06	4.95E–04	1.00E+06	4.95E–04	1.00E+06	4.95E–04
		U-234	1.29E+05	2.02E–03	1.29E+05	2.09E–03	1.29E+05	2.12E–03
		Th-230	5.64E+05	2.77E+01	5.59E+05	1.91E+01	5.69E+05	2.86E+01
		Ra-226	5.64E+05	3.59E+04	5.59E+05	2.64E+04	5.74E+05	3.62E+04
	4N + 3	Am-243	4.88E+04	4.05E–02	4.88E+04	3.72E–02	4.88E+04	5.52E–02
		Pu-239	5.88E+04	2.21E+02	5.88E+04	2.20E+02	5.88E+04	3.04E+02
		U-235	1.00E+06	3.60E–05	9.99E+05	4.27E–05	1.00E+06	4.11E–05
		Pa-231	1.00E+06	3.27E+01	1.00E+06	2.63E+01	1.00E+06	3.74E+01

* Zirconium originating from the fuel matrix only.

Figures 5-10 and 5-11 show the near-field and geosphere release rates as functions of time in cases PD-VVER and PD-EPR for all radionuclides for which calculations were made. Differences in the near-field and geosphere release rates between the various cases are only minor. In particular, in the case of the near field, the results show:

- somewhat lower peak releases of C-14 in cases PD-VVER and PD-EPR compared with the Base Case;
- fairly minor differences in peak release of other key radionuclides, including Ni-59 and I-129, at 10,000 years;
- a similar long-term release rate of Ra-226 after several hundred thousand years.

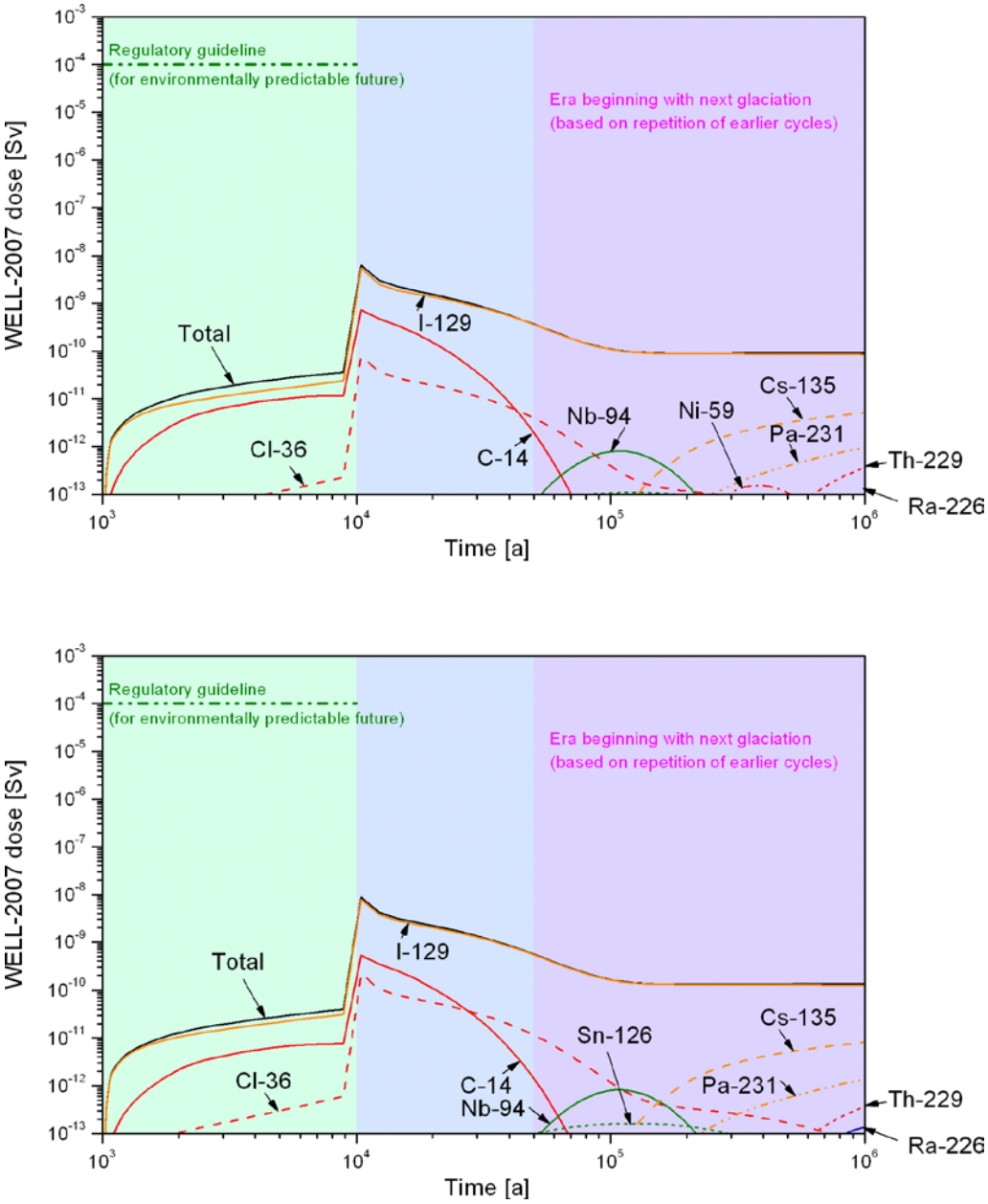

Figure 5-10. *WELL-2007 dose as a function of time in case PD-VVER (upper figure) and case PD-EPR (lower figure).*

Regarding C-14, Tables 5-12 and 5-13 show that the fraction of this radionuclide not embedded in the fuel matrix is assumed to be 55% (inventory in IRF, Zircaloy and other metal parts), compared with 70% in the Base Case. The inventories in the Zircaloy and other metal parts, as well as the IRF, are completely released to solution by 10,000 years (see the fractional dissolution rates in Table 5-5). The resulting higher concentrations of C-14 in solution in the canister interior at 10,000 years explains the higher peak releases in cases PD-VVER and PD-EPR compared with the Base Case.

Figure 5-10 shows the releases from the geosphere to the biosphere as a function of time in cases PD-VVER and PD-EPR expressed as WELL-2007 dose based on the dose conversion factors given in Table 3-1. Figure 5-11 shows time-dependent releases from the geosphere to the biosphere divided by the geo-bio flux constraints specified by the Finnish regulator and given in Table 1-1, and the sum of these releases over all calculated radionuclides.

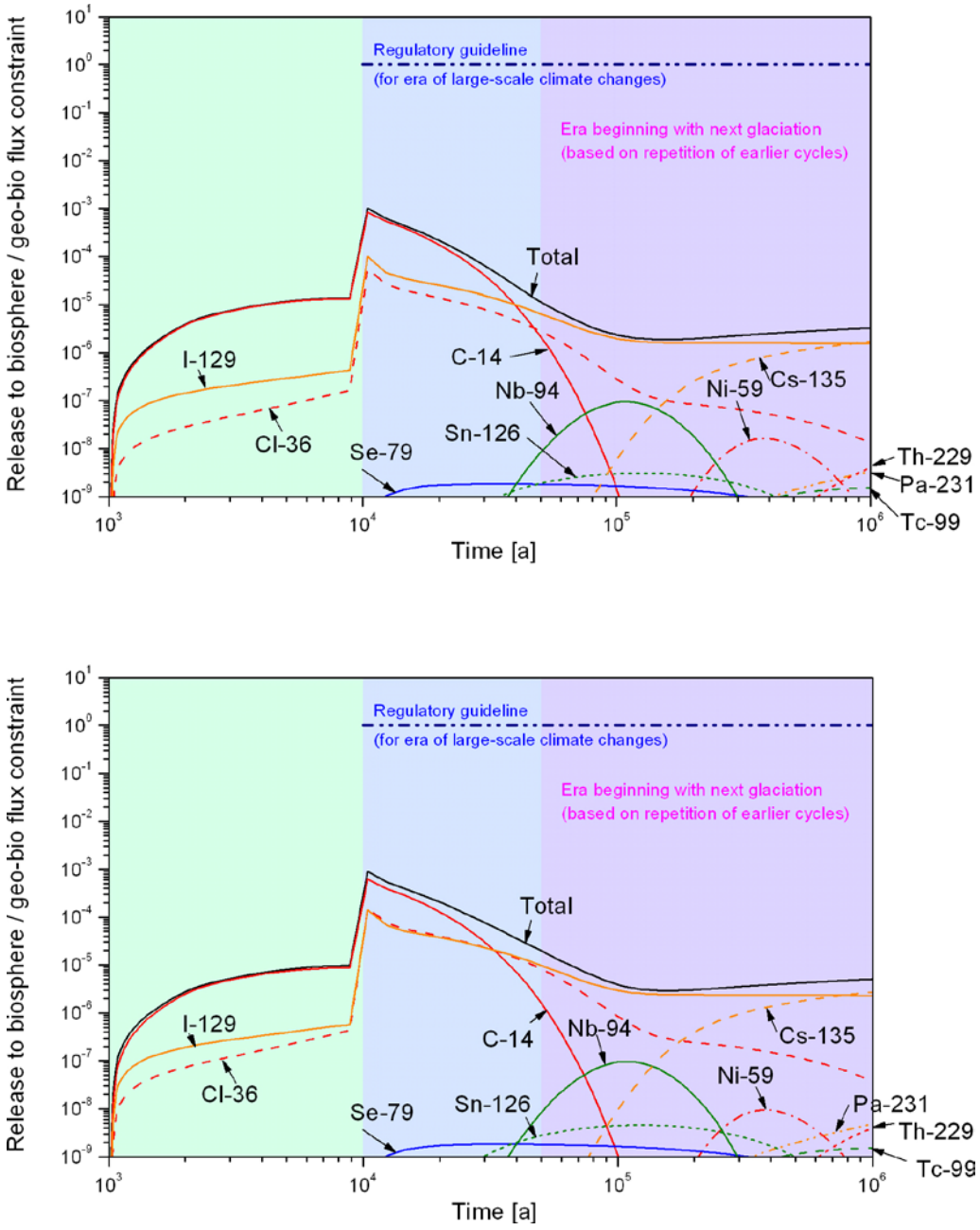

Figure 5-11. *Ratios of nuclide-specific activity releases to their respective geo-bio flux constraints in case PD-VVER (upper figure) and case PD-EPR (lower figure).*

In both PD-VVER and PD-EPR, as in the Base Case, the dose maximum occurs shortly after loss of transport resistance of the defect at 10,000 years, is about four orders of magnitude below the regulatory dose guideline of 10^{-4} Sv per year, and is dominated by I-129. The sum of time-dependent releases from the geosphere to the biosphere divided by their respective geo-bio flux constraints also has its maximum shortly after 10,000 years, is about three orders of magnitude below the regulatory guideline of one, and is dominated by C-14.

5.4 Cases addressing uncertainties in the evolution of the fuel and the release of radionuclides from the fuel and metallic components

5.4.1 Differences compared with the Base Case

In the Base Case, fuel dissolution subsequent to contact of the fuel with water is assumed to take place at a constant fuel matrix fractional dissolution rate of 10^{-7} per year (Table 5-5). In order to assess the impact of uncertainties in the mechanism of the dissolution process, alternative increased and decreased rates are considered in cases **PD-HIFDR** and **PD-LOFDR**, respectively.

Another significant source of uncertainty is the size and, for some radionuclides, the very existence of a segregated and rapidly released fraction – the instant release fraction (IRF). In order to elucidate the relative importance of the IRF and other radionuclide inventory components, a case **PD-IRF** considered in which only the Base Case IRF is included in the calculation.

5.4.2 Radionuclide inventories, half-lives and partitioning

In cases PD-HIFDR and PD-LOFDR, radionuclide inventories and half-lives are as in the Base Case, and are given in Table 5-2. As noted above, in case PD-IRF, only the Base Case IRF is included in the calculation. The inventory fractions in the spent fuel matrix, in Zircaloy and in other metal parts are disregarded in order to elucidate the IRF contribution to the Base Case results.

5.4.3 Near-field model

The geometry of near-field model domain is as in the Base Case, and is defined in Figure 5-1 and Table 5-4.

Fuel matrix fractional dissolution rates for cases addressing uncertainties in the evolution of the fuel are given in Table 5-17. The increased and decreased rates assumed (10^{-6} and 10^{-8} per year) correspond to the upper and lower limits of the triangular distribution recommended for use in SR-Can by /Werme et al. 2004/.

Table 5-17. Fuel matrix fractional dissolution rates for cases addressing uncertainties in the evolution of the fuel.

Case	Fuel matrix fractional dissolution rate [a^{-1}]
PD-HIFDR	10^{-6}
PD-LOFDR	10^{-8}
PD-IRF	Not relevant (IRF only)

Other parameter values related to radionuclide release, as well as parameter values related to the processes of:

- water ingress;
- solubility limitation and radionuclide transport inside the canister;
- radionuclide transfer to the buffer/evolution of the defect;
- radionuclide transport in the buffer; and
- radionuclide transfer to the geosphere;

are as in the Base Case, and are given in Tables 5-5 to 5-7. Near-field model boundary conditions and transfer coefficients are also unchanged with respect to the Base Case.

5.4.4 Geosphere model

The geosphere model is as in the Base Case. Parameter values that apply to all migrating species are given in Table 5-8. Element-dependent parameters are given in Tables 5-9 and 5-10.

5.4.5 Results

Table 5-18 gives calculated maximum near-field release rates in Bq per year for each radionuclide in the Base Case for an initial penetrating defect (case PD-BC) and in cases PD-HIFDR and PD-LOFDR. It also gives the times at which these maxima occur (t_{max}).

Some similarities and differences between the results apparent from Table 5-18 include:

- the similar peak release of several radionuclides, including C-14, Ni-59 and I-129, at 10,000 years; and
- the sensitivity of peak release rates to fuel dissolution rate, e.g. in the case of certain actinide chain members, such as Pu-239.

Figure 5-12 shows the releases from the geosphere to the biosphere as a function of time in cases PD-HIFDR and PD-LOFDR expressed as WELL-2007 dose based on the dose conversion factors given in Table 3-1. Figure 5-13 shows time-dependent releases from the geosphere to the biosphere divided by the geo-bio flux constraints specified by the Finnish regulator and given in Table 1-1, and the sum of these releases over all calculated radionuclides. In both PD-HIFRD and PD-LOFDR, as in the Base Case, the dose maximum occurs shortly after loss of transport resistance of the defect at 10,000 years, and is about four orders of magnitude below the regulatory dose guideline of 10^{-4} Sv per year. The sum of time-dependent releases from the geosphere to the biosphere divided by their respective geo-bio flux constraints also has its maximum shortly after 10,000 years, and is about three orders of magnitude below the regulatory guideline of one.

The figures also show that, although the dose maximum and summed release maximum, which are dominated by I-129 and C-14, respectively, are insensitive to fuel dissolution rates, long-term releases to the biosphere are significantly higher in case PD-HIFDR compared with PD-LOFDR.

Table 5-18. Calculated maximum near-field release rates for each radionuclide in the Base Case for an initial penetrating defect (case PD-BC) and in cases PD-HIFDR and PD-LOFDR, and the times at which these maxima occur. Full results are presented in Appendix G.

Radionuclide			Base Case (PD-BC)		PD-HIFDR		PD-LOFDR	
			t_{max} [a]	Bq/a	t_{max} [a]	Bq/a	t_{max} [a]	Bq/a
Activation/fission products		C-14	1.01E+04	6.77E+05	1.01E+04	6.79E+05	1.01E+04	6.76E+05
		Cl-36	1.03E+04	1.10E+05	1.03E+04	1.11E+05	1.03E+04	1.10E+05
		Ni-59	1.23E+04	3.44E+05	1.23E+04	3.44E+05	1.23E+04	3.44E+05
		Se-79	2.15E+04	2.08E–01	2.15E+04	2.08E–01	2.15E+04	2.08E–01
		Mo-93	1.08E+04	3.67E–01	1.08E+04	3.67E–01	1.08E+04	3.67E–01
		Zr-93	2.20E+05	5.03E–02	2.20E+05	5.03E–02	2.20E+05	5.03E–02
		Zr-93p*	2.35E+05	3.68E+00	2.35E+05	3.68E+00	2.35E+05	3.68E+00
		Nb-94	1.99E+04	7.70E+03	1.99E+04	7.70E+03	1.99E+04	7.70E+03
		Tc-99	8.85E+05	2.25E+01	8.85E+05	2.25E+01	8.15E+05	2.24E+01
		Pd-107	8.90E+05	3.02E+01	8.60E+05	1.29E+02	1.54E+04	1.99E+01
		Sn-126	1.15E+05	4.84E+00	1.15E+05	4.80E+01	1.05E+05	5.17E–01
		I-129	1.03E+04	1.27E+04	1.03E+04	1.46E+04	1.03E+04	1.25E+04
		Cs-135	1.01E+04	7.78E+03	8.90E+05	1.10E+04	1.01E+04	7.66E+03
Actinide chains	4N	Pu-240	3.44E+04	1.65E+01	3.44E+04	1.53E+02	3.44E+04	1.64E+00
		U-236	1.00E+06	5.79E–04	1.00E+06	5.79E–04	1.00E+06	5.79E–04
	4N + 1	Cm-245	5.38E+04	6.05E–04	5.38E+04	6.05E–03	5.38E+04	6.05E–05
		Am-241	5.38E+04	6.38E–04	5.38E+04	6.37E–03	5.38E+04	6.37E–05
		Np-237	1.00E+06	8.21E–01	1.00E+06	8.21E–01	1.00E+06	8.21E–01
		U-233	1.00E+06	1.30E+00	1.00E+06	1.30E+00	1.00E+06	1.30E+00
		Th-229	1.00E+06	7.65E–01	1.00E+06	7.65E–01	1.00E+06	5.57E–01
	4N + 2	Cm-246	3.88E+04	6.19E–06	3.88E+04	6.19E–05	3.88E+04	6.19E–07
		Pu-242	3.94E+05	3.01E+01	3.94E+05	3.01E+02	3.94E+05	3.01E+00
		U-238	1.00E+06	4.95E–04	1.00E+06	4.95E–04	1.00E+06	4.95E–04
		U-234	1.29E+05	2.02E–03	1.29E+05	2.02E–03	1.29E+05	2.02E–03
		Th-230	5.64E+05	2.77E+01	7.44E+05	2.88E+01	5.64E+05	2.77E+00
		Ra-226	5.64E+05	3.59E+04	7.44E+05	3.63E+04	5.74E+05	3.78E+03
	4N + 3	Am-243	4.88E+04	4.05E–02	4.88E+04	4.12E–01	4.88E+04	4.07E–03
		Pu-239	5.88E+04	2.21E+02	5.88E+04	2.20E+03	5.88E+04	2.20E+01
		U-235	1.00E+06	3.60E–05	1.00E+06	3.60E–05	1.00E+06	3.60E–05
		Pa-231	1.00E+06	3.27E+01	1.00E+06	3.27E+02	1.00E+06	3.27E+00

* Zirconium originating from the fuel matrix only.

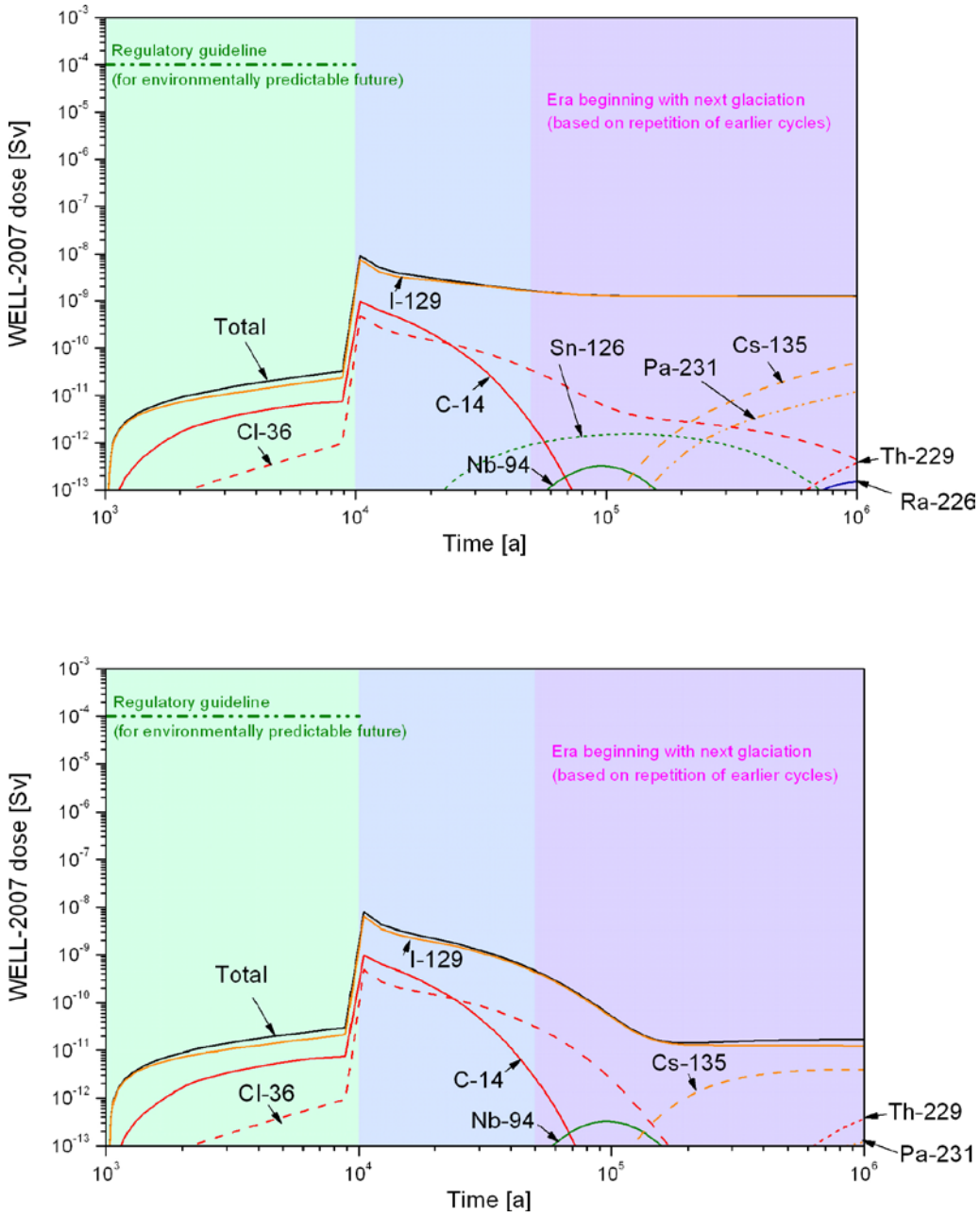

Figure 5-12. *WELL-2007 dose as a function of time in case PD-HIFDR (upper figure) and case PD-LOFDR (lower figure).*

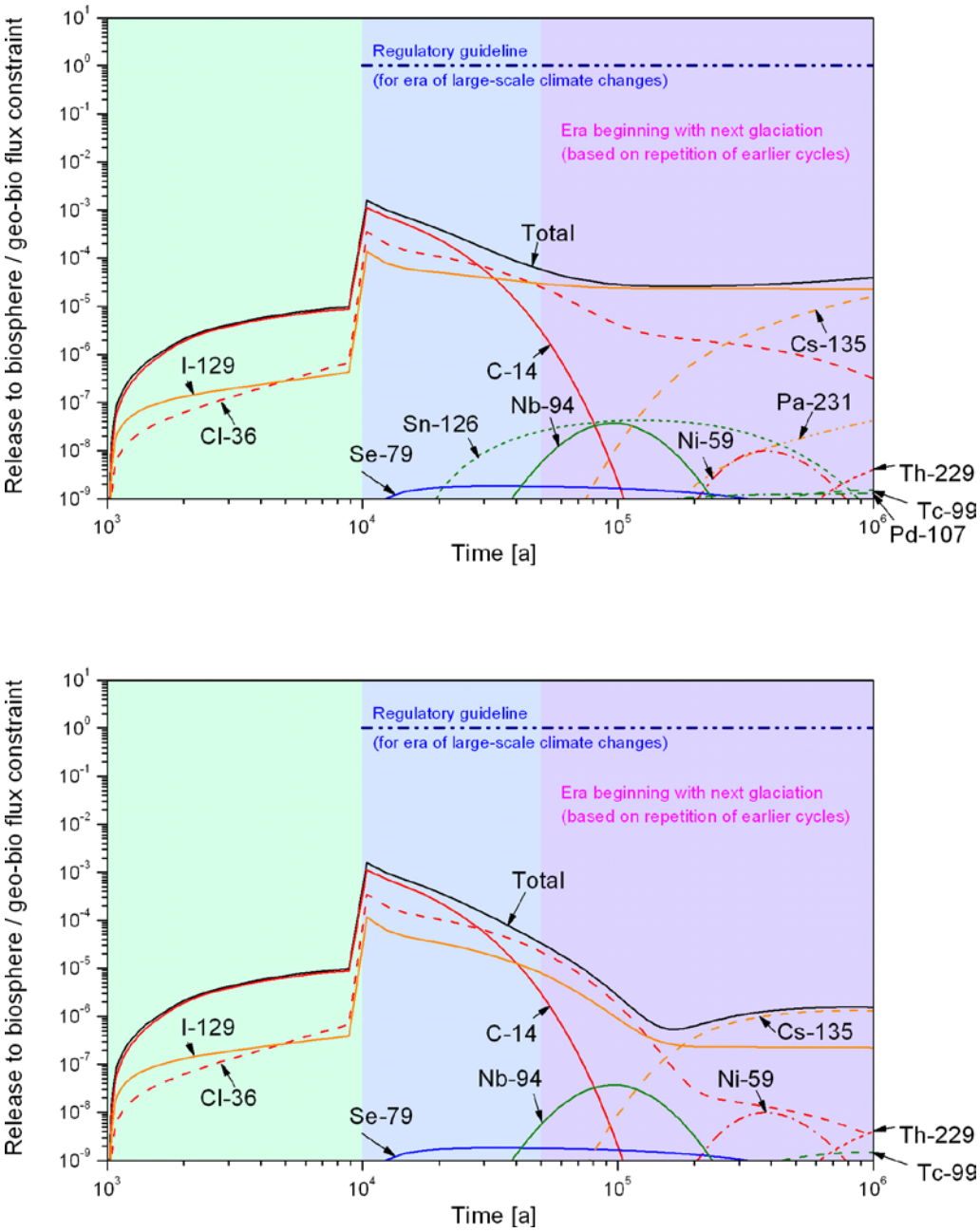

Figure 5-13. *Ratios of nuclide-specific activity releases to their respective geo-bio flux constraints in case PD-HIFDR (upper figure) and case PD-LOFDR (lower figure).*

Table 5-19 gives calculated maximum near-field release rates in Bq per year for each radionuclide in the Base Case for an initial penetrating defect (case PD-BC) and in case PD-IRF (in which only the Base Case IRF is calculated). It also gives the times at which these maxima occur (t_{max}). The table also shows the IRF as a fraction of total radionuclide inventory (from Table 5-2). Figure 5-14 shows the near-field release rates as functions of time for all radionuclides for which calculations were made.

Table 5-19 and Figure 5-14 show that, in the cases of I-129, Cs-135 and Se-79, there is little difference in the peak release at 10,000 years, when the transport resistance of the canister defect is assumed to be lost in the Base Case and in case PD-IRF, indicating that the IRF is the major contributor to this peak. Some other radionuclides, including Cl-36 and C-14, show a significantly higher peak release at 10,000 years in the Base Case compared with case PD-IRF. Significant fractions of these radionuclides are initially present in Zircaloy and other metal parts (not included in case PD-IRF) and accumulate in solution in the void space inside the canisters before the transport resistance of the defect is assumed to be lost.

Table 5-19. Calculated maximum near-field release rates for each radionuclide in the Base Case for an initial penetrating defect (case PD-BC) and in case PD-IRF, and the times at which these maxima occur.

Radionuclide	IRF [%]	Base Case (PD-BC)		PD-IRF	
		t_{max} [a]	Bq/a	t_{max} [a]	Bq/a
C-14	3	1.01E+04	6.77E+05	1.01E+04	3.36E+04
Cl-36	5	1.03E+04	1.10E+05	1.03E+04	1.07E+04
Ni-59	0	1.23E+04	3.44E+05	–	–
Se-79	0.1	2.15E+04	2.08E–01	2.26E+04	2.08E–01
Mo-93	0	1.08E+04	3.67E–01	–	–
Zr-93	0	2.20E+05	5.03E–02	–	–
Zr-93p*	0	2.35E+05	3.68E+00	–	–
Nb-94	0	1.99E+04	7.70E+03	–	–
Tc-99	1	8.85E+05	2.25E+01	6.49E+05	2.22E+01
Pd-107	1	8.90E+05	3.02E+01	1.53E+04	1.98E+01
Sn-126	0.01	1.15E+05	4.84E+00	3.88E+04	1.01E–01
I-129	5	1.03E+04	1.27E+04	1.03E+04	1.24E+04
Cs-135	5	1.01E+04	7.78E+03	1.01E+04	7.65E+03

* Zirconium originating from the fuel matrix only.

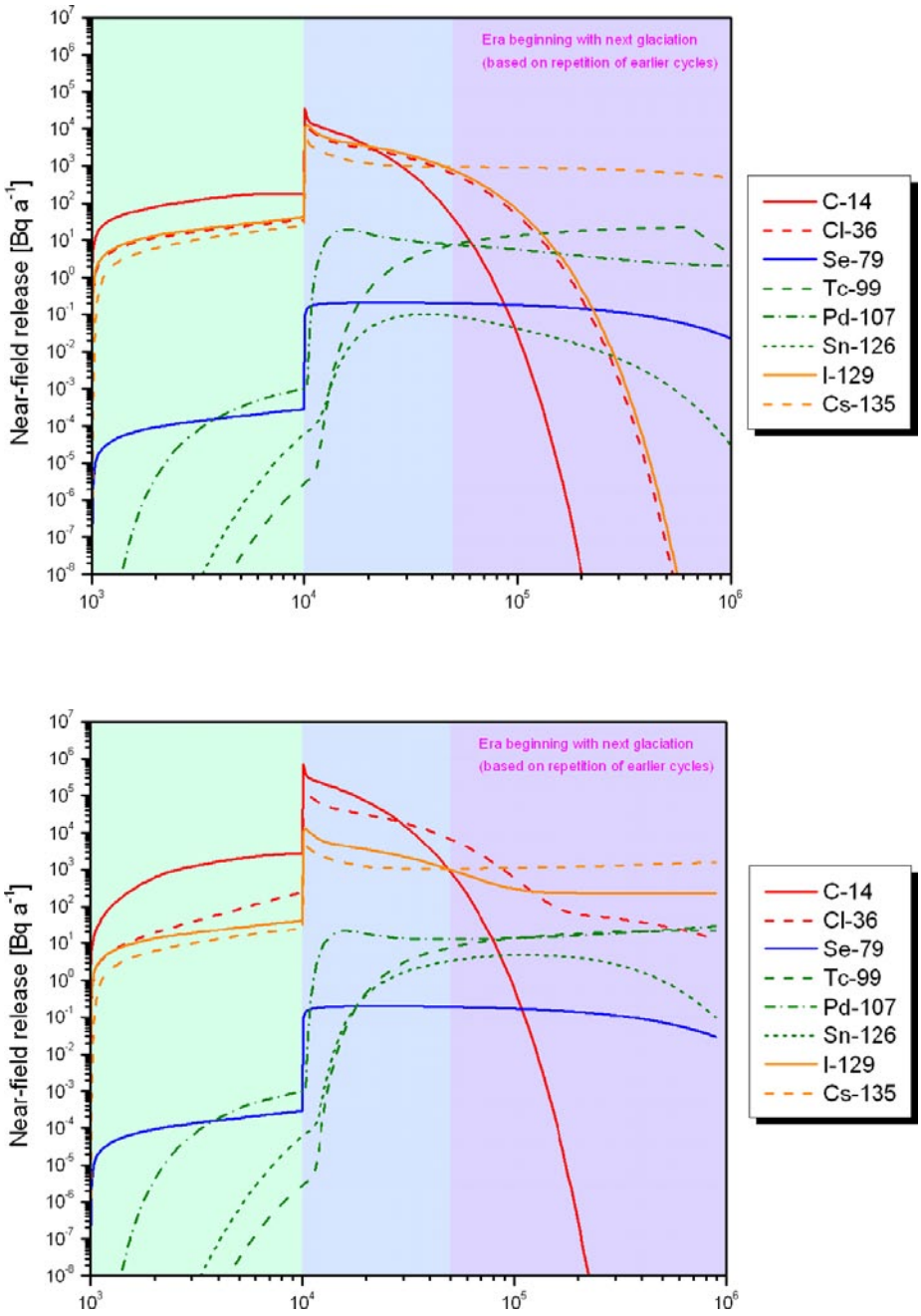

Figure 5-14. *Release rates of individual radionuclides from the near field in case PD-IRF (upper figure) and in the Base Case (lower figure).*

5.5 Cases addressing uncertainties in the characteristics and evolution of the defect

5.5.1 Differences compared with the Base Case

In the Base Case, the diameter of the initial penetrating defect is taken to be 1 mm, corresponding roughly to the maximum defect size that might not escape detection using current non-destructive testing (NDT) quality control techniques. The defect ceases to provide transport resistance at 10,000 years after canister emplacement.

In order to assess the impact of a possibly larger defect, an alternative higher defect diameter is considered in case **PD-BIGHOLE**. Cases **PD-HIDELAY** and **PD-LODELAY** are defined in order to illustrate the impact of uncertainties in the evolution of the hole, which affect the time at which the defect is modelled as ceasing to provide transport resistance. Cases PD-HIDELAY and PD-LODELAY consider, respectively, increased and decreased times at which the defect is modelled as ceasing to provide transport resistance, but assume that the initial size of the defect is as in the Base Case.

Finally in this section, Case **PD-BHLD** considers a decrease in the time at which the defect is modelled as ceasing to provide transport resistance, together with an increased initial defect size (motivated by the high likelihood that an increased initial defect size will result in more rapid corrosion and volume expansion of the insert).

5.5.2 Radionuclide inventories, half-lives and partitioning

Radionuclide inventories and half-lives and partitioning between fuel matrix, IRF, Zircaloy and other metal parts are as in the Base Case, and are given in Table 5-2.

5.5.3 Near-field model

In cases PD-BIGHOLE and PD-BHLD, a defect diameter of 4 mm is assumed (the Base Case diameter is 1 mm). Such defects are considered likely to be detected by quality control measures, and the canisters rejected for emplacement. The cases, nevertheless, allows the impact of transport resistances associated with the (smaller) hole to be better understood. A hypothetical 4 mm defect diameter was assumed in SR-Can, where it was considered to be large, given the observed distribution of pore sizes from friction stir welding, which is the current reference canister sealing technique in the Swedish programme.

Otherwise, the geometry of near-field model domain is as in the Base Case, and is defined in Figure 5-1 and Table 5-4.

According to SR-Can Data Report /SKB 2006b/, loss of transport resistance of the defect may occur at any time between 1,000 and 100,000 years after radionuclide transport pathways from the canister interior are established (which in turn is assumed to take 1,000 years). In order to explore the impact of this uncertainty, loss of transport resistance is defined as occurring at 100,000 years in case PD-HIDELAY, and at 2,000 years after emplacement (1,000 years after radionuclide transport pathways from the canister interior are established) in cases PD-LODELAY and PD-BHLD.

Parameter values related to:

- radionuclide release;
- solubility limitation and radionuclide transport inside the canister;
- radionuclide transfer to the buffer/evolution of the defect;
- radionuclide transport in the buffer; and
- radionuclide transfer to the geosphere;

are as in the Base Case, and are given in Tables 5-5 to 5-7. Near-field model boundary conditions are also unchanged with respect to the Base Case (with the exception of transfer coefficients related to transport through the defect, which are calculated internally by the code REPCOM).

5.5.4 Geosphere model

The geosphere model is as in the Base Case. Parameter values that apply to all migrating species are given in Table 5-8. Element-dependent parameters are given in Table 5-9 and 5-10.

5.5.5 Results

Table 5-20 gives calculated maximum near-field release rates in Bq per year for each radionuclide in the Base Case for an initial penetrating defect (case PD-BC), in case PD-BIGHOLE and in case PD-BHLD. It also gives the times at which these maxima occur (t_{max}). There is little difference in the magnitude of the peak release in cases PD-BC and PD-BIGHOLE for many radionuclides, including C-14, Ni-59, Cl-36, Nb-94 and I-129. In case PD-BHLD, on the other hand, some maxima are increased (e.g. C-14), some reduced (e.g. Cl-36) and some little changed (e.g. Ni-59 and I-129). The increase in the case of C-14 is explained by the fact that, because of its half-life of 5,730 years, there is less decay of this radionuclides by the time of loss of transport resistance by the defect in base PD-BHLD than in the Base Case, The decrease in the case of Cl-36 is explained by the fact that 50% of the inventory of this radionuclide is assumed to be present initially in the Zircaloy cladding, which has a fractional dissolution rate of 10^{-4} per year. There is, therefore, less Cl-36 released to solution at the time of loss of transport resistance by the defect in case PD-BHLD compared with the Base Case.

Figure 5-15 shows the releases from the geosphere to the biosphere as a function of time in case PD-BIGHOLE and in case PD-BHLD expressed as WELL-2007 dose based on the dose conversion factors given in Table 3-1. Figure 5-16 shows time-dependent releases from the geosphere to the biosphere divided by the geo-bio flux constraints specified by the Finnish regulator and given in Table 1-1, and the sum of these releases over all calculated radionuclides.

In both cases, as in the Base Case, the dose maximum occurs shortly after loss of transport resistance of the defect at 10,000 years, is about four orders of magnitude below the regulatory dose guideline of 10^{-4} Sv per year and is dominated by I-129. The sum of time-dependent releases from the geosphere to the biosphere divided by their respective geo-bio flux constraints also has its maximum shortly after 10,000 years, is about three orders of magnitude below the regulatory guideline of one in case PD-BIGHOLE and more than two orders of magnitude below the regulatory guideline in case PD-BHLD, and is dominated by C-14 in both cases. Comparing with Figures 5-5 and 5-6, there are, as expected, higher releases in case PD-BIGHOLE compared with the Base Case in the period prior to loss of transport resistance of the defect at 10,000 years. In case PD-BHLD, Figures 5-15 and 5-16 show how that release rate of Cl-36 to the biosphere continues to rise after loss of transport resistance of the defect at 2,000 years, due to the continuing dissolution of the Zircaloy cladding which, as noted above, initially contains 50% of the Cl-36 inventory.

Table 5-21 gives calculated maximum near-field release rates in Bq per year for each radionuclide in the Base Case for an initial penetrating defect (case PD-BC) and in cases PD-HIDELAY and PD-LODELAY. It also gives the times at which these maxima occur (t_{max}). The peak release of C-14 is increased with respect to the Base Case in case PD-LODELAY, and decreased in case PD-HIDELAY. In the latter case, much of the C-14 initially present has decayed by the time the defect is assumed to lose its transport resistance (as noted above, the half-life of C-14 is 5,730 years). The magnitudes of the peak releases of many other safety relevant radionuclides are less strongly affected, although the time of peak release, which in many cases coincides with the loss of transport resistance of the defect, is clearly reduced in case PD-LODELAY and increased in case PD-HIDELAY.

Table 5-20. Calculated maximum near-field release rates for each radionuclide in the Base Case for an initial penetrating defect (case PD-BC), in case PD-BIGHOLE and in case PD-BHLD, and the times at which these maxima occur. Full results are presented in Appendix G.

Radionuclide			Base Case (PD-BC)		PD- BIGHOLE		PD-BHLD	
			t_{max} [a]	Bq/a	t_{max} [a]	Bq/a	t_{max} [a]	Bq/a
Activation/fission products		C-14	1.01E+04	6.77E+05	1.01E+04	6.33E+05	2.02E+03	1.33E+06
		Cl-36	1.03E+04	1.10E+05	1.03E+04	1.09E+05	1.10E+04	4.92E+04
		Ni-59	1.23E+04	3.44E+05	1.23E+04	3.45E+05	4.53E+03	3.86E+05
		Se-79	2.15E+04	2.08E–01	2.15E+04	2.08E–01	1.30E+04	2.11E–01
		Mo-93	1.08E+04	3.67E–01	1.08E+04	3.67E–01	2.77E+03	1.47E+00
		Zr-93	2.20E+05	5.03E–02	2.20E+05	5.03E–02	2.05E+05	5.05E–02
		Zr-93p*	2.35E+05	3.68E+00	2.35E+05	3.68E+00	2.30E+05	3.69E+00
		Nb-94	1.99E+04	7.70E+03	1.99E+04	7.70E+03	1.18E+04	1.01E+04
		Tc-99	8.85E+05	2.25E+01	8.85E+05	2.25E+01	9.20E+05	2.25E+01
		Pd-107	8.90E+05	3.02E+01	8.90E+05	3.02E+01	9.25E+05	3.08E+01
		Sn-126	1.15E+05	4.84E+00	1.15E+05	4.84E+00	1.15E+05	4.83E+00
		I-129	1.03E+04	1.27E+04	1.03E+04	1.24E+04	2.25E+03	1.26E+04
		Cs-135	1.01E+04	7.78E+03	1.01E+04	6.89E+03	2.10E+03	7.86E+03
Actinide chains	4N	Pu-240	3.44E+04	1.65E+01	3.44E+04	1.65E+01	3.12E+04	1.97E+01
		U-236	1.00E+06	5.79E–04	1.00E+06	5.79E–04	1.00E+06	5.80E–04
	4N + 1	Cm-245	5.38E+04	6.05E–04	5.38E+04	6.08E–04	5.12E+04	6.92E–04
		Am-241	5.38E+04	6.38E–04	5.38E+04	6.41E–04	5.12E+04	7.29E–04
		Np-237	1.00E+06	8.21E–01	1.00E+06	8.21E–01	1.00E+06	8.23E–01
		U-233	1.00E+06	1.30E+00	1.00E+06	1.30E+00	1.00E+06	1.31E+00
		Th-229	1.00E+06	7.65E–01	1.00E+06	7.65E–01	1.00E+06	7.66E–01
	4N + 2	Cm-246	3.88E+04	6.19E–06	3.88E+04	6.31E–06	3.62E+04	9.29E–06
		Pu-242	3.94E+05	3.01E+01	3.94E+05	3.01E+01	3.86E+05	3.01E+01
		U-238	1.00E+06	4.95E–04	1.00E+06	4.95E–04	1.00E+06	4.96E–04
		U-234	1.29E+05	2.02E–03	1.29E+05	2.02E–03	1.21E+05	2.06E–03
		Th-230	5.64E+05	2.77E+01	5.64E+05	2.77E+01	5.61E+05	2.77E+01
		Ra-226	5.64E+05	3.59E+04	5.64E+05	3.59E+04	5.61E+05	3.59E+04
	4N + 3	Am-243	4.88E+04	4.05E–02	4.88E+04	4.07E–02	4.62E+04	4.87E–02
		Pu-239	5.88E+04	2.21E+02	5.88E+04	2.21E+02	6.12E+04	2.21E+02
		U-235	1.00E+06	3.60E–05	1.00E+06	3.60E–05	1.00E+06	3.60E–05
		Pa-231	1.00E+06	3.27E+01	1.00E+06	3.27E+01	1.00E+06	3.27E+01

* Zirconium originating from the fuel matrix only.

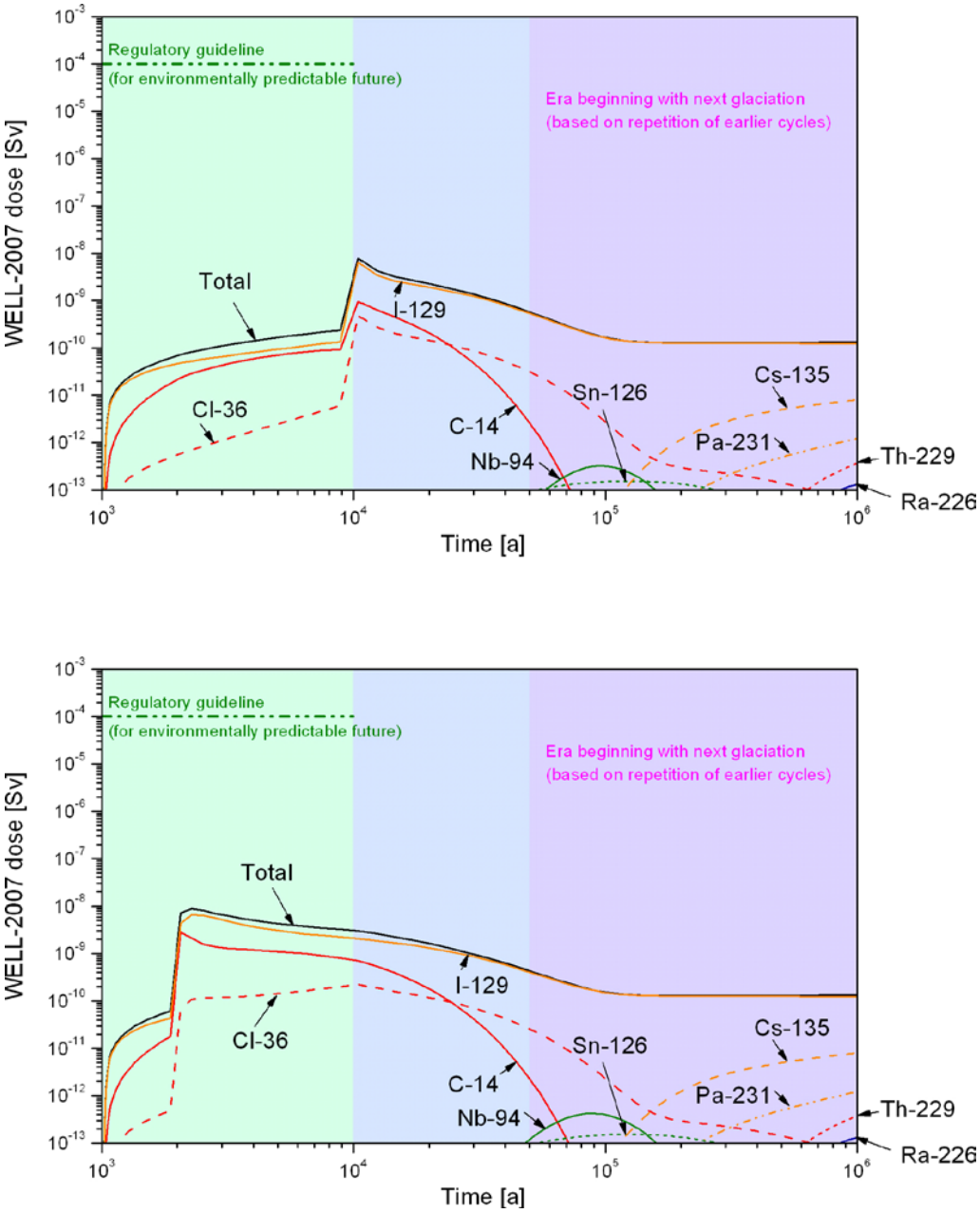

Figure 5-15. *WELL-2007 dose as a function of time in case PD-BIGHOLE (upper figure) and case PD-BHLD (lower figure).*

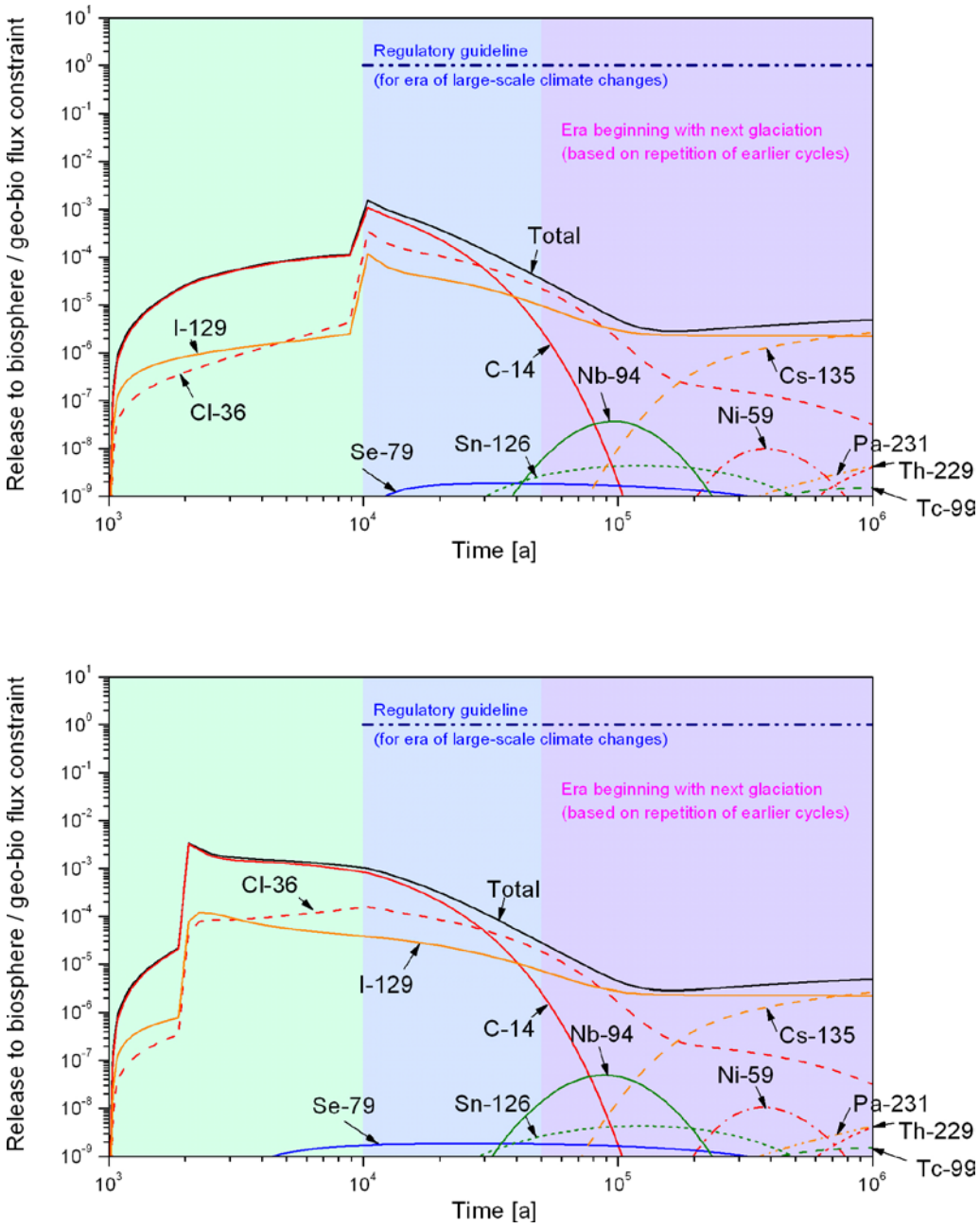

Figure 5-16. *Ratios of nuclide-specific activity releases to their respective geo-bio flux constraints in case PD-BIGHOLE (upper figure) and case PD-BHLD (lower figure).*

Table 5-21. Calculated maximum near-field release rates for each radionuclide in the Base Case for an initial penetrating defect (case PD-BC) and in cases PD-HIDELAY and PD-LODELAY, and the times at which these maxima occur. Full results are presented in Appendix G.

Radionuclide			Base Case (PD-BC)		PD-HIDELAY		PD-LODELAY	
			t_{max} [a]	Bq/a	t_{max} [a]	Bq/a	t_{max} [a]	Bq/a
Activation/fission products		C-14	1.01E+04	6.77E+05	1.10E+04	2.70E+03	2.02E+03	1.34E+06
		Cl-36	1.03E+04	1.10E+05	1.01E+05	6.65E+04	1.10E+04	4.92E+04
		Ni-59	1.23E+04	3.44E+05	1.02E+05	1.57E+05	4.53E+03	3.86E+05
		Se-79	2.15E+04	2.08E–01	1.12E+05	1.71E–01	1.30E+04	2.11E–01
		Mo-93	1.08E+04	3.67E–01	3.81E+03	1.11E–03	2.77E+03	1.47E+00
		Zr-93	2.20E+05	5.03E–02	3.04E+05	4.83E–02	2.05E+05	5.05E–02
		Zr-93p*	2.35E+05	3.68E+00	3.24E+05	3.55E+00	2.30E+05	3.69E+00
		Nb-94	1.99E+04	7.70E+03	1.10E+05	3.40E+02	1.18E+04	1.01E+04
		Tc-99	8.85E+05	2.25E+01	8.38E+05	2.24E+01	9.20E+05	2.25E+01
		Pd-107	8.90E+05	3.02E+01	1.10E+05	3.55E+01	9.25E+05	3.08E+01
		Sn-126	1.15E+05	4.84E+00	1.34E+05	6.36E+00	1.15E+05	4.83E+00
		I-129	1.03E+04	1.27E+04	1.01E+05	1.02E+04	2.25E+03	1.26E+04
		Cs-135	1.01E+04	7.78E+03	1.01E+05	3.38E+03	2.10E+03	7.93E+03
Actinide chains	4N	Pu-240	3.44E+04	1.65E+01	1.19E+05	8.84E–03	3.12E+04	1.97E+01
		U-236	1.00E+06	5.79E–04	1.00E+06	5.74E–04	1.00E+06	5.80E–04
	4N + 1	Cm-245	5.38E+04	6.05E–04	6.12E+04	9.44E–06	5.12E+04	6.92E–04
		Am-241	5.38E+04	6.38E–04	6.12E+04	9.95E–06	5.12E+04	7.29E–04
		Np-237	1.00E+06	8.21E–01	1.00E+06	8.03E–01	1.00E+06	8.23E–01
		U-233	1.00E+06	1.30E+00	1.00E+06	1.25E+00	1.00E+06	1.31E+00
		Th-229	1.00E+06	7.65E–01	1.00E+06	7.61E–01	1.00E+06	7.66E–01
	4N + 2	Cm-246	3.88E+04	6.19E–06	4.12E+04	7.34E–08	3.62E+04	9.29E–06
		Pu-242	3.94E+05	3.01E+01	3.68E+05	3.04E+01	3.86E+05	3.01E+01
		U-238	1.00E+06	4.95E–04	1.00E+06	4.91E–04	1.00E+06	4.96E–04
		U-234	1.29E+05	2.02E–03	2.24E+05	1.64E–03	1.21E+05	2.06E–03
		Th-230	5.64E+05	2.77E+01	5.58E+05	2.77E+01	5.61E+05	2.77E+01
		Ra-226	5.64E+05	3.59E+04	5.64E+05	3.59E+04	5.61E+05	3.59E+04
	4N + 3	Am-243	4.88E+04	4.05E–02	5.62E+04	5.77E–04	4.62E+04	4.87E–02
		Pu-239	5.88E+04	2.21E+02	1.34E+05	7.13E+01	6.12E+04	2.21E+02
		U-235	1.00E+06	3.60E–05	1.00E+06	3.56E–05	1.00E+06	3.60E–05
		Pa-231	1.00E+06	3.27E+01	1.00E+06	3.27E+01	1.00E+06	3.27E+01

* Zirconium originating from the fuel matrix only.

Figure 5-17 shows the releases from the geosphere to the biosphere as a function of time in cases PD-HIDELAY and PD-LODELAY expressed as WELL-2007 dose based on the dose conversion factors given in Table 3-1. Figure 5-18 shows time-dependent releases from the geosphere to the biosphere divided by the geo-bio flux constraints specified by the Finnish regulator and given in Table 1-1, and the sum of these releases over all calculated radionuclides.

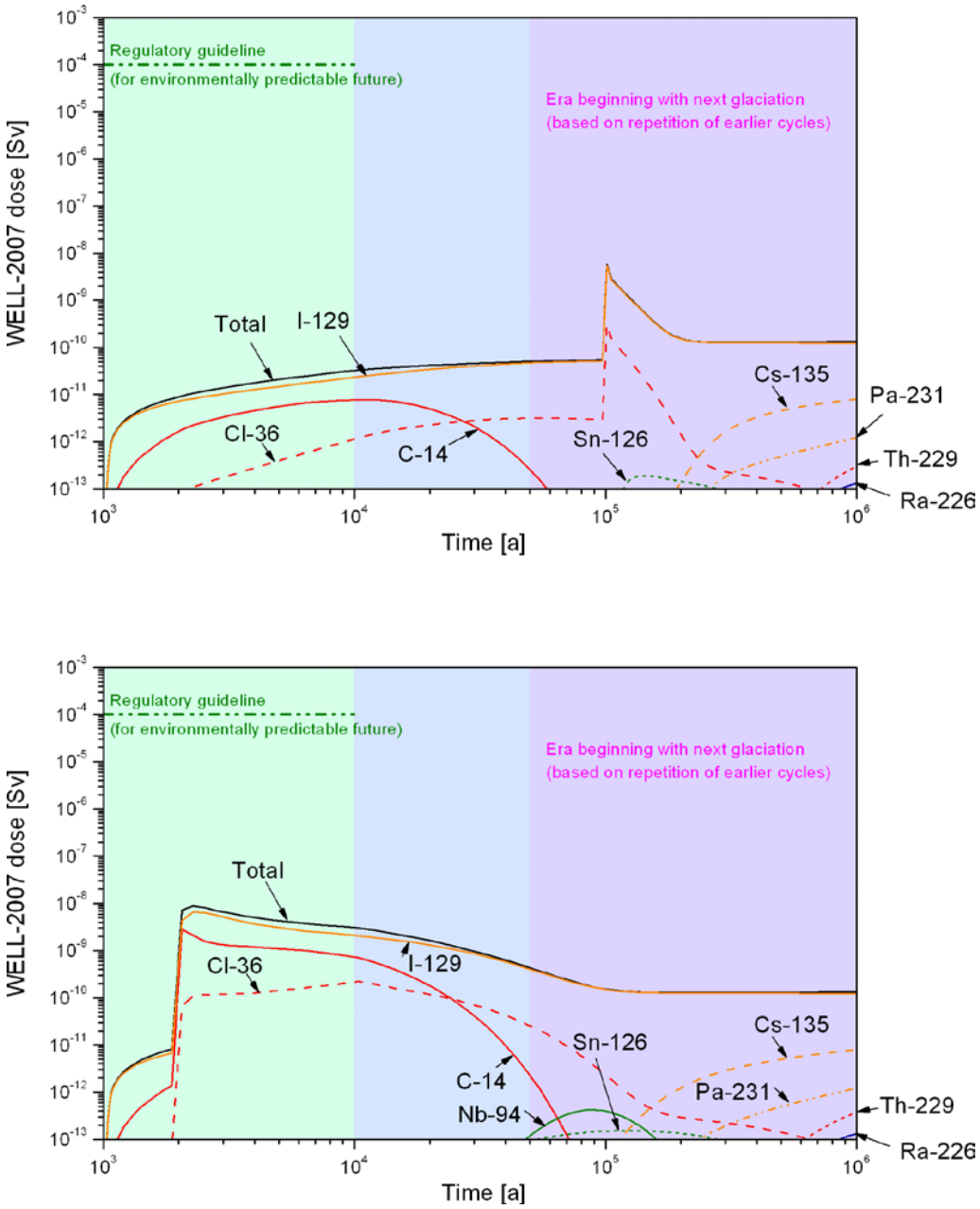

Figure 5-17. *WELL-2007 dose as a function of time in case PD-HIDELAY (upper figure) and case PD-LODELAY (lower figure).*

In both PD-HIDELAY and PD-LODELAY, as in the Base Case, the dose maximum occurs shortly after loss of transport resistance of the defect, and is about four orders of magnitude below the regulatory dose guideline of 10^{-4} Sv per year. The sum of time-dependent releases from the geosphere to the biosphere divided by their respective geo-bio flux constraints also has its maximum shortly after loss of transport resistance of the defect. The maximum is more than two orders of magnitude below the regulatory guideline of one in case PD-LODEAY (similar to case PD-BHLD), and more than three orders of magnitude below the regulatory guideline of one in case PD-HIDELAY. The difference is accounted for largely by the impact of delay on C-14 release, which is discussed above.

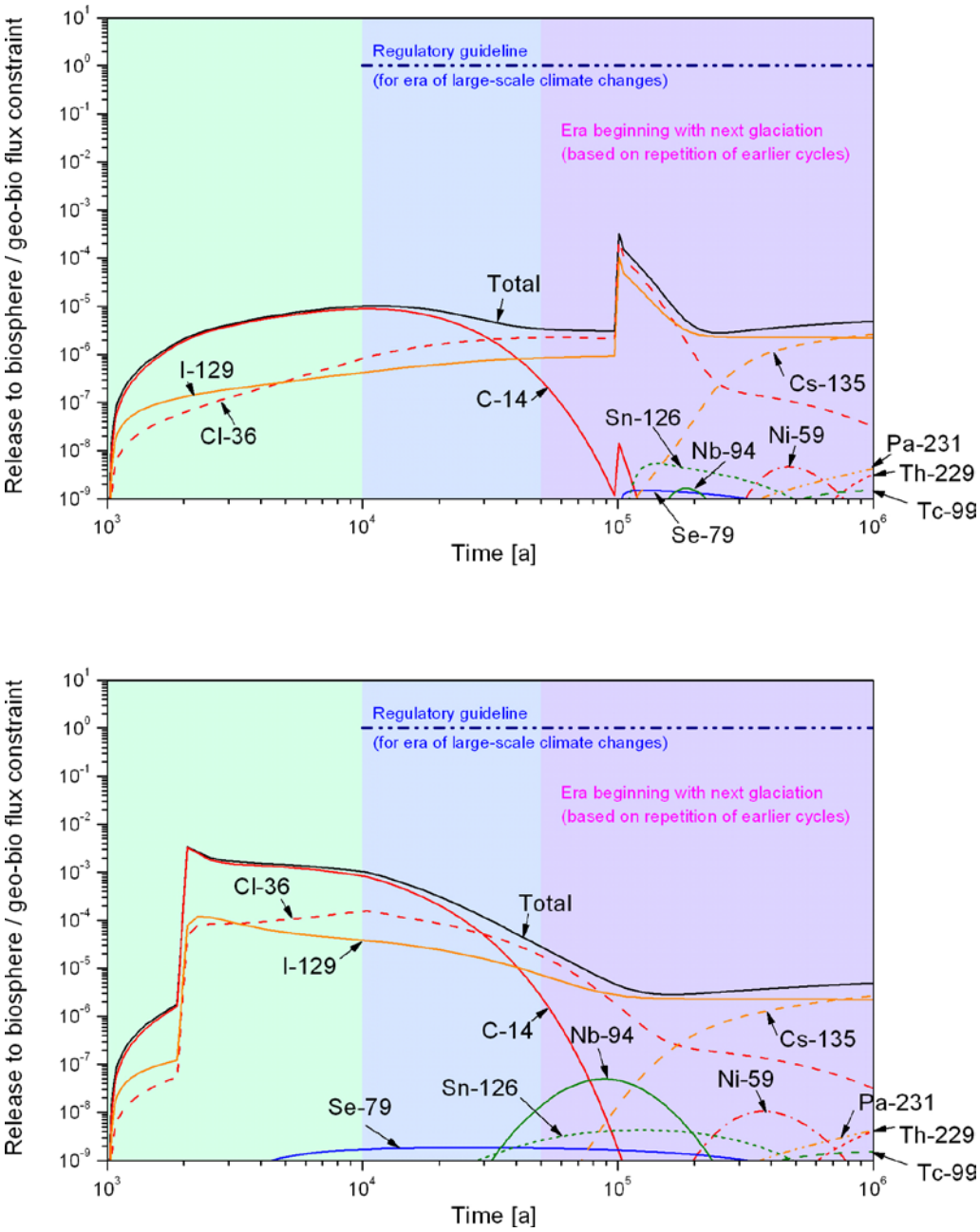

Figure 5-18. *Ratios of nuclide-specific activity releases to their respective geo-bio flux constraints in case PD-HIDELAY (upper figure) and case PD-LODELAY (lower figure).*

Finally, Figure 5-19 shows both the calculated annual landscape dose to the most exposed individual and the WELL-2007 dose in case PD-LODELAY. The highest annual landscape dose occurs at a similar time to the highest WELL-2007 dose, and, as in the Base Case, is less than 10^{-6} Sv, compared with about 10^{-8} Sv in the case of WELL-2007 dose.

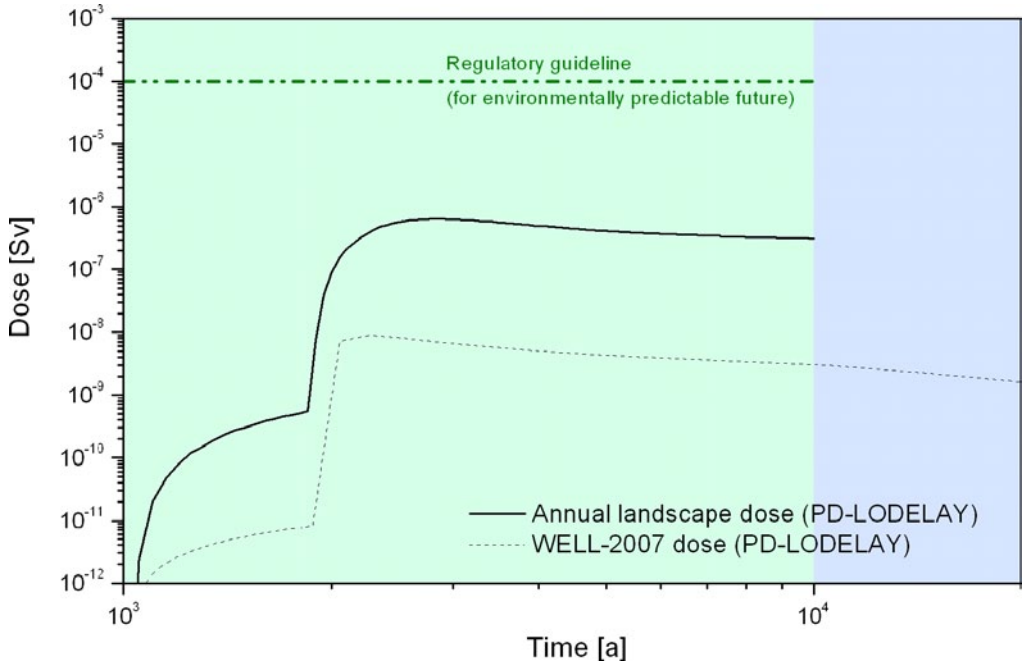

Figure 5-19. *Annual landscape dose and WELL-2007 dose as functions of time in case PD-LODELAY.*

5.6 Cases addressing potential loss or redistribution of buffer mass during the operational phase and in the course of buffer saturation

5.6.1 Differences compared with the Base Case

The Process Report /Gribi et al. 2007/ and the Evolution Report /Smith et al. 2007a/ identify a number of processes specific to KBS-3H that could lead to a loss of bentonite mass from, or redistribution of bentonite mass in, a drift compartment especially in the early phase of repository evolution including the operational phase. The processes addressed include:

- axial displacements of distance blocks and supercontainers caused by differential saturation and swelling along the deposition drift;
- water flows between wet and dry supercontainer due to piping along the bentonite/rock interface units and causing erosion and redistribution of bentonite;
- bentonite erosion into fractures, which may be of concern during the operational phase, namely if a sealed compartment is hydraulically connected to some nearby open rock excavation (in contrast, long-term erosion of bentonite into fractures has been investigated in previous studies and found to be of less concern); and
- bentonite compaction due to volume changes arising from the formation of iron corrosion products (mainly magnetite, but also some iron sulphide and siderite).

A loss of swelling pressure at the drift wall could also lead to enhanced thermal spalling due to reduction in confining pressure associated with time-dependent degradation of rock strength; this is treated in the PD-SPALL case (Section 5.7).

Scoping calculations have been performed to estimate the impact of these processes on buffer density (see Appendix B in the Evolution Report). In the Base Case, it is assumed that these processes have negligible impact on the transport properties of the buffer. The above-mentioned scoping calculations indicted that any density changes resulting from these processes will be less than those required for significant advective transport in the buffer or for the colloid filtration function of the buffer to be compromised. Furthermore, buffer sorption coefficients are expected to be unaffected by these processes. There is, however, more significant uncertainty in the impact of buffer mass loss or redistribution on the diffusion coefficients for transported radionuclides. Case **PD-HIDIFF** addresses the possibility of an increased diffusion coefficient as a result, for example, of transient water flow (including piping) and erosion.

5.6.2 Radionuclide inventories, half-lives and partitioning

Radionuclide inventories and half-lives and partitioning between fuel matrix, IRF, Zircaloy and other metal parts are as in the Base Case, and are given in Table 5-2.

5.6.3 Near-field model

The geometry of near-field model domain is as in the Base Case, and is defined in Figure 5-1 and Table 5-4.

For modelling radionuclide transport in the buffer, the effective diffusion coefficient for the various species in bentonite is increased from the Base Case values Section 5.2.3 to a species-independent, higher value of 8.6×10^{-10} m^2 s^{-1}, which is considered to be a bounding value at the high end of the range of possibilities. Major ions found in groundwater have diffusion coefficients in free water in the range 10^{-9} to 2×10^{-9} m^2 s^{-1} at 25 ºC, see, e.g. Section 3.4 in /Freeze and Cherry 1979/. The transport porosity for this case is taken to be 0.43 for all migrating species. The effective diffusion coefficient, D_e, is calculated from the diffusion coefficient in free water (2×10^{-9} m^2 s^{-1}) multiplied by the transport porosity, $D_e = 8.6 \times 10^{-10}$ m^2 s^{-1}.

Parameter values related to:

- water ingress;
- radionuclide release;
- solubility limitation and radionuclide transport inside the canister;
- radionuclide transfer to the buffer/evolution of the defect;
- radionuclide transport in the buffer; and
- radionuclide transfer to the geosphere;

are as in the Base Case and are given in Tables 5-5 to 5-7. Near-field model boundary conditions are also unchanged with respect to the Base Case (with the exception of transfer coefficients at the mouth of the defect, which are calculated internally by the code REPCOM and are functions of the diffusion coefficient in the buffer).

5.6.4 Geosphere model

Buffer erosion by transient water flows could give rise to a period of colloidal silica formation at the buffer/rock interface that could, in principle, affect geosphere transport if radionuclides were released during the period of erosion. It is, however, assumed that transient water flows giving rise to erosion have ceased before 1,000 years, when the first radionuclide releases to the geosphere take place. The geosphere model is, therefore, as in the Base Case.

Parameter values that apply to all migrating species are given in Table 5-8. Element-dependent parameters are given in Table 5-9 and 5-10.

5.6.5 Results

Table 5-22 gives calculated maximum near-field release rates in Bq per year for each radionuclide in the Base Case for an initial penetrating defect (case PD-BC) and in case PD-HIDIFF. It also gives the times at which these maxima occur (t_{max}).

Table 5-22. Calculated maximum near-field release rates for each radionuclide in the Base Case for an initial penetrating defect (case PD-BC) and in case PD-HIDIFF, and the times at which these maxima occur. Full results are presented in Appendix G.

Radionuclide			Base Case (PD-BC)		PD-HIDIFF	
			t_{max} [a]	Bq/a	t_{max} [a]	Bq/a
Activation/fission products		C-14	1.01E+04	6.77E+05	1.01E+04	3.19E+05
		Cl-36	1.03E+04	1.10E+05	1.01E+04	2.89E+04
		Ni-59	1.23E+04	3.44E+05	1.03E+04	3.52E+05
		Se-79	2.15E+04	2.08E–01	1.06E+04	2.38E–01
		Mo-93	1.08E+04	3.67E–01	1.03E+04	5.51E+00
		Zr-93	2.20E+05	5.03E–02	1.05E+05	5.86E–02
		Zr-93p*	2.35E+05	3.68E+00	1.10E+05	4.26E+00
		Nb-94	1.99E+04	7.70E+03	1.14E+04	1.03E+04
		Tc-99	8.85E+05	2.25E+01	8.90E+05	3.87E+01
		Pd-107	8.90E+05	3.02E+01	8.90E+05	2.21E+01
		Sn-126	1.15E+05	4.84E+00	9.47E+04	2.81E+00
		I-129	1.03E+04	1.27E+04	1.01E+04	3.36E+03
		Cs-135	1.01E+04	7.78E+03	1.01E+04	5.75E+03
Actinide chains	4N	Pu-240	3.44E+04	1.65E+01	1.63E+04	1.46E+02
		U-236	1.00E+06	5.79E–04	9.99E+05	7.11E–04
	4N + 1	Cm-245	5.38E+04	6.05E–04	2.48E+04	1.72E–02
		Am-241	5.38E+04	6.38E–04	2.48E+04	1.82E–02
		Np-237	1.00E+06	8.21E–01	1.00E+06	1.17E+00
		U-233	1.00E+06	1.30E+00	1.00E+06	8.06E–01
		Th-229	1.00E+06	7.65E–01	5.79E+05	2.23E+01
	4N + 2	Cm-246	3.88E+04	6.19E–06	2.06E+04	7.74E–04
		Pu-242	3.94E+05	3.01E+01	3.29E+05	1.62E+01
		U-238	1.00E+06	4.95E–04	9.84E+05	5.60E–04
		U-234	1.29E+05	2.02E–03	5.88E+04	2.98E–03
		Th-230	5.64E+05	2.77E+01	5.14E+05	2.14E+01
		Ra-226	5.64E+05	3.59E+04	5.69E+05	2.55E+04
	4N + 3	Am-243	4.88E+04	4.05E–02	1.63E+04	2.27E+00
		Pu-239	5.88E+04	2.21E+02	2.48E+04	3.19E+02
		U-235	1.00E+06	3.60E–05	9.89E+05	5.40E–05
		Pa-231	1.00E+06	3.27E+01	1.00E+06	1.65E+01

* Zirconium originating from the fuel matrix only.

There are two competing effects, such that releases of some radionuclides are decreased in case PD-HIDIFF compared with the Base Case, whereas releases of other radionuclides are increased. The increased diffusion coefficient in the buffer in case PD-HIDIFF means that radionuclides migrate further in the axial direction along the drift, as well as radially towards the drift wall. This provides more dilution of radionuclides in buffer pore water, which tends to decrease peak releases and extend the tailing parts of the release curves. The most pronounced effects occur with non-solubility-limited anions, such as C-14, Cl-36 and I-129, since anionic exclusion is not considered in case PD-HIDIFF, consistent with the assumption of a bounding value for the diffusion coefficient at the high end of the range of possibilities. On the other hand, the increased diffusion coefficient in the buffer in case PD-HIDIFF also reduces the minimum transport time across the buffer. This leads to less radionuclide decay during transport, and leads to increased near-field release rates. In most cases, increases or decreases in the near-field release rate are not large compared with other uncertainties (a factor of about 3 or less). There are a few shorter-lived actinides, such as Am-241, Am-243, Cm-245 and Cm-246 for which the release rate from the near field is more than an order of magnitude higher than in the Base Case, but these radionuclides in any case largely decay during geosphere transport.

Figure 5-20 shows the releases from the geosphere to the biosphere as a function of time in case PD-HIDIFF expressed as WELL-2007 dose based on the dose conversion factors given in Table 3-1. Figure 5-21 shows time-dependent releases from the geosphere to the biosphere divided by the geo-bio flux constraints specified by the Finnish regulator and given in Table 1-1, and the sum of these releases over all calculated radionuclides. As in the Base Case, the dose maximum occurs shortly after loss of transport resistance of the defect at 10,000 years, and is about four orders of magnitude below the regulatory dose guideline of 10^{-4} Sv per year. The sum of time-dependent releases from the geosphere to the biosphere divided by their respective geo-bio flux constraints also has its maximum shortly after 10,000 years, and is about three orders of magnitude below the regulatory guideline of one.

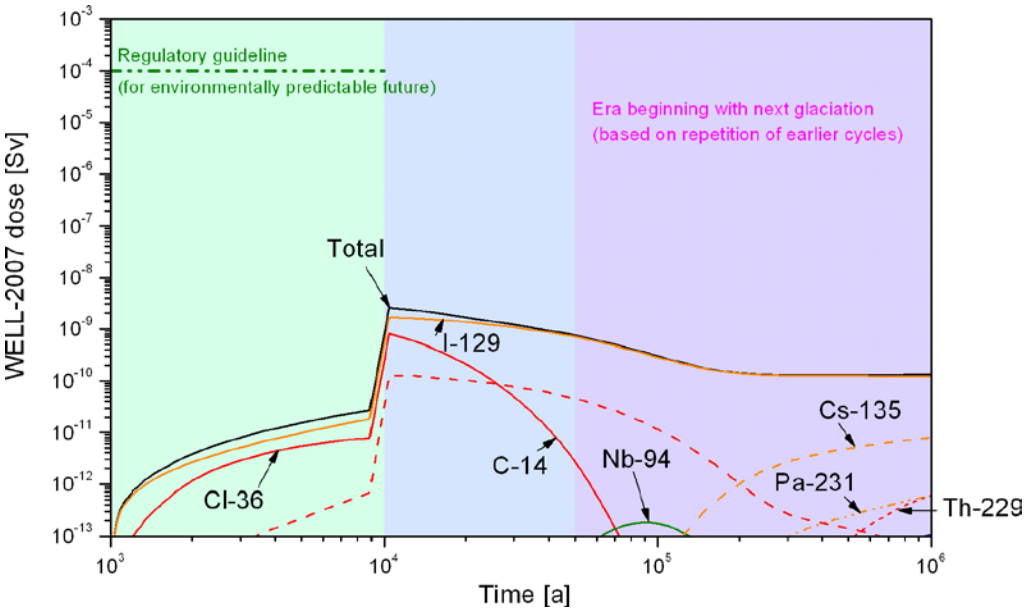

Figure 5-20. *WELL-2007 dose as a function of time in case PD-HIDIFF.*

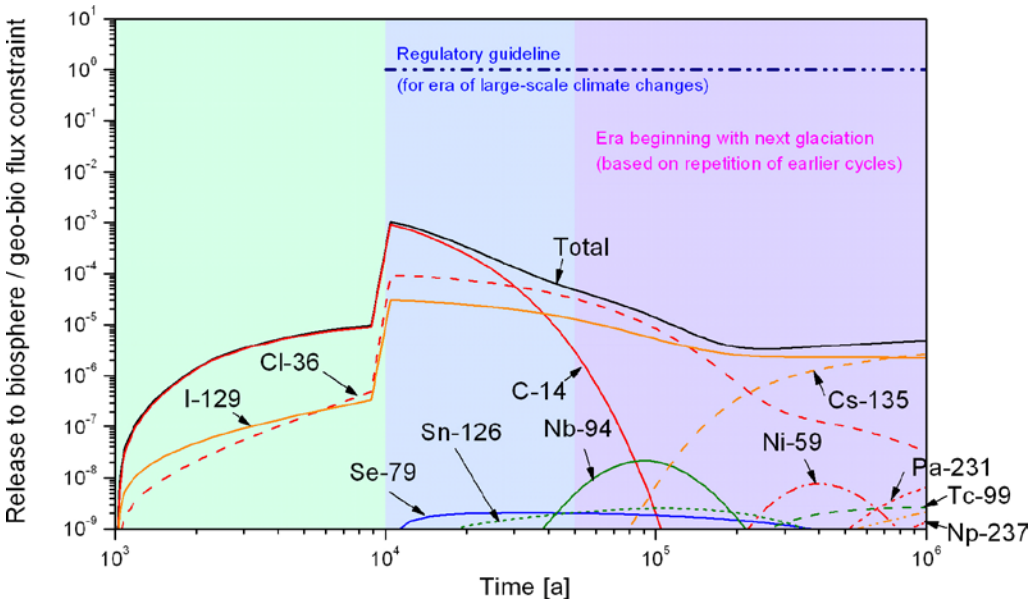

Figure 5-21. *Ratios of nuclide-specific activity releases to their respective geo-bio flux constraints in case PD-HIDIFF.*

5.7 Cases addressing processes originating at the buffer/rock interface

5.7.1 Differences compared with the Base Case

There are a number of processes identified in the Process and Evolution Reports /Gribi et al. 2007, Smith et al. 2007a/ that could significantly affect the transport properties of the buffer/rock interface. These are:

- thermally induced rock spalling;
- the presence of potentially porous or fractured corrosion products from the steel supercontainers in contact with the drift wall in tighter drift sections;
- chemical interactions of the buffer with these corrosion products; and
- chemical interactions of the buffer with leachates from cementitious repository components, including grout used to limit groundwater inflow to the drift during operations.

There are also other processes that could potentially alter buffer transport properties and mass transfer across the buffer/rock interface (e.g. cementation due to silica precipitation, strain due to deformation of the supercontainer shell).

In the Base Case, it is assumed that the impact of these processes is negligible. The degree to which system properties will, in reality, be affected and the spatial extent of the effects is, however, highly uncertain. Thus, four variant cases are considered in which the impact of these processes is assumed to be more significant. All four cases are similar in that the perturbing processes are assumed to create a high-permeability zone at the interface. The extent of the zone, and the groundwater flow within the zone, is, however, case dependent.

In all cases, the perturbation to the buffer/rock interface is assumed to be restricted to the drift sections in which supercontainers are emplaced, with the distance blocks in between being unaffected. Thus, in none of the cases does the perturbed buffer/rock interface a continuous flow and transport pathways along the drift. In the case of thermally-induced rock spalling, for example, although the hydraulic conductivity of the host rock near the drift wall in affected drift sections may be substantially increased, the pressure on the drift wall exerted by the distance blocks adjacent to the affected sections is expected to suppress spalling (Section 5.4.5 of the Evolution Report).

Case **PD-SPALL** addresses the case of a perturbed buffer/rock interface in a relatively tight drift section. This is, for example, relevant to the case of thermally-induced rock spalling, since, in such drift sections, buffer swelling pressure at the drift wall is less likely to be developed rapidly enough to prevent this process from taking place compared with less tight drift sections. It could also be considered to address the impact of porous/fractured iron corrosion products being in direct contact with the drift wall – this is also a greater possibility in relatively tight drift sections (Section 5.5.3 in the Evolution Report). Although the hydraulic conductivity of the host rock near the drift wall in affected drift sections is assumed to be substantially increased by thermally induced spalling, the pressure on the drift wall exerted by the distance blocks is assumed to suppress spalling where the distance blocks contact the rock and to prevent the formation of continuous flow and transport pathways along the drift. Note that the narrow initial gap between the distance blocks and the drift wall is expected top lead to a relatively fast development of swelling pressure compared with the adjacent buffer originally inside the supercontainers, where the gap to the drift wall is larger.

Cases **PD-FEBENT1**, **PD-FEBENT2** and **PD-FE-BENT3** primarily address chemical interaction of the buffer with the iron of the supercontainer (or with high-pH leachates from cementitious repository components). In case PD-FEBENT1, the extent of the affected buffer zone is assumed to be limited to a region around the supercontainer of vanishingly small thickness but with very high (effectively infinite) hydraulic conductivity. In case PD-FEBENT2, the affected buffer zone is assumed to extend across 10% of the entire thickness of the buffer (4 cm). This is consistent, for example, with the results of iron/bentonite reactive transport modelling, which indicate that the extent of the zone potentially undergoing mineral transformation due to iron/bentonite interaction is likely to remain spatially limited (a few centimetres) for hundreds of thousands of years or more /Wersin et al. 2007/ (Section 6.5.3 of the Evolution Report /Smith et al. 2007a/). In case PD-FEBENT3, the affected buffer zone is conservatively assumed to extend across half the entire thickness of the buffer (20 cm).

The possibility of rock spalling occurring at locations where water inflow and intersecting fracture transmissivity are higher than those in case PD-SPALL is covered implicitly by case PD-FEBENT1. This is considered relevant because current knowledge about the swelling pressures that are sufficient to suppress spalling is quite weak (SKB is currently spending significant effort on this issue). Furthermore, the impact that heating and cooling may have on water inflow and transmissivity in the adjacent rock is uncertain.

5.7.2 Radionuclide inventories, half-lives and partitioning

Radionuclide inventories and half-lives and partitioning between fuel matrix, IRF, Zircaloy and other metal parts are as in the Base Case, and are given in Table 5-2.

5.7.3 Near-field model

In case PD-SPALL, the transmissivity of the intersecting fracture is set to $10^{-10}\,m^2\,s^{-1}$. The corresponding fracture aperture obtained from Eq. 5-1 is 5 µm. It is argued in the KBS-3H Evolution Report that thermally-induced rock spalling is unlikely to occur in the drift sections with an initial inflow of about 0.1 litres per minute (the maximum allowed in an ~ 10 m long drift section used for canister and buffer emplacement in the current reference design). An intersecting fracture with a transmissivity of $10^{-10}\,m^2\,s^{-1}$ is likely to give an more than an order of magnitude lower than this, although there is some uncertainty in the relationship between transmissivity and initial inflow, as discussed is Section 5.2.3. In cases PD-FEBENT1, PD-FEBENT2 and PD-FEBENT3, the transmissivity and aperture of the intersecting fracture are as in the Base Case of ($3 \times 10^{-9}\,m^2\,s^{-1}$ and 3×10^{-5} m, respectively).

While in reality a perturbed buffer/rock interface may provide a hydraulic connection between several neighbouring fractures intersecting the drift, it is assumed in all cases that all release from the buffer to the perturbed zone is captured by the nearest intersecting fracture (i.e. the fracture depicted in Figure 5-1).

Thus, the geometry of near-field model domain is also as in the Base Case (see Figure 5-1 and Table 5-4), with the exception of the fracture aperture in case PD-SPALL, and the outer radius of the (unaltered) buffer in cases PD-FEBENT2 and PD-FEBENT3. In cases PD-SPALL and PD-FEBENT1, the buffer outer radius (r_b [m]) is identical to the drift radius (r_t). In PD-FEBENT2 and PD-FEBENT3, however, r_b is given by:

$$r_b = (r_t - r_c)(1 - P) + r_c \qquad \text{(Eq. 5-12)}$$

where P is the proportion of the buffer thickness affected, i.e. r_b takes a values of 0.885 m and 0.725 m in PD-FEBENT2 and PD-FEBENT3, respectively.

Parameter values related to:

- water ingress;
- radionuclide release;
- solubility limitation and radionuclide transport inside the canister;
- radionuclide transfer to the buffer/evolution of the defect;
- radionuclide transport in the buffer; and
- radionuclide transfer to the geosphere (with the exception of fracture transmissivity and aperture in case PD-SPALL);

are as in the Base Case, and are given in Tables 5-5 to 5-7.

Near-field model boundary conditions and transfer coefficients are, however, modified with respect to the Base Case. In the Base Case, the buffer/rock interface is treated as a zero flux boundary (Eq. 5-4), except where it is intersected by the fracture. The perturbed buffer/rock interface is treated instead as a mixing tank – i.e. radionuclides entering this region are considered to become uniformly mixed with the groundwater flowing through the region. This mixing tank approach has also been used in some other safety assessments to treat the effects of the excavation disturbed/damaged zone (EdZ/EDZ) around a repository drift /e.g. Nagra 1994, JNC 2000/[26]. In the mixing tank approach, the boundary condition given by Eq. 5-4 is replaced by:

$$Q_F C\big|_{r=r_b} = 2\pi r_t D_e \int_{z=-p_c/2}^{p_c/2} \left.\frac{\partial C}{\partial r}\right|_{r=r_b} dz \qquad \text{(Eq. 5-13)}$$

where $z = 0$ lies at the centre of the canister, and Q_F is the flow through the mixing tank (and is also the transfer coefficient from the buffer into the rock, as defined in Section 5.2.3). If the mixing tank is assumed to have a hydraulic conductivity far in excess of either the buffer or the rock:

$$Q_F = 4 r_t T i \qquad \text{(Eq. 5-14)}$$

i.e. the mixing tank "captures" the flow from a portion of the fracture that is twice the drift diameter (the factor of 2 is due to a convergence of flow lines towards the drift). Q_F takes a value of 1×10^{-4} m^3 a^{-1} in case PD-SPALL and 3.1×10^{-3} m^3 a^{-1} in cases PD-FEBENT1, PD-FEBENT2 and PD-FEBENT3. The Base Case value of Q_F given in Section 5.2.3 is 2×10^{-4} m^3 a^{-1}. Thus, conditions at the buffer/rock interface are more favourable to limiting releases in case PD-SPALL than in the Base Case. This is because, although the interface is perturbed unfavourably in case PD-SPALL, the type of drift section in which thermally-induced spalling is assumed to occur is tighter than in the drift section considered in the Base Case.

[26] As demonstrated in Appendix 9 of /Nagra 1994/, any non-uniformity in the groundwater flow around the outer boundary of the buffer gives only a second-order effect on the total diffusive flux from the repository near field.

The treatment of the perturbed buffer/rock interface as a mixing tank is highly conservative. In reality, for example, buffer affected by iron-bentonite interactions is expected to have an increased, but still low, hydraulic conductivity. It should be noted that the modelling of flow and solute transport in a zone damaged due to rock spalling has been addressed in the case of a KBS-3V repository in /Neretnieks 2006/. Neretnieks also considers the capture of flow due to a conductive layer at the buffer/rock interface, and includes the effects of different fracture orientations with respect to the deposition hole. Neretnieks notes that the situation considered here, in which the damaged zone is treated as a mixing tank, can be considered a "worst case". He shows that, in terms of its impact on flow around the drift, the high conductivity mixing tank approximation applies where the hydraulic conductivity of the perturbed zone (K [m s^{-1}]) satisfies the condition (Eq. 14 in /Neretnieks 2006/):

$$K >> 10\frac{T}{(r_t - r_b)} \qquad \text{(Eq. 5-15)}$$

For a transmissivity of 3×10^{-9} m^2 s^{-1}, and assuming a perturbed zone with of 20 cm (as in PD-FEBENT2), the condition is that $K >> 1.5 \times 10^{-7}$ m s^{-1}. This an increase of 6 to 7 orders of magnitude above the hydraulic conductivity of the unperturbed saturated buffer (see, e.g. Figure 4-8 of /SKB 2006a/).

/Neretnieks 2006/ also considers the less pessimistic case where solute exchange between the damaged zone and the buffer takes place by diffusion. Diffusive mixing in the damaged zone may, however, be enhanced by mixing by advection in the complex fracture network that may exist within the zone (i.e. by dispersion), and so the more pessimistic mixing tank approximation is used here.

5.7.4 Geosphere model

The geosphere model is as in the Base Case. Parameter values that apply to all migrating species are given in Table 5-8. Element-dependent parameters are given in Table 5-9 and 5-10. Although the assumed transmissivity of the intersecting fracture in case PD-SPALL is less than that of the Base Case by a factor of about 30, the transport resistance of the geosphere is the result of a network of fractures with a range of transmissivities, and so is assumed to be unaffected by assumptions regarding the transmissivity of the one individual fracture within that network that intersects the drift near the failed canister. Hence, WL/Q is 50,000 years per metre as in the Base Case. The impact of a reduced geosphere transport resistance (with the Base Case value of Q_F) is illustrated by Case PD-LOGEOR (Section 5.12).

5.7.5 Results

Table 5-23 gives calculated maximum near-field release rates in Bq per year for each radionuclide in the Base Case for an initial penetrating defect (case PD-BC) and in cases PD-SPALL and PD-FEBENT1. It also gives the times at which these maxima occur (t_{max}). Table 5-24 gives results for PD-FEBENT1, PD-FEBENT2 and PD-FEBENT3.

Near-field release rate maxima in case PD-SPALL are reduced with respect to the Base Case, is generally by a factor of 2, which is the factor by which the transfer coefficient from the buffer to the rock (Q_F) is reduced. As noted above, conditions at the buffer/rock interface are assumed to more favourable to limiting releases in case PD-SPALL than in the Base Case because, although the interface is perturbed unfavourably in case PD-SPALL, the intersecting fracture is assumed to be tighter than in the Base Case. Near-field release rates in the three bentonite alteration cases for most safety relevant radionuclides are increased with respect to the Base Case by more than an order of magnitude, in line with the increase by a factor of about 16 in the transfer coefficient from the buffer to the rock.

Table 5-23. Calculated maximum near-field release rates for each radionuclide in the Base Case for an initial penetrating defect (case PD-BC) and in cases PD-SPALL and PD-FEBENT1, and the times at which these maxima occur. Full results are presented in Appendix G.

Radionuclide			Base Case (PD-BC)		PD-SPALL		PD-FEBENT1	
			t_{max} [a]	Bq/a	t_{max} [a]	Bq/a	t_{max} [a]	Bq/a
Activation/fission products		C-14	1.01E+04	6.77E+05	1.01E+04	3.40E+05	1.01E+04	9.00E+06
		Cl-36	1.03E+04	1.10E+05	1.03E+04	5.77E+04	1.02E+04	7.96E+05
		Ni-59	1.23E+04	3.44E+05	1.23E+04	1.73E+05	1.23E+04	4.97E+06
		Se-79	2.15E+04	2.08E–01	2.15E+04	1.09E–01	1.99E+04	1.32E+00
		Mo-93	1.08E+04	3.67E–01	1.08E+04	1.92E–01	1.06E+04	2.54E+00
		Zr-93	2.20E+05	5.03E–02	2.10E+05	2.53E–02	2.00E+05	6.94E–01
		Zr-93p*	2.35E+05	3.68E+00	2.35E+05	1.85E+00	2.30E+05	5.07E+01
		Nb-94	1.99E+04	7.70E+03	1.99E+04	3.86E+03	1.99E+04	1.12E+05
		Tc-99	8.85E+05	2.25E+01	8.65E+05	1.13E+01	8.80E+05	3.21E+02
		Pd-107	8.90E+05	3.02E+01	8.90E+05	1.53E+01	1.62E+04	3.25E+02
		Sn-126	1.15E+05	4.84E+00	1.15E+05	2.42E+00	1.10E+05	7.05E+01
		I-129	1.03E+04	1.27E+04	1.03E+04	6.62E+03	1.02E+04	9.22E+04
		Cs-135	1.01E+04	7.78E+03	1.01E+04	3.89E+03	1.01E+04	1.19E+05
Actinide chains	4N	Pu-240	3.44E+04	1.65E+01	3.44E+04	8.23E+00	3.44E+04	2.50E+02
		U-236	1.00E+06	5.79E–04	9.99E+05	2.91E–04	1.00E+06	7.99E–03
	4N + 1	Cm-245	5.38E+04	6.05E–04	5.38E+04	3.03E–04	5.38E+04	9.27E–03
		Am-241	5.38E+04	6.38E–04	5.38E+04	3.19E–04	5.38E+04	9.76E–03
		Np-237	1.00E+06	8.21E–01	1.00E+06	4.12E–01	1.00E+06	1.16E+01
		U-233	1.00E+06	1.30E+00	1.00E+06	6.56E–01	1.00E+06	1.76E+01
		Th-229	1.00E+06	7.65E–01	9.99E+05	3.83E–01	9.99E+05	1.15E+01
	4N + 2	Cm-246	3.88E+04	6.19E–06	3.88E+04	3.09E–06	3.88E+04	9.51E–05
		Pu-242	3.94E+05	3.01E+01	3.94E+05	1.51E+01	3.74E+05	4.31E+02
		U-238	1.00E+06	4.95E–04	1.00E+06	2.49E–04	1.00E+06	6.83E–03
		U-234	1.29E+05	2.02E–03	1.29E+05	1.01E–03	1.29E+05	2.86E–02
		Th-230	5.64E+05	2.77E+01	5.59E+05	1.39E+01	5.69E+05	4.08E+02
		Ra-226	5.64E+05	3.59E+04	5.74E+05	1.80E+04	5.64E+05	4.22E+05
	4N + 3	Am-243	4.88E+04	4.05E–02	4.88E+04	2.03E–02	4.88E+04	6.21E–01
		Pu-239	5.88E+04	2.21E+02	5.88E+04	1.10E+02	5.88E+04	3.32E+03
		U-235	1.00E+06	3.60E–05	9.99E+05	1.81E–05	1.00E+06	4.96E–04
		Pa-231	1.00E+06	3.27E+01	1.00E+06	1.64E+01	1.00E+06	4.46E+02

* Zirconium originating from the fuel matrix only.

Differences between cases PD-FEBENT1, PD-FEBENT2 and PD-FEBENT3 are mostly relatively minor. There is, for example, an 8% increase in the maximum release rate of I-129 in moving from case PD-FEBENT1 (40 cm of unperturbed buffer) to case PD-FEBENT2 (36 cm of unperturbed buffer), and a further 60% increase in moving to case PD-FEBENT3 (20 cm of unperturbed buffer). For some shorter-lived and more highly sorbing radionuclides, there is more sensitivity to the thickness of unperturbed buffer. Thus, for example, there is a 45% increase in the maximum release rate of Pu-239 in moving from case PD-FEBENT1 to case PD-FEBENT2, and a further increase of almost a factor of 5 in moving to case PD-FEBENT3.

Table 5-24. Calculated maximum near-field release rates for each radionuclide in case PD-FEBENT1, PD-FEBENT2 and PD-FEBENT3, and the times at which these maxima occur. Full results are presented in Appendix G.

Radionuclide			PD-FEBENT1		PD-FEBENT2		PD-FEBENT3	
			t_{max} [a]	Bq/a	t_{max} [a]	Bq/a	t_{max} [a]	Bq/a
Activation/fission products		C-14	1.01E+04	9.00E+06	1.01E+04	9.77E+06	1.01E+04	1.43E+07
		Cl-36	1.02E+04	7.96E+05	1.02E+04	8.57E+05	1.01E+04	1.37E+06
		Ni-59	1.23E+04	4.97E+06	1.23E+04	5.73E+06	1.34E+04	9.78E+06
		Se-79	1.99E+04	1.32E+00	1.84E+04	1.35E+00	1.62E+04	1.65E+00
		Mo-93	1.06E+04	2.54E+00	1.05E+04	2.68E+00	1.03E+04	3.62E+00
		Zr-93	2.00E+05	6.94E–01	1.70E+05	7.10E–01	7.97E+04	7.95E–01
		Zr-93p*	2.30E+05	5.07E+01	1.95E+05	5.18E+01	8.47E+04	5.76E+01
		Nb-94	1.99E+04	1.12E+05	1.99E+04	1.33E+05	1.46E+04	2.62E+05
		Tc-99	8.80E+05	3.21E+02	8.90E+05	3.62E+02	8.80E+05	5.69E+02
		Pd-107	1.62E+04	3.25E+02	1.54E+04	4.16E+02	1.40E+04	1.20E+03
		Sn-126	1.10E+05	7.05E+01	1.05E+05	8.68E+01	7.47E+04	2.25E+02
		I-129	1.02E+04	9.22E+04	1.01E+04	9.97E+04	1.01E+04	1.60E+05
		Cs-135	1.01E+04	1.19E+05	1.01E+04	1.57E+05	1.01E+04	3.94E+05
Actinide chains	4N	Pu-240	3.44E+04	2.50E+02	3.07E+04	4.64E+02	2.06E+04	5.90E+03
		U-236	1.00E+06	7.99E–03	1.00E+06	8.17E–03	1.00E+06	8.93E–03
	4N + 1	Cm-245	5.38E+04	9.27E–03	4.88E+04	2.02E–02	3.07E+04	5.19E–01
		Am-241	5.38E+04	9.76E–03	4.88E+04	2.13E–02	3.07E+04	5.47E–01
		Np-237	1.00E+06	1.16E+01	9.99E+05	1.26E+01	9.94E+05	1.69E+01
		U-233	1.00E+06	1.76E+01	1.00E+06	1.65E+01	1.00E+06	8.72E+00
		Th-229	9.99E+05	1.15E+01	9.99E+05	2.03E+01	2.19E+05	2.62E+02
	4N + 2	Cm-246	3.88E+04	9.51E–05	3.88E+04	2.49E–04	2.48E+04	1.58E–02
		Pu-242	3.74E+05	4.31E+02	3.54E+05	5.11E+02	2.54E+05	1.15E+03
		U-238	1.00E+06	6.83E–03	1.00E+06	6.98E–03	1.00E+06	7.62E–03
		U-234	1.29E+05	2.86E–02	1.14E+05	3.09E–02	5.88E+04	4.28E–02
		Th-230	5.69E+05	4.08E+02	5.54E+05	5.31E+02	6.44E+05	1.51E+03
		Ra-226	5.64E+05	4.22E+05	5.69E+05	4.58E+05	8.39E+05	5.46E+05
	4N + 3	Am-243	4.88E+04	6.21E–01	4.38E+04	1.40E+00	2.75E+04	4.26E+01
		Pu-239	5.88E+04	3.32E+03	5.38E+04	4.81E+03	3.88E+04	2.29E+04
		U-235	1.00E+06	4.96E–04	1.00E+06	5.07E–04	9.99E+05	5.53E–04
		Pa-231	1.00E+06	4.46E+02	1.00E+06	5.13E+02	1.00E+06	9.86E+02

* Zirconium originating from the fuel matrix only.

Figures 5-22 and 5-23 show the releases from the geosphere to the biosphere as a function of time in cases PD-SPALL, PD-FEBENT1, PD-FEBENT2 and PD-FEBENT3 expressed as WELL-2007 dose based on the dose conversion factors given in Table 3-1. Figures 5-24 and 5-25 show time-dependent releases from the geosphere to the biosphere divided by the geo-bio flux constraints specified by the Finnish regulator and given in Table 1-1, and the sum of these releases over all calculated radionuclides.

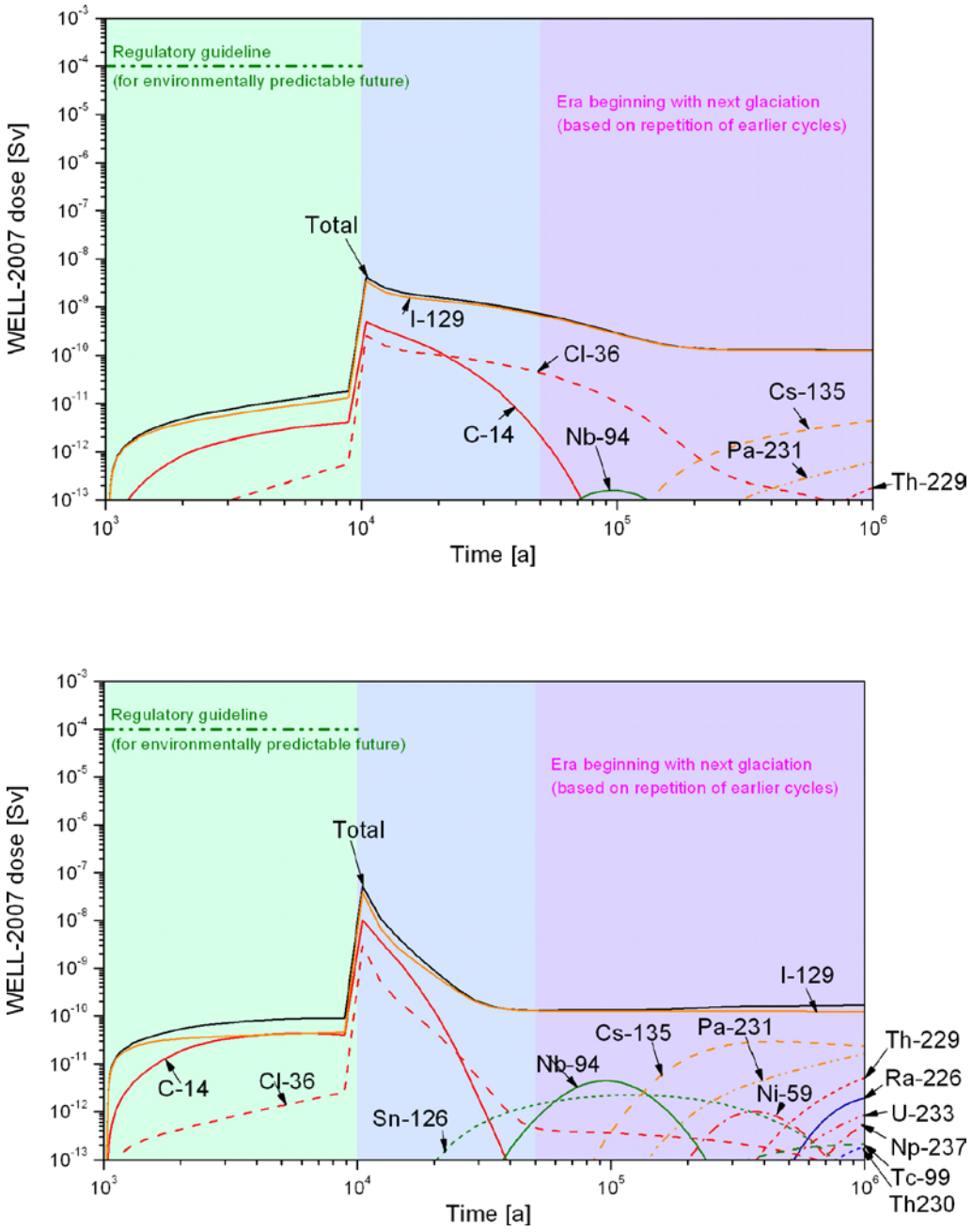

Figure 5-22. *WELL-2007 dose as a function of time in case PD-SPALL (upper figure) and case PD-FEBENT1 (lower figure).*

In all four cases, as in the Base Case, the dose maxima occur shortly after loss of transport resistance of the defect at 10,000 years. They are more than four orders of magnitude below the regulatory dose guideline of 10^{-4} Sv per year in case PD-SPALL, and about three orders of magnitude below the guideline in cases PD-FEBENT1, PD-FEBENT2 and PD-FEBENT3. The sums of time-dependent releases from the geosphere to the biosphere divided by their respective geo-bio flux constraints also have their maxima shortly after 10,000 years. The maxima are more than three orders of magnitude below the regulatory guideline of one in case PD-SPALL, and about two orders of magnitude below the guideline in cases PD-FEBENT1, PD-FEBENT2 and PD-FEBENT3.

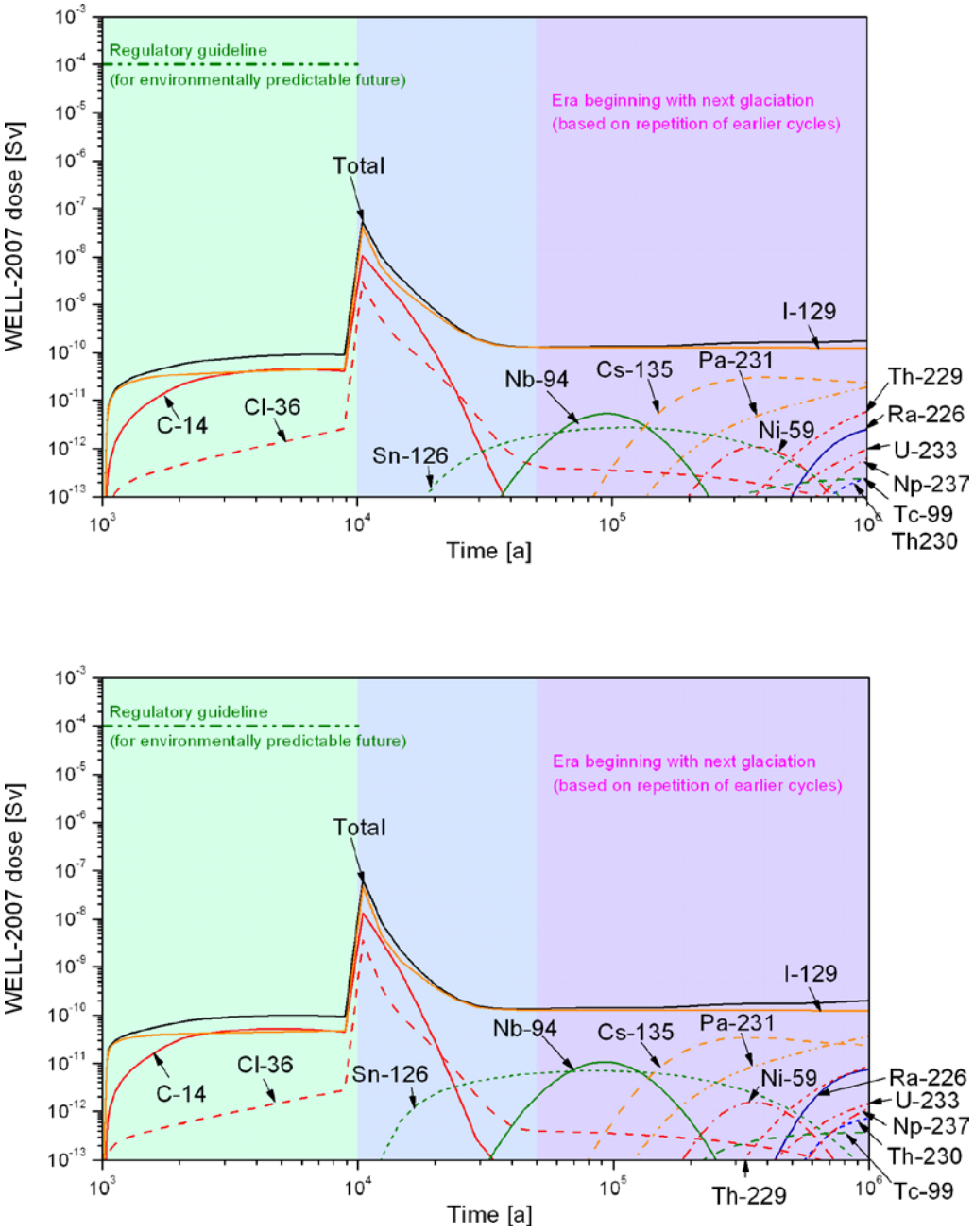

Figure 5-23. *WELL-2007 dose as a function of time in case PD-FEBENT2 (upper figure.) and case PD-FEBENT3 (lower figure).*

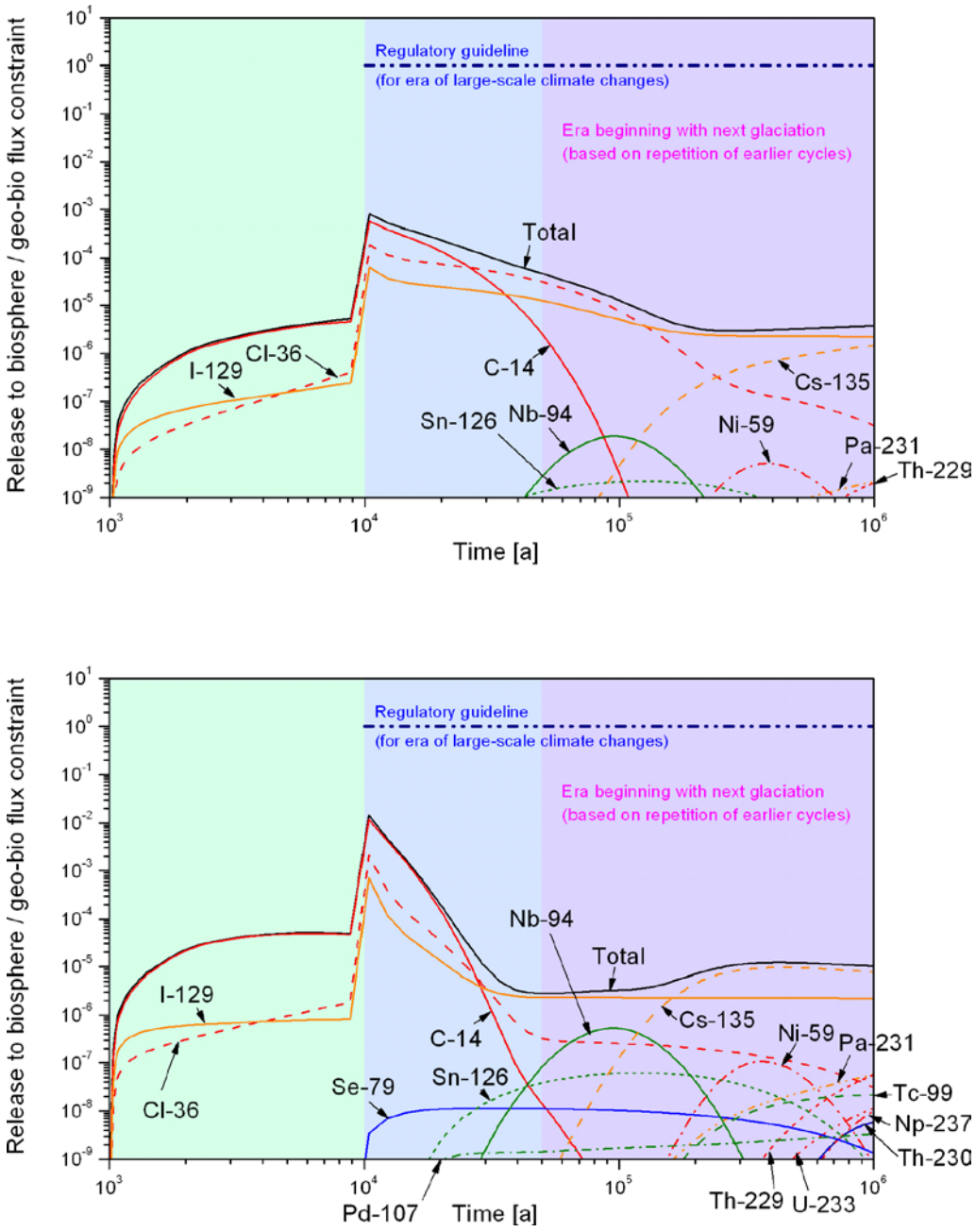

Figure 5-24. *Ratios of nuclide-specific activity releases to their respective geo-bio flux constraints in case PD-SPALL (upper figure) and case PD-FEBENT1 (lower figure). Curves for Th-230 and its daughter Ra-226 overlie each other.*

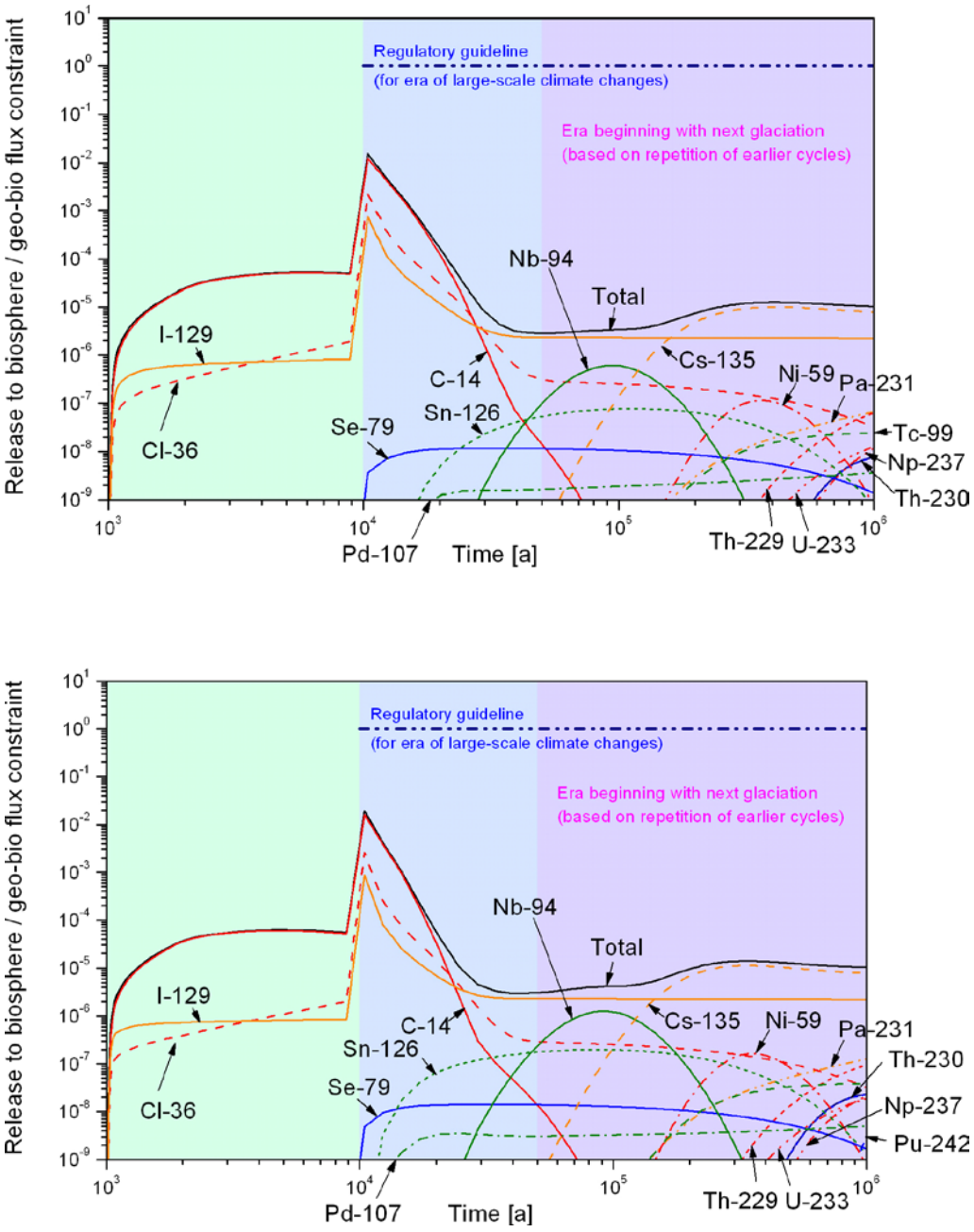

Figure 5-25. *Ratios of nuclide-specific activity releases to their respective geo-bio flux constraints in case PD-FEBENT2 (upper figure) and case PD-FEBENT3 (lower figure). Curves for Th-230 and its daughter Ra-226 overlie each other.*

Finally, Figure 5-26 shows both the calculated annual landscape dose to the most exposed individual and the WELL-2007 dose in case PD-FEBENT3. The highest annual landscape dose occurs at the end of the 10,000 period over which biosphere modelling was carried out, and is less than 10^{-5} Sv, compared with less than 10^{-7} Sv in the case of WELL-2007 dose.

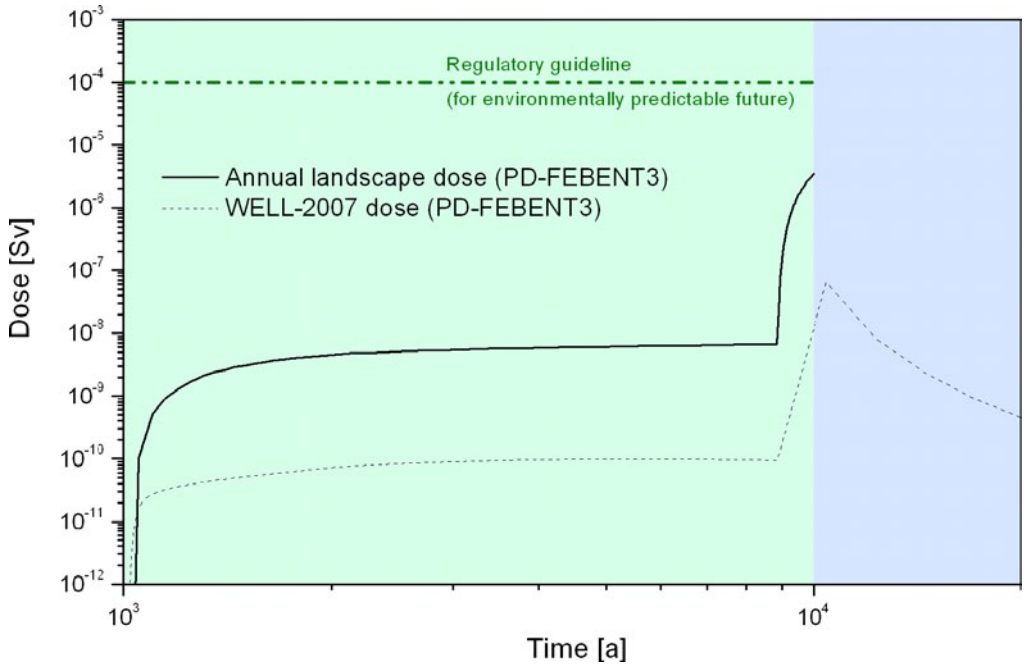

Figure 5-26. *Annual landscape dose and WELL-2007 dose as functions of time in case PD-FEBENT3.*

5.8 Case addressing expulsion of contaminated water by gas

5.8.1 Differences compared with the Base Case

In the Base Case, it is assumed that gas generated inside a defective canister, principally hydrogen from the corrosion of steel, has no impact on radionuclide transport. As discussed in the Process and Evolution Reports /Gribi et al. 2007, Smith et al. 2007a/, however, if the defect is unfavourably located on the underside of the canister, the possibility of gas-induced release of contaminated water from the canister interior to the buffer cannot be excluded. This situation is addressed in case **PD-EXPELL**. It is emphasised, however, that an actual defect may be located anywhere around the canister (no significance should be attached to the depiction of the location of the defect at the upper side of the canister in Figure 5-1). Furthermore, as in all cases addressing an initial penetrating defect, the water inflows may be much reduced due to sealing of the hole by bentonite and corrosion products, making this variant case less likely.

5.8.2 Radionuclide inventories, half-lives and partitioning

Radionuclide inventories and half-lives and partitioning between fuel matrix, IRF, Zircaloy and other metal parts are as in the Base Case, and are given in Table 5-2.

5.8.3 Near-field model

The geometry of the near-field model domain is as in the Base Case and is defined in Figure 5-1 and Table 5-4.

In case PD-EXPELL, it is assumed that a gas-driven water pulse, beginning at 2,800 years after emplacement and lasting for a further 1,300 years, propels water from the canister interior through the buffer to the fracture. These assumptions are based on the most pessimistic case from a range of model calculations of the fate of water/vapour/gas and radionuclides in a canister with an initial penetrating defect described in the KBS-3H Process Report (Section 2.5 of /Gribi et al. 2007/.

Expelled water will, in reality, contain a mixture of IRF radionuclides and radionuclides released to the water by fuel matrix dissolution and by the corrosion of Zircaloy and other metal parts, such as stainless steel and Inconel. In the case of the fuel matrix, given its slow 10^{-7} per year fractional dissolution rate in the Base Case and most variants in the present study, it is assumed that amounts of radionuclides released by the time of the gas-driven water pulse are negligible compared with the IRF amounts. On the other hand, for simplicity, it is assumed that the Zircaloy and other metal parts have corroded and released their radionuclides to solution by the time that the gas-driven water pulse starts, i.e. all radionuclides in the Zircaloy and other metal parts are, in the model, combined with the IRF and, commencing 2,800 years after emplacement, are released directly from the canister interior to the geosphere at a fractional rate of 7.7×10^{-4} per year (i.e. complete release in 1,300 years).

The assumption of complete corrosion of Zircaloy and other metal parts in this time frame is conservative. The low corrosion rates of the Zircaloy and other metal parts, may, in reality, mean that some radionuclides, including potentially significant amounts of Nb-94 and C-14, are retained within these components beyond the period of gas expulsion. Indeed, the water inflow rate on which the calculated gas-driven water pulse is based is insufficent to support complete corrosion of these components before the gas-driven water pulse starts. The assumed inflow rate is also higher that expected in reality since the possible plugging of the hole with bentonite or corrosion products and the decrease of hydraulic gradient due to gas pressure build-up are not taken into account.

Parameter values related to:

- water ingress;
- radionuclide release;
- radionuclide transport in the buffer (for radionuclides released from the fuel matrix); and
- radionuclide transfer to the geosphere;

are as in the Base Case, and are given in Tables 5-5 to 5-7. However, for reasons of conservatism (and to simplify the calculations), solubility limits are not applied.

Near-field model boundary conditions and transfer coefficients are also unchanged with respect to the Base Case.

5.8.4 Geosphere model

The impact of repository-generated gas on geosphere transport in case PD-EXPELL is assumed to be negligible and therefore geosphere transport modelled is as in the Base Case. In reality, there may still be gas being generated by the corrosion of supercontainers and other steel components external to the canister between 2,800 and 4,100 years following emplacement (Section 5.5 of the Evolution Report), but this is assumed to be dissipated (e.g. by two-phase flow in the intersecting fracture) without significantly perturbing the transport of dissolved radionuclides in the geosphere. The impact of this assumption is, however, small, as illustrated by the limited attenuation of releases of key radionuclides by the geosphere transport barrier in this case (see Figure 5-29).

Geosphere parameter values that apply to all migrating species are given in Table 5-8. Element-dependent parameters are given in Table 5-9 and 5-10.

5.8.5 Results

Table 5-25 gives calculated maximum near-field release rates in Bq per year for radionuclides that are initially present in the IFR, Zircaloy and other metal parts in the Base Case for an initial penetrating defect (case PD-BC) and in case PD-EXPELL. It also gives the times at which these maxima occur (t_{max}). Maximum near-field release rates are significantly higher than in the Base Case, for some radionuclides by several orders of magnitude.

Table 5-25. Calculated maximum near-field release rates in the Base Case for an initial penetrating defect (case PD-BC) and in case PD-EXPELL, and the times at which these maxima occur. Full results are presented in Appendix G.

Radionuclide	Base Case (PD-BC)		PD-EXPELL	
	t_{max} [a]	Bq/a	t_{max} [a]	Bq/a
C-14	1.01E+04	6.77E+05	2.80E+03	2.29E+07
Cl-36	1.03E+04	1.10E+05		9.04E+05
Ni-59	1.23E+04	3.44E+05		2.12E+08
Se-79	2.15E+04	2.08E–01		5.40E+03
Mo-93	1.08E+04	3.67E–01		1.15E+07
Zr-93	2.20E+05	5.03E–02		1.34E+07
Nb-94	1.99E+04	7.70E+03		4.49E+07
Tc-99	8.85E+05	2.25E+01		9.99E+06
Pd-107	8.90E+05	3.02E+01		7.07E+04
Sn-126	1.15E+05	4.84E+00		3.52E+03
I-129	1.03E+04	1.27E+04		9.39E+04
Cs-135	1.01E+04	7.78E+03		1.78E+06

Figure 5-27 shows the releases from the geosphere to the biosphere as a function of time in case PD-EXPELL expressed as WELL-2007 dose based on the dose conversion factors given in Table 3-1. Figure 5-28 shows time-dependent releases from the geosphere to the biosphere divided by the geo-bio flux constraints specified by the Finnish regulator and given in Table 1-1, and the sum of these releases over all calculated radionuclides.

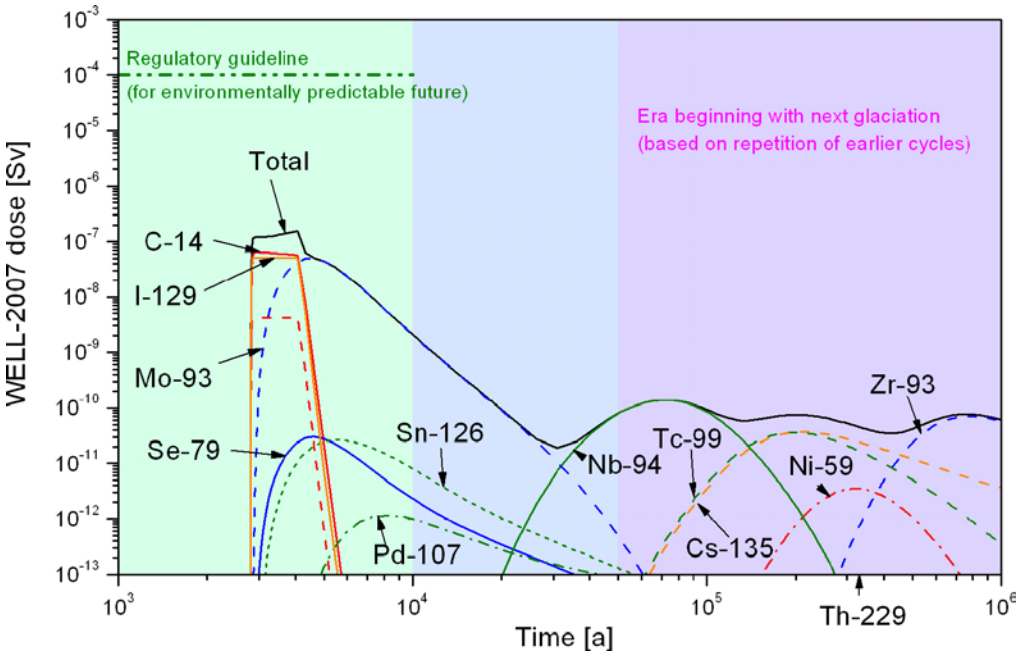

Figure 5-27. *WELL-2007 dose as a function of time in case PD-EXPELL.*

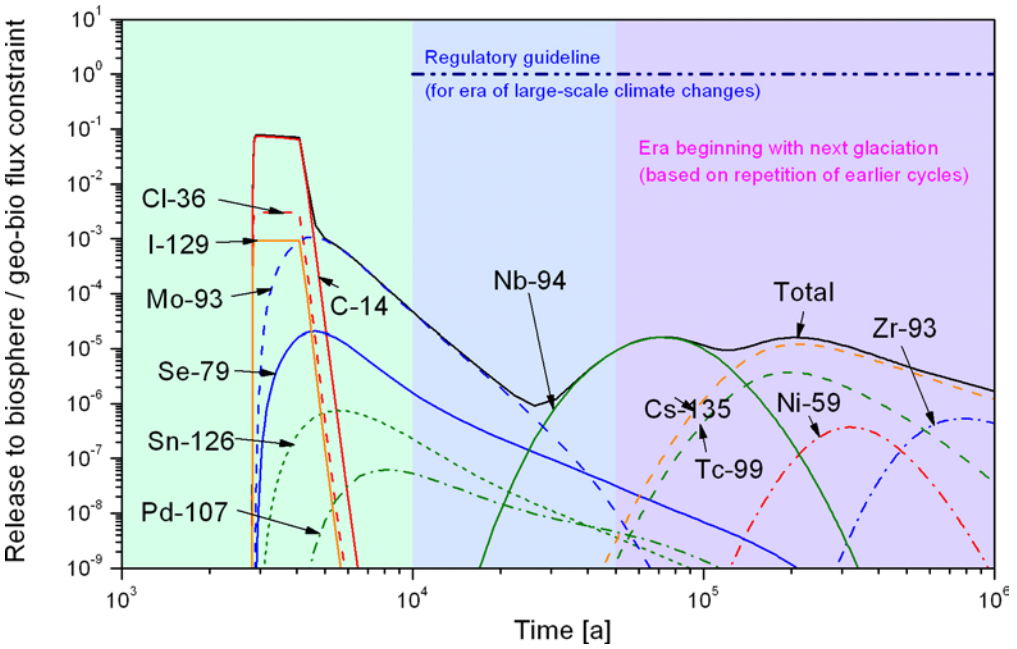

Figure 5-28. *Ratios of nuclide-specific activity releases to their respective geo-bio flux constraints in case PD-EXPELL.*

The dose maximum occurs at about 3,000 years, and is more than two orders of magnitude below the regulatory dose guideline of 10^{-4} Sv per year. Up to the end of the gas pulse, total dose is dominated by I-129, C-14 and, towards the end of the pulse, Mo-93. The I-129 and C-14 contributions decline rapidly after the end of the pulse, whereas Nb-94 continues to increase. The three radionuclides contribute similarly to the dose maximum. The sum of time-dependent releases from the geosphere to the biosphere divided by their respective geo-bio flux constraints also has its maximum at about three thousand years, is about one order of magnitude below the regulatory guideline (applicable at times beyond about 10,000 years) of one, and is dominated by C-14.

As noted above, there is some uncertainty in the impact of repository-generated gas on the geosphere transport barrier. Figure 5-29 compares the near-field and geosphere release rates of some key radionuclides in this case: C-14, I-129 and Mo-93.

The figure shows that the maximum release rates of C-14 and I-129 to the biosphere would be unaffected if the most pessimistic view were taken of the performance of the geosphere transport barrier, with direct release from the near field to the biosphere, and that the maximum release rate of Mo-93 would be increased only moderately (by less than an order of magnitude).

Finally, Figure 5-30 shows both the calculated annual landscape dose to the most exposed individual and the WELL-2007 dose for this case. The highest annual landscape dose is about 2×10^{-5} Sv, compared with about 2×10^{-7} Sv in the case of WELL-2007 dose.

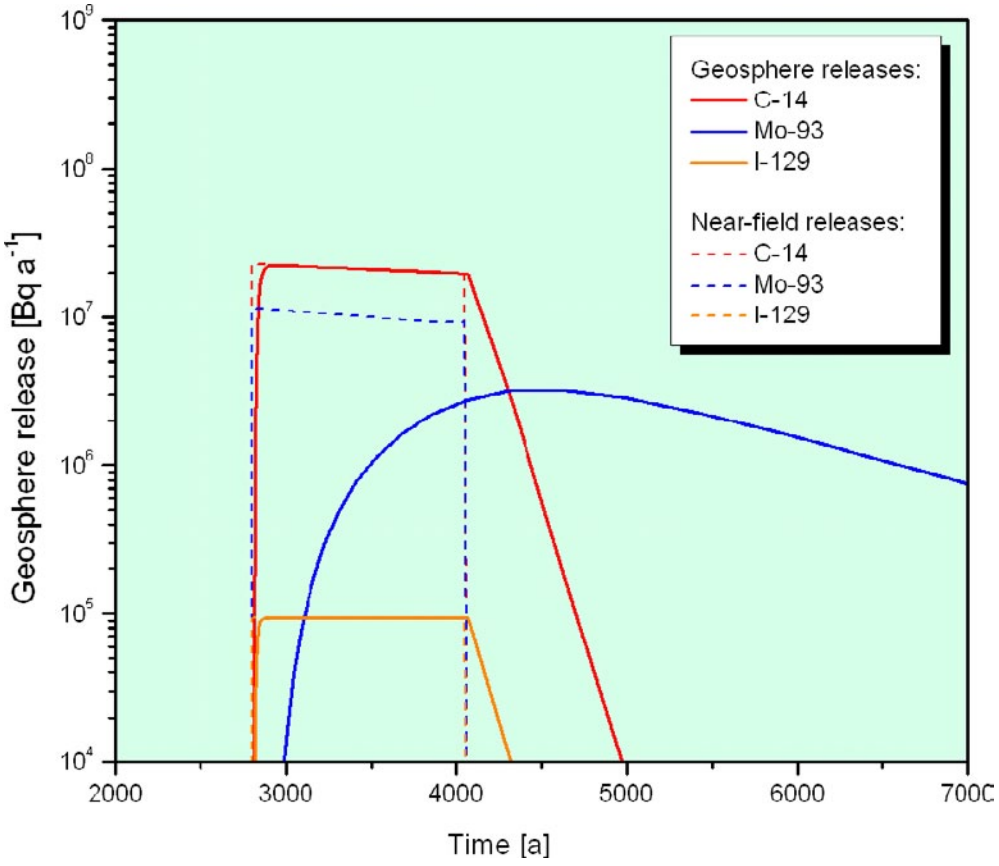

Figure 5-29. *Comparison of the near-field and geosphere release rates of some key radionuclides in case PD-EXPELL.*

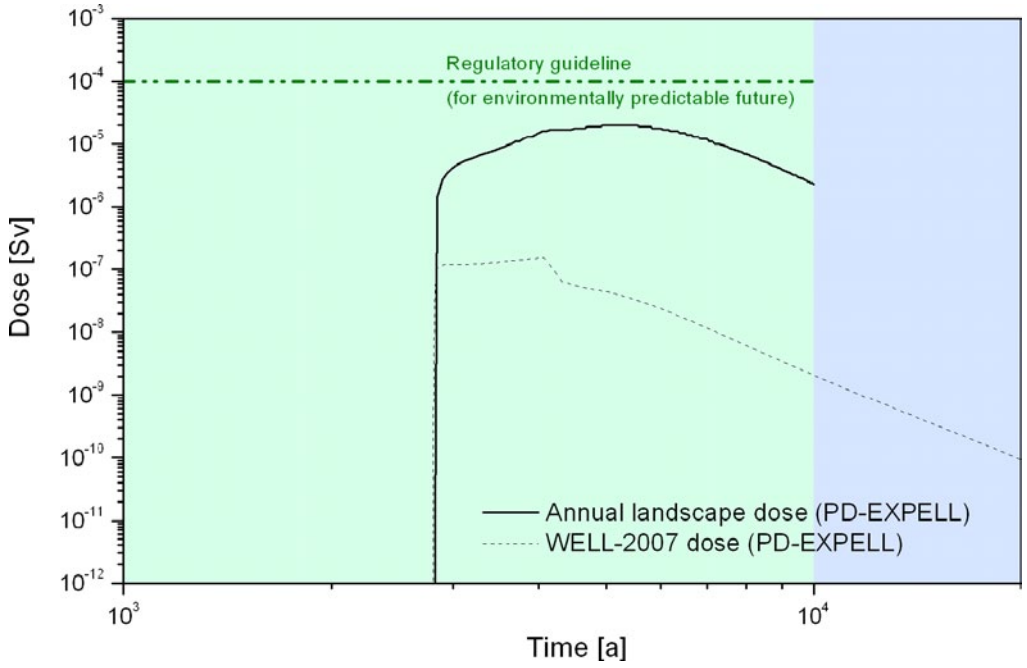

Figure 5-30. *Annual landscape dose and WELL-2007 dose as functions of time in case PD-EXPELL.*

5.9 Case addressing transport of radionuclides as volatile species by gas

5.9.1 Differences compared with the Base Case

In the Base Case, it is assumed that radionuclides are transported entirely as dissolved species. This includes gaseous radionuclides such as Rn-222, and radionuclides such as C-14 that can form volatile species (C-14 is considered to be present either as organic acid or as methane in the Base Case). Such radionuclides could, however, also be transported by repository generated gas.

The formation of pathways for advective gas flow from the canister interior to the geosphere is described in Section 9.10.4 of the Evolution Report /Smith et al. 2007a/. As the canister insert corrodes, hydrogen gas will be produced and gas pressure inside the canister will rise until it exceeds the gas breakthrough pressure of the buffer. In some experiments, this pressure has been found to be above 20 MPa for bentonite with a swelling pressure of ~ 6 MPa (Section 2.3.3 of /SKB 2006c/). After breakthrough, gas pressure will fall to a lower value ('shut-in pressure' of about 10 MPa), sufficient to support the pathways for gas flow and prevent their closure due to swelling pressure. About half the gas contained within the canister at the moment of breakthrough is thus released as a pulse. The gas pathways will remain open, transporting gas at a rate equal to the rate of gas generation, until gas production ceases or is greatly reduced such that it can be dissipated solely by diffusion, at which time the pathways are expected to close and re-seal.

Transport of C-14 by gas is considered in cases **PD-VOL-1 and PD-VOL-2**, which consider high and low rates of repository gas generation, respectively. C-14 is assumed to mix with gas generated in the interior of the canister and to be transported with this gas through the buffer to the geosphere.

5.9.2 Radionuclide inventories, half-lives and partitioning

For C-14, the only radionuclide considered in this case, data are as in the Base Case and given in Table 5-2.

5.9.3 Near-field model

The geometry of near-field model domain is as in the Base Case, and is defined in Figure 5-1 and Table 5-4.

In cases PD-VOL-1 and PD-VOL-2, it is assumed that all liquid water entering through the defect is consumed by corrosion of the cast iron insert. Release of C-14 in gaseous form, however, continues due to alteration of the fuel matrix and corrosion of the Zircaloy and other metal parts in the presence of water vapour. Base Case rates of alteration and corrosion are assumed (Table 4-4). The gaseous C-14 released from the Zircaloy and other metal parts mixes with IRF C-14 and the hydrogen generated by steel corrosion. The other metal parts are mostly stainless steel (53 kg/tU) and Inconel (2.9 kg/tU), which likely have significant Nb-94 and C-14 inventories /Anttila 2005/. In TILA-99, it was assumed that the fractional corrosion rate of all other metal parts (cast iron, stainless steel, Inconel) was 10^{-3} per year (as presented in Table 5-5). In realty, the corrosion rate of stainless steel is less than that of cast iron and, as cast iron is lower in the galvanic series than stainless steel, the stainless steel will be protected against corrosion for as long as cast iron is present.

The rate of steel corrosion assumed in case PD-VOL-1 is 1 μm per year, representing a long-term conservative rate value. As discussed in the Process Report /Gribi et al. 2007/ and Evolution Reports /Smith et al. 2007a/, the expected initial corrosion product of steel in the

presence of bentonite is magnetite, which is expected to form as a thin adherent layer with a thickness that is constant in time and an outer, looser layer with poor adhesion. The corrosion rate will decrease rapidly as the surface film of magnetite develops.Corrosion experiments performed in compacted bentonite /Smart et al. 2004/ for a period of about 1 year gave rates of 1–2 µm per year. The assumption of a 1 µm per year corroson rate is further supported by various natural analogue studies, as discussed in SR-Can's Fuel and Canister Process report /SKB 2006b/.

The possibility that the downward trend observed in corrosion experiments continues beyond the duration of the experiments is considered in case PD-VOL-2, which assumes a lower long-term steel corrosion rate of 0.1 µm per year. Although higher steel corrosion rates have been observed, they subsequently decrease to value generally in the range discussed above.

Steel corrosion to magnetite proceeds by the reaction:

$3Fe + 4H_2O \rightarrow Fe_3O_4 + 4H_2$,

Thus, three moles of iron produce four models of hydrogen gas, and the rate of gas generation, r_g [mol a^{-1}] inside a canister is given by:

$$r_g = \frac{4}{3} RF \frac{\rho_{Fe}}{M_{Fe}} \qquad \text{(Eq. 5-16)}$$

where:

F is the steel corrosion rate, taken to be 1 µm per year in case PD-VOL-1 and 0.1 µm per year in case PD-VOL-2;

R is the total inner surface of the cast iron insert – about 34 m^2 for BWR canisters;

ρ_{Fe} is the density of the insert, taken to be 7,800 kg m^{-3};

M_{Fe} is the atomic mass of iron, 0.056 kg mol^{-1}.

It is assumed to take 1,000 years for the canister insert to become breached and for corrosion of the inner surfaces of the cast iron insert to begin (the same as the time required for contact of water with the fuel/metallic parts to take place and for transport pathways to be established in the Base Case). At a later time t_g [a], the gas pressure inside the canister reaches the gas break-through pressure of the bentonite, and one half of the C-14 inventory present in gaseous form in the void space inside the canister is assumed to be transferred directly and instantaneously to the geosphere.

Time t_g is calculated from the following equations, assuming negligible dissipation of gas pressure by mechanisms other than advection along pathways created when the gas breakthrough pressure is exceeded:

$$t_g = 1{,}000 \text{ years} + \frac{P_g}{r_g} \frac{V_0}{R_0 T_0} \qquad \text{(Eq. 5-17)}$$

where:

P_g is the gas breakthrough pressure of the bentonite, taken to be 20 MPa (see Section 5.9.1, above);

V_0 is the internal void space in the canisters (assumed to become completely gas filled, and equated to the water volume for dissolution, as given in Table 5-4);

R_0 is the ideal gas constant, 8.315 J mol^{-1} K^{-1};

T_0 is temperature, taken to be 303 K.

At times greater than t_g, all C-14 released in gaseous form to the canister interior mixes with gas in the void space inside the canister, migrates through gas pathways in the bentonite, and is released to the geosphere. Assuming negligible dissipation of gas pressure by mechanisms other than advection along pathways created when the gas breakthrough pressure is exceeded, the equivalent flow rate, Q_g [m^3 a^{-1}], with which the C-14 in the void space inside the canister is released is:

$$Q_g = r_g \frac{R_0 T_0}{P_0} \qquad \text{(Eq. 5-18)}$$

This continues until gas production ceases at a time t_c [a], whereupon the calculation is terminated. t_c is given by:

$$\text{tc} = 1{,}000 \text{ years} + \frac{M}{RF\rho_{Fe}} \qquad \text{(Eq. 5-19)}$$

where:

M is the mass of iron and steel in the canister interior, taken to be 13.4×10^3 kg for BWR canisters (Table 3.1 in the Process Report, /Gribi et al. 2007/).

Applying the above data, the model parameter values given in Table 5-26 are obtained.

5.9.4 Geosphere model

The geosphere model is as in the Base Case. All gaseous C-14 reaching the geosphere is assumed to dissolve in the relatively large amounts of water present in the rock. It is then transported with flowing water, with the Base Case geosphere transport resistance (WL/Q) of 50,000 years per metre. Even if some C-14 remained in gaseous form and were transported more rapidly through the geosphere, the impact on calculated release rates to the biosphere would be small, because of the limited attenuation of releases of C-14 by the Base Case geosphere transport barrier (see, e.g., Figure 5-29).

5.9.5 Results

Figure 5-31 shows the C-14 releases from the geosphere to the biosphere as a function of time in the Base Case and in cases PD-VOL-1 and PD-VOL-2 expressed as WELL-2007 dose based on the dose conversion factors given in Table 3-1. Figure 5-32 shows time-dependent releases of C-14 from the geosphere to the biosphere divided by the geo-bio flux constraint specified by the Finnish regulator and given in Table 1-1.

Table 5-26. Times when the gas pressure inside the canister reaches the gas breakthrough pressure of the bentonite (t_g) and when gas generation ceases (t_c) in cases PD-VOL-1 and PD-VOL-2.

	PD-VOL-1	PD-VOL-2
Q_g	8×10^{-4} m^3 a^{-1}	8×10^{-5} m^3 a^{-1}
t_g	1,900 a	10,000 a
t_c	51,000 a	510,000 a

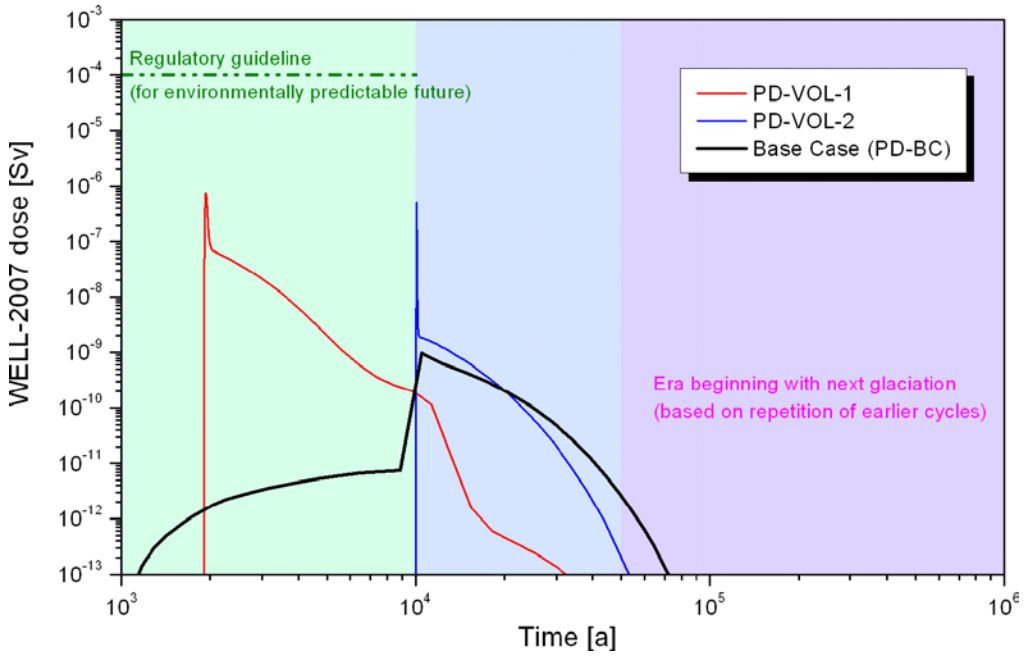

Figure 5-31. *WELL-2007 C-14 dose as a function of time in the Base Case (PD-BC) and in cases PD-VOL-1 and PD-VOL-2.*

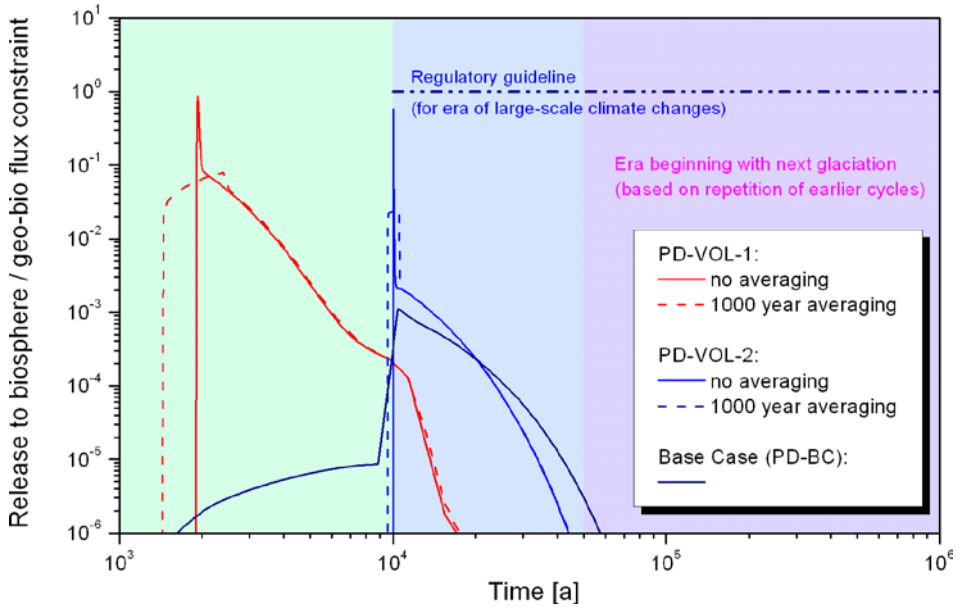

Figure 5-32. *Ratios of C-14 activity release to the geo-bio flux constraint in the Base Case (PD-BC) and in cases PD-VOL-1 and PD-VOL-2.*

The maximum C-14 dose is about two orders of magnitude below the regulatory guideline in both cases (about three orders of magnitude higher than in the Base Case). However, the maximum release rate of C-14 to the biosphere divided by the geo-bio flux constraint for C-14 is only slightly below the regulatory guideline, compared with more than three orders of magnitude below in the Base Case. Doses and releases are a little lower in case PD-VOL-2 than in case PD-VOL-1, since gas pressure build-up is slower in case PD-VOL-1, allowing more time for C-14 to decay before it is expelled to the geosphere (the half-life of C-14 is 5,730 years).

It should be noted that an artefact of the FTRANS code is some additional spreading (numerical dispersion) of the sharp peaks occurring at time t_g. To test the possible magnitude of this affect, an alternative geosphere transport model using an analytical solution has also been applied to the near-field release. The problem solved by the two models is not identical. In particular, the alternative model assumes a homogeneous rock matrix that extends an infinite distance on either side of the model fracture, with properties set equal to those of the first centimetre of rock matrix in the FTRANS model (Table 5-9). The impact of this difference is not, however, expected to be large. The result is that the alternative geosphere transport model gives a peak release which is a factor of about 4 times higher than the FTRANS result, with the lower release calculated using FTRANS attributed mainly to numerical dispersion. The maximum release rate of C-14 to the biosphere divided by the geo-bio flux constraint for C-14 may thus exceed the regulatory guideline.

No averaging of release rates over time has been applied in the calculations. The regulatory guideline YVL 8.4, on the other hand, allows averaging over a maximum interval of 1,000 years when comparing releases with geo-bio flux constraints. Such averaging spreads and reduces the magnitudes of the peak releases, as also illustrated in Figure 5-32. With averaging, release maxima are more than an order of magnitude below the guideline. Furthermore, longitudinal dispersion due, for example, to the variability in transport times along differnt paths through the geosphere fracture network, would, in reality, result in the spreading of the radionuclide pulse and the lowering of the geosphere release maximum. Longitudinal dispersion is not, however, included in the geosphere transport model used in the present safety assessment. This is becuase the decision was taken to base the representation of the geosphere largely on the earlier TILA-99 assessment, where longitudinal dispersion was omitted in the majority of geosphere transport calculations.

Finally, Figure 5-33 shows both the calculated annual landscape dose to the most exposed individual and the WELL-2007 dose in case PD-VOL-1. As in the Base Case, the highest annual landscape dose occurs shortly after 1,900 years. The maximum takes a value of 6.4×10^{-5} Sv, which is close to, though slightly below, the 10^{-4} Sv regulatory guideline.

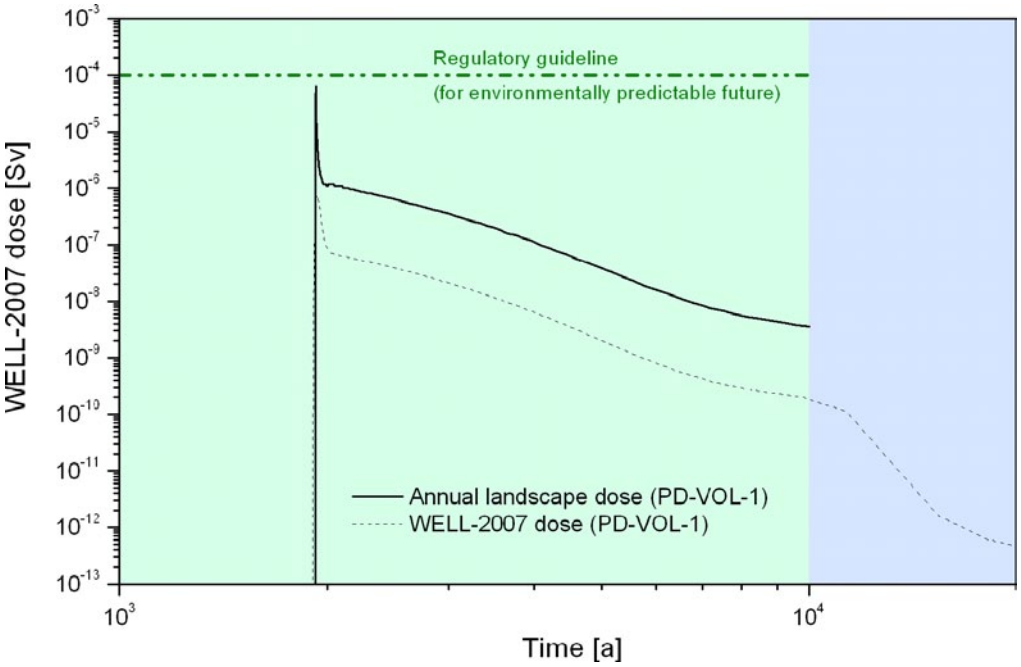

Figure 5-33. *Annual landscape dose and WELL-2007 dose as functions of time in case PD-VOL-1.*

5.10 Case addressing uncertainties in chemical speciation, solubilities and redox conditions

5.10.1 Differences compared with the Base Case

Uncertainties in the values assigned to solubilities and sorption coefficients arise in part from uncertainties in the speciation of the migrating elements. Speciation in the near field and geosphere is affected by a range of incompletely understood features and processes, including, for example, the presence of hydrogen gas and iron corrosion products, and the impact of the hydrogen gas on the bentonite porewater chemistry, as well as variability in groundwater composition in space and time.

Uncertainties regarding the speciation and sorption of several specific elements are discussed in Appendix E. Uncertainties in C speciation are of particular interest, given the significant contribution the C-14 makes to calculated releases and doses in the Base Case and many variant cases. Appendix E notes that the proportion of organic C to inorganic C released by the corrosion of activated metal parts is high, and that the fate of the organic molecules is uncertain. They could remain as organic molecules, undergo oxidation to CO_2 or reduction to methane. In the Base Case, it is assumed that all C is transported in methanic form in both the near field and geosphere, and that it does not sorb on solid surfaces. In cases **PD-BCC**, **PD-VVERC** and **PD-EPRC**, it is assumed that microbial oxidation of methane takes place in the geosphere, which is possible, for example, if brackish, sulphate-rich water reaches repository depth during future evolution of the Olkiluoto site. This leads to the formation of CO_2, and to weakly sorbing carbonate, increasing C-14 retardation (the possibility that calcite will precipitate is, however, not addressed in these cases). PD-BCC addresses release from a BWR-type canister. Cases PD-VVERC and PD-EPRC address C-14 releases from a VVER-440-type canister and from an EPR-type canister, respectively.

Nb speciation is also uncertain. As noted in Section 5.2.3, speciation calculations indicate that Nb will be present as anionic complexes in buffer pore water, although, in the Base Case, Nb is treated as neutral. In case **PD-BCN**, however, Nb is treated as anionic in the near field and the geosphere.

Base Case near-field solubilities for redox-sensitive elements are based on an assumption of long-term dynamic equilibrium between magnetite and hematite formed in the system around the corroding iron insert, with a pH_2 of 10^{-7} atm. As noted in Section 5.2.3, the system has an Eh of –230 mV vs. SHE for a buffer porewater pH of 7.4. The Base Case redox state gives generally the highest solubilities for the different redox conditions considered in Appendix E, and is therefore likely to be conservative for most, though not all, elements. As an alternative assumption, redox conditions in the near field in variant case **PD-NFSLV** are assumed to be determined by the corrosion products of the supercontainer steel shell. In particular, an equilibrium in buffer porewater between magnetite and siderite in a system of corroding iron is assumed, which gives an Eh of –202 mV vs. SHE for the dilute/brackish water system with a bentonite water pH of 7.4 /Grivé et al. 2007/. Although the redox conditions in the Base Case and the variant case PD-NFSLV are essentially the same, the less negative Eh value assumed in PD-NFSLV gives some significant differences in calculated solubilities for some elements. In particular, U and Mo solubilities are higher in case **PD-NFSLV** compared with the Base Case, and Se and Pu solubilities are lower (calculated Tc solubility remains constant and very low until the Eh vs. SHE is greater than zero).

5.10.2 Radionuclide inventories, half-lives and partitioning

Radionuclide inventories and half-lives and partitioning between fuel matrix, IRF, Zircaloy and other metal parts are as in the Base Case in cases PD-NFSLV and PD-BCC, and are given in Table 5-2 (inventories of stable nuclides in Table 5-3). Values for case PD-VVERC and PD-EPRC are the same as in cases PD-VVER and PD-EPR and are given in Tables 5-12 and 5-13, respectively. For these cases, the inventories of stable nuclides are given in Table 5-14.

5.10.3 Near-field model

The geometry of the near-field model domain is as in the Base Case (see Figure 5-1 and Table 5-4).

Parameter values related to:

- water ingress;
- radionuclide release; and
- evolution of the defect;

are as in the Base Case, and are given in Tables 5-5 to 5-7. As in the Base Case, I, Cl, Se and Mo are treated as anionic when assigning porosities and effective diffusion coefficients in the buffer, with remaining elements being treated as neutral and cationic species, based on expert judgement, supported by the speciation calculations given in Appendix D and in /Grivé et al. 2007/. Nb is treated as anionic in case PD-BCN, and is assumed not to sorb on buffer pore surfaces. Near-field model boundary conditions and transfer coefficients are also unchanged with respect to the Base Case.

Near-field solubilities for case PD-NFSLV are given in Table 5-27. As in the Base Case, values are based on estimates by /Grivé et al. 2007/. Of the redox-sensitive elements, Se and Pu have lower solubilities in case PD-NFSLV compared with the Base Case, whereas Mo and U have higher solubilities in case PD-NFSLV compared with the Base Case. Near-field solubilities for cases PD-BCC, PD-BCN, PD-VVERC and PD-EPRC are as in the Base Case (Table 5-6).

5.10.4 Geosphere model

Because Nb is assumed to be anionic in the geosphere in case PD-BCN, the K_d value for Nb is reduced by a factor of 20 with respect to its value in TILA-99, as given in Table 5-10, where it was considered to be present as neutral or cationic species in the geosphere.

In cases PD-BCC, PD-VVERC and PD-EPRC, C is assumed to be transported in the geosphere as carbonate and to sorb in the geosphere with a K_d of 0.0001 $m^3\ kg^{-1}$, which is the value assumed in TILA-99 (Table 11-9 in /Vieno and Nordman 1999/; conservative value, applicable

Table 5-27. Near-field solubilities for case PD-NFSLV addressing uncertainties in the redox state of the near field. Values are for a system with an Eh vs. SHE of –202 mV, compared with –230 mV in the Base Case. Further details on oxidation states, speciation and uncertainties are presented in Appendix E, Table E-2.

Element	Solubility [mol dm^{-3}]	Element	Solubility [mol dm^{-3}]
Am	BC	Pd	BC
C	BC	Pu	3.7×10^{-7}
Cl	BC	Ra	BC
Cm	BC	Th	BC
Cs	BC	Se	1.0×10^{-10}
I	BC	Sm	BC
Mo	2.4×10^{-8}	Sn	BC
Ni	BC	Sr	BC
Nb	BC	Tc	BC
Np	BC	U	3.3×10^{-9}
Pa	BC	Zr	BC

Note: BC indicates that the values are the same as in the Base Case (Table 5-5).

in non-saline and saline groundwaters and in both oxidizing and reducing conditions). The porosity and effective diffusion coefficient used to calculate C transport in these cases are those for anions in Table 5-9. Otherwise, the geosphere model is again as in the Base Case.

The geosphere model for case PD-NFSLV is as in the Base Case. Parameter values that apply to all migrating species are given in Table 5-8. Element-dependent parameters are given in Tables 5-9 and 5-10. As in the Base Case, geosphere solubilities are not applied (in effect, geosphere solubilities are assumed to be greater than or equal to those in the near field).

5.10.5 Results

Figure 5-34 shows the Nb-94 releases from the geosphere to the biosphere as a function of time in the Base Case and in cases PD-BCN and in the Base Case (PD-BC) expressed as WELL-2007 dose based on the dose conversion factors given in Table 3-1. Figure 5-35 shows time-dependent releases of Nb-94 from the geosphere to the biosphere in the same two cases, divided by the geo-bio flux constraint specified by the Finnish regulator and given in Table 1-1.

The assumption that Nb-94 is anionic and does not sorb on buffer pore surfaces in case PD-BCN results in an earlier and higher Nb-94 dose maximum. The release maximum is higher by almost three orders of magnitude in case PD-BCN compared with case PD-BC. The well-2007 dose is, however, still almost six orders of magnitude below the regulatory guideline, and the release to the biosphere divided by the geo-bio flux constraint for Nb-94 almost five orders of magnitude below the regulatory guideline, in case PD-BCN.

Figure 5-36 shows the C-14 releases from the geosphere to the biosphere as a function of time in cases PD-BCC, PD-VVERC and PD-EPRC expressed as WELL-2007 dose based on the dose conversion factors given in Table 3-1. Figure 5-37 shows time-dependent releases of C-14 from the geosphere to the biosphere in the same three cases, divided by the geo-bio flux constraint specified by the Finnish regulator and given in Table 1-1. In the two figures, comparison is made with cases PD-BC, PD-VVER and PD-EPR, in which there is no C-14 sorption in the geosphere.

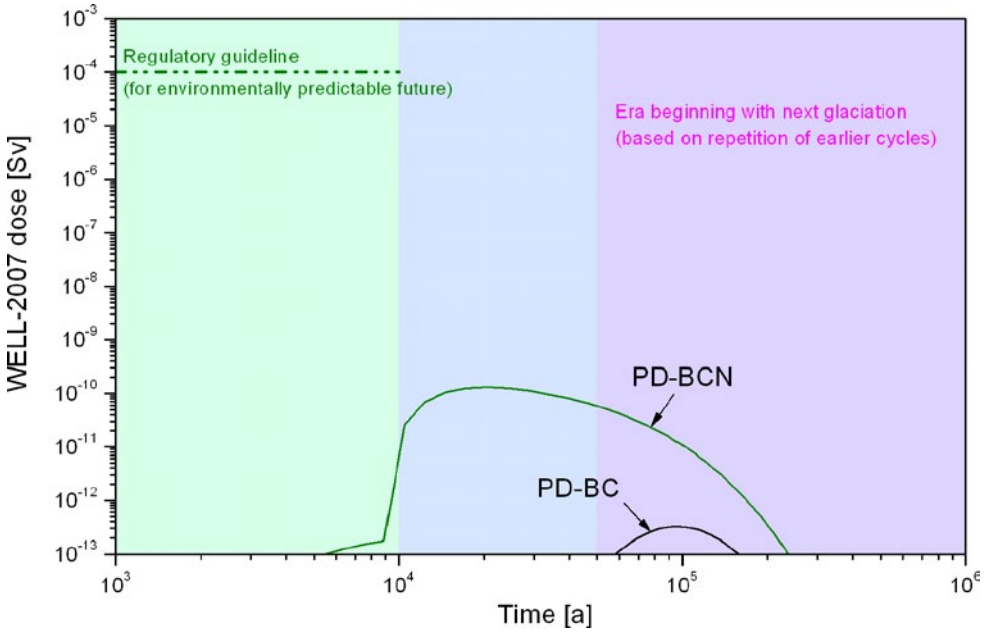

Figure 5-34. *WELL-2007 Nb-94 dose as a function of time in the Base Case (PD-BC) and in cases PD-BCN.*

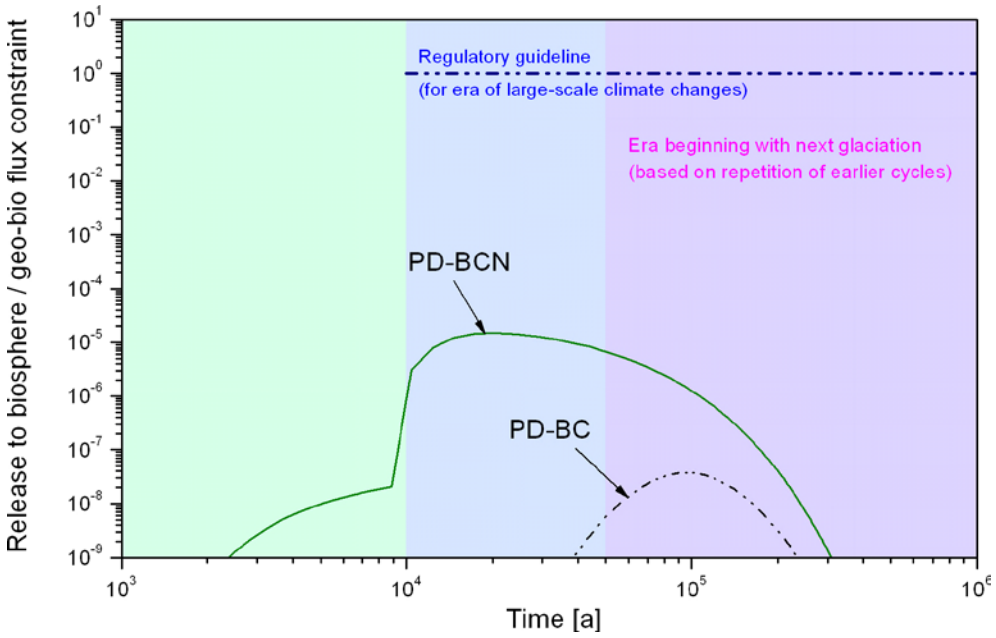

Figure 5-35. *Ratios of Nb-93 activity release to the geo-bio flux constraint in the Base Case (PD-BC) and in case PD-BCN.*

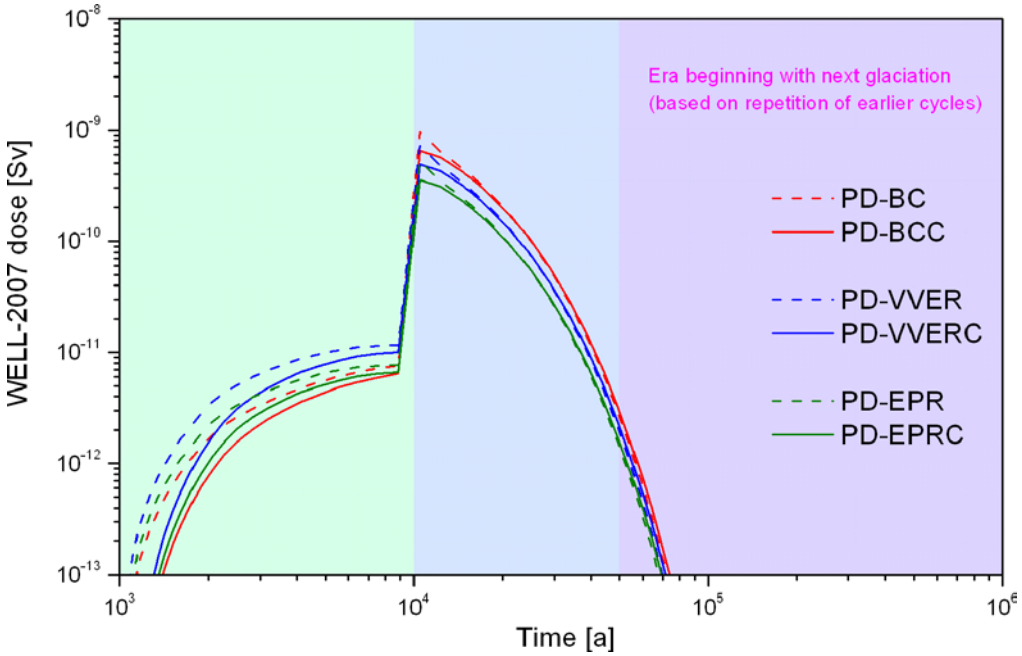

Figure 5-36. *WELL-2007 C-14 dose as a function of time in the Base Case (PD-BC) and in cases PD-BCC, PD-VVER, PD-VVERC, PD-EPR and PD-EPRC.*

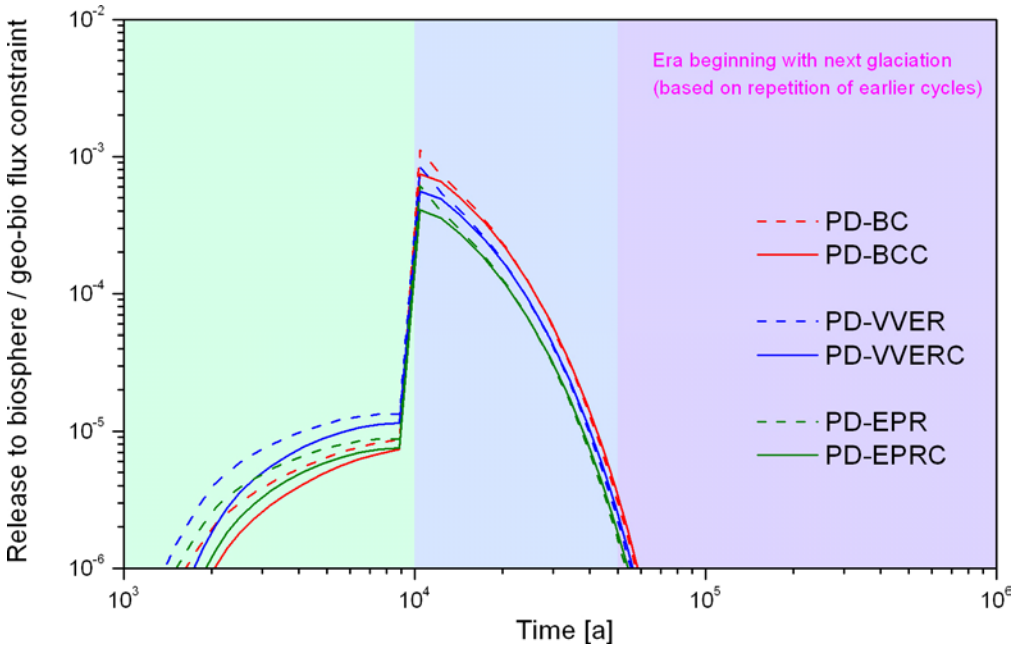

Figure 5-37. *Ratios of C-14 activity release to the geo-bio flux constraint in the Base Case (PD-BC) and in cases PD-BCC, PD-VVER, PD-VVERC, PD-EPR and PD-EPRC.*

The small additional retardation due to sorption in the geosphere (K_d = 0.0001 m^3 kg^{-1}) in cases PD-BCC, PD-VVERC and PD-EPRC has very little impact. The maxima occur at the same time as in the cases without geosphere sorption but there is a small reduction in the magnitude of releases to the biosphere.

Table 5-28 gives calculated maximum near-field release rates in Bq per year for each radionuclide in the Base Case for an initial penetrating defect (case PD-BC) and in case PD-NFSLV, indicating where there are differences with respect to the Base Case.

Solubility limits are different for Se, Mo, U and Pu in the two cases. However, in neither case do Pu concentrations in solution reach the Pu solubility limit, and the release maxima of Pu isotopes are unchanged in case PD-NFSLV compared with the Base Case. Mo solubility is reduced from 2.6 × 10^{-8} mol. dm^{-3} in the Base Case to 2.4 × 10^{-8} mol. dm^{-3} in case PD-NFSLV, giving a small decrease in the maximum near-field release rate. The solubility of Se is reduced by about a factor of three from 3.1 × 10^{-10} mol. dm^{-3} in the Base Case to 1.0 × 10^{-10} mol. dm^{-3} in case PD-NFSLV, giving a corresponding factor of three decrease in the maximum near-field release rate. U solubility is increased by more than a factor of three from 9.5 × 10^{-10} mol. dm^{-3} in the Base Case to 3.3 × 10^{-9} mol dm^{-3} in case PD-NFSLV, giving a corresponding factor of more than three increase in the release rates of U-238, U-234, U-235 and U-236. The maximum release rate of U-233 is virtually unchanged with respect to the Base Case, since U-233 release is dominated by radioactive ingrowth from its parent Np-237.

Figure 5-38 shows the releases of Se-79, Mo-93 and various U isotopes from the geosphere to the biosphere as functions of time the two cases expressed as WELL-2007 dose based on the dose conversion factors given in Table 3-1. Figure 5-39 shows time-dependent releases from the geosphere to the biosphere divided by the geo-bio flux constraints specified by the Finnish regulator and given in Table 1-1, and the sum of these releases over all radionuclides for which calculations were made. The figures confirm that Mo-93 release is virtually unchanged in the two cases, that the release of Se-79 is reduced by a factor of about three, and that the releases of U isotopes (with the exception of U-233) are increased by a similar factor.

Table 5-28. Calculated maximum near-field release rates for each radionuclide in the Base Case for an initial penetrating defect (case PD-BC) and in case PD-NFSLV. BC indicates same value as in the Base Case. Full results are presented in Appendix G.

Radionuclide			Base Case (PD-BC)		PD-NFSLV	
			t_{max} [a]	Bq/a	t_{max} [a]	Bq/a
Activation/fission products		C-14	1.01E+04	6.77E+05	BC	BC
		Cl-36	1.03E+04	1.10E+05	BC	BC
		Ni-59	1.23E+04	3.44E+05	BC	BC
		Se-79	2.15E+04	2.08E–01	2.15E+04	6.70E–02
		Mo-93	1.08E+04	3.67E–01	1.08E+04	3.39E–01
		Zr-93	2.20E+05	5.03E–02	BC	BC
		Zr-93p*	2.35E+05	3.68E+00	BC	BC
		Nb-94	1.99E+04	7.70E+03	BC	BC
		Tc-99	8.85E+05	2.25E+01	BC	BC
		Pd-107	8.90E+05	3.02E+01	BC	BC
		Sn-126	1.15E+05	4.84E+00	BC	BC
		I-129	1.03E+04	1.27E+04	BC	BC
		Cs-135	1.01E+04	7.78E+03	BC	BC
Actinide chains	4N	Pu-240	3.44E+04	1.65E+01	BC	BC
		U-236	1.00E+06	5.79E–04	9.99E+05	2.01E–03
	4N + 1	Cm-245	5.38E+04	6.05E–04	BC	BC
		Am-241	5.38E+04	6.38E–04	BC	BC
		Np-237	1.00E+06	8.21E–01	BC	BC
		U-233	1.00E+06	1.30E+00	BC	BC
		Th-229	1.00E+06	7.65E–01	BC	BC
	4N + 2	Cm-246	3.88E+04	6.19E–06	BC	BC
		Pu-242	3.94E+05	3.01E+01	BC	BC
		U-238	1.00E+06	4.95E–04	9.99E+05	1.72E–03
		U-234	1.29E+05	2.02E–03	1.34E+05	7.02E–03
		Th-230	5.64E+05	2.77E+01	BC	BC
		Ra-226	5.64E+05	3.59E+04	BC	BC
	4N + 3	Am-243	4.88E+04	4.05E–02	BC	BC
		Pu-239	5.88E+04	2.21E+02	BC	BC
		U-235	1.00E+06	3.60E–05	9.94E+05	1.25E–04
		Pa-231	1.00E+06	3.27E+01	BC	BC

* Zirconium originating from the fuel matrix only.

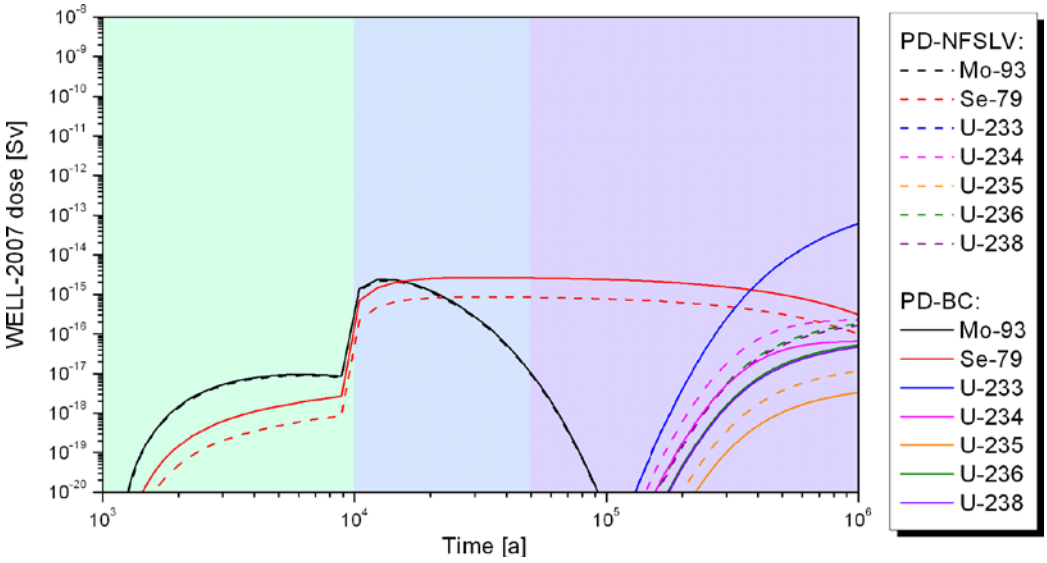

Figure 5-38. *WELL-2007 dose as a function of time in case PD-NFSLV.*

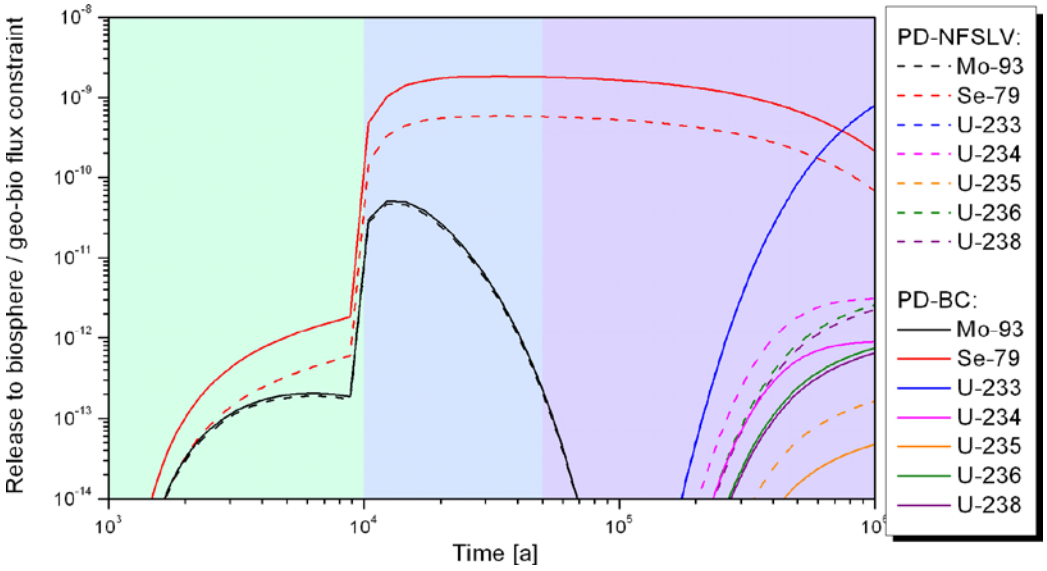

Figure 5-39. *Ratios of nuclide-specific activity releases to their respective geo-bio flux constraints in case PD-NFSLV.*

5.11 Case addressing variability in groundwater salinity

5.11.1 Differences compared with the Base Case

Groundwater salinity affects geochemical retention in the host rock. If also affects bentonite water composition, and hence it affects retention processes in the buffer. Furthermore, a sufficient reduction in salinity can lead to the possibility of significant buffer erosion by flowing groundwater, potentially leading to canister failure by corrosion and subsequently increased radionuclide transport rates from the failed canister to the geosphere (see Chapter 6).

Groundwater salinity is expected to vary considerably over time. There is currently about 12 g per litre of total dissolved solids (TDS) at repository depth (420 m below ground) at Olkiluoto, which, according to the results of modelling of groundwater flow and composition, may rise transiently to around 25 g per litre as a result of the upconing associated with excavations, before decreasing again as a result of land uplift (Figure 6-19 of /Pastina and Hellä 2006/ and Figure 4-1 of the Evolution Report, /Smith et al. 2007a/). A transient reduction in salinity in association with glacial retreat is also possible (and is one of the scenarios identified as potentially leading to canister failure by corrosion in a million year time frame – see Chapter 6). Ongoing site characterisation work is exploring whether or not such transient reduction in salinity has happened in the past.

Variability of salinity in time is not explicitly modelled in radionuclide release and transport calculations (except for a step change in case PD-GMWC – see below). In the Base Case, groundwater conditions are assumed to be reducing and dilute/brackish at all times. In case **PD-SAL**, reducing and brackish/saline groundwater is assumed (comparable in salinity to the present-day groundwater at repository depth). In case **PD-HISAL**, reducing and saline water is assumed, which covers, for example, the impact of upconing (these Olkiluoto groundwaters are described in Appendix D). In both cases, these waters are assumed to be in equilibrium with bentonite porewater. Cases **PD-GMW**, **PD-GMWV**, **PD-GMWC** consider a change from reference (dilute/brackish) water to glacial meltwater at repository depth.

Large uncertainties exist with respect to the composition of glacial meltwater that could potentially penetrate at repository depth. To address these uncertainties, two alternative glacial meltwater compositions are considered, one in cases PD-GMW and PD-GMWC and another in case PD-GMWV. PD-GMW and PD-GMWC consider dilute granitic groundwater from ice melting at Grimsel, Switzerland, sampled at the Grimsel Test Site, as an analogue for the dilute groundwater composition expected from ice melting processes (the "ice melting groundwater" used in SR-Can, as described in /Duro et al. 2006/). It has a pH of 9.6 and an Eh of –200 mV. PD-GMWV considers the estimated Quaternary glacial melt water composition expected from ice melting processes. This is the "glacial meltwater" described in /Pitkänen et al. 2004/, which accounts for the fact that pyrite/pyrrhotite are very common in fractures at Olkiluoto and that pyrite dissolution due to oxygen present in the glacial meltwater will result in a lower pH than is the case if only calcite equilibrium is considered. The glacial meltwater in this case has an assumed pH of 5.8 and an Eh of –136 mV, the redox state being determined (as in the Base Case) the magnetite/hematite equilibrium at a pH_2 of 10^{-7} atm. The chemical compositions of both groundwaters are given in Appendix D, Table D-3.

The next glacial retreat, and hence the next possibility for penetration of glacial meltwater to repository depth, is expected in 70,000 years time, based on a repetition of previous glacial cycles (see Chapter 7 of the Evolution Report, /Smith et al. 2007a/ and Chapter 5 of /Pastina and Hellä 2006/), and this is the time at which the change in groundwater composition at repository depth is assumed to occur. Canister failure (water ingress through the penetrating defect) is also assumed to occur at 70,000 years in cases PD-GMW and PD-GMWV, with loss of transport resistance of the defect 9,000 years later. Since there is no radionuclide release in the first 70,000 years, the change in groundwater composition at 70,000 years is not explicitly modelled in these cases. In case PD-GWMC, there is assumed to be an initial penetrating defect that allows water ingress and radionuclide release after 1,000 years, as in the Base Case. The change in groundwater composition at 70,000 years is, therefore, explicitly modelled in this case.

Glacial meltwater is assumed to be reducing when it reaches repository depth, but sorption of released radionuclides along geosphere transport paths is evaluated based on the assumption that conditions along these paths are predominantly oxidising. Although infiltrating meltwater will contain dissolved oxygen, the intrusion of oxygen dissolved in glacial meltwater to repository depth is unlikely due to possible microbial consumption of oxygen and the interaction of oxygen with fracture minerals in the geosphere. Furthermore, recent interpretation of hydrogeochemical site data, and especially gas data, from Olkiluoto give no evidence for such intrusion in the past (Section 7.3.5 of /Smith et al. 2007a/), although more information to support this tentative finding will be sought in future studies. Reducing conditions will also be favoured by the iron present in the near field (especially the canister insert). It is therefore assumed that reducing conditions are present within and around the repository.

No modification of the glacial meltwater due to interaction with the buffer has been considered in any of these cases, (although the buffer is still assumed to be present and not eroded away).

5.11.2 Radionuclide inventories, half-lives and partitioning

Radionuclide inventories, half-lives and partitioning between fuel matrix, IRF, Zircaloy and other metal parts are as in the Base Case, and are given in Table 5-2.

5.11.3 Near-field model

The geometry of near-field model domain is as in the Base Case (see Figure 5-1 and Table 5-4).

As noted above, water ingress through the penetrating defect is assumed to occur at 70,000 years in cases PD-GMW and PD-GMWV, with loss of transport resistance of the defect 9,000 years later. Otherwise, parameter values related to:

- water ingress; and
- radionuclide release;

are as in the Base Case and are given in Table 5-5.

In cases PD-SAL, PD-HISAL and PD-GMWV, as in the Base Case, I, Cl, Se and Mo are treated as anionic when assigning porosities and effective diffusion coefficients in the buffer, with remaining elements being treated as neutral and cationic species, based on expert judgement, supported by the speciation calculations given in Appendix E and in /Grivé et al. 2007/. In cases PD-GMW and (PD-GMWC after 70,000 years), again based on speciation calculations, Sn, Sm, Am and Cm are also considered to be predominantly anionic in the near field, but neutral in the geosphere. The speciation calculations also indicate that Th and Nb are anionic in the near field, but, as in the Base Case, Th and Nb are treated as neutral species in the assessment cases. As noted in Section 5.2.3, Th speciation and Nb speciation are particularly uncertain, because of limited thermodynamic data for Nb and limited data for the dominating anionic hydroxyl carbonate Th complexes. Both of Th and Nb are reported to sorb in clays and thus should be present in non-anionic form; see the further discussions in Appendix E.

In cases PD-SAL and PD-GMWV, buffer sorption coefficients are also as in the Base Case. Values are given in Table 5-7. K_d values for use in the other cases are given in Table 5-29. In case PD-HISAL, these are based on the lower limit values given in Table A-13 of the SR-Can Data Report /SKB 2006b/. In cases PD-GMW (and PD-GMWC after 70,000 years) the K_d values of Sn, Sm, Am and Cm are set to zero, which conservatively takes account of their anionic form.

In cases PD-GMW and PD-GMWV, a transport pathway from the canister interior to the buffer is assumed to form at 70,000 years (coinciding with an influx of glacial meltwater to repository depth), compared with 1,000 years in the Base Case and in Case PD-GMWC. In all cases, the canister is assumed to lose its transport resistance after a further 9,000 years (see Table 5-5).

Table 5-29. Sorption coefficients (K_d values) for the near field in cases PD-SAL, PD-HISAL, PD-GMW, PD-GMWV and PD-GMWC (after 70,000 years); BC = Base Case value.

	K_d [m^3 kg^{-1}] PD-SAL and D-GMWV	PD-HISAL	PD-GMW and PD-GMWC		K_d [m^3 kg^{-1}] PD-SAL and PD-GMWV	PD-HISAL	PD-GMW and PD-GMWC
Am		4	0	Pd		BC	BC
C		BC	BC	Pu		2	BC
Cl		BC	BC	Ra		0.0002	BC
Cm		4	0	Th		4	BC
Cs		0.006	BC	Se		BC	BC
I	All BC	BC	BC	Sm	All BC	0.5	0
Mo		BC	(*)	Sn		1.4	0
Ni		0.01	BC	Sr		0.0002	BC
Nb		BC	BC	Tc		1.4	BC
Np		2	BC	U		BC	BC
Pa		BC	BC	Zr		0.2	BC

* Not calculated in these cases because of the short half-life of Mo-93 (4,000 years).

Near-field solubilities for cases PD-SAL, PD-HISAL and PD-GMW, PD-GMWV and PD-GMWC are given in Table 5-30. As in the Base Case, values for PD-SAL and PD-HISAL are based on estimates by /Grivé et al. 2007/. In these cases, as in the Base Case, the redox state is determined by a long-term dynamic equilibrium between magnetite and hematite formed in the system around the corroding iron insert, with a pH_2 of 10^{-7} atm. The PD-SAL system has an Eh of –171 mV (vs. SHE) for a buffer porewater pH of 7.82, and the PD-HISAL system has an Eh of –160 mV (vs. SHE) for a buffer porewater pH of 7.66 (/Grivé et al. 2007/ and Appendix D, Table D-2).

For a few elements, there are significant differences between cases PD-GMW (and PD-GMWC) and PD-GMWV in the solubility values assigned. For Mo, for example, the large difference is due to the different solubility limiting solids, with $CaMoO_4$ assumed in case PD-GMW (and PD-GMWC) and MoO_2 assumed in case PD-GMWV. It should be noted, however, that the pH of near-field porewater will be buffered by the bentonite present, and is expected to be slightly alkaline, with a pH of around 8, which is nearer to the value in PD-GMW and PD-GMWC than that in PD-GMWV. It should also be noted that the glacial meltwater in case PD-GMWV has a very low ionic strength, which causes large uncertainties in the solubilities assigned. In particular, charge balance errors can occur due to the high solubility of the solid compared with the low ionic strength of the water.

5.11.4 Geosphere model

Geosphere parameter values that apply to all migrating species are as in the Base Case and are given in Table 5-8. Element-dependent porosities and effective diffusion coefficients for anions and for neutral and cationic species are given in Table 5-31. Values are taken from Table 11-10 in TILA-99. TILA-99 values for saline groundwater are adopted in Cases PD-SAL and PD-HISAL. TILA-99 values for non-saline groundwater are adopted for the glacial meltwater cases PD-GMW, PD-GMWV and PD-GMWC. In cases PD-SAL and PD-HISAL, as in the Base Case, Cl, Se, Mo and I are assumed to be present as anions. In addition, in cases PD-GMW, PD-GMWV and PD-GMWC, Tc, U, Pu and Np are also assumed to be present as anions. This is consistent with the treatment of geosphere migration in oxidising conditions in TILA-99.

Table 5-30. Near-field solubilities in cases PD-SAL, PD-HISAL, PD-GMW, PD-GMWV and PD-GMWC (after 70,000 years). Further details regarding oxidation states and speciation, as well as on uncertainties, are presented in Appendix E, Tables E-3 (PD-SAL), E-4 (PD-HISAL), E-5 (PD-GMW and PD-GMWC) and E-6 (PD-GMWV).

Element	Solubility [mol dm^{-3}]			
	PD-SAL	PD-HISAL	PD-GMW and PD-GMWC	PD-GMWV
Am	4.5×10^{-7}	9.2×10^{-7}	5.6×10^{-8}	5.3×10^{-9}
C	High	High	High	High
Cl	High	High	High	High
Cm	4.5×10^{-7}	9.2×10^{-7}	5.6×10^{-8}	5.3×10^{-9}
Cs	High	High	High	High
I	High	High	High	High
Mo	2.0×10^{-8}	9.2×10^{-9}	(*)	(*)
Nb	8.1×10^{-5}	6.2×10^{-5}	2.9×10^{-3}	1.5×10^{-5}
Ni	3.9×10^{-4}	7.4×10^{-4}	4.1×10^{-7}	High
Np	7.8×10^{-10}	7.2×10^{-10}	8.2×10^{-10}	1.3×10^{-9}
Pa	2.9×10^{-7}	2.8×10^{-7}	3.2×10^{-7}	3.3×10^{-7}
Pd	2.5×10^{-6}	2.8×10^{-6}	2.7×10^{-6}	2.7×10^{-6}
Pu	1.8×10^{-8}	2.9×10^{-8}	1.3×10^{-10}	8.3×10^{-9}
Ra	3.5×10^{-8}	5.9×10^{-8}	8.8×10^{-7}	7.1×10^{-5}
Se	1.2×10^{-9}	5.2×10^{-6}	4.5×10^{-11}	1.5×10^{-8}
Sm	2.1×10^{-8}	3.8×10^{-8}	1.8×10^{-9}	1.0×10^{-8}
Sn	1.2×10^{-7}	1.0×10^{-7}	2.7×10^{-6}	8.4×10^{-8}
Sr	1.9×10^{-4}	3.7×10^{-4}	1.1×10^{-5}	High
Tc	4.0×10^{-9}	4.0×10^{-9}	4.5×10^{-9}	4.0×10^{-9}
Th	9.8×10^{-10}	6.8×10^{-10}	8.1×10^{-10}	6.4×10^{-10}
U	6.5×10^{-10}	6.2×10^{-10}	2.3×10^{-9}	1.6×10^{-9}
Zr	1.7×10^{-8}	1.6×10^{-8}	1.8×10^{-8}	1.8×10^{-8}

* Not calculated in these cases because of the short half-life of Mo-93 (4,000 years).

Table 5-31. Geosphere matrix porosity and effective diffusion coefficients (based on Table 11-10 in /Vieno and Nordman 1999/).

Parameter	Distance from fracture	Species	Cases	Value
Porosity	0–1 cm	Anions	PD-SAL, PD-HISAL	0.2%
			PD-GMW, PD-GMWV	0.1%
		Neutral and cationic species	All cases	0.5%
	1–10 cm	Anions	PD-SAL, PD-HISAL	0.04%
			PD-GMW, PD-GMWV	0.02%
		Neutral and cationic species	All cases	0.1%
Effective diffusion coefficient	0–1 cm	Anions	PD-SAL, PD-HISAL	5×10^{-14} m^2 s^{-1}
			PD-GMW, PD-GMWV	1×10^{-14} m^2 s^{-1}
		Neutral and cationic species	All cases	10^{-13} m^2 s^{-1}
	1–10 cm	Anions	PD-SAL, PD-HISAL	5×10^{-15} m^2 s^{-1}
			PD-GMW, PD-GMWV	1×10^{-15} m^2 s^{-1}
		Neutral and cationic species	All cases	10^{-14} m^2 s^{-1}

Geosphere sorption coefficients (K_d values) are given in Table 5-32. Values are, for the most part, taken from Table 11-9 in TILA-99. TILA-99 conservative values for saline reducing conditions are adopted in cases PD-SAL and PD-HISAL. TILA-99 conservative values for non-saline oxidising groundwater are adopted for the glacial meltwater cases PD-GMW, PD-GMWV and PD-GMWC (for times after 70,000 years, with Base Case values used at earlier times). As in the Base Case, exceptions to the use of TILA-99 data are C and Mo. For C, Base Case K_d values are used. For Mo, the K_d value has been reduced by a factor of 5 in the saline groundwaters as compared to the Base Case. The K_d value for Mo should, in principle, also be adjusted downwards to take account of the altered redox conditions in glacial meltwater. However, the half-life of Mo-93 (4,000 years) is much less than the earliest time at which glacial meltwater is assumed to enter the geosphere (70,000 years), and thus release and transport of Mo-93 is not calculated in cases PD-GMW, PD-GMWV and PD-GMWC.

5.11.5 Results

Table 5-33 gives calculated maximum near-field release rates in Bq per year for each radionuclide in the Base Case for an initial penetrating defect (case PD-BC) and in cases PD-SAL and PD-HISAL, indicating where there are differences with respect to the Base Case. It also gives the times at which the maxima occur (t_{max}).

Figure 5-40 shows the releases from the geosphere to the biosphere as a function of time in cases PD-SAL and PD-HISAL expressed as WELL-2007 dose based on the dose conversion factors given in Table 3-1. Figure 5-41 shows time-dependent releases from the geosphere to the biosphere divided by the geo-bio flux constraints specified by the Finnish regulator and given in Table 1-1, and the sum of these releases over all calculated radionuclides. Total doses and summed releases in both cases are virtually unchanged compared with the Base Case. There are some changes, however, in the release rates of certain radionuclides that make only minor contributions to the total doses and summed releases. The near-field and geosphere releases of Se-79 are, for example, significantly higher in PD-HISAL compared with either PD-SAL or the Base Case. This is attributable to the much higher solubility of Se in PD-HISAL compared with the other two cases (Table 5-30).

Table 5-32. Geosphere sorption coefficients (K_d values) in cases PD-SAL, PD-HISAL, PD-GMW, PD-GMWV and PD-GMWC (after 70,000 years); BC = Base Case value.

	K_d [m^3 kg^{-1}]			K_d [m^3 kg^{-1}]	
	PD-SAL, PD-HISAL	PD-GMW, PD-GMWV, PD-GMWC		PD-SAL, PD-HISAL	PD-GMW, PD-GMWV, PD-GMWC
Am	BC	BC	Pd	0.0001	BC
C	BC	BC	Pu	BC	0.2
Cl	BC	BC	Ra	0.02	BC
Cm	BC	BC	Th	BC	BC
Cs	0.01	BC	Se	0.0001	BC
I	BC	BC	Sm	BC	BC
Mo	0.0001	(*)	Sn	0.0001	BC
Ni	0.005	BC	Sr	0.0001	BC
Nb	BC	BC	Tc	BC	0
Np	BC	0.002	U	BC	0.001
Pa	BC	BC	Zr	BC	BC

* Not calculated in these cases because of the short half-life of Mo-93 (4,000 years).

Table 5-33. Calculated maximum near-field release rates for each radionuclide in the Base Case for an initial penetrating defect (case PD-BC) and in cases PD-SAL and PD-HISAL. BC indicates same value as in the Base Case. Full results are presented in Appendix G.

Radionuclide			Base Case (PD-BC)		PD-SAL		PD-HISAL	
			t_{max} [a]	Bq/a	t_{max} [a]	Bq/a	t_{max} [a]	Bq/a
Activation/fission products		C-14	1.01E+04	6.77E+05	BC	BC	BC	BC
		Cl-36	1.03E+04	1.10E+05	BC	BC	BC	BC
		Ni-59	1.23E+04	3.44E+05	2.58E+04	5.21E+04	2.15E+04	1.13E+05
		Se-79	2.15E+04	2.08E–01	2.15E+04	8.04E–01	1.03E+04	1.36E+03
		Mo-93	1.08E+04	3.67E–01	1.08E+04	2.82E–01	1.08E+04	1.30E–01
		Zr-93	2.20E+05	5.03E–02	BC	BC	2.25E+05	4.42E–02
		Zr-93p*	2.35E+05	3.68E+00	BC	BC	2.45E+05	3.23E+00
		Nb-94	1.99E+04	7.70E+03	1.46E+04	1.16E+04	1.62E+04	1.06E+04
		Tc-99	8.85E+05	2.25E+01	8.85E+05	2.14E+01	8.90E+05	2.57E+01
		Pd-107	8.90E+05	3.02E+01	BC	BC	BC	BC
		Sn-126	1.15E+05	4.84E+00	BC	BC	1.05E+05	7.04E+00
		I-129	1.03E+04	1.27E+04	BC	BC	BC	BC
		Cs-135	1.01E+04	7.78E+03	BC	BC	1.01E+04	1.68E+04
Actinide chains	4N	Pu-240	3.44E+04	1.65E+01	3.88E+04	3.19E+00	3.07E+04	2.39E+01
		U-236	1.00E+06	5.79E–04	1.00E+06	3.96E–04	1.00E+06	3.78E–04
	4N + 1	Cm-245	5.38E+04	6.05E–04	BC	BC	3.88E+04	1.21E–02
		Am-241	5.38E+04	6.38E–04	BC	BC	3.88E+04	1.27E–02
		Np-237	1.00E+06	8.21E–01	1.00E+06	5.82E–01	1.00E+06	6.40E–01
		U-233	1.00E+06	1.30E+00	1.00E+06	9.25E–01	1.00E+06	5.74E–01
		Th-229	1.00E+06	7.65E–01	1.00E+06	1.78E–01	9.99E+05	2.68E–01
	4N + 2	Cm-246	3.88E+04	6.19E–06	BC	BC	3.07E+04	2.78E–04
		Pu-242	3.94E+05	3.01E+01	2.79E+05	3.11E+01	3.74E+05	4.96E+01
		U-238	1.00E+06	4.95E–04	9.99E+05	3.39E–04	1.00E+06	3.23E–04
		U-234	1.29E+05	2.02E–03	1.29E+05	1.38E–03	1.29E+05	1.32E–03
		Th-230	5.64E+05	2.77E+01	8.19E+05	4.48E+00	9.39E+05	4.27E+00
		Ra-226	5.64E+05	3.59E+04	5.74E+05	3.83E+04	5.74E+05	7.46E+04
	4N + 3	Am-243	4.88E+04	4.05E–02	BC	BC	3.44E+04	9.78E–01
		Pu-239	5.88E+04	2.21E+02	8.38E+04	7.33E+01	6.88E+04	2.54E+02
		U-235	1.00E+06	3.60E–05	9.99E+05	2.46E–05	1.00E+06	2.35E–05
		Pa-231	1.00E+06	3.27E+01	BC	BC	BC	BC

* Zirconium originating from the fuel matrix only.

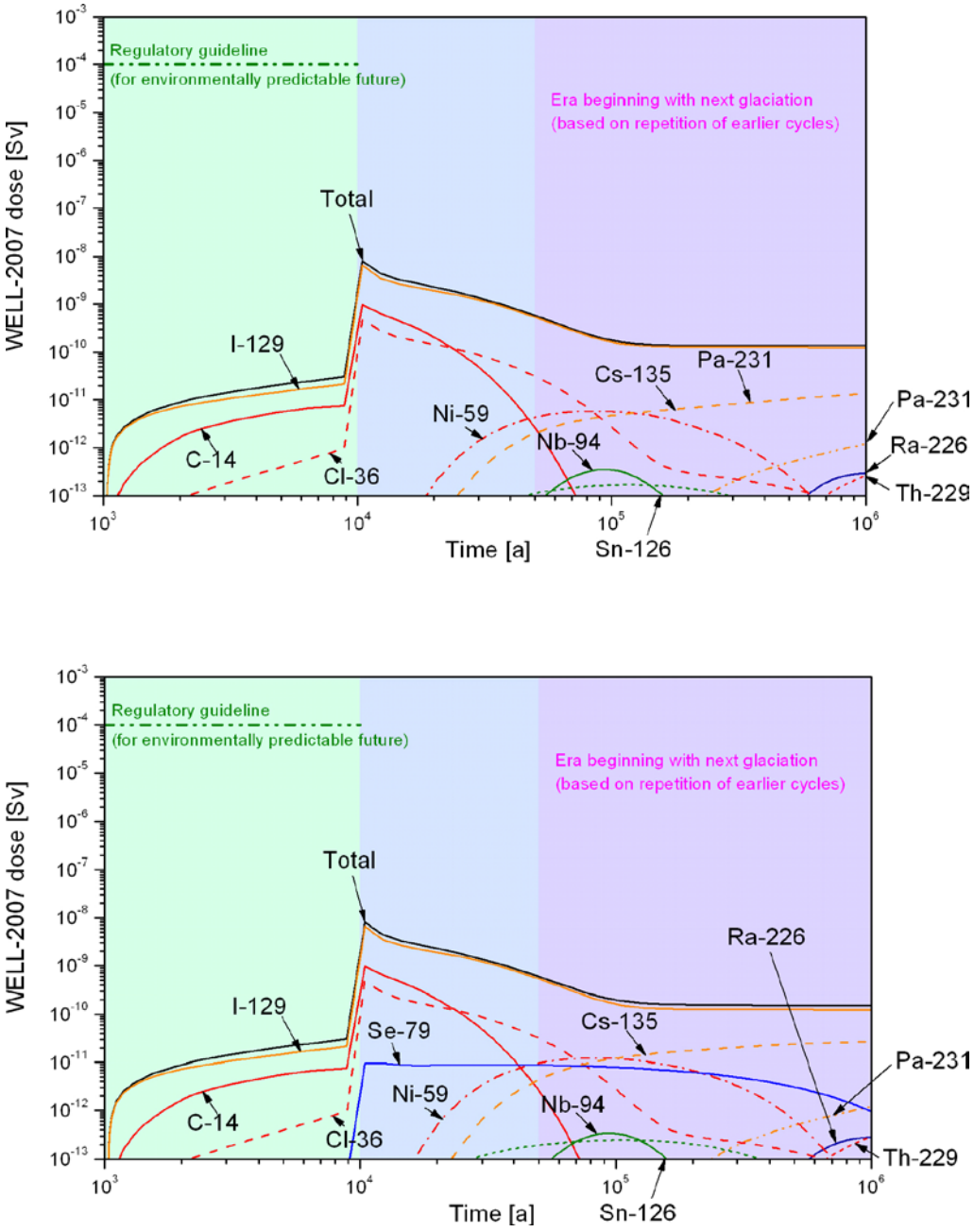

Figure 5-40. *WELL-2007 dose as a function of time in case PD-SAL (upper figure) and case PD-HISAL (lower figure).*

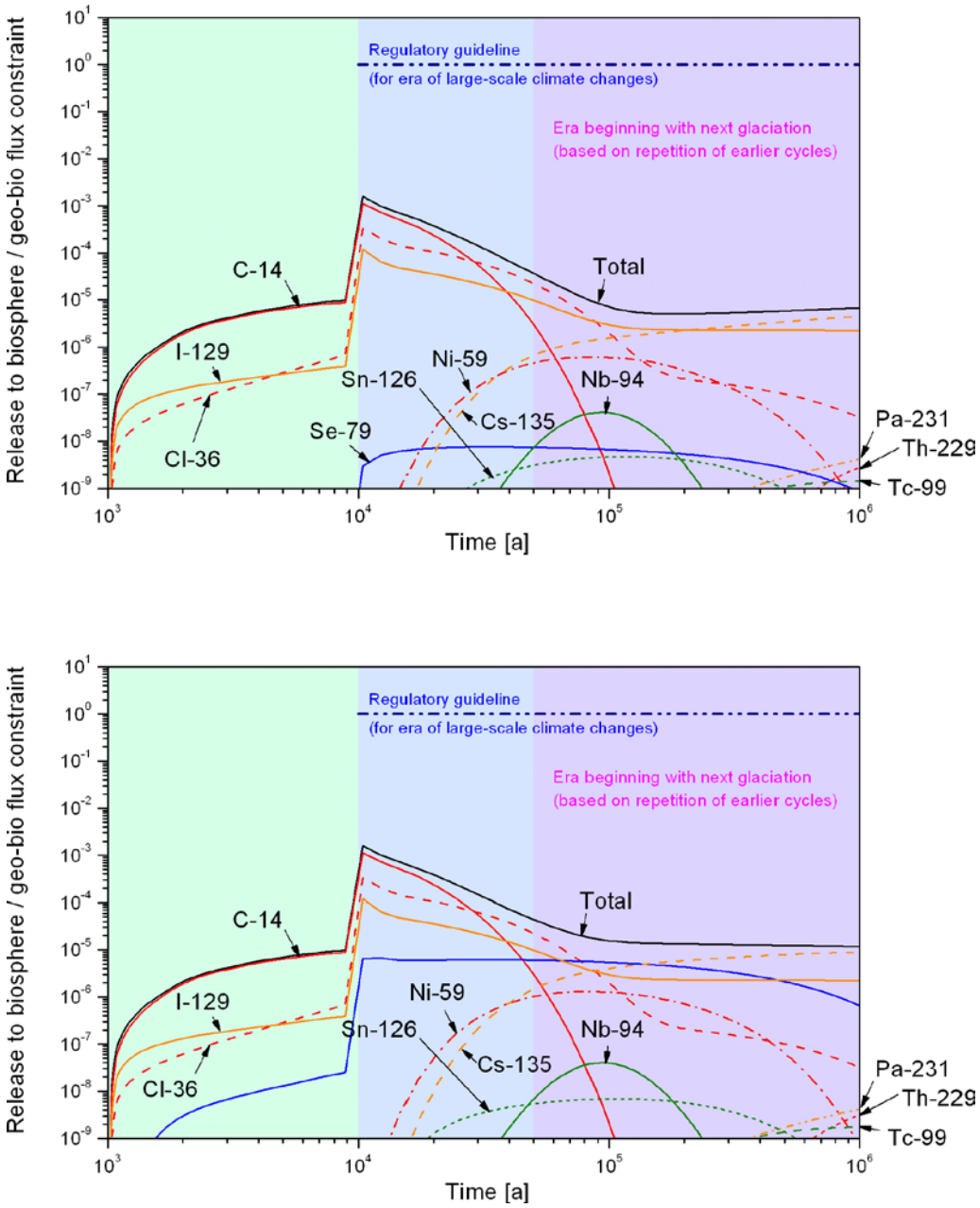

Figure 5-41. *Ratios of nuclide-specific activity releases to their respective geo-bio flux constraints in case PD-SAL (upper figure) and case PD-HISAL (lower figure).*

Figure 5-42 shows both the calculated annual landscape dose to the most exposed individual and the WELL-2007 dose in case PD-HISAL. As in the Base Case, the highest annual landscape dose occurs at the end of the 10,000 period over which biosphere modelling was carried out, and is less than 10^{-6} Sv, compared with about 10^{-8} Sv in the case of WELL-2007 dose.

Table 5-34 gives calculated maximum near-field release rates in Bq per year for each radionuclide in the Base Case for an initial penetrating defect (case PD-BC) and in cases PD-GMW, PD-GMWV and PD-GMWC. Again, it also gives the times at which these maxima occur (t_{max}). Figure 5-43 shows the releases from the geosphere to the biosphere as a function of time in cases PD-GMW and PD-GMWV expressed as WELL-2007 dose based on the dose conversion factors given in Table 3-1. Figure 5-44 shows time-dependent releases from the geosphere to the biosphere in the same cases, divided by the geo-bio flux constraints specified by the Finnish regulator and given in Table 1-1, and the sum of these releases over all radionuclides for which calculations were made.

As in the Base Case, the dose maxima in cases PD-GMW and PD-GMWV are dominated by I-129. Although the timing of the maxima is later than in the Base Case, the magnitude is little changed at about 4 orders of magnitude below the regulatory guideline. The sum of time-dependent releases from the geosphere to the biosphere divided by their respective geo-bio flux constraints has a maximum that is about three orders of magnitude below the regulatory guideline of one in all three cases. In both cases PD-GMW and PD-GMWV, it is dominated by Cl-36 and I-129, C-14 having substantially decayed by the time radionuclides are released from the canister. Cs-135 also makes a significant contribution at later times. Total doses and summed releases are virtually the same in both cases, although there are some differences in the release rates of certain radionuclides that make only minor contributions to the total doses and summed releases.

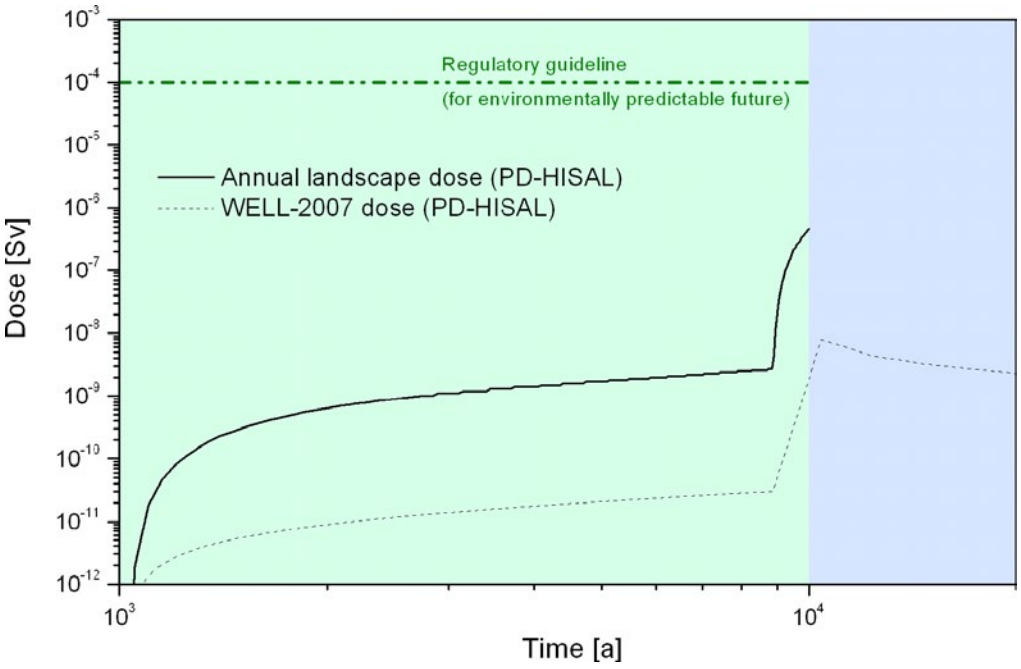

Figure 5-42. *Annual landscape dose and WELL-2007 dose as functions of time in case PD-HISAL.*

Table 5-34. Calculated maximum near-field release rates for each radionuclide in cases PD-GMW, PD-GMWV and PD-GMWC, and the times at which these maxima occur. Full results are presented in Appendix G.

Radionuclide			PD-GMW		PD-GMWV		PD-GMWC	
			t_{max} [a]	Bq/a	t_{max} [a]	Bq/a	t_{max} [a]	Bq/a
Activation/fission products		C-14	7.91E+04	1.54E+02	7.91E+04	1.54E+02	1.01E+04	6.77E+05
		Cl-36	7.93E+04	9.41E+04	7.93E+04	9.41E+04	1.03E+04	1.10E+05
		Ni-59	9.48E+04	3.02E+01	7.95E+04	2.99E+05	1.23E+04	3.44E+05
		Se-79	9.05E+04	2.60E–02	9.05E+04	8.66E+00	2.15E+04	2.08E–01
		Mo-93**	–	–	–	–	1.08E+04	3.67E–01
		Zr-93	2.89E+05	5.16E–02	2.89E+05	5.16E–02	2.20E+05	5.32E–02
		Zr-93p*	3.09E+05	3.79E+00	3.09E+05	3.79E+00	2.45E+05	3.89E+00
		Nb-94	8.08E+04	1.12E+03	9.25E+04	2.88E+02	1.99E+04	7.70E+03
		Tc-99	9.59E+05	2.41E+01	9.54E+05	2.14E+01	8.80E+05	2.41E+01
		Pd-107	9.59E+05	3.00E+01	9.59E+05	3.00E+01	8.90E+05	3.02E+01
		Sn-126	7.91E+04	5.50E+02	1.84E+05	3.00E+00	7.07E+04	5.74E+02
		I-129	7.93E+04	1.26E+04	7.93E+04	1.26E+04	1.03E+04	1.27E+04
		Cs-135	7.91E+04	7.62E+03	7.91E+04	7.62E+03	1.01E+04	7.78E+03
Actinide chains	4N	Pu-240	1.03E+05	6.58E–05	1.03E+05	4.20E–03	3.44E+04	1.65E+01
		U-236	1.07E+06	1.40E–03	1.00E+06	9.75E–04	9.95E+05	1.40E–03
	4N +1	Cm-245	7.91E+04	3.50E+00	1.23E+05	2.19E–06	7.07E+04	4.57E+01
		Am-241	7.91E+04	3.69E+00	1.23E+05	2.31E–06	7.07E+04	4.81E+01
		Np-237	1.07E+06	6.12E–01	1.00E+06	9.70E–01	1.00E+06	6.15E–01
		U-233	1.07E+06	9.74E–01	1.00E+06	1.54E+00	1.00E+06	9.84E–01
		Th-229	1.07E+06	1.64E–01	1.00E+06	1.93E–01	1.00E+06	1.65E–01
	4N + 2	Cm-246	7.91E+04	4.11E–03	1.08E+05	2.62E–10	7.07E+04	8.41E–02
		Pu-242	1.07E+06	3.82E–01	8.38E+05	2.37E+01	7.00E+04	1.06E+01
		U-238	1.07E+06	1.20E–03	1.00E+06	8.34E–04	1.00E+06	1.20E–03
		U-234	2.08E+05	3.86E–03	2.08E+05	2.68E–03	1.75E+05	3.58E–03
		Th-230	9.58E+05	3.70E+00	8.33E+05	2.93E+00	8.30E+05	3.70E+00
		Ra-226	1.07E+06	3.32E+04	1.00E+06	3.32E+04	5.70E+05	3.84E+04
	4N + 3	Am-243	7.91E+04	1.60E+02	1.18E+05	6.15E–05	7.07E+04	1.90E+03
		Pu-239	1.38E+05	2.37E–01	1.38E+05	1.52E+01	5.88E+04	2.21E+02
		U-235	1.07E+06	8.71E–05	1.00E+06	6.06E–05	1.00E+06	8.68E–05
		Pa-231	1.07E+06	3.27E+01	1.00E+06	3.27E+01	1.00E+06	3.27E+01

* Zirconium originating from the fuel matrix only.

** Molybdenum is not considered in cases PD-GMW and PD-GMWV because its half-life is about 4,000 years and after 70,000 years, when the calculations of cases PD-GMW and PD-GMWV start, it will have essentially completely decayed away.

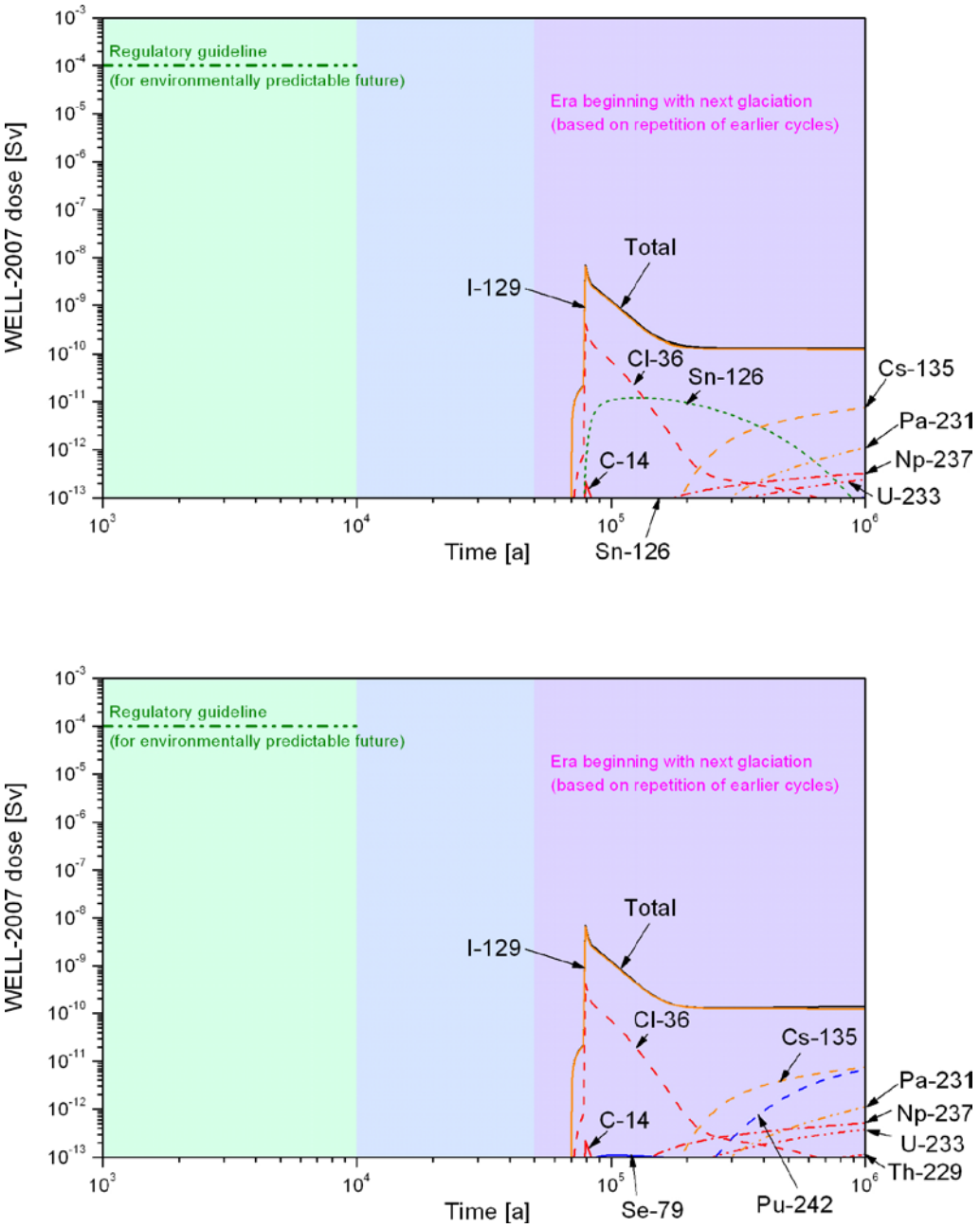

Figure 5-43. *WELL-2007 dose as a function of time in case PD-GMW (upper figure) and case PD-GMWV (lower figure).*

Sn-126 makes a larger contribution to both the near-field and geosphere releases in case PD-GMW compared with case PD-GMWV, which is attributable to its higher assumed solubility in buffer porewater in case PD-GMW compared with case PD-GMWV (Table 5-30). Pu-242, on the other hand, makes a larger contribution in case PD-GMWV than it does in case PD-GMW, because its solubility is higher in case PD-GMWV. Note that the solubility of Pu-242 in both cases is significantly lower than in the Base Case (Table 5-6), where Pu concentrations do not reach the Pu solubility limit. The near-field release maximum of Pu-242 is similar in case PD-GMWV and in the Base Case (indicating that the Pu solubility limit is also not reached in either of these cases) but higher by almost two orders of magnitude than the near-field release maximum in case PD-GMW. The lower release to the biosphere in the Base Case compared with case PD-GMWV is attributable to the lower geosphere sorption coefficient in the latter case (Table 5-32). The discussion of the Base Case in Section 5.2.5 indicates significant

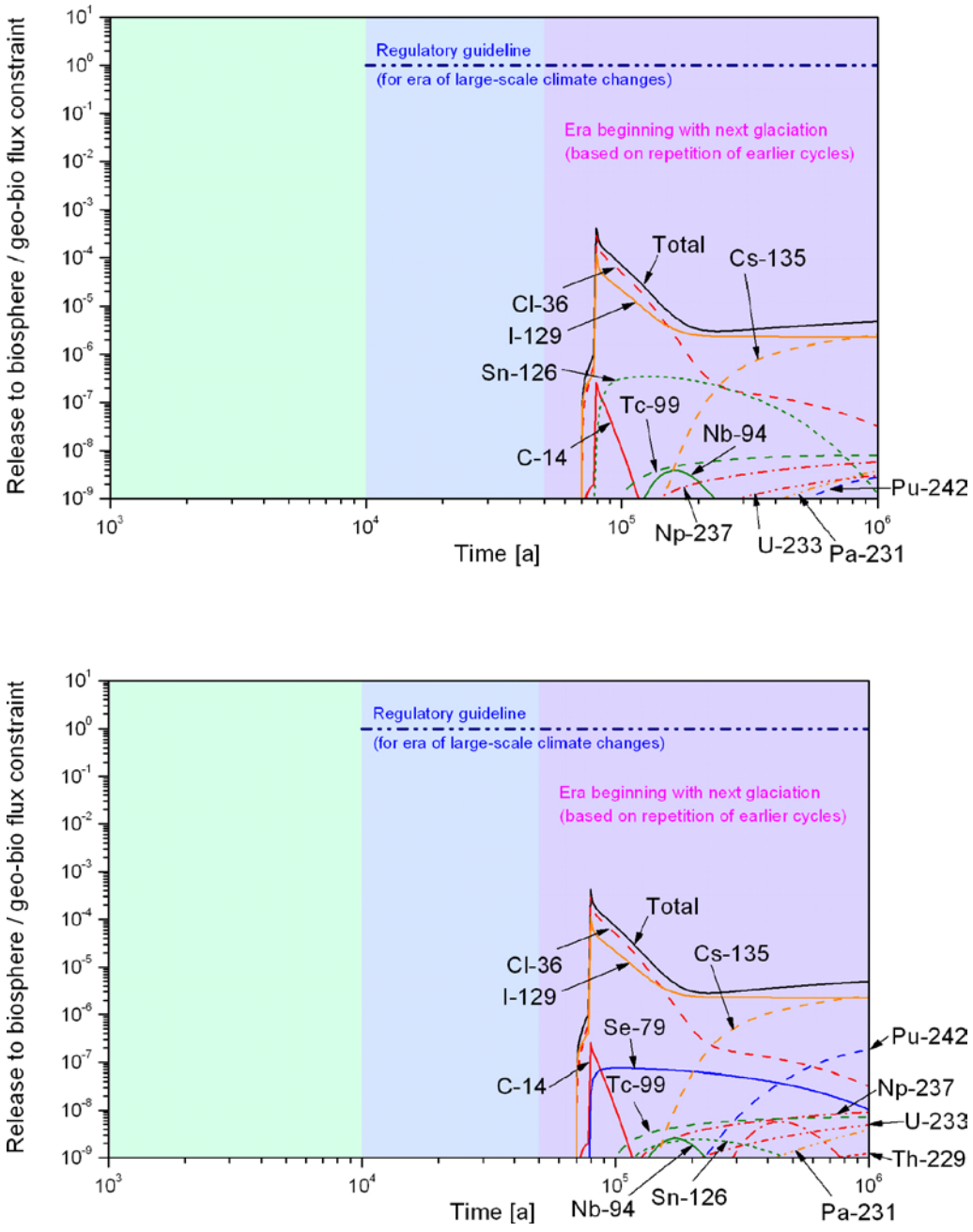

Figure 5-44. *Ratios of nuclide-specific activity releases to their respective geo-bio flux constraints in case PD-GMW (upper figure) and case PD-GMWV (lower figure).*

attenuation of Pu-242 release by radioactive decay during geosphere transport (see Figure 5-6), and the amount of decay during transport is expected to be sensitive to retardation of transport by sorption in the geosphere.

Figure 5-45 shows the releases from the geosphere to the biosphere as a function of time in the Base Case (PD-BC) and in case PD-GMWC, in which there is a transition to glacial meltwater at 70,000 years, expressed as WELL-2007 dose based on the dose conversion factors given in Table 3-1. Figure 5-46 shows time-dependent releases from the geosphere to the biosphere in the same cases, divided by the geo-bio flux constraints specified by the Finnish regulator and given in Table 1-1, and the sum of these releases over all radionuclides for which calculations were made.

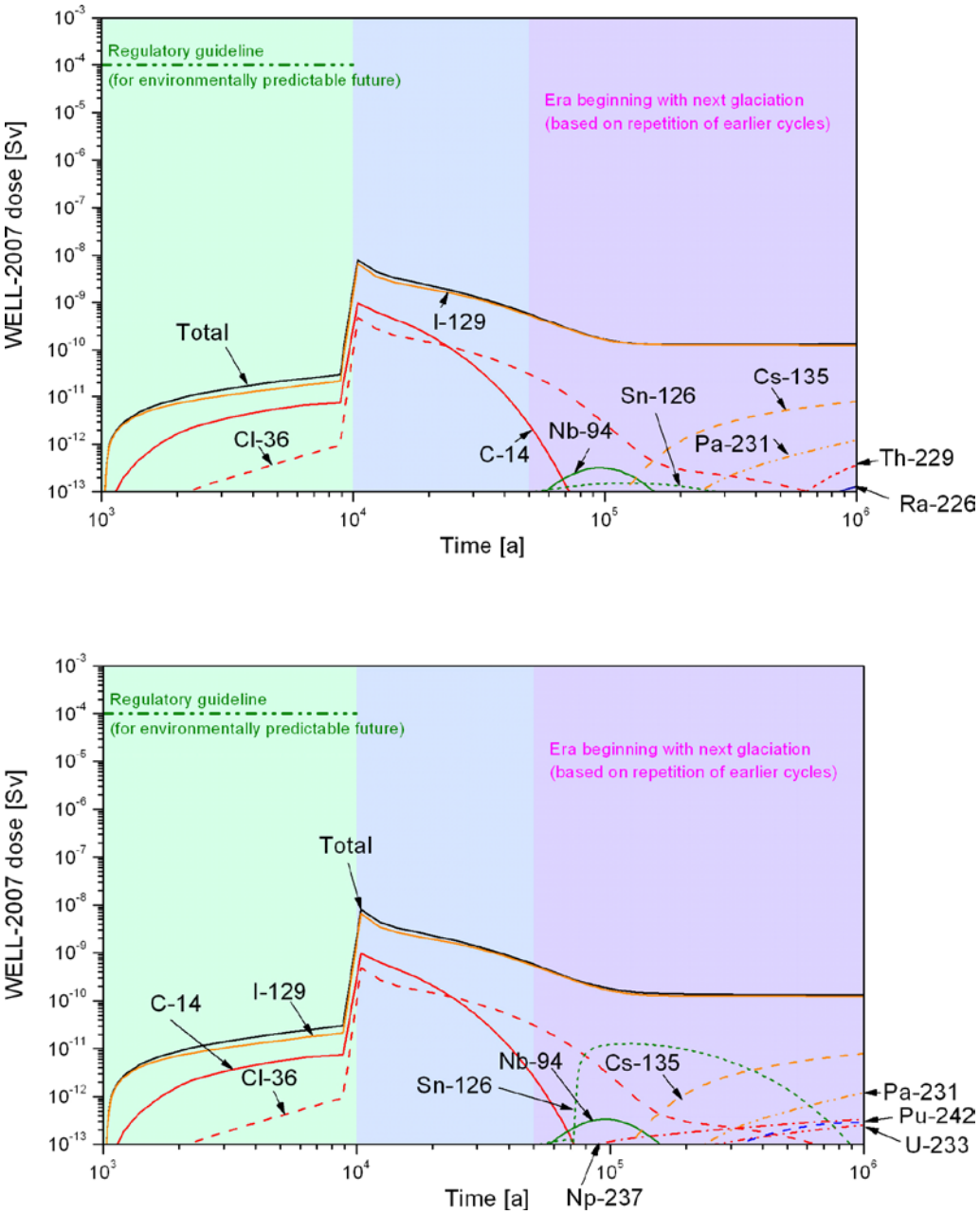

Figure 5-45. *WELL-2007 dose as a function of time in the Base Case (PD-BC) (upper figure) and case PD-GMWC (lower figure).*

The radionuclides contributing most to dose and summed releases – I-129, C-14, Cl-36 and Cs-135 – are insensitive to the transition to glacial meltwater, and thus the total dose and summed releases are virtually unchanged in case PD-GMWC compared with the Base Case. There are, however, differences in the case of radionuclides making relatively minor contributions to the totals. For example, Figure 5-45 shows a sudden increase in Sn-126 release at 70,000 years as the Sn solubility changes from 1.2×10^{-7} mol dm^{-3} (its Base case value, see Table 5-6) to 2.7×10^{-6} (its value in case PD-GMWC after 70,000 years, see Table 5-30).

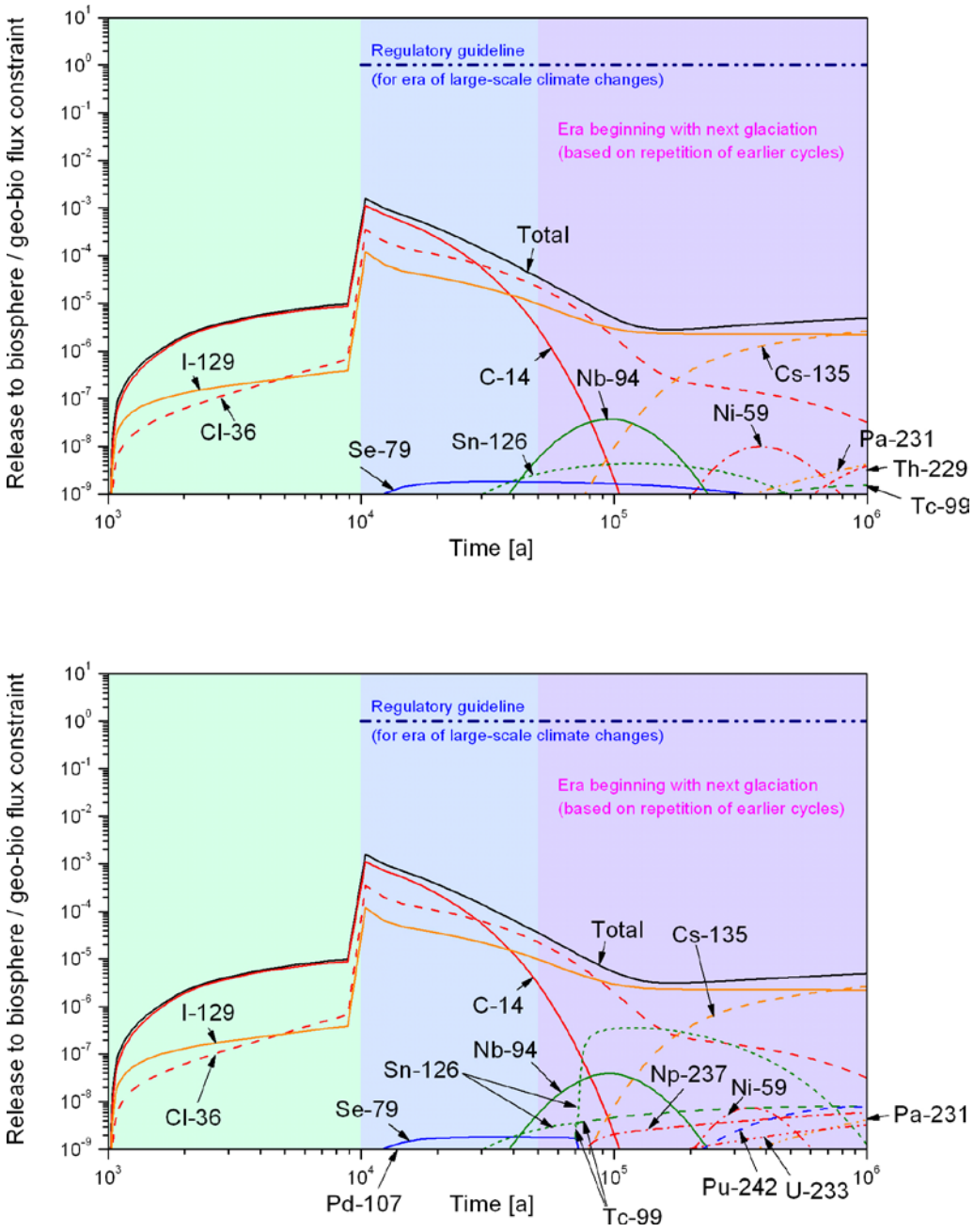

Figure 5-46. *Ratios of nuclide-specific activity releases to their respective geo-bio flux constraints in the Base Case (PD-BC) (upper figure) and case PD-GMWC (lower figure).*

5.12 Cases addressing uncertainty in groundwater flow and geosphere transport resistance

5.12.1 Differences compared with the Base Case

There are a number of uncertainties concerning groundwater flow at the buffer/rock interface and geosphere transport resistance (WL/Q), including, for example:

- uncertainties in the characterisation of the network of water-conducting fractures in the host rock; and
- the degradation of characterisation borehole backfill and seals, which could lead to the formation of new water conducting features.

Groundwater flow may also vary significantly, and in an uncertain manner, with time. For example, in the event of a warm-based ice sheet covering the site, the pressure exerted by the overlying ice on the liquid water between the ice and the rock could, over an uncertain but limited period, force large volumes of glacial meltwater into deeper parts of the bedrock. Additional uncertainties are associated with the possibility of processes such as colloid facilitated radionuclide transport and two-phase flow, which are not accounted for in the models used in the present safety assessment, but will need to be considered in future studies. Finally, scoping calculations presented in the Evolution Report suggest that corrosion of the canister insert and the resulting compaction of the buffer could lead to swelling pressures that could damage the rock (Appendix B.4 in /Smith et al. 2007a/). Although the calculations are conservative, disregarding, for example, relaxation of the increased density by buffer creep along the drift, the possibility of higher flows and reduced geosphere transport resistance cannot currently be discounted.

In the Base Case, groundwater flow at the buffer/rock interface and the geosphere transport resistance are taken from TILA-99. Although more recent developments in the understanding of the Olkiluoto site, and, in particular, discrete fracture network modelling carried out in support of the KBS-3H safety studies /Lanyon and Marschall 2006/, have been used to provide additional support for the parameter values selected (see Sections 5.2.3 and 5.2.4), a comprehensive evaluation of recent site data and modelling in terms of their impact on the assessment of groundwater flow and geosphere transport has yet to be carried out. This is because the focus of the present safety studies has been on differences between KBS-3H and KBS-3V, which mainly concern the near field. Furthermore, the discrete fracture network modelling and the Base Case for radionuclide release and transport calculations are both based on the assumption that fractures with transmissivities above 3×10^{-9} m^2 s^{-1} will not intersect the deposition drifts and canister of buffer emplacement locations. As noted in Section 5.2.3, this assumption, which is based on a relationship between observed initial inflow and transmissivity, has yet to be confirmed and is associated with some significant uncertainties, including those related to perturbations to inflow caused by repository excavation.

No detailed analysis to quantify or bound these various uncertainties and perturbing processes has been carried out, and the impact of time-varying flow, and associated variations in groundwater composition, on radionuclide release and transport is an issue for future studies. However, four assessment cases are defined and analysed so as to provide an indication of the importance of groundwater flow and geosphere transport resistance in delaying and attenuating releases from the near field in the event of an initial penetrating defect.

Flow at the buffer/rock interface is increased with respect to the Base Case in cases **PD-HIFLOW**, with no assumed change to the geosphere transport resistance. The geosphere transport resistance is decreased with respect to the Base Case resistance in case **PD-LOGEOR**, and increased with respect to the Base Case resistance in case **PD-HIGEOR**, with no assumed change to flow at the buffer/rock interface. In case **PD-HIFLOWR**, flow at the buffer/rock interface is increased with respect to the Base Case, and geosphere transport resistance is decreased with respect to the Base Case.

Matrix diffusion (coupled to sorption on matrix pore surfaces) is a key process retarding radionuclide transport through the geosphere. A sensitivity analysis of the impact of varying matrix diffusion depth is reported in Appendix C.

5.12.2 Radionuclide inventories, half-lives and partitioning

Radionuclide inventories and half-lives and partitioning between fuel matrix, IRF, Zircaloy and other metal parts are as in the Base Case, and are given in Table 5-2.

5.12.3 Near-field model

The near-field model is identical to that of the Base Case, as described in Section 5.2.3, with the exception of the transfer coefficient Q_f, which is set to an increased value of 6.3×10^{-4} m^3 a^{-1} in cases PD-HIFLOW and PD-HIFLOWR. This represents an increase of a factor of $\sqrt{(10)}$ with respect to the Base-case value of 2×10^{-4} m^3 a^{-1}, which corresponds, for example, to an order of magnitude increase in either the transmissivity (T) or hydraulic gradient (i) in Eq. 5-10. Q_f is set to the Base-case value of 2×10^{-4} m^3 a^{-1} in cases PD-LOGEOR and PD-HIGEOR.

5.12.4 Geosphere model

The geosphere model is identical to that of the Base Case, as described in Section 5.2.4, with the exception of the transport resistance of the geosphere (WL/Q) which is assigned a value of 5,000 years per metre in cases PD-LOGEOR and PD-HIFLOWR and 500,000 years per metre in case PD-HIGEOR (the Base-case value is 50,000 years per metre). Geosphere transport resistance is set to the Base-case value in case PD-HIFLOW.

5.12.5 Results

Table 5-35 gives calculated maximum geosphere release rates in Bq per year for each radionuclide in the Base Case for an initial penetrating defect (case PD-BC) and in cases PD-HIFLOW and PD-HIFLOWR. It also gives the times at which these maxima occur (t_{max}). Figure 5-47 shows the releases from the geosphere to the biosphere as a function of time in cases PD-HIFLOW and PD-HIFLOWR expressed as WELL-2007 doses based on the dose conversion factors given in Table 3-1. Figure 5-48 shows time-dependent releases from the geosphere to the biosphere in the same cases, divided by the geo-bio flux constraints specified by the Finnish regulator and given in Table 1-1, and the sum of these releases over all radionuclides for which calculations were made.

The magnitude of the peak release of radionuclides dominating peak dose and peak summed release – C-14, Cl-36 and I-129 – are increased by a factor of about 3 in case PD-HIFLOW compared with the Base Case (PD-BC). This is approximately the same as the factor of $\sqrt{(10)}$ by which the transfer coefficient Q_f is increased. The timing of the peak releases remains the same (a little over 10,000 years).

There is only a small additional increase in the peak release of these radionuclides in case PD-HIFLOWR, in which the transport resistance of the geosphere is reduced by a factor of 10 with respect to its Base-case value. There is, however, a more significant increase in the release rates of some of the actinide chain members, such as Ra-226 and Pa-231, which decay substantially in the geosphere in the Base Case. These come to dominate total dose at later times in case PD-HIFLOWR, such that the calculated dose at a million years is higher by almost an order of magnitude than in the Base Case (although still substantially less than the peak dose shortly after 10,000 years).

Table 5-35. Calculated maximum geosphere release rates for each radionuclide in the Base Case for an initial penetrating defect (case PD-BC) and in cases PD-HIFLOW and PD-HIFLOWR, and the times at which these maxima occur. Full results are presented in Appendix G.

Radionuclide			Base Case (PD-BC)		PD-HIFLOW		PD-HIFLOWR	
			t_{max} [a]	Bq/a	t_{max} [a]	Bq/a	t_{max} [a]	Bq/a
Activation/fission products		C-14	1.04E+04	3.35E+05	1.04E+04	9.90E+05	1.04E+04	1.02E+06
		Cl-36	1.04E+04	1.05E+05	1.04E+04	2.72E+05	1.04E+04	2.77E+05
		Ni-59	3.80E+05	2.98E+02	3.76E+05	8.81E+02	4.42E+04	1.48E+05
		Se-79	3.42E+04	1.82E–01	3.42E+04	4.72E–01	2.45E+04	5.30E–01
		Mo-93	1.23E+04	1.52E–01	1.23E+04	4.04E–01	1.04E+04	8.24E–01
		Zr-93	1.00E+06	6.68E–03	1.00E+06	2.07E–02	4.10E+05	1.28E–01
		Zr-93p*	1.00E+06	4.89E–01	1.00E+06	1.51E+00	4.56E+05	9.44E+00
		Nb-94	9.73E+04	3.77E+01	9.73E+04	1.17E+02	2.45E+04	1.05E+04
		Tc-99	1.00E+06	4.56E+00	1.00E+06	1.42E+01	9.96E+05	5.98E+01
		Pd-107	1.00E+06	3.15E+01	1.00E+06	9.31E+01	1.00E+06	9.45E+01
		Sn-126	1.46E+05	3.92E+00	1.46E+05	1.22E+01	1.16E+05	1.48E+01
		I-129	1.04E+04	1.19E+04	1.04E+04	3.08E+04	1.04E+04	3.13E+04
		Cs-135	1.00E+06	7.97E+02	1.00E+06	1.72E+03	4.86E+05	2.97E+03
Actinide chains	4N	Pu-240	2.92E+04	3.01E–17	2.92E+04	9.47E–17	6.42E+04	3.60E–02
		U-236	1.00E+06	2.25E–04	1.00E+06	6.96E–04	1.00E+06	1.68E–03
	4N + 1	Cm-245	1.56E+05	3.04E–09	1.56E+05	9.56E–09	6.42E+04	5.30E–04
		Am-241	1.56E+05	3.20E–09	1.56E+05	1.01E–08	6.42E+04	5.59E–04
		Np-237	1.00E+06	6.79E–02	1.00E+06	2.12E–01	1.00E+06	2.19E+00
		U-233	1.00E+06	2.38E–01	1.00E+06	7.39E–01	1.00E+06	3.76E+00
		Th-229	1.00E+06	1.19E–01	1.00E+06	3.69E–01	1.00E+06	1.88E+00
	4N + 2	Cm-246	1.20E+05	6.85E–14	1.20E+05	2.15E–13	4.92E+04	2.79E–06
		Pu-242	1.00E+06	1.48E–03	1.00E+06	4.64E–03	5.96E+05	5.43E+01
		U-238	1.00E+06	1.95E–04	1.00E+06	6.04E–04	1.00E+06	1.43E–03
		U-234	1.00E+06	2.68E–04	1.00E+06	8.30E–04	1.96E+05	4.80E–03
		Th-230	1.00E+06	1.17E–02	1.00E+06	3.65E–02	6.36E+05	4.02E+01
		Ra-226	1.00E+06	1.19E–02	1.00E+06	3.73E–02	6.40E+05	6.19E+01
	4N + 3	Am-243	1.46E+05	6.03E–08	1.46E+05	1.90E–07	5.92E+04	3.12E–02
		Pu-239	8.36E+05	6.93E–13	8.36E+05	2.17E–12	1.30E+05	2.01E+01
		U-235	1.00E+06	1.42E–05	1.00E+06	4.38E–05	9.96E+05	1.04E–04
		Pa-231	1.00E+06	1.26E–01	1.00E+06	3.91E–01	1.00E+06	5.80E+01

* Zirconium originating from the fuel matrix only.

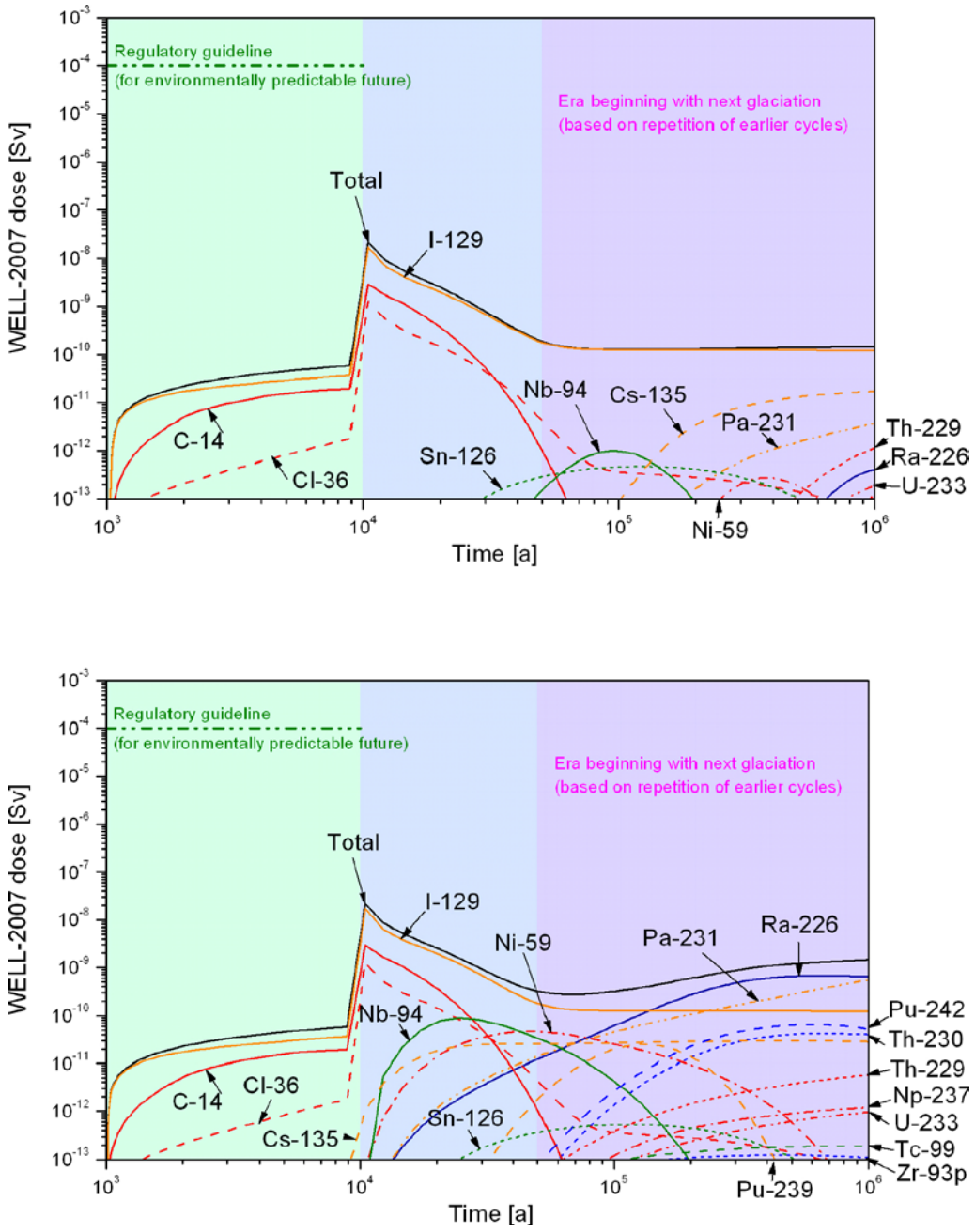

Figure 5-47. *WELL-2007 dose as a function of time in case PD-HIFLOW (upper figure) and case PD-HIFLOWR (lower figure).*

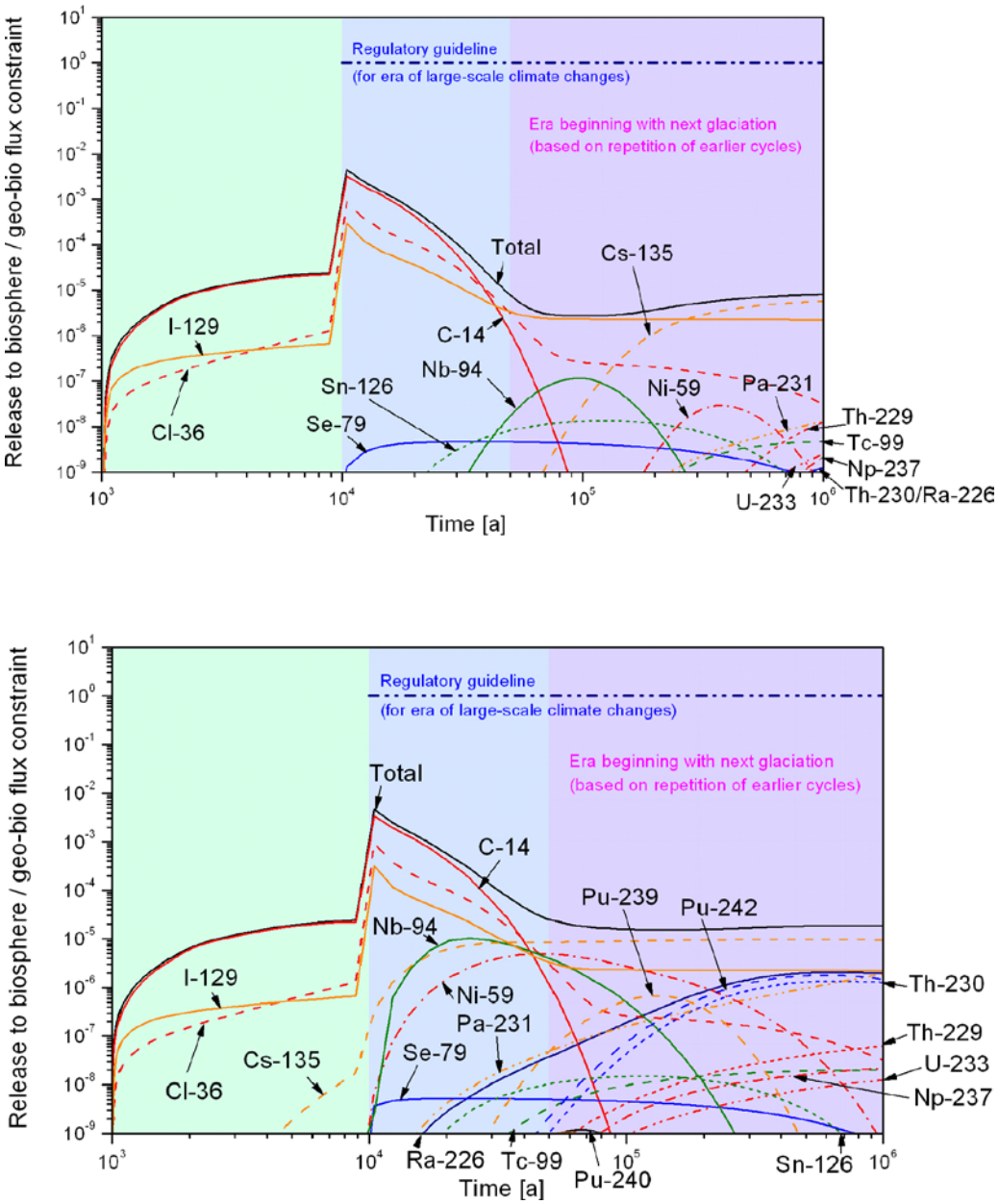

Figure 5-48. *Ratios of nuclide-specific activity releases to their respective geo-bio flux constraints in case PD-HIFLOW (upper figure) and case PD-HIFLOWR (lower figure).*

Table 5-36 gives calculated maximum geosphere release rates in Bq per year for each radionuclide in the Base Case for an initial penetrating defect (case PD-BC) and in cases PD-LOGEOR and PD-HIGEOR. It also gives the times at which these maxima occur (t_{max}). Figure 5-49 shows the releases from the geosphere to the biosphere as a function of time in cases PD-LOGEOR and PD-HIGEOR expressed as WELL-2007 doses based on the dose conversion factors given in Table 3-1. Figure 5-50 shows time-dependent releases from the geosphere to the biosphere in the same cases, divided by the geo-bio flux constraints specified by the Finnish regulator and given in Table 1-1, and the sum of these releases over all radionuclides for which calculations were made.

Table 5-36. Calculated maximum geosphere release rates for each radionuclide in the Base Case for an initial penetrating defect (case PD-BC) and in cases PD-LOGEOR and PD-HIGEOR, and the times at which these maxima occur. Full results are presented in Appendix G.

Radionuclide			Base Case (PD-BC)		PD-LOGEOR		PD-HIGEOR	
			t_{max} [a]	Bq/a	t_{max} [a]	Bq/a	t_{max} [a]	Bq/a
Activation/fission products		C-14	1.04E+04	3.35E+05	1.04E+04	3.44E+05	1.04E+04	2.58E+05
		Cl-36	1.04E+04	1.05E+05	1.04E+04	1.07E+05	1.04E+04	8.97E+04
		Ni-59	3.80E+05	2.98E+02	4.92E+04	4.86E+04	1.23E+04	2.87E–08
		Se-79	3.42E+04	1.82E–01	2.45E+04	2.05E–01	1.10E+05	7.65E–02
		Mo-93	1.23E+04	1.52E–01	1.04E+04	3.06E–01	2.92E+04	9.60E–04
		Zr-93	1.00E+06	6.68E–03	4.30E+05	4.15E–02	1.00E+06	4.61E–15
		Zr-93p*	1.00E+06	4.89E–01	4.50E+05	3.05E+00	1.00E+06	3.33E–13
		Nb-94	9.73E+04	3.77E+01	2.45E+04	3.35E+03	2.06E+04	2.38E–11
		Tc-99	1.00E+06	4.56E+00	9.96E+05	1.92E+01	8.60E+05	6.23E–12
		Pd-107	1.00E+06	3.15E+01	1.00E+06	3.20E+01	1.00E+06	2.65E+01
		Sn-126	1.26E+05	4.33E+00	1.16E+05	4.78E+00	2.00E+05	1.64E+00
		I-129	1.04E+04	1.19E+04	1.04E+04	1.21E+04	1.04E+04	1.02E+04
		Cs-135	1.00E+06	7.97E+02	1.00E+06	1.50E+03	8.00E+05	6.15E–09
Actinide chains	4N	Pu-240	2.92E+04	3.01E–17	6.42E+04	1.14E–02	All releases approx. zero	
		U-236	1.00E+06	2.25E–04	1.00E+06	5.42E–04		
	4N +1	Cm-245	1.56E+05	3.04E–09	6.42E+04	1.69E–04		
		Am-241	1.56E+05	3.20E–09	6.42E+04	1.78E–04		
		Np-237	1.00E+06	6.79E–02	1.00E+06	7.04E–01		
		U-233	1.00E+06	2.38E–01	1.00E+06	1.22E+00		
		Th-229	1.00E+06	1.19E–01	1.00E+06	6.08E–01		
	4N + 2	Cm-246	1.20E+05	6.85E–14	4.92E+04	8.86E–07		
		Pu-242	1.00E+06	1.48E–03	5.90E+05	1.75E+01		
		U-238	1.00E+06	1.95E–04	1.00E+06	4.64E–04		
		U-234	1.00E+06	2.68E–04	1.90E+05	1.55E–03		
		Th-230	1.00E+06	1.17E–02	6.36E+05	1.29E+01		
		Ra-226	1.00E+06	1.19E–02	6.40E+05	1.99E+01		
	4N + 3	Am-243	1.46E+05	6.03E–08	5.92E+04	9.91E–03		
		Pu-239	8.36E+05	6.93E–13	1.30E+05	6.41E+00		
		U-235	1.00E+06	1.42E–05	1.00E+06	3.37E–05		
		Pa-231	1.00E+06	1.26E–01	1.00E+06	1.88E+01		

* Zirconium originating from the fuel matrix only.

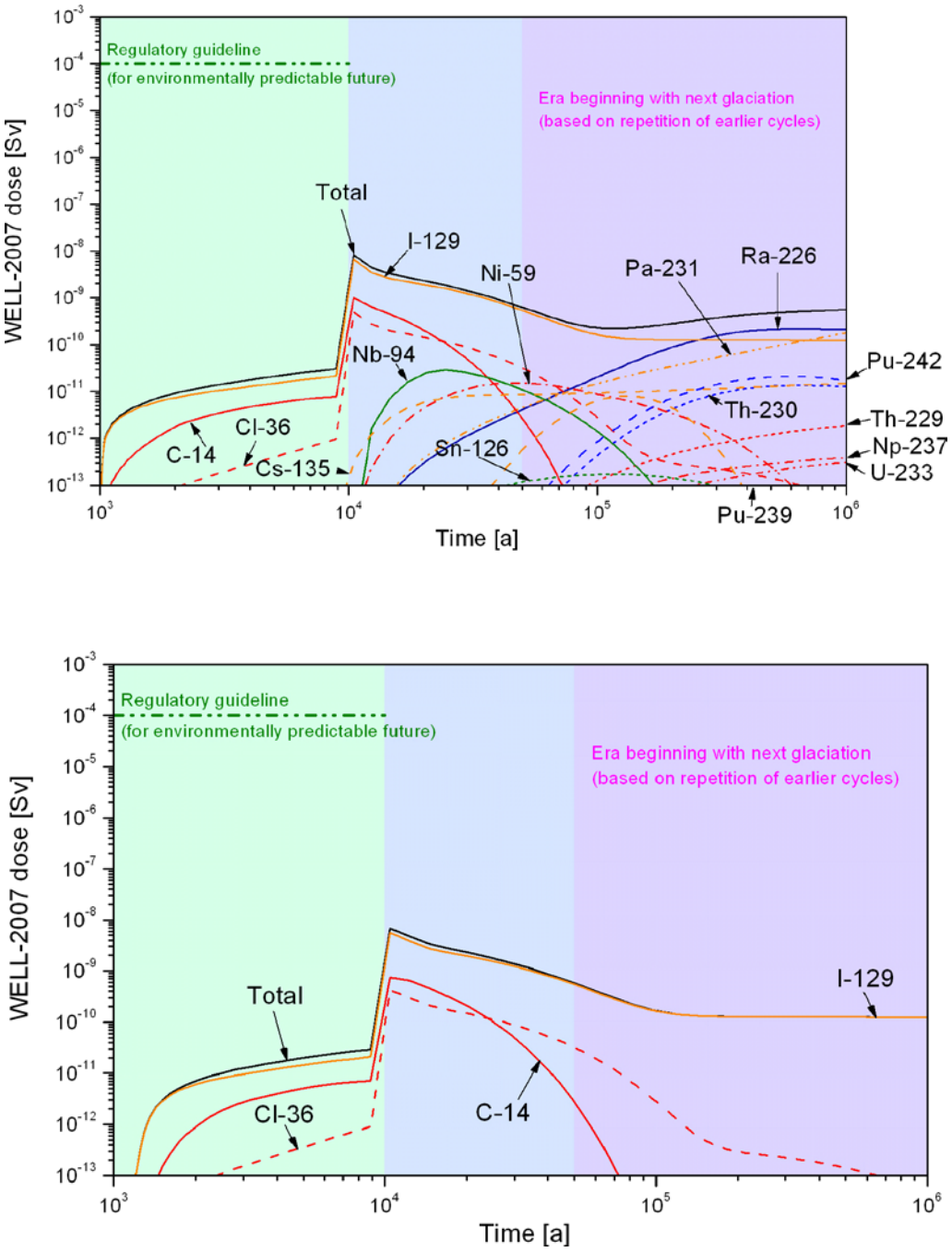

Figure 5-49. *WELL-2007 dose as a function of time in case PD-LOGEOR (upper figure) and case PD-HIGEOR (lower figure).*

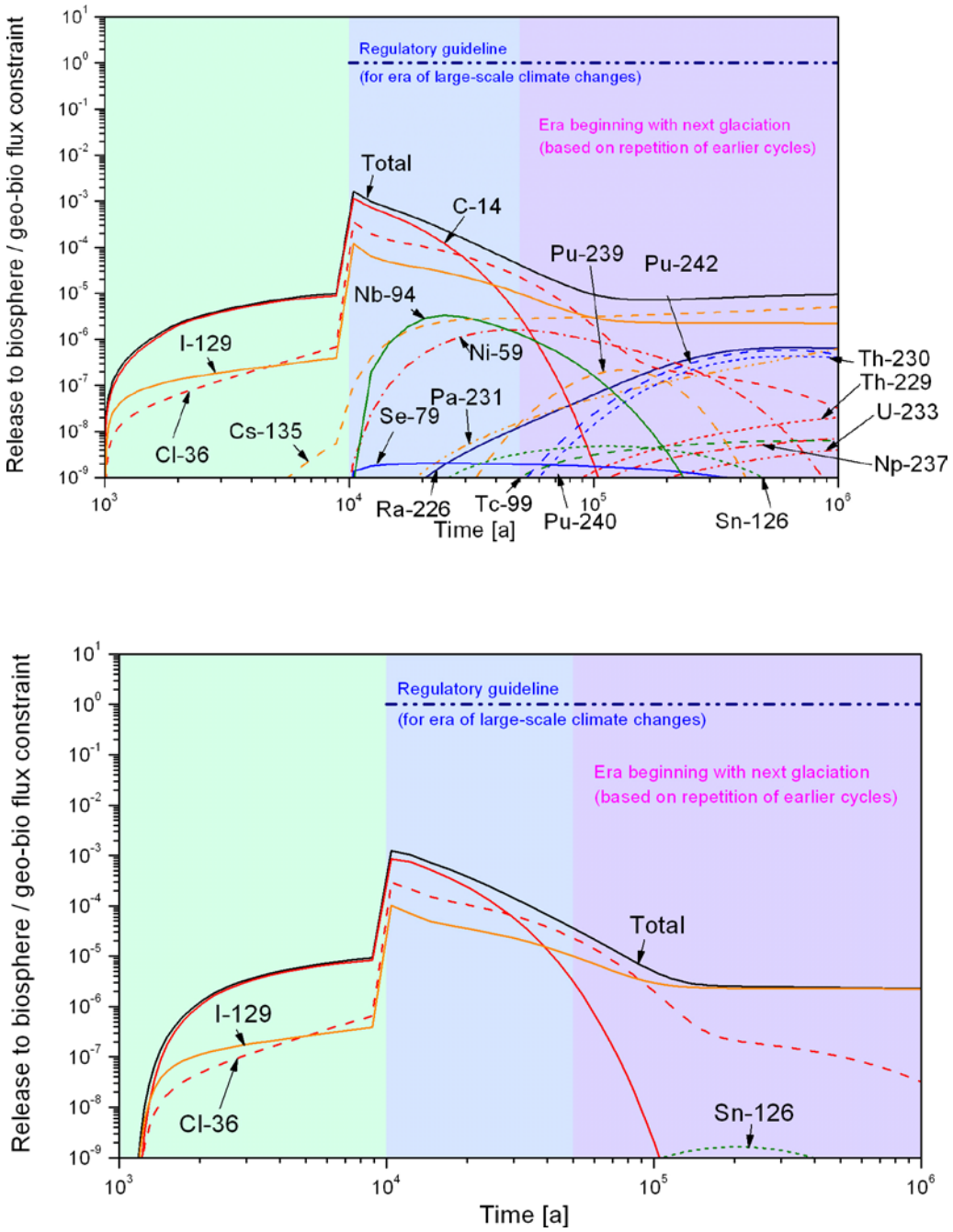

Figure 5-50. *Ratios of nuclide-specific activity releases to their respective geo-bio flux constraints in case PD-LOGEOR (upper figure) and case PD-HIGEOR (lower figure).*

These results confirm that releases of C-14, Cl-36 and I-129 are little affected by the transport resistance of the geosphere over the range investigated. There are, however, numerous other radionuclides that decay substantially during geosphere transport in case PD-HIGEOR, but are released to the biosphere and contribute significantly to dose and summed release, especially at later times, in case PD-LOGEOR. To further illustrate this behaviour, Figures 5-51 and 5-52 shows release rate maxima from the near-field and geosphere, expressed in terms of

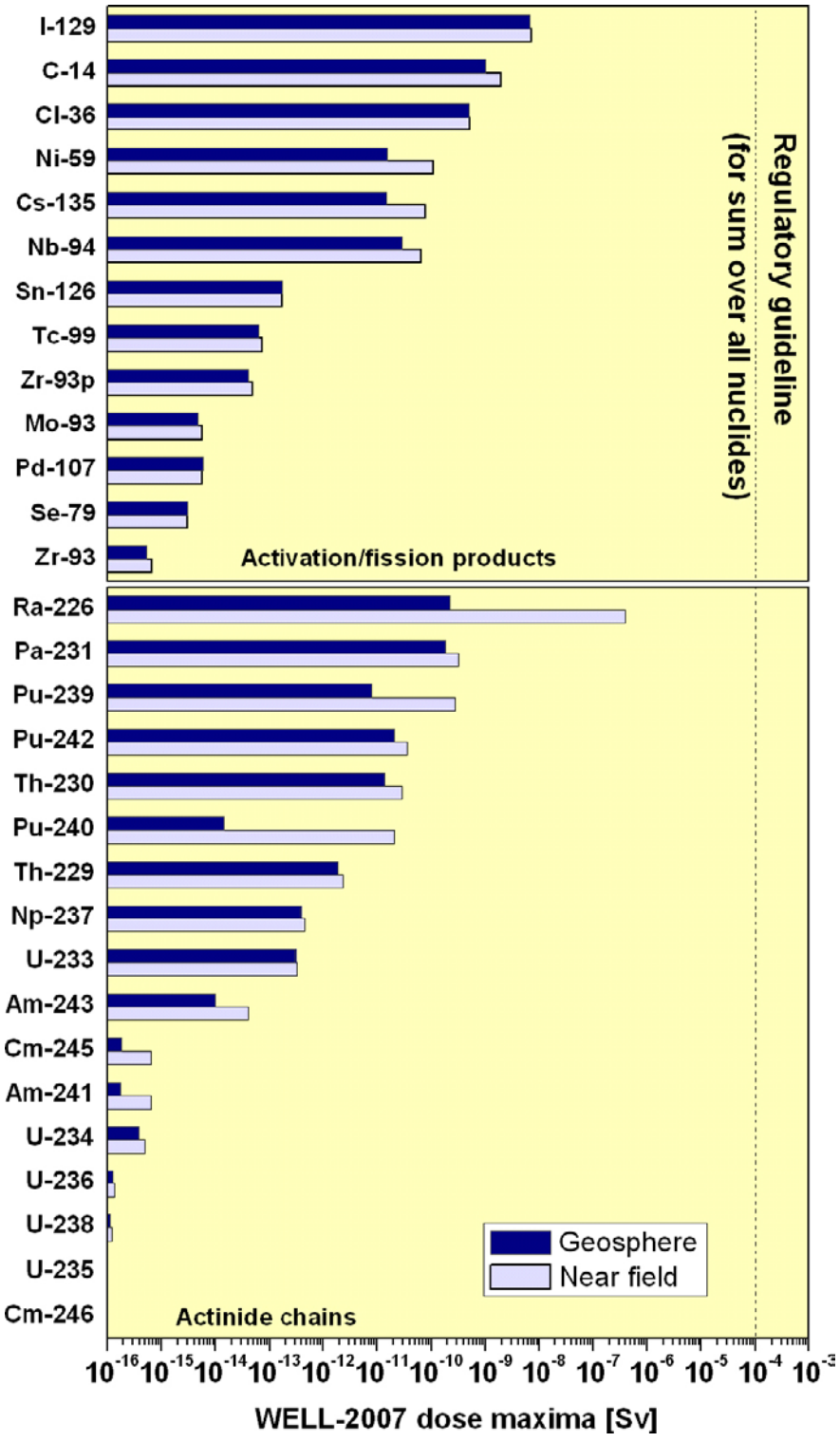

Figure 5-51. *Release rate maxima from the near field and geosphere, expressed as WELL-2007 dose, for all the radionuclides considered in the PD-LOGEOR calculation.*

WELL-2007 dose, for all the radionuclides considered in the PD-LOGEOR and PD-HIGEOR calculations, respectively. The figure shows that none of the actinides and only a few of the activation and fission products penetrate the geosphere in case PD-HIGEOR, but that some actinide chain members and all the activation and fission products are able to penetrate the geosphere with relatively little decay in case PD-LOGEOR.

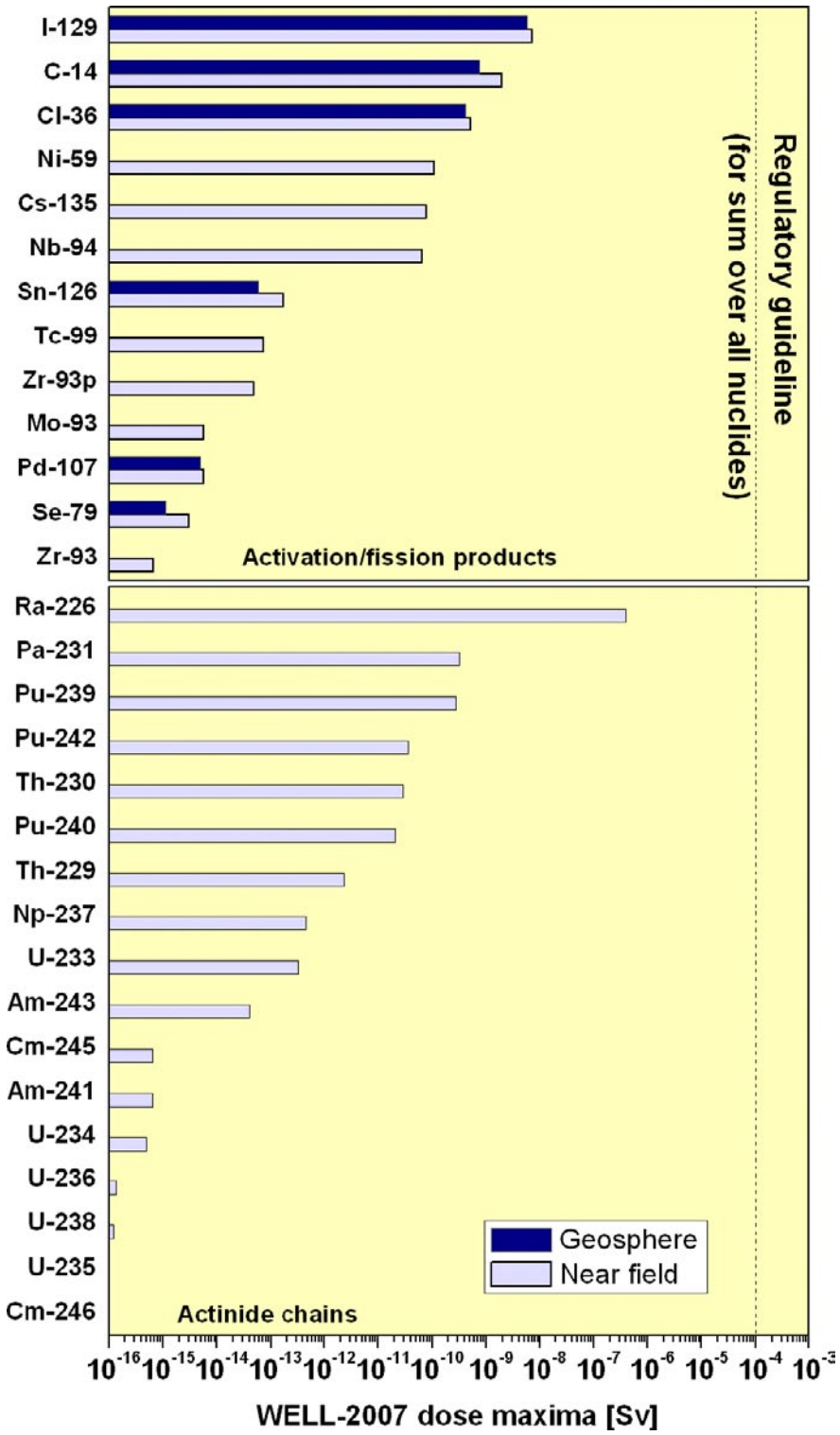

Figure 5-52. *Release rate maxima from the near field and geosphere, expressed as WELL-2007 dose, for all the radionuclides considered in the PD-HIGEOR calculation.*

Finally, Figure 5-53 both the calculated annual landscape dose to the most exposed individual and the WELL-2007 dose in case PD-LOGEOR. The highest annual landscape dose occurs at the end of the 10,000 period over which biosphere modelling was carried out, and is less than 10^{-6} Sv, compared with about 10^{-8} Sv at 10,000 years in the case of WELL-2007 dose.

5.13 Summary of results for cases assuming an initial penetrating defect

Table 5-37 gives a summary of results for all cases assuming an initial penetrating defect. The table shows, for each case, the calculated WELL-2007 dose maxima and the summed geosphere release maxima (which each maximum divided by its respective geo-bio flux constraint), and the times of occurrence of these maxima.

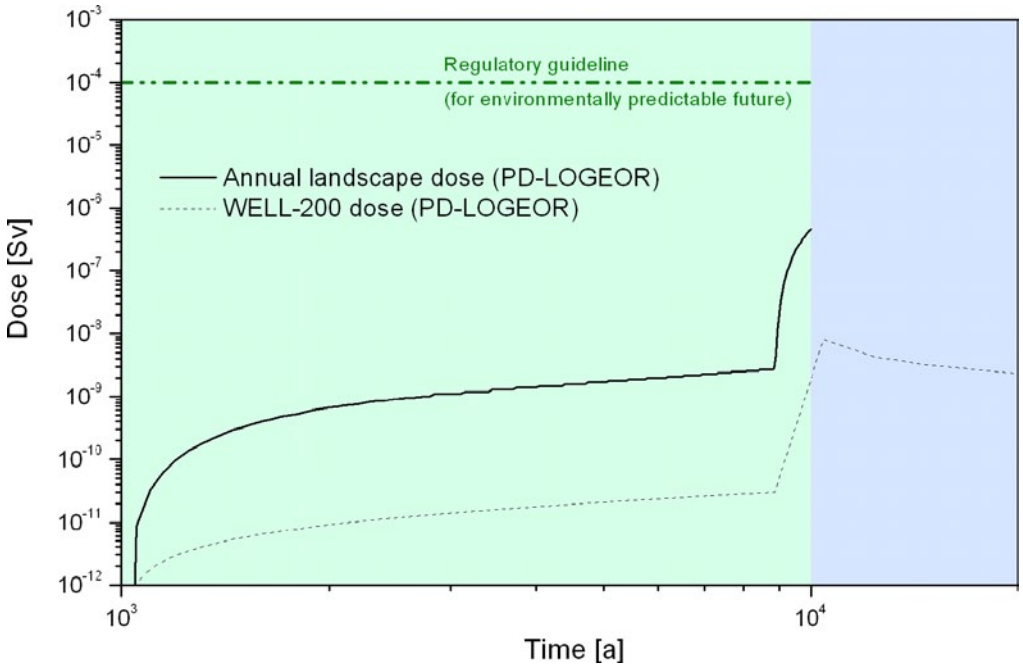

Figure 5-53. *Annual landscape dose and WELL-2007 dose as functions of time in case PD-LOGEOR.*

Table 5-37. WELL-2007 dose maxima, maxima of the summed nuclide-specific activity releases divided by their respective geo-bio flux constraints, and the times of occurrence of these maxima for all cases assuming an initial penetrating defect.

Case	WELL-2007 dose		Activity release	
	Maximum [Sv]	Time [a]	Maximum	Time [a]
PD-BC	8.0×10^{-9}	1.0×10^{4}	1.6×10^{-3}	1.0×10^{4}
PD-VVER	6.3×10^{-9}	1.0×10^{4}	9.9×10^{-4}	1.0×10^{4}
PD-EPR	8.6×10^{-9}	1.0×10^{4}	9.1×10^{-4}	1.0×10^{4}
PD-HIFDR	9.1×10^{-9}	1.0×10^{4}	1.6×10^{-3}	1.0×10^{4}
PD-LOFDR	7.9×10^{-9}	1.0×10^{5}	1.6×10^{-3}	1.0×10^{5}
PD-IRF	6.5×10^{-9}	1.0×10^{4}	2.1×10^{-4}	1.0×10^{4}
PD-BIGHOLE	7.8×10^{-9}	1.0×10^{4}	1.6×10^{-3}	1.0×10^{4}
PD-HIDELAY	5.8×10^{-9}	1.0×10^{5}	3.2×10^{-4}	1.0×10^{5}
PD-LODELAY	8.9×10^{-9}	2.3×10^{3}	3.4×10^{-3}	2.1×10^{3}
PD-BHLD	8.9×10^{-9}	2.3×10^{3}	3.4×10^{-3}	2.1×10^{3}
PD-HIDIFF	2.6×10^{-9}	1.0×10^{4}	1.0×10^{-3}	1.0×10^{4}
PD-SPALL	4.2×10^{-9}	1.0×10^{4}	8.1×10^{-4}	1.0×10^{4}
PD-FEBENT1	5.3×10^{-8}	1.0×10^{4}	1.4×10^{-2}	1.0×10^{4}
PD-FEBENT2	5.5×10^{-8}	1.0×10^{4}	1.5×10^{-2}	1.0×10^{4}
PD-FEBENT3	6.5×10^{-8}	1.0×10^{4}	1.9×10^{-2}	1.0×10^{4}
PD-EXPELL	1.6×10^{-7}	4.1×10^{3}	7.9×10^{-2}	2.9×10^{3}
PD-VOL–1	7.5×10^{-7}	1.9×10^{3}	7.9×10^{-2} (8.6×10^{-1})*	2.4×10^{3} (1.9×10^{3})*
PD-VOL-2	5.1×10^{-7}	1.0×10^{4}	2.4×10^{-2} (5.8×10^{-1})*	1.1×10^{4} (1.0×10^{4})*
PD-BCN	8.0×10^{-9}	1.0×10^{4}	1.6×10^{-3}	1.0×10^{4}
PD-BCC	7.7×10^{-9}	1.0×10^{4}	1.2×10^{-3}	1.0×10^{4}
PD-VVERC	6.1×10^{-9}	1.0×10^{4}	7.1×10^{-4}	1.0×10^{4}
PD-EPRC	8.4×10^{-9}	1.0×10^{-4}	7.0×10^{-4}	1.0×10^{-4}
PD-NFSLV	8.0×10^{-9}	1.0×10^{4}	1.6×10^{-3}	1.0×10^{4}
PD-SAL	8.0×10^{-9}	1.0×10^{4}	1.6×10^{-3}	1.0×10^{4}
PD-HISAL	8.0×10^{-9}	1.0×10^{4}	1.6×10^{-3}	1.0×10^{4}
PD-GMW	7.0×10^{-9}	7.9×10^{4}	4.2×10^{-4}	7.9×10^{4}
PD-GMWV	7.0×10^{-9}	7.9×10^{4}	4.2×10^{-4}	7.9×10^{4}
PD-GMWC	8.0×10^{-9}	1.0×10^{4}	1.6×10^{-3}	1.0×10^{4}
PD-HIFLOW	2.1×10^{-8}	1.0×10^{4}	4.5×10^{-3}	1.0×10^{4}
PD-LOGEOR	8.2×10^{-9}	1.0×10^{4}	1.6×10^{-3}	1.0×10^{4}
PD-HIGEOR	6.8×10^{-9}	1.0×10^{4}	1.3×10^{-3}	1.0×10^{4}
PD-HIFLOWR	2.1×10^{-8}	1.0×10^{4}	4.6×10^{-3}	1.0×10^{4}

* Values before 1,000 year averaging (see Section 5.9).

6 Cases addressing failure due to copper corrosion

6.1 General considerations

As discussed in Section 2.2.5, two scenarios can be envisaged in which canister failure by corrosion occurs before a million years. These are scenarios in which:

1. the buffer/rock interface is perturbed, leading to enhanced mass transfer at the interface; and
2. dilute glacial meltwater penetrates to repository depth, leading to chemical erosion of the buffer and to advective conditions becoming established within it.

In the assessment cases described in this chapter, which all involve canister failure by corrosion before a million years, radionuclide release is assumed to begin at 100,000 years. As also discussed in Section 2.2.5, this failure time is regarded as pessimistic, given the slow rate of canister corrosion even in these scenarios. Some radionuclides will decay to insignificance within this time frame. Thus, Mo-93 in particular, which has a half-life of 4,000 years, is not included in the calculations.

Radionuclide release and transport calculations are again carried out for a Base Case and a set of variant cases, all of which are based on the assumption of a single canister failing at 100,000 years. In reality, multiple canister failures occurring at similar times is possible in either of the above scenarios, although a distribution of failure times is more likely, since corrosion due to transfer of sulphide from the host rock to the canister surface will be affected by the heterogeneity of the rock. The consequences of multiple canister failures at around the same time can in principle be obtained by multiplying the results by the number of canister failures postulated. For both scenarios leading to this mode of canister failure, the canister positions most vulnerable to failure will be those associated with the highest groundwater flows at the buffer/rock interface, although in neither scenario can an estimate currently be made of the likelihood or rate of canister failure by corrosion in a million year time frame, given the limited quantitative understanding of relevant processes, such as chemical erosion of the buffer and the impact of methane and hydrogen on the microbial reduction of groundwater sulphate to sulphide. The possibility of multiple failures occurring within a limited time interval will, however, need to be assessed in the course of future studies.

The assessment cases addressing canister failure due to copper corrosion are summarised in Table 6-1. Detailed case definitions are given in the following sections. The cases address uncertainties in fuel dissolution rate (release of radionuclides to the geosphere is controlled principally by the dissolution rate of the fuel in this canister failure mode, see Section 10.6.3 in SR-Can Main Report /SKB 2006a/) and in groundwater flow and composition.

6.2 Base Case

6.2.1 Radionuclide inventories, half-lives and partitioning

Radionuclide inventories and half-lives and partitioning between fuel matrix, IRF, Zircaloy and other metal parts are as in the Base Case for an initial penetrating defect (case PD-BC), and are given in Table 5-2.

Table 6-1. Identifiers and summary descriptions of each of the assessment cases that assume canister failure due to copper corrosion, with references to report sections where detailed case definitions are provided. Groundwater chemistry and its impact on buffer porewater chemistry (bentonite water) are discussed in Appendix D. The concepts of equivalent flow rate (Q_F) and geosphere transport resistance (WL/Q) are discussed in Section 5.2.3 in the context of the Base Case. In all cases, CC-BC means same as Base Case.

Identifier	Summary description	Groundwater chemistry	Q_F [$m^3\ a^{-1}$]	*WL/Q* [$a\ m^{-1}$]	Full definition (report section)
CC-BC	Base Case (BC) for failure due to copper corrosion (CC)	Dilute/brackish	3.1×10^{-3}	5×10^{4}	Section 6.2
Cases addressing uncertainties in the fuel dissolution rate					
CC-HIFDR	Increased fuel dissolution rate	CC-BC	CC-BC	CC-BC	Section 6.3
CC-LOFDR	Reduced fuel dissolution rate				
Cases addressing uncertainties in groundwater flow and composition in combination with an increased fuel dissolution rate					
CC-GMW	Glacial meltwater present at repository depth (impact on near-field solubilities and geosphere retention parameters)	Dilute glacial meltwater type GWM	CC-BC	CC-BC	Section 6.4
CC-LOGEOR	Reduced transport resistance in geosphere	CC-BC	CC-BC	5×10^{3}	Section 6.4
CC-LOGEORG	Reduced transport resistance in geosphere, glacial meltwater	Dilute glacial meltwater type GWM	CC-BC	5×10^{3}	Section 6.4
CC-LOGEORS	Reduced transport resistance in geosphere and saline groundwater	Saline/brackish	CC-BC	5×10^{3}	Section 6.4

6.2.2 Near-field model

(v) Geometry

The geometry of near-field model domain is as in the Base Case for an initial penetrating defect (case PD-BC) – Figure 5-1 and Table 5-4 – except that the initial defect is absent.

(vi) Processes and material properties

A single representative canister, with no initial penetrating defect, is assumed to fail completely at 100,000 years following emplacement. The failed canister and insert are assumed to offer no resistance to water ingress and radionuclide release[27].

There could, in reality, be a delay of some thousands of years from the time that the copper shell fails before the insert also fails due to corrosion. This delay is, however, likely to be small compared with the overall failure time, assumed to be 100,000 years. As in the case of an initial penetrating defect, loss of transport resistance is also, in reality, likely to be a process that occurs gradually over time, rather than as a discrete event. However, an instantaneous loss of transport resistance is a conservative assumption, since a gradual loss of transport resistance would spread the peak release over a longer period of time, reducing its magnitude.

[27] This assumption is conservative. In reality, there will be a delay of some thousands of years before the insert also fails due to corrosion, although this delay is likely to be small compared with the failure time.

Following the ingress of water, IRF radionuclides are conservatively modelled as being transferred directly to the geosphere. The buffer is assumed to provide no delay or attenuation of radionuclide releases (advective conditions prevail in the buffer in the scenario where the buffer is severely eroded by glacial meltwater). Thereafter, it is further conservatively assumed that, with the exception of uranium isotopes, all radionuclides released by fuel matrix dissolution and corrosion of the Zircaloy and other metal parts are transferred directly and instantaneously to the geosphere at the rate that they are released from these components. The same rates of dissolution and corrosion are assumed as in the Base Case for an initial penetrating defect (case PD-BC – Table 5-5). Solubility limitation is not taken into account for these radionuclides because of their low concentrations in the case of advective flow in the eroded buffer, and because the capacity of the eroded buffer to filter colloids formed if precipitation does take place is uncertain.

Uranium, on the other hand, is present in relative large amounts, and may be precipitated as the fuel matrix dissolves. Although it is uncertain whether or not uranium colloids would be filtered by an eroded buffer, it is argued in SR-Can that, in terms of calculated individual doses or risks, it is conservative to assume that all precipitated uranium remains within the canister, where it continues to produce daughter radionuclides, such as the Th-230, Th-229 and Pa-231 generated by U-234, U-233 and U-235, respectively. This is because, without uranium precipitation, the uranium isotopes are released to and dispersed in the biosphere before more radiotoxic daughters are produced. This approach is also followed in the present safety assessment. The solubility limit for uranium is given in Table 5-6. Uranium daughters and dissolved uranium are modelled as being transferred directly to the geosphere, as described above.

In order to calculate the amount of dissolved uranium released to the geosphere, the transfer coefficient from the canister interior to the geosphere, Q_F [$m^3\ a^{-1}$], is set equal to the groundwater flow rate through the eroded buffer. If the eroded buffer is assumed to have a hydraulic conductivity far in excess of that of the rock:

$$Q_F = 4 r_t T i \qquad \text{(Eq. 6-1)}$$

i.e. the perturbed buffer "captures" the flow from a portion of the fracture that is twice the drift diameter. Q_F takes a value of $3.1 \times 10^{-3}\ m^3\ a^{-1}$.

6.2.3 Geosphere model

The geosphere model is as in the Base Case for an initial penetrating defect. Parameter values that apply to all migrating species are given in Table 5-8. Element-dependent parameters are given in Table 5-9 and 5-10.

6.2.4 Results

Table 6-2 gives calculated maximum near-field release rates in Bq per year for all radionuclides for which calculations were made in the Base Case for an initial penetrating defect (case PD-BC) and in the Base Case for canister rupture due to canister corrosion (CC-BC). It also gives the times at which these maxima occur (t_{max}).

For shorter-lived radionuclides, such as C-14 with a half-life of 5,700 years, near-field release maxima are lower in CC-BC than in PD-BC, since this radionuclide substantially decays before canister failure in case CC-BC. On the other hand, the increase in Q_F in case CC-BC compared with PD-BC results in generally higher near-field release maxima for radionuclides longer half-lives. The increase for sorbing radionuclides, such as Cs-135, is greater than that for non-sorbing radionuclide, such as I-129. This is because the transport barrier provided by the buffer in case PD-BC provides greater attenuation of releases by decay for sorbing compared with non-sorbing radionuclides. The assumption of direct transfer from the canister interior to the geosphere means that this transport barrier is by-passed for all radionuclides in case CC-BC.

Table 6-2. Calculated maximum near-field release rates for each radionuclide in the Base Case for an initial penetrating defect (case PD-BC) and in Base Case for canister failure due to corrosion (CC-BC), and the times at which these maxima occur. The calculation begins at 100,000 years (see main text). Full results are presented in Appendix G.

	Radionuclide	PD-BC t_{max} [a]	PD-BC Bq/a	CC-BC t_{max} [a]	CC-BC Bq/a
Activation/fission products	C-14	1.01E+04	6.77E+05	1.01E+05	1.02E+02
	Cl-36	1.03E+04	1.10E+05	1.00E+05	3.78E+05
	Ni-59	1.23E+04	3.44E+05	1.01E+05	1.16E+08
	Se-79	2.15E+04	2.08E–01	1.00E+05	2.47E+04
	Mo-93	1.08E+04	3.67E–01	–	–
	Zr-93	2.20E+05	5.03E–02	1.02E+05	1.68E+06
	Zr-93p*	2.35E+05	3.68E+00	1.02E+05	1.69E+04
	Nb-94	1.99E+04	7.70E+03	1.01E+05	1.92E+06
	Tc-99	8.85E+05	2.25E+01	1.00E+05	4.17E+07
	Pd-107	8.90E+05	3.02E+01	1.00E+05	4.02E+05
	Sn-126	1.15E+05	4.84E+00	1.00E+05	1.03E+04
	I-129	1.03E+04	1.27E+04	1.00E+05	5.38E+05
	Cs-135	1.01E+04	7.78E+03	1.00E+05	9.93E+06
Actinide chains	Pu-240	3.44E+04	1.65E+01	1.01E+05	8.84E+01
	U-236	1.00E+06	5.79E–04	1.00E+05	3.53E–02
	Cm-245	5.38E+04	6.05E–04	1.01E+05	3.47E–01
	Am-241	5.38E+04	6.38E–04	1.01E+05	3.61E–01
	Np-237	1.00E+06	8.21E–01	1.02E+05	8.77E+03
	U-233	1.00E+06	1.30E+00	1.00E+05	8.46E–02
	Th-229	1.00E+06	7.65E–01	9.90E+05	1.57E+05
	Cm-246	3.88E+04	6.19E–06	1.01E+05	9.60E–05
	Pu-242	3.94E+05	3.01E+01	1.02E+05	1.35E+04
	U-238	1.00E+06	4.95E–04	1.00E+05	3.01E–02
	U-234	1.29E+05	2.02E–03	1.00E+05	1.79E–01
	Th-230	5.64E+05	2.77E+01	1.10E+06	3.20E+04
	Ra-226	5.64E+05	3.59E+04	2.25E+05	1.27E+04
	Am-243	4.88E+04	4.05E–02	1.01E+05	1.22E+01
	Pu-239	5.88E+04	2.21E+02	1.01E+05	1.17E+05
	U-235	1.00E+06	3.60E–05	1.00E+05	2.19E–03
	Pa-231	1.00E+06	3.27E+01	1.10E+06	5.47E+03

* Zirconium originating from the fuel matrix only.

Figure 6-1 shows the releases from the geosphere to the biosphere as a function of time in case CC-BC expressed as WELL-2007 dose based on the dose conversion factors given in Table 3-1. Figure 6-2 shows time-dependent releases from the geosphere to the biosphere divided by the geo-bio flux constraints specified by the Finnish regulator and given in Table 1-1, and the sum of these releases over all calculated radionuclides.

The peak dose, which is dominated by I-129, occurs shortly after canister failure at 100,000 years, and is more than two orders of magnitude below the regulatory dose guideline of 10^{-4} Sv per year. At later times, dose continues firstly to be dominated by I-129, and later by

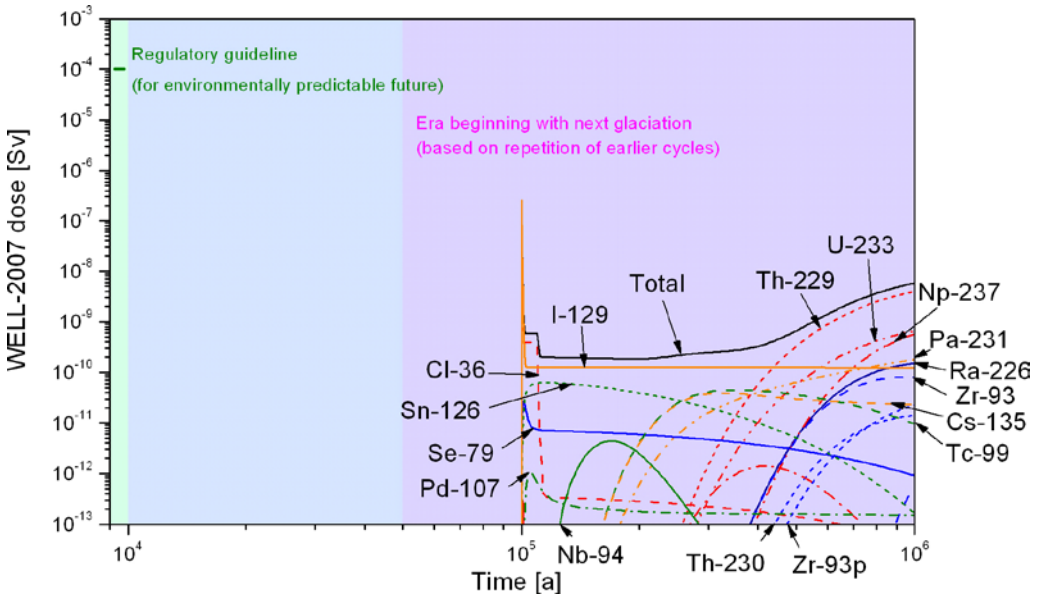

Figure 6-1. *WELL-2007 dose as a function of time in case CC-BC.*

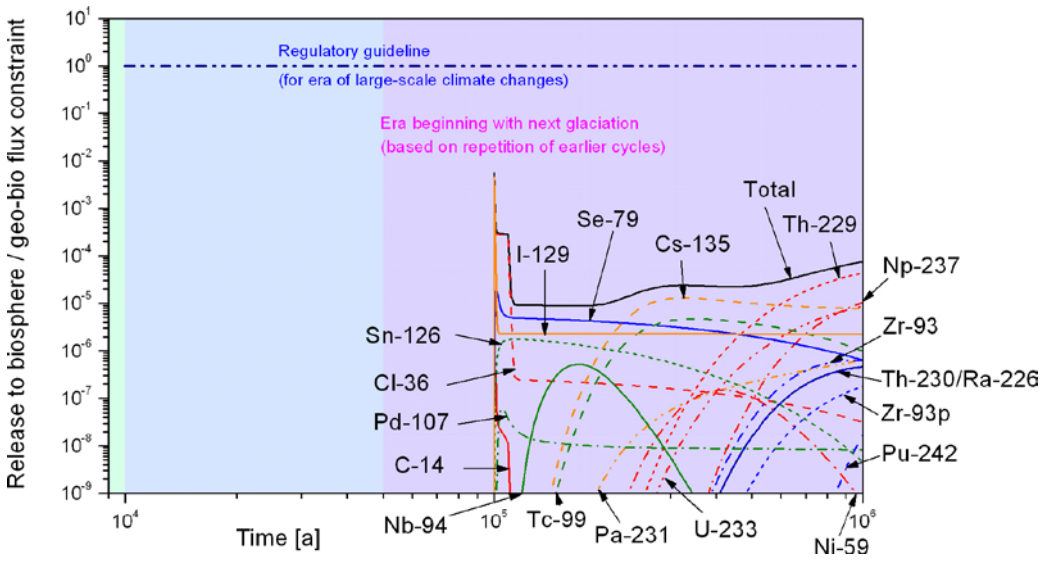

Figure 6-2. *Ratios of nuclide-specific activity releases to their respective geo-bio flux constraints in case CC-BC.*

Th-229 (a decay product of Np-237). The sum of time-dependent releases from the geosphere to the biosphere divided by their respective geo-bio flux constraints also has its maximum shortly after 100,000 years, and takes a value of 6×10^{-3} (i.e. it would require in excess of one hundred canisters failing at similar times for the regulatory guideline to be exceeded; as noted earlier, the estimation of the number of canister that may fail at similar times by this mode is an issue for future work).

It should be noted that the magnitude of the peak shortly after 100,000 years is increased by the conservative assumption that the canister fails completely and instantaneously at this time. In reality, some mass transport resistance may be retained following the initial failure of a canister.

6.3 Cases addressing uncertainties in the fuel dissolution rate

6.3.1 Differences compared with the Base Case

In the Base Case CC-BC, fuel dissolution subsequent to the fuel being contacted by water is assumed to take place at a constant fractional fuel dissolution rate of 10^{-7} per year. In order to assess the impact of uncertainties in the rate of the dissolution process, alternative increased and decreased rates are considered in cases **CC-HIFDR** and **CC-LOFDR**, respectively.

6.3.2 Radionuclide inventories, half-lives and partitioning

Radionuclide inventories and half-lives and partitioning between fuel matrix, IRF, Zircaloy and other metal parts are as in the Base Case.

6.3.3 Near-field model

The geometry of near-field model domain is also as in the Base Case. Increased and decreased fuel matrix fractional dissolution rates of 10^{-6} and 10^{-8} per year (compared with the Base Case value of 10^{-7} per year) are assumed in variant cases CC-HIFDR and CC-LOFDR, respectively. These values correspond to the upper and lower limits of the triangular distribution recommended for use in SR-Can by /Werme et al. 2004/.

Other parameter values related to radionuclide release, as well as parameter values related to the processes of:

- water ingress;
- solubility limitation and radionuclide transport inside the canister;
- radionuclide transfer to the buffer/evolution of the defect;
- radionuclide transport in the buffer; and
- radionuclide transfer to the geosphere;

are as in the Base Case. Near-field model boundary conditions and transfer coefficients are also unchanged with respect to the Base Case.

6.3.4 Geosphere model

The geosphere model is as in the Base Case.

6.3.5 Results

Table 6-3 gives calculated maximum near-field release rates in Bq per year for each radionuclide for which calculations were made in the Base Case for canister failure due to copper corrosion (case CC-BC) and in cases CC-HIFDR and CC-LOFDR. It also gives the times at which these maxima occur (t_{max}).

Figure 6-3 shows the releases from the geosphere to the biosphere as a function of time in cases CC-HIFDR and CC-LOFDR expressed as WELL-2007 dose based on the dose conversion factors given in Table 3-1. Figure 6-4 shows time-dependent releases from the geosphere to the biosphere divided by the geo-bio flux constraints specified by the Finnish regulator and given in Table 1-1, and the sum of these releases over all calculated radionuclides.

The higher long-term doses and releases of, for example, I-129, Cl-36, Ra-226, Th-229 and Cs-135 in CC-HIFDR compared with CC-LOFDR are clearly shown. The maximum dose, which is dominated by the I-129 instant release fraction, is, however, virtually unchanged.

Table 6-3. Calculated maximum near-field release rates for each radionuclide in the Base Case for canister failure due to copper corrosion (case CC-BC) and in cases CC-HIFDR and CC-LOFDR, and the times at which these maxima occur. BC – same as Base Case. Full results are presented in Appendix G.

Radionuclide			CC-BC		CC-HIFDR		CC-LOFDR	
			t_{max} [a]	Bq/a	t_{max} [a]	Bq/a	t_{max} [a]	Bq/a
Activation/fission products		C-14	1.01E+05	1.02E+02	BC	BC	BC	BC
		Cl-36	1.00E+05	3.78E+05	BC	BC	BC	BC
		Ni-59	1.01E+05	1.16E+08	BC	BC	BC	BC
		Se-79	1.00E+05	2.47E+04	BC	BC	BC	BC
		Mo-93	–	–	–	–	–	–
		Zr-93	1.02E+05	1.68E+06	1.02E+05	1.83E+06	1.02E+05	1.67E+06
		Zr-93p*	1.02E+05	1.69E+04	1.02E+05	1.69E+05	1.02E+05	1.69E+03
		Nb-94	1.01E+05	1.92E+06	BC	BC	BC	BC
		Tc-99	1.00E+05	4.17E+07	BC	BC	BC	BC
		Pd-107	1.00E+05	4.02E+05	BC	BC	BC	BC
		Sn-126	1.00E+05	1.03E+04	1.01E+05	2.31E+04	BC	BC
		I-129	1.00E+05	5.38E+05	BC	BC	BC	BC
		Cs-135	1.00E+05	9.93E+06	BC	BC	BC	BC
Actinide chains	4N	Pu-240	1.01E+05	8.84E+01	1.01E+05	8.84E+02	1.01E+05	8.84E+00
		U-236	1.00E+05	3.53E–02	BC	BC	BC	BC
	4N + 1	Cm-245	1.01E+05	3.47E–01	1.01E+05	3.47E+00	1.01E+05	3.47E–02
		Am-241	1.01E+05	3.61E–01	1.01E+05	3.61E+00	1.01E+05	3.61E–02
		Np-237	1.02E+05	8.77E+03	1.02E+05	8.77E+04	1.02E+05	8.77E+02
		U-233	1.00E+05	8.46E–02	BC	BC	BC	BC
		Th-229	9.90E+05	1.57E+05	9.90E+05	1.57E+06	9.70E+05	1.57E+04
	4N + 2	Cm-246	1.01E+05	9.60E–05	1.01E+05	9.60E–04	1.01E+05	9.60E–06
		Pu-242	1.02E+05	1.35E+04	1.02E+05	1.35E+05	1.02E+05	1.35E+03
		U-238	1.00E+05	3.01E–02	BC	BC	BC	BC
		U-234	1.00E+05	1.79E–01	BC	BC	BC	BC
		Th-230	1.10E+06	3.20E+04	1.10E+06	3.20E+05	1.10E+06	3.20E+03
		Ra-226	2.25E+05	1.27E+04	2.25E+05	1.27E+05	2.25E+05	1.27E+03
	4N + 3	Am-243	1.01E+05	1.22E+01	1.01E+05	1.22E+02	1.01E+05	1.22E+00
		Pu-239	1.01E+05	1.17E+05	1.01E+05	1.17E+06	1.01E+05	1.17E+04
		U-235	1.00E+05	2.19E–03	BC	BC	BC	BC
		Pa-231	1.10E+06	5.47E+03	1.10E+06	5.47E+04	1.10E+06	5.47E+02

* Zirconium originating from the fuel matrix only.

In both CC-HIFDR and CC-LOFDR, as in the Base Case, the dose maximum occurs shortly after loss of transport resistance of the defect at 100,000 years, and is more than two orders of magnitude below the regulatory dose criterion of 10^{-4} Sv per year (although, according to Finnish regulations, this criterion is applicable at earlier times – i.e. the environmentally predictable future). The sum of time-dependent releases from the geosphere to the biosphere divided by their respective geo-bio flux constraints also has its maximum shortly after 100,000 years, and is a little over two orders of magnitude below the regulatory guideline of one.

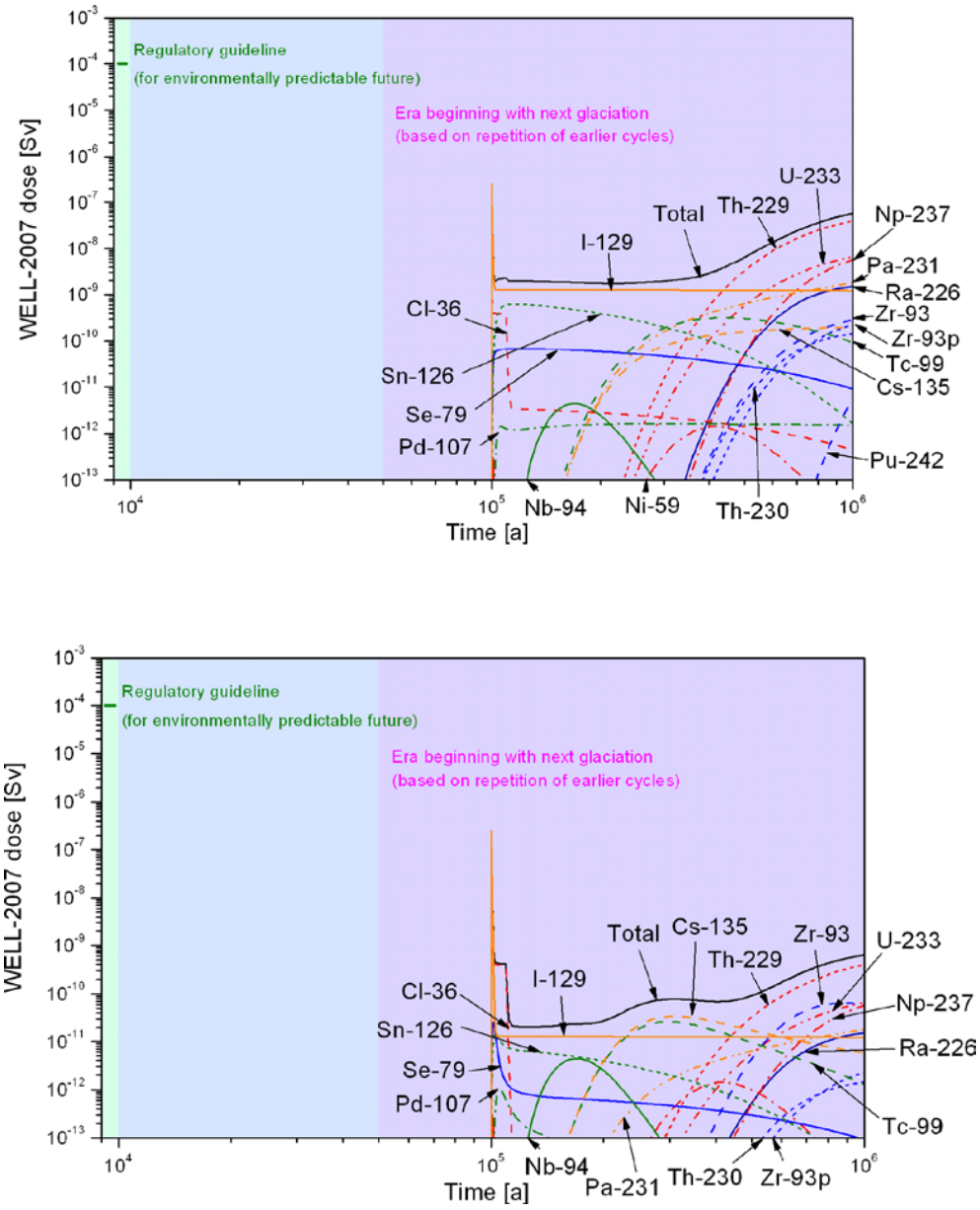

Figure 6-3. *WELL-2007 dose as a function of time in case CC-HIFDR (upper figure) and case CC-LOFDR (lower figure).*

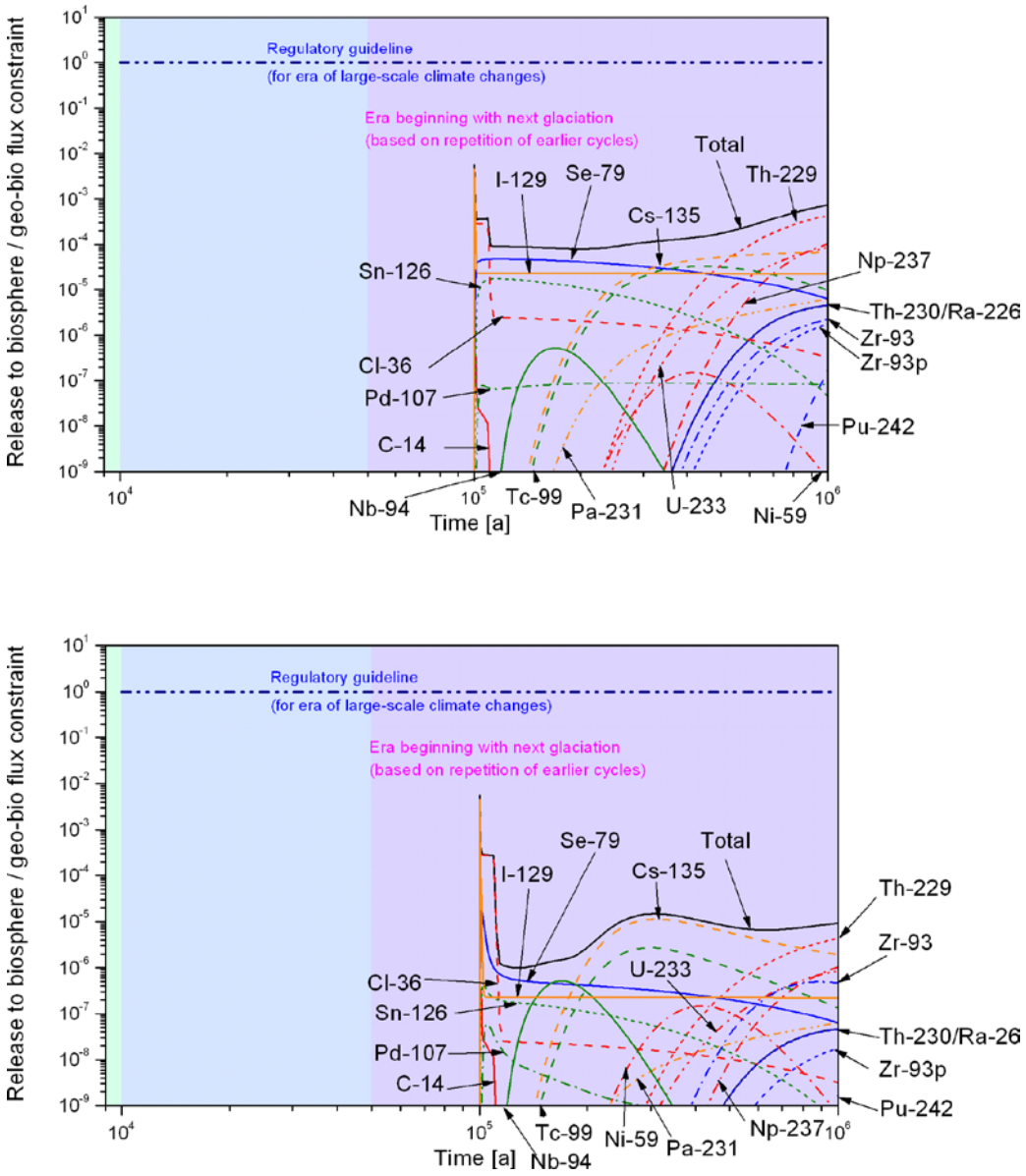

Figure 6-4. *Ratios of nuclide-specific activity releases to their respective geo-bio flux constraints in case CC-HIFDR (upper figure) and case CC-LOFDR (lower figure).*

6.4 Cases addressing uncertainties in geosphere transport resistance and groundwater composition

6.4.1 Differences compared with the Base Case

As discussed in Chapter 5 in the context of a canister with an initial penetrating defect, there are numerous uncertainties associated with groundwater flow and composition. Groundwater flow and the geosphere transport resistance may be affected, for example, by:

- uncertainties in the characterisation of the network of water-conducting fractures in the host rock; and
- the degradation of characterisation borehole backfill and seals, which could lead to the formation of new water conducting features.

Groundwater composition, and particularly salinity, may also be affected by repository excavation and, in the far longer-term, by the possible influx of glacial meltwater to repository depth.

As in the case of canister failure due to an initial, penetrating defect, no detailed analysis to quantify or bound these various uncertainties and perturbing processes has been carried out. However, a limited set of four assessment cases is defined and analysed to provide an indication of the importance of groundwater flow and geosphere transport resistance in delaying and attenuating releases from the near field in the event of canister failure by corrosion. Because glaciation and chemical erosion of the buffer by glacial meltwater are key concerns in discussion of canister failure by corrosion, three out of four of these cases consider potential effects of glaciation on groundwater flow and composition.

As noted in Chapter 5, groundwater flow may, in reality, vary significantly with time, particularly in association with glacial advance and retreat, and the impact of time-varying flow and associated variations in groundwater composition on radionuclide release and transport are issues for future studies.

In case **CC-GMW**, dilute glacial meltwater is assumed to be present at all times after canister failure. The geosphere transport resistance is decreased with respect to the Base Case resistance in case **CC-LOGEOR**, while groundwater conditions are assumed to remain reducing and dilute/brackish, as in the Base Case. This case was selected because of the potential effects of glaciations/permafrost on the hydraulic properties of the geosphere (e.g. taliks, hydraulic jacking). In case **CC-LOGEORS**, geosphere transport resistance is also decreased with respect to the Base Case, while in addition saline/brackish water is assumed. This case was selected because there is a potential for upconing of saline/brackish groundwater during periods of permafrost and in the presence of a warm-based ice sheet, as discussed in the KBS-3V Evolution Report /Pastina and Hellä 2006/. Finally, in case **CC-LOGEORG**, geosphere transport resistance is again decreased with respect to the Base Case, while in addition low salinity glacial meltwater water is assumed to be present throughout the geosphere. In all of these cases, an increased fuel dissolution rate is assumed to address the uncertainty due to the fuel dissolution rate in the case of low geosphere transport resistance (WL/Q).

It is assumed that 100,000 years remains a conservative choice of canister failure time, irrespective of these uncertainties in groundwater flow and composition. Another issue for further study is, however, whether the number of canisters that may fail at similar times by corrosion is affected by these uncertainties.

6.4.2 Radionuclide inventories, half-lives and partitioning

Radionuclide inventories and half-lives and partitioning between fuel matrix, IRF, Zircaloy and other metal parts are as in the Base Case, and are given in Table 5-2.

6.4.3 Near-field model

A fractional fuel matrix dissolution rate identical to that in case CC-HIFDR (10^{-6} per year) is assumed in all four variant cases. U solubility for case CC-LOGEORS is the same as that in case PD-SAL, and U solubility in cases CC-GMW and CC-LOGEORG is the same as those in case PD-GMW (Table 5-30). In other respects, the near-field model in all four variant cases is identical to that of the Base Case.

6.4.4 Geosphere model

In case CC-LOGEOR, the geosphere model is identical to that of the Base Case, with the exception of the transport resistance of the geosphere (WL/Q) which is assigned a value of 5,000. The transport resistance of geosphere is also set to 5,000 in cases CC-LOGEORS and CC-LOGEORG. The transport resistance of the geosphere takes the base Case value (50,000) in case PD-GMW.

In case CC-LOGEORS, element-dependent porosities and effective diffusion coefficients for anions and for neutral and cationic species, as well as geosphere sorption coefficients, are the same as those in case PD-SAL. In cases CC-GMW and CC-LOGEORG, values are the same as in case PD-GMW, respectively (Tables 5-31 and 5-32). In case CC-LOGEOR, they are identical to those of the Base Case.

6.4.5 Results

Table 6-4 gives calculated maximum near-field release rates in Bq per year for each radionuclide in the Base Case for canister failure due to copper corrosion (case CC-BC) and in cases CC-LOGEOR and CC-LOGEORS, indicating where there are differences between these latter two cases. It also gives the times at which the maxima occur (t_{max}).

Figure 6-5 shows the releases from the geosphere to the biosphere as a function of time in cases CC-LOGEOR and CC-LOGEORS expressed as WELL-2007 dose based on the dose conversion factors given in Table 3-1. Figure 6-6 shows time-dependent releases from the geosphere to the biosphere divided by the geo-bio flux constraints specified by the Finnish regulator and given in Table 1-1, and the sum of these releases over all calculated radionuclides.

There is a pulse release dominated by the I-129 IRF at 100,000 years. The sharpness and height of this initial peak are due to the assumption of complete loss of transport resistance of the canister immediately upon failure. Higher doses and summed releases, however, occur some hundreds of thousands of years later (and are still increasing slightly at a million years). These are dominated by Ra-226, and are higher in case CC-LOGEORS (saline groundwater) than in CC-LOGEOR (dilute/brackish groundwater) because of the lower geosphere sorption coefficient of Ra-226 in case CC-LOGEORS (0.02 for saline groundwater, see Table 5-32, compared with 0.2 for dilute/brackish groundwater, see Table 5-10).

The WELL-2007 dose at a million years is less than an order of magnitude below the regulatory dose criterion of 10^{-4} Sv per year in case CC-LOGEORS (although, according to Finnish regulations, this criterion is applicable at earlier times – i.e. the environmentally predictable future). The Ra-226 releases from the geosphere to the biosphere divided by its geo-bio flux constraint is, however, more than an order of magnitude below the regulatory guideline of one at a million years.

Table 6-4. Calculated maximum geosphere release rates for each radionuclide in the Base Case for canister failure due to copper corrosion (case CC-BC) and in cases CC-LOGEOR and CC-LOGEORS, and the times at which these maxima occur. LOGEOR indicates same magnitude of release maximum as case CC-LOGEOR. Full results are presented in Appendix G.

Radionuclide			Base Case (CC-BC)		CC-LOGEOR		CC-LOGEORS	
			t_{max} [a]	Bq/a	t_{max} [a]	Bq/a	t_{max} [a]	Bq/a
Activation/fission products		C-14	1.01E+05	1.02E+02	1.01E+05	1.02E+02	LOGEOR	LOGEOR
		Cl-36	1.00E+05	3.30E+05	1.00E+05	3.68E+05	1.00E+05	3.63E+05
		Ni-59	4.14E+05	4.50E+03	1.20E+05	1.69E+06	1.02E+05	3.33E+07
		Se-79	1.01E+05	1.88E+03	1.00E+05	1.24E+04	1.00E+05	1.64E+04
		Mo-93	–	–	–	–	–	–
		Zr-93	9.74E+05	6.26E+03	1.58E+05	1.93E+05	LOGEOR	LOGEOR
		Zr-93p*	1.10E+06	2.12E+03	3.70E+05	1.25E+05	LOGEOR	LOGEOR
		Nb-94	1.68E+05	5.22E+02	1.05E+05	1.40E+05	LOGEOR	LOGEOR
		Tc-99	3.50E+05	1.41E+04	1.33E+05	6.59E+05	LOGEOR	LOGEOR
		Pd-107	1.05E+05	6.11E+03	1.00E+05	1.00E+05	1.00E+05	2.40E+05
		Sn-126	1.43E+05	1.36E+03	1.05E+05	2.07E+04	1.04E+05	2.22E+04
		I-129	1.00E+05	4.56E+05	1.00E+05	5.22E+05	1.00E+05	5.14E+05
		Cs-135	3.24E+05	3.91E+03	1.11E+05	8.67E+04	1.02E+05	3.82E+05
Actinide chains	4N	Pu-240	1.00E+05	4.96E–12	1.38E+05	2.47E–01	LOGEOR	LOGEOR
		U-236	1.10E+06	1.56E–02	1.10E+06	3.34E–02	LOGEOR	LOGEOR
	4N +1	Cm-245	2.04E+05	5.39E–07	1.14E+05	5.25E–01	LOGEOR	LOGEOR
		Am-241	2.04E+05	5.68E–07	1.14E+05	5.53E–01	LOGEOR	LOGEOR
		Np-237	1.10E+06	1.26E+03	4.20E+05	6.74E+04	LOGEOR	LOGEOR
		U-233	1.10E+06	2.96E+03	7.30E+05	2.42E+04	LOGEOR	LOGEOR
		Th-229	1.10E+06	1.48E+03	1.00E+06	4.92E+04	LOGEOR	LOGEOR
	4N + 2	Cm-246	1.88E+05	2.93E–13	1.09E+05	6.91E–05	LOGEOR	LOGEOR
		Pu-242	1.10E+06	1.65E+00	3.74E+05	5.44E+04	LOGEOR	LOGEOR
		U-238	1.10E+06	1.35E–02	1.09E+06	2.85E–02	LOGEOR	LOGEOR
		U-234	1.10E+06	1.73E–02	1.93E+05	1.12E–01	LOGEOR	LOGEOR
		Th-230	1.10E+06	1.43E+01	1.10E+06	1.47E+05	LOGEOR	LOGEOR
		Ra-226	1.10E+06	1.46E+01	1.10E+06	1.50E+05	1.10E+06	1.45E+06
	4N + 3	Am-243	2.00E+05	5.40E–06	1.14E+05	1.57E+01	LOGEOR	LOGEOR
		Pu-239	1.00E+05	6.14E–09	1.78E+05	1.56E+04	LOGEOR	LOGEOR
		U-235	1.10E+06	9.82E–04	1.10E+06	2.07E–03	LOGEOR	LOGEOR
		Pa-231	1.10E+06	2.13E+01	1.10E+06	3.14E+04	LOGEOR	LOGEOR

* Zirconium originating from the fuel matrix only.

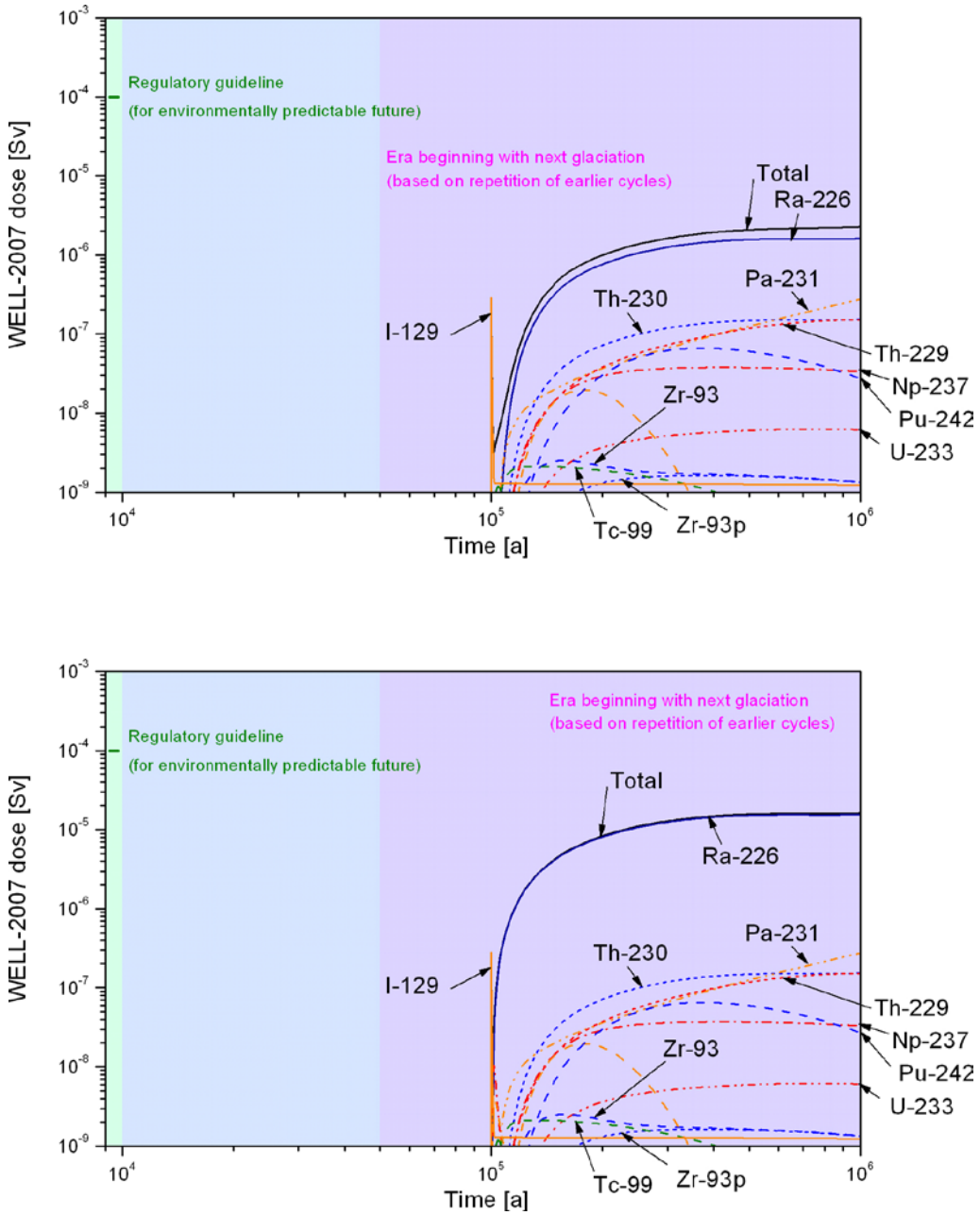

Figure 6-5. *WELL-2007 dose as a function of time in case CC-LOGEOR (upper figure) and case CC-LOGEORS (lower figure).*

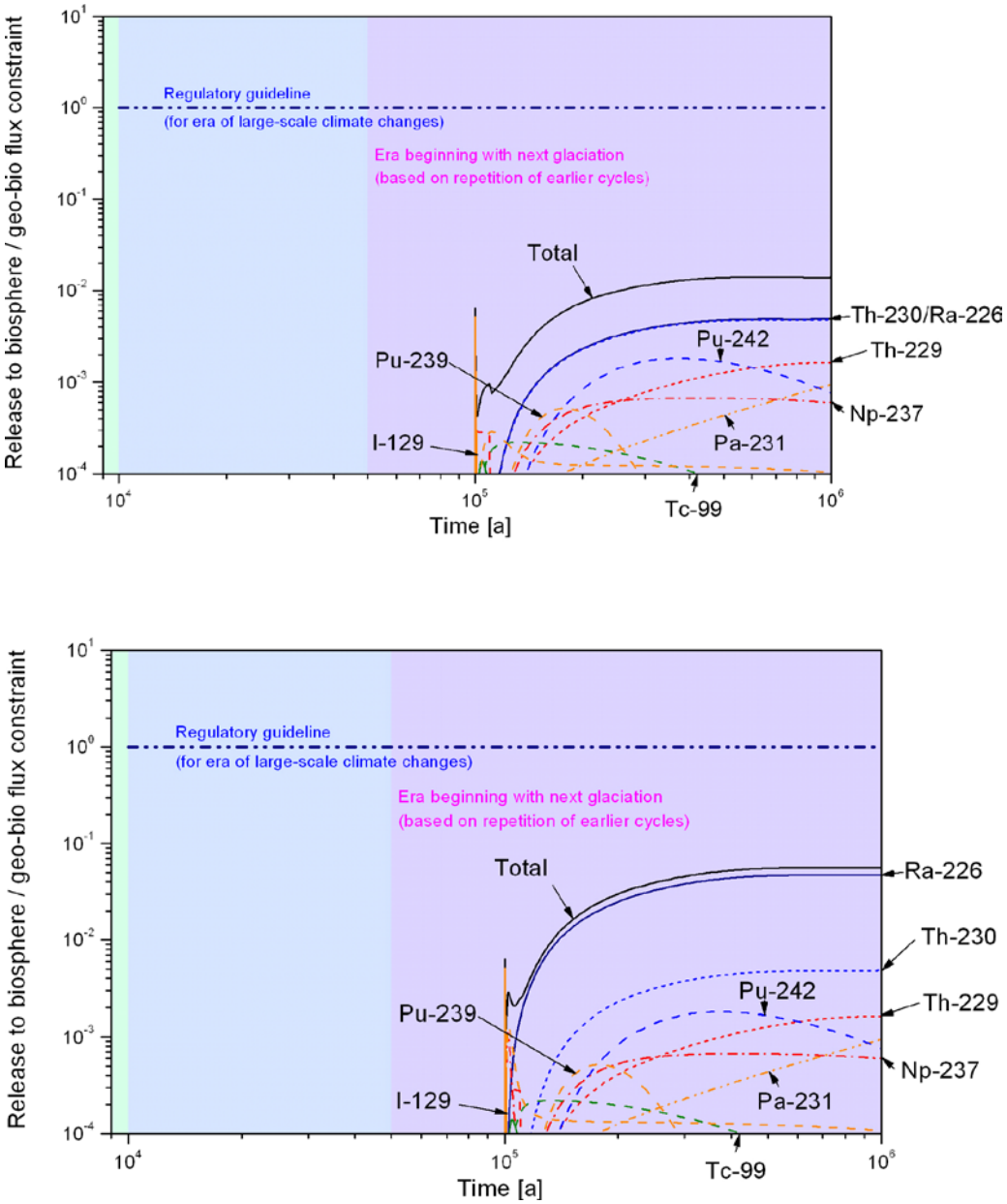

Figure 6-6. *Ratios of nuclide-specific activity releases to their respective geo-bio flux constraints in case CC-LOGEOR (upper figure) and case CC-LOGEORS (lower figure).*

Table 6-5 gives calculated maximum near-field release rates in Bq per year for each radionuclide in the Base Case for canister failure due to copper corrosion (case CC-BC) and in the glacial meltwater cases CC-GMW and CC-LOGEORG, indicating where there are differences between CC-GMW and CC-HIFDR (both assume increase fuel dissolution rates compared with the Base Case) and between CC-LOGEORG and CC-LOGEOR. It also gives the times at which the maxima occur (t_{max}).

Figure 6-7 shows the releases from the geosphere to the biosphere as a function of time in cases CC-GMW and CC-LOGEORG expressed as WELL-2007 dose based on the dose conversion factors given in Table 3-1. Figure 6-8 shows time-dependent releases from the geosphere to the biosphere divided by the geo-bio flux constraints specified by the Finnish regulator and given in Table 1-1, and the sum of these releases over all calculated radionuclides.

In both cases, there is a pulse release dominated by the I-129 IRF at 100,000 years. In case CC-GMW, this gives highest dose (a little less than two orders of magnitude below the regula-

Table 6-5. Calculated maximum geosphere release rates for each radionuclide in the Base Case for canister failure due to copper corrosion (case CC-BC) and in cases CC-GMW and CC-LOGEORG, and the times at which these maxima occur. HIFDR indicates release maxima are the same as in CC-HIFDR. LOGEOR indicates release maxima are the same as in case CC-LOGEOR. Full results are presented in Appendix G.

Radionuclide			Base Case (CC-BC)		CC-GMW		CC-LOGEORG	
			t_{max} [a]	Bq/a	t_{max} [a]	Bq/a	t_{max} [a]	Bq/a
Activation/fission products		C-14	1.01E+05	1.02E+02	HIFDR	HIFDR	LOGEOR	LOGEOR
		Cl-36	1.00E+05	3.30E+05	HIFDR	HIFDR	LOGEOR	LOGEOR
		Ni-59	4.14E+05	4.50E+03	HIFDR	HIFDR	LOGEOR	LOGEOR
		Se-79	1.01E+05	1.88E+03	HIFDR	HIFDR	LOGEOR	LOGEOR
		Mo-93	–	–	–	–	–	–
		Zr-93	9.74E+05	6.26E+03	HIFDR	HIFDR	LOGEOR	LOGEOR
		Zr-93p*	1.10E+06	2.12E+03	HIFDR	HIFDR	LOGEOR	LOGEOR
		Nb-94	1.68E+05	5.22E+02	HIFDR	HIFDR	LOGEOR	LOGEOR
		Tc-99	3.50E+05	1.41E+04	1.00E+05	3.54E+07	1.00E+05	4.04E+07
		Pd-107	1.05E+05	6.11E+03	HIFDR	HIFDR	LOGEOR	LOGEOR
		Sn-126	1.43E+05	1.36E+03	1.43E+05	1.35E+04	LOGEOR	LOGEOR
		I-129	1.00E+05	4.56E+05	HIFDR	HIFDR	LOGEOR	LOGEOR
		Cs-135	3.24E+05	3.91E+03	1.10E+06	1.98E+04	LOGEOR	LOGEOR
Actinide chains	4N	Pu-240	1.00E+05	4.96E–12	1.68E+05	1.78E–04	1.08E+05	1.15E+02
		U-236	1.10E+06	1.56E–02	1.08E+06	3.52E–02	8.34E+05	2.46E–02
	4N + 1	Cm-245	2.04E+05	5.39E–07	HIFDR	HIFDR	LOGEOR	LOGEOR
		Am-241	2.04E+05	5.68E–07	HIFDR	HIFDR	LOGEOR	LOGEOR
		Np-237	1.10E+06	1.26E+03	2.24E+05	7.84E+04	1.24E+05	8.56E+04
		U-233	1.10E+06	2.96E+03	1.02E+06	7.29E+03	9.80E+05	7.62E+02
		Th-229	1.10E+06	1.48E+03	1.03E+06	2.19E+02	1.01E+06	3.84E+04
	4N + 2	Cm-246	1.88E+05	2.93E–13	HIFDR	HIFDR	LOGEOR	LOGEOR
		Pu-242	1.10E+06	1.65E+00	7.24E+05	1.86E+04	2.04E+05	8.92E+04
		U-238	1.10E+06	1.35E–02	1.09E+06	3.00E–02	1.07E+06	2.10E–02
		U-234	1.10E+06	1.73E–02	1.28E+05	1.49E–01	1.07E+05	1.20E–01
		Th-230	1.10E+06	1.43E+01	HIFDR	HIFDR	LOGEOR	LOGEOR
		Ra-226	1.10E+06	1.46E+01	HIFDR	HIFDR	LOGEOR	LOGEOR
	4N + 3	Am-243	2.00E+05	5.40E–06	2.00E+05	5.40E–05	LOGEOR	LOGEOR
		Pu-239	1.00E+05	6.14E–09	2.34E+05	2.59E+02	1.16E+05	3.39E+05
		U-235	1.10E+06	9.82E–04	1.09E+06	2.18E–03	9.84E+05	1.52E–03
		Pa-231	1.10E+06	2.13E+01	HIFDR	HIFDR	LOGEOR	LOGEOR

* Zirconium originating from the fuel matrix only.

tory guideline) and the highest value of release divided be geo-bio flux constraint (more than two orders of magnitude below the regulatory guideline). The most significant contributions at later times come from Np-237 and Pu-242. In case CC-LOGEORG, the pulse at 100,000 years also the highest value of release divided be geo-bio flux constraint (a little less than two orders of magnitude below the regulatory guideline), but only slightly lower values are found at later times use to Th-230 and its daughter, Ra-226. The highest doses in case CC-LOGEORG are more than an order of magnitude below the regulatory guideline, are dominated by Ra-226 and occur some hundreds of thousands of years after the pulse, but are still increasing slightly at a million years.

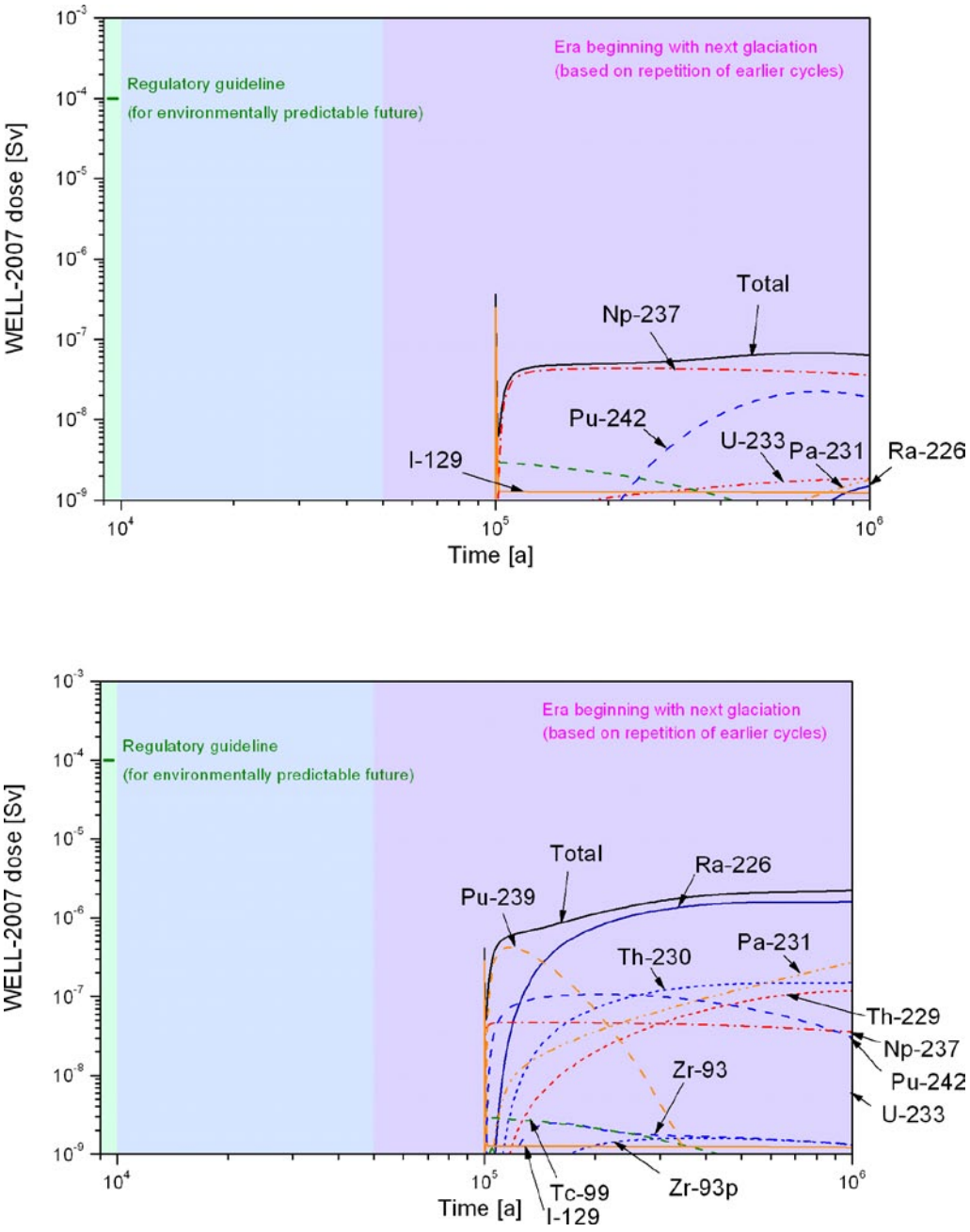

Figure 6-7. *WELL-2007 dose as a function of time in case CC-GMW (upper figure) and case CC-LOGEORG (lower figure).*

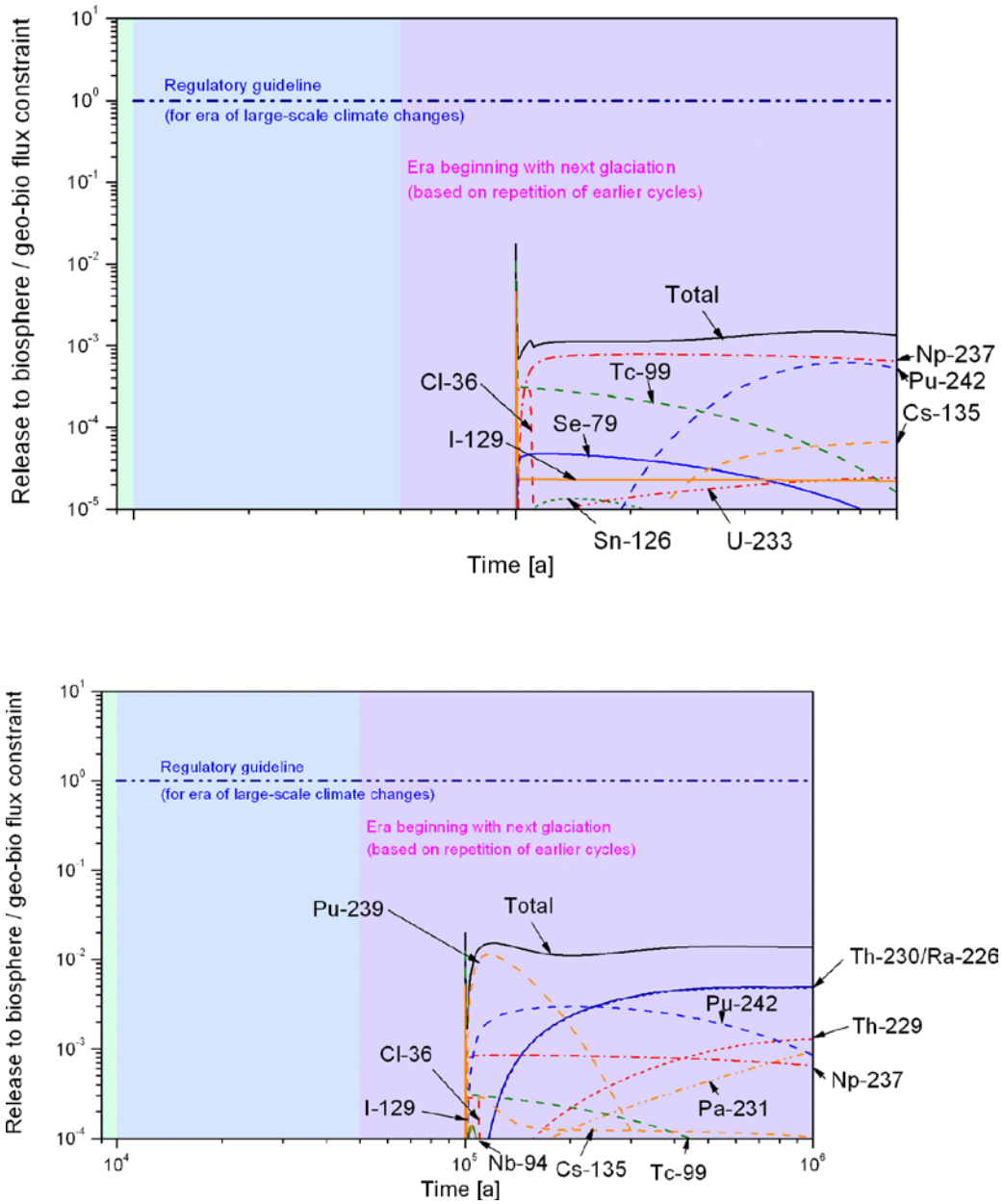

Figure 6-8. *Ratios of nuclide-specific activity releases to their respective geo-bio flux constraints in case CC-GMW (upper figure) and case CC-LOGEORG (lower figure).*

6.5 Summary of results for cases addressing failure due to copper corrosion

Table 6-6 gives a summary of results for all cases addressing failure due to copper corrosion. The table shows, for each case, the calculated WELL-2007 dose maxima and the summed geosphere release maxima (which each maximum divided by its respective geo-bio flux constraint), and the times of occurrence of these maxima.

Table 6-6. WELL-2007 dose maxima, maxima of the summed nuclide-specific activity releases divided by their respective geo-bio flux constraints, and the times of occurrence of these maxima for all cases addressing failure due to copper corrosion.

Case	WELL-2007 dose		Activity release	
	Maximum [Sv]	Time [a]	Maximum	Time [a]
CC-BC	2.5×10^{-7}	1.0×10^{5}	5.7×10^{-3}	1.0×10^{5}
CC-HIFDR	2.5×10^{-7}	1.0×10^{5}	5.7×10^{-3}	1.0×10^{5}
CC-LOFDR	2.5×10^{-7}	1.0×10^{5}	5.7×10^{-3}	1.0×10^{5}
CC-GMW	3.7×10^{-7}	1.0×10^{5}	1.7×10^{-2}	1.0×10^{5}
CC-LOGEOR	2.3×10^{-6} (at 10^{6} yrs)	$> 10^{6}$	1.4×10^{-2}	6.3×10^{5}
CC-LOGEORG	2.3×10^{-6} (at 10^{6} yrs)	$> 10^{6}$	2.0×10^{-2}	1.0×10^{5}
CC-LOGEORS	1.6×10^{-5} (at 10^{6} yrs)	$> 10^{6}$	5.7×10^{-2} (at 10^{6} yrs)	$> 10^{6}$

7 Cases addressing rupture due to rock shear

7.1 General considerations

As described in Section 2.2.6, large earthquakes, if they were to occur in the vicinity of the repository, could lead to shear movements on some of the larger fractures in the host rock that intersect the repository drifts. In the Base Case (**RS-BC**) and variant case for this canister failure mode, the location of the affected canister is assumed to coincide with the location of the shearing fracture. This follows the definition of a similar case in SR-Can (Section 10.7 of SR-Can, /SKB 2006b/). Any residual resistance provided by the canister to water ingress and radionuclide release following rupture due to rock shear is not considered quantifiable and is conservatively neglected. There is also assumed to be no delay between failure and the establishment of a radionuclide pathway from the canister interior to the buffer.

A shear movement of 10 cm is assumed to reduce the minimum transport distance for radionuclides through the buffer by 20 cm (see Figure 7-1 in Section 7.2.2). Note that 10 cm is a conservative estimate of the minimum shear movement required to cause canister failure; see Section 7.4.5 of the Evolution Report of /Smith et al. 2007a/.

The same dilute/brackish geochemical conditions are assumed in this Base Case as in the Base Case for a canister with an initial penetrating defect. However, because of the uncertain effects of shear movement on the transport properties of the geosphere, a high rate of groundwater flow (modelled by a "zero concentration" boundary condition) is assumed at the buffer/rock interface, and a lower geosphere transport resistance is assumed compared with the Base Case for a canister with an initial penetrating defect. A variant case (**RS-GMW**) with low-salinity glacial meltwaters also evaluated.

A single canister failing due to rock shear at 70,000 years is postulated, this being the time of the next glacial retreat, assuming a repetition of the last glacial cycle. As noted in connection with canister failure due to copper corrosion, some radionuclides will decay to insignificance within this time frame. Thus, Mo-93 in particular, which has a half-life of 4,000 years, is not included in the calculations.

The consequences of multiple canister failures at around the same time can be obtained by multiplying the results for single canister failure by the number of canister failures postulated. As described in Section 2.2.6, the expectation value of the number of canisters in the repository that could potentially be damaged by rock shear in the event of a large earthquake is currently estimated at 16 out of the total number of 3,000 canisters, although there are some significant uncertainties associated with the parameter values for the model by which this estimate is calculated that could lead to it being either an underestimate or an overestimate of the actual likelihood of damage. The probability an earthquake occurring that is sufficiently large to cause such damage in a 100,000 year time frame has been estimated at 0.02.

7.2 Base Case

7.2.1 Radionuclide inventories, half-lives and partitioning

Radionuclide inventories and half-lives and partitioning between fuel matrix, IRF, Zircaloy and other metal parts are as in the Base Case for an initial penetrating defect (case PD-BC), and are given in Table 5-2.

7.2.2 Near-field model

(i) Geometry

Radionuclides are assumed to be released to the buffer at the inner surface of an annular cylindrical region (indicated by dashed lines in Figure 7-1) with its axis lying along that of the drift. It has an inner radius equal to $r_c + d_s$ – i.e. the canister radius plus the assumed shear displacement of 10 cm, and an outer radius equal to $r_t - d_s$ – i.e. the drift radius minus 10 cm. A shear movement of 10 cm thus reduces the minimum transport distance for radionuclides through the buffer by 20 cm. These simplifications are made to maintain the cylindrical symmetry of the near field, which facilitates near-field transport modelling.

(ii) Processes and material properties

The canister is assumed to be ruptured by rock shear at 70,000 years after emplacement. Thereafter, the supply of water to the canister interior is conservatively assumed to be unlimited. Following the ingress of water, radionuclide release to the canister interior as well as solubility limitation of radionuclide concentration are treated as in the Base Case for an initial penetrating defect (PD-BC).

The ruptured canister is conservatively assumed to provide no resistance to radionuclide release. In reality, the ruptured canister may continue for some time to limit the ingress of water and the release of radionuclides, but, given their uncertainty, no credit is taken for these effects in the calculations.

Radionuclides diffuse from the canister interior to the buffer across the inner boundary of the annular cylindrical region shown by dashed lines in Figure 7-1, with its axis lying along that of the drift. The treatment of diffusion in the buffer is otherwise as in the Base Case for an initial penetrating defect, except that, due to the uncertainty in the properties of the intersecting fracture, the radionuclide concentration at the outer boundary of the buffer is conservatively set to zero.

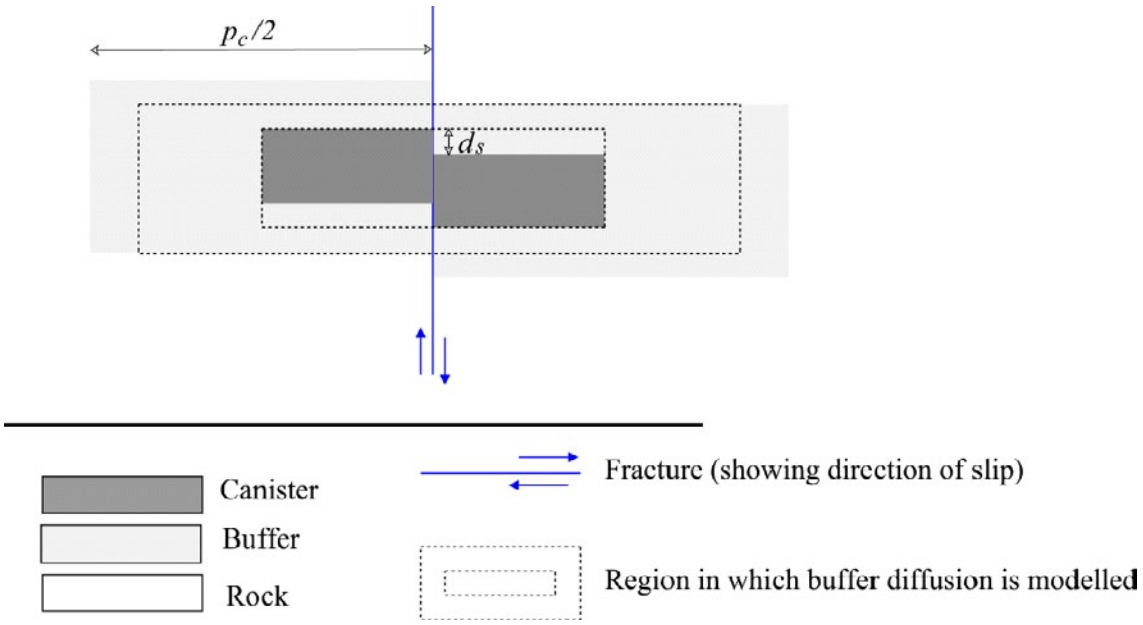

Figure 7-1. *Geometrical domain of the near-field model in the Base Case for canister rupture due to rock shear. The canister has a length of 4.835 m and an outer diameter of 1.05 m. The drift diameter is 1.85 m. The canister pitch (p_c) is 11 m. The displacement due to rock shear (d_s) is 10 cm.*

7.2.3 Geosphere model

The likely correlation between fracture size and transmissivity means that, at drift locations where rupture by rock shear occurs, the transport resistance provided by the host rock is likely to be relatively low, and may be further reduced by the effects of rock shear on the fracture. The flow in the fracture is therefore assumed to be high, leading to relatively rapid transport of radionuclides released from the buffer through the geosphere to the biosphere. The geosphere transport resistance is set to WL/Q = 1,000, which is a factor of 50 lower than in the Base Case for an initial penetrating defect (case PD-BC). The reduction in transport resistance with respect to PD-BC is greater than in other cases illustrating low geosphere transport resistances (e.g. PD-LOGEOR). This reflects the fact that shear movement is potentially a major event for the geosphere transport barrier. However, the value WL/Q = 1,000 is somewhat arbitrary and not based on site understanding. Developing a better understanding of the impart of shear movements on the properties of fractures is an issue for further studies.

7.2.4 Results

Table 7-1 gives calculated maximum near-field release rates in Bq per year for each calculated radionuclide in the Base Case for an initial penetrating defect (case PD-BC) and in the Base Case for canister rupture due to rock shear (RS-BC). It also gives the times at which these maxima occur (t_{max}). Although canister failure is much delayed with respect to case PD-BC, the near field provides a less effective transport barrier than in case PD-BC because of its reduced thickness and the assumption of zero concentration at the buffer/rock interface. Thus, the table shows that, for longer-lived radionuclides, and especially those with half-lives of 100,000 years or more, near-field releases are significantly increased in case RS-BC compared with case PD-BC.

Figure 7-2 shows the releases from the geosphere to the biosphere as a function of time in case RS-BC expressed as WELL-2007 dose based on the dose conversion factors given in Table 3-1. Figure 7-3 shows time-dependent releases from the geosphere to the biosphere divided by the geo-bio flux constraints specified by the Finnish regulator and given in Table 1-1, and the sum of these releases over all radionuclides for which calculations were made. There is a peak in dose of about 2×10^{-7} Sv for single canister failure that occurs shortly after canister failure at 70,000 years, which is almost three orders of magnitude below the regulatory dose guideline of 10^{-4} Sv per year. The highest dose, however, occurs at later times, and is due to Ra-226. The sum of time-dependent releases from the geosphere to the biosphere divided by their respective geo-bio flux constraints also has a peak shortly after 70,000 years, which more than two orders of magnitude below the regulatory guideline of one. The highest values, however, again occur at later times and are due to Ra-226. At a million years, these remain more than two orders of magnitude below the regulatory guideline.

The dose will clearly still be below the regulatory guideline if 16 canisters fail in the event of a single large earthquake. However, the number of canisters that might fail over a million year time frame (and contribute to the Ra-226 dose at a million years) due to multiple earthquakes has not so far been evaluated

Figures 7-4 and 7-5 shows release rate maxima from the near-field and geosphere, expressed in terms of WELL-2007 dose and in terms of releases divided by geo-bio flux constraints, respectively, for all the radionuclides considered in the case RS-BC. The figures show the very limited attenuation of near-field releases by the geosphere in this case. They also indicate that, at least for a single canister failure, regulatory guidelines are not exceeded even in the extreme hypothetical case of direct release from the near field to the biosphere.

Table 7-1. Calculated maximum near-field release rates for each radionuclide in the Base Case for an initial penetrating defect (case PD-BC) and in Base Case for canister rupture due to rock shear (RS-BC), and the times at which these maxima occur. Full results are presented in Appendix G.

Radionuclide			PD-BC t_{max} [a]	PD-BC Bq/a	RS-BC t_{max} [a]	RS-BC Bq/a
Activation/fission products		C-14	1.01E+04	6.77E+05	7.00E+04	1.26E+04
		Cl-36	1.03E+04	1.10E+05	7.00E+04	2.60E+05
		Ni-59	1.23E+04	3.44E+05	7.16E+04	6.94E+07
		Se-79	2.15E+04	2.08E–01	7.52E+04	2.67E+00
		Mo-93	1.08E+04	3.67E–01	–	–
		Zr-93	2.20E+05	5.03E–02	1.09E+05	8.90E+00
		Zr-93p*	2.35E+05	3.68E+00	1.14E+05	6.46E+02
		Nb-94	1.99E+04	7.70E+03	7.21E+04	4.76E+05
		Tc-99	8.85E+05	2.25E+01	8.49E+05	7.28E+03
		Pd-107	8.90E+05	3.02E+01	7.28E+04	1.87E+04
		Sn-126	1.15E+05	4.84E+00	1.01E+05	1.55E+03
		I-129	1.03E+04	1.27E+04	7.00E+04	3.41E+05
		Cs-135	1.01E+04	7.78E+03	7.00E+04	3.00E+07
Actinide chains	4N	Pu-240	3.44E+04	1.65E+01	8.15E+04	1.58E+02
		U-236	1.00E+06	5.79E–04	1.04E+06	1.01E–01
	4N + 1	Cm-245	5.38E+04	6.05E–04	9.19E+04	1.07E–01
		Am-241	5.38E+04	6.38E–04	9.19E+04	1.13E–01
		Np-237	1.00E+06	8.21E–01	1.06E+06	2.02E+02
		U-233	1.00E+06	1.30E+00	1.07E+06	4.84E+01
		Th-229	1.00E+06	7.65E–01	2.55E+05	9.74E+03
	4N + 2	Cm-246	3.88E+04	6.19E–06	8.58E+04	6.19E–05
		Pu-242	3.94E+05	3.01E+01	1.45E+05	8.80E+03
		U-238	1.00E+06	4.95E–04	1.07E+06	8.57E–02
		U-234	1.29E+05	2.02E–03	1.00E+05	4.30E–01
		Th-230	5.64E+05	2.77E+01	1.07E+06	1.77E+04
		Ra-226	5.64E+05	3.59E+04	1.07E+06	6.02E+05
	4N + 3	Am-243	4.88E+04	4.05E–02	9.19E+04	4.18E+00
		Pu-239	5.88E+04	2.21E+02	9.57E+04	6.73E+04
		U-235	1.00E+06	3.60E–05	1.07E+06	6.23E–03
		Pa-231	1.00E+06	3.27E+01	1.07E+06	4.63E+03

* Zirconium originating from the fuel matrix only.

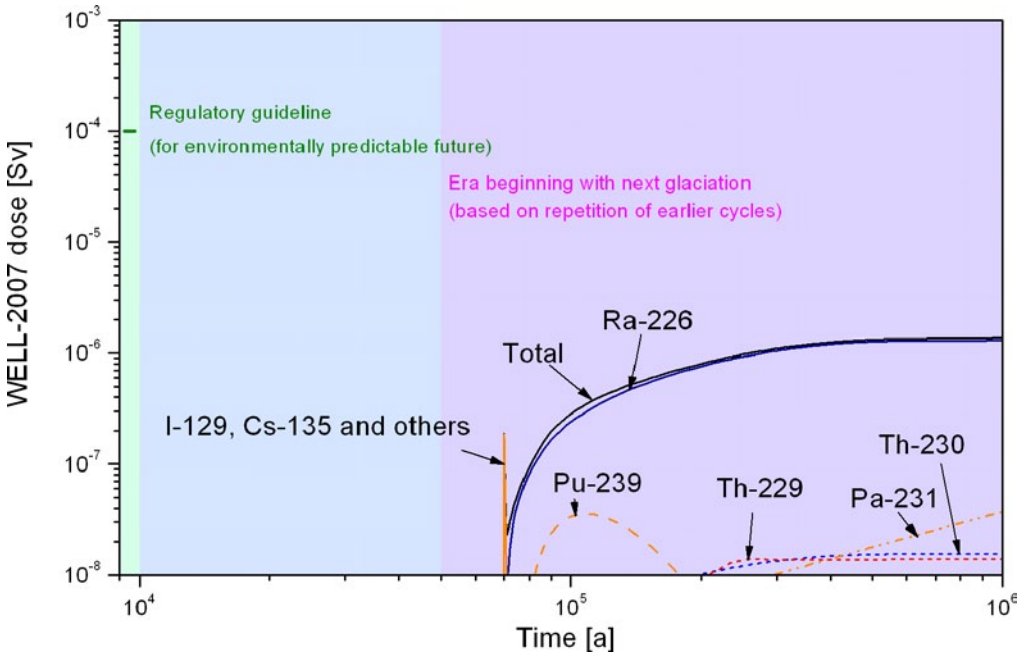

Figure 7-2. *WELL-2007 dose as a function of time in case RS-BC.*

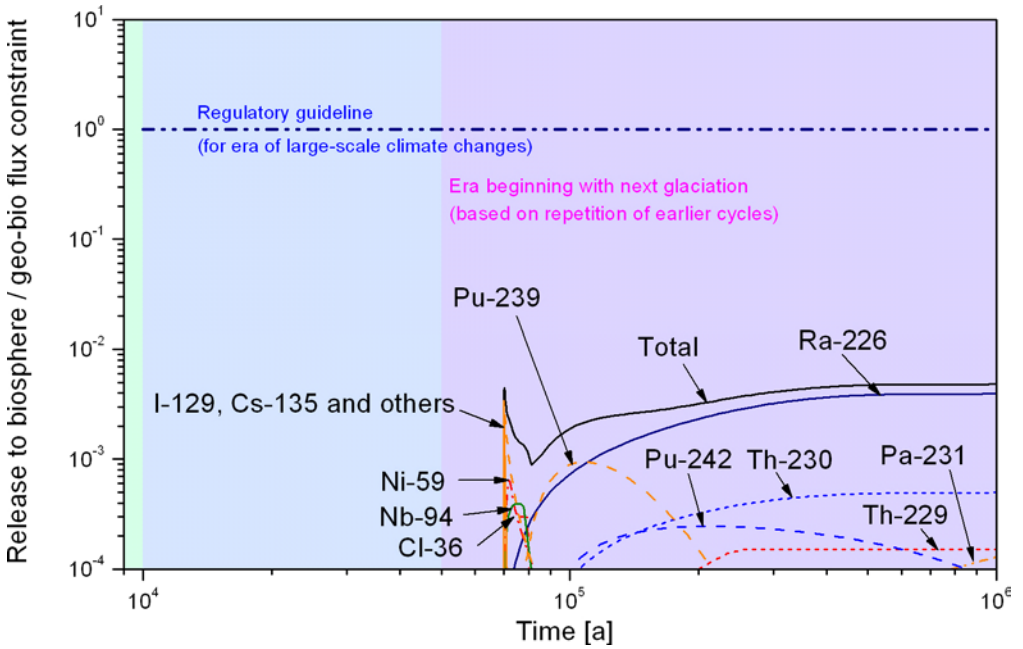

Figure 7-3. *Ratios of nuclide-specific activity releases to their respective geo-bio flux constraints in case RS-BC.*

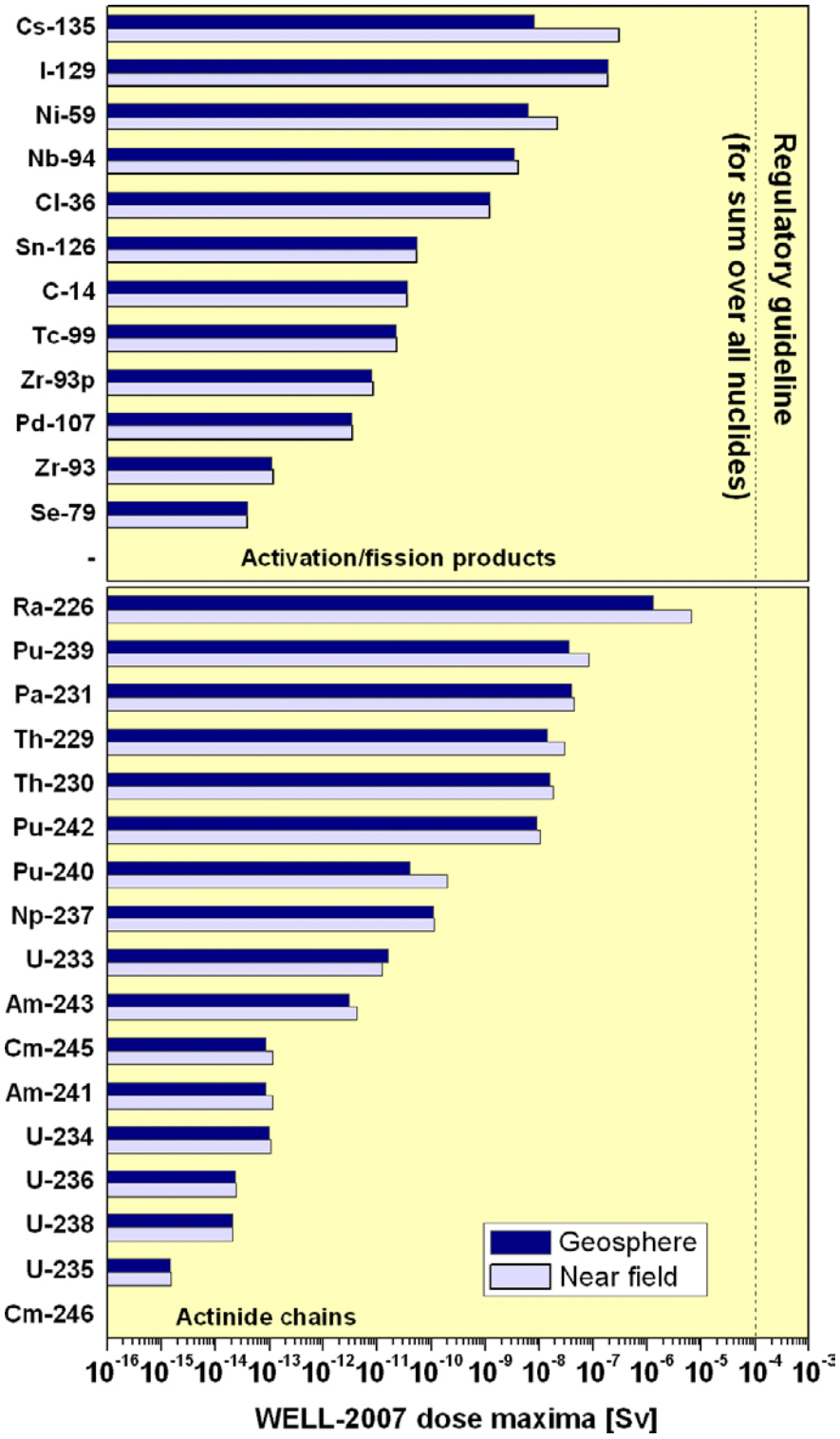

Figure 7-4. *Release rate maxima from the near field and geosphere, expressed as WELL-2007 dose, for all the radionuclides considered in the RS-BC calculation.*

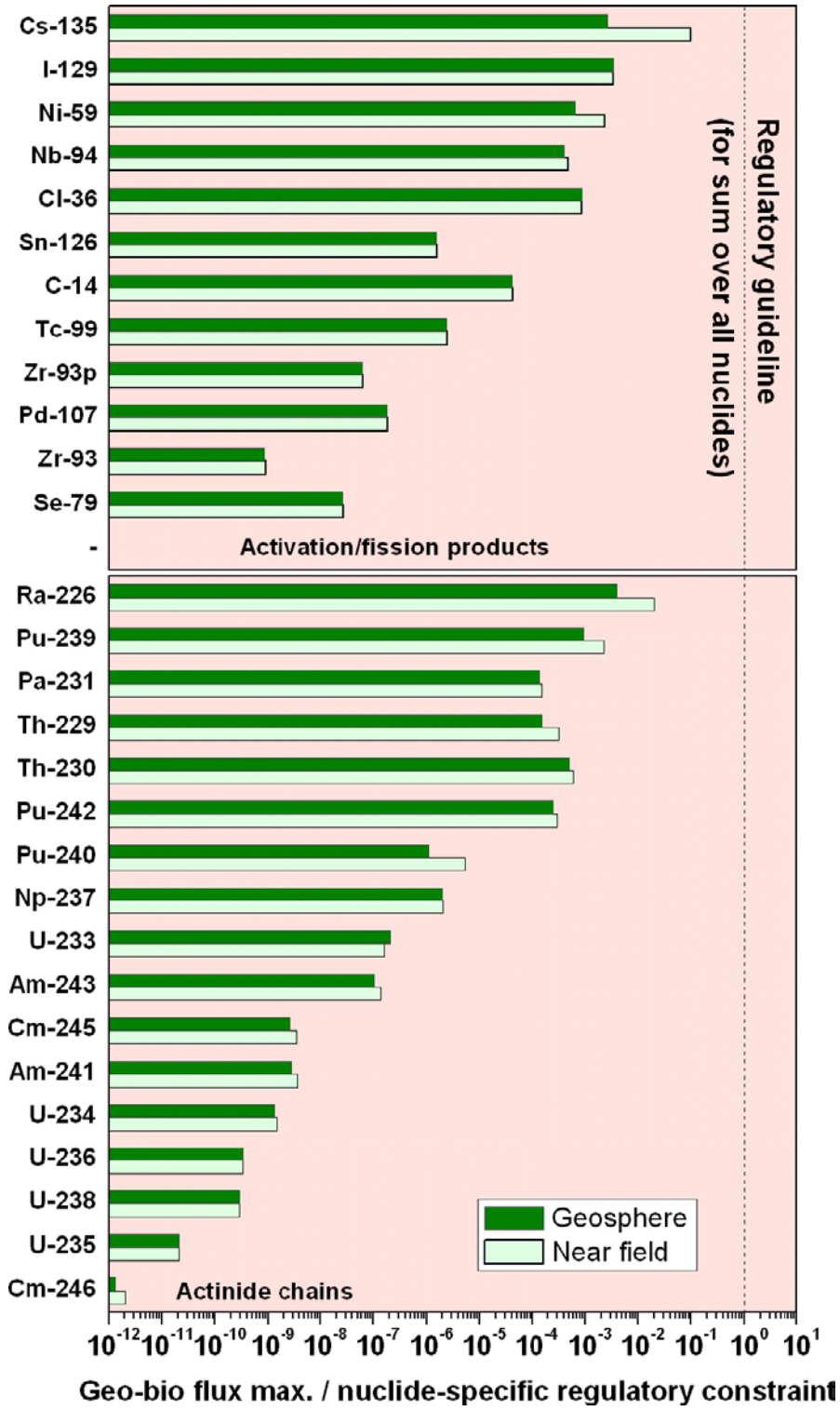

Figure 7-5. *Release rate maxima from the near field and geosphere divided by the geo-bio flux constraints specified by the Finnish regulator for all the radionuclides considered in the PD-BC calculation.*

7.3 Cases addressing uncertainties in groundwater composition

7.3.1 Differences compared with the Base Case

In case **RS-GMW**, dilute glacial meltwater is assumed to be present at all times after canister failure (earthquakes large enough to give rise to damaging shear movements being most likely to occur shortly after a period of glaciation).

7.3.2 Radionuclide inventories, half-lives and partitioning

Radionuclide inventories and half-lives and partitioning between fuel matrix, IRF, Zircaloy and other metal parts are as in the Base Case, and are given in Table 5-2.

7.3.3 Near-field model

Near-field solubilities for case RS-GMW are the same as those in case PD-GMW (Table 5-30). Otherwise, the near field model is as in the Base Case.

7.3.4 Geosphere model

In case RS-GMW, element-dependent porosities and effective diffusion coefficients for anions and for neutral and cationic species, as well as geosphere sorption coefficients, are the same as in case PD-GMW (Tables 5-31 and 5-32).

7.3.5 Results

Table 7-2 gives calculated maximum near-field release rates in Bq per year for each radionuclide in the Base Case canister failure due to rock shear (case RS-BC) and in case RS-GMW. It also gives the times at which these maxima occur (t_{max}). Figure 7-6 shows the releases from the geosphere to the biosphere as a function of time in case RS-GMW expressed as WELL-2007 dose based on the dose conversion factors given in Table 3-1. Figure 7-7 shows time-dependent releases from the geosphere to the biosphere in the same cases, divided by the geo-bio flux constraints specified by the Finnish regulator and given in Table 1-1, and the sum of these releases over all radionuclides for which calculations were made.

As in the Base Case, there is a peak in dose that occurs shortly after canister failure at 70,000 years. The highest dose, however, again occurs at later times, and is due to Ra-226. The sum of time-dependent releases from the geosphere to the biosphere divided by their respective geo-bio flux constraints also has a peak shortly after 100,000 years, which more than two orders of magnitude below the regulatory guideline of one. Once again, the highest values, however, occur at later times due to Ra-226. At a million years, these remain more than two orders of magnitude below the regulatory guideline.

Table 7-2. Calculated maximum geosphere release rates for each radionuclide in the Base Case for canister failure due to rock shear (case RS-BC) and in cases RS-GMW, and the times at which these maxima occur. BC – same as Base Case. Full results are presented in Appendix G.

Radionuclide			RS-BC t_{max} [a]	RS-BC Bq/a	RS-GMW t_{max} [a]	RS-GMW Bq/a
Activation/fission products		C-14	7.00E+04	1.23E+04	BC	BC
		Cl-36	7.00E+04	2.59E+05	BC	BC
		Ni-59	7.18E+04	1.94E+07	8.96E+04	5.36E+03
		Se-79	7.55E+04	2.66E+00	7.55E+04	3.86E–01
		Mo-93	–	–	–	–
		Zr-93	1.84E+05	8.27E+00	1.84E+05	8.76E+00
		Zr-93p*	1.94E+05	6.03E+02	1.94E+05	6.39E+02
		Nb-94	7.55E+04	3.93E+05	7.15E+04	1.09E+06
		Tc-99	1.05E+06	7.06E+03	1.03E+06	7.80E+03
		Pd-107	7.26E+04	1.81E+04	7.22E+04	1.90E+04
		Sn-126	1.03E+05	1.53E+03	7.01E+04	5.78E+03
		I-129	7.00E+04	3.40E+05	BC	BC
		Cs-135	7.04E+04	7.83E+05	BC	BC
Actinide chains	4N	Pu-240	8.96E+04	3.21E+01	8.13E+04	1.45E+00
		U-236	1.06E+06	9.95E–02	1.07E+06	2.44E–01
	4N + 1	Cm-245	9.35E+04	7.98E–02	7.38E+04	2.28E+00
		Am-241	9.35E+04	8.40E–02	7.46E+04	2.41E+00
		Np-237	1.06E+06	1.98E+02	1.04E+06	1.51E+02
		U-233	1.07E+06	6.21E+01	1.07E+06	3.68E+01
		Th-229	2.60E+05	4.55E+03	7.14E+05	5.79E+02
	4N + 2	Cm-246	8.63E+04	4.01E–05	7.32E+04	3.87E–03
		Pu-242	2.10E+05	7.35E+03	1.03E+06	1.22E+02
		U-238	1.07E+06	8.48E–02	1.05E+06	2.08E–01
		U-234	1.18E+05	3.95E–01	9.82E+04	1.04E+00
		Th-230	1.07E+06	1.51E+04	5.74E+05	2.70E+03
		Ra-226	1.07E+06	1.20E+05	1.07E+06	2.31E+05
	4N + 3	Am-243	9.35E+04	3.06E+00	7.38E+04	1.11E+02
		Pu-239	1.08E+05	2.84E+04	9.35E+04	5.15E+02
		U-235	1.07E+06	6.16E–03	1.05E+06	1.51E–02
		Pa-231	1.07E+06	4.14E+03	BC	BC

* Zirconium originating from the fuel matrix only.

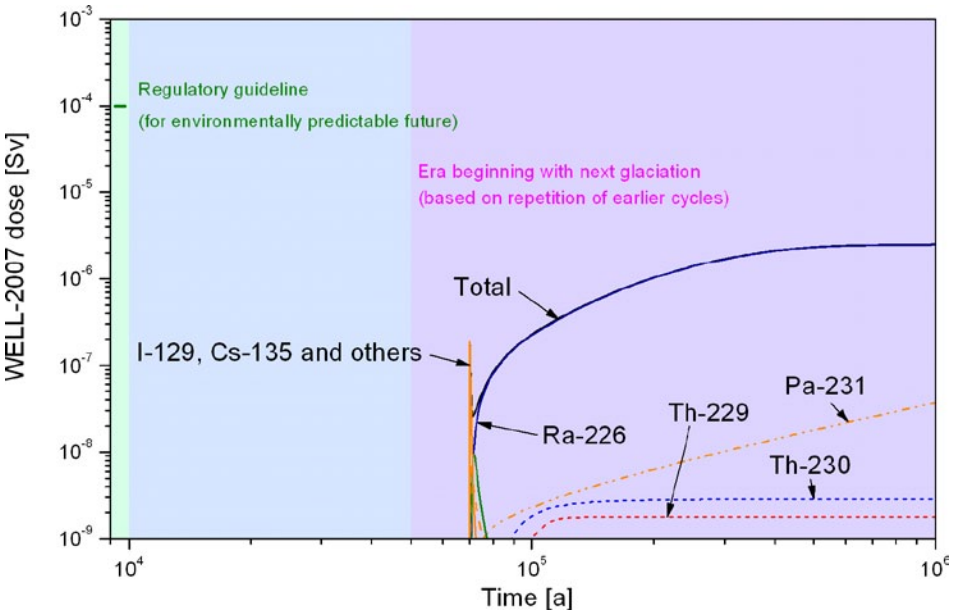

Figure 7-6. *WELL-2007 dose as a function of time in case RS-GMW.*

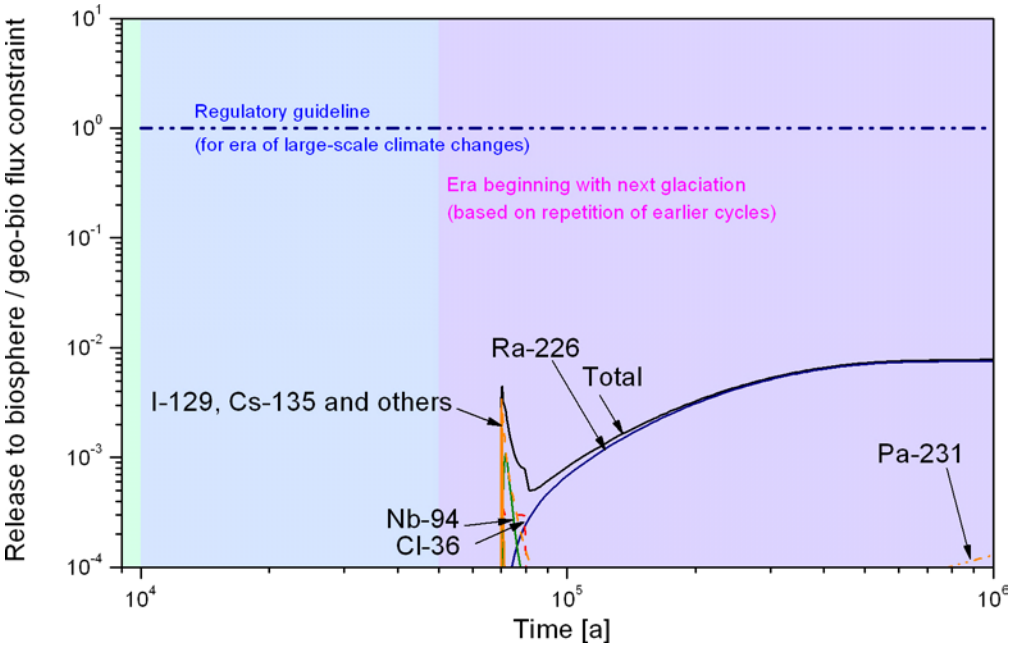

Figure 7-7. *Ratios of nuclide-specific activity releases to their respective geo-bio flux constraints in case RS-GMW.*

7.4 Summary of results for cases addressing rupture due to rock shear

Table 7-3 gives a summary of results for all cases addressing canister rupture due to rock shear. The table shows, for each case, the calculated WELL-2007 dose maxima and the summed geosphere release maxima (which each maximum divided by its respective geo-bio flux constraint), and the times of occurrence of these maxima.

Table 7-3. WELL-2007 dose maxima, maxima of the summed nuclide-specific activity releases divided by their respective geo-bio flux constraints, and the times of occurrence of these maxima for all cases addressing canister rupture due to rock shear.

Case	WELL-2007 dose		Activity release	
	Maximum [Sv]	Time [a]	Maximum	Time [a]
RS-BC	1.4×10^{-6} (at 10^6 yrs)	> 10^6	4.9×10^{-3} (at 10^6 yrs)	> 10^6
RS-GMW	2.6×10^{-6} (at 10^6 yrs)	> 10^6	8.0×10^{-3} (at 10^6 yrs)	> 10^6

8 Overview of results and evaluation of compliance

8.1 Annual landscape dose maxima

Annual landscape dose is the primary assessment endpoint for the environmentally predictable future. This quantity has been calculated for all assessment cases where calculated releases to the biosphere occur in the first 10,000 years after repository closure. These include all the assessment cases for a canister with an initial penetrating defect, with the exceptions of PD-HIDELAY and PD-VOL-2.

Results from seven representative assessment cases have been presented in Chapter 5. An overview of these results is given in Figure 8-1. Other cases assuming an initial penetrating defect have been treated by scaling approaches or qualitative arguments, as described in the Biosphere Analysis Report /Broed et al. 2007/. Other canister failure modes occur after the "environmentally predictable future" and so no evaluation of annual landscape dose is required.

The highest calculated annual landscape dose for the most exposed individual is about 6×10^{-5} Sv, occurs at about 1,900 years, and arises in the assessment case PD-VOL-1. This is a little less than a factor of two below the regulatory constraint of 10^{-4} Sv. The case includes some pessimistic assumptions. As discussed in section 5.9.3, the corrosion rates of steel components assumed in this case may err on the high side, and the effects of longitudinal dispersion, which would result in the spreading of the radionuclide pulse and the lowering of the geosphere release maximum, have not been taken into account.

For all other assessment cases, the annual landscape dose maxima range from 5×10^{-7} to 2×10^{-5} Sv, and are thus around an order of magnitude or more below the regulatory constraint. The second highest maximum, 2×10^{-5} Sv, arises in the assessment case PD-EXPELL. The case again includes some pessimistic assumptions. It considers the consequences of a gas-driven

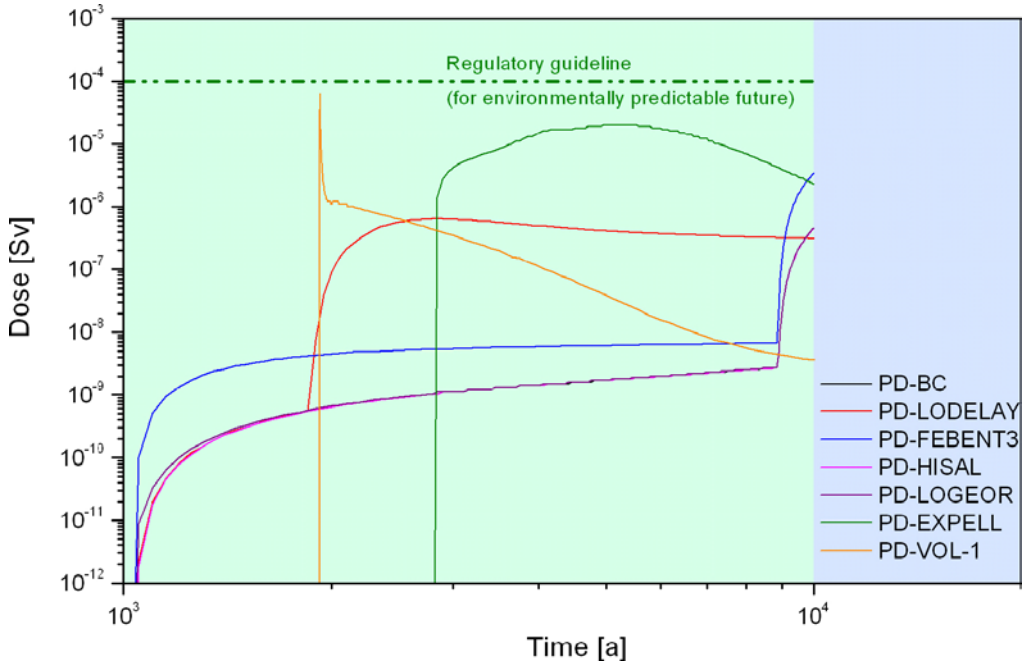

Figure 8-1. *Annual landscape dose as a function of time in seven representative cases (results for PD-BC, PD-HISAL and PD-LOGEOR approximately coincide).*

water pulse, beginning at 2,800 years after emplacement and lasting for a further 1,300 years, which propels water from the canister interior through the buffer to the fracture. The parameter values describing the pulse are based on the most pessimistic case from a range of model calculations of the fate of water/vapour/gas and radionuclides in a canister with an initial penetrating defect described in the KBS-3H Process Report. Furthermore, the assumption of complete corrosion of Zircaloy and other metal parts in this time frame is conservative, as discussed in section 5.8.3. In reality, some radionuclides, including potentially significant amounts of Nb-94 and C-14, may be retained within these components beyond the period of gas expulsion. Indeed, the water inflow rate on which the calculated gas-driven water pulse is based is insufficient to support complete corrosion of these components before the gas-driven water pulse starts. The assumed inflow rate is also higher that expected in reality, since the possible plugging of the hole with bentonite or corrosion products and the decrease of hydraulic gradient due to gas pressure build-up are not taken into account. It should, however, again be noted that only a single failed canister is considered in this and other cases.

8.2 WELL-2007 dose maxima

WELL-2007 dose – a safety indicator based on an indicative stylised well scenario – has been calculated for all assessment cases over a million year time frame. Table 8-1 gives WELL-2007 dose maxima and the times of occurrence of these maxima for all the cases considered in the safety assessment.

In most cases, the calculated dose maxima occur at slightly more than 10,000 years in the future, 10,000 years being the assumed time when an initial penetrating defect loses its transport resistance in the majority of cases dealing with this failure mode, and is also roughly the start of the era of extreme climate changes, when the Finnish regulatory dose constraint of 10^{-4} Sv per year no longer applies. Given this assumption, the only cases involving an initial penetrating defect in which the dose maxima occur significantly later than 10,000 years in the future are PD-HIDELAY and the glacial meltwater cases PD-GMW and PD-GMWV, in which the loss of transport resistance of the defect is assumed to occur at 79,000 years in the future (9,000 years following initial water ingress at 70,000 years). In assessment cases assuming the alternative canister failure modes of canister corrosion and rock shear, the dose maxima occur at around 70,000 years or beyond. Only in cases PD-EXPELL, PD-VOL-1, PD-LODELAY and PD-BHLD do the calculated dose maxima occur earlier than 10,000 years (between 2,000 and 4,000) years.

These results should not, however, be taken to imply that 10,000 years is the most likely time for the dose maximum to occur in reality. It is important to note that the SR-Can Data Report (Section 4.4.7 of /SKB 2006b/) suggests that loss of transport resistance could occur at any time between 1,000 and 100,000 years after radionuclide transport pathways from the canister interior are established, and the choice of 10,000 years for many of the cases analysed in the present safety assessment is somewhat arbitrary, and is made for the purposes of illustration only. Uncertainty in the time when an initial penetrating defect loses its transport resistance is such that the maxima could equally well occur in the environmentally predictable future – i.e. before the era of extreme climate changes – or much later, up to a million years in the future. The large number of cases analysed involving an initial penetrating defect should also not be taken to imply that the presence of an initial penetrating defect is the most likely failure mode. As noted in Section 2.2.4, Posiva is not yet taking any position on the likelihood of occurrence of canisters with initial penetrating defects.

Table 8-1. WELL-2007 dose maxima and the times of occurrence of these maxima for all the cases considered in the safety assessment.

Case	Maximum Magnitude [Sv]	Time [a]	Case	Maximum Magnitude [Sv]	Time [a]
Initial penetrating defect in canister			PD-EPRC	8.4×10^{-9}	1.0×10^{-4}
PD-BC	8.0×10^{-9}	1.0×10^{4}	PD-NFSLV	8.0×10^{-9}	1.0×10^{4}
PD-VVER	6.3×10^{-9}	1.0×10^{4}	PD-SAL	8.0×10^{-9}	1.0×10^{4}
PD-EPR	8.6×10^{-9}	1.0×10^{4}	PD-HISAL	8.0×10^{-9}	1.0×10^{4}
PD-HIFDR	9.1×10^{-9}	1.0×10^{4}	PD-GMW	7.0×10^{-9}	7.9×10^{4}
PD-LOFDR	7.9×10^{-9}	1.0×10^{5}	PD-GMWV	7.0×10^{-9}	7.9×10^{4}
PD-IRF	6.5×10^{-9}	1.0×10^{4}	PD-GMWC	8.0×10^{-9}	1.0×10^{4}
PD-BIGHOLE	7.8×10^{-9}	1.0×10^{4}	PD-HIFLOW	2.1×10^{-8}	1.0×10^{4}
PD-HIDELAY	5.8×10^{-9}	1.0×10^{5}	PD-LOGEOR	8.2×10^{-9}	1.0×10^{4}
PD-LODELAY	8.9×10^{-9}	2.3×10^{3}	PD-HIGEOR	6.8×10^{-9}	1.0×10^{4}
PD-BHLD	8.9×10^{-9}	2.3×10^{3}	PD-HIFLOWR	2.1×10^{-8}	1.0×10^{4}
PD-HIDIFF	2.6×10^{-9}	1.0×10^{4}	**Canister failure due to copper corrosion**		
PD-SPALL	4.2×10^{-9}	1.0×10^{4}	CC-BC	2.5×10^{-7}	1.0×10^{5}
PD-FEBENT1	5.3×10^{-8}	1.0×10^{4}	CC-HIFDR	2.5×10^{-7}	1.0×10^{5}
PD-FEBENT2	5.5×10^{-8}	1.0×10^{4}	CC-LOFDR	2.5×10^{-7}	1.0×10^{5}
PD-FEBENT3	6.5×10^{-8}	1.0×10^{4}	CC-GMW	3.7×10^{-7}	1.0×10^{5}
PD-EXPELL	1.6×10^{-7}	4.1×10^{3}	CC-LOGEOR	2.3×10^{-6} (at 10^{6} yrs)	$> 10^{6}$
PD-VOL-1	7.5×10^{-7}	1.9×10^{3}	CC-LOGEORG	2.3×10^{-6} (at 10^{6} yrs)	$> 10^{6}$
PD-VOL-2	5.1×10^{-7}	1.0×10^{4}	CC-LOGEORS	1.6×10^{-5} (at 10^{6} yrs)	$> 10^{6}$
PD-BCN	8.0×10^{-9}	1.0×10^{4}	**Canister failure due to rock shear**		
PD-BCC	7.7×10^{-9}	1.0×10^{4}	RS-BC	1.4×10^{-6} (at 10^{6} yrs)	$> 10^{6}$
PD-VVERC	6.1×10^{-9}	1.0×10^{4}	RS-GMW	2.6×10^{-6} (at 10^{6} yrs)	$> 10^{6}$

Figure 8-2 shows the magnitudes of the dose maxima in all the assessment cases considered in the safety assessment. The cases are arranged in two groups: at the top are those cases where the dose maximum occurs in the era of extreme climate changes and, at the bottom, the last four are those cases where the dose maximum occurs in the environmentally predictable future, which is taken to extend to 10,000 years post closure. (see, however, the caveats above). Within each group, cases are arranged in order of descending magnitude of the dose maximum.

The figure shows that, in all cases, the calculated WELL-2007 dose maxima for single canister failures are below the regulatory guideline of 10^{-4} Sv per year (although, as noted above, in most cases the maxima occur beyond the time frame in which this guideline applies). The possibility of multiple canister failures remains an issue for future studies. The highest calculated dose maxima are in the cases involving canister failure by corrosion or by rock shear, in which there is no assumed period in which the failed canister provides a transport resistance. The entire instant release fraction from the fuel is thus released to the buffer as a pulse in these cases, whereas there is more spreading in time in cases involving a small, initial penetrating defect.

In cases PD-EXPELL, PD-VOL-1, PD-LODELAY and PD-BHLD, in which calculated dose maxima occur in the environmentally predictable future when the regulatory dose constraint applies, the maxima are 2–4 orders of magnitude below the guideline.

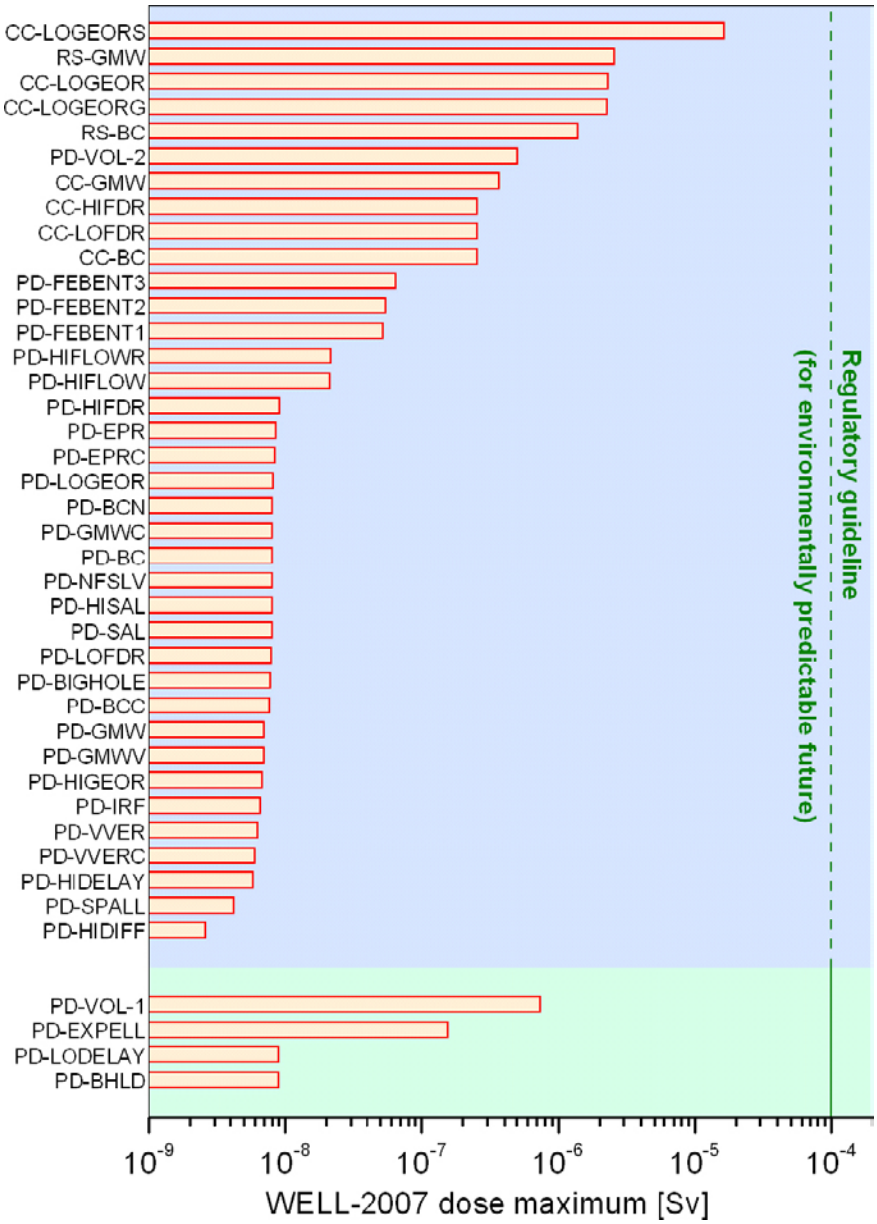

Figure 8-2. *Calculated WELL-2007 dose maxima in all assessment cases. Green background shading indicates the maxima that occur within the first 10,000 years following closure, which is interpreted in the present study as the "environmentally predictable future".*

8.3 Calculated releases in the era of large-scale climate changes

Geo-bio fluxes have also been calculated for all assessment cases over a million year time frame. Table 8-2 gives calculated summed geosphere release maxima (with each maximum divided by its respective geo-bio flux constraint) and the times of occurrence of these maxima for all the cases considered in the safety assessment.

Table 8-2. Maxima of the summed nuclide-specific activity releases divided by their respective geo-bio flux constraints and the times of occurrence of these maxima for all the cases considered in the safety assessment.

Case	Maximum Magnitude	Time [a]	Case	Maximum Magnitude	Time [a]
Initial penetrating defect in canister			PD-EPRC	7.0×10^{-4}	1.0×10^{-4}
PD-BC	1.6×10^{-3}	1.0×10^{4}	PD-NFSLV	1.6×10^{-3}	1.0×10^{4}
PD-VVER	9.9×10^{-4}	1.0×10^{4}	PD-SAL	1.6×10^{-3}	1.0×10^{4}
PD-EPR	9.1×10^{-4}	1.0×10^{4}	PD-HISAL	1.6×10^{-3}	1.0×10^{4}
PD-HIFDR	1.6×10^{-3}	1.0×10^{4}	PD-GMW	4.2×10^{-4}	7.9×10^{4}
PD-LOFDR	1.6×10^{-3}	1.0×10^{5}	PD-GMWV	4.2×10^{-4}	7.9×10^{4}
PD-IRF	2.1×10^{-4}	1.0×10^{4}	PD-GMWC	1.6×10^{-3}	1.0×10^{4}
PD-BIGHOLE	1.6×10^{-3}	1.0×10^{4}	PD-HIFLOW	4.5×10^{-3}	1.0×10^{4}
PD-HIDELAY	3.2×10^{-4}	1.0×10^{5}	PD-LOGEOR	1.6×10^{-3}	1.0×10^{4}
PD-LODELAY	3.4×10^{-3}	2.1×10^{3}	PD-HIGEOR	1.3×10^{-3}	1.0×10^{4}
PD-BHLD	3.4×10^{-3}	2.1×10^{3}	PD-HIFLOWR	4.6×10^{-3}	1.0×10^{4}
PD-HIDIFF	1.0×10^{-3}	1.0×10^{4}	**Canister failure due to copper corrosion**		
PD-SPALL	8.1×10^{-4}	1.0×10^{4}	CC-BC	5.7×10^{-3}	1.0×10^{5}
PD-FEBENT1	1.4×10^{-2}	1.0×10^{4}	CC-HIFDR	5.7×10^{-3}	1.0×10^{5}
PD-FEBENT2	1.5×10^{-2}	1.0×10^{4}	CC-LOFDR	5.7×10^{-3}	1.0×10^{5}
PD-FEBENT3	1.9×10^{-2}	1.0×10^{4}	CC-GMW	1.7×10^{-2}	1.0×10^{5}
PD-EXPELL	7.9×10^{-2}	2.9×10^{3}	CC-LOGEOR	1.4×10^{-2}	6.3×10^{5}
PD-VOL-1	7.9×10^{-2}	2.4×10^{3}	CC-LOGEORG	2.0×10^{-2}	1.0×10^{5}
	(8.6×10^{-1})*	(1.9×10^{3})*			
PD-VOL-2	2.4×10^{-2}	1.1×10^{4}	CC-LOGEORS	5.7×10^{-2} (at 10^{6} yrs)	$> 10^{6}$
	(5.8×10^{-1})*	(1.0×10^{4})*			
PD-BCN	1.6×10^{-3}	1.0×10^{4}	**Canister failure due to rock shear**		
PD-BCC	1.2×10^{-3}	1.0×10^{4}	RS-BC	4.9×10^{-3} (at 10^{6} yrs)	$> 10^{6}$
PD-VVERC	7.1×10^{-4}	1.0×10^{4}	RS-GMW	8.0×10^{-3} (at 10^{6} yrs)	$> 10^{6}$

* Values before 1,000 year averaging (see Section 5.9).

As with calculated doses, in most cases the calculated maxima occur at slightly more than 10,000 years in the future, at the start of the era of extreme climate changes. According to the Finnish regulator, the sum of the ratios of nuclide-specific activity releases to their respective constraints should be less than one in order to satisfy regulatory requirements in this time frame. Again, the fact than many cases give maxima at about 10,000 years does not imply that 10,000 years is the most likely time for the dose maximum to occur in reality, nor does the large number of cases analysed involving an initial penetrating defect imply that the presence of an initial penetrating defect is the most likely failure mode.

Figure 8-3 shows the magnitudes of the summed release maxima in all the assessment cases considered in the safety assessment. The cases are again arranged in two groups: at the top are those cases where the release maximum occurs in the era of extreme climate changes, and at the bottom (the last four) are those cases where the release maximum occurs in the environmentally predictable future. Within each group, cases are arranged in order of descending magnitude of the release maximum.

The highest calculated release maxima occur in cases PD-VOL-1 and PD-VOL-2, i.e. expulsion of C-14 in volatile form by repository generated gas through an initial penetrating defect. In case PD-VOL-1 in particular, the maximum release divided by the geo-bio flux constraint is only slightly below the regulatory guideline value of one, although it should be noted that, in case PD-VOL-1, since the maximum occurs at about 2,000 years, it is the dose constraint, rather than the geo-bio flux constraint, that is applicable.

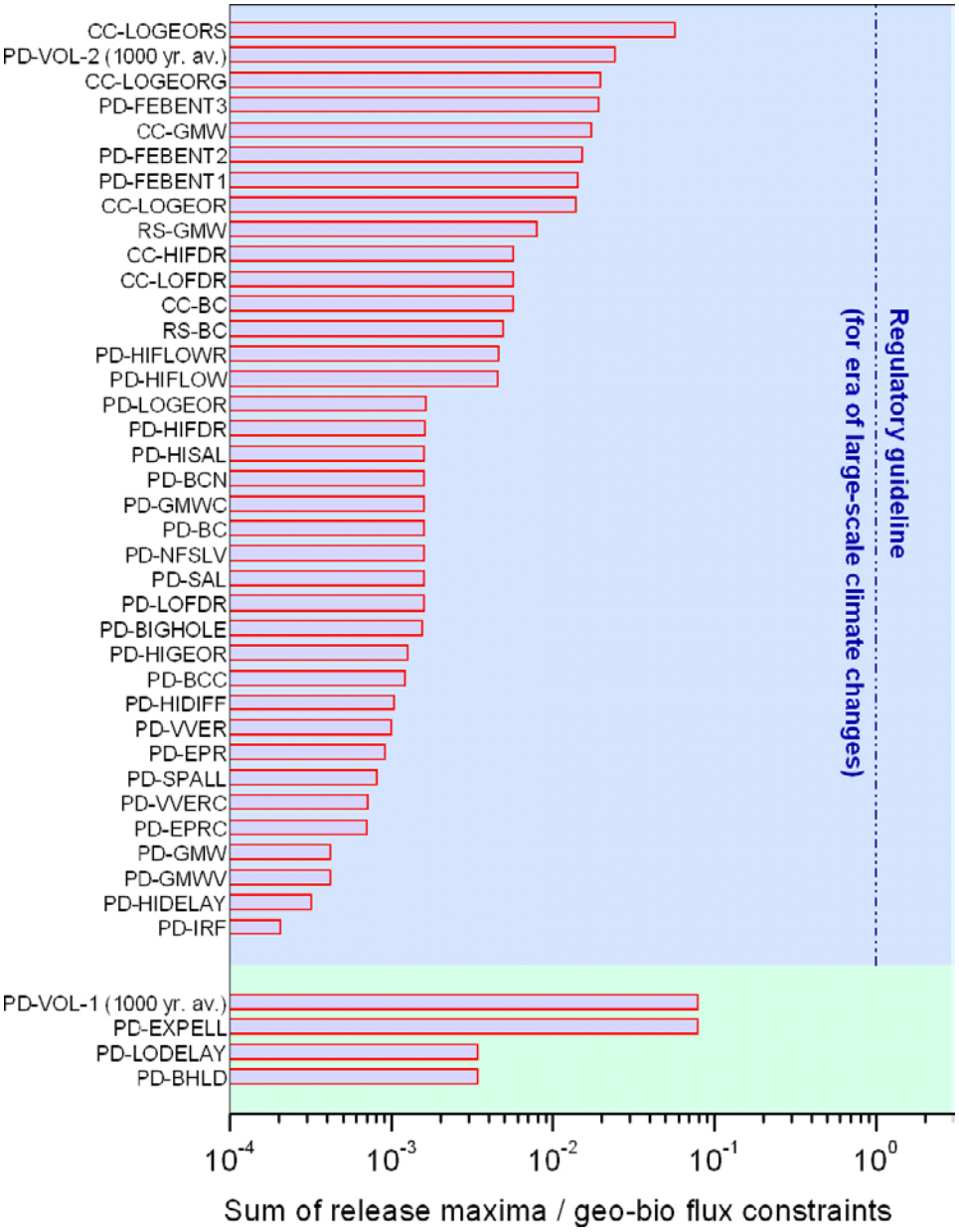

Figure 8-3. *Calculated summed release rate maxima in all assessment cases. Before carrying out the summation, nuclide-specific activity releases are divided by their respective geo-bio flux constraints. Green background shading indicates the maxima that occur within the first 10,000 years following closure, which is interpreted in the present study as the "environmentally predictable future".*

The highest calculated summed release maximum occurs in case CC-LOGEORS, i.e. canister failure by copper corrosion, in association, for example, with an influx of glacial meltwater and loss of buffer mass by chemical erosion, coupled to an assumption of low transport resistance and saline geochemical conditions in the geosphere. In this case, the summed release maximum is more than an order of magnitude below the regulatory guideline. Nevertheless, there are significant uncertainties associated with this scenario, i.e. whether substantial buffer mass loss by chemical erosion could occur at all, and, if it does, the number of canister positions that are likely to be affected (case CC-LOGEORS deals with only a single canister failure). The development of a better understanding of chemical erosion is a priority for future work for both the KBS-3H and KBS-3V design alternatives.

8.4 Compliance with regulatory criteria in different time frames and the issue of multiple canister failures

Overall, the release and transport calculations indicate compliance with Finnish regulations both for the "environmentally predictable future" and for later times, assuming single canister failure by any of the identified modes.

In all cases, the calculated dose maxima are below the regulatory guideline of 10^{-4} Sv per year (although, as noted above, in most cases the maxima occur beyond the time frame in which this guideline applies). The highest calculated WELL-2007 dose maxima are in the cases involving canister failure by corrosion or by rock shear, in which there is no assumed subsequent period in which the failed canister provides a transport resistance and the geosphere transport resistance is assumed to be lower than in other cases, allowing sorbing radionuclides, such as Th-230 and Ra-226, to migrate across the geosphere without substantial attenuation by radioactive decay. The entire instant release fraction from the fuel is thus released to the buffer as a pulse in these cases, whereas there is more spreading in time in cases involving a small, initial penetrating defect.

In cases PD-EXPELL, PD-VOL-1, PD-LODELAY and PD-BHLD, in which calculated dose maxima occur in the environmentally predictable future when the regulatory dose guideline applies, the WELL-2007 dose maxima are 2–4 orders of magnitude below the guideline. The annual landscape dose is, however, less than a factor of two below that guideline in case PD-VOL-1 and less than a factor of five below the guideline in case PD-EXPELL. As discussed in section 8.1, both of these cases are based on a number of pessimistic assumptions. These include, in case PD-VOL-1, the high assumed corrosion rates of steel components and the omission of longitudinal dispersion, which would result in the spreading of the radionuclide pulse and the lowering of the geosphere release maximum in this case.. In case PD-EXPELL, the parameter values describing the gas pulse are based on the most pessimistic case from a range of model calculations of the fate of water/vapour/gas and radionuclides in a canister with an initial penetrating defect. Furthermore, although the water inflow rate on which the calculated gas-driven water pulse is based is insufficient to support complete corrosion of Zircaloy and other metal parts before the gas-driven water pulse starts, complete corrosion of these parts and release of associated radionuclides to solution is conservatively assumed in the assessment case. The assumed inflow rate is also higher that expected in reality, since the possible plugging of the hole with bentonite or corrosion products and the decrease of hydraulic gradient due to gas pressure build-up are not taken into account.

The differences between the WELL-2007 doses and the landscape doses are most likely due to different conceptual assumptions, particularly those concerning the biosphere, e.g. accumulation in the biosphere, identification of the most exposed subgroup of the population, radionuclide-specific biosphere transport processes. Work is still ongoing to analyse the different results and identify key assumptions affecting the doses at different end points.

A key issue for future safety assessments will be to better quantify the probability of the failure of several canisters with a million year time frame, and the likelihood that such failures will occur at similar times. The probability of multiple canisters failures at similar times has been evaluated only in the case of canister failure due to rock shear – the expectation value of the number of canisters in the repository that could potentially be damaged by rock shear in the event of a large earthquake has been estimated to be 16 out of the total number of 3,000 canisters (Section 2.2.6). The geo-bio flux constraint will still be met in cases RS-BC and RS-GMW if 16 canisters fail in the event of a single large earthquake. However, the number of canisters that might fail over a million year time frame (and contribute to the Ra-226 dose at a million years) has not so far been evaluated; see, however, the discussion of the hazards arising from radionuclide releases in the Complementary Evaluations of Safety Report /Neall et al. 2007/, where a bounding analysis with all canisters failing is presented.

More generally, a key issue for future safety assessments will, however, be to better quantify the probability of the failure of several canisters at similar times. This and other issues requiring further work are discussed in Chapter 9.

9 Ongoing work and issues for further consideration

This chapter lists issues for further consideration that have been identified during the KBS-3H safety assessment. Many of issues below are relevant to both the KBS-3V and KBS-3H. Some of these issues are already the object of ongoing work and some are included in the next phase of the KBS-3H programme (2008-2009). The issues are not prioritised and are to be considered in the context of the development of the KBS-3H alternative, taking into account programmatic objectives and constraints, such as schedules and resources both in Posiva and SKB.

There remain several general safety assessment issues, issues related to radionuclide release and transport processes and modelling, and issues of code development that will need to be considered in future RD&D and safety assessment exercises.

In addition to these, there are a number of issues related to the scientific understanding of the evolution of the repository and its environment that indirectly affect radionuclide release and transport calculations, through their effects on the likelihood, timing and mode of canister failure, and the transport and retention properties of the system subsequent to canister failure. Some have already been mentioned in the present report. They include the need for a better understanding of:

- the evolution of conditions external to the repository (the Olkiluoto Site Description 2006, for example, identifies a range of issues and uncertainties concerning the current site model, and discusses the activities being undertaken or proposed to address them);
- the early evolution of the buffer;
- iron/bentonite interaction;
- gas pressurisation and migration in the repository near field;
- microbial activity;
- interactions involving cement;
- rock spalling; and
- buffer erosion by dilute glacial meltwater (the related issue of colloid facilitated radionuclide transport is mentioned in Section 9.2.8).

The reader is referred to the KBS-3H Process Report /Gribi et al. 2007/ and Evolution Report /Smith et al. 2007a/ for a discussion of these issues and associated uncertainties.

9.1 General safety assessment issues

Although a broad range of assessment cases has been considered in the present safety assessment, the range of cases analysed is significantly smaller than that considered, for example, in either the TILA-99 or SR-Can safety assessments and not all conceivable uncertainties and combinations of uncertainties are covered. For example, uncertainties in the transport barrier provided by the geosphere, biosphere uncertainties and uncertainties related to future human actions are either not addressed or are analysed in less detail than others.

While use has been made, as far as possible, of well-tested and thoroughly reviewed models, computer codes and databases in analysing the assessment cases, each of these may involve significant simplification of the real system. For example, a significant limitation of the present

safety assessment is the assumption of steady groundwater flow and (with the exception of one assessment case – PD-GMWV) composition. Furthermore, data for analysing assessment cases are based on the preliminary information available at the time of writing the present report. The motivation for and plausibility (or conservatism) of selected parameter values and model assumptions used have been reported as much as possible given the time constraints in this and other reports dealing with KBS-3H safety studies. This discussion is, however, often limited and largely qualitative. In the case of geosphere transport modelling, the modelling approach and parameter values used are based largely on TILA-99, and more recent developments in the understanding of the Olkiluoto site are used only to provide additional support for the parameter values selected (e.g. in terms of their conservatism). Uncertainties related to the geosphere transport barrier do not fall within the main focus of the present safety assessment, since most of the key differences between KBS-3V and KBS-3H repositories relate to the evolution and performance of the near field. A detailed analysis of the current understanding of the geosphere transport model parameters such as the flow and transport properties of the bedrock in terms of the transport resistance of the geosphere is, however, being undertaken in the context of the safety case for a KBS-3V repository at Olkiluoto.

In the biosphere part of the assessment, most of the ecosystem-specific models are largely unchanged compared with SR-97. However, the concept of landscape modelling, or chaining the ecosystems into a network, is rather new and has been previously applied only in SR-Can and in some case studies by Posiva. The studies have shown that, to track the fate and consequences of radionuclide releases to the biosphere, it is important to model the entire area of the biosphere – not just the first contaminated area affected by releases, but also areas downstream. Biosphere assessments conducted in this way are, however, time consuming. Thus, a tiered approach is envisaged for future safety assessments where first safety indicators like the WELL-2007 dose are used, with detailed simulations carried out only for those few radionuclides contributing most to the dose.

The biosphere data applied in the present safety assessment are mainly the same data as those used previously in the SR-97 safety assessment, as well as in SR-Can, with only limited effort to ensure their consistency with the assumptions made for the near field and geosphere simulations in the present safety assessment. In the future, by concentrating on the most significant radionuclides, more resources could be spent on affirming the validity of the best estimate parameter values and distributions that contribute to the dose. Several tools to facilitate the process are already available, most importantly the Biosphere Assessment Database of Posiva with reviewing functions /Hjerpe 2006/, and the Eikos tool for sensitivity analyses /Ekström and Broed 2006/.

A comprehensive data report along the lines of that prepared for SR-Can /SKB 2006b/, with structured procedures for handling input data to radionuclide release and transport calculations, will be considered in any future safety studies for both the KBS-3V and KBS-3H designs, and is likely to be required in support of a future safety case.

9.2 Issues related to radionuclide release and transport processes and modelling

9.2.1 Radionuclide inventory

The partitioning of radionuclide inventories between the fuel matrix, instant release fraction, Zircaloy and other metal parts is uncertain; the values used in the present safety assessment are based on expert judgement, guided by considerations in /Anttila 2005/. Further information on this issue will be required in future safety assessments.

9.2.2 Probability of canister failure

Three different canister failure modes are judged to be plausible in a million year time frame for a KBS-3H (or KBS-3V) repository at Olkiluoto: (i), the presence of an initial, penetrating defect in the copper shell, (ii), canister failure by corrosion following perturbation of the buffer or buffer/rock interface and (iii), canister failure due to secondary shear movements on rock fractures in the event of a large earthquake.

Posiva is not yet taking any position on the likelihood of occurrence of canisters with initial penetrating defects. A qualification programme for the applicable examination procedures for Finnish canister component manufacture and sealing will be developed by the end of 2009 and executed by the end of 2012, before the application for the encapsulation plant construction license is submitted.

Canister failure by corrosion in a million year time frame is judged to be possible only if there is significant perturbation of the buffer or buffer/rock interface, for example due to chemical erosion by dilute glacial meltwater, allowing an increased rate of migration of sulphide from the groundwater to the canister surface. There is, however, currently no adequate quantitative understanding of chemical erosion on which to base a reliable estimate of the rate of canister failure by this mechanism. There is also uncertainty in the evolution of sulphide concentrations in the groundwater, which is associated with the potential for microbial activity at the boundary between sulphate rich water and the deeper, methane rich zone at the Olkiluoto site.

Only in the case of canister failure by rock shear has an estimate been made of the number of canisters potentially affected. This estimate, however, has some significant limitations, being based, for example, on fracture network data that have since been updated. Furthermore, the cumulative effect of the impact of many earthquakes over a prolonged period on the buffer and canisters is an issue for further investigation. Finally, methods to identify and avoid potentially problematic fractures during repository construction have not, so far, been evaluated in detail.

In the present safety assessment, each assessment case postulates a single canister failure by one or other of the above failure modes at a given time, and the resultant releases of radionuclides to the biosphere are evaluated. The likelihood or frequency of canister failure by each mode must, however, be evaluated in any future safety case.

9.2.3 Internal evolution of a failed canister

There are many uncertainties in the internal evolution of a failed canister, most of which are treated in safety assessment calculations using conservative assumptions. It is possible that a better understanding of, for example, processes leading to water ingress, fuel matrix dissolution and the establishment of a transport pathway from the canister interior to the buffer could allow some of these uncertainties to be reduced. An improved understanding of the corrosion rates of, and gas generation from, the different metals inside the canister could also allow some of the uncertainties associated with the modelling of the expulsion of dissolved radionuclides by gas and with the release of radionuclides as volatile species to be reduced.

9.2.4 Solubility limitation and speciation

Solubility limits, which are applied in the present safety assessment inside a failed canister and at the buffer/rock interface, are subject to a number of significant uncertainties (see Appendix E).

One important issue related to solubility limits is element speciation. For some elements, including carbon, the chemical form is currently not precisely known. A few elements (e.g. niobium, plutonium, thorium and uranium) are thought to be present in anionic, neutral, or cationic

forms depending on the groundwater composition, and especially on pH and redox conditions and concentration of dissolved carbonate in the groundwater. This is an issue, therefore, that is dependent on both the knowledge of the correct groundwater composition and accuracy of available thermodynamic data.

In the present safety assessment, the transport of one dominant chemical species is considered for each element, while, in reality, there may be a mixture of different species, each with different transport properties. The species that are determined to be the most abundant in the repository near field following release to solution are, in most cases, the ones for which transport calculations are performed. It is, however, possible that some of the less abundant species will be the more mobile and so, in reality, will be released at greater rates to the biosphere. Thus, in some uncertain cases, e.g. thorium, the dominant species is selected conservatively based on the known sorption properties of the element, rather than on abundance. The kinetics of transformation of chemical species during transport is also uncertain. These are issues that will require consideration in future safety assessments.

Solubility limits used in the evaluation of assessment cases are based on a set of reference waters, corresponding to different possible groundwater compositions. In reality, however, groundwater composition, and, therefore, solubilities, will vary in space and time. The salinity of the water at Olkiluoto site during different periods has been modelled in the 3V Evolution Report/Pastina and Hellä 2006/, and the impact of the time-dependence of groundwater components of importance in the estimation of solubility limit will be addressed in the coming 3V studies.

For a given reference water, uncertainties in solubility limits arise from the fact that the concentrations are not known or the concentrations are associated with large uncertainties for some important groundwater components, such as phosphates and organic acids. The lack of data on phosphate concentration (or the fact that phosphate concentration is below the detection limit) has an important impact on the solubility limiting phases and the solubility limits. Organic compounds and formation of organic complexes have not been considered in the assessment of solubilities and speciation of the elements. Uncertainties also arise due to the limited overall understanding and quantification of the redox- and pH-buffering capacity of the rock during different periods. Furthermore, some of the thermodynamic data for the radionuclides of interest are still associated with significant uncertainties, as exemplified by the recent data published for Ni /Gamsjäger et al. 2005/.

Finally, the possibility of precipitation or co-precipitation at the boundary between the buffer and rock, leading to colloid formation and migration in the geosphere has not been taken into account in the present study and needs to be addressed in the future.

9.2.5 Sorption

There are a number of uncertainties affecting the sorption values used in the present safety assessment. There is a general lack of experimental data for some elements under relevant conditions, in particular Nb and Mo. In the near field, organic substances or their degradation products could, for example, form complexes with radionuclides, which would lower radionuclide sorption and thus increase radionuclide transport rates. Another source of uncertainty is the impact of Fe(II) from the corrosion of the insert of a failed canister on the capacity of the buffer to sorb some radionuclides. Fe(II) could, in particular, compete with the sorption of species such as Ni(II) and Sr(II), and weaken the barrier function of the buffer with respect to Ni and Sr radionuclides. In the present safety assessment, however, it is argued on the basis of scoping calculations that the impact of such uncertainties on overall release rates to the biosphere is limited. Iron corrosion products may not only perturb the sorption properties of the buffer, but may themselves sorb radionuclides. Although this process is favourable to safety, it is also possible that changes in geochemical conditions and/or ageing and transformation of the surfaces of the corrosion products could release sorbed radionuclides. This is also particularly relevant in the case of Ni(II).

Overall, there is a need to update geosphere parameter values based on more recent information on the host rock at Olkiluoto, including the changes caused by the evolution of groundwater chemistry. These need to be considered in parallel with the improvements in knowledge regarding the speciation of different elements, including an assessment of the role of organic compounds and formation of colloids.

9.2.6 Buffer transport properties

It has been assumed in radionuclide release and transport calculations that transport properties throughout most of the buffer correspond to those of saturated MX-80 bentonite. In reality, the clay can undergo a variety of changes during its early evolution, especially in drift sections where saturation of the buffer is very slow, as discussed in the KBS-3H Evolution Report /Smith et al. 2007a/. A better understanding of the transport properties of the buffer is required, taking into account its evolution from virgin plastic clay to clay that is potentially altered, for example by the presence of iron, precipitated silica and stray materials.

9.2.7 Treatment of the buffer/rock interface

Various features and processes have been identified that may lead to detrimental changes in the mass transfer properties of the buffer/rock interface (e.g. iron/bentonite interactions, thermally-induced rock spalling). In considering the effects of such changes on radionuclide release and transport, the approach taken is to treat the perturbed zone as a mixing tank, and to evaluate groundwater flow through this mixing tank based on the highly conservative assumption that it has a high (effectively infinite) hydraulic conductivity. In reality, even if the perturbed zone has a hydraulic conductivity that is higher than either the rock matrix or the unperturbed buffer, hydraulic conductivity may remain sufficiently low to limit the flow of water through the zone. It is even possible that a buffer transformed, for example, by iron/bentonite interaction could have a negligible permeability and thus continue to limit mass transfer across the buffer/rock interface significantly. Determining some bounding estimates for the hydraulic properties of the perturbed buffer/rock interface is an issue for future studies.

9.2.8 Geosphere transport properties and processes

In the present safety assessment, the dominant radionuclide transport mechanism in the geosphere is assumed to be advection of dissolved radionuclides in flowing groundwater, retarded by matrix diffusion and sorption. The possible impact of groundwater or repository-derived colloids on radionuclide transport has not been assessed. Steady groundwater flow and transport properties that are constant in space and time are assumed. These assumptions are not well supported. They are made to simplify the present assessment, the focus of which is on the repository near field, since this is where most of the differences between KBS-3H and KBS-3V arise. As noted earlier, a detailed analysis of the current understanding of the geosphere transport model parameters is being undertaken in the context of the safety case for a KBS-3V repository at Olkiluoto, and the findings should also be applicable to KBS-3H.

9.3 Development of computer codes

In future safety assessments, Posiva aims to use commercial and internationally used radionuclide transport codes complemented by simple calculations and reasoned arguments to build understanding, enhance transparency and facilitate peer review.

References

Ahonen L, Vieno T, 1994. Effects of glacial meltwater on corrosion of copper canisters. Report YJT-95-19. Nuclear Waste Commission of Finnish Power Companies. Helsinki.

Andersson J, Hermansson J, Elert M, Gylling B, Moreno L, Selroos J-O, 1998. Derivation and treatment of the flow wetted surface and other geosphere parameters in the transport models FARF31 and COMP23 for use in safety assessment. SKB R-98-60, Svensk Kärnbränslehantering AB.

Andersson J, Ahokas H, Hudson J A, Koskinen L, Luukkonen A, Löfman J, Keto V, Pitkänen P, Mattila J, Ikonen A T K, Ylä-Mella M, 2007. Olkiluoto Site Description (2 vols.). Posiva Report 2007-03. Posiva Oy, Olkiluoto, Finland.

Anttila M, 2005. Radioactive characteristics of the spent fuel of the Finnish nuclear power plants. Posiva Working Report 2005-71. Posiva Oy, Olkiluoto, Finland.

Autio J, 2007. KBS-3H Design Description 2005. Posiva Working Report 2007-11 and SKB R-08-29. Posiva Oy, Olkiluoto, Finland and Svensk Kärnbränslehantering AB, Sweden.

Autio J, Börgesson L, Sandén T, Rönnqvist P-E, Berghäll J, Kotola R, Parkkinen I, Johansson E, Hagros A, Eriksson M, 2007. KBS-3H Design Description 2006. Posiva Working Report 2007-107 and SKB R-08-32. Posiva Oy, Olkiluoto, Finland and Svensk Kärnbränslehantering AB, Sweden.

Autio J, Anttila P, Börgesson L, Sandén T, Rönnqvist P-E, Johansson E, Hagros A, Eriksson M, Halvarson B, Berghäll J, Kotola R, Parkkinen I, 2008. KBS-3H Design Description 2007. Posiva 2008-01 and SKB R-08-44. Posiva Oy, Olkiluoto, Finland and Svensk Kärnbränslehantering AB, Sweden.

Eriksson M, Halvarson B, Berghäll J, Kotola R, Parkkinen I, 2008. KBS-3H Design Description 2007. POSIVA 2008-01 and SKB R-08-44, Posiva Oy, Olkiluoto, Finland and Svensk Kärnbränslehantering AB, Sweden.

Avila R, Bergström U, 2006. Methodology for calculation of doses to man and implementation in PANDORA. SKB R-06-68, and Posiva Working Report 2006-56. Svensk Kärnbränslehantering AB, Sweden and Posiva Oy, Olkiluoto, Finland.

Avila R, Pröhl G, 2007. Models used in the SFR1 SAR-08 and KBS-3H safety assessments for calculation of C-14 doses. Posiva Working report 2007-107. Posiva Oy, Olkiluoto, Finland.

Broed R, 2007. Landscape model configuration for biosphere analysis of selected cases in TILA-99 and in KBS-3H safety evaluation, 2007. Posiva Working report 2007-108. Posiva Oy, Olkiluoto, Finland.

Broed R, Avila,R, Bergström U, Hjerpe T, Ikonen A T K, 2007. Biosphere analysis for selected cases in TILA-99 and in KBS-3H safety evaluation, 2007. Posiva Working Report 2007-109. Posiva Oy, Olkiluoto, Finland.

Brydsten L, 2004. A mathematical model for lake ontogeny in terms of filling with sediments and macrophytic vegetation. SKB TR-04-09, Svensk Kärnbränslehantering AB.

Börgesson L, Johannesson L-E, Hernelind J, 2004. Earthquake induced rock shear through a deposition hole. Effect on the canister and the buffer. SKB TR-04-02, Svensk Kärnbränslehantering AB.

Börgesson L, Sandén T, Fälth B, Åkesson M, Lindgren E, 2005. Studies of buffers behaviour in KBS-3H concept; Work during 2002-2004. SKB R-05-50, Svensk Kärnbränslehantering AB.

Carlson L, Karnland O, Olsson S, Rance A, Smart N, 2006. Experimental studies on the interactions between anaerobically corroding iron and bentonite. Posiva Working Report 2006-60 and SKB R-08-28. Posiva Oy, Olkiluoto, Finland and Svensk Kärnbränslehantering AB, Sweden.

Cramer J, Smellie J, 1994. Final report of the AECL/SKB Cigar Lake Analog Study (Also published as AECL-10851 COG-93-147). SKB TR-94-04, Svensk Kärnbränslehantering AB.

Duro L, Grivé M, Cera E, Gaona X, Domènech C, Bruno J, 2006. Determination and assessement of the concentration limits to be used in SR-Can. SKB TR-06-30. Svensk Känrbränslehantering AB.

Ekström P-A, Broed R, 2006. Senstivity analysis methods and a biosphere test case implemented in EIKOS. Posiva Working Report 2006-31. Posiva Oy, Olkiluoto, Finland.

Freeze R A, Cherry J A, 1979. Groundwater. Prentice Hall, Inc., Englewood Cliffs, USA.

FTRANS, 1983. A two-dimensional code for simulating fluid flow and transport of radioactive nuclides in fractured rock for repository performance assessment. Report ONWI-426. Intera Environmental Consultants Inc., Houston, USA.

Gamsjäger H, Bugajski J, Lemire R, Gajda T, Preis W, 2005. Chemical Thermodynamics 6. Chemical Thermodynamics of Nickel. NEA OECD, Elsevier.

Gribi P, Johnson L, Suter D, Smith P, Pastina B, Snellman M, 2007. Safety assessment for a KBS-3H spent nuclear fuel repository at Olkiluoto – Process Report, Posiva Report 2007-09 and SKB R-08-36. Posiva Oy, Olkiluoto, Finland and Svensk Kärnbränslehantering AB, Sweden.

Grivé M, Montoya V, Duro L, 2007. Assessment of the concentration limits for radionuclides for Posiva. Posiva Working Report 2007-103. Posiva Oy, Olkiluoto, Finland.

Hakanen M, Hölttä P, 1992. Review of sorption and diffusion parameters for TVO-92. Report YJT-92-14. Nuclear Waste Commission of Finnish Power Companies, Helsinki, Finland.

Hartley L, Hoch A, Jackson P, Joyce S, Mc Carthy R, Rodwell W, Swift B, Marsic N, 2006a. Groundwater flow and transport modelling during the temperate period for the SR-Can assessment Forsmark area – version 1.2. SKB R-06-98, Svensk Kärnbränslehantering AB.

Hartley L, Hoch A, Jackson P, Joyce S, Mc Carthy R, Swift B, Gylling B, Marsic N, 2006b. Groundwater flow and transport modelling during the temperate period for the SR-Can assessment. Laxemar subarea – version 1.2. SKB R-06-99, Svensk Kärnbränslehantering AB.

Hjerpe T, 2006. Overall Strategy for Management of Parameters and Data in the Biosphere Assessment Portfolio. Posiva Working Report 2006-109. Posiva Oy, Olkiluoto, Finland.

Hellä P, Ahokas H, Palmén J, Tammisto E, 2006. Analysis of geohydrological data for design of KBS-3H repository layout. Posiva Working Report 2006-16 and SKB R-08-27. Posiva Oy, Olkiluoto, Finland and Svensk Kärnbränslehantering AB, Sweden.

IAEA, 2003. "Reference biospheres" for solid radioactive waste disposal. Report of the BIOMASS Theme 1 of the BIOsphere Modelling ASSessment (BIOMASS) Programme. IAEA-BIOMASS-6. IAEA, Vienna, Austria.

IAEA, 2007. IAEA Safety Glossary – Terminology Used in Nuclear Safety and Radiation Protection, 2007 Edition, International Atomic Energy Agency, Vienna.

ICRP (International Commission on Radiological Protection), 1991. 1990 Recommendations of the International Commission on Radiological Protection, ICPR Publication 60. Annals of the ICRP Volume 21/1-3. Elsevier Science Ltd, Oxford.

ICRP (International Commission on Radiological Protection), 1996. Age-dependent dose to members of the public from intake of radionuclides: Part 5 compilation of ingestion and inhalation dose coefficients. Annals of the ICRP Volume 26(1). Elsevier Science Ltd, Oxford.

Ikonen K, 2003. Thermal analysis of KBS-3H type repository. Posiva Report 2003-11. Posiva Oy, Olkiluoto, Finland.

Ikonen K, 2005. Thermal conditions of open KBS-3H tunnel. Posiva Report 2005-04 and SKB R-08-24. Posiva Oy, Olkiluoto, Finland and Svensk Kärnbränslehantering AB, Sweden.

Ikonen A T K, Hjerpe T, Aro L, Leppänen V, 2007. Terrain and ecosystems development model of Olkiluoto site, version 2006. Posiva Working report 2007-110. Posiva Oy, Olkiluoto, Finland.

Johnson L H, McGinnes D F, 2002. Partitioning of radionuclides in Swiss power reactor fuels. Nagra Technical Report NTB 02-07. Nagra, Wettingen, Switzerland.

Johnson L, Marschall P, Wersin P, Gribi P, 2005. HMCBG processes related to the steel components in the KBS-3H disposal concept. Posiva Working Report 2005-09 and SKB R-08-25. Posiva Oy, Olkiluoto, Finland and Svensk Kärnbränslehantering AB, Sweden.

JNC, 2000. H12 project to establish technical basis for HLW disposal in Japan, Supporting Report 3: Safety assessment of the geological disposal system, 2nd progress report on research and development for the geological disposal of HLW in Japan. JNC TN1410 2000-004. JNC, Tokai, Japan.

La Pointe P, Hermanson J, 2002. Estimation of Rock Movements due to Future Earthquakes at Four Candidate Sites for a Spent Fuel Repository in Finland. Posiva Report 2002-02. Posiva Oy, Helsinki, Finland.

Lanyon G W, Marschall P, 2006. Discrete fracture network modelling of a KBS-3H repository at Olkiluoto. POSIVA 2006-06 and SKB R-08-26. Posiva Oy, Olkiluoto, Finland and Svensk Kärnbränslehantering AB, Sweden.

Liu J, Löfgren M, Neretnieks I, 2006. SR-Can Data and uncertainty assessment. Matrix diffusivity and porosity in situ. SKB R-06-111, Svensk Kärnbränslehantering AB.

Löfgren M, Neretnieks I, 2003. Formation factor logging by electrical methods: Comparison of formation factor logs obtained in situ and in the laboratory. J. Contaminant Hydrology, 61, 107–115.

Löfman J, 1996. Groundater flow modelling at the Olkiluoto site – Flow under natural conditions. Posiva Working Report PATU-96-76e. Posiva Oy, Helsinki, Finland.

Löfman J, 1999. Site scale groundwater flow in Olkiluoto. Posiva Report 99-03. Posiva Oy, Helsinki, Finland.

Lönnqvist M, Hökmark H, 2007. Thermo-mechanical analyses of a KBS-3H deposition drift at the Olkiluoto site, Posiva Working Report 2007-66 and SKB R-08-30. Posiva Oy, Olkiluoto, Finland and Svensk Kärnbränslehantering AB, Sweden.

Motta M M, Miranda C F, 1989. Molybdate adsorption on kaolinite, montmorillonite and illite: constant capacitance modelling. Soil Sci. Soc. Am. J., 53, 380-385.

Müller Ch, Elagin M, Scharmach M, Bellon C, Jaenisch G-R, Bär S, Redmer B, Goebbels J, Ewert U, Zscherpel U, Boehm R, Brekow G, Erhard A, Heckel T, Tessaro U, Tscharntke D, Ronneteg U, 2006. Reliability of nondestructive testing (NDT) of the copper canister seal weld. SKB R-06-08, Svensk Kärnbränslehantering AB.

Nagra, 1994. Kristallin-I safety assessment report. Nagra Technical Report NTB 93-22. Nagra, Wettingen, Switzerland.

Nagra, 2002. Project Opalinus Clay: Safety Report. Demonstration of disposal feasibility for spent fuel, vitrified high-level waste and long-lived intermediate-level waste (Entsorgungsnachweis). Nagra Technical Report NTB 02-05. Nagra, Wettingen, Switzerland.

Neall F, Pastina B, Smith P, Gribi P, Snellman M, Johnson L, 2007. KBS-3H Complementary evaluations of safety. Posiva Report 2007-10 and SKB R-08-35 Posiva Oy, Olkiluoto, Finland and Svensk Kärnbränslehantering AB, Sweden.

Neretnieks I, 2006. Flow and solute transport in a zone damaged due to spalling. SKB R-06-91, Svensk Kärnbränslehantering AB.

Nordman H, Vieno T, 1994. Near-field model REPCOM. Report YJT-94-12. Nuclear Waste Commission of Finnish Power Companies (YJT), Helsinki, Finland.

Nordman H, Vieno T, 2003. Modelling of near-field transport in KBS-3V/H type repositories with PORFLOW and REPCOM codes. Posiva Working Report 2003-07. Posiva Oy, Olkiluoto, Finland.

NRC (National Research Council), 1999. Risk Assessment of Radon in Drinking Water. Committee on Risk Assessment of Exposure to Radon in Drinking Water. National Academy Press, Washington, DC.

Ojala A E K, Virkki H, Palmu J-P, Hokkanen K, Kaija J, 2006. Regional development of river basins in the Olkiluoto-Pyhäjärvi area, SW Finland, 2000 BP – 8000 AP. Posiva Working report 2006-113. Posiva Oy, Olkiluoto, Finland.

Pastina B, Hellä P, 2006. Expected evolution of a spent fuel repository at Olkiluoto. Posiva Report 2006-05. Posiva Oy, Olkiluoto, Finland.

Pitkänen P, Partamies S, Luukkonen A, 2004. Hydrogeochemical interpretation of baseline groundwater conditions at the Olkiluoto site. Posiva Report 2003-07. Posiva Oy, Olkiluoto, Finland.

Posiva, 2003. Baseline Conditions at Olkiluoto. Posiva Report 2003-02. Posiva Oy, Olkiluoto, Finland.

Posiva, 2005. Olkiluoto Site Description 2004. Posiva Report 2005-03. Posiva Oy, Olkiluoto, Finland.

Posiva, 2006. Nuclear waste management of the Olkiluoto and Loviisa power plants: Programme for research, development and technical design for 2007-2009. Posiva TKS-2006. Posiva Oy, Olkiluoto, Finland.

Raiko H, 2005. Disposal Canister for Spent Nuclear Fuel – Design Report. Posiva Report 2005-02. Posiva Oy, Olkiluoto, Finland.

Ronneteg U, Cederqvist L, Rydén H, Öberg T, Müller C, 2006. Reliability in sealing of canister for spent nuclear fuel. SKB R-06-26, Svensk Kärnbränslehantering AB.

Ruokola E, 2002. Consideration of timescales in the Finnish safety regulations for spent fuel disposal. Proc. of Workshop on the handling of timescales in assessing post-closure safety of deep geological repositories. Organisation for Economic Co-operation and Development, Nuclear Energy Agency, 85–89. Issy-les-Moulineaux, France.

SKB, 2006a. Long-term safety for KBS-3 repositories at Forsmark and Laxemar – a first evaluation – Main report of the SR-Can project, SKB TR-06-09, Svensk Kärnbränslehantering AB.

SKB, 2006b. Data report for the safety assessment SR-Can. SKB TR-06-25, Svensk Kärnbränslehantering AB.

SKB, 2006c. Buffer and backfill process report for the safety assessment SR-Can. SKB TR-06-18, Svensk Kärnbränslehantering AB.

SKB, 2006d. Geosphere process report for the safety assessment SR-Can. SKB TR-06-19, Svensk Kärnbränslehantering AB.

SKB, 2006e. Fuel and canister process report for the safety assessment SR-Can. SKB TR-06-22, Svensk Kärnbränslehantering AB.

Smart N R, Rance A P, Werme L O, 2004. Anaerobic corrosion of steel in bentonite. Mat. Res. Soc. Symp. Proc. 807, 441-446.

Smith P, Johnson L, Snellman M, Pastina B, Gribi P, 2007a. Safety assessment for a KBS-3H spent nuclear fuel repository at Olkiluoto – Evolution report. Posiva Report 2007-08 and SKB R-08-37. Posiva Oy, Olkiluoto, Finland and Svensk Kärnbränslehantering AB, Sweden.

Smith P, Neall F, Snellman M, Pastina B, Nordman H, Johnson L, Hjerpe T, 2007b. Safety assessment for a KBS-3H spent nuclear fuel repository at Olkiluoto – Summary report. Posiva Report 2007-06 and SKB R-08-39. Posiva Oy, Olkiluoto, Finland and Svensk Kärnbränslehantering AB, Sweden.

SSI, 2005. The Swedish Radiation Protection Authority's guidelines on the application of the regulations (SSI FS 1998:1) concerning protection of human health and the environment in connection with the final management of spent nuclear fuel and nuclear waste. SSI FS 2005:1. Statens strålskyddsinstitut (SSI), Stockholm, Sweden.

STUK, 1999. Government decision on the safety of disposal of spent nuclear fuel (478/1999). Radiation and Nuclear Safety Authority (STUK) Report STUK-B-YTO 195. STUK, Helsinki, Finland.

STUK, 2001. Long-term safety of disposal of spent nuclear fuel. Radiation and Nuclear Safety Authority (STUK). Guide YVL 8.4. STUK, Helsinki, Finland.

Vieno T, Nordman H, 1999. Safety assessment of spent fuel disposal in Hästholmen, Kivetty, Olkiluoto and Romuvaara TILA-99. Posiva Report 99-07. Posiva Oy, Helsinki, Finland.

Vieno T, Ikonen A T K, 2005. Plan for Safety Case of spent fuel repository at Olkiluoto. POSIVA 2005-01. Posiva Oy, Olkiluoto, Finland.

Werme L O, Johnson L H, Oversby V M, King F, Spahiu K, Grambow B, Shoesmith D W, 2004. Spent fuel performance under repository conditions: A model for use in SR-Can. SKB TR 04-19, Svensk Kärnbränslehantering AB.

Wersin P, Birgersson M, Olsson S, Karnland O, Snellman M, 2007. Impact of corrosion-derived iron on the bentonite buffer within the KBS-3H disposal concept. The Olkiluoto site as case study. POSIVA 2007-11 and SKB R-08-34. Posiva Oy, Olkiluoto, Finland and Svensk Kärnbränslehantering AB, Sweden.

Åstrand P-G, Jones J, Broed R, Avila R, 2005. PANDORA technical description and user guide. Posiva Working report 2005-64. Posiva Oy, Olkiluoto, Finland.

Appendix A

Computer codes

A.1 The REPCOM code

Near-field analyses have been performed with the REPCOM code. REPCOM has been developed by the Technical Research Centre of Finland (VTT) for radionuclide transport analyses in the near field of repositories for low and intermediate level waste or spent fuel. The phenomena that can be modelled using REPCOM are:

- release from the waste – several waste types, each with different release functions, can be included;
- advective and/or diffusive transport within a system of engineered barriers;
- sorption on solid surfaces;
- solubility limitation of concentrations; and
- radionuclide decay and ingrowth.

Detailed descriptions of how these phenomena are treated, including the governing equations solved by REPCOM, are given in /Nordman and Vieno 1994/.

In order to simulate the migration of radionuclides through a system of engineered barriers and their release to the geosphere, the repository is discretised into small volumes termed "compartments". In setting up a problem to be solved using REPCOM, compartment sizes must be chosen that are sufficiently small that instantaneous mixing can be assumed in each compartment[28].

Stepwise changes in the properties and geometry of the compartments can be accommodated, and different boundary conditions at the interface with the geosphere can be applied by means of user-specified mass transfer coefficients[29]. The derivation of the transfer coefficients is presented in detail in Section 11.6 of TILA-99 /Vieno and Nordman 1999/, and discussed further in /Vieno and Nordman 2000/, where the transfer coefficients used in TILA-99 are compared with those used in the Swedish SR 97 assessment /SKB 1999/.

REPCOM has been verified against analytical models /Nordman 1986, Vieno et al. 1992, Nordman and Vieno 1994/. It has also been verified against the commercial PORFLOW code, a computational fluid dynamics tool used by nuclear waste management and research organisations in several countries /Nordman and Vieno 2003/. This exercise included preliminary near-field transport analyses for KBS-3H, as well as KBS-3V. In Appendix B, REPCOM is compared against the Nagra near-field calculation code SPENT.

A.2 The FTRANS code

Geosphere analyses have been performed with the FTRANS code /FTRANS 1983, Nordman and Vieno 1994/. FTRANS is a dual-porosity model for flow and transport. In the flowing porosity domain, phenomena that can be modelled with FTRANS are:

- groundwater flow;
- advective radionuclide transport; and
- longitudinal dispersion.

---

[28] A concept for the discretisation of the near field of KBS-3V type repository for use with REPCOM is described in /Vieno and Nordman 2000/. This represents an update of the discretisation used in TILA-99 and earlier assessments.

[29] The applicability of the transfer coefficient approach has been assessed using transient three-dimensional modelling of the repository near field in /Pereira 2006/.

In the matrix porosity domain, phenomena that can be modelled are:

- diffusion; and
- sorption on solid surfaces.

Radioactive decay and ingrowth are represented in both domains, and transfer of radionuclides across the boundary between the domains takes place by diffusion.

Flow porosity in the analyses carried out for KBS-3H/Olkiluoto takes the form of a representative planar fracture of width W [m], length L [m] and flow rate Q [m^3 a^{-1}]. FTRANS input parameters are chosen in such a way as to give the required value for the lumped parameter WL/Q, which, as discussed for example in Section 11.5 of TILA-99 /Vieno and Nordman 1999/, represents the "transport resistance" of the geosphere.

Matrix porosity in the rock adjacent to the fracture can be subdivided into different subdomains, each with different transport properties. This can be used, for example, to differentiate between mineralogically altered rock immediately adjacent to the fracture, and more distant, unaltered rock.

FTRANS has been verified using test cases as part of the INTRACOIN and INTRAVAL projects /INTRACOIN 1984, Rasilainen 1989/. Additional verification tests against an analytical model have been presented in TVO-92 /Vieno et al. 1992/.

A.3 Auxiliary computer codes

Besides the main codes described above, the auxiliary codes Apu1a and Apu2a have been used. These are, respectively, pre- and post-processing routines which are used, among other things, to convert REPCOM output into FTRANS input format and to convert the results from FTRANS into a more user-friendly format.

Pre-processor Apu1a

FTRANS uses four main input files: Files 24, 35, 20 and 17. Apu1a reads these files as follows.

Data from File 24:

- The first line gives the number of materials (typically two different layers of rock matrix) and number of nuclides in the file.
- The second line gives the porosity and D_e values for the two layers of rock used, one layer (e.g. 1 cm thick in file 35) represents the rock matrix close to the fracture surface and the second (e.g. 9 cm thick in file 35) represents the rock matrix further away from the surface. The entire rock matrix thickness would thus be 10 cm. The first four values are for neutral and cationic species and next four values for anions.
- The next lines give the names and K_d values of nuclides. Negative K_d values indicated that the nuclide is an anion but the absolute value is used in calculations. With Apu1a, it is possible to assign different porosities and De values (in the rock matrix) for chain elements thereby adding flexibility to the model.
- The following lines give the names and half-lives of nuclides.

Example of file 24.

Additional data, which are not used, are in the file because of historical reasons. These data are shaded in the example below.

```
2  2
 5.00E-03  1.00E-13  1.00E-03  1.00E-14  1.00E-03  1.00E-14  2.00E-04  1.00E-15
C-14     0.00E-04  2.00E-09  0.00E-01  2.00E-10  5.00E-02  1.00E-12  1.00E-01  2.00E-14  2.50E-02  2.00E-12
Cl-36   -1.00E-99  2.00E-09  0.00E-01  2.00E-10  5.00E-02  1.00E-12  1.00E-01  2.00E-14  2.50E-02  2.00E-12
C-14     5.70E+03  2.90E-15  1.00E+33  1.28E+10  1.44e+09  1.44e+08  1.09E+10  7.84e+09  0.00E+00
Cl-36    3.00E+05  4.70E-15  1.00E+33  0.00E+00  0.00E+05  0.00E+00  6.72e+08  0.00e+00  0.00e+00
```

Data from File 35

- The first line gives the velocity of water (e.g. 24 m/y), the half aperture of the fracture (e.g. 2.5×10^{-4} m), the length of the migration route (e.g. 600 m), the number of nodes in the migration direction (e.g. 20) and the increase factor of the distance between nodes in the flow direction (e.g. 1.02 for a 2% increase).
- the second line gives the number of rock material layers (2 layers in our case), the thickness of the first layer of rock matrix (e.g. 0.01 m near the fracture), the number of nodes of the first layer (e.g. 7) and the factor with the distance between nodes is increased (e.g. 1.5 for a 50% increase between successive nodes). Next on the second line is the thickness of the second layer (e.g. 0.09 m), the number of nodes in the second layer (e.g. 12) and the factor by which the distance between successive nodes is increased. The three last variables on this second line are read if a two-layer system is used, as is the case in this report.
- The next two lines do not contain variables and provide guidance for the mathematical solution to be used in calculating the results. Therefore it is important that these lines remain unchanged if the results are to be reproduced. Further information on the lines that do not contain any variable parameter values, but rather information on the mathematical models is provided in the FTRANS manual /FTRANS 1983/.
- In the fifth line, the third variable gives the number of time steps that may be changed (e.g. 120). The rest of the line must remain unchanged for the same reasons discussed above.
- On the sixth line, there are five variables, four of which may be changed by the user: the length of first time step (e.g. 0.1), start time of calculation (always zero), increase factor of time step (e.g. 1.2), the maximum length of a time step (e.g. 20,000 years) and the end time of calculation (e.g. 106 years).
- The next lines in the file must remain unchanged for the same reasons discussed above.

Example of File 35 (the contents of this file are described in the FTRANS manual)

```
24.  2.5e-4  600. 20  1.02
2   0.01  7   1.5  0.09  12  1.5
   1
FTRANS TEST: LASKENTATAPAUS HENKKA (korjaus 1) VARIAATIO 1
 861  800  120   1   2   8   1   6   0  40   1   0
  1.0E-1   0.0E+4   1.2E+0   2.0E+4   1.0E+6
    0.0
  0  -1  10   1   1   1   0   0   0
  0   0   0   0
  0.0E00   0.0E00  0.00E00  3.155E-9   5.0E-9   3.0E-0   0.0E+0   2.0E+4
       1.00e+00 1.000e+00 1.000e+00
  0.0E+2   0.0E00   1.0E00   2.5E-4  0.00E+4   0.0E+0
       1.00e+00 1.000e+00 1.000e+00
  0  2.888E-5  1.000E+0  1.000E+0  1.000E-7   1.0E+5
```

Data from Files 17 and 20

File 20 and file 17 are the output files from REPCOM. They include the release pulses from the near field. Files 17 and 20 must be in the same directory where the calculation is carried out. The nuclide names must be the same as in file 24. In file 20, the start time is zero, but in file 17 the real start time, i.e. the time of the event triggering the release is specified (e.g. 1,000 years, the time for a defective canister to become penetrated).

Example of File 17
Output file for C-14 in the penetrating defect-base case (PD-BC)

```
C-14         299  EM=    6.7675E+05  T=       1.01E+04  A=       1.96E-09
2.21E+09
  1.000E+03 9.779E-10
  1.000E+03 3.818E-06[…]
  2.000E+03 6.096E+02[…]
  3.087E+03 1.227E+03[…]
  5.521E+03 2.109E+03[…]
  1.000E+04 2.687E+03[…]
  5.469E+04 4.397E+02[…]
  1.047E+05 2.939E-01[…]
  2.047E+05 1.534E-07[…]
  3.047E+05 1.998E-13[…]
  4.047E+05 7.834E-19[…]
  5.047E+05 3.985E-24[…]
  6.047E+05 2.081E-29[…]
  7.047E+05 1.089E-34[…]
  8.047E+05 5.697E-40[…]
  9.047E+05 2.982E-45[…]
1.001E+06 2.444E-50
```

Example of File 20
Carbon-14 data for PD-BC case
In the first line, the number "1" means that nuclide number one in a chain is considered. The number "299" indicates that there are 299 time steps in the release pulse. Following lines: time (years from emplacement) and release (Bq)

```
    1     299           C-14
  0.000E+00 9.779E-10
  2.749E-01 3.818E-06
  4.804E-01 2.690E-04
  7.218E-01 3.478E-03
  1.005E+00 1.936E-02
  1.730E+01 6.840E+00[…]
  1.250E+02 4.470E+01[…]
  1.000E+03 6.096E+02[…]
  1.000E+04 2.745E+05[…]
  5.369E+04 4.397E+02[…]
  1.037E+05 2.939E-01[…]
  5.037E+05 3.985E-24[…]
  9.037E+05 2.982E-45[…]
  1.000E+06 2.444E-50
```

From files 24, 35, 17 and 20 data, Apu1a produces the input file for FTRANS (File 25, see example below, the contents of which is described in the FTRANS manual, /FTRANS 1983/) and the release pulse from the near field to File 11. FTRANS then is run using File 25. The results from FTRANS are stored into File 10 (the output pulse).

Example of File 25

FTRANS input for C-14 in PD-BC (penetrating defect-base case)

```
    1
FTRANS TEST: LASKENTATAPAUS HENKKA (korjaus 1) VARIAATIO 1
  420  380  120    1    2    8    1    6    0   20    1    0
    1.0E-1    0.0E+4    1.2E+0    2.0E+4    1.0E+6
       0.0
    0   -1   10    1    1    1    0    0    0
    0    0    0    0
    1    1    1    1    1    1    1    2    2    2    2    2    2    2    2    2
    2    2    2    1    1    1    1    1    1    2    2    2    2    2    2    2
    2    2    2    2    2    2    1    1    1    1    1    1    1    2    2    2
    2    2    2    2    2    2    2    2    2    1    1    1    1    1    1    1
    2    2    2    2    2    2    2    2    2    2    2    2    1    1    1    1
    1    1    1    2    2    2    2    2    2    2    2    2    2    2    2    1
    1    1    1    1    1    1    2    2    2    2    2    2    2    2    2    2
    2    2    1    1    1    1    1    1    1    2    2    2    2    2    2    2
    2    2    2    2    2    1    1    1    1    1    1    1    2    2    2    2
    2    2    2    2    2    2    2    2    1    1    1    1    1    1    1    2
    2    2    2    2    2    2    2    2    2    2    2    1    1    1    1    1
    1    1    2    2    2    2    2    2    2    2    2    2    2    2    1    1
    1    1    1    1    1    2    2    2    2    2    2    2    2    2    2    2
    2    1    1    1    1    1    1    1    2    2    2    2    2    2    2    2
    2    2    2    2    1    1    1    1    1    1    1    2    2    2    2    2
    2    2    2    2    2    2    2    1    1    1    1    1    1    1    2    2
    2    2    2    2    2    2    2    2    2    2    1    1    1    1    1    1
    1    2    2    2    2    2    2    2    2    2    2    2    2    1    1    1
    1    1    1    1    2    2    2    2    2    2    2    2    2    2    2    2
    1    1    1    1    1    1    1    2    2    2    2    2    2    2    2    2
    2    2    2    1    1    1    1    1    1    1    2    2    2    2    2    2
    2    2    2    2    2    2    1    1    1    1    1    1    2    2    2    2
    2    2    2    2    2    2    2    2    2    1    1    1    1    1    1    1
    2    2    2    2    2    2    2    2    2    2    2    2
 0.000E+00 0.000E+00 0.000E+00 1.000E+00 1.000E+00 3.000E+00 0.000E+00 2.000E+04
           1.000E+00
           3.156E-06
           5.000E-03
 0.000E+00 0.000E+00 0.000E+00 1.000E+00 1.000E+00 3.000E+00 0.000E+00 2.000E+04
           1.000E+00
           3.156E-07
           1.000E-03
 0.000E+00 0.000E+00 1.000E+00 2.500E-04 0.000E+00 0.000E+00
           1.000E+00
    0 1.216E-04 1.000E+00 1.000E+00 1.000E-07 1.000E+05
   20   21   600.000   600.000    1
     0.000    24.694    49.882    75.574   101.779   128.509   155.773   183.582
   211.948   240.881   270.393   300.495   331.199   362.517   394.461   427.044
   460.279   494.179   528.756   564.025   600.000
 0.000E+00 3.108E-04 7.771E-04 1.476E-03 2.525E-03 4.099E-03 6.459E-03 1.000E-02
 1.035E-02 1.087E-02 1.166E-02 1.284E-02 1.461E-02 1.726E-02 2.124E-02 2.722E-02
 3.617E-02 4.961E-02 6.977E-02 1.000E-01
    1    1   21    1 2.500E-04
    2   21   41    1 2.500E-04
    3   41   61    1 2.500E-04
    4   61   81    1 2.500E-04
    5   81  101    1 2.500E-04
    6  101  121    1 2.500E-04
    7  121  141    1 2.500E-04
    8  141  161    1 2.500E-04
    9  161  181    1 2.500E-04
   10  181  201    1 2.500E-04
   11  201  221    1 2.500E-04
   12  221  241    1 2.500E-04
   13  241  261    1 2.500E-04
   14  261  281    1 2.500E-04
   15  281  301    1 2.500E-04
   16  301  321    1 2.500E-04
   17  321  341    1 2.500E-04
   18  341  361    1 2.500E-04
   19  361  381    1 2.500E-04
   20  381  401    1 2.500E-04
    0    1    1
    1    1    1 1.000E+00 6.000E-03
     0.000     0.000     0.000     0.000
    24.000    24.000    24.000    24.000    24.000    24.000    24.000    24.000
    24.000    24.000    24.000    24.000    24.000    24.000    24.000    24.000
    24.000    24.000    24.000    24.000
    1    0
  401    0
 0.600E-02
```

Post processor Apu2a

The post processor reads File 24 to find the radionuclide names and reads the FTRANS output pulse from File 10. Apu2a writes the release pulse from the far field into File 3 and the maximum value of release and the timing of the release into File 19. It also writes the time at which 90% of maximum of the release is observed into File 19. The final results are thus from File 3 and File 19.

Example of File 3
Carbon-14 data from PD-BC case.
First line: radionuclide name, maximum dose (Bq), time of maximum release,
Following lines: time (years from canister emplacement and release (Bq).

```
C-14       113 EM=    3.351E+05 tm=    1.044E+04
  1.000E+03 1.487E-20[…]
 1.005E+03 7.965E-15
  1.006E+03 1.041E-11[…]
  1.027E+03 4.203E-01[…]
  1.170E+03 4.746E+01[…]
  5.550E+03 2.095E+03
  6.460E+03 2.300E+03
  7.552E+03 2.481E+03
  8.862E+03 2.615E+03
  1.044E+04 3.351E+05[…]
  2.056E+04 6.557E+04
  2.448E+04 3.724E+04
  2.917E+04 1.881E+04
  3.481E+04 8.275E+03
  4.157E+04 3.193E+03[…]
  5.942E+04 2.255E+02
  7.110E+04 4.220E+01
  8.469E+04 5.542E+00
  1.010E+05 5.373E-01[…]
  5.006E+05 6.861E-24[…]
  1.001E+06 0.000E+00
  1.001E+06 0.000E+00
```

Example of File 19
Carbon-14 results
First line: time at which 90% of the maximum release rate has been reached and the release rate at that instant. The shaded word is not relevant.
Second line; time of maximum, maximum release rate, indicative dose rate (sv/yr) and total integrated release.

```
C-14       1.04E+04     3.35E+05   yli 90 %, oikein
C-14       1.04E+04     3.35E+05     9.72E-10     2.33E+09
```

How to run Apu1a and Apu2a

Apu1a and Apu2a are run using the following UNIX command strings:

- “1 1” means that one single nuclide is calculated and it is number 1 in file 24
  e.g. command echo “1 1” |$HOME/kpa94a/apu2a
- “3 4 5 6 “ means that a chain of 3 nuclides is calculated and they are numbers 4, 5 and 6 in file 24. The same nuclides must also exist in files 17 and 20. e.g. command echo “3 4 5 “ |$HOME/kpa94a/apu1a

Traceability and reproducibility of results

In the interest of traceability and reproducibility of the results, the scripts for all calculation cases are kept in the directory named “scasejob” as the scripts of TILA-99 are still in directory “tila99job”. An example of a script can be found in /Nordman and Vieno 2003/. The scripts also contain links to all input data that were used in the calculation.

References

FTRANS, 1983. A two-dimensional code for simulating fluid flow and transport of radioactive nuclides in fractured rock for repository performance assessment. Report ONWI-426. Intera Environmental Consultants Inc., Houston, USA.

INTRACOIN, 1984. INTRACOIN – International nuclide transport intercomparison study – Final report level 1. Swedish Nuclear Power Inspectorate (SKI) Technical Report 84:3. SKI, Stockholm, Sweden.

Nordman H, 1986. REPCOM – a compartment model of a repository for nuclear waste. Technical Report TUMA-12/86 (In Finnish). Technical Research Centre of Finland, Nuclear Engineering Laboratory, Helsinki, Finland.

Nordman H, Vieno T 1994. Near-field model REPCOM. Report YJT-94-12. Nuclear Waste Commission of Finnish Power Companies (YJT), Helsinki, Finland.

Nordman H, Vieno T, 2003. Modelling of near-field transport in KBS-3V/H type repositories with PORFLOW and REPCOM codes. Posiva Working Report 2003-07. Posiva Oy, Helsinki, Finland.

Pereira A, 2006. Three dimensional modelling of a KBS-3 canister for spent nuclear fuel – some migration studies. Swedish Nuclear Power Inspectorate (SKI) Report 2006:17. SKI, Stockholm, Sweden.

Rasilainen K, 1989. Installation and testing of the migration model FTRANS. Teollisuuden Voima Oy (TVO), TVO/Safety and Technology, Work Report 89-24. (In Finnish). TVO, Helsinki, Finland.

SKB, 1999. SR 97 – Processes in the repository evolution. SKB TR-99-07, Svensk Kärnbränslehantering AB.

Vieno T, Hautojärvi A, Koskinen L, Nordman H, 1992. TVO-92 safety analysis of spent fuel disposal. Report YJT-92-33E. Nuclear Waste Commission of Finnish Power Companies. (YJT), Helsinki, Finland.

Vieno T, Nordman H, 1999. Safety assessment of spent fuel disposal in Hästholmen, Kivetty, Olkiluoto and Romuvaara TILA-99. Posiva Report 99-07. Posiva Oy, Helsinki, Finland.

Vieno T, Nordman H, 2000. Updated compartment model for near-field transport in a KBS-3 type repository. Posiva Working Report 2000-41. Posiva Oy, Helsinki, Finland.

Appendix B

Results obtained using an alternative near-field code

B.1 The SPENT code and its application in the present safety assessment

SPENT is a near-field release and transport code for a spent fuel waste form developed for safety assessments in Switzerland by Nagra. It is described in detail, for example, in Appendix 1 of /Nagra 2002/.

SPENT represents the cylindrical canister containing the fuel and an annular buffer region around this as a radially symmetric system. The outer boundary of the region considered in SPENT is the interface to the geosphere and is handled through the use of an appropriate boundary condition, whereby the diffusive radionuclide flux from the buffer is set equal to the advective flux entering the geosphere. At the inner boundary, a penetrating defect of a given radius can be assumed to be present. The canister may also be assumed to "disappear" (or the defect to lose its transport resistance) after a given time.

In addition to providing release rates from the near-field, SPENT provides output that gives insights as to where different parts of the overall inventory of a given radionuclides reside at any given time (e.g. incorporated in the fuel matrix, sorbed on the buffer, released to the geosphere). This can enhance understanding of how the repository near field limits the release rates of different radionuclides.

The principal differences from REPCOM are that:

- SPENT models diffusion in the buffer as a 1-D radial transport process, whereas REPCOM considers both radial diffusion and diffusion parallel to the canister axis;
- the analytical expression used for the transport resistance of the defect is different in the two codes; and
- the handling of solubility limitation of concentration is also different in the two codes.

These differences are explained in more detail in Section B.2.

In this appendix, SPENT is applied to the Base Case for an initial penetrating defect (Case PD-BC), and the results compare with those of REPCOM. The purpose is, on the one hand, to provide a quality check of the correctness of application of REPCOM and, on the other, a check of the consequences of some of the various model differences noted above.

The results of the comparison are presented in Section B.3, and some conclusions drawn in Section B.4.

B.2 Principal differences between SPENT and REPCOM

(i) Diffusion in one and two dimensions

SPENT models diffusion in the buffer as a 1-D radial process, whereas REPCOM considers both radial diffusion and diffusion parallel to the canister axis. In applying SPENT in the present safety assessment (as in Nagra safety assessments) the volume of buffer considered accessible to diffusion is that surrounding the failed canister between the canister outer surface and the drift wall. The buffer between the failed canister and the adjacent canisters is conservatively assumed to be inaccessible. In applying REPCOM, diffusion into this part of the buffer is, on the other hand, taken into account. In this respect, REPCOM can be considered more realistic than SPENT.

(ii) Transport resistance of the defect

REPCOM internally calculates a steady-state transfer coefficient for the defect. It comprises two parts: the transfer coefficient for mass transport along the length of the defect (Q_h) and the transport coefficient for mass transport from the hole into the buffer (Q_m). The expression for the combined transfer coefficient (Q) is:

$$Q = \left(\frac{1}{Q_h} + \frac{1}{Q_m} \right)^{-1} = \left(\frac{d_h}{\pi r_h^2 D_h} + \frac{1}{2\pi r_h D_e} \right)^{-1} \qquad \text{(Eq. B-1)}$$

where r_h [m] is the defect radius, d_h [m] is the length of the defect, D_h [m^2 a^{-1}] is the effective diffusion coefficient of the species in the defect and D_e [m^2 a^{-1}] is the effective diffusion coefficient of the species in the buffer /Vieno and Nordman 2000/.

In SPENT, the release rate to the buffer from the pinhole defect, J, is time dependent, and is calculated from the model proposed by /Chambré et al. 1986/, in which the transport resistance of the path through the defect is neglected.

According to this formulation:

$$J = 4 D_e r_h C \left[1 + \frac{2 r_h}{\pi} \sqrt{\left(\frac{\varepsilon R}{\pi D_e t} \right)} \right] \qquad \text{(Eq. B-2)}$$

where ε is the buffer porosity, t [a] is the time after the onset of releases, C [mol m^{-3}] is the radionuclide concentration inside the canister and R is a retardation factor that accounts for sorption in the buffer.

Eq. B-2 implies a steady state ($t \rightarrow \infty$) transfer coefficient, Q_a [m^3 a^{-1}]:

$$Q_a = 4 D_e r_h \qquad \text{(Eq. B-3)}$$

Comparing Eqs. B-1 and B-3 suggests that, provided transport through the defect is well approximated as a steady state, the transport resistance of the path through the defect can be included in SPENT calculations if an effective defect radius r_{eff} [m] is used as the input parameter, given by:

$$r_{eff} = \frac{1}{4 D_e} \left(\frac{d_h}{\pi r_h^2 D_h} + \frac{1}{2\pi r_h D_e} \right)^{-1} \qquad \text{(Eq. B-4)}$$

(note that r_{eff} and r_h differ by a factor of $\pi/2$, even in the case of an infinitesimally short hole).

Using the data from the near-field model of case PD-BC given in Section 5.2.3, Eq. B-4 gives an effective defect radius for SPENT calculations in the present safety assessment of 4×10^{-4} m for anions and 6×10^{-5} m for cations (excluding Cs, which, according to Table 5-7, has a higher effective diffusion coefficient than other cations).

(iii) Handling of solubility limitation of concentration

SPENT applies solubility limits internally within the canister and throughout the modelled part of the buffer. If the concentration of an element exceeds its solubility limit, then the isotopes of that element are precipitated *in situ*. Precipitates redissolve if the concentration falls. In REPCOM, solubility limits are applied in this way only internally within the canister. REPCOM does not apply solubility limits within the buffer, except at its interface with the rock. In this case, however, precipitates are not formed *in situ*, but rather they are transferred back to the canister interior. In this respect, SPENT can be considered more realistic than REPCOM.

B.3 Comparison of SPENT and REPCOM results

(i) Single radionuclides: I-129 and Se-79

Figure B-1 shows a comparison of the single radionuclide release rates from the PD-BC near field calculated using the codes REPCOM and SPENT, taking the examples of I-129 and Se-79.

Agreement between REPCOM and SPENT results is reasonable, with the minor differences being attributable to the modelling of diffusion in one dimension in SPENT and two dimensions in REPCOM, and the difference in the treatment of the transport resistance of the defect.

Figures B-2 and B-3 show the distributions of I-129 and Se-79 inventory between different forms in the near field (and released to the geosphere) as functions of time, calculated using SPENT.

The inventories of both radionuclides are contained predominantly in the slowly dissolving fuel matrix throughout the million year calculational period. After water ingress to the canister interior at 1,000 years and prior to loss of transport resistance of the defect at 10,000 years, I-129 released from the waste form and the I-129 instant release fraction (IRF) are present mainly in aqueous solution inside the canister, with relatively small but increasing amounts present in the buffer and in the geosphere. In the case of Se-79, in addition to aqueous solution, this radionuclide is present in precipitated form inside the canister (no solubility limit is applied in the case of I-129).

After loss of transport resistance of the defect at 10,000 years, the inventory inside the canister in aqueous solution (and, in the case of Se-79, in the form of precipitate) starts to fall, as the rate of mass transfer to the buffer is increased. The inventory in solution in the buffer sharply increases at 10,000 years, and then slowly decreases as inventory accumulated inside the canister is transferred first to the buffer, and then to the geosphere.

Neither I-129 nor Se-79 are assumed to sorb on buffer pore surfaces. Furthermore, Se-79 does not exceed its solubility limit at any time in buffer pore water.

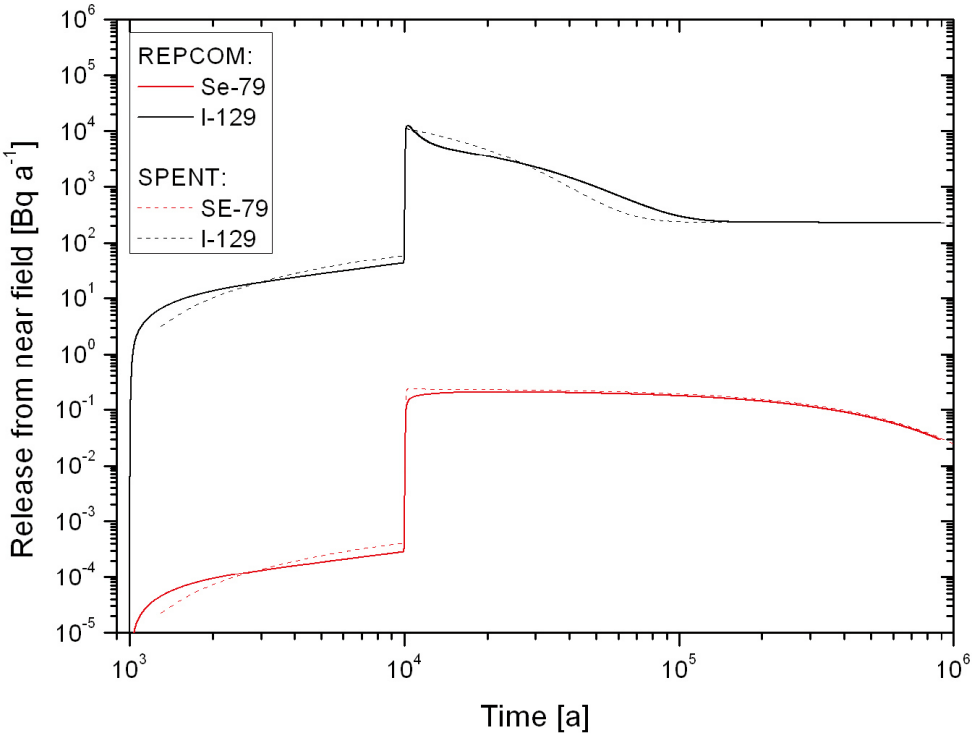

Figure B-1. *I-129 and Se-79 release rates from the PD-BC near field calculated using the codes REPCOM and SPENT.*

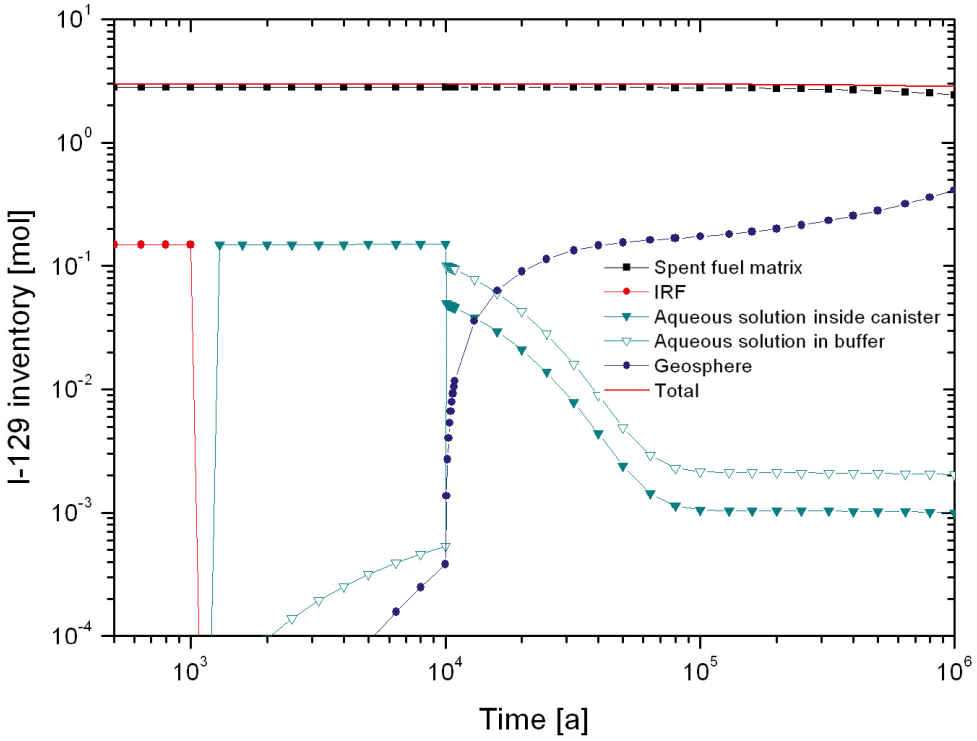

Figure B-2. *Distribution of I-129 inventory between different forms in the near field, and released to the geosphere, as a function of time, calculated using SPENT.*

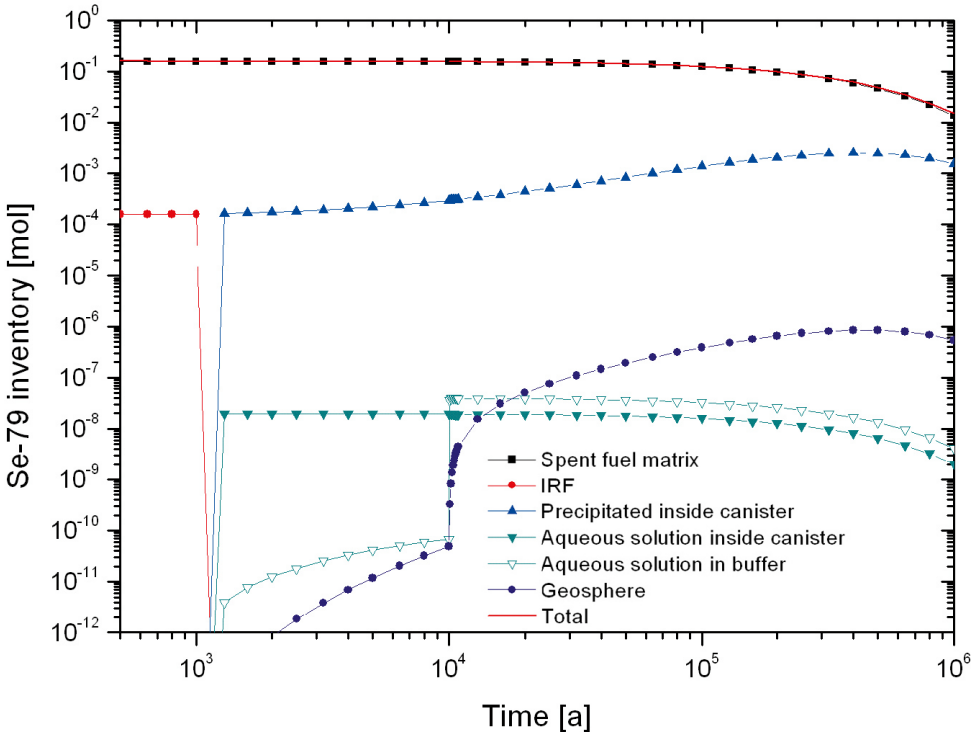

Figure B-3. *Distribution of Se-79 inventory between different forms in the near field, and released to the geosphere, as a function of time, calculated using SPENT.*

(ii) U-238 and its decay products

Figure B-4 shows a comparison of the release rates of U-238 and its decay products from the PD-BC near field using the codes REPCOM and SPENT.

Agreement between REPCOM and SPENT results is reasonable in the cases of U-238, U-234 and Ra-226. There is a greater discrepancy in the case of Th-230, with REPCOM giving higher release rates of this radionuclide at all calculated times.

Much of the Th-230 released to the geosphere is the result of the decay of U-234 near the buffer/rock interface. Th is strongly sorbed, and Th-230 decays significantly during transport through the buffer, so only Th-230 generated by decay of U-234 near the buffer/rock interface reaches the geosphere in significant amounts. The difference in the calculated releases of Th-230 between REPCOM and SPENT may at least partly be explained by the difference in the treatment of solubility limitation of the concentration of its parent radionuclides U-234 and other isotopes of U. U rapidly reaches its solubility limit internally within the canister (see Figure B-5, which is discussed further, below). Furthermore, shortly after the loss of transport resistance of the defect at 10,000 years, the solubility limit of U is exceeded in the buffer, due to ingrowth (e.g. the decay of Pu-242 in the buffer to U-238 and Np-237 to U-233). In SPENT, the rate of transport of U-234 to the buffer/rock interface is reduced, because part of the U-234 inventory in the buffer is modelled as immobile precipitates. This in turn reduces the release rate of Th-230 to the geosphere. In REPCOM, on the other hand, solubility limits are applied at the buffer/rock interface, and not internally within the buffer. This gives rise to a higher transport rate of U-234 to the interface. Thus, although the release rate of U-234 to the geosphere is still limited by U solubility, the release rate of Th-230 is increased.

Figure B-5 shows the distribution of U-234 inventory between different forms in the near field (and released to the geosphere) as a function of time, calculated using SPENT. The figure confirms that U exceeds its solubility limit inside the canister shortly after water ingress at 1,000 years, resulting in U-234 precipitation inside the canister. The figure further shows that U also exceeds its solubility limit inside the buffer shortly after loss of transport resistance of the defect at 10,000 years.

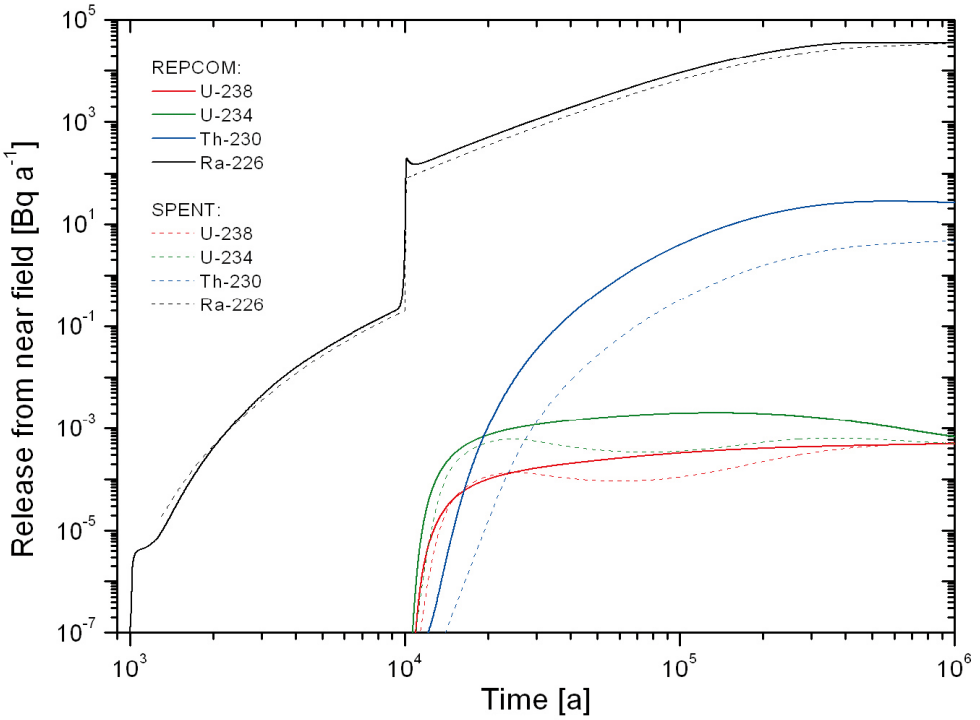

Figure B-4. *Release rates of U-238 and its decay products from the PD-BC near field calculated using the codes REPCOM and SPENT.*

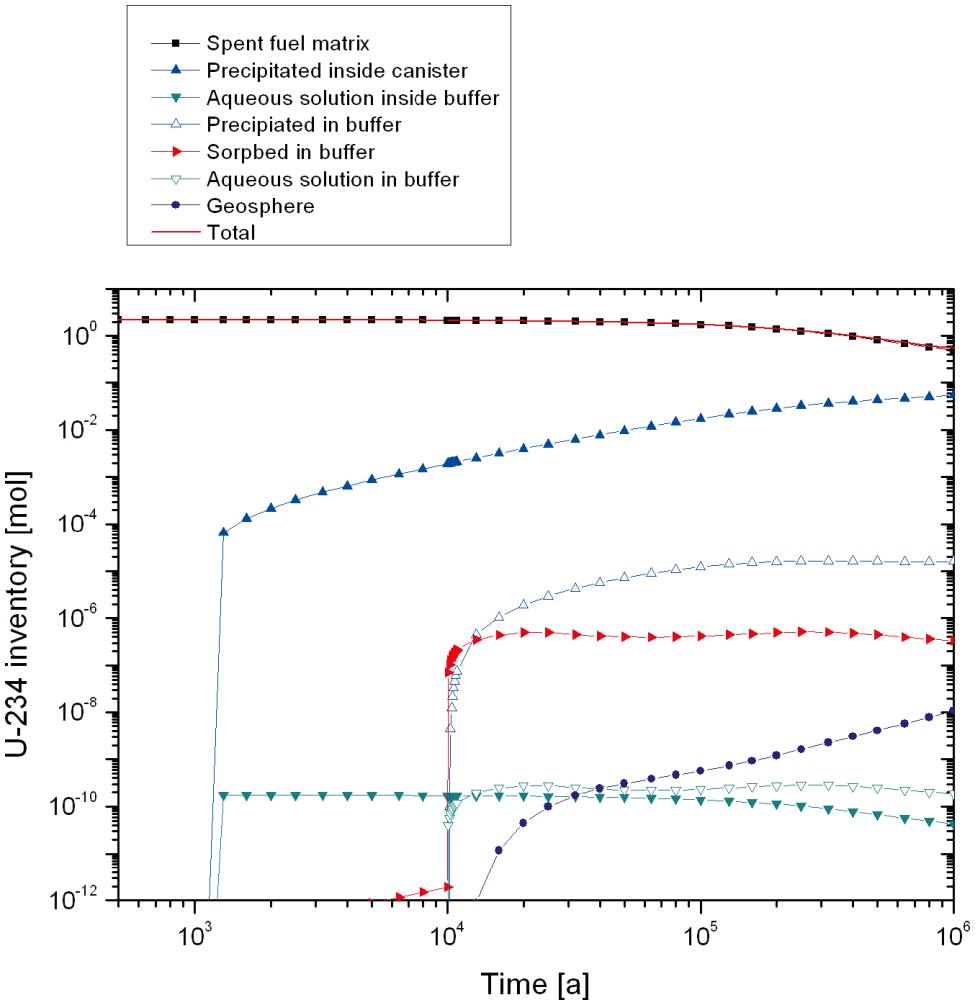

Figure B-5. *Distribution of U-234 inventory between different forms in the near field, and released to the geosphere, as a function of time, calculated using SPENT.*

(iii) Np-237 and its decay products

As a further example of chain decay, Figure B-6 shows a comparison of the release rates of Np-237 and its decay products from the PD-BC near field using the codes REPCOM and SPENT.

Agreement between REPCOM and SPENT results is reasonable in for all three radionuclides, although the levelling of Th-229 release calculated by REPCOM after about 200,000 years is not shown in the SPENT results.

B.4 Conclusions

The principal differences between the Nagra code SPENT and the REPCOM code used in the present safety assessment are that:

- SPENT models diffusion in the buffer as a 1-D radial process, whereas REPCOM considers both radial diffusion and diffusion parallel to the canister axis;
- the analytical expression used for the transport resistance of the defect is different in the two codes; and
- the handling of solubility limitation of concentration is also different in the two codes.

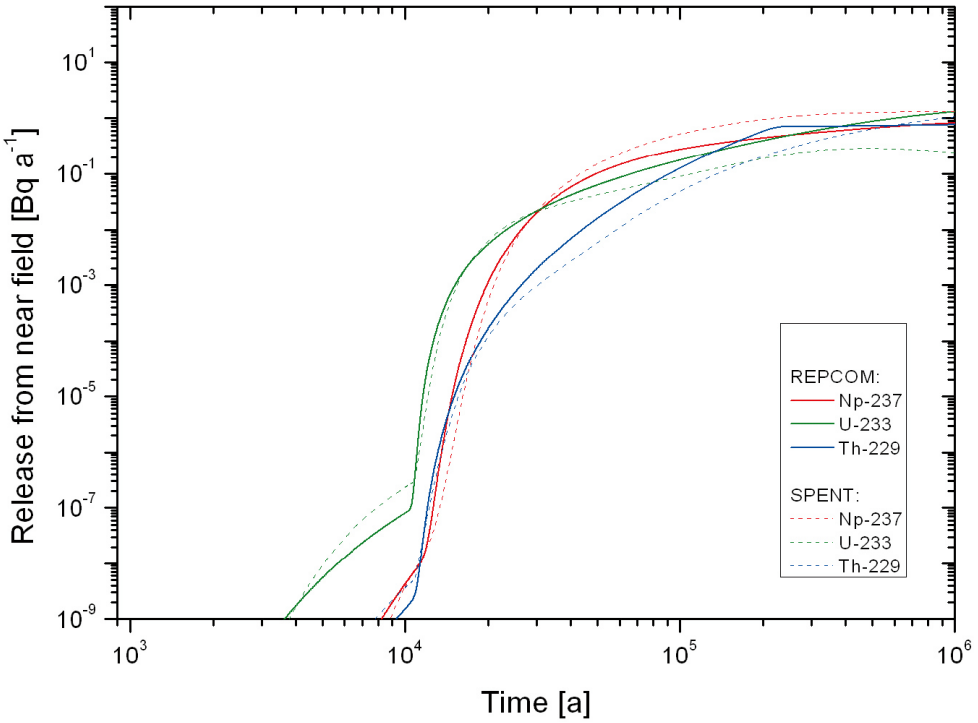

Figure B-6. *Release rates of Np-237 and its decay products from the PD-BC near field calculated using the codes REPCOM and SPENT.*

From the comparisons made of the results obtained by evaluating the same case (PD-BC) with the two codes, it appears that the first two differences, which apply to all radionuclides, have only minor consequences for calculated radionuclide releases. The differences in the handling of the solubility limitation of concentration, on the other hand, can give rise to significant differences in the behaviour of U isotopes and their daughters. Although these radionuclides are not generally among those that dominate calculated doses in the present safety assessment, the handling of the solubility limitation of concentration in the repository near field is an issue that deserves further consideration in future safety assessments.

References

Chambré P L, Lee W, Kim C L, Pigford T H, 1986. Steady-state and transient radionuclide transport through penetrations in nuclear waste containers, Lawrence Berkeley Laboratories Report LBL-21806, Berkeley, CA, USA.

Nagra, 2002. Project Opalinus Clay: Models, Codes and Data for Safety Assessment. Nagra Technical Report Series, NTB 02-06, Nagra, Wettingen, Switzerland.

Vieno T, Nordman H, 2000. Updated compartment model for near-field transport in a KBS-3 type repository. Posiva Working Report 2000-41. Posiva Oy, Helsinki, Finland.

Appendix C

Illustration of the impact of matrix diffusion on radionuclide release from the geosphere

In addition to the assessment cases defined in the main text, three additional cases, **MD-1**, **MD-2** and **MD-3**, have been defined in order to illustrate the impact on radionuclide release from the geosphere of the assumed maximum depth to which radionuclides can diffuse into the rock matrix.

These cases assume a hypothetical pulse release of a unit mass of a stable non-anion from the near field to the geosphere. The geosphere model is as in the Base Case, with the exception of the maximum rock matrix depth, which is set to 10 cm (as in the Base Case) in case MD-1, 30 cm in case MD-2 and 1 m in case MD-3. In addition to a transport resistance (WL/Q) of 50,000 a m^{-1}, a groundwater travel time of 50 years is assumed (corresponding, for example, to a mean fracture aperture along the transport path of 1 mm, the groundwater travel time being the product of aperture and transport resistance).

Results are shown in Figure C-1. The figure shows that the height of the release maximum is insensitive to matrix diffusion depth across the range considered.

The depth to which a non-sorbing nuclide will penetrate the matrix in time Δt [s] is given approximately as:

$$\sqrt{2D\Delta t} \qquad \text{(Eq. C-1)}$$

where D [m^2 s^{-1}] is the matrix diffusion coefficient. For cations and neutral species, D for the first centimetre matrix adjacent to a fracture is 10^{-13} m^2 s^{-1} (Table 5-9) Figure C-1 indicates that Δt – the pulse width – is in the order of 5 years (about 1.5×10^8 s) by the time the pulse has migrated across the geosphere. The matrix penetration depth is therefore in the order of a few millimetres. Insensitivity to the maximum depth of diffusion accessible rock matrix in the range 10 cm to 1 m is therefore to be expected.

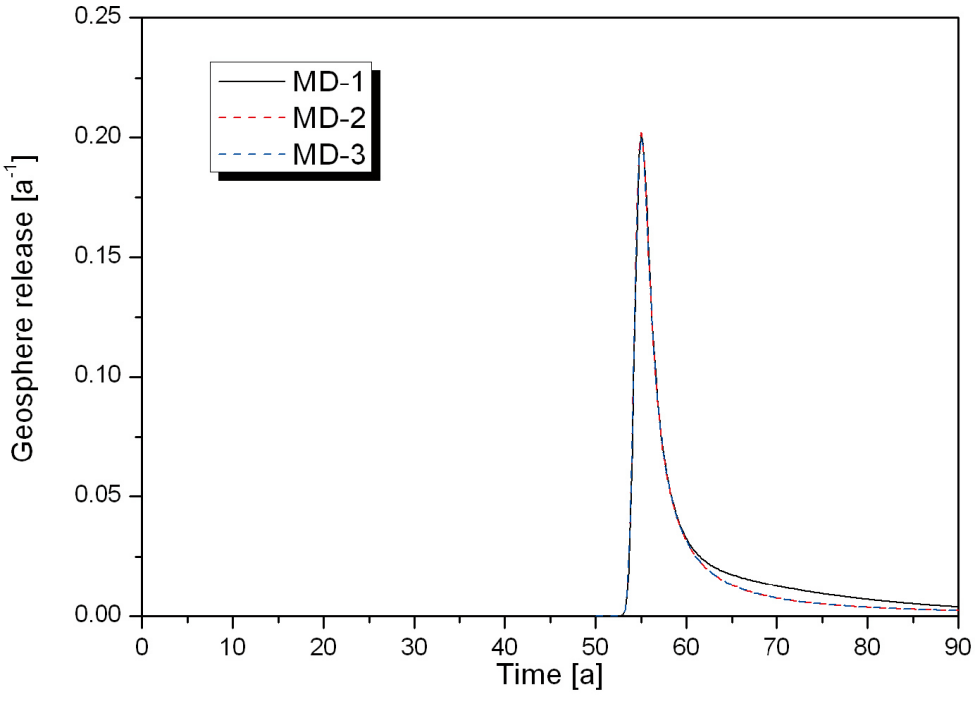

Figure C-1. *Geosphere release as a function of time for three different matrix diffusion depths and a pulse release of unit mass from the near field.*

Appendix D

Olkiluoto reference waters

D.1 Groundwater types

Three different broad types of waters, and a number of variants within these broad types, have been considered for the assessment of solubility limits and for the selection of diffusion and sorption parameters to be used in the radionuclide transport modelling:

- Groundwater types currently found at the Olkiluoto site and are either present at repository depth now, or may occur at repository depth in the future as the distribution of groundwater types evolves: *Olkiluoto groundwaters*;
- Olkiluoto groundwater modified by interaction with bentonite: *Bentonite waters*; and
- *Glacial meltwaters*.

D.2 Olkiluoto groundwaters

Based on the available data from deep boreholes /Pitkänen et al. 2004, 2007/ four reference groundwaters representative of repository conditions at Olkiluoto have been defined:

i. Brackish/saline groundwater (water sample reference: KR20/465/1);

ii. saline groundwater (water sample reference: KR10/498/1);

iii. brine groundwater (water sample reference: KR12/741/1); and

iv. dilute/brackish groundwater (water sample reference: KR6/58/1).

The first two waters reflect the expected range of compositions at repository depth reasonably well for the present site conditions and the conditions once the site is constructed and natural conditions have been restored, based on the discussion presented in the KBS-3V Evolution report /Pastina and Hellä 2006/. The third and fourth types are considered to be limiting compositions at either end of the range of variations in groundwater salinity in the future. The dilute/brackish groundwater is closest in terms of total dissolved solids (TDS) to the expected undisturbed conditions at repository depth in the period up to 10,000 years in the future.

The properties assigned to these reference groundwaters are listed in Table D-1, based on groundwater samples from Olkiluoto that have been classified as “valid”, with no significant sampling or analysis uncertainties /Pitkänen et al. 2007/.

D.3 Bentonite waters

The compositions of the bentonite waters, which are given in Table D-2, correspond to those of the different Olkiluoto groundwaters, modified to take into account their interaction with the buffer and (with respect to redox conditions) with the canister.

The compositions have been obtained using the conventional model of /Bradbury and Baeyens 1997/, as applied by /Curti and Wersin 2002/, under the constraint of constant pCO_2, determined by the pCO_2 of the groundwater (it should be noted that diffusion of CO_2 in the buffer bentonite is fast relative to the timescales of interest, which are generally greater than 10,000 years). According to this model, there are some differences between bentonite water compositions and those of the corresponding groundwaters. These differences, which are due to cation exchange and the dissolution of calcite and gypsum in the buffer, are greatest in the case dilute/brackish groundwater, where the equilibrium with the ion exchanger leads to increased cation concentrations. On the other hand, because of the strong buffering of the clay surfaces and the presence of calcite, pH conditions are predicted to remain rather stable (pH approx. 8). The main change predicted on long timescales is the enrichment of Ca relative to Na on the montmorillonite ion exchangeable sites.

Table D-1. Compositions of groundwaters taken from selected measurements in /Pitkänen et al. 2007/. Calculated values obtained with PHREEQC assuming T = 15°C. Concentrations in mmole l^{-1} unless otherwise indicated. SI: saturation index. (After Table 3.2.2 of /Wersin et al. 2007/, but with the addition of phosphate and fluoride).

	Brackish/saline groundwater	Saline groundwater	Brine groundwater	Dilute/brackish groundwater
Sample	**KR20/465/1**	**KR10/498/1**	**KR12/741/1**	**KR6/58/1**
Depth (m)	**465**	**498**	**741**	**58**
Solution composition				
TDS (mg/l)	10,544	22,099	49,483	1,026
Ionic strength (meq/l)	218	478	1,180	20
pH	7.4	8.0	8.2	7.6
Alkalinity	0.66	0.11	0.12	2.79
DIC	0.55	0.11	0.04	2.72
SO_4^{2-}	0.21	0.01	0.05	1.31
Cl(-I)	180.5	380.8	863.2	10.4
Na(I)	114.8	210.0	360.9	9.8
K(I)	0.28	0.36	0.49	0.20
Ca(II)	32.4	89.1	254.5	2.1
Mg(II)	2.6	1.6	1.5	1.1
Sr(II)	0.16	0.37	1.14	0.01
SiO_2	0.36	0.28	0.21	0.41
Mn(I)	5.8E–03	7.3E–03	9.3E–03	
Fe tot	2.5E–03	2.0E–03	3.8E–04	0.024
S^{2-}tot	5.61E–03	< 3.12E–04	1.25E–03	6.24E–04
F(-I)	1E–05	9.8E–05	6.3E–05	3.2E–05
$PO_{4\ tot}$	< 3E–07	1E–07	2.6E–06	5E–06
Calculated data				
Eh (mV)	–217 S(6)/S(-2)	–258 S(6)/S(-2)	–299 C(4)/C(-4)	–35 $Fe(OH)_3$/Fe(2)
SI(calcite)	0.03	0.06	0.57	0.00
SI(FeS_{am})	–0.34	–1.06	–0.11	0.00
SI(pyrite)	8.80	6.05	6.40	16.2
SI(siderite)	–1.72	–2.16	–2.11	0.34

The redox conditions for the bentonite waters have been calculated based on equilibrium with the corrosion products of the steel supercontainer in Olkiluoto groundwater conditions. Magnetite is the stable Fe phase at pH values higher than 8, and pyrite is also thermodynamically stable under the conditions expected in the repository. Siderite formation is, in principle, also possible, but requires high carbonate and low sulphide activities in the groundwater, such as in the case of the dilute/brackish type groundwater.

It should also be noted that there are other sources of iron in the system in addition to the steel supercontainer shell and other steel repository components. In particular, the smectite fraction in MX-80 bentonite typically contains about 2 wt% of structural iron, most of which is Fe(III) /Vogt and Köster 1978/. MX-80 also generally contains Fe(II) mineral impurities, such as pyrite and siderite /e.g. Müller-Vonmoos and Kahr 1983/, as well as traces of iron oxides /Baeyens and Bradbury 1997/. Because of the variability in MX-80 composition and possible oxidation of Fe^{2+} during processing of the raw material, however, the relative amounts of reactive iron phases may vary considerably.

Table D-2. Calculated bentonite porewater composition (bentonite waters) for different groundwater compositions. Concentrations in mmole l^{-1} unless otherwise indicated (after /Wersin et al. 2007/.

	Brackish/saline groundwater	Saline groundwater	Brine groundwater	Dilute/brackish groundwater
Solution composition				
Ionic strength (meq/l)	315	507	1,169	220
pH	7.82	7.66	8.03	7.39
Alkalinity	0.52	0.40	0.072	2.50
SO_4^{2-}	34.9	22.6	11.9	74.2
Cl(-I)	185	386	924	15.1
Na(I)	271	384	645	167
K(I)	0.85	1.24	2.3	0.53
Ca(II)	20.8	42.9	167	10.4
Mg(II)	6.32	10.9	24.9	1.1
Surface species				
NaX	1,990	1,980	1,890	1,990
CaX_2	249	247	324	248
MgX_2	69.3	63.8	49.8	70.3
KX	23.4	23.0	22.1	23.5
SOH	221	234	203	250
SO^-	68.2	54.4	86.1	35.4
SOH_2^+	2.14	3.12	1.3	5.68
Eh calculation				
Fe tot	2.3E–3	4.2E–3	4E–03	0.04
S^{2-}tot	5.3E–3	4.8E–3	1.3E–03	–
Eh (mV)	–171 Fe_3O_4/FeS	–160 Fe_3O_4/FeS	–280 Fe_3O_4/FeS	–202 Fe_3O_4/$FeCO_3$

D.4 Glacial meltwaters

Large uncertainties exist regarding the composition of glacial meltwater that may, in the future, penetrate at repository depth, in view of which two different glacial water compositions have been used to carry out the solubility limit calculations: a “glacial meltwater”, as defined by /Pitkänen et al. 2004/, which is used in the present safety assessment in assessment case PD-GMWV, and an “ice melting groundwater”, as defined by /Duro et al. 2006/, which is used in the present safety assessment in assessment cases PD-GMW, PD-GMWC, CC-GMW and RS-GMW, and was also used in SR-Can. The former is the estimated Quaternary glacial melt water composition expected from ice melting processes, and the latter corresponds to the composition of a dilute granitic groundwater from ice melting at Grimsel, Switzerland, sampled at the Grimsel Test Site, which is considered to provide an analogue for the dilute groundwater composition expected from ice melting processes. The chemical compositions of both groundwaters are given in Table D-3.

Table D-3. Two alternative glacial meltwater compositions, (i), ice melting water, as used in assessment case PD-GMW, PD-GMWC, CC-GMW and RS-GMW, and (ii), glacial meltwater, as used in assessment case PD-GMWV. All values in mmol/l unless otherwise stated.

	Ice melting groundwater (as used in assessment case PD-GMW and others)	Glacial meltwater (as used in assessment case PD-GMWV)
T (°C)	15	1
pH	9.6	5.8
Alkalinity (meq/l)	0.45	2.6×10^{-3}
SO_4^{2-}	6.1×10^{-2}	5.2×10^{-4}
Cl(-I)	0.16	0.020
Na(I)	0.69	6.5×10^{-3}
K(I)	5×10^{-3}	3.8×10^{-3}
Ca(II)	0.14	3.2×10^{-3}
Mg(II)	6.2×10^{-4}	4.1×10^{-3}
Sr(II)	2×10^{-3}	1×10^{-6}
SiO_2	0.25	1.7×10^{-4}
Mn(II)	5×10^{-6}	
Fe tot	3×10^{-6}	1.8×10^{-6}
F(-I)	0.36	
Eh (mV)	–200	920*
Eh (calculated)		–136* (magnetite/hematite)

* In case of glacial meltwater, as used in assessment case PD-GMWV, the Eh of 920 mV was calculated taking into account the oxygen present in the original infiltrating glacial meltwater (7.2 mg/l). If the oxygen consumption by iron compounds and the long-term equilibrium between magnetite/hematite ($pH_2 = 10^{-7}$atm) are taken into account, the calculated Eh is –136 mV.

References

Baeyens B, Bradbury M H, 1997. A mechanistic description of Ni and Zn sorption on Na-montmorillonite. Part I: Titration and sorption measurements. J. Contam. Hydrology 27, 199–222.

Bradbury M H, Baeyens B, 1997. A mechanistic description of Ni and Zn sorption on Na-montmorillonite. J. Contam. Hydrol. 27, 223–248.

Curti E, Wersin P, 2002. Assessment of porewater chemistry in the bentonite backfill for the Swiss SF/HLW repository. Nagra Technical Report NTB 02-09, Wettingen, Switzerland.

Duro L, Grivé M, Cera E, Gaona X, Domènech C, Bruno J, 2006. Determination and assessment of the concentration limits to be used in SR-Can. SKB TR-06-30, Svensk Kärnbränslehantering AB.

Müller-Vonmoos M, Kahr G, 1983. Mineralogische Untersuchungen von Wyoming Bentonit MX-80 und Montigel. Nagra Technical Report NTB 83-12, Wettingen, Switzerland.

Pastina B, Hellä P, 2006. Expected evolution of a spent fuel repository at Olkiluoto, Posiva Report 2006-05. Posiva Oy, Olkiluoto, Finland.

Pitkänen P, Partamies S, Luukkonen A, 2004. Hydrogeochemical interpretation of baseline groundwater conditions at the Olkiluoto site. Posiva Report 2003-07. Posiva Oy, Olkiluoto, Finland.

Pitkänen P, Ahokas H, Ylä-Mella M, Partamies S, Snellman M, Hellä P 2007. Quality Review of Hydrochemical Baseline Data from the Olkiluoto Site, Posiva Report 2007-05. Posiva Oy, Olkiluoto, Finland.

Vogt K, Köster H M, 1978. Zur Mineralogie, Kristallchemie und Geochemie einiger Montmorillonite aus Bentoniten. Clay Minerals, 13, 25–43.

Wersin P, Birgersson M, Olsson S, Karnland O, Snellman M, 2007. Impact of corrosion-derived iron on the bentonite buffer within the KBS-3H disposal concept. The Olkiluoto site as case study. Posiva Report 2007-11 and SKB R-08-34. Posiva Oy, Olkiluoto, Finland and Svensk Kärnbränslehantering AB, Sweden.

Appendix E

Evaluation of chemical speciation and solubility limits

This appendix summarises the results of the evaluations of chemical speciation and solubility limits carried out by /Grivé et al. 2007/. Key assumptions and related uncertainties are identified and recommended solubility limits are given for the elements of interest in various conditions as assumed in the radionuclide release and transport calculations. Near-field and geosphere speciation and solubility limits have been assessed for all the elements of interest in the present safety assessment, although only near-field solubilities are used in the evaluation of assessment cases (See Sections 5.2.3 and 5.2.4). Chemical speciation in the geosphere is, however, relevant to the evaluation of matrix diffusion and sorption on rock matrix pore surfaces.

E.1 General approach and overview of results

The conceptual model used by /Grivé et al. 2007/ for the assessment of chemical speciation and solubility limits in the near field is shown in Figure E-1. The same conceptual model was used in SR-Can /Duro et al. 2006/. Void spaces inside the canister are assumed to be filled with water of a specified composition. The solid phases considered in the assessment are those produced by the anoxic corrosion of the canister, its cast iron insert and the fuel itself. The hydrogen produced by the corrosion of the insert on the redox state of the system is also considered.

The first step was to assess which are the main solid phases that could precipitate in this system from a chemical thermodynamic point of view. Given the uncertainties described in the following sections, this assessment included the use of sensitivity analysis to study the influence of groundwater composition and redox conditions on the chemical speciation of the elements of interest. If more than one solid phase was identified, expert judgement was used to select the phase that is kinetically more likely to form.

Once the solubility-limiting phases had been identified, the solubility limits for elements of interest were evaluated for each of the various reference water compositions defined in Appendix D. An overview of evaluated solubility limits is give in Table E-1.

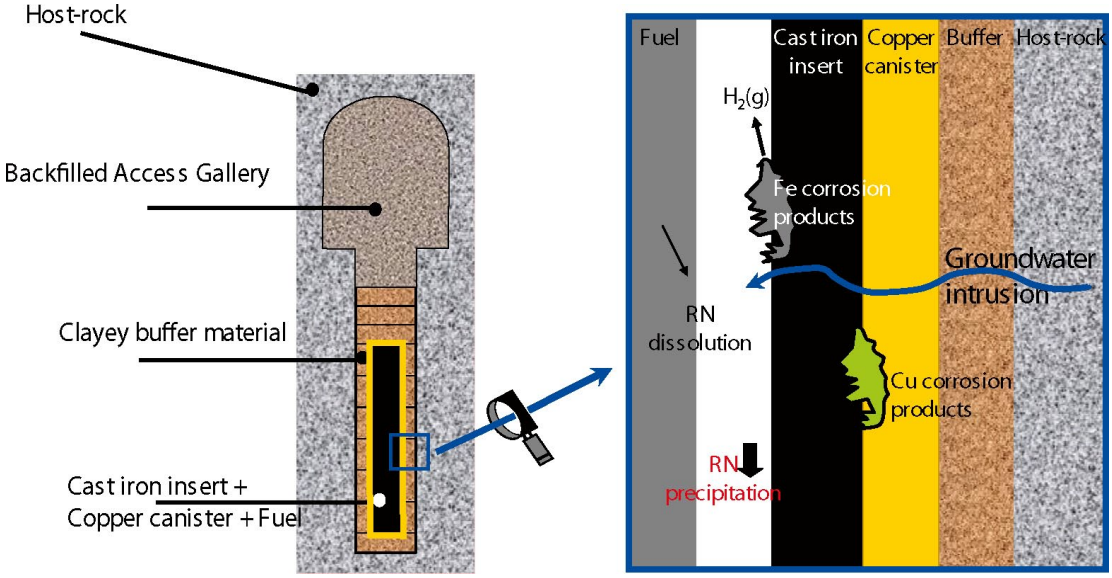

Figure E-1. *Illustration of the system under study. This figure shows the KBS-3V design, but the features of interest, which are those close to the fuel, are common to KBS-3H and KBS-3V /after Grivé et al. 2007/.*

Table E-1. Solubility limits for elements of interest for the different groundwaters and different redox conditions relevant to the Olkiluoto site and its evolution /after Grivé et al. 2007/. gw = groundwater.

		Solubility limit (mol × dm^{-3})								
		Olkiluoto groundwater				Bentonite waters			Glacial waters	
Element	Redox state	Brackish/ Saline	Saline	Dilute/ brackish	Brine	Brackish/ Saline	Saline	Dilute/ brackish	Glacial meltwater	Ice melting water
Am/Cm	Eh gw	1.7×10^{-7}	4.4×10^{-7}	3.2×10^{-9}	1.2×10^{-8}	4.5×10^{-7}	9.2×10^{-7}	4.0×10^{-7}	5.4×10^{-9}	5.6×10^{-8}
	$pH_2(g)=10^{-7}$ atm	1.7×10^{-7}	4.4×10^{-7}	3.2×10^{-9}	1.2×10^{-8}	4.5×10^{-7}	9.2×10^{-7}	4.0×10^{-7}	5.3×10^{-9}	
	$pH_2(g)= 10^{2}$ atm	1.7×10^{-7}	4.4×10^{-7}	3.2×10^{-9}	1.2×10^{-8}	4.5×10^{-7}	9.2×10^{-7}	4.0×10^{-7}		
Cs	Eh gw	n.s.l	n.s.l	n.s.l	n.s.l	n.s.l	n.s.l	n.s.l	n.s.l	n.s.l
	$pH_2(g)=10^{-7}$ atm	n.s.l	n.s.l	n.s.l	n.s.l	n.s.l	n.s.l	n.s.l	n.s.l	
	$pH_2(g)=10^{2}$ atm	n.s.l	n.s.l	n.s.l	n.s.l	n.s.l	n.s.l	n.s.l		
Mo	Eh gw	7.9×10^{-9}	8.5×10^{-8}	1.9×10^{-5}	1.3×10^{-8}	8.9×10^{-6}	4.1×10^{-6}	2.4×10^{-8}	n.s.l	1.5×10^{-4}
	$pH_2(g)=10^{-7}$ atm	2.8×10^{-9}	4.5×10^{-8}	3.7×10^{-9}	6.7×10^{-8}	2.0×10^{-8}	9.2×10^{-9}	2.6×10^{-9}	5.6×10^{-13}	
	$pH_2(g)= 10^{2}$ atm									
Nb	Eh gw	3.9×10^{-5}	1.2×10^{-4}	4.6×10^{-5}	2.0×10^{-4}	8.1×10^{-5}	6.2×10^{-5}	3.8×10^{-5}	1.5×10^{-5}	2.9×10^{-3}
	$pH_2(g)=10^{-7}$ atm	3.9×10^{-5}	1.2×10^{-4}	4.6×10^{-5}	2.0×10^{-4}	8.1×10^{-5}	6.2×10^{-5}	3.8×10^{-5}	1.5×10^{-5}	
	$pH_2(g)= 10^{2}$ atm	3.9×10^{-5}	1.2×10^{-4}	4.6×10^{-5}	2.0×10^{-4}	8.1×10^{-5}	6.2×10^{-5}	3.8×10^{-5}		
Ni	Eh gw	2.0×10^{-3}	1.4×10^{-4}	4.4×10^{-4}	4.4×10^{-5}	3.9×10^{-4}	7.4×10^{-4}	4.3×10^{-3}	n.s.l	4.1×10^{-7}
	$pH_2(g)=10^{-7}$ atm	2.0×10^{-3}	1.4×10^{-4}	4.4×10^{-4}	4.4×10^{-5}	3.9×10^{-4}	7.4×10^{-4}	4.3×10^{-3}	n.s.l	
	$pH_2(g)= 10^{2}$ atm	2.0×10^{-3}	1.4×10^{-4}	4.4×10^{-4}	4.4×10^{-5}	3.9×10^{-4}	7.4×10^{-4}	4.1×10^{-3}		
Np	Eh gw	8.0×10^{-10}	6.9×10^{-10}	1.2×10^{-9}	5.7×10^{-10}	7.8×10^{-10}	7.2×10^{-10}	1.1×10^{-9}	n.s.l	8.2×10^{-10}
	$pH_2(g)=10^{-7}$ atm	8.0×10^{-10}	6.9×10^{-10}	1.2×10^{-9}	5.7×10^{-10}	7.8×10^{-10}	7.2×10^{-10}	1.1×10^{-9}	1.3×10^{-9}	
	$pH_2(g)= 10^{2}$ atm	8.0×10^{-10}	6.9×10^{-10}	1.2×10^{-9}	5.7×10^{-10}	7.8×10^{-10}	7.2×10^{-10}	1.1×10^{-9}		
Pa	Eh gw	3.0×10^{-7}	2.8×10^{-7}	3.1×10^{-7}	2.4×10^{-7}	2.9×10^{-7}	2.8×10^{-7}	3.0×10^{-7}	3.3×10^{-7}	3.2×10^{-7}
	$pH_2(g)=10^{-7}$ atm	3.0×10^{-7}	2.8×10^{-7}	3.1×10^{-7}	2.4×10^{-7}	2.9×10^{-7}	2.8×10^{-7}	3.0×10^{-7}	3.3×10^{-7}	
	$pH_2(g)= 10^{2}$ atm	3.0×10^{-7}	2.8×10^{-7}	3.1×10^{-7}	2.3×10^{-7}	2.9×10^{-7}	2.8×10^{-7}	3.0×10^{-7}		
Pd	Eh gw	2.6×10^{-6}	2.5×10^{-6}	2.7×10^{-6}	2.4×10^{-6}	2.5×10^{-6}	2.8×10^{-6}	2.5×10^{-6}	2.7×10^{-6}	2.7×10^{-6}
	$pH_2(g)=10^{-7}$ atm	2.6×10^{-6}	2.5×10^{-6}	2.7×10^{-6}	2.4×10^{-6}	2.5×10^{-6}	2.8×10^{-6}	2.5×10^{-6}	2.7×10^{-6}	
	$pH_2(g)= 10^{2}$ atm	2.6×10^{-6}	2.5×10^{-6}	2.7×10^{-6}	2.4×10^{-6}	2.5×10^{-6}	2.8×10^{-6}	2.5×10^{-6}		
Pu	Eh gw	8.0×10^{-9}	1.3×10^{-9}	1.5×10^{-10}	2.3×10^{-10}	8.0×10^{-10}	1.0×10^{-9}	3.7×10^{-7}	1.6×10^{-5}	1.3×10^{-10}
	$pH_2(g)=10^{-7}$ atm	8.0×10^{-9}	1.8×10^{-9}	5.1×10^{-10}	2.7×10^{-10}	1.8×10^{-8}	2.9×10^{-8}	1.1×10^{-6}	8.3×10^{-9}	
	$pH_2(g)= 10^{2}$ atm	8.0×10^{-9}	9.5×10^{-9}	5.1×10^{-10}	2.0×10^{-10}	3.4×10^{-6}	5.4×10^{-6}	1.5×10^{-5}		

Element	Redox state	Solubility limit (mol × dm^{-3}) Olkiluoto groundwater				Bentonite waters			Glacial waters	
		Brackish/ Saline	Saline	Dilute/ brackish	Brine	Brackish/ Saline	Saline	Dilute/ brackish	Glacial meltwater	Ice melting water
Ra	Eh gw	3.2×10^{-6}	1.1×10^{-4}	1.1×10^{-7}	3.0×10^{-5}	3.5×10^{-8}	5.9×10^{-8}	2.2×10^{-8}	2.010^{-4}	8.8×10^{-7}
	$pH_2(g)=10^{-7}$ atm	3.2×10^{-6}	1.1×10^{-4}	1.1×10^{-7}	3.0×10^{-5}	3.5×10^{-8}	5.9×10^{-8}	2.2×10^{-8}	7.1×10^{-5}	
	$pH_2(g)= 10^{2}$ atm	3.3×10^{-6}	1.1×10^{-4}	1.1×10^{-7}	3.0×10^{-5}	3.6×10^{-8}	6.0×10^{-8}	2.2×10^{-8}		
Se	Eh gw	6.0×10^{-10}	8.8×10^{-10}	6.6×10^{-14}	6.3×10^{-9}	4.3×10^{-11}	3.0×10^{-11}	1.0×10^{-10}	n.s.l	4.5×10^{-11}
	$pH_2(g)=10^{-7}$ atm	1.0×10^{-9}	1.2×10^{-9}	2.1×10^{-10}	2.7×10^{-9}	1.2×10^{-9}	8.8×10^{-10}	3.1×10^{-10}	1.5×10^{-8}	
	$pH_2(g)= 10^{2}$ atm	1.4×10^{-5}	4.5×10^{-6}	3.8×10^{-7}	1.7×10^{-5}	6.4×10^{-6}	5.2×10^{-6}	1.2×10^{-6}		
Sn	Eh gw	9.6×10^{-8}	1.4×10^{-7}	1.1×10^{-7}	1.5×10^{-7}	1.2×10^{-7}	1.0×10^{-7}	9.6×10^{-8}	8.4×10^{-8}	2.7×10^{-6}
	$pH_2(g)=10^{-7}$ atm	9.6×10^{-8}	1.4×10^{-7}	1.1×10^{-7}	1.5×10^{-7}	1.2×10^{-7}	1.0×10^{-7}	9.6×10^{-8}	8.4×10^{-8}	
	$pH_2(g)= 10^{2}$ atm	1.2×10^{-7}	1.7×10^{-7}	1.4×10^{-7}	1.8×10^{-7}	1.5×10^{-7}	1.3×10^{-7}	1.2×10^{-7}		
Sm	Eh gw	9.3×10^{-9}	7.8×10^{-9}	9.2×10^{-10}	1.2×10^{-10}	2.1×10^{-8}	3.8×10^{-8}	7.5×10^{-8}	1.0×10^{-8}	1.8×10^{-9}
	$pH_2(g)=10^{-7}$ atm	9.3×10^{-9}	7.8×10^{-9}	9.2×10^{-10}	1.2×10^{-10}	2.1×10^{-8}	3.8×10^{-8}	7.5×10^{-8}	1.0×10^{-8}	
	$pH_2(g)= 10^{2}$ atm	9.3×10^{-9}	7.8×10^{-9}	9.2×10^{-10}	1.2×10^{-10}	2.1×10^{-8}	3.8×10^{-8}	7.2×10^{-8}		
Sr	Eh gw	5.9×10^{-3}	9.2×10^{-3}	3.1×10^{-4}	1.6×10^{-2}	1.9×10^{-4}	3.6×10^{-4}	9.1×10^{-5}	n.s.l	1.4×10^{-5}
	$pH_2(g)=10^{-7}$ atm	5.9×10^{-3}	9.2×10^{-3}	3.1×10^{-4}	1.6×10^{-2}	1.9×10^{-4}	3.6×10^{-4}	9.1×10^{-5}	n.s.l	
	$pH_2(g)=10^{2}$ atm	5.9×10^{-3}	9.2×10^{-3}	3.1×10^{-4}	1.6×10^{-2}	1.9×10^{-4}	3.7×10^{-4}	9.3×10^{-5}		
Tc	Eh gw	4.0×10^{-9}	4.0×10^{-9}	5.0×10^{-9}	4.1×10^{-9}	4.0×10^{-9}	4.0×10^{-9}	4.2×10^{-9}	n.s.l	4.5×10^{-9}
	$pH_2(g)=10^{-7}$ atm	4.0×10^{-9}	4.0×10^{-9}	4.2×10^{-9}	4.1×10^{-9}	4.0×10^{-9}	4.0×10^{-9}	4.2×10^{-9}	4.0×10^{-9}	
	$pH_2(g)= 10^{2}$ atm	4.0×10^{-9}	4.0×10^{-9}	4.2×10^{-9}	4.0×10^{-9}	4.0×10^{-9}	4.0×10^{-9}	4.2×10^{-9}		
Th	Eh gw	1.0×10^{-9}	2.0×10^{-10}	6.9×10^{-9}	7.5×10^{-11}	9.8×10^{-10}	6.8×10^{-10}	6.3×10^{-9}	6.4×10^{-10}	8.1×10^{-10}
	$pH_2(g)=10^{-7}$ atm	1.0×10^{-9}	2.0×10^{-10}	6.9×10^{-9}	7.5×10^{-11}	9.8×10^{-10}	6.8×10^{-10}	6.3×10^{-9}	6.4×10^{-10}	
	$pH_2(g)= 10^{2}$ atm	1.0×10^{-9}	2.0×10^{-10}	6.9×10^{-9}	7.5×10^{-11}	9.8×10^{-10}	6.8×10^{-10}	6.3×10^{-9}		
Zr	Eh gw	1.7×10^{-8}	1.6×10^{-8}	1.8×10^{-8}	1.4×10^{-8}	1.7×10^{-8}	1.6×10^{-8}	1.7×10^{-8}	1.8×10^{-8}	1.8×10^{-8}
	$pH_2(g)=10^{-7}$ atm	1.7×10^{-8}	1.6×10^{-8}	1.8×10^{-8}	1.4×10^{-8}	1.7×10^{-8}	1.6×10^{-8}	1.7×10^{-8}	1.8×10^{-8}	
	$pH_2(g)= 10^{2}$ atm	1.7×10^{-8}	1.6×10^{-8}	1.8×10^{-8}	1.4×10^{-8}	1.7×10^{-8}	1.6×10^{-8}	1.7×10^{-8}		
U	Eh gw	7.0×10^{-10}	6.1×10^{-10}	2.7×10^{-7}	5.2×10^{-10}	6.7×10^{-9}	2.5×10^{-9}	3.3×10^{-9}	1.3×10^{-7}	2.3×10^{-9}
	$pH_2(g)=10^{-7}$ atm	6.8×10^{-10}	6.1×10^{-10}	8.0×10^{-10}	5.2×10^{-10}	6.5×10^{-10}	6.2×10^{-10}	9.5×10^{-10}	1.6×10^{-9}	
	$pH_2(g)= 10^{2}$ atm	6.5×10^{-10}	6.1×10^{-10}	6.8×10^{-10}	5.1×10^{-10}	6.3×10^{-10}	6.1×10^{-10}	6.6×10^{-10}		

The computer modelling tool used for these studies was the geochemical computer program PHREEQC /Parkhurst and Appelo 2001/. The reason for selecting this code, rather than any of the others that are available, is that it is an open code developed by the USGS that has been extensively tested in many different types of applications. The PHREEQC code also has an advantage over some alternative codes in that it has the capability of calculating the solubility for all elements simultaneously, thus considering possible competition among complexes.

There are limitations in the thermodynamic database used by PHREEQC. For some elements, the database contains slightly out-dated information (e.g. on nickel) or no information (e.g. in the case of molybdenum). Updates to the thermodynamic database (TDB) published within the NEA-TBD project have been used in the current application, as described in /Grivé et al. 2007/, and concern Se, Ni, Zr, Mo and Th. Furthermore, given these limitations and other uncertainties described in Section E.2 and E.3, expert judgement was also used to supplement or modify calculated chemical speciation and solubility limits where these were considered to be unreliable.

The elicitation of expert judgement is described in Section E.4. The uncertainties judged to be most relevant for each element are identified in the following sections in Tables E-2 to E-6.

E.2 Key assumptions and related uncertainties

E.2.1 Key assumptions

Some key assumptions made in evaluating chemical speciation and solubility limits for use in radionuclide release and transport calculations are that:

- the chemical composition of the water in the canister interior is known, and no significant variations in the chemical composition of the water occur over time;
- redox conditions in the canister interior are known, and no significant variations in redox conditions occur over time;
- no significant variations in water temperature occur over the time frame of interest, which extends from the time of formation of transport pathways from the canister interior to the buffer up to a million years in the future;
- where more than one solid phase can form, the more amorphous phase is kinetically favoured and thus is considered the solubility-limiting phase; and
- solubility limits calculated for the canister interior are also applicable at the buffer/rock interface.

The validity of these assumptions and related uncertainties are discussed in the following sections.

E.2.2 Uncertainty and variability in water composition

/Grivé et al. 2007/ list the uncertainty of the composition of the water inside the canister as one of the most important in the evaluation of solubility limits, and especially uncertainties in the concentrations of iron and phosphate (redox conditions are also important for sole elements – the impact of hydrogen on Eh is discussed in Section E.1.3, below). The uncertainty in the iron concentration mainly affects elements that might be co-precipitated with iron sulphides, such as selenium. The uncertainty in phosphate concentration, which arises both from a lack of data and the fact that the phosphate concentrations in groundwater are in some cases below the detection limit, has a broader impact on the assumed solubility limiting phases and on the evaluated solubility limits. In some cases, a zero phosphate concentration has been assumed (note that phosphate does not appear in the solution compositions given in Table D-2).

The composition of the water inside the canister is strongly affected by that of the groundwater around repository, which will vary over time due, for example, to perturbing effects of repository construction, to land uplift and, in the longer term, to major climatic changes (especially glaciation). In general, variability and the associated uncertainties in groundwater composition have been handled in the safety assessment by deriving solubility limits for a range of different groundwaters and bentonite waters that may arise during the evolution of the repository and its environment. Each solubility limit is selected as realistically as possible for a given water composition.

E.2.3 Uncertainty associated with the redox state of the system

The redox state of the system inside the canister is affected by that of the groundwater or bentonite water that enters the canister (Appendix D), and by the hydrogen produced by the corrosion of the insert. The hydrogen pressure (pH_2) inside the canister is, however, subject to significant uncertainty. This source of uncertainty has been handled in the safety assessment by deriving solubility limits by using different assumptions of hydrogen partial pressure (see Section E.6).

E.2.4 Uncertainty associated with temperature evolution

Temperature affects the stability of aqueous phases and solid compounds, and the chosen activity corrections and solvers used in PHREEQC and other codes. In /Grivé et al. 2007/, a selection of reaction enthalpies is included, although in some cases no enthalpy data are available. The approach to correct the equilibrium constants for temperature effects follows the Van't Hoff equation, where a constant $\Delta_r H^0$ is considered. In all cases, the solubilities are calculated at 15°C. As discussed in /Pastina and Hellä 2006/ in the context of a KBS-3V repository at Olkiluoto, the decay heat of spent nuclear fuel raises the temperature of the repository and the surrounding bedrock by several tens of degrees for many centuries and by a few degrees for several thousand years. In the radionuclide release and transport calculations, transport pathways from the canister interior to the buffer are assumed to be formed no earlier than 1,000 years after repository closure. However, /Pastina and Hellä 2006/ note that five thousand years after disposal, the temperature of the canister has been calculated to be between 11 and 6ºC higher than the undisturbed ambient temperature at repository depth. These results are also expected to be broadly representative of a KBS-3H repository. Elevated temperatures at early times therefore introduce a source of uncertainty into speciation and solubility limit calculations.

E.2.5 Uncertainty associated with the effects of higher ionic strength water

The PHREEQC code can use two different equations to calculate the activity coefficients (γ_i) of species i in a solution of ionic strength I. By default, it applies the Davies equation:

$$\log(\gamma_i) = -0.5102\, z_i^2 \left(\frac{\sqrt{I}}{1+\sqrt{I}} - 0.3I \right) \qquad \text{(Eq. E-1)}$$

where z_i is the charge number of species i.

Alternatively, if the necessary parameter values (a_i and b_i) are known, it can also apply the Debye-Hückel equation:

$$\log(\gamma_i) = -z_i^2 \left(\frac{A\sqrt{I}}{1+Ba_i\sqrt{I}} \right) + b_i I \qquad \text{(Eq. E-2)}$$

where A and B are constants.

These equations are generally considered applicable at ionic strengths (I) lower than 0.1 eq/l, and may, in some cases, provide good approximations up to ionic strengths of 0.2 eq/l. They are, therefore, applicable to the dilute/brackish and brackish/saline reference groundwaters, dilute/brackish bentonite water, ice melting water and glacial meltwater, as defined in Appendix D. They are not, however, necessarily applicable at ionic strengths as high as those of the saline and brine groundwaters and the other bentonite waters defined in Appendix D, which introduces uncertainty into the solubility limits calculated for these waters. For these cases, according to the NEA guidelines, the Specific Ion Interaction Theory (SIT) is preferred. Unfortunately, none of the geochemical codes used can apply the SIT methodology to calculate the activity coefficient of a species as a function of the ionic strength.

Differences in ionic strengths as a function of the groundwater composition lead us to assess the extent of disagreement between different activity correction approaches. In general, we do not expect significant variations (within ± 0.3 log units for log solubility) in solubility calculations due to different activity corrections. The main differences are expected in the brine water, where the ionic strength is I=1.2 M. For these high ionic strength waters further effort is needed to address the activity correction properly.

E.2.6 Uncertainty associated with the precipitation of multiple solid phases

When more than one solid phase can precipitate, the less crystalline phase is assumed to be kinetically favoured and is consequently assumed to be the solubility limiting solid phase. This assumption is partly based on the Ostwald Step Rule. This rule postulates that the precipitate with the highest solubility, that is, the least stable solid phase, will form first. The nucleation of a more soluble phase is kinetically favoured over that of the less soluble phase. Small particles have a higher ratio surface area to particle mass than large particles and therefore will have high surface energy, thus dissolving preferentially. The higher solubility of small particles produces solutions that are supersaturated relative to large particles. No metallic form of native phases has been considered, except for Se(0). This assumption is made in the light of the very slow formation kinetics of this type of phases under the conditions of interest, but is nonetheless affected by significant uncertainties.

E.2.7 Applicability of the solubility limits at the buffer/rock interface

Although solubility limits are derived for the system (water and solid phases) inside the canister very close the fuel surfaces (Figure E-1), they are applied in the present safety assessment both inside the canister, and also at the buffer/rock interface. In reality, the water at the buffer/rock interface is likely to have an uncertain transitional composition between that of groundwater and bentonite water. As noted in Appendix D, the compositions of groundwater and bentonite water may be different, due to cation exchange and the dissolution of calcite and gypsum in the buffer. In addition, solid phases other than the ones produced by the corrosion of the canister and the fuel may form within the buffer, but have not been considered in calculating solubility limits. These include phases formed by co-precipitation or sorption of radionuclides on iron corrosion products or other solids in the buffer/rock interface and subsequent dissolution of these due to changing conditions.

Solubility limits have not be derived for the conditions that might actually prevail at the buffer/rock interface. Geosphere solubilities (applicable away from the interface) have been calculated, but their use in safety assessment at the buffer/rock interface would potentially be non-conservative in cases where geosphere solubilities are lower than near-field solubilities. As discussed in Section 5.2.3, applying a lower, geosphere solubility at the interface implies that any precipitates formed at the interface because geosphere solubilities are exceeded would be immobile. Applying a higher, near-field solubility at the interface, on the other hand, is equivalent to assuming conservatively that any such precipitates are mobilised as colloids, but redissolve a short distance into the geosphere as a result of dilution.

E.3 Other assumptions and modelling simplifications

(i) Precipitation of pure solid phases

The precipitation of pure solid phases of the elements has been assumed in all cases. The possible formation of mixed solid phases has not been included, although /Grivé et al. 2007/ discuss it for those elements likely to be incorporated in other major solids, such as selenium.

(ii) Sulphate to sulphide reduction

The possibility of microbiologically mediated reduction of sulphate involving either hydrogen or methane has not been taken into account, although the potential effect of this process has been discussed in /Grivé et al. 2007/. This simplification will mainly affect those elements whose solubility is considered to be limited by sulphate or sulphide solids, such as Sr, Ra, Se or Sn.

(iii) Co-precipitation or sorption on iron oxides

The potential co-precipitation of radionuclides with the iron corrosion products formed either inside the canister or at the buffer-rock interface due to the supercontainer corrosion products present has not been taken into account in the calculations. This is because of the lack of quantitative understanding of the co-precipitation process, including the effect of changing groundwater composition.

E.4 Use of expert judgement

The main experts from whom judgement was elicited included the authors of /Grivé et al. 2007/ from ENVIROS (Spain), who were also involved in the solubility calculations for SR-Can /SKB 2006a/. Margit Snellman (Saanio and Riekkola Oy) and Lawrence Johnson (NAGRA) also provided expert judgment on the selection of relevant processes, groundwater compositions, oxidation states and chemical forms of the species of interest and recommended solubility limits to be applied in the different assessment cases. Expert judgement was based in all cases on information from laboratory experiments and natural systems, and experience from other relevant safety assessments, e.g., SR-Can, TILA-99 and the Swiss Project Opalinus Clay /Nagra 2002ab/.

Expert judgement was specifically used in determining the solubility limiting solids, chemical speciation and solubility limits of the following elements:

Carbon	Molybdenum
Niobium	Selenium
Americium	Thorium
Curium	Uranium
Samarium	Nickel
Tin	Palladium

(iv) Carbon speciation

The proportion of organic to inorganic C-14 released by the corrosion of activated metals has been found to be high /Johnson and Schwyn 2004/. Identified organic compounds are e.g., short chain carboxylic acids, alcohols and aldehydes. The fate of these organic molecules is unclear: they can either be transported without chemical change, undergo oxidation to CO_2 or reduction to methane by microbial activity. The same authors have pointed out that, in addition to the formation of organic acids, direct formation of methane from metal carbides is also possible.

The timing and the substrate in which these oxidation/reduction reactions occur are not known. Microbial reactions are not likely to occur in the buffer because of the high swelling pressure, but might occur at the buffer-rock interface, in the geosphere and, most likely, in the biosphere. In case of oxidation to CO_2, the precipitation of calcite ($CaCO_3$) is a likely process resulting in the retardation of C-14, but this has conservatively been neglected in the transport calculations in the present safety assessment.

In view of these uncertainties, it is conservatively assumed in the majority of assessment cases that all carbon is present as neutral species, such as methane or organic acids (hence the K_d is set to zero). The alternative assumption that C-14 is present in geosphere in anionic form (carbonate) is, however, considered in assessment cases PD-BCC, PD-VVERV and PD-EPRC (Section 5.10).

(v) Niobium speciation and solubility

There is a general lack of thermodynamic data in the literature on niobium, which gives rise to major uncertainties in its chemical speciation and solubility limit. In the calculations performed by Grivé et al. the solubility-limiting solid is assumed to be $Nb_2O_5(s)$. Nb speciation and solubility are strongly dependent on the pH of the water, which is also subject to variability and uncertainty (Appendix D). The main aqueous species in equilibrium with this solid assuming glacial melt-water composition (pH 5.8) is the neutral penta-hydroxide $Nb(OH)_5$. For the Olkiluoto ground-water and bentonite water compositions (pH 7.4 to 8.2), the proportion of NbO_3^- increases with pH from 64% to 90% and up to 100% for the ice melting water (pH 9.6). The highest solubility limit is also found to arise for the high pH ice melting water composition. The limited available data for sorption of niobium on bentonite /Ochs and Talerico 2004/, indicates that niobium is either neutral or cationic in the buffer.

Due to the limitations and uncertainties noted above, Nb is treated as neutral in the majority of assessment cases. The recognised possibility of anionic speciation of Nb in the near field and far field is, however, considered is considered in the variant case PD-BCN (Section 5.10).

The niobium solubility limit used in the present safety assessment in case PD-BC and the majority of other cases has been revised downwards by almost two orders downwards from the TILA-99 conservative value for non-saline reducing conditions (Table 11-2 in TILA-99, /Vieno and Nordman 1999/. This is largely because the solubility of niobium is much greater at the high pH (pH 10) that was considered to represent the upper end of the range for this groundwater in TILA-99 /Vuorinen et al. 1998/. In the present study, the bentonite water corresponding to dilute brackish groundwater in has a pH of 7.8. The limited thermodynamic data for niobium, however, remains a major source of uncertainty in the solubility limit for this element.

(vi) Americium and curium

In the present safety assessment, the solubility limit for curium has been based on the chemical analogy with americium. In most TDBs and other data compilations, americium and curium are considered equivalent and data for the two elements may be used interchangeably /Grivé et al. 2007/.

The main species expected in the case of the reference groundwaters are free Am^{3+} and Cm^{3+}, and mainly cationic sulphate and carbonate complexes. The anionic carbonate complex dominates only in case of the high pH ice melting water. It is, however, likely that the pH in the geosphere during a future influx of glacial meltwater will be closer to that of glacial meltwater (pH 5.8), which is buffered by interaction with fracture minerals. Thus the speciation of americium and curium in the geosphere in assessment case PD-GMW and other assessment cases dealing with glacial meltwater is assumed to be dominated by the free cations Am^{3+} and Cm^{3+}.

The solubility limit for curium used in the present safety assessment has been revised upwards by one order of magnitude compared with the TILA-99 conservative value for non-saline reducing conditions (Table 11-2 in /Vieno and Nordman 1999/). This is largely because the solubility of curium is much greater at the high pH (pH 10) that was considered to represent the upper end of the range for this groundwater in TILA-99 /Vuorinen et al. 1998/. As noted above, in the present study, the bentonite water corresponding to dilute brackish groundwater in has a pH of 7.8. Other

factors contributing to the upward revision may include the different thermodynamic data, solubility limiting solid ($CmOHCO_3$ in TILA-99), and the omission of carbonate complexes (species in solution) for curium in the case of TILA-99.

(vii) Samarium

As in the case of americium and curium, the main samarium species in the groundwater is free Sm^{3+}, and mainly cationic sulphate and carbonate complexes. Anionic carbonate complexes dominate in the high pH ice melting water. The anionic carbonate complex dominates only in case of the high pH ice melting water. It is, however, likely that the pH in the geosphere during a future influx of glacial meltwater will be closer to that of glacial meltwater (pH 5.8), which is buffered by interaction with fracture minerals. Thus the speciation of samarium in the geosphere in assessment case PD-GMW and other assessment cases dealing with glacial meltwater is assumed to be dominated by the free cation Sm^{3+}.

The solubility limit for samarium used in the present safety assessment has been revised downwards by more than two orders of magnitude compared with the TILA-99 conservative solubility values for non-saline reducing conditions (Table 11-2 in /Vieno and Nordman 1999/). This may be due to the different thermodynamic data, and solubility limiting solid ($Sm_2(CO_3)_3$ in TILA-99). Additional relevant factors are the more realistic approach taken here, as well as the different groundwater conditions. In the fresh reducing groundwater conditions in TILA-99, phosphate complexes are formed at high pH (pH 10), increasing the solubility of samarium /Vuorinen et al. 1998/.

(viii) Tin

In the case of tin, aqueous speciation is dominated by the hydrolysis complexes of Sn(IV), namely $Sn(OH)_4$, with some contribution of the anionic species $Sn(OH)_5^-$ in some of the groundwaters. The proportion of this anionic species increases with pH, and, in the high pH ice melting water, is the dominating species formed. It is, however, likely that the pH in the geosphere during a future influx of glacial meltwater will be closer to that of glacial meltwater (pH 5.8), which is buffered by interaction with fracture minerals. Thus the speciation of tin in the geosphere in assessment case PD-GMW and other assessment cases dealing with glacial meltwater is assumed to be dominated by neutral $Sn(OH)_4$.

(ix) Selenium

According to /Grivé et al. 2007/, the presence of Fe(II) in aqueous solution may cause the precipitation of $FeSe_x(s)$ solid phases. This means that the solubility limit of selenium is very much dependent on the assumed Fe(II) concentration, in cases where the precipitation of $FeSe_x(s)$ is assumed to occur. Another possibility would be the formation of native Se, which would imply the oxidation of Se(-II) released from the fuel to Se(0). It has recently been shown that both Se(0) and $FeSe_2(s)$ form in $FeSe_x(s)$ dissolution experiments /Iida et al. 2007/. The concentrations of aqueous Se measured in the experiments were, nevertheless, much higher than those expected on the assumption that they are driven by the Se(0) solubility control. Due to the reducing environment of interest in the present safety assessment, ferrous selenide solids have been selected as the solubility limiting phases, although the formation of Se(0) cannot be completely ruled out, and this gives rise to an important uncertainty in the selected solubility control. Additional uncertainties arise from the possibility of co-precipitation effects and the definition of redox states of the system.

The solubility of selenium used in the present safety assessment has been revised downwards by four orders of magnitude compared with the TILA-99 conservative solubility values for non-saline reducing conditions (Table 11-2 in /Vieno and Nordman 1999/). In addition to the more realistic approach taken in the present safety assessment, the change in the solubility limit also reflects the changes in the thermodynamic data, as well as the different groundwater conditions, including redox. Selenium solubility depends very strongly on redox conditions (Eh). The Eh in TILA-99 groundwaters ranged from about –250 to –410 mV (vs. SHE), where the lowest value

gives the highest solubility. The effect of lower Eh is also seen in the solubility calculations for the present safety assessment. Again, the solubility of selenium is highest for the lowest Eh, which, in the present assessment, is around –500 mV (vs. SHE), corresponding to a pH_2 of 100 atm. (see Section E.2.3).

(x) Molybdenum, Thorium, Uranium and Nickel

Molybdenum has not been included in the speciation and solubility calculations in either TILA-99 or in SR-Can. For the present safety assessment, new thermodynamic data were selected and added to the database by /Grivé et al. 2007/.

The solubility limits of both uranium and thorium used in the present safety assessment have been revised downwards by about two orders of magnitude compared with the TILA-99 values (3×10^{-7} M and 5×10^{-7} M, respectively). This makes thorium, in particular, significantly less soluble than in other recent safety assessments, including SR-Can, where the range is 1×10^{-7} to 4×10^{-5} M, and the Swiss Project Opalinus Clay /Nagra 2002ab/, which used a value of 7×10^{-7} M. The change to the thorium solubility limit reflects the work by /Grivé et al. 2007/ in updating the solubility database for the present safety assessment. A more consistent and coherent selection of thorium data was made compared with that of /Duro et al. 2006/, which was used in SR-Can. Furthermore, recently published data for aqueous hydroxides and solids has been taken into account, including data for thorium aqueous hydroxides from /Altmaier et al. 2005/, in which previous values from /Neck and Kim 2001/ have been checked and slightly revised.

In the case of thorium, chemical speciation is still uncertain and there is limited data for the anionic hydroxy-carbonate thorium complexes formed, which dominate in the waters of interest in this safety assessment. The assumption of anionic speciation would contradict the well-known sorption properties of thorium on various materials, both clays and the minerals found on fracture surfaces in crystalline rock. Thus, thorium is treated as a non-anionic species in the present safety assessment. Thorium is also treated as neutral species in SR-Can and in TILA-99.

In the case of uranium, the calculated solubility limit is much closer to other recent safety assessments, such as Project Opalinus Clay /Nagra 2002ab/. As in the case of thorium, there remain uncertainties associated with the speciation of uranium which may affect the results, e.g. the possible formation of hydroxides and the stabilisation of $UO_2(CO_3)_3^{4-}$ in the negative redox regime, especially at higher pH. Uranium solubility is also very sensitive to redox conditions, which also might be reflected in the different results for the groundwaters in TILA-99 and in the present safety assessment.

The significantly higher solubility limit assigned to nickel requires some comment, as it is some 40 times higher than the TILA-99 conservative value, and higher even than the "very conservative value" (1×10^{-3} M). A consequence of the new database applied for nickel is that the solubility limiting solid phase under relevant conditions is found to be not the carbonate but the hydroxide. In addition, changes to the stability product for the species $NiCO_3(aq)$, which was the dominant nickel species in SR-97 /SKB 1999/, mean that, in Olkiluoto groundwaters, the main aqueous nickel species is not $NiCO_3(aq)$, but Ni^{2+}. As a result, the main solubility limiting reaction becomes:

$$Ni(OH)_{2(s)} + 2\ H^+ = Ni^{2+} + 2\ H_2O, \qquad \text{(Eq. E-3)}$$

which has log K_{sp} of 11.03. In the pH range of 7 to 8, this implies a nickel solubility of 10^{-3} to 10^{-4} M, justifying a higher solubility limit used in the present assessment. Future effort is, however, needed to better establish the solubility of nickel under near-field conditions.

(xi) Palladium

The solubility limit for palladium has been revised upwards by a factor of 250 compared with the TILA-99 value of 1×10^{-8} M. This upward revision is largely due to the different solubility limiting solid – amorphous $Pd(OH)_2$ – as compared with the oxide PdO, which was assumed in TILA-99.

E.5 Solubility limits for bentonite water equilibrated with dilute/brackish groundwater

The solubility limits used in the present safety assessment in the Base Case for an initial penetrating defect (PD-BC) and the majority of other assessment cases are given in the main text in Table 5-6 and in Table E-2 (values in bold). Table E-2 also shows the solubility limiting solid, oxidation states and main complexes formed, as described further in Section E.8, and the main uncertainties in the evaluated speciation and solubility limits.

These are evaluated for bentonite water equilibrated with dilute/brackish groundwater under the assumption of redox conditions determined by the long-term dynamic equilibrium between magnetite and hematite formed in a system in which, for example, the iron of the insert corrodes to magnetite in a first step and to hematite in a second step. pH_2 is assumed to be limited by the hematite/magnetite stability boundary, and takes a value of 10^{-7} atm. This system has an Eh of –230 mV (vs. SHE) for a bentonite water pH of 7.4.

This redox state generally gives the highest solubilities for the different redox conditions considered by /Grivé et al. 2007/, and is therefore likely to be conservative for most elements. In fact, with the exceptions of U, Mo, Se and Pu, the solubility-limiting solids and calculated solubility limits the elements considered in the safety assessment are fairly insensitive to redox conditions over the range considered (Table E-1). Tc solubility is known to be redox sensitive, but has been calculated as remaining constant and very low until the Eh vs. SHE is greater than zero.

As noted in Section E.2, both water composition and redox state are subject to variability and uncertainty, and alternative assumptions regarding both are considered in the safety assessment (see Sections E.6 and E.7).

E.6 Solubility limits for alternative redox conditions

Table E-2 shows alternative solubility limits (values not shown in bold) for the redox-sensitive elements Se, Mo, U and Pu, which are also used in assessment case PD-NFSLV. In this case, it has been assumed that the corrosion products of the KBS-3H supercontainer steel shell determines the Eh of the system. In particular, an equilibrium in buffer porewater between magnetite and siderite in a system of corroding iron, gives an Eh of –202 mV vs. SHE for the dilute/brackish water system with a bentonite water pH of 7.4. Pu solubility is about one order of magnitude lower in these alternative redox conditions as compared to the Base Case conditions. For Se there is a slight decrease in solubility in the alternative redox conditions. Mo and U solubility increases, and uranium carbonate complexes dominates in the alternative redox conditions. Sn solubility shows some minor sensitivity to redox conditions (not shown in Table E-2), but, for convenience, the same value (1.2×10^{-7} M) has been used for Sn in the case PD-NFSLV as in the Base Case (PD-BC).

/Grivé et al. 2007/ also calculated solubility limits under the assumption that hydrogen pressure inside the canister is determined by the gas breakthrough pressure of the buffer. As discussed in the Evolution Report /Smith et al. 2007/, gas breakthrough within bentonite has been observed to occur at a pressure approximately equal to the sum of the bentonite swelling pressure (7–8 MPa at full saturation) and the hydrostatic pressure (4 MPa at a depth of 400 m), i.e. at approximately 11–12 MPa (in the order of 100 atm.) at full saturation[30], in which case, according to /Grivé et al. 2007/, the redox potential inside the canister ranges from Eh= –497 to –544 mV for the groundwater pH range 7.4 to 8.2 (Table D-1).

[30] As also discussed in the Evolution Report, some recent experiments have, however, shown that the breakthrough pressure of gas through bentonite can be substantially higher than this (above 20 MPa for bentonite with a swelling pressure of ~ 6MPa).

Table E-2. Solubility limiting solids, solubility limits, oxidation states and main complexes formed, and associated uncertainties in the case of bentonite water equilibrated with dilute/brackish groundwater. Values used in the Base Case for an initial penetrating defect (PD-BC) and the majority of other assessment cases in the present safety assessment are shown in bold. Alternative values for the redox-sensitive elements Se, Mo, U and Pu used in assessment case PD-NFSLV are also shown.

Element/Solubility limiting solid	Solubility (mol/L)	Oxidation state/ main complexes formed	Associated uncertainty
C	n.s.l.	C(IV)/CO_3^{2-}, HCO_3^-	Carbonate reduction to methane
Cl	n.s.l.	Cl (-I)/Cl^-	
Ni/$Ni(OH)_2$	4.3×10^{-3}	Ni(II)/Ni^{2+}, $NiSO_4$ (43%), $Ni(SO_4)_2^{2-}$ (11%)	SO_4^{2-} to HS^- reduction
Se/$FeSe_2$	**3.1×10^{-10}** (pH_2 10^{-7})	Se(-II)/HSe^- (100%)	Effect of iron in water Formation of native Se°. Possibility of co-precipitation with sulphides
$FeSe_2$	1.0×10^{-10}	HSe^- (100%)	
Sr/Celestite $SrSO_4$	**9.1×10^{-5}** (pH_2 10^{-7})	Sr(II)/Sr^{2+}(55%), $SrSO_4$ (44%)	Possibility of co-precipitation with other elements' carbonates SO_4^{2-} to HS^- reduction
Mo/MoO_2	**2.6×10^{-9}** (pH_2 10^{-7})	Mo(VI)/MoO_4^{2-} (100%)	Scarcity of thermodynamic data
	2.4×10^{-8}	MoO_4^{2-} (100%)	
Zr/$Zr(OH)_4$ (aged)	1.7×10^{-8}	Zr(IV)/$Zr(OH)_4$ (100%)	Crystallinity of the solid phase
Nb/Nb_2O_5	3.8×10^{-5}	Nb(V)/NbO_3^-(63%), $Nb(OH)_5$ (37%)	Scarcity of thermodynamic data
Tc/$TcO_2 \times 1{,}6H_2O$	4.2×10^{-9}	Tc(IV)/$TcO(OH)_2$ (99.9%)	Formation of metallic Tc°
Pd/$Pd(OH)_2$	2.5×10^{-6}	Pd(II)/$Pd(OH)_2$ (100%)	Formation of metallic Pd°
Sn/SnO_2 (am)	1.2×10^{-7}	Sn(IV)/$Sn(OH)_4$(82%), $Sn(OH)_5^-$ (18%)	SO_4^{2-} to HS^- reduction
I	n.s.l.	I(-I)	
Cs	n.s.l.	Cs(I)	
Sm/$SmOHCO_3$	7.5×10^{-8}	Sm(III)/$SmSO_4^+$ (39%), $Sm(SO_4)_2^-$ (28%), $Sm(CO_3)_2^-$ (14%), Sm^{3+} (10%), $SmCO_3^+$ (9%)	Effects of phosphates in water; stability of the solid hydroxo-carbonate
Ra/$RaSO_4$	2.2×10^{-8}	Ra(II)/$RaSO_4$(71%), Ra^{2+}(29%)	Possibility of co-precipitation with other elements' carbonates SO_4^{2-} to HS^- reduction
Th/$ThO_2 \times 2H_2O$	6.3×10^{-9}	Th(IV)/$ThCO_3(OH)_3^-$ (65%), $Th(CO3)_2(OH)_2^{2-}$ (30%)	Stability of the solid phase Uncertain thermodynamic data for aqueous carbonates
Pa/Pa_2O_5	3.0×10^{-7}	Pa(V)/PaO_2OH (100%)	Lack of thermodynamic data
U/$UO_2 \times 2H_2O$	**9.5×10^{-10}** (pH_2 10^{-7})	U(IV), U(VI)/$U(OH)_4$ (69%), $UO_2(CO_3)_3^{4-}$ (30%)	Silicate solid precipitation Thermodynamic data on solid stability
	3.3×10^{-9}	$UO_2(CO_3)_3^{4-}$ (78%), $U(OH)_4$ (19%),	
Pu/$Pu(OH)_4$(am)	**1.1×10^{-6}** (pH_2 10^{-7}) 3.7×10^{-7}	Pu(III)/$Pu(SO_4)_2^-$(45%), $PuSO_4^+$ (42%) $Pu(SO_4)_2^-$(45%), $PuSO_4^+$ (42%)	Effect of phosphates in water; stability of the solid hydroxo-carbonate; SO_4^{2-} to HS^- reduction
Np/ $NpO_2 \times 2H_2O$(am)	1.1×10^{-9}	Np(IV)/$Np(OH)_4$ (66%), $NpCO_3(OH)_3^-$ (32%)	Crystallinity of the solid phase
Am/ $Am(CO_3)_2Na \times 5H_2O$	4.0×10^{-7}	Am(III)/$AmSO_4^+$ (33%), $Am(CO_3)_2^-$ (23%), $AmCO_3^+$ (21%), Am^{3+} (13%)	Effect of phosphates in water; Stability of the solid hydroxo-carbonate
Cm	4.0×10^{-7}	Cm(III)	Assumed analogy with Am

Results are shown in the summary table (Table E-1). It was found that:

- Se shows a higher solubility at the high pH_2 at about 10^2 atm. for the different solubility limiting solid $Fe_{1.04}Se$;
- U shows a lower solubility for the pH_2 10^2 atm. and 10^{-7} atm. cases, which is due to the more reducing conditions, and change in proportion of main complexes formed;
- Pu shows a highest solubility for the pH_2 10^2 case for the bentonite waters and for the oxygen-rich glacial meltwater case where Pu(V) dominates. As compared to the Base case where $Pu(OH)_4$ is the solubility limiting solid $PuCO_3OH$ and $PuO_2(OH)_2$ are the solubility limiting solids in the bentonite water at high pH_2 and the oxygen-rich glacial meltwater, respectively.

The solubility limits calculated under these redox conditions have not, however, been considered further in this safety assessment.

E.7 Solubility limits for alternative groundwater compositions

E.7.1 Brackish-saline and saline groundwater types

Solubility limits for bentonite water equilibrated with the brackish/saline and saline groundwater are shown in Tables E-3 and E-4. These values are used to evaluate assessment cases PD-SAL, and PD-HISAL, respectively.

As in the majority of assessment cases, the redox state is determined by a long-term dynamic equilibrium between magnetite and hematite formed in the system around the corroding iron insert, with a pH_2 of 10^{-7} atm. The PD-SAL system has an Eh of –171 mV (vs. SHE) for a buffer porewater pH of 7.82, and the PD-HISAL system has an Eh of –160 mV (vs. SHE) for a buffer porewater pH of 7.66.

E.7.2 Glacial meltwater intrusion

Two variant compositions of glacial meltwater have been considered in the safety assessment as a way to address the uncertainty in the composition of glacial meltwater potentially intruding at repository depth.

The pH in buffer water is likely to be buffered by bentonite present and thus the expected pH is in the region of slightly alkaline conditions, and closer to the ice melting water variant – (i), below. This is, therefore, the main variant used in the safety assessment in assessment cases PD-GMW and other glacial meltwater cases, but excluding PD-GMWV, which is based on the glacial meltwater composition – variant (ii), below.

(i) Ice melting water (as used in assessment case PD-GMW and other glacial meltwater cases)

Water resulting from the infiltration of glacial meltwater (ice melting water) to depth is expected to be rather diluted. As discussed in Appendix D, the glacial meltwater used in SR-Can /Duro et al. 2006/ and in the present assessment in assessment cases PD-GMW and other glacial meltwater cases (excluding PD-GMWV, see below) is based on a Grimsel groundwater composition, i.e. discharging groundwater from the Migration Shear Zone at the Grimsel Test Site (GTS) in Switzerland, which is subject to interaction with granitic minerals. The pH of the water is 9.6 and its Eh is –200 mV. Solubility limits in this glacial meltwater are presented in Table E-5.

Table E-3. Solubility limits in the case of bentonite porewater equilibrated with brackish/ saline groundwater. Data from this table are used in Table 5-30 (assessment case PD-SAL).

Element/Solubility limiting solid	Solubility (mol/L)	Oxidation state/main complexes formed	Associated uncertainty
C	n.s.l.	C(IV)/CO_3^{2-}, HCO_3^-	Carbonate reduction to methane
Cl	n.s.l.	Cl (-I)/Cl^-	
Ni/$Ni(OH)_2$	3.9×10^{-4}	Ni(II)/Ni^{2+} (70%), $NiSO_4$ (22%)	SO_4^{2-} to HS^- reduction
Se/$FeSe_2$	1.2×10^{-9}	Se(-II)/HSe^- (100%)	Effect of iron in water Formation of native Se°. Possibility of co-precipitation with sulphides
Sr/$SrSO_4$	1.9×10^{-4}	Sr(II)/Sr^{2+}(99.7%), $SrSO_4$ (21%)	Possibility of co-precipitation with other elements' carbonates SO_4^{2-} to HS^- reduction
Mo/MoO_2	2.0×10^{-8}	Mo(VI)/MoO_4^{2-} (100%)	Scarcity of TDB
Zr/ $Zr(OH)_4$(am)	1.7×10^{-8}	Zr(IV)/$Zr(OH)_4$ (100%)	Crystallinity of the solid phase
Nb/Nb_2O_5 (cr)	8.1×10^{-5}	Nb(V)/NbO_3^-(83%), $Nb(OH)_5$ (17%)	Scarcity of TDB
Tc/$TcO_2 \times 1{,}6H_2O$	4.0×10^{-9}	Tc(IV)/$TcO(OH)_2$ (99.4%)	Formation of metallic Tc°
Pd/$Pd(OH)_2$	2.5×10^{-6}	Pd(II)/$Pd(OH)_2$ (99.4%)	Formation of metallic Pd°
Sn/SnO_2 (am)	1.2×10^{-7}	Sn(IV)/$Sn(OH)_4$(62%), $Sn(OH)_5^-$ (38%)	SO_4^{2-} to HS^- reduction
I	n.s.l.	I(-I)	
Cs	n.s.l.	Cs(I)/Cs^+ (93%), CsCl (7%)	
Sm/$SmOHCO_3$	2.1×10^{-8}	Sm(III)/$SmSO_4^+$(35%), $Sm(CO_3)_2^-$ (10%), Sm^{3+} (29%), $SmCO_3^+$ (13%), $Sm(SO_4)_2^-$(9%)	Effects of phosphates in water; stability of the solid hydroxo-carbonate
Ra/$RaSO_4$	3.5×10^{-8}	Ra(II)/Ra^{2+}(55%), $RaSO_4$ (43%)	Possibility of co-precipitation with other elements' carbonates SO_4^{2-} to HS^- reduction
Th/$ThO_2 \times 2H_2O$	9.8×10^{-10}	Th(IV)/$ThCO_3(OH)_3^-$ (84%), $Th(CO_3)_2(OH)_2^{2-}$ (8%) $Th(OH)_4$ (5%)	Stability of the solid phase Uncertain thermodynamic data for aqueous carbonates
Pa/Pa_2O_5	2.9×10^{-7}	Pa(V)/PaO_2OH (100%)	Lack of thermodynamic data
U/$UO_2 \times 2H_2O$	6.5×10^{-10}	U(IV)/$U(OH)_4$ (99.4%)	Silicate solid precipitation TDB data on solid stability
Pu/$Pu(OH)_4$(am)	1.8×10^{-8}	Pu(III)/$PuSO_4^+$ (48%), $Pu(SO_4)_2^-$ (18%), Pu^{3+}(16%), $PuOH^{2+}$ (9%),$PuCO_3^+$(5%),	Stability of the solid hydroxo-carbonate, SO_4^{2-} to HS^- reduction
Np/ NpO_22H_2O	7.8×10^{-10}	Np(IV)/$Np(OH)_4$ (90%), $NpCO_3(OH)_3^-$ (9%)	Crystallinity of the solid phase
Am/ $Am(CO_3)_2Na \times 5H_2O$	4.5×10^{-7}	Am(III)/$AmSO_4^+$ (23%), $Am(CO_3)_2^-$ (13%), $AmCO_3^+$ (22%), Am^{3+} (29%), $AmOH^{2+}$ (9%)	Reliability of phosphate measurements
Cm	4.5×10^{-7}	Cm(III)	Assumed analogy with Am.

Table E-4. Solubility limits in the case of bentonite porewater equilibrated with saline groundwater. Data from this table are used in Table 5-30 (assessment case PD-HISAL).

Element/Solubility limiting solid	Solubility (mol/L)	Oxidation state/ main complexes formed	Associated uncertainty
C	n.s.l.	C(IV)/CO_3^{2-}, HCO_3^-	Carbonate reduction to methane
Cl	n.s.l.	Cl (-I)/Cl^-	
Ni/$Ni(OH)_2$	7.4×10^{-4}	Ni(II)/Ni^{2+} (79%), $NiSO_4$ (11%), $NiCl^+$ (10%)	SO_4^{2-} to HS^- reduction
Se/$FeSe_2$	8.8×10^{-10}	Se(-II)/HSe^- (100%)	Effect of iron in water Formation of native Se°. Possibility of co-precipitation with sulphides
Sr/$SrSO_4$	3.6×10^{-4}	Sr(II)/Sr^{2+}(89%), $SrSO_4$ (11%)	Possibility of co-precipitation with other elements' carbonates SO_4^{2-} to HS^- reduction
Mo/MoO_2	9.2×10^{-9}	Mo(VI)/MoO_4^{2-} (100%)	Scarcity of TDB
Zr/ $Zr(OH)_4$(am)	1.6×10^{-8}	Zr(IV)/$Zr(OH)_4$ (100%)	Crystallinity of the solid phase
Nb/Nb_2O_5	6.2×10^{-5}	Nb(V)/NbO_3^-(80%), $Nb(OH)_5$ (20%)	Scarcity of TDB
Tc/$TcO_2 \times 1{,}6H_2O$	4.0×10^{-9}	Tc(IV)/$TcO(OH)_2$ (100%)	Formation of metallic Tc°
Pd/$Pd(OH)_2$	2.8×10^{-6}	Pd(II)/$Pd(OH)_2$ (87%),$PdCl_4^{2-}$ (13%)	Formation of metallic Pd°
Sn/SnO_2 (am)	1.0×10^{-7}	Sn(IV)/$Sn(OH)_4$(69%), $Sn(OH)_5^-$ (31%)	SO_4^{2-} to HS^- reduction
I	n.s.l.	I(-I)	
Cs	n.s.l.	Cs(I)/Cs^+ (88%), CsCl (12%)	
Sm/$SmOHCO_3$	3.8×10^{-8}	Sm(III)/$SmSO_4^+$(28%), Sm^{3+} (48%), $SmCO_3^+$ (10%),	Effects of phosphates in water; stability of the solid hydroxo-carbonate
Ra/$RaSO_4$	5.9×10^{-8}	Ra(II)/Ra^{2+}(69%), $RaSO_4$ (25%), $RaCl^+$ (6%)	Possibility of co–precipitation with other elements' carbonates SO_4^{2-} to HS^- reduction
Th/$ThO_2 \times 2H_2O$	6.8×10^{-10}	Th(IV)/$ThCO_3(OH)_3^-$ (84%), $Th(CO_3)_2(OH)_2^{2-}$ (8%) $Th(OH)_4$ (5%)	Stability of the solid phase Uncertain thermodynamic data for aqueous carbonates
Pa/Pa_2O_5	2.8×10^{-7}	Pa(V)/PaO_2OH (100%)	Lack of thermodynamic data
U/$UO_2 \times 2H_2O$	6.2×10^{-10}	U(IV), $U(OH)_4$ (97%)	Silicate solid precipitation TDB data on solid stability
Pu/$Pu(OH)_4$(s)	2.9×10^{-8}	Pu(III)/$PuSO_4^+$ (44%), $Pu(SO_4)_2^-$ (7%), Pu^{3+}(30%), $PuOH^{2+}$ (12%),$PuCO_3^+$(5%)	Effects of phosphates in water; stability of the solid hydroxy-carbonate; SO_4^{2-} to HS^- reduction
Np/ $NpO_2 2H_2O$	7.2×10^{-10}	Np(IV)/$Np(OH)_4$ (92%), $NpCO_3(OH)_3^-$ (6%)	Crystallinity of the solid phase
Am/ $Am(CO_3)_2Na \times 5H_2O$	9.2×10^{-7}	Am(III)/$AmSO_4^+$ (17%), $AmCO_3^+$ (17%), Am^{3+} (57%)?, $AmOH^{2+}$ (9%)	Reliability of phosphate measurements
Cm	9.2×10^{-7}	Cm(III)	Assumed analogy with Am.

Table E-5. Solubility limits in the case of ice melting groundwater. Data from this table are used in Table 5-30 (assessment case PD-GMW).

Element/Solubility limiting solid	Solubility (mol/L)	Oxidation state/ main complexes formed	Associated uncertainty
C	n.s.l.	C(IV)/CO_3^{2-}, HCO_3^-	Carbonate reduction to methane
Cl	n.s.l.	Cl (-I)/Cl^-	
Ni/$Ni(OH)_2$	4.1×10^{-7}	Ni(II)/Ni^{2+} (7%), $Ni(OH)_2$ (93%)	SO_4^{2-} to HS^- reduction
Se/$FeSe_2$	4.5×10^{-11}	Se(-II)/HSe^- (100%)	Effect of iron in water Formation of native Seº. Possibility of co-precipitation with sulphides
Sr/$SrCO_3$	1.1×10^{-5}	Sr(II)/Sr^{2+}(97%)	Possibility of co-precipitation with other elements' carbonates SO_4^{2-} to HS^- reduction
Mo/$CaMoO_4$	1.5×10^{-4}	Mo(VI)/MoO_4^{2-} (100%)	Scarcity of TDB
Zr/ $Zr(OH)_4$(aged)	1.8×10^{-8}	Zr(IV)/$Zr(OH)_4$ (100%)	Crystallinity of the solid phase
Nb/Nb_2O_5	2.9×10^{-3}	Nb(V)/NbO_3^-(100%),	Scarcity of TDB
Tc/$TcO_2 \times 1{,}6H_2O$	4.5×10^{-9}	Tc(IV)/$TcO(OH)_2$ (89.7%), TcO_4^- (7%), $TcO(OH)_3^-$ (5%)	Formation of metallic Tcº
Pd/$Pd(OH)_2$	2.7×10^{-6}	Pd(II)/$Pd(OH)_2$ (100%)	Formation of metallic Pdº
Sn/SnO_2(am)	2.7×10^{-6}	Sn(IV))/$Sn(OH)_6^{2-}$(15%), $Sn(OH)_5^-$ (82%)	SO_4^{2-} to HS^- reduction
I	n.s.l.	I(-I)	
Cs	n.s.l.	Cs(I)/Cs^+ (100%),	
Sm/$SmPO_4$	1.8×10^{-9}	Sm(III)/$Sm(CO_3)_2^-$ (100%)	Effects of phosphates in water; stability of the solid hydroxo-carbonate
Ra/$RaSO_4$	8.8×10^{-7}	Ra(II)/Ra^{2+}(97%),	Possibility of co-precipitation with other elements' carbonates SO_4^{2-} to HS^- reduction
Th/$ThO_2 \times 2H_2O$	8.1×10^{-10}	Th(IV)/$ThCO_3(OH)_3^-$ (88%), $Th(OH)_4$(7%)	Stability of the solid phase Uncertain thermodynamic data for aqueous carbonates
Pa/Pa_2O_5	3.2×10^{-7}	Pa(V)/PaO_2OH (100%)	Lack of thermodynamic data
U/Uranophane $Ca(UO_2)_2(SiO_3OH)_2 \times 5H_2O$	2.3×10^{-9}	U(VI)/$UO_2(CO_3)_3^{4-}$(97%)	Silicate solid precipitation TDB data on solid stability
Pu/$Pu(OH)_4$(am)	1.3×10^{-10}	Pu(IV)/$Pu(OH)_4$(100%),	Effect of phosphates in water;
Np/ $NpO_2 \times 2H_2O$(am)	8.2×10^{-10}	Np(IV)/$Np(OH)_4$ (93%), $NpCO3(OH)_3^-$ (7%)	Crystallinity of the solid phase
Am/Am(OH)3	5.6×10^{-8}	Am(III)/$Am(CO_3)^{2-}$ (54%), $AmOSi(OH)_3^{2+}$ (46%),	Effect of phosphates in water;
Cm	5.6×10^{-8}	Cm(III)	Assumed analogy with Am

(ii) Glacial meltwater (as used in assessment case PD-GMWV)

Pyrite/pyrrhotite are very common in fractures in the Olkiluoto bedrock. If pyrite dissolution due to oxygen present in glacial meltwater is taken into account, this results in a lower pH water than is the case with pure calcite equilibrium. These conditions are considered in assessment case PD-GMWV by using the estimated glacial meltwater composition by /Pitkänen et al. 2004/ (Appendix D). No oxygen is expected to be transported down to the repository level, and the Eh has been evaluated assuming a long-term, dynamic equilibrium between the magnetite and hematite formed in the system of corroding iron insert, the boundary of which is at about $pH_2=10^{-7}$ atm., which at a pH of 5.8, results in an Eh of –136 mV. Solubilities for this variant of the glacial meltwater are presented in Table E-6.

Table E-6. Solubility limits in the case of glacial meltwater. Data from this table are used in Table 5-30 (assessment case PD-GMWV).

Element/Solubility limiting solid	Solubility (mol/L)	Oxidation state/ main complexes formed	Associated uncertainty
C	n.s.l.	C(IV)/CO_3^{2-}, HCO_3^-	Carbonate reduction to methane
Cl	n.s.l.	Cl (-I)/Cl^-	
Ni/$Ni(OH)_2$	n.s.l.	Ni(II)/Ni^{2+} (100%)	SO_4^{2-} to HS^- reduction
Se/$FeSe_2$	1.5×10^{-8}	Se(-II)/HSe^- (99%)	Formation of native Se°. Possibility of co-precipitation with sulphides
Sr/$SrCO_3$	n.s.l.	Sr(II)/Sr^{2+}(100%)	Possibility of co-precipitation with other elements' carbonates SO_4^{2-} to HS^- reduction
Mo/MoO_2	5.6×10^{-13}	Mo(VI)/MoO_4^{2-} (99%)	Scarcity of TDB
Zr/ $Zr(OH)_4$(aged)	1.8×10^{-8}	Zr(IV)/$Zr(OH)_4$ (100%)	Crystallinity of the solid phase
Nb/Nb_2O_5	1.5×10^{-5}	Nb(V)/$Nb(OH)_5$(97%),	Scarcity of TDB
Tc/$TcO_2 \times 1{,}6H_2O$	4.0×10^{-9}	Tc(IV)/$TcO(OH)_2$ (100%)	Formation of metallic Tc°
Pd/$Pd(OH)_2$	2.7×10^{-6}	Pd(II)/$Pd(OH)_2$ (100%)	Formation of metallic Pd°
Sn/SnO_2(am)	8.4×10^{-8}	Sn(IV))/$Sn(OH)_4$ (99%)	SO_4^{2-} to HS^- reduction
I	n.s.l.	I(-I)	
Cs	n.s.l.	Cs(I)/Cs^+ (100%),	
Sm/$SmPO_4$	1.0×10^{-8}	Sm(III)/Sm^{3+} (100%)	
Ra/$RaSO_4$	7.1×10^{-5}	Ra(II)/Ra^{2+}(100%),	Possibility of co-precipitation with other elements' carbonates SO_4^{2-} to HS^- reduction
Th/$ThO_2 \times 2H_2O$	6.4×10^{-10}	Th(IV)/$Th(OH)_3^+$ (72%), $Th(OH)_2^{2+}$ (18%), $Th(OH)_4$(9%)	Stability of the solid phase Uncertain thermodynamic data for aqueous carbonates
Pa/Pa_2O_5	3.3×10^{-7}	Pa(V)/PaO_2OH (100%)	Lack of thermodynamic data
U/UO_2 $2H_2O$	1.6×10^{-9}	U(IV), U(VI)/$U(OH)_4$ (42%), UO_2^{2+} (40%), $U(OH)_3^+$ (20%)	Silicate solid precipitation TDB data on solid stability
Pu/$Pu(PO_4)$	8.3×10^{-9}	Pu(III)/Pu^{3+}(97%),	Effect of phosphates in water;
Np/ $NpO_2 \times 2H_2O$(am)	1.3×10^{-9}	Np(IV)/$Np(OH)_4$ (58%), $Np(OH)_3^+$ (42%)	Crystallinity of the solid phase
Am/ $AmPO_4xH_2O$ (am)	5.3×10^{-9}	Am(III)/Am^{3+} (99%)	Effect of phosphates in water; Reliability of phosphate measurements
Cm	5.3×10^{-9}	Cm(III)	Assumed analogy with Am

E.8 Chemical speciation and oxidation states

Whether chemical species are modelled as, on the one hand, anionic, or, on the other hand, neutral or cationic, affects the modelling of diffusive transport in the buffer and matrix diffusion in the host rock, as described in Section 5.3.2 and 5.3.3. Table E-7 summarises the chemical forms assumed in the various assessment cases of the present safety assessment.

The evaluations of /Grivé et al. 2007/ show that the elements Cs, Sr, Ra, Zr, Ni, Pd and Pa form neutral or cationic complexes (defined as more than 50% of the speciation as neutral or cationic complexes) in all waters, as do Sn, Tc, Sm, U, Np and Am in all but a few cases. For Pu about 50% anionic and 50% cationic complexes are formed in bentonite water equilibrated with dilute/ brackish groundwater (see Table E-2).

Table E-7. Summary of the chemical forms assumed in the various assessment cases of the present safety assessment. A = anionic; others are neutral or cationic

Assessment case		Element																				
		Am	C	Cl	Cm	Cs	I	Mo	Ni	Nb	Np	Pa	Pd	Pu	Ra	Th	Se	Sm	Sn	Sr	Tc	U	Zr
PD-BC and others (excluding those below)	Near field			A			A	A									A						
	Geosphere			A			A	A									A						
PD-BCC, PD-VVERC and PD-EPRC	Near field			A			A	A									A						
	Geosphere		A	A			A	A									A						
PD-BCN	Near field			A			A	A		A							A						
	Geosphere			A			A	A		A							A						
PD-SAL, PD-HISAL	Near field			A			A	A									A						
	Geosphere			A			A	A									A						
CC-LOGEORS	Near field	Not applicable – direct release of radionuclides to geosphere (but U solubility as in case PD-SAL)																					
	Geosphere			A			A	A									A						
PD-GMW, PD-GMWC, CC-GMW, RS-GMW	Near field	A			A													A	A				
	Geosphere			A			A	A			A			A			A				A	A	
CC-GMW, CC-LOGEORG	Near field	Not applicable – direct release of radionuclides to geosphere (but U solubility as in case PD-GMW)																					
	Geosphere			A			A	A			A			A			A				A	A	
PD-GMWV	Near field			A			A	A									A						
	Geosphere			A			A	A			A			A			A				A	A	

The evaluations also show I, Cl, Se and Mo as forming mainly anionic complexes in most waters. In addition, Nb and Th are shown to be anionic in all waters except for glacial meltwater (as used in assessment case PD-GMWV). However, as discussed in Section E.4, the speciation of Nb and Th is associated with large uncertainties, due to limited data. Both elements are also known to sorb on bentonite. Thus, Th and Nb are treated in the safety assessment as non-anionic species in all waters.

Carbon is shown as being present as carbonate in all waters, but, as discussed earlier in Section E.4, carbon is treated as a neutral complex (methane) in the majority of assessment cases. Oxidation of carbon to carbon dioxide and subsequent dissolution as carbonate in the geosphere is treated in variant cases PD-BCC, PD-VVERC and PD-EPRC.

In the case of ice melting groundwater (as used, e.g., assessment case PD-GMW), Sn, Am, Cm, and Sm are shown to be anionic in the near field, which is due largely to the high pH (pH 9.6) of the water, such that speciation is dominated by anionic hydroxides or hydrocycarbonate complexes formed. The glacial meltwater (as used in assessment case PD-GMWV) is a water with lower pH (pH 5.8), which is closer to the expected pH (close to neutral pH) range for infiltrating glacial water being buffered by interaction with fracture minerals. Thus, geosphere speciation in all assessment cases addressing glacial meltwater (PD-GMW, PD-GMWV and other glacial meltwater cases) is assumed to be the same as near-field speciation assessment case PD-GMWV. This means that Sn, Am, Cm and Sm are cations in the geosphere for all glacial meltwater cases. This is also in line with the interpretation of speciation of these elements in TILA-99 /Vuorinen et al. 1998/. In addition, in the present safety assessment, for the purpose of comparison with TILA-99, oxidising condtions and anionic speciation of Tc, U, Np and Pu have been assumed in the geosphere in cases dealing with glacial meltwater.

The speciation calculations indicate that some elements, notably U, Pu and Np, may be present in the buffer in more than one oxidation state. Speciation also changes depending on the oxidation state, which can vary according to groundwater composition. For example, U(VI) is dominant in carbonate-rich waters, even under reducing conditions, due to the stability of the carbonate complexes formed, whereas, in low-carbonate groundwaters, the U(IV) will become dominant under similar redox conditions.

Np(IV) dominates in the case of Np and is the assumed oxidation state in the safety assessment. In the case of Pu, Pu(III) dominates in all waters except for ice melting water, which has a higher pH, where Pu(IV) dominates. However, according to Table A-12 of the SR-Can Data Report /SKB 2006b/, Pu(IV), with a lower limit K_d of 4, is less sorbing than Pu(III), which has a K_d of 10. For reasons of conservatism, and to be consistent with SR-Can, the oxidation state Pu(IV) is the assumed oxidation state evaluating geosphere transport parameters.

References

Altmaier M, Neck V, Müller R, Fanghänel Th, 2005. Solubility of $ThO_2 \cdot xH_2O$ in carbonate solution and the formation of ternary Th(IV) hydroxide-carbonate complexes. Radiochim. Acta, 93, 83–92.

Duro L, Grivé M, Cera E, Gaona X, Domènech C, Bruno J, 2006. Determination and assessment of the concentration limits to be used in SR-Can. SKB TR-06-30, Svensk Kärnbränslehantering AB.

Grivé M, Montoya V, Duro L, 2007. Determination and assessment of the concentration limits for radionuclides for Posiva. Posiva working report 2007-103. Posiva Oy, Olkiluoto, Finland.

Iida Y, Yamaguchi T, Tanaka T, Kitamura A, Nakayama S, 2007. Determination of the solubility limiting solid of Se in the presence of Fe under anoxic conditions. In Book of Abstracts of Mobile Fision and Activation Products in Nuclear Waste Disposal International Workshop. La Baule (France) January 16–19 2007.

Johnson L H, Schwyn B (eds.), 2004. Proceedings of a workshop on the release and transport of C-14 in repository environments. NAGRA report Interner Bericht 04-03. Nagra, Wettingen, Switzerland.

Nagra, 2002a. Project Opalinus Clay: Safety Report. Demonstration of disposal feasibility for spent fuel, vitrified high-level waste and long-lived intermediate-level waste (Entsorgungsnachweis). Nagra Technical Report NTB 02-05. Nagra, Wettingen, Switzerland.

Nagra, 2002b. Project Opalinus Clay: Models, codes and data for safety assessment. Demonstration of disposal feasibility for spent fuel, vitrified high-level waste and long-lived intermediate-level waste (Entsorgungsnachweis). Nagra Technical Report NTB 02-06. Nagra, Wettingen, Switzerland.

Neck V, Kim J I, 2001. Solubility and hydrolysis of tetravalent actinides. Radiochim. Acta, 89, 1–16.

Ochs M, Talerico C, 2004. SR-Can. Data and uncertainty assessment. Migration parameters for the bentonite buffer in the KBS-3H concept. SKB TR-04-18, Svensk Kärnbränslehantering AB.

Parkhurst D L, Appelo C A J, 2001. User's guide to PHREEQC (Version 2.4.6). A computer program for speciation, batch reaction, one dimensional transport and inverse geochemical calculations. U.S. Department of the Interior. U.S. Geological Survey, Water-Resources Investigations, Washington, DC, USA.

Pastina B, Hellä P, 2006. Expected evolution of a spent fuel repository at Olkiluoto, Posiva Report 2006-05. Posiva Oy, Olkiluoto, Finland.

Pitkänen P, Partamies S, Luukkonen A, 2004. Hydrogeochemical interpretation of baseline groundwater conditions at the Olkiluoto site. Posiva Report 2003-07. Posiva Oy, Olkiluoto, Finland.

Smith P A, Johnson L H, Snellman M, Pastina B, Gribi P, 2007. Safety assessment for a KBS-3H spent nuclear fuel repository at Olkiluoto – Evolution report. Posiva Report 2007-08 and SKB R-08-37. Posiva Oy, Olkiluoto, Finland and Svensk Kärnbränslehantering AB, Sweden.

SKB, 1999. Deep repository for spent nuclear fuel, SR 97 – Post closure safety. SKB TR-99-06, Svensk Kärnbränslehantering AB.

SKB 2006a. Long-term safety for KBS-3 repositories at Forsmark and Laxemar – a first evaluation. Main Report of the SR-Can project. SKB TR-06-09, Svensk Kärnbränslehantering AB.

SKB, 2006b. Data report for the safety assessment SR-Can. SKB TR-06-25, Svensk Kärnbränslehantering AB.

Vieno T, Nordman H, 1999. Safety assessment of spent fuel disposal in Hästholmen, Kivetty, Olkiluoto and Romuvaara TILA-99. Posiva Report 99-07. Posiva Oy, Helsinki, Finland.

Vuorinen U, Kulmala S, Hakanen M, Ahonen L, Carlsson T, 1998. Solubility database for TILA-99. Posiva Report 98-14. Posiva Oy, Helsinki, Finland.

Appendix F

Biosphere modelling and the evaluation of dose

There has been significant progress in Posiva's biosphere assessment /Ikonen 2006/ since the publication of TILA-99 /Vieno and Nordman 1999/. Much planning has gone into developing a biosphere assessment that is genuinely site-specific. In the following, the biosphere analysis applied to the relevant cases of the KBS-3H radionuclide transport analysis is outlined. Full discussion on the biosphere analysis will be published separately /Broed et al. 2007/, and in the subsequent sections of this report the preliminary key results are summarised.

Posiva's biosphere assessment is based on the description of present-day conditions of the existing site /Haapanen et al. 2007/, on the terrain and ecosystems development model of the future site /Ikonen et al. 2007/, and on radionuclide transport simulations with a system of connected ecosystem-specific biosphere object modules, or a landscape model, based on those (Figure F-1). The biosphere objects are generic but also applicable to the site, i.e. they can use either site-specific parameter values or data from appropriate reference areas and literature. The use of parameter values, biosphere objects and the landscape model in the biosphere analysis is described in detail in /Broed et al. 2007/ and references therein.

Due to post-glacial land uplift, the sea is expected to retreat to a significant distance from the site during the time frame of the biosphere analysis (Figure F-2). The landscape model consists of a number of biosphere objects, each emerging and changing geometrical properties with time /Broed et al. 2007/. Along with the land uplift, new terrestrial and limnic objects are formed from the basins of the sea, inheriting the radionuclide inventory of the corresponding compartments of the former sea objects. As calculated within the terrain and ecosystems

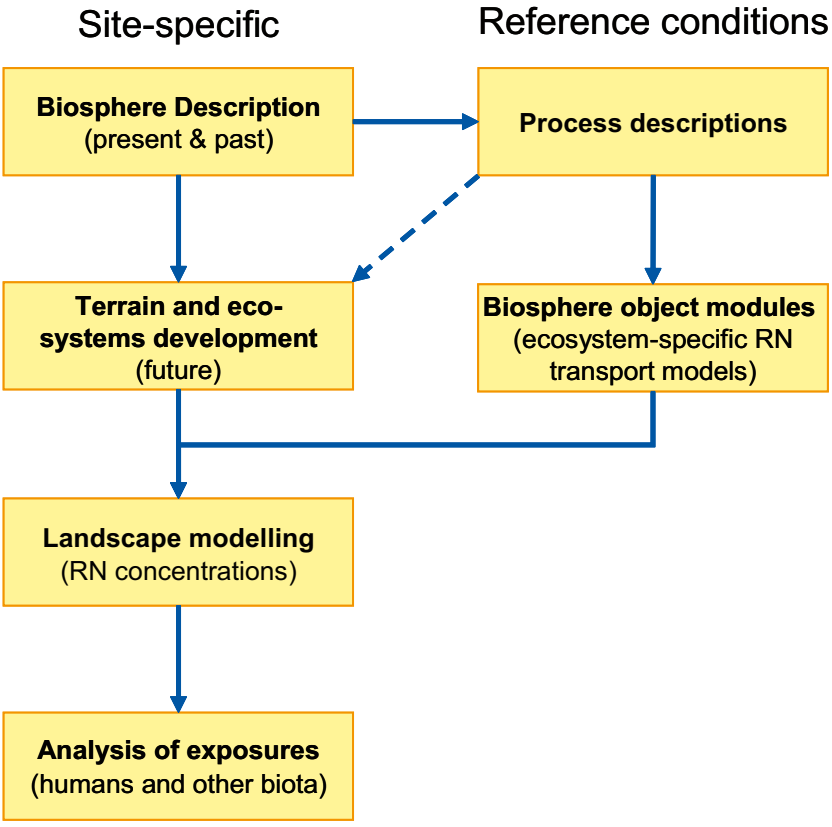

Figure F-1. *Modelling stages in Posiva's biosphere analysis.*

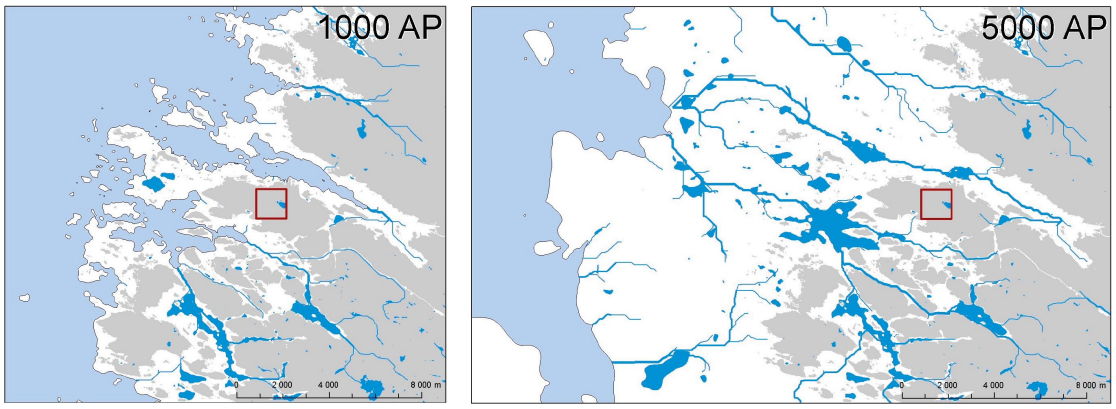

Figure F-2. *Change of landscape at Olkiluoto site from about 1,000 to 5,000 years after present due to the land uplift /Ikonen et al. 2007/. Present land areas are shown in grey and the repository area is indicated by the red rectangles. The scale of the maps is such that their vertical extent on the page corresponds to a distance of 17 km.*

development model /Ikonen et al. 2007/, an enlarging wetland area, inheriting the respective activity inventory, will develop on the borders of each lake object as it decreases in volume due to macrophyte colonisation and sedimentation processes dependent on the object properties. Terrain and ecosystem forecasts are used to estimate the object-specific parameter values for time steps of 500 years, in between which the values are interpolated in the landscape model. In the base case of the biosphere analysis, no significant anthropogenic climate change is assumed. Rather, the future climate assumed to undergo a repetition of the last glacial cycle (from the Eemian interglacial to the end of the Weichselian glaciation (see the description of the Weichselian-R scenario in the Evolution Reports for KBS-3H /Smith et al. 2007/ and KBS-3V /Pastina and Hellä 2006/. In addition, an evaluation of an alternative climate scenario of moderate anthropogenic CO_2 emissions is discussed in /Broed et al. 2007/. Base on Finnish regulatory guidance, vegetation types and other ecosystem conditions are assumed to be similar to those of the present day.

Since little information is available on the release locations to the biosphere, a nominal discharge pattern is used in the base case, supported by variants based on earlier discharge areas used in the TILA-99 assessment /Vieno and Nordman 1999/ and on other more recent indications and assumptions of potential release locations. These include observed fracturing at the potential bedrock lineaments /Kuivamäki 2005/, and hydraulic bedrock features /Ahokas et al. 2007/, boreholes and shafts intersecting or close to the repository volume. Based on earlier case studies, radionuclide inputs to lake and coast objects are directed by default only to the water body, but discharges through sediments are analysed in variant cases /Broed et al. 2007/.

In the evaluation of dose to humans, the intake of food by an adult was set to correspond to the standard nutritional demand of 110 kg carbon per year. Use of over-estimated occupancy factors (usually a minor contributor to the dose) and concentration ratios representative over a wide enough selection of possible sources of food avoids speculation about details of future food habits and exploitation of the landscape /Avila and Bergström 2006, Broed et al. 2007/. Caloric intake was used to weight different food items proportionally to their nutritional value, as is commonly done in ecosystem studies. Nutritional demand was assumed to stay rather constant even in the relatively far future. Another important assumption is that humans will exploit the contaminated landscape maximally, i.e. eating all potentially edible food produced within the biosphere objects; the number of persons living on the production from an area is constrained by the annual productivity of edible products and the size of the area. The production of naturally occurring food items is constrained by the primary production of the object and can be assessed separately on a generic basis. The same approach was also used in the recent SR-Can assessment /SKB 2006, and references therein/.

Exposures and potential effects to the other biota will be assessed on the basis of the maximum concentration in a medium and an ecosystem among all the cases in the biosphere analysis. The ERICA approach and threshold values /Beresford et al. 2007/ will then be applied and results reported in /Broed et al. 2007/. However, the concentrations are expected to be insignificantly low relative to those that would be of significance in inducing deleterious effects in other biota.

To compare the dose implications of the different cases to previous assessments and other safety cases irrespective of the details of the biosphere at the time of the release, a stylised safety indicator based on a drinking water well (WELL-2007) is used in this report. The indicator is similar to the WELL-97 used in the TILA-99 assessment /Vieno and Nordman 1999/, but incorporates updated ingestion dose coefficients. In the biosphere analysis report /Broed et al. 2007/, a second safety indicator is also used: an agricultural well (AgriWELL-2007) representing the annual dose arising from the use of contaminated well water for drinking and irrigation at an average farm of the region and from the subsequent consumption of agricultural products produced. There the results obtained by using these two safety indicators are compared with each other and to the more realistic doses calculated as described above.

References

Ahokas H, Vaittinen T, Tammisto E, Nummela J, 2007. Modelling of hydro-zones for the layout planning and numerical flow model in 2006. Working Report 2007-01. Posiva Oy, Olkiluoto, Finland.

Avila R, Bergström U, 2006. Methodology for calculation of doses to man and implementation in PANDORA. Posiva Working Report 2006-56 and SKB R-06-68. Posiva Oy, Olkiluoto, Finland and Svensk Kärnbränslehantering AB, Sweden.

Beresford N, Brown J, Copplestone D, Garnier-Laplace J, Howard B, Larsson C-M, Oughton D, Pröhl G, Zinger I (eds.) 2007. D-ERICA: An integrated approach to the assessment and management of environmental risks from ionising radiation. Description of purpose, methodology and application. Report from European Commission project ERICA, contract number FI6R-CT-2004-508847.

Broed R, Avila R, Bergström U, Hjerpe T, Ikonen A T K, 2007. Biosphere analysis for selected cases in TILA-99 and in KBS-3H safety evaluation, 2007. Posiva Working Report 2007-109. Posiva Oy, Olkiluoto, Finland.

Haapanen R, Aro L, Ilvesniemi H, Kareinen T, Kirkkala T, Lahdenperä A-M, Mykrä S, Turkki H, Ikonen A T K, 2007. Olkiluoto biosphere description 2006. Posiva Report 2007-02. Posiva Oy, Olkiluoto, Finland.

Ikonen A T K, 2006. Posiva Biosphere Assessment: Revised structure and status 2006. Posiva Report 2006-07. Posiva Oy, Olkiluoto, Finland.

Ikonen A T K, Hjerpe T, Aro L, Leppänen V, 2007. Terrain and ecosystems development model of Olkiluoto site, version 2006. Posiva Working report 2007-110. Posiva Oy, Olkiluoto, Finland.

Kuivamäki A, 2005. Revision of the lineament interpretations of the Olkiluoto area in the light of acoustic-seismic data from the adjacent marine areas. Posiva Working Report 2005-16. Posiva Oy, Olkiluoto, Finland.

Pastina B, Hellä P, 2006. Expected evolution of a spent nuclear fuel repository at Olkilutoto. Posiva Report 2006-05. Posiva Oy, Olkiluoto, Finland.

SKB, 2006. Long-term safety for KBS-3 repositories at Forsmark and Laxemar – a first evaluation. Main Report of the SR-Can project. SKB TR-06-09, Svensk Kärnbränslehantering AB.

Smith P A, Johnson L H, Snellman M, Pastina B, Gribi P, 2007. Safety assessment for a KBS-3H spent nuclear fuel repository at Olkiluoto – Evolution report. Posiva Report 2007-08 and SKB R-08-37. Posiva Oy, Olkiluoto, Finland and Svensk Kärnbränslehantering AB, Sweden.

Vieno T, Nordman H, 1999. Safety assessment of spent fuel disposal in Hästholmen, Kivetty, Olkiluoto and Romuvaara TILA-99. Posiva Report 99-07. Posiva Oy, Helsinki, Finland.

Appendix G

Calculated radionuclide release rates

This appendix presents the calculated releases from the near field and from the geosphere as functions of time for all calculated cases. Table G-1 gives an overview of the figures in this appendix.

Table G-1. Overview of near-field and geosphere release curves in this appendix.

Case	Fission and activation products	Actinide chains	Case	Fission and activation products	Actinide chains
Initial penetrating defect in canister			PD-EPRC	None calculated	Only C-14 calculated
PD-BC	Figure G-1	Figure G-2	PD-NFSLV	Figure G-31	Figure G-32
PD-VVER	Figure G-3	Figure G-4	PD-SAL	Figure G-33	Figure G-34
PD-EPR	Figure G-5	Figure G-6	PD-HISAL	Figure G-35	Figure G-36
PD-HIFDR	Figure G-7	Figure G-8	PD-GMW	Figure G-37	Figure G-38
PD-LOFDR	Figure G-9	Figure G-10	PD-GMWV	Figure G-39	Figure G-40
PD-IRF	Figure G-11 (near-field only)	None calculated	PD-GMWC	Figure G-41	Figure G-42
PD-BIGHOLE	Figure G-12	Figure G-13	PD-HIFLOW	Figure G-43	Figure G-44
PD-HIDELAY	Figure G-14	Figure G-15	PD-LOGEOR	Figure G-45	Figure G-46
PD-LODELAY	Figure G-16	Figure G-17	PD-HIGEOR	Figure G-47	Figure G-48
PD-BHLD	Figure G-18	Figure G-19	PD-HIFLOWR	Figure G-49	Figure G-50
PD-HIDIFF	Figure G-20	Figure G-21	**Canister failure due to copper corrosion**		
PD-SPALL	Figure G-22	Figure G-23	CC-BC	Figure G-51	Figure G-52
PD-FEBENT1	Figure G-24	Figure G-25	CC-HIFDR	Figure G-53	Figure G-54
PD-FEBENT2	Figure G-26	Figure G-27	CC-LOFDR	Figure G-55	Figure G-56
PD-FEBENT3	Figure G-28	Figure G-29	CC-GMW	Figure G-57	Figure G-58
PD-EXPELL	Figure G-30 (geosphere only)	None calculated	CC-LOGEOR	Figure G-59	Figure G-60
PD-VOL-1	Only C-14 calculated	None calculated	CC-LOGEORG	Figure G-61	Figure G-62
PD-VOL-2	Only C-14 calculated	None calculated	CC-LOGEORS	Figure G-63	Figure G-64
PD-BCN	Only Nb-94 calculated	None calculated	**Canister failure due to rock shear**		
PD-BCC	Only C-14 calculated	None calculated	RS-BC	Figure G-65	Figure G-66
PD-VVERC	Only C-14 calculated	None calculated	RS-GMW	Figure G-67	Figure G-68

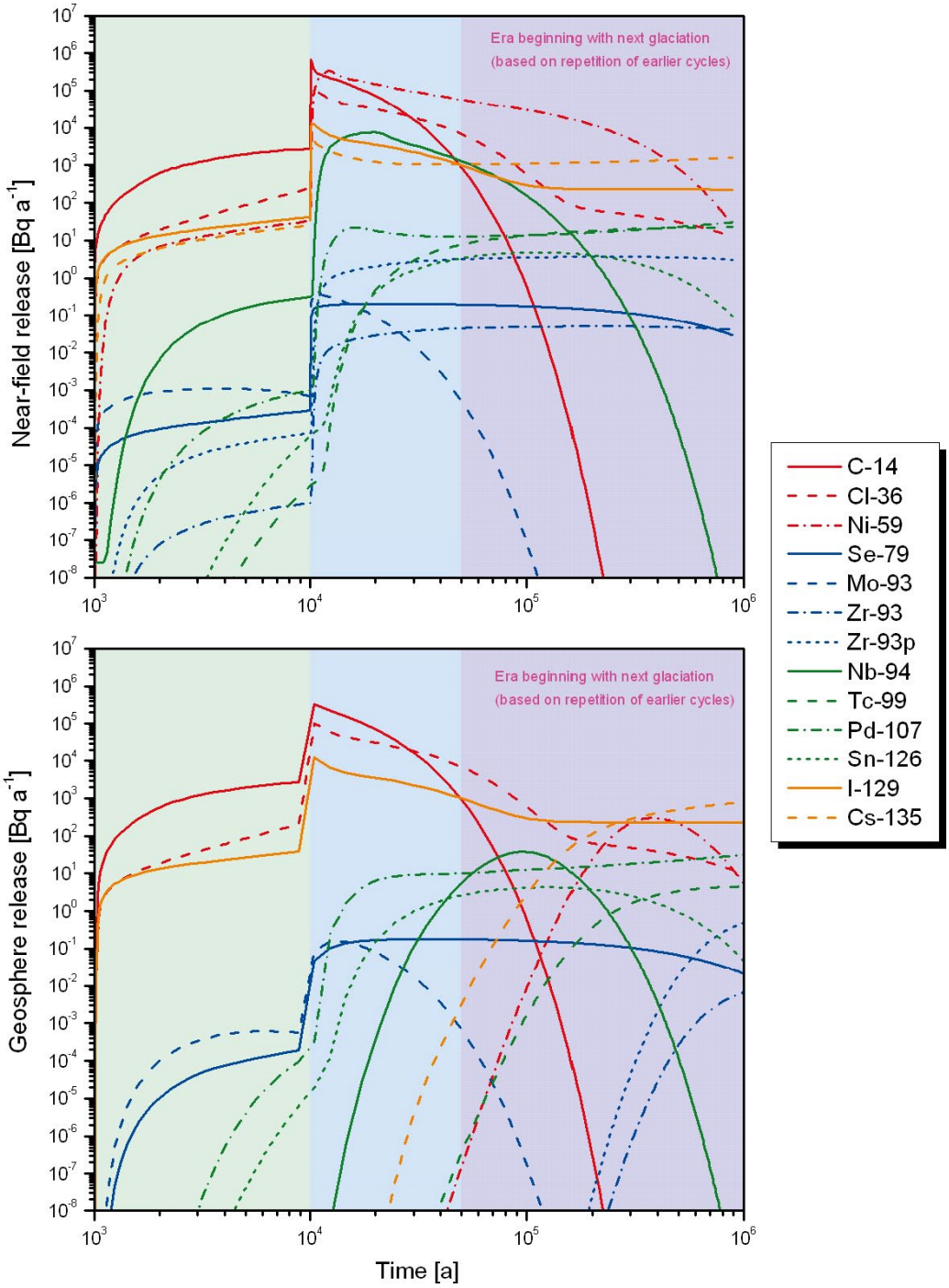

Figure G-1. *Release rates of activation and fission products from the near field (upper figure) and geosphere (lower figure) as functions of time in case PD-BC.*

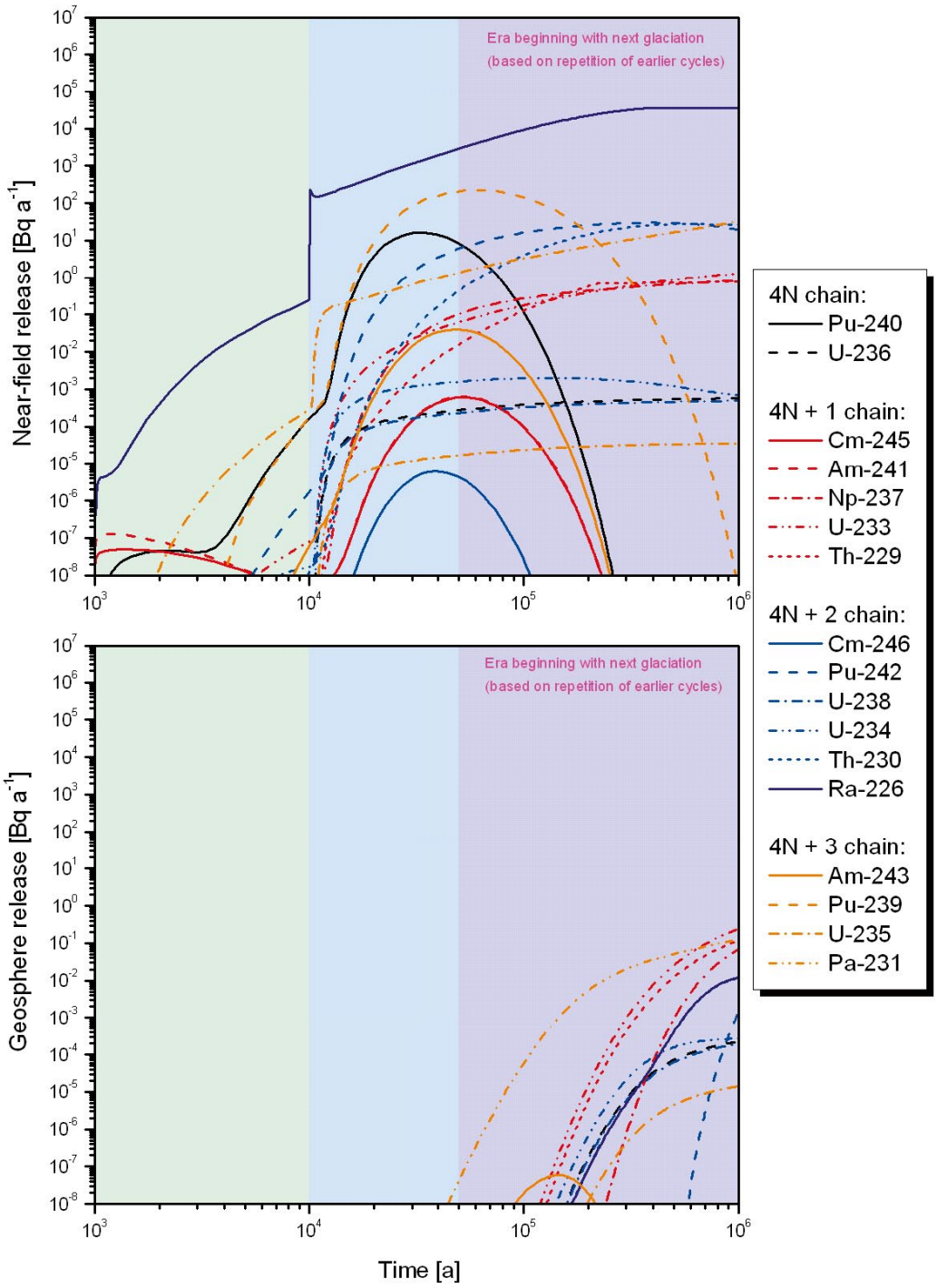

Figure G-2. *Release rates of actinide chain members from the near field (upper figure) and geosphere (lower figure) as functions of time in case BD-BC.*

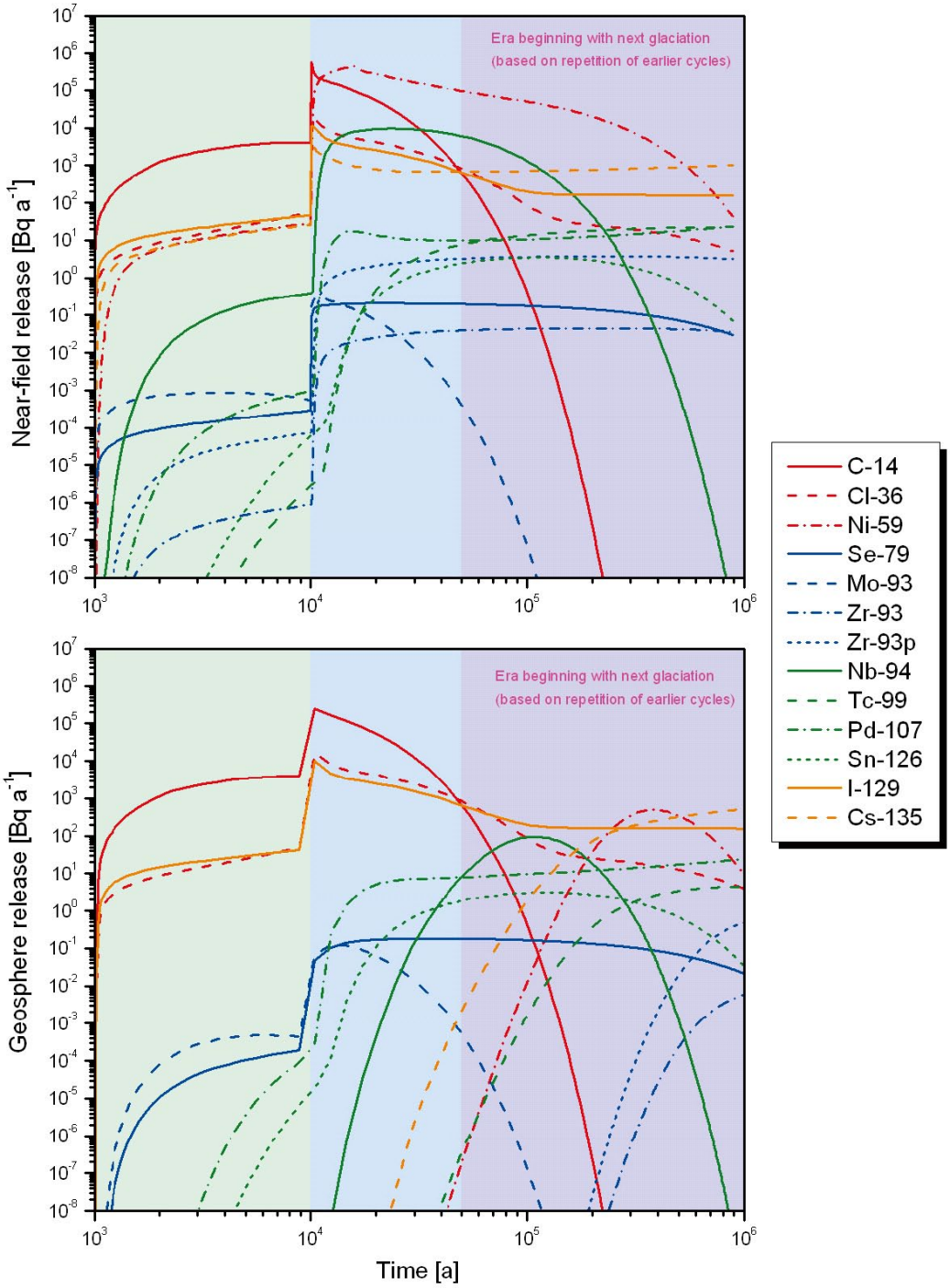

Figure G-3. *Release rates of activation and fission products from the near field (upper figure) and geosphere (lower figure) as functions of time in case PD-VVER.*

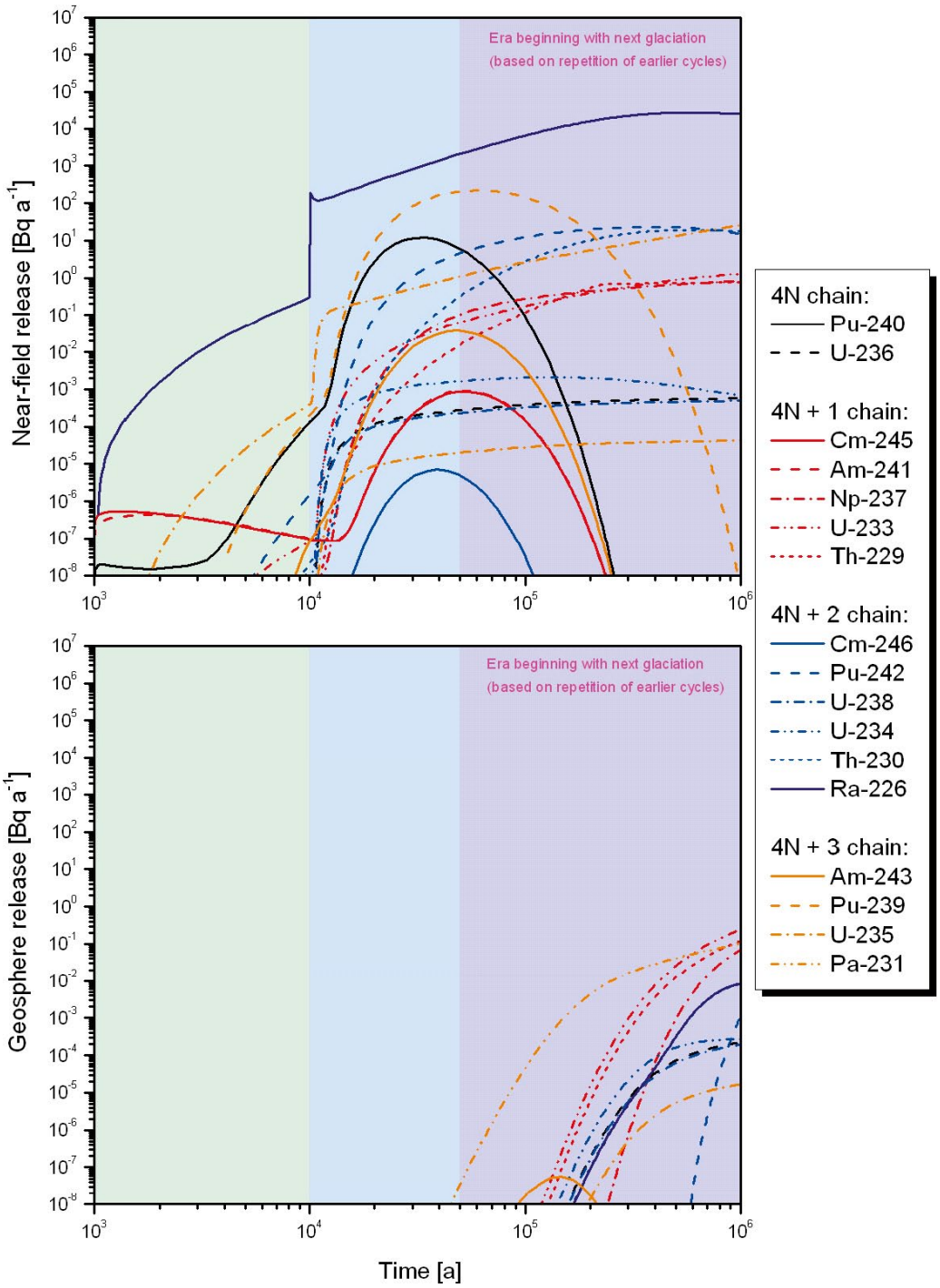

Figure G-4. *Release rates of actinide chain members from the near field (upper figure) and geosphere (lower figure) as functions of time in case PD-VVER.*

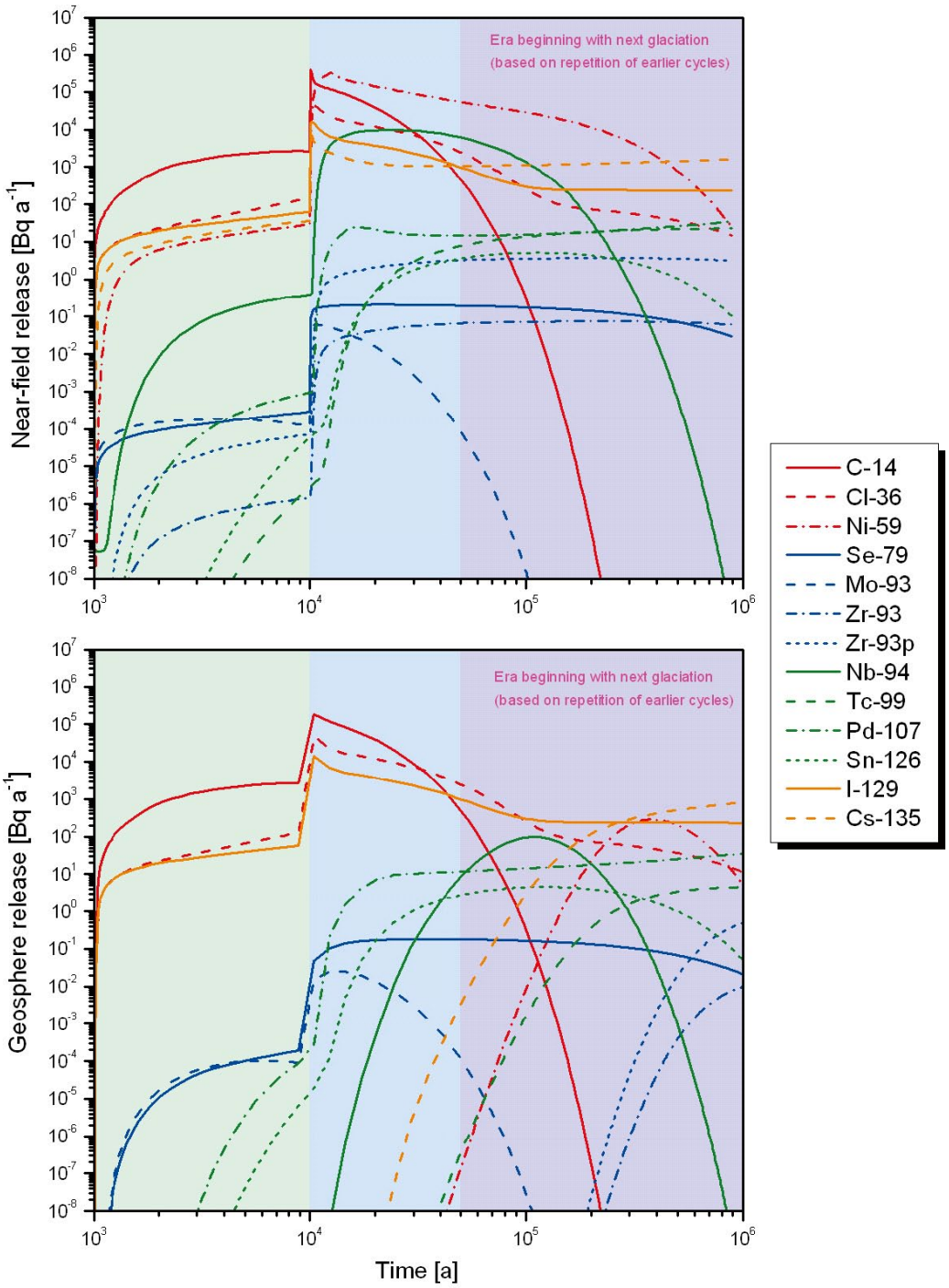

Figure G-5. *Release rates of activation and fission products from the near field (upper figure) and geosphere (lower figure) as functions of time in case PD-EPR.*

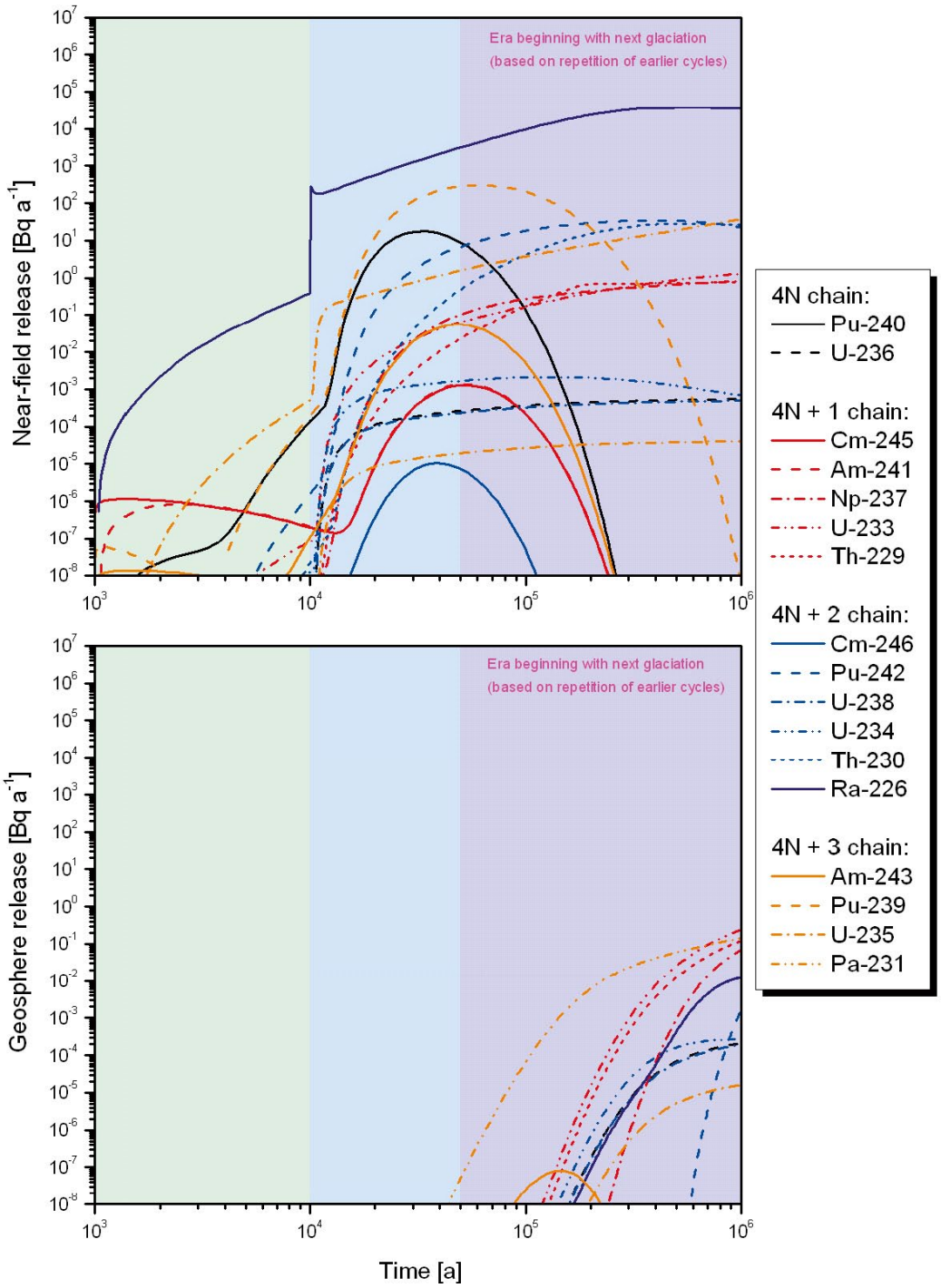

Figure G-6. *Release rates of actinide chain members from the near field (upper figure) and geosphere (lower figure) as functions of time in case PD-EPR.*

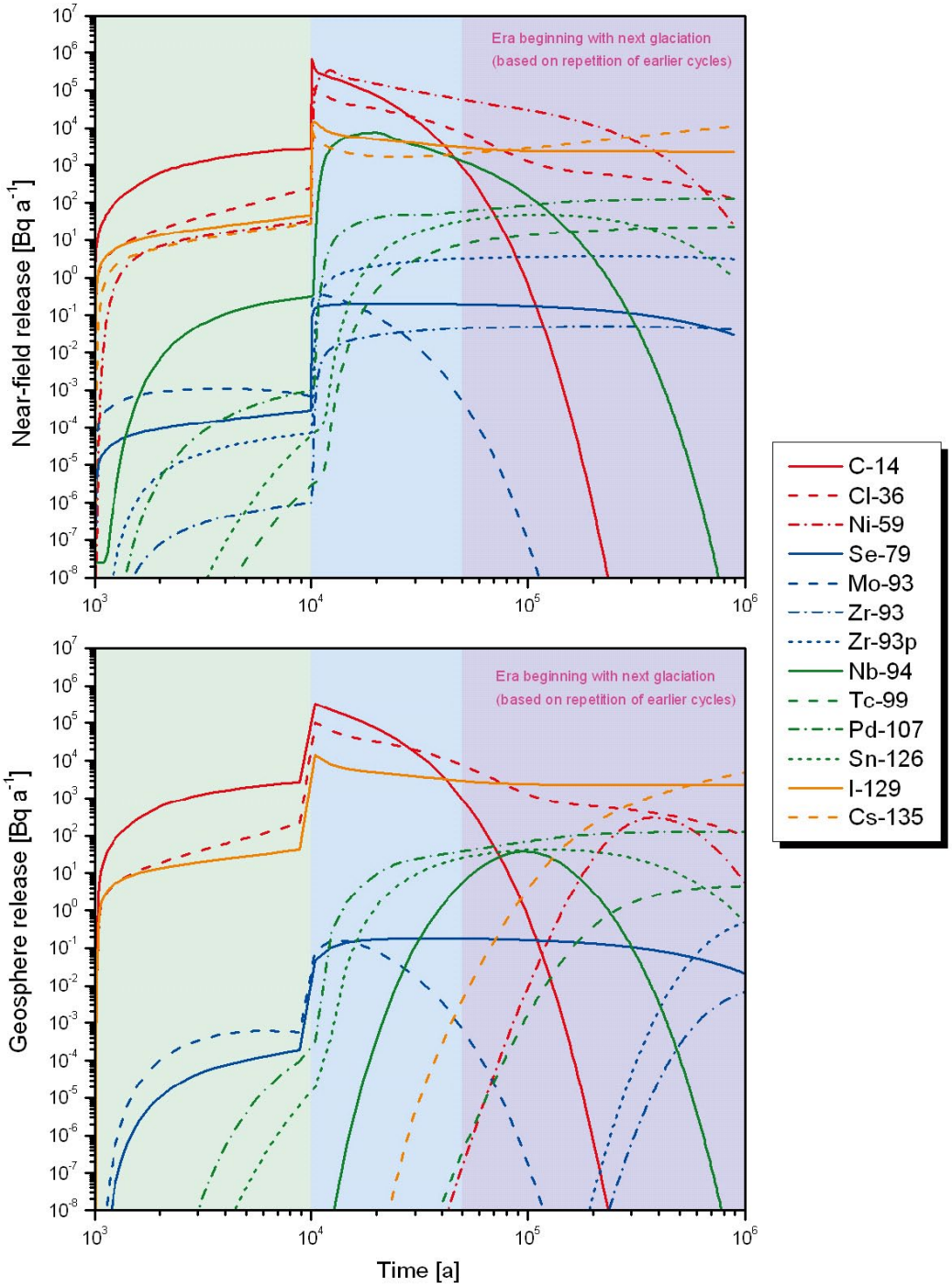

Figure G-7. *Release rates of activation and fission products from the near field (upper figure) and geosphere (lower figure) as functions of time in case PD-HIFDR.*

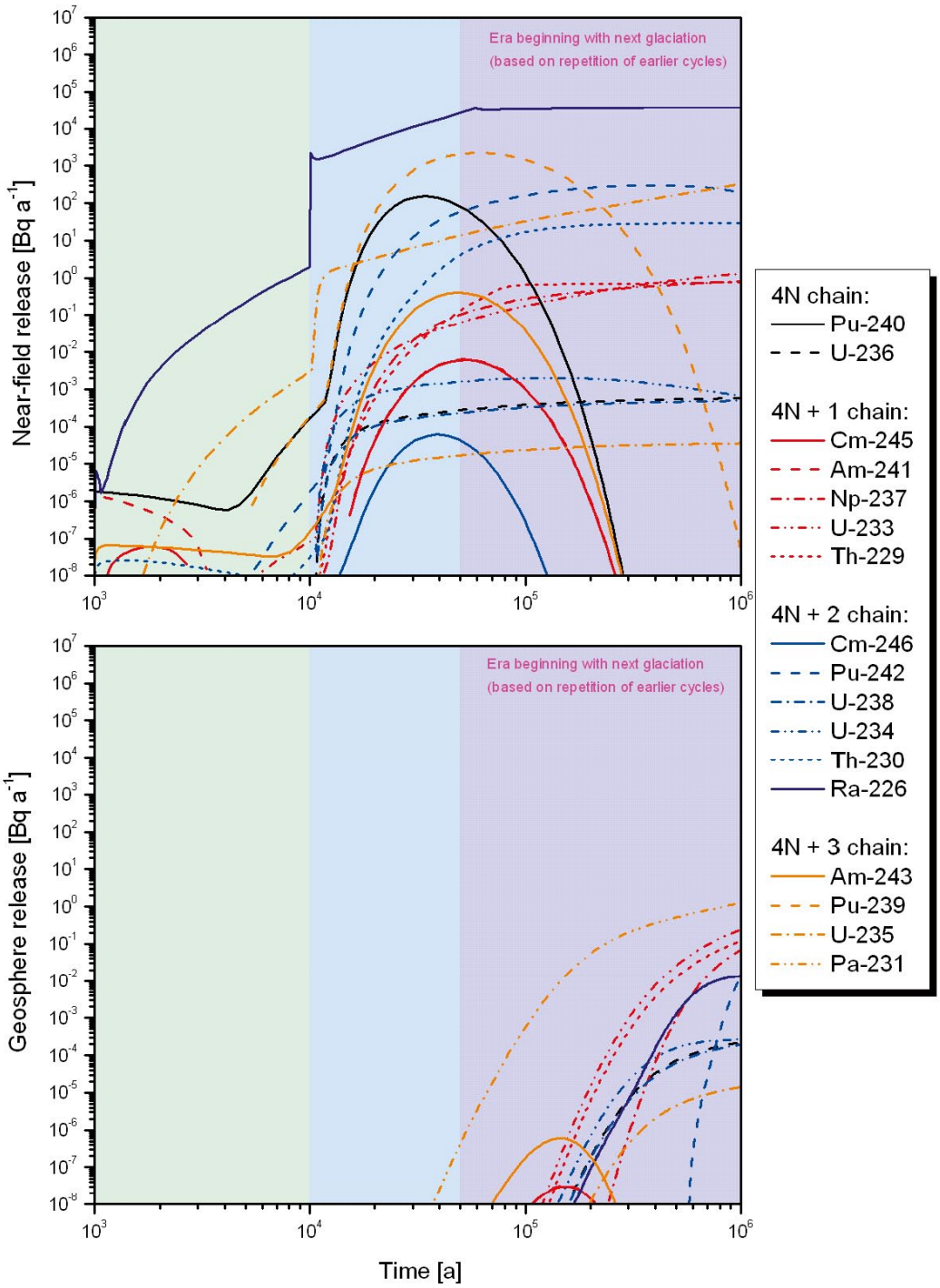

Figure G-8. *Release rates of actinide chain members from the near field (upper figure) and geosphere (lower figure) as functions of time in case PD-HIFDR.*

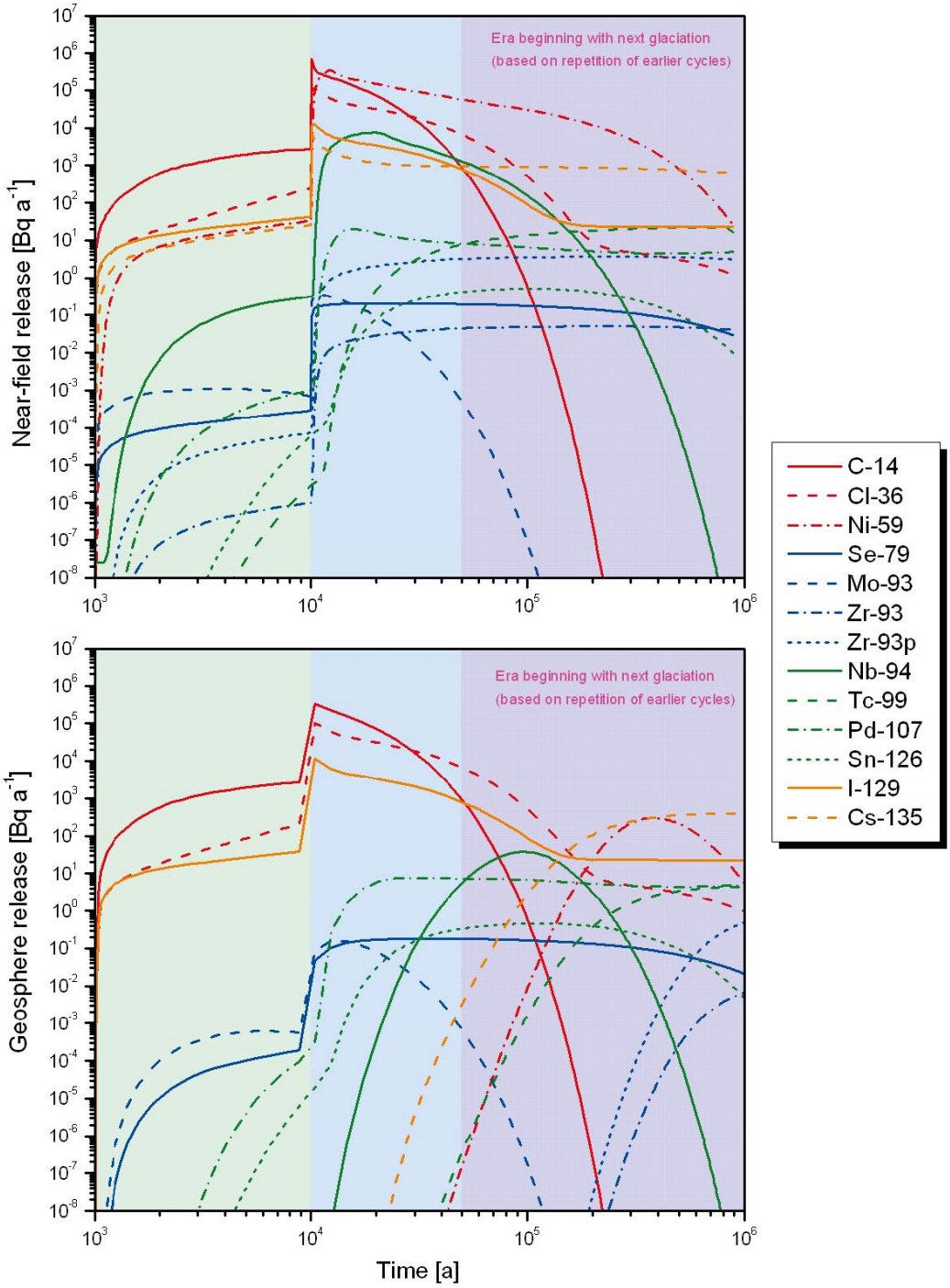

Figure G-9. *Release rates of activation and fission products from the near field (upper figure) and geosphere (lower figure) as functions of time in case PD-LOFDR.*

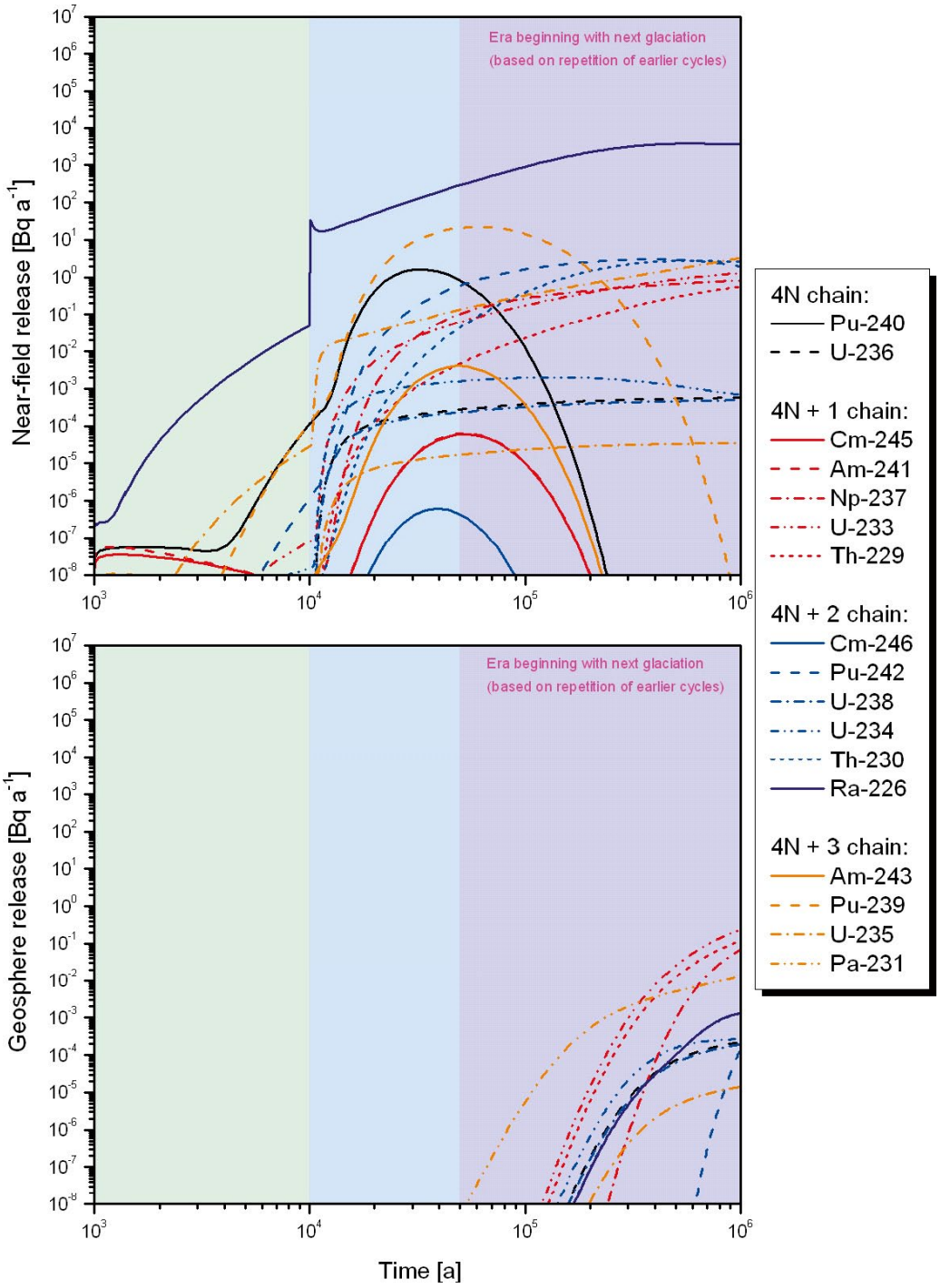

Figure G-10. *Release rates of actinide chain members from the near field (upper figure) and geosphere (lower figure) as functions of time in case PD-LOFDR.*

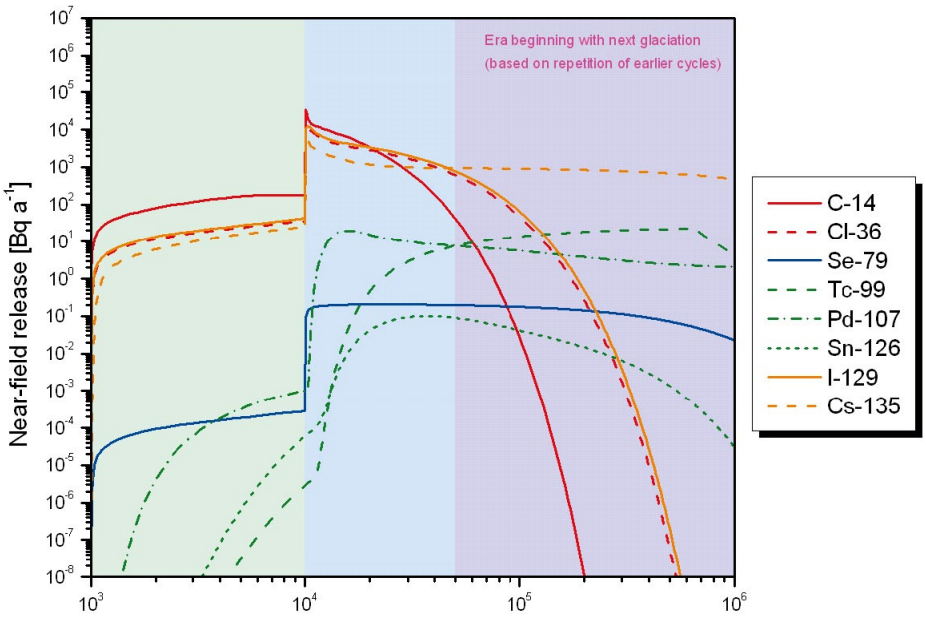

Figure G-11. *Release rates of individual radionuclides from the near field in case PD-IRF.*

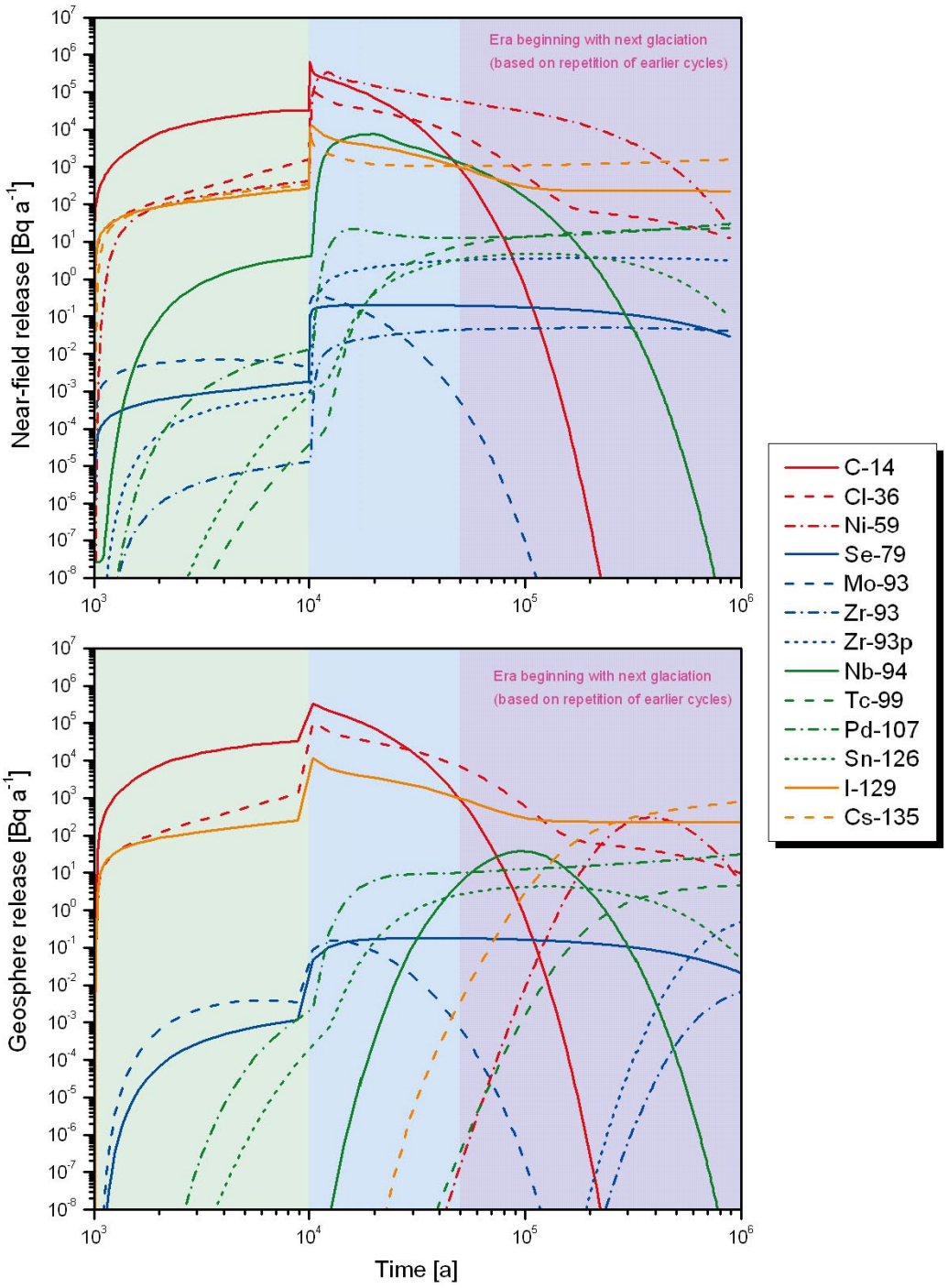

Figure G-12. *Release rates of activation and fission products from the near field (upper figure) and geosphere (lower figure) as functions of time in case PD-BIGHOLE.*

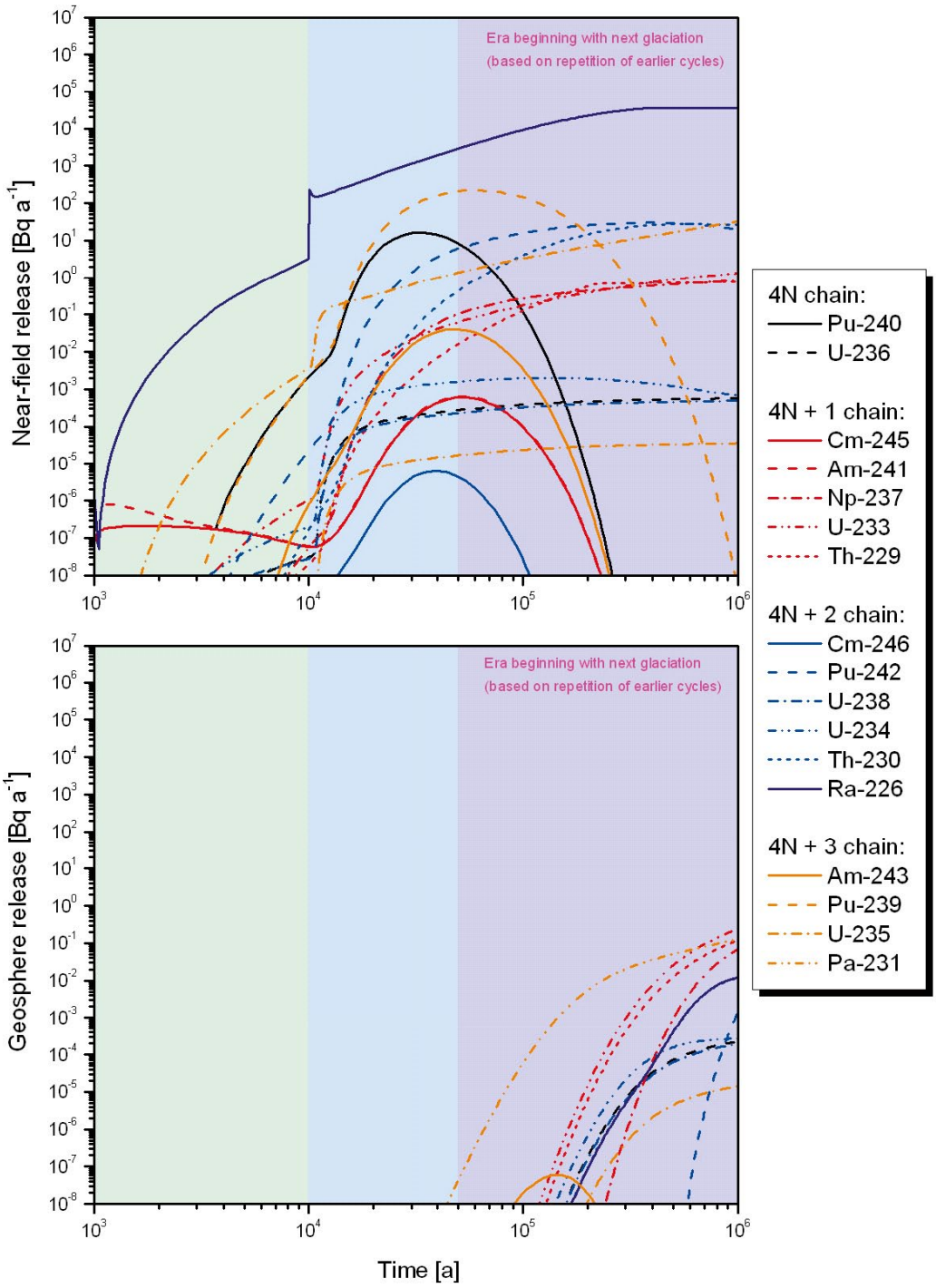

Figure G-13. *Release rates of actinide chain members from the near field (upper figure) and geosphere (lower figure) as functions of time in case PD-BIGHOLE.*

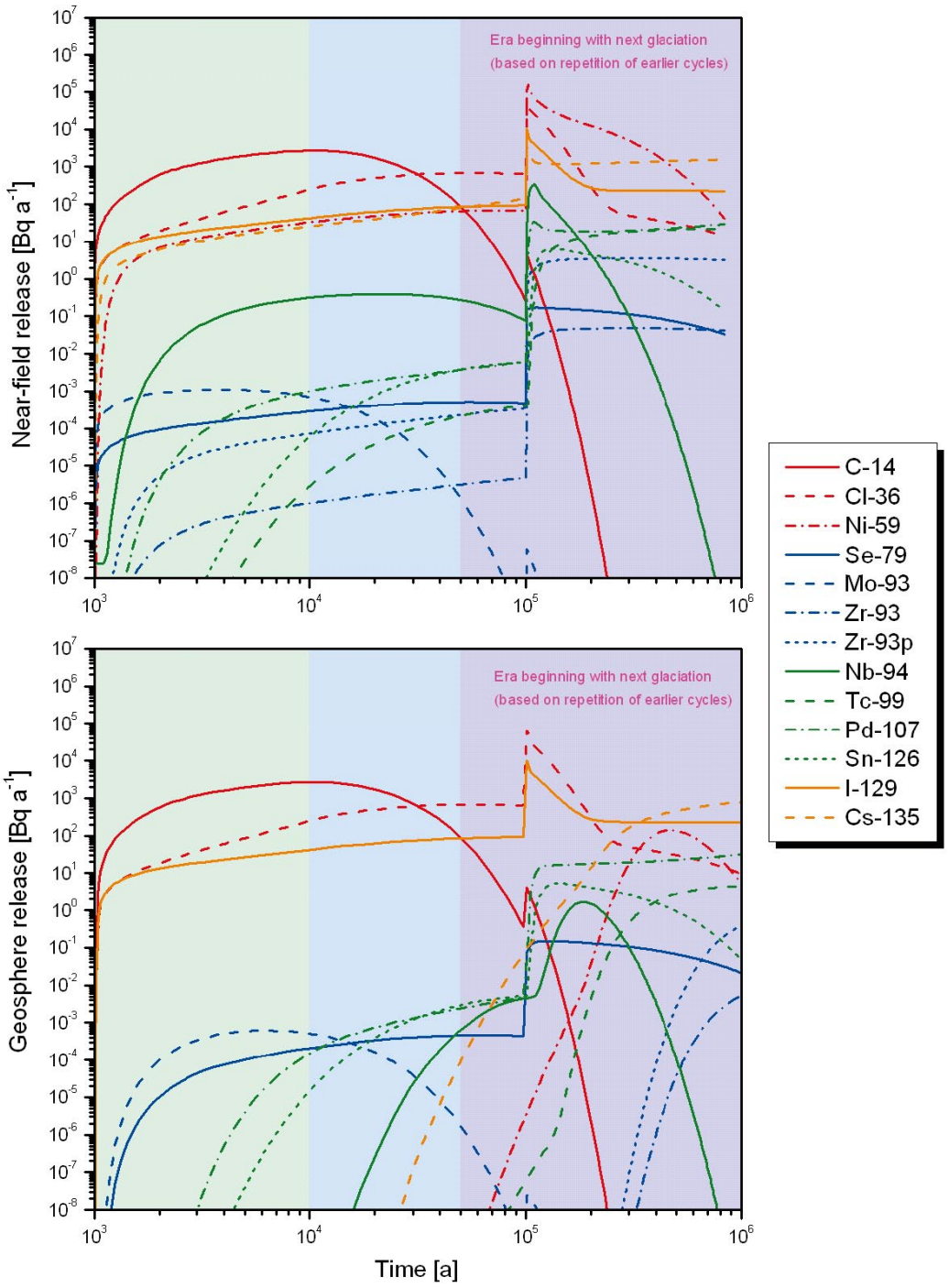

Figure G-14. *Release rates of activation and fission products from the near field (upper figure) and geosphere (lower figure) as functions of time in case PD-HIDELAY.*

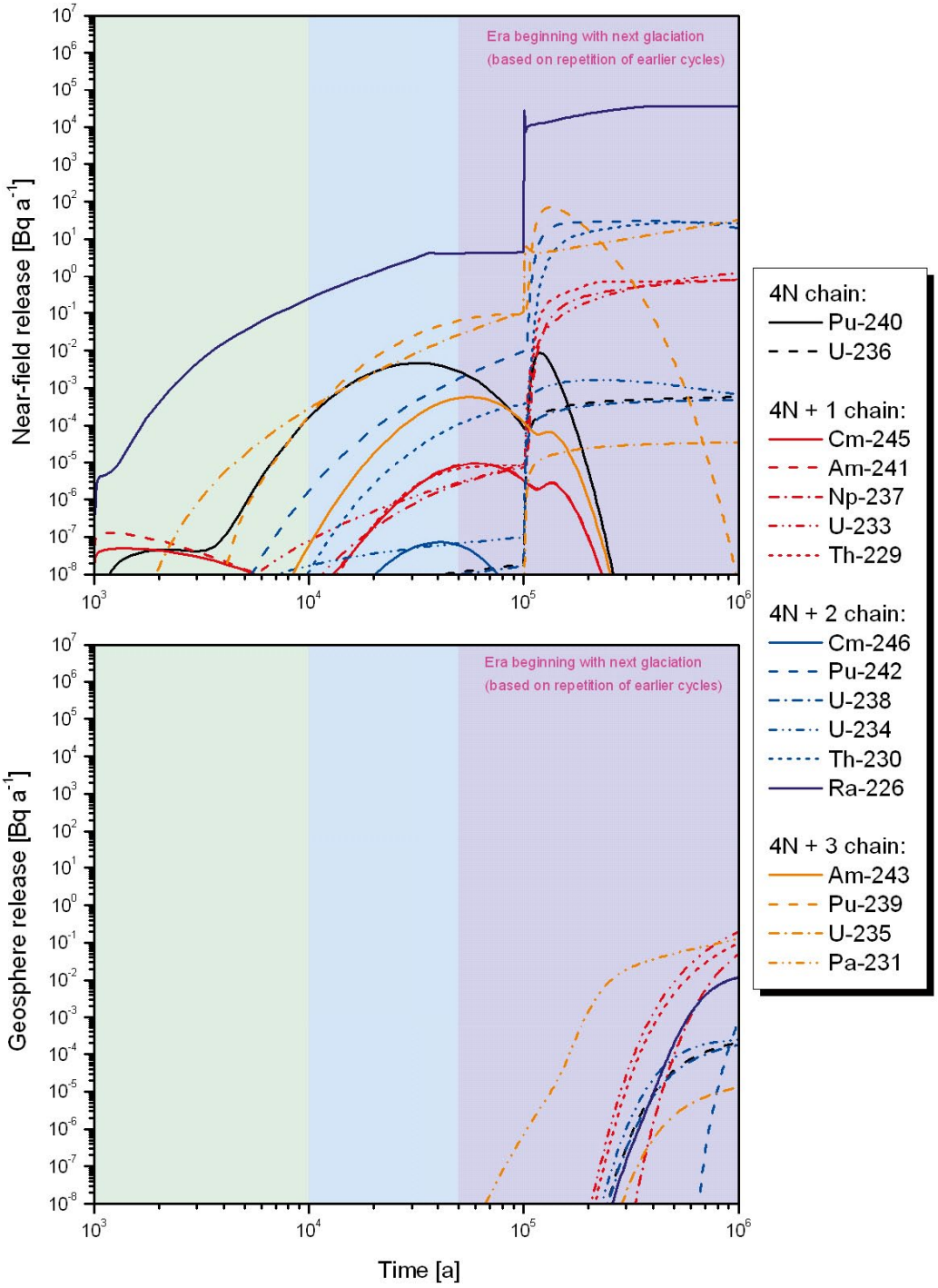

Figure G-15. *Release rates of actinide chain members from the near field (upper figure) and geosphere (lower figure) as functions of time in case PD-HIDELAY.*

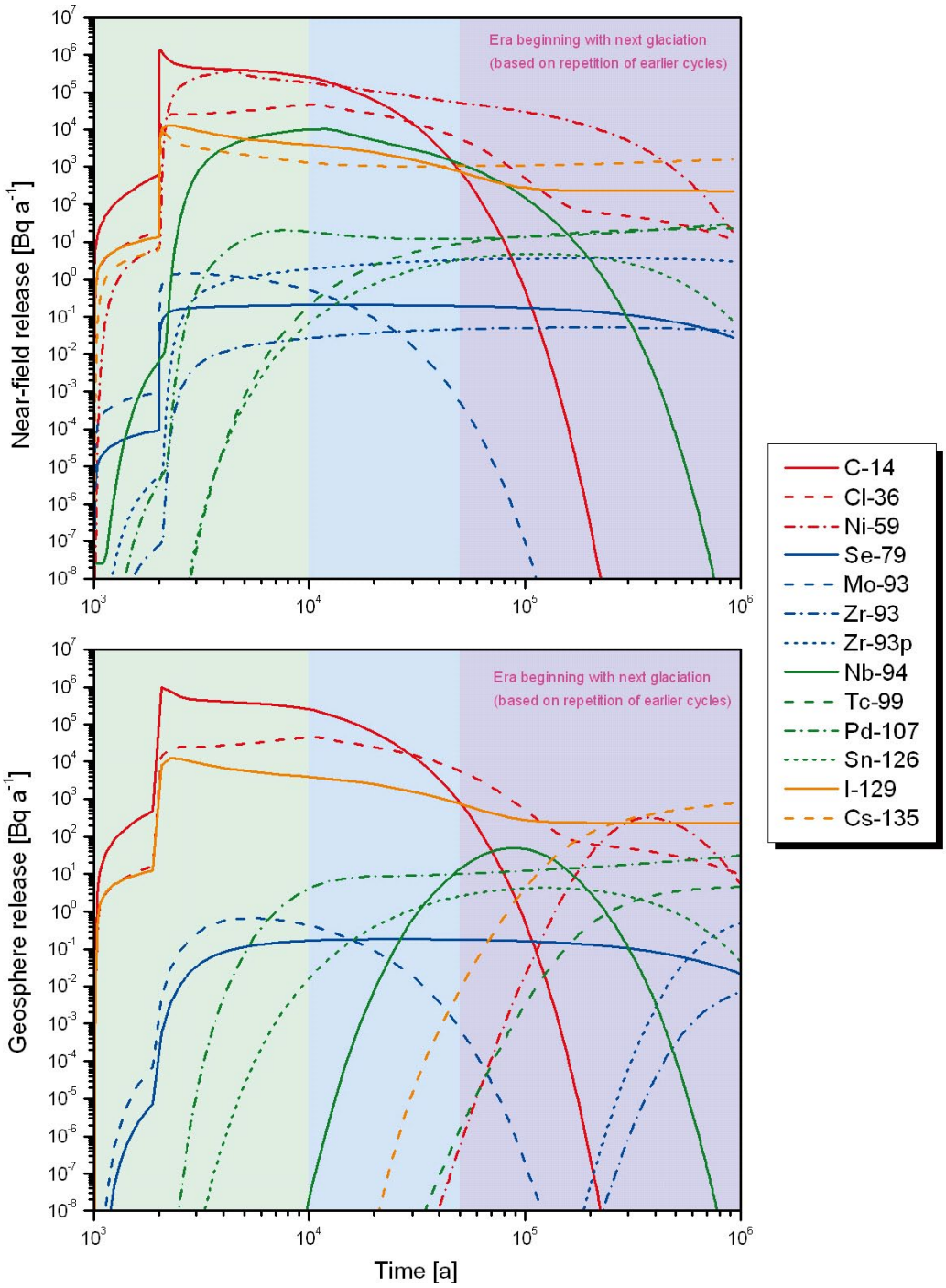

Figure G-16. *Release rates of activation and fission products from the near field (upper figure) and geosphere (lower figure) as functions of time in case PD-LODELAY.*

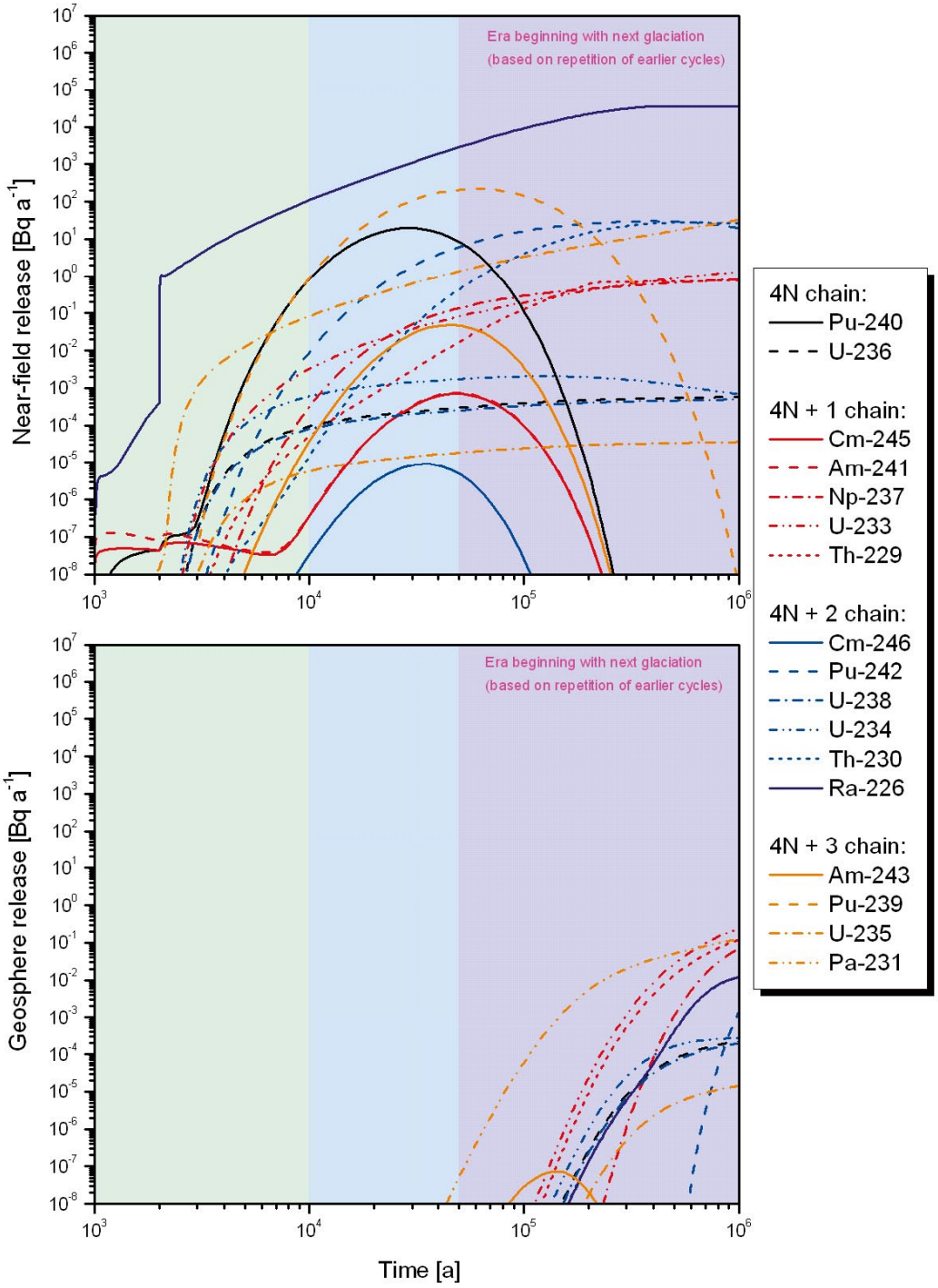

Figure G-17. *Release rates of actinide chain members from the near field (upper figure) and geosphere (lower figure) as functions of time in case PD-LODELAY.*

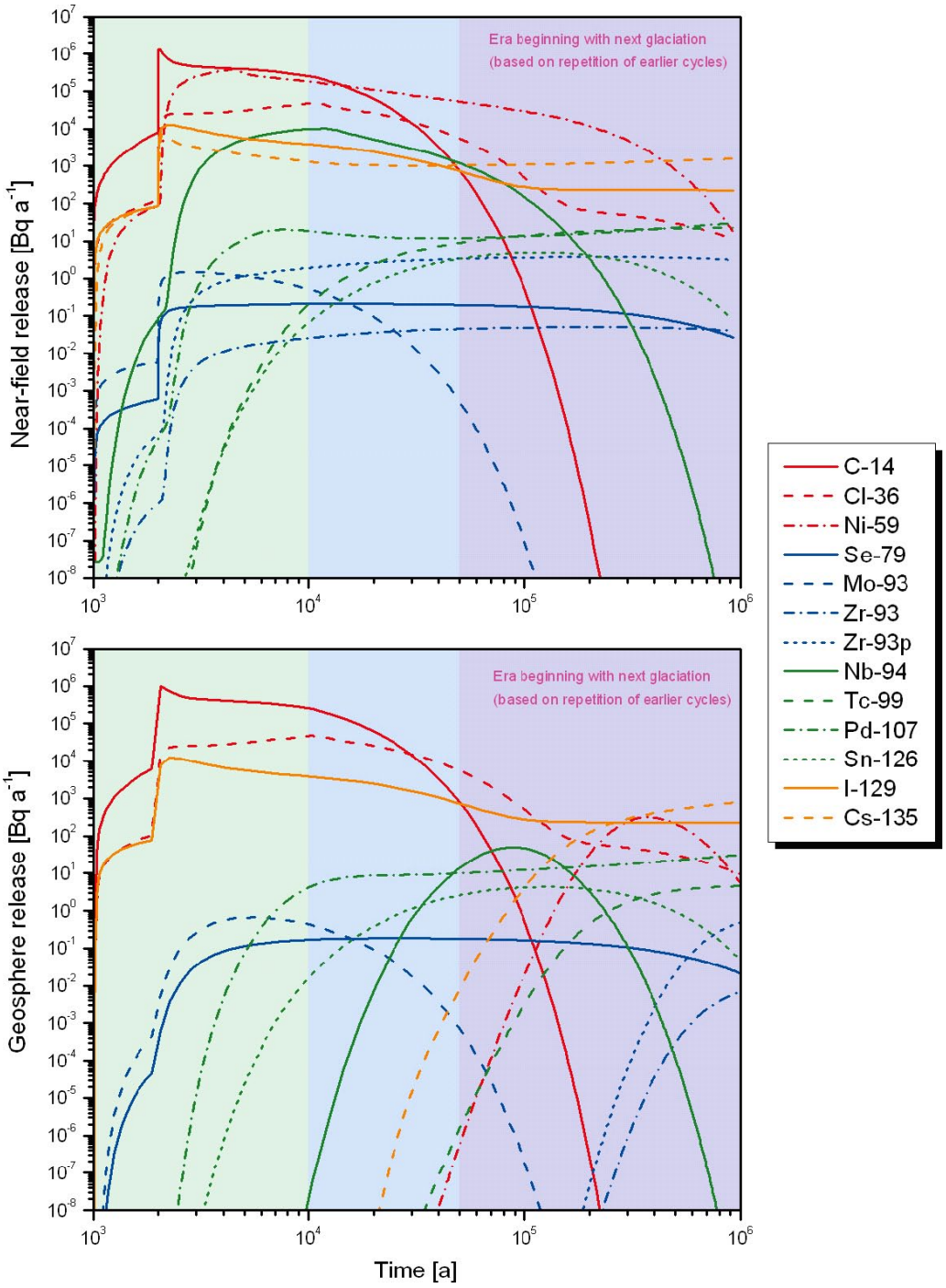

Figure G-18. *Release rates of activation and fission products from the near field (upper figure) and geosphere (lower figure) as functions of time in case PD-BHLD.*

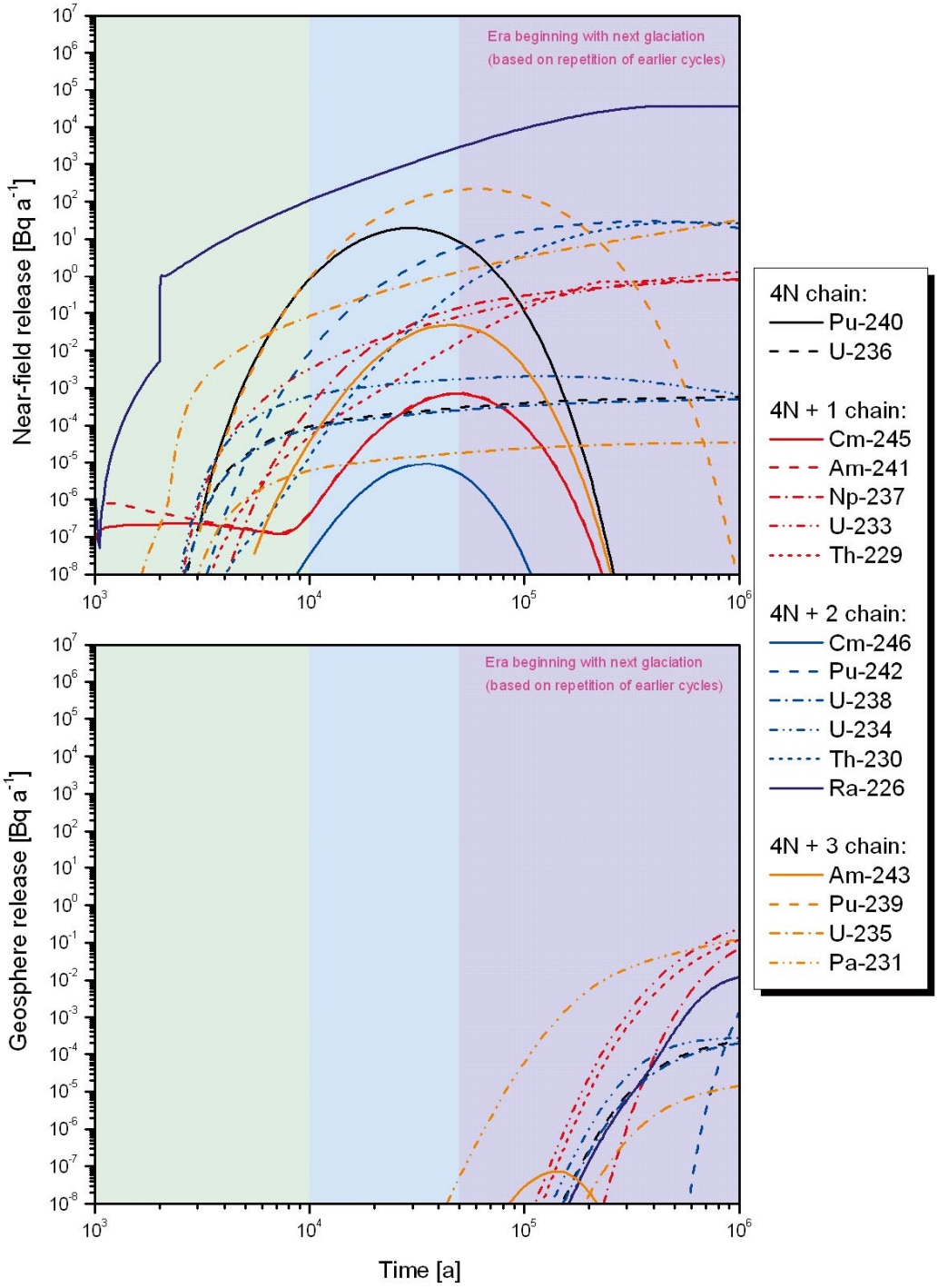

Figure G-19. *Release rates of actinide chain members from the near field (upper figure) and geosphere (lower figure) as functions of time in case PD-BHLD.*

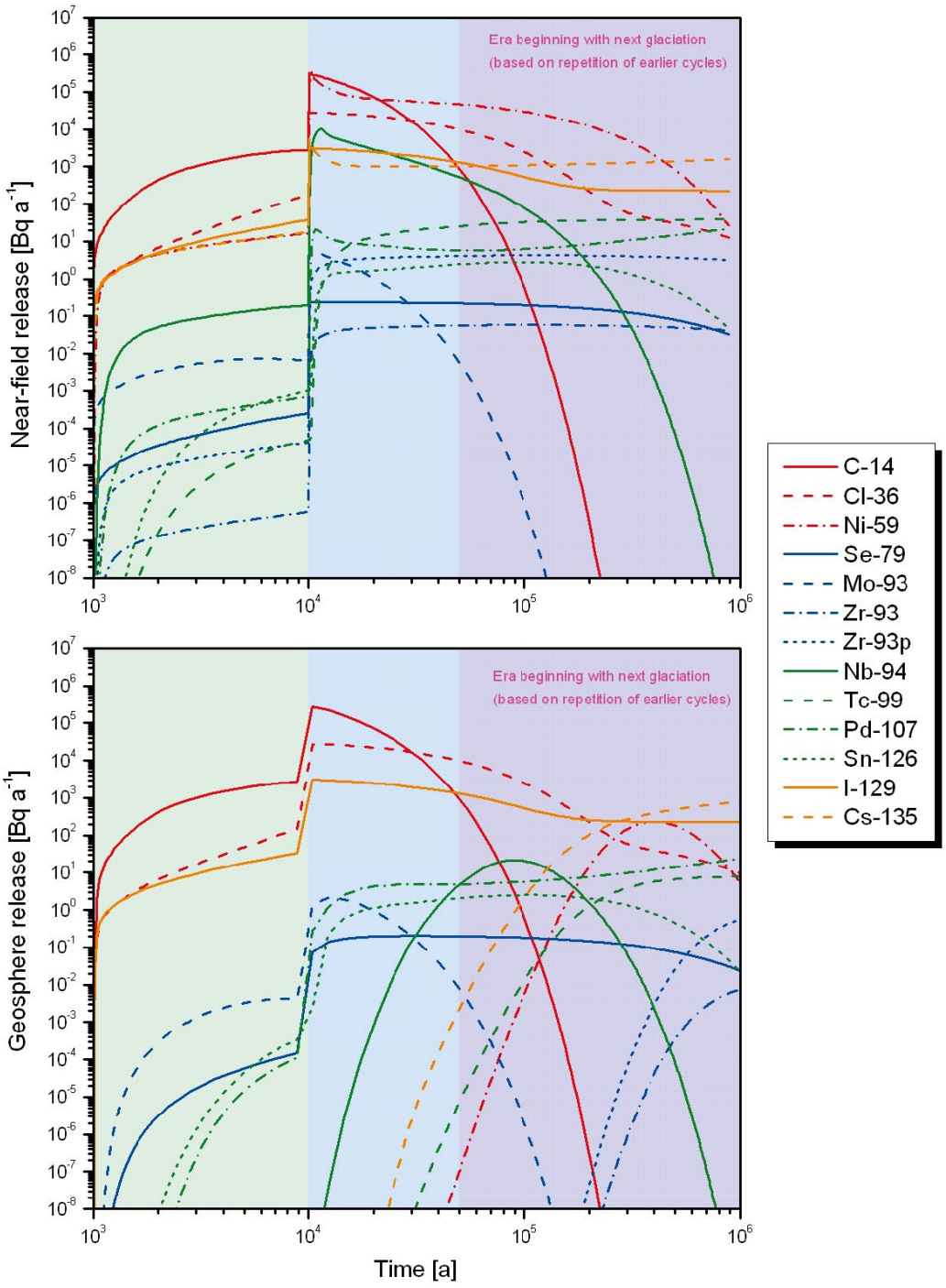

Figure G-20. *Release rates of activation and fission products from the near field (upper figure) and geosphere (lower figure) as functions of time in case PD-HIDIFF.*

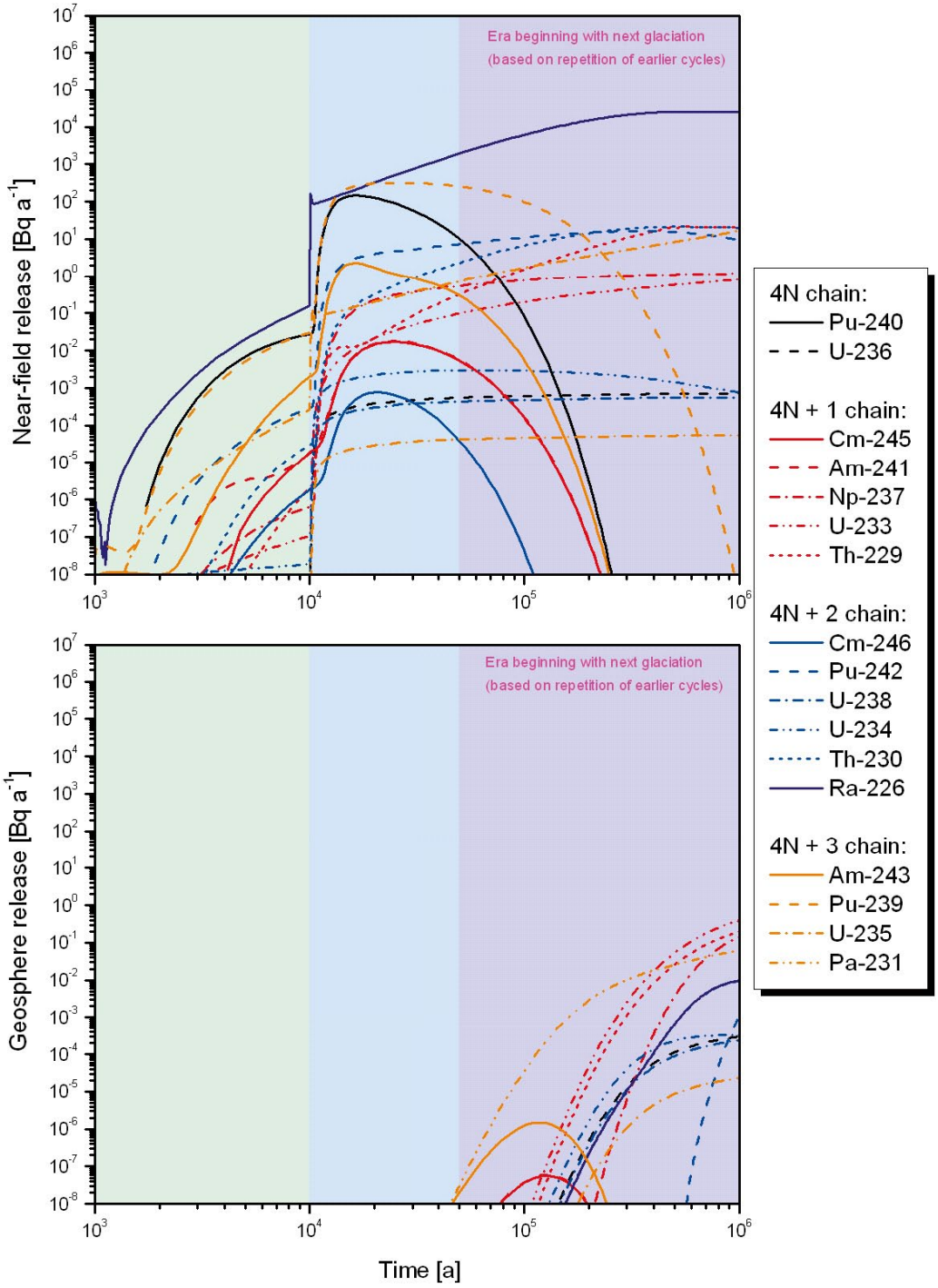

Figure G-21. *Release rates of actinide chain members from the near field (upper figure) and geosphere (lower figure) as functions of time in case PD-HIDIFF.*

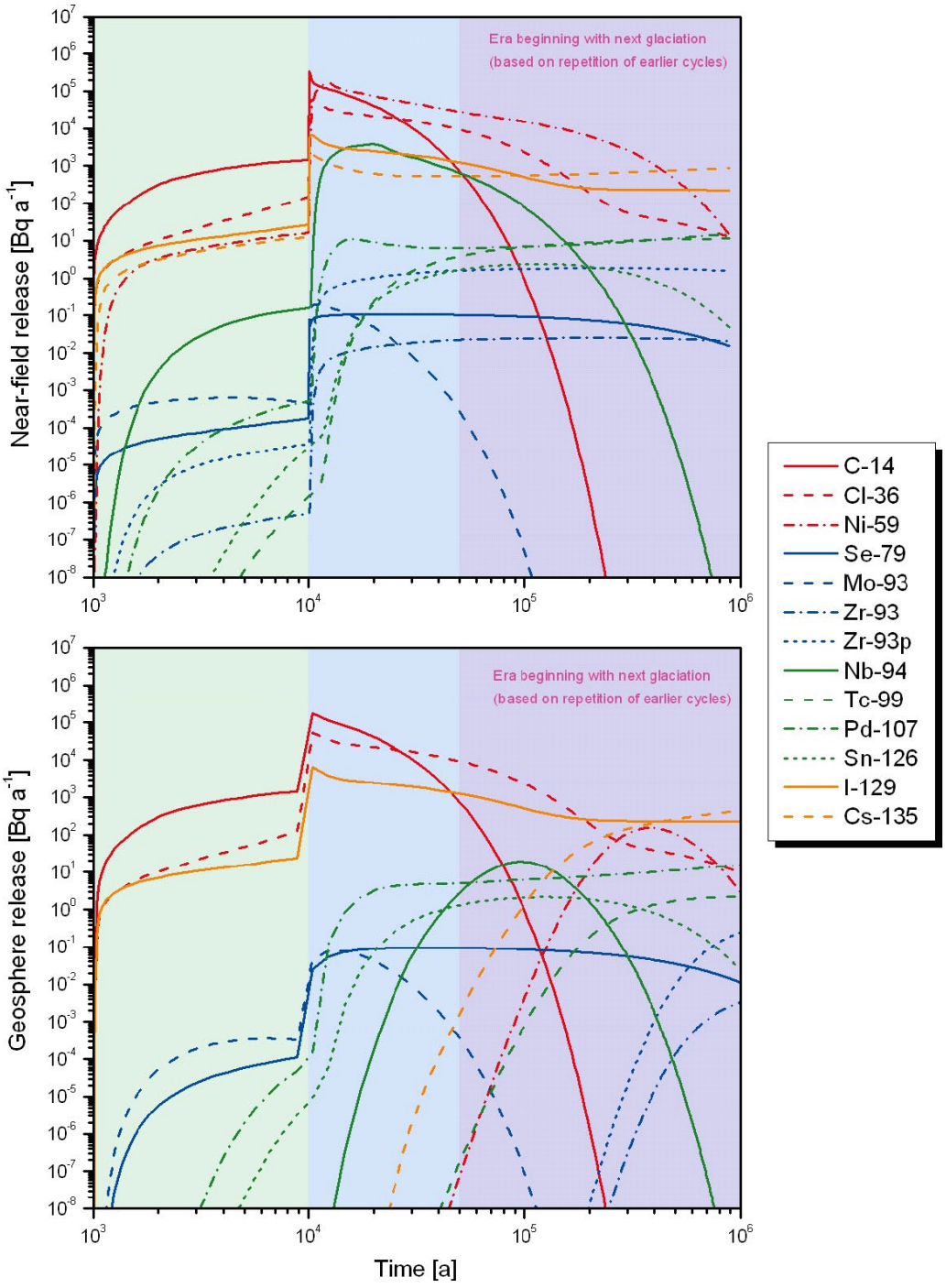

Figure G-22. *Release rates of activation and fission products from the near field (upper figure) and geosphere (lower figure) as functions of time in case PD-SPALL.*

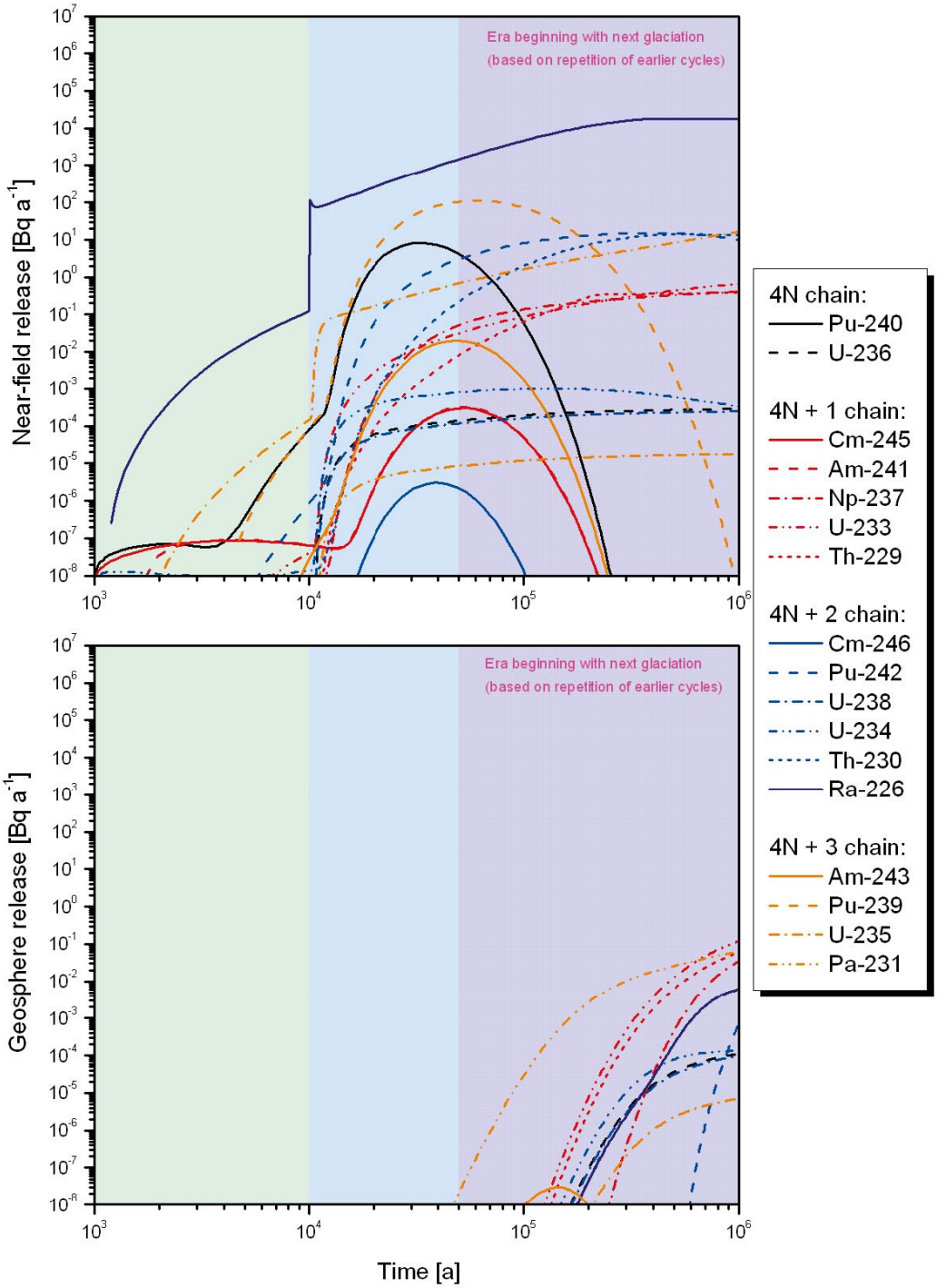

Figure G-23. *Release rates of actinide chain members from the near field (upper figure) and geosphere (lower figure) as functions of time in case PD-SPALL.*

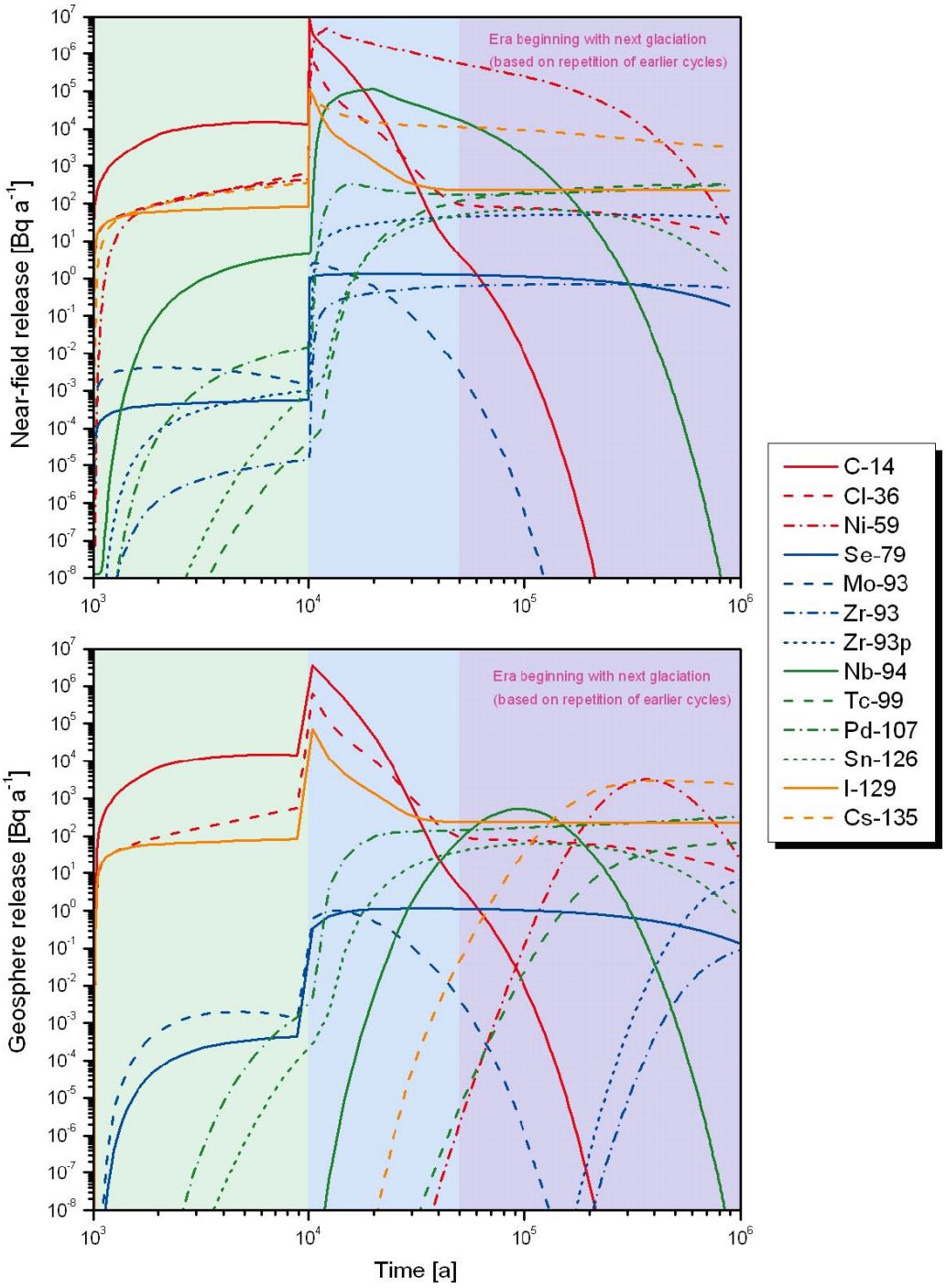

Figure G-24. *Release rates of activation and fission products from the near field (upper figure) and geosphere (lower figure) as functions of time in case PD-FEBENT1.*

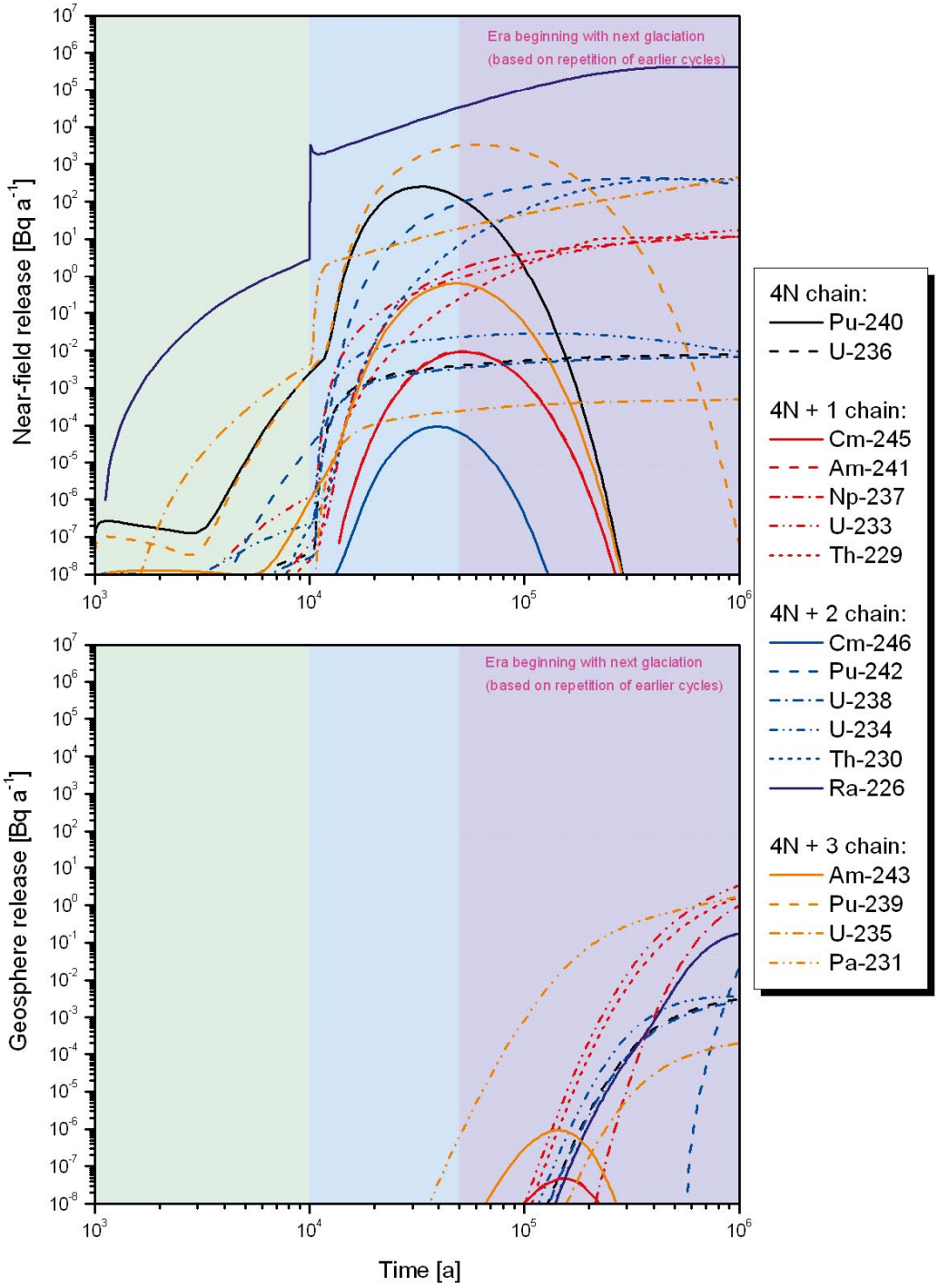

Figure G-25. *Release rates of actinide chain members from the near field (upper figure) and geosphere (lower figure) as functions of time in case PD-FEBENT1.*

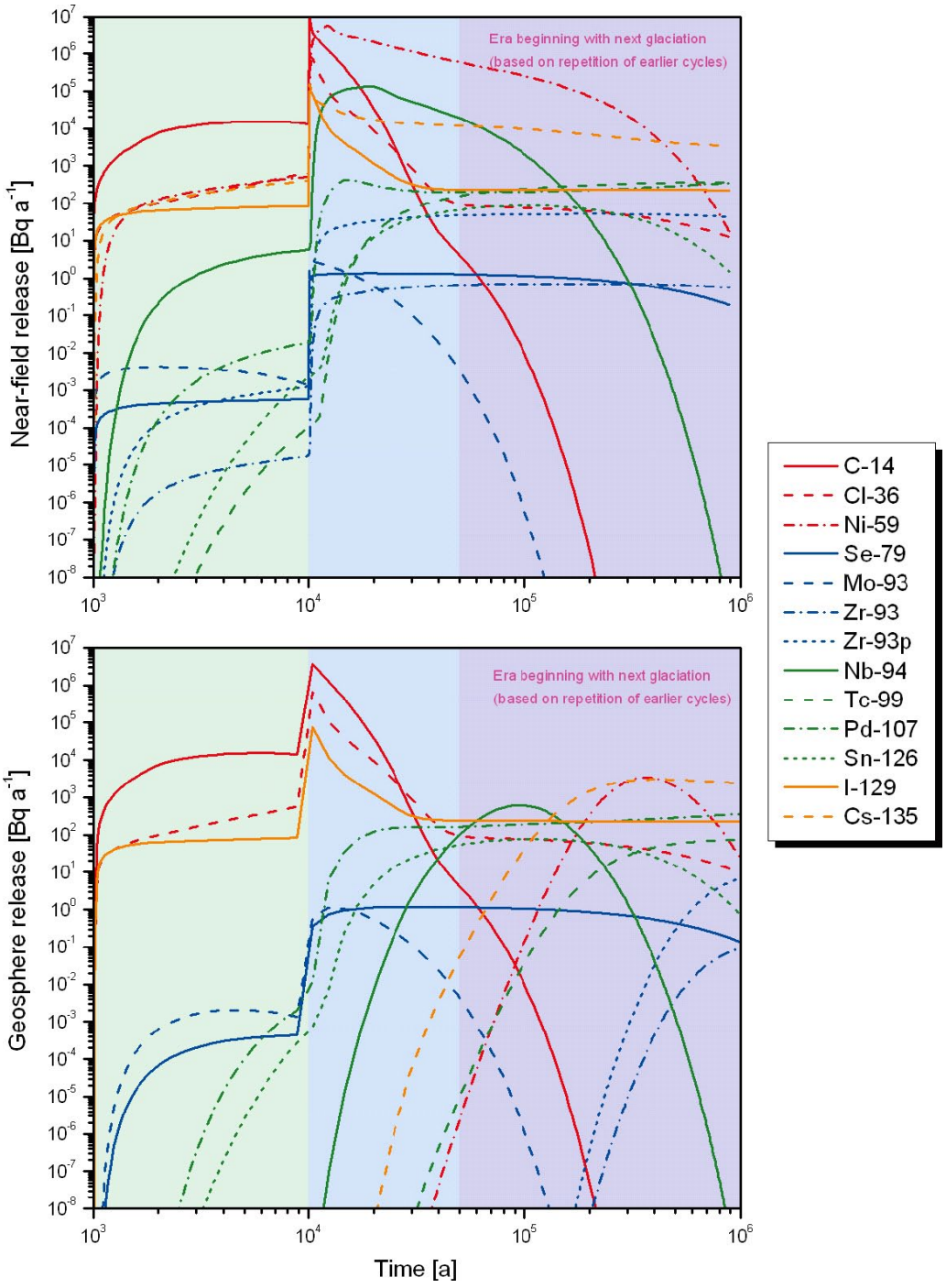

Figure G-26. *Release rates of activation and fission products from the near field (upper figure) and geosphere (lower figure) as functions of time in case PD-FEBENT2.*

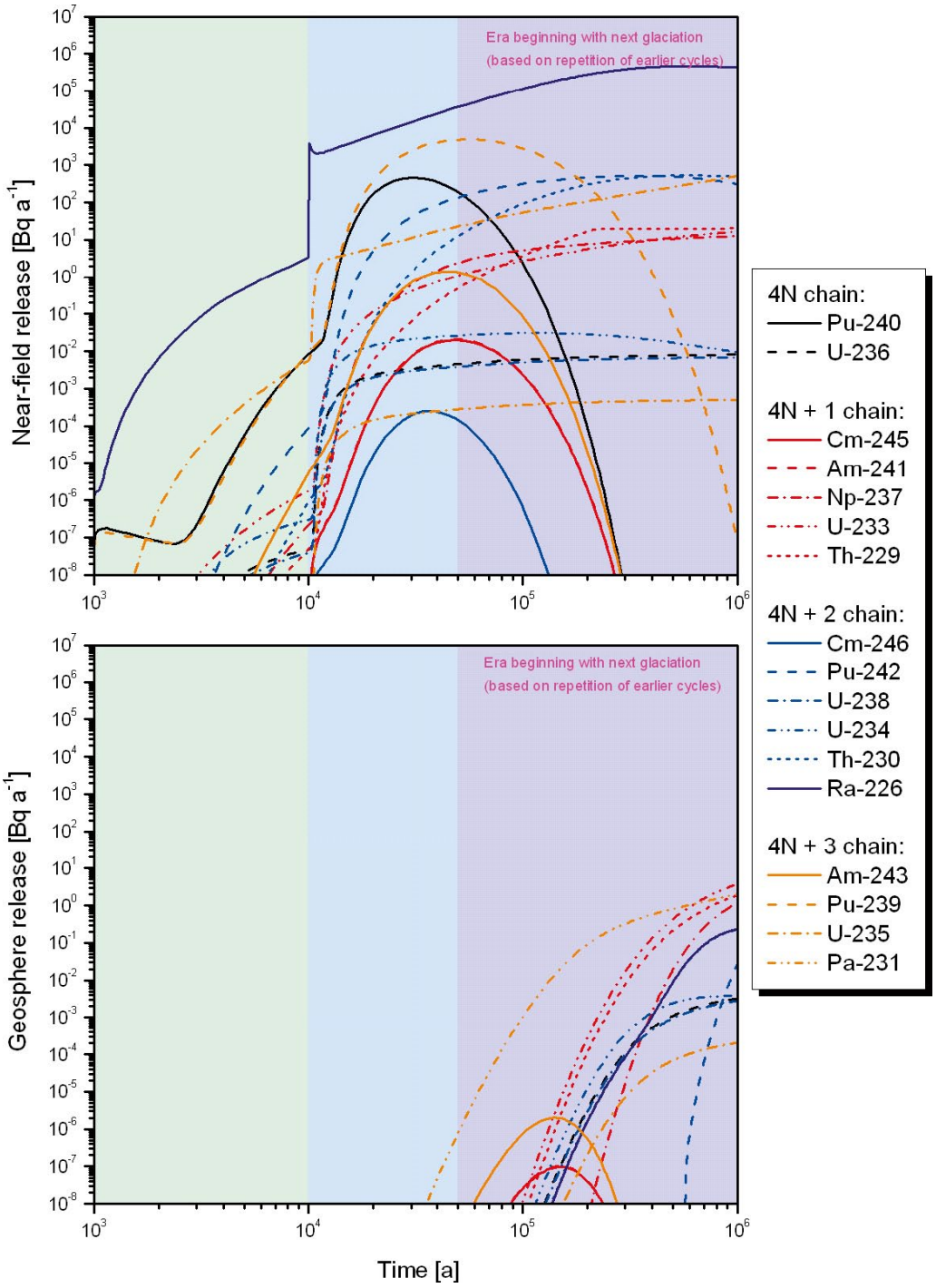

Figure G-27. *Release rates of actinide chain members from the near field (upper figure) and geosphere (lower figure) as functions of time in case PD-FEBENT2.*

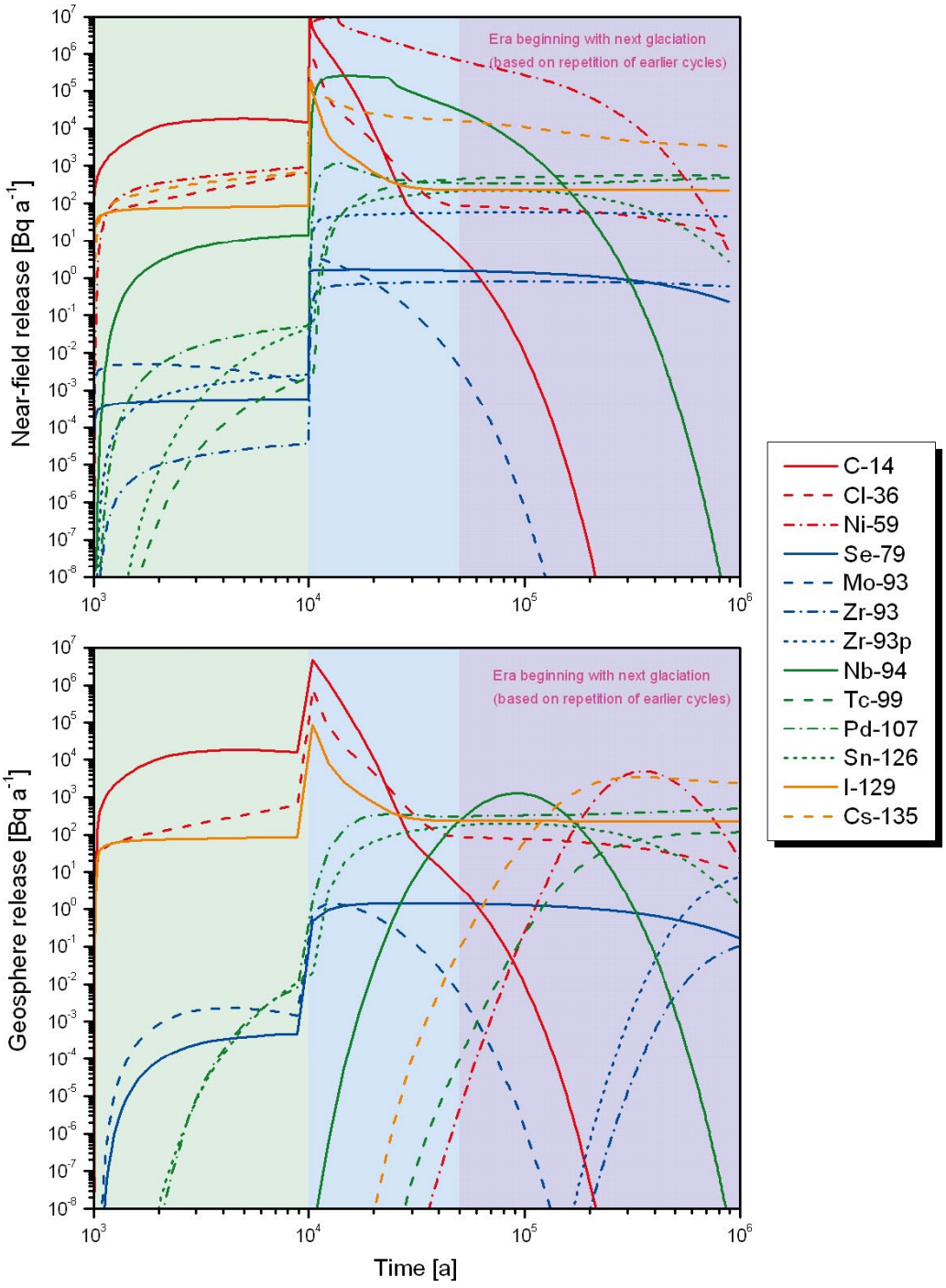

Figure G-28. *Release rates of activation and fission products from the near field (upper figure) and geosphere (lower figure) as functions of time in case PD-FEBENT3.*

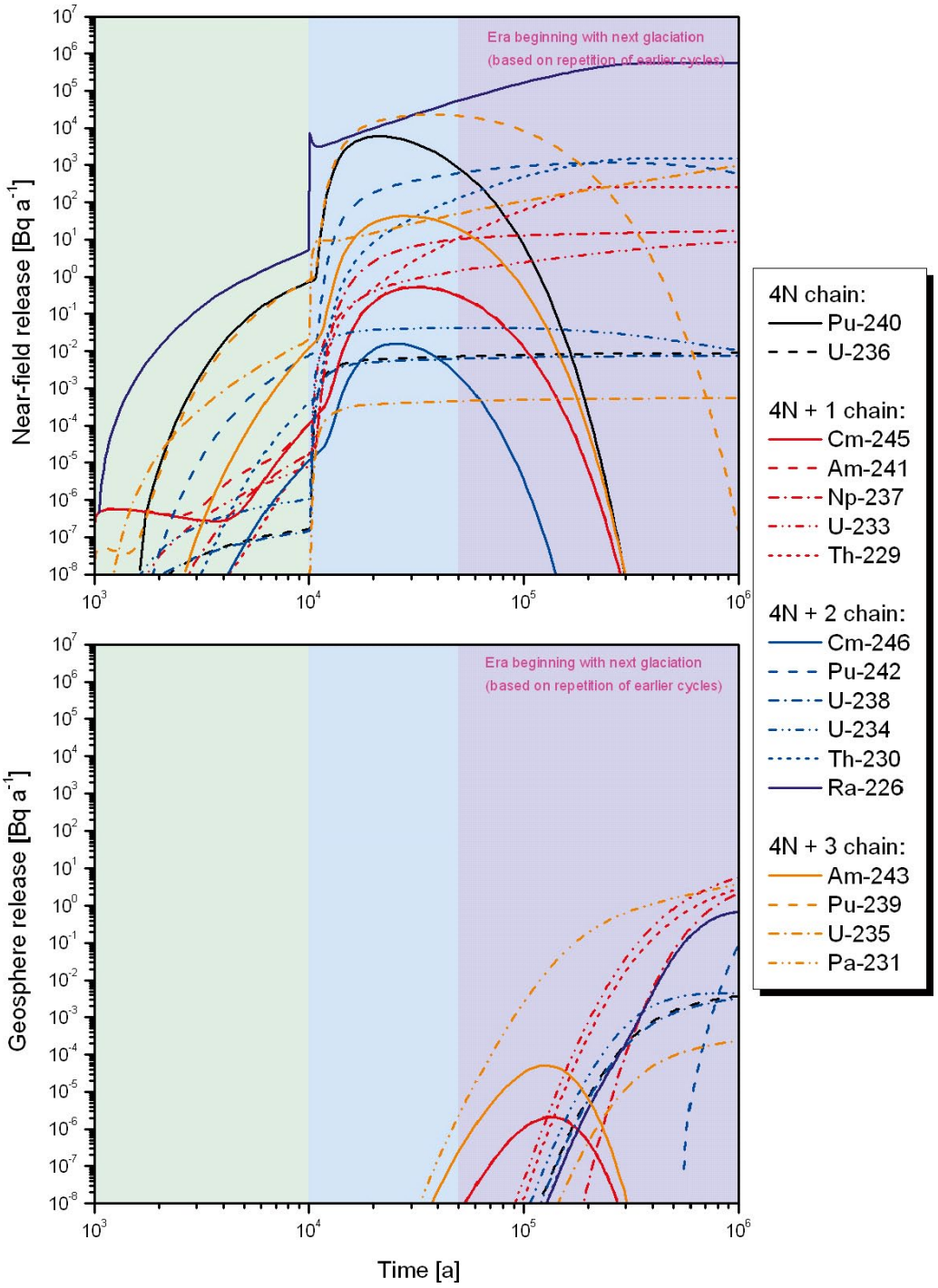

Figure G-29. *Release rates of actinide chain members from the near field (upper figure) and geosphere (lower figure) as functions of time in case PD-FEBENT3.*

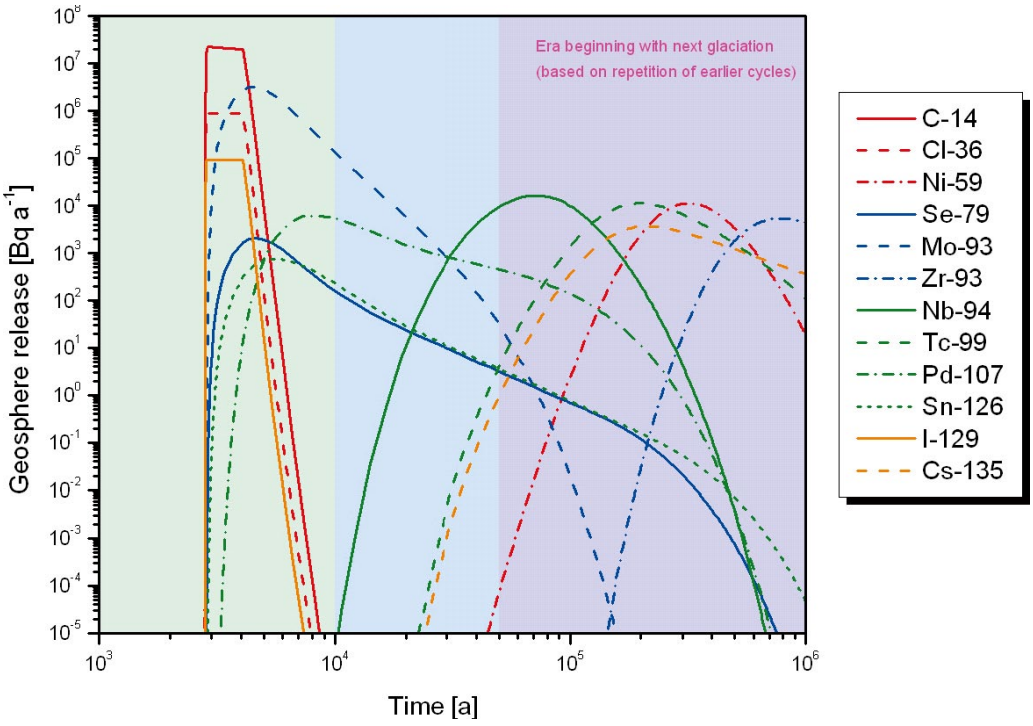

Figure G-30. *Release rates of actinide chain members from the geosphere as functions of time in case PD-EXPELL.*

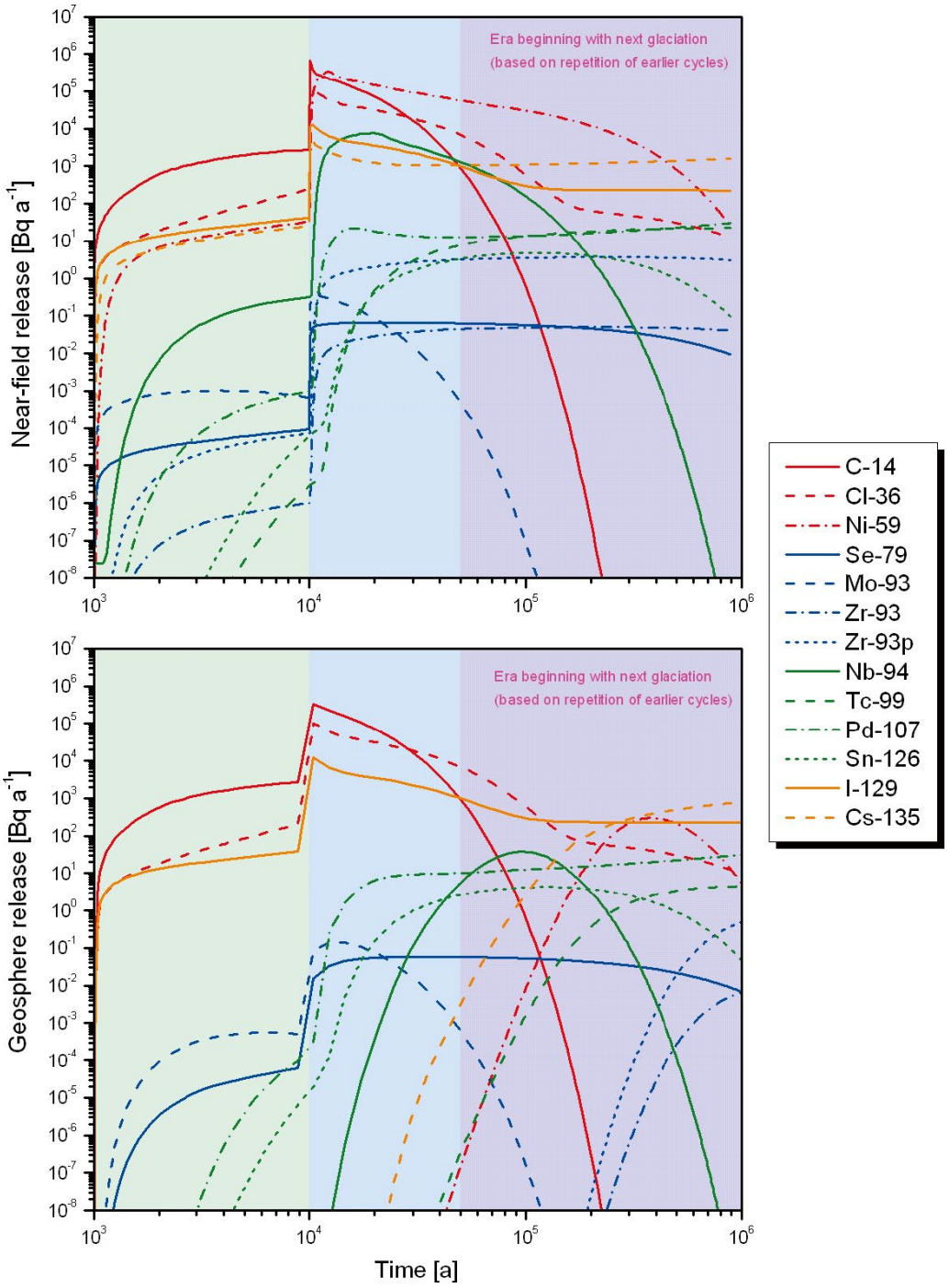

Figure G-31. *Release rates of activation and fission products from the near field (upper figure) and geosphere (lower figure) as functions of time in case PD-NFSLV.*

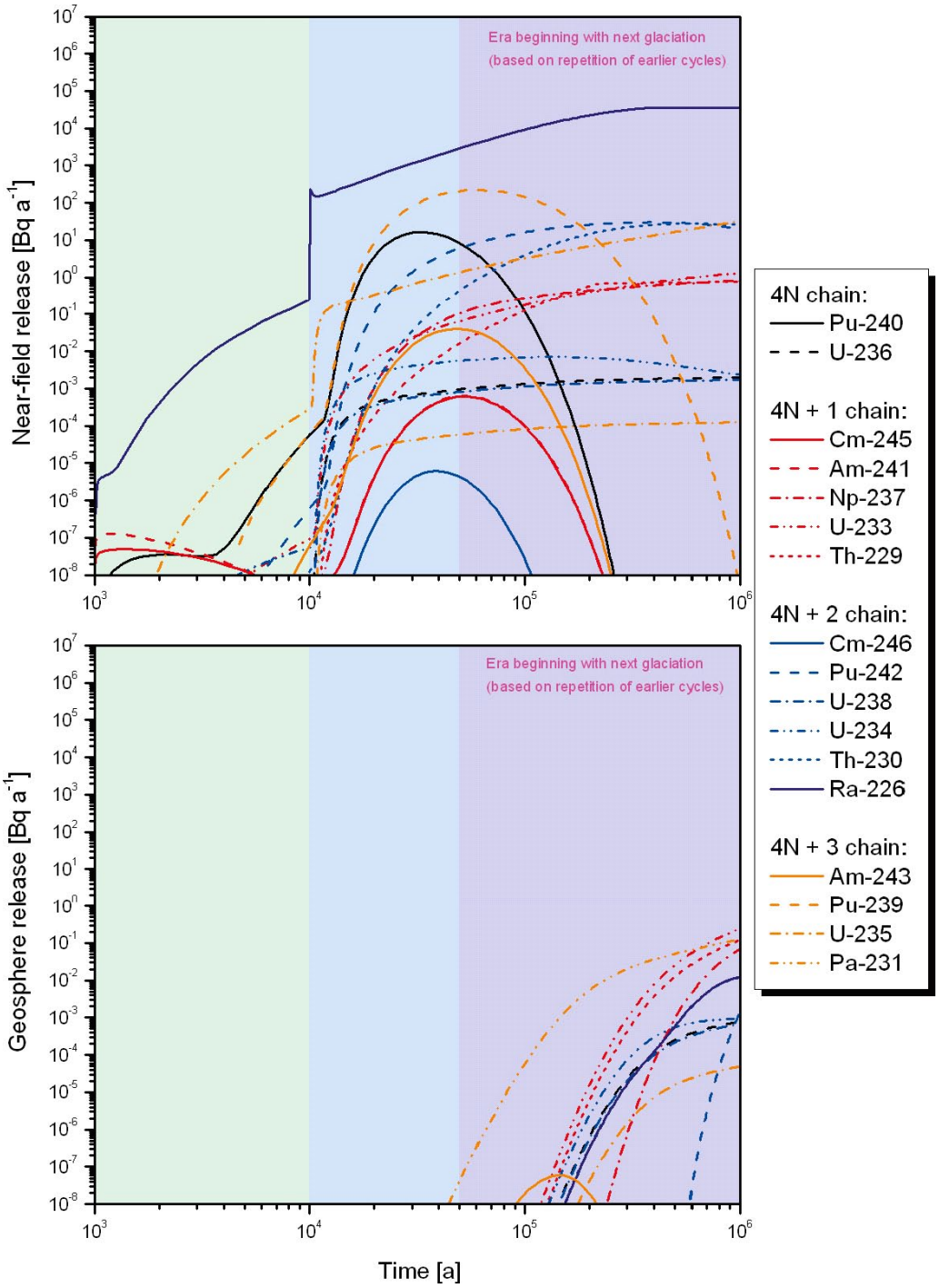

Figure G-32. *Release rates of actinide chain members from the geosphere as functions of time in case PD-NFSLV.*

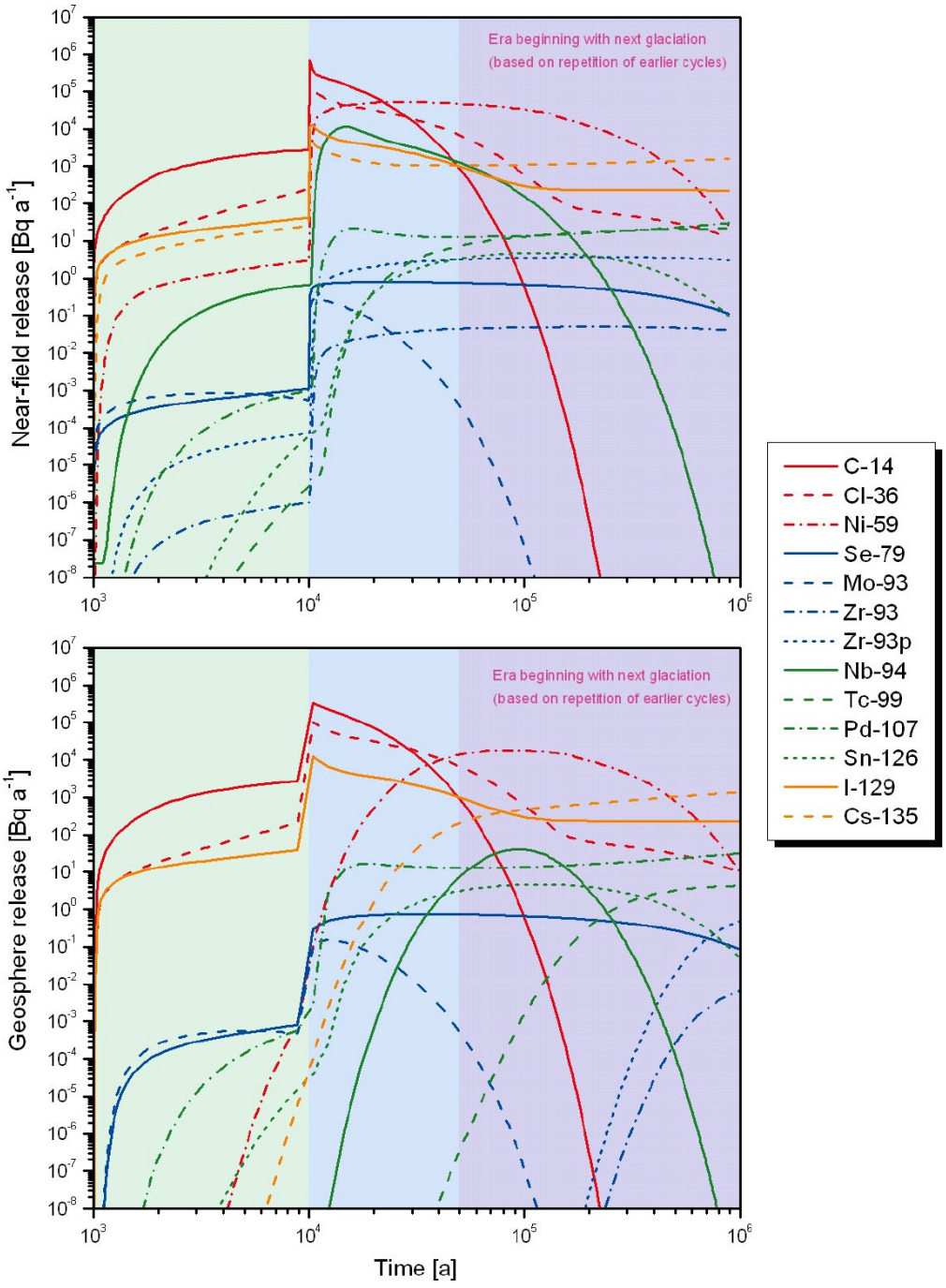

Figure G-33. *Release rates of activation and fission products from the near field (upper figure) and geosphere (lower figure) as functions of time in case PD-SAL.*

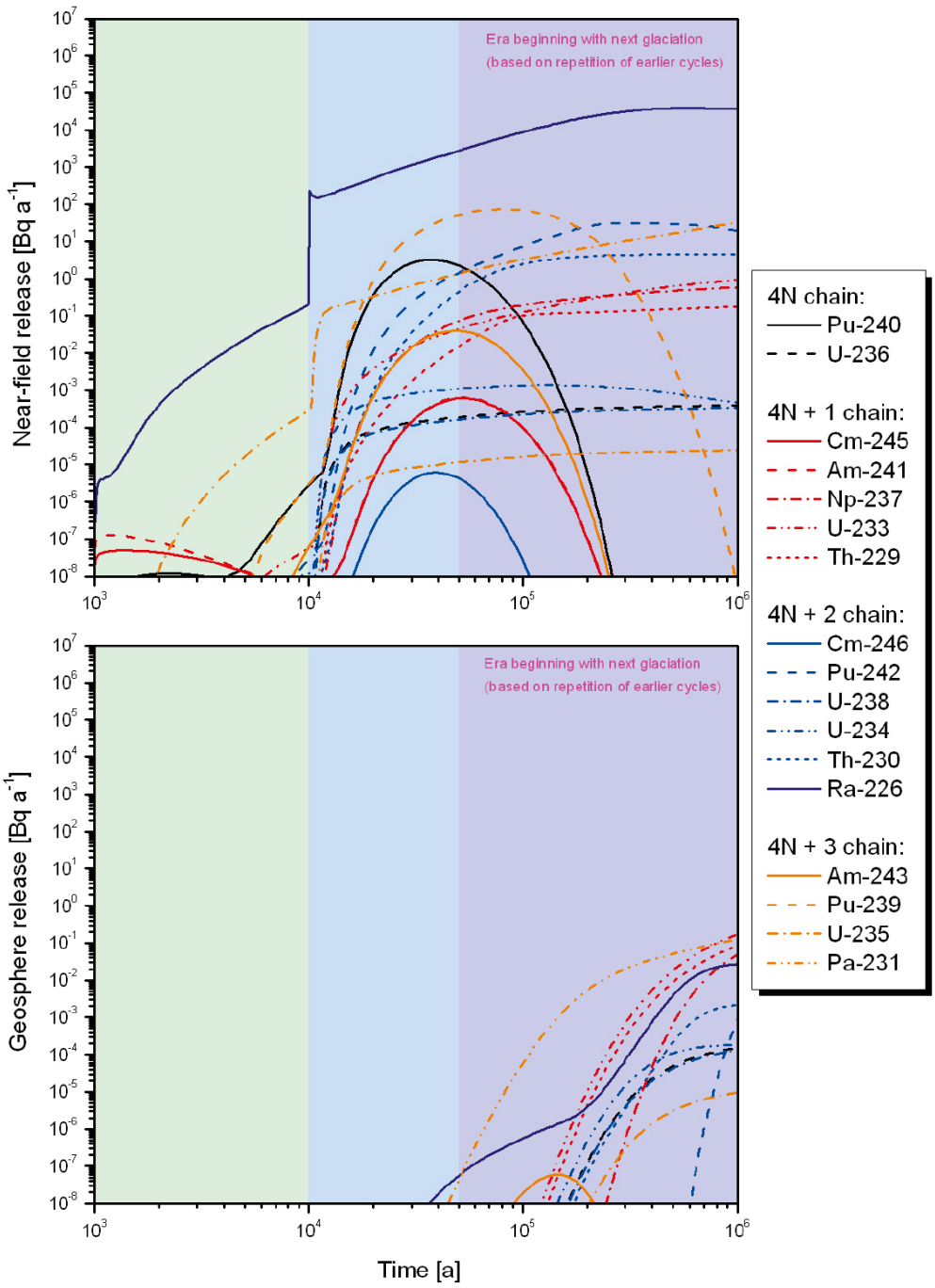

Figure G-34. *Release rates of actinide chain members from the geosphere as functions of time in case PD-SAL.*

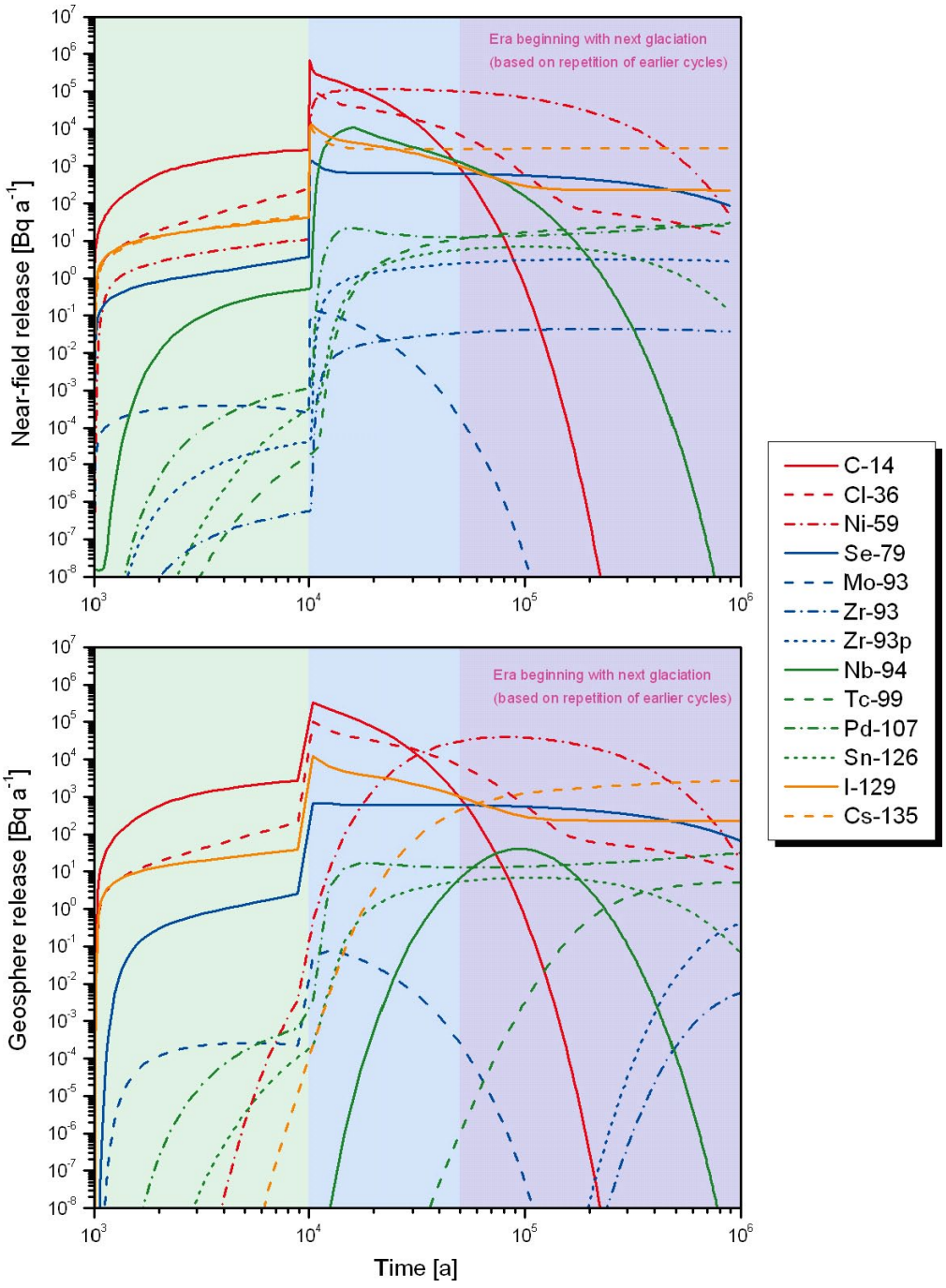

Figure G-35. *Release rates of activation and fission products from the near field (upper figure) and geosphere (lower figure) as functions of time in case PD-HISAL.*

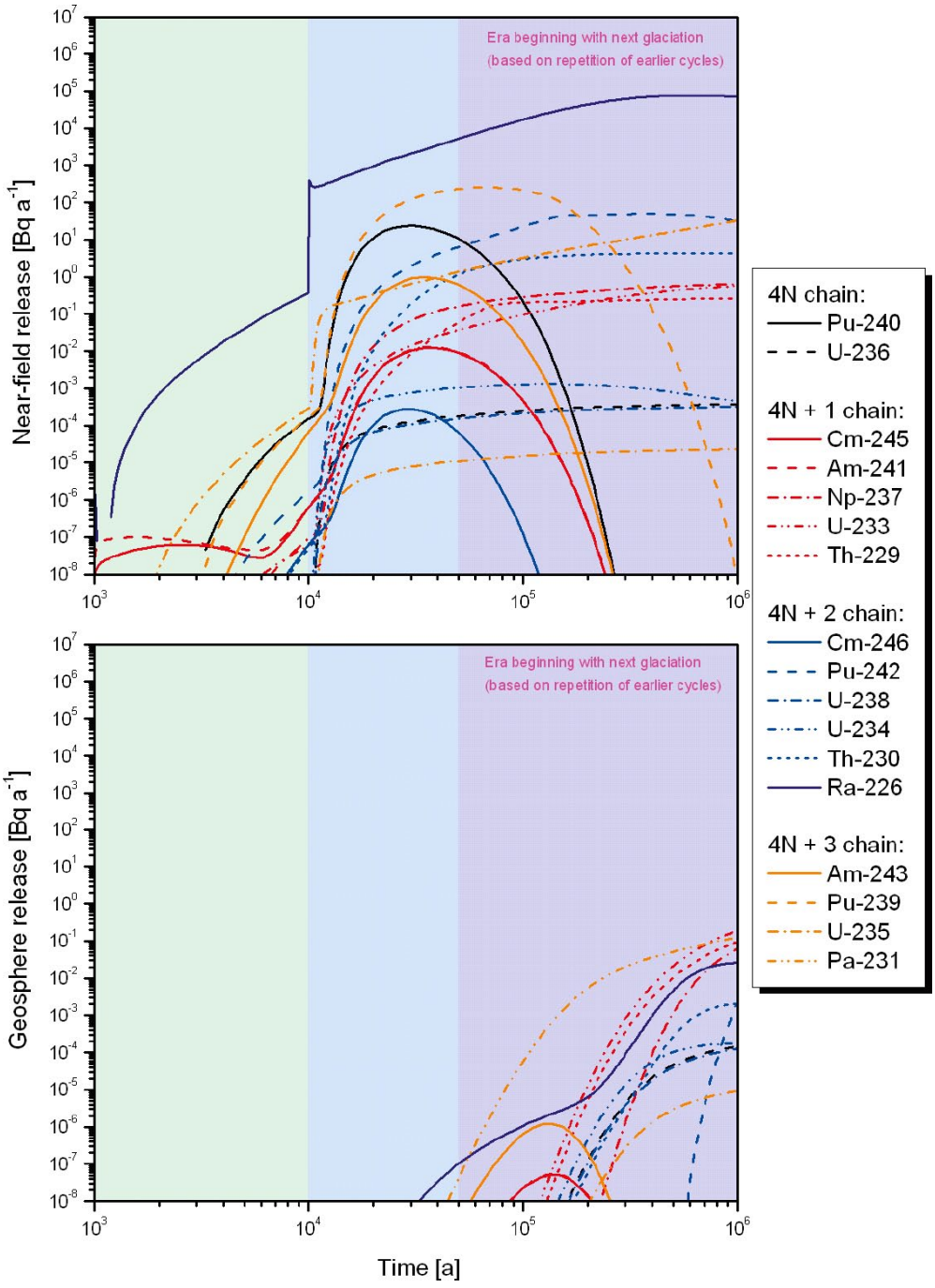

Figure G-36. *Release rates of actinide chain members from the geosphere as functions of time in case PD-HISAL.*

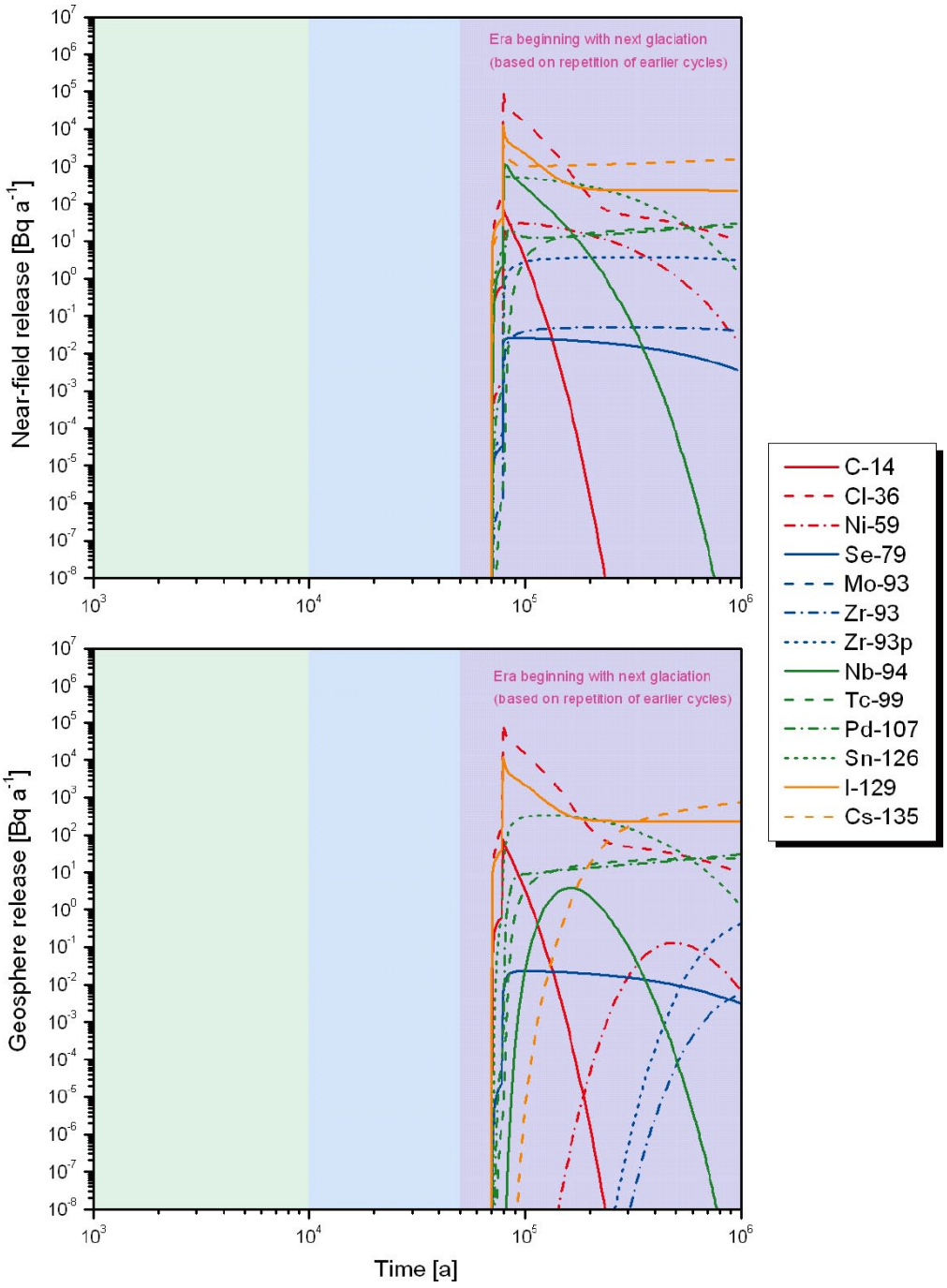

Figure G-37. *Release rates of activation and fission products from the near field (upper figure) and geosphere (lower figure) as functions of time in case PD-GMW.*

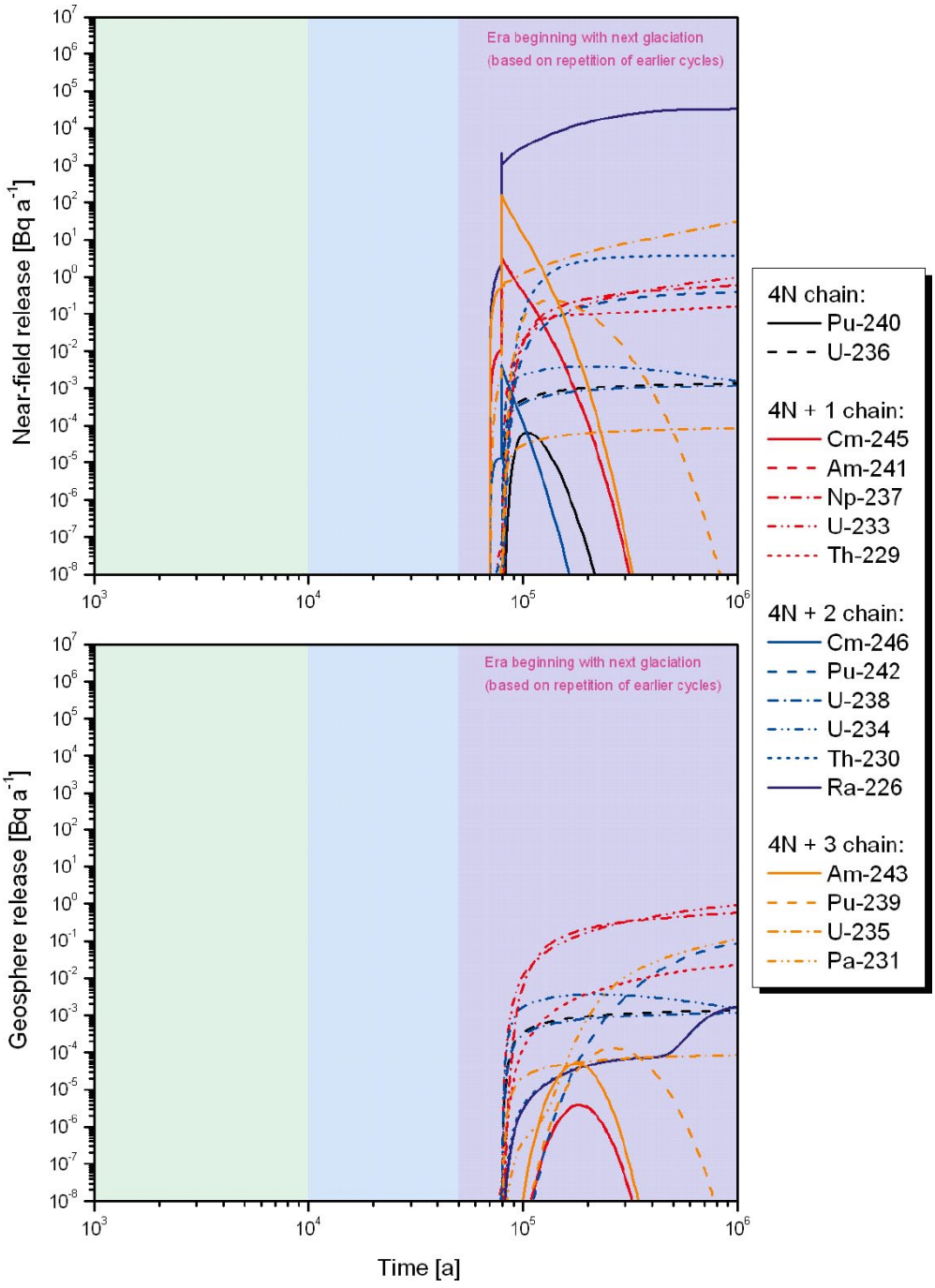

Figure G-38. *Release rates of actinide chain members from the geosphere as functions of time in case PD-GMW.*

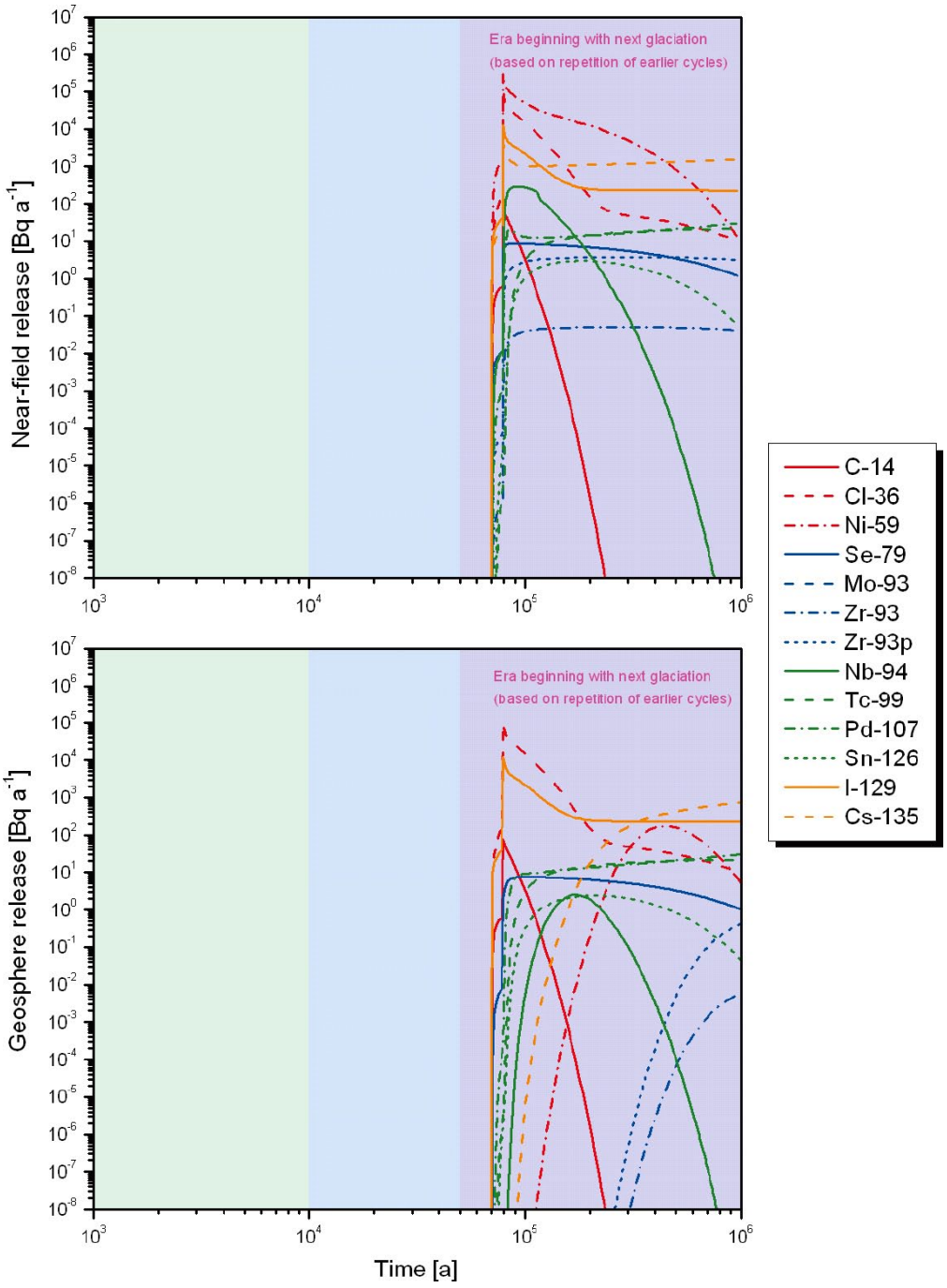

Figure G-39. *Release rates of activation and fission products from the near field (upper figure) and geosphere (lower figure) as functions of time in case PD-GMWV.*

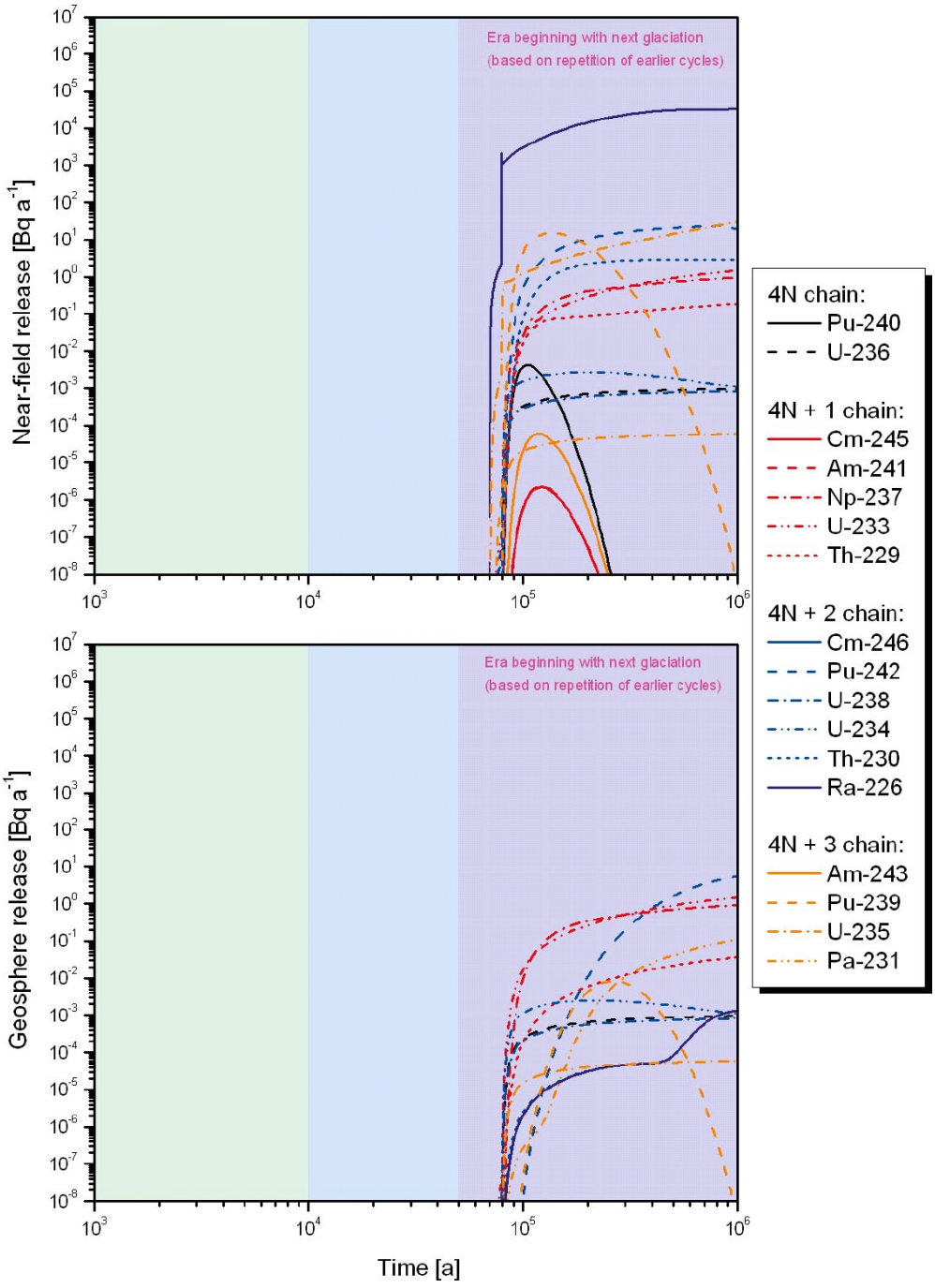

Figure G-40. *Release rates of actinide chain members from the geosphere as functions of time in case PD-GMWV.*

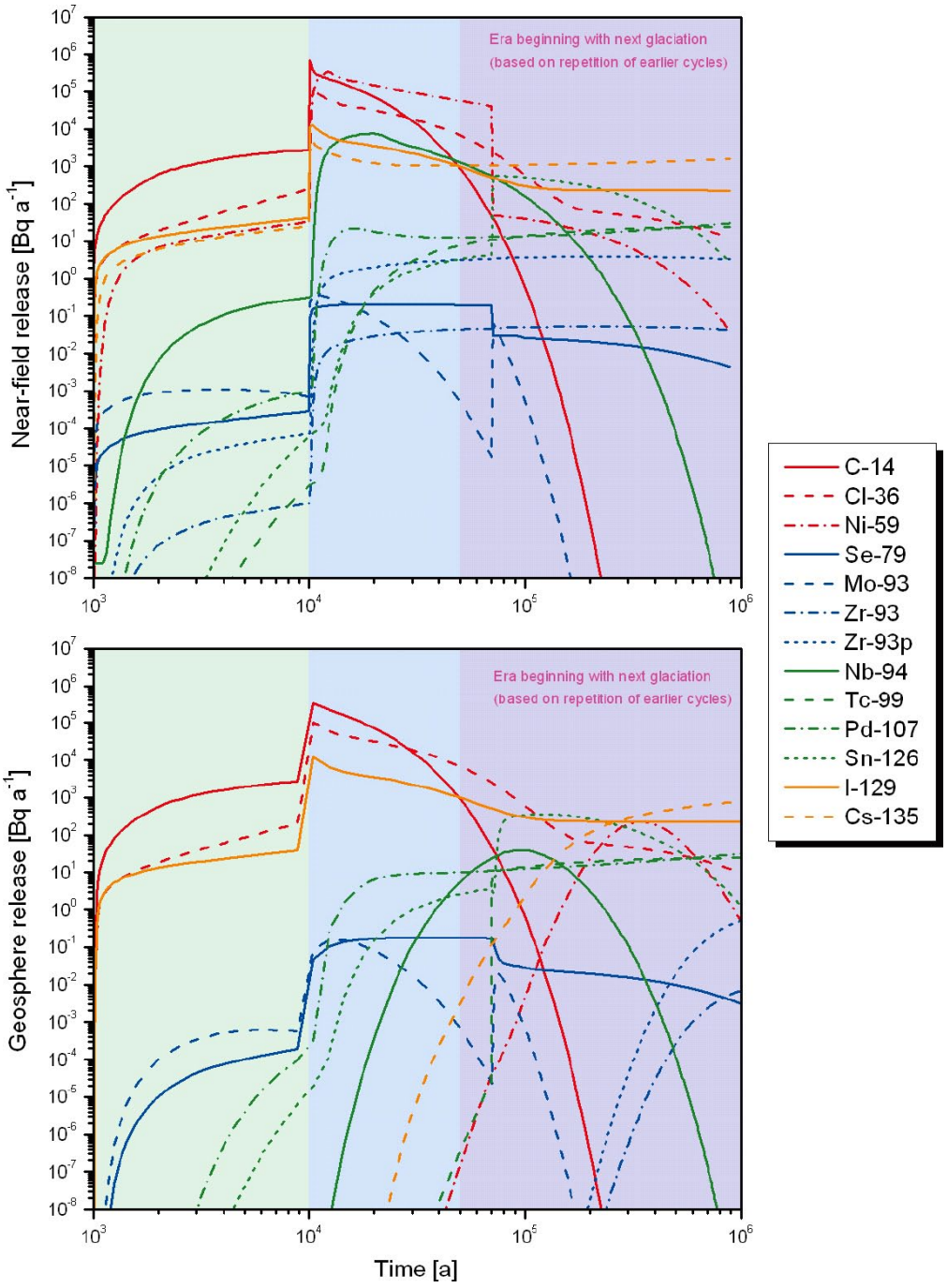

Figure G-41. *Release rates of activation and fission products from the near field (upper figure) and geosphere (lower figure) as functions of time in case PD-GMWC.*

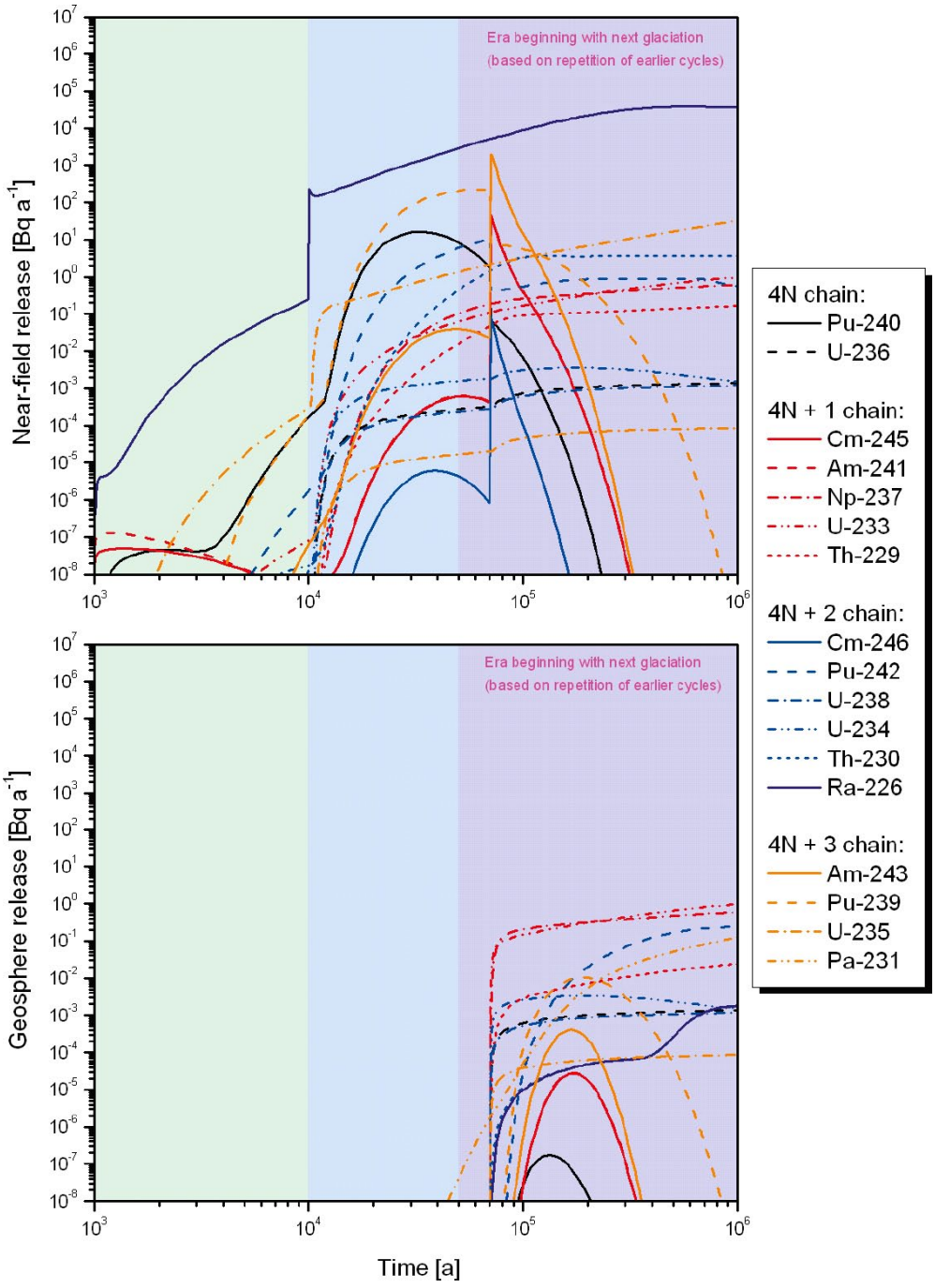

Figure G-42. *Release rates of actinide chain members from the geosphere as functions of time in case PD-GMWC.*

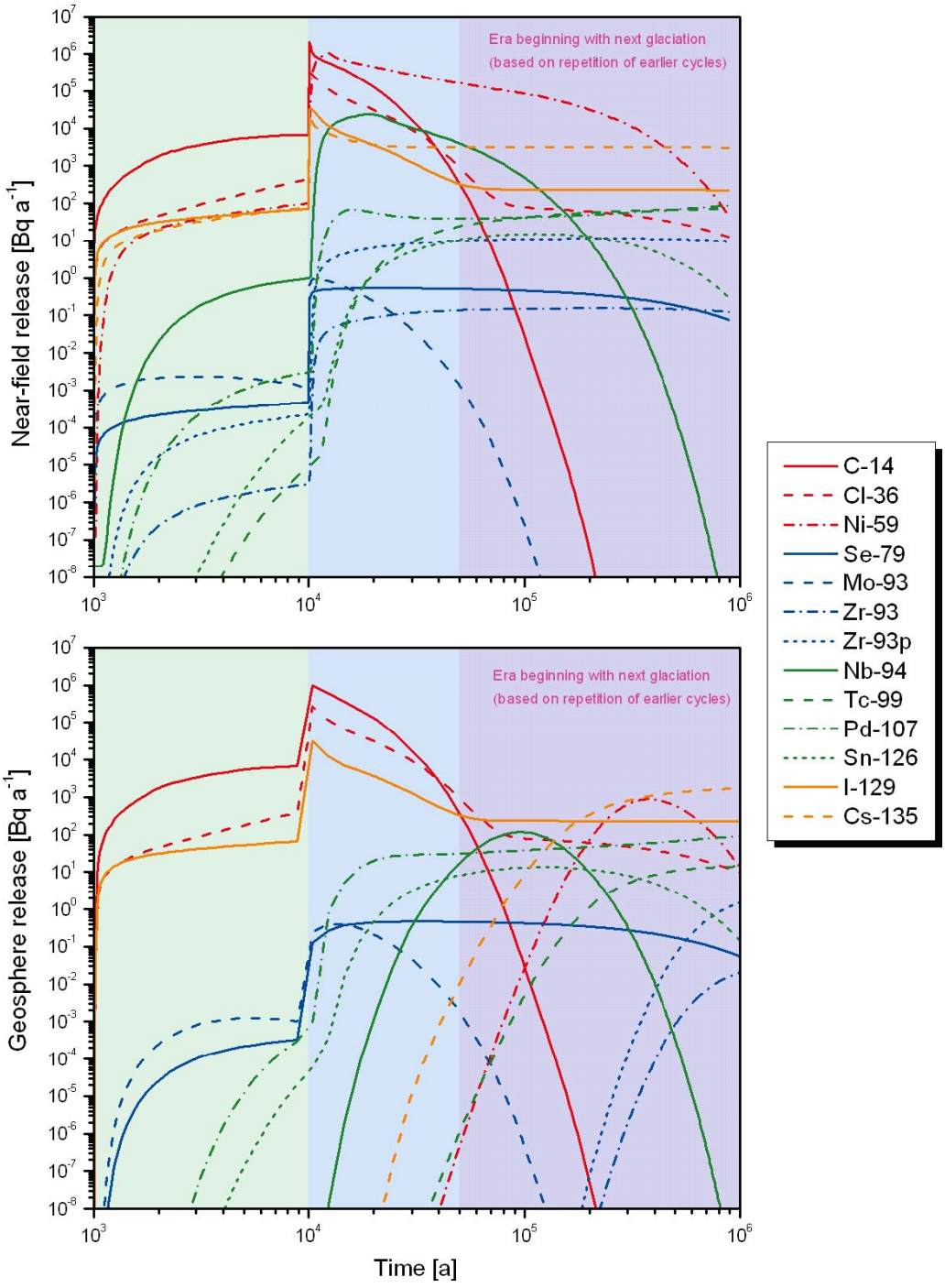

Figure G-43. *Release rates of activation and fission products from the near field (upper figure) and geosphere (lower figure) as functions of time in case PD-HIFLOW.*

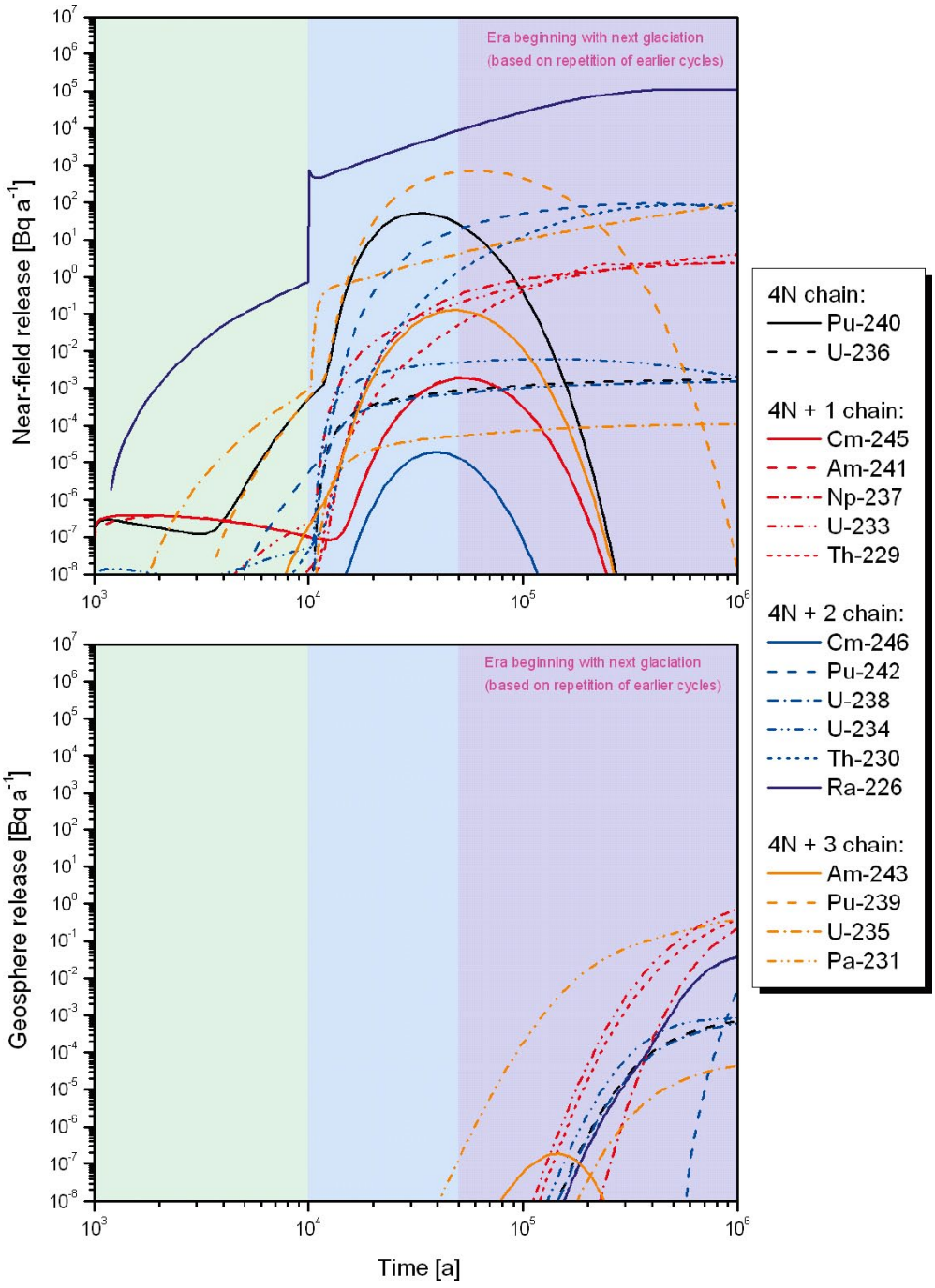

Figure G-44. *Release rates of actinide chain members from the geosphere as functions of time in case PD-HIFLOW.*

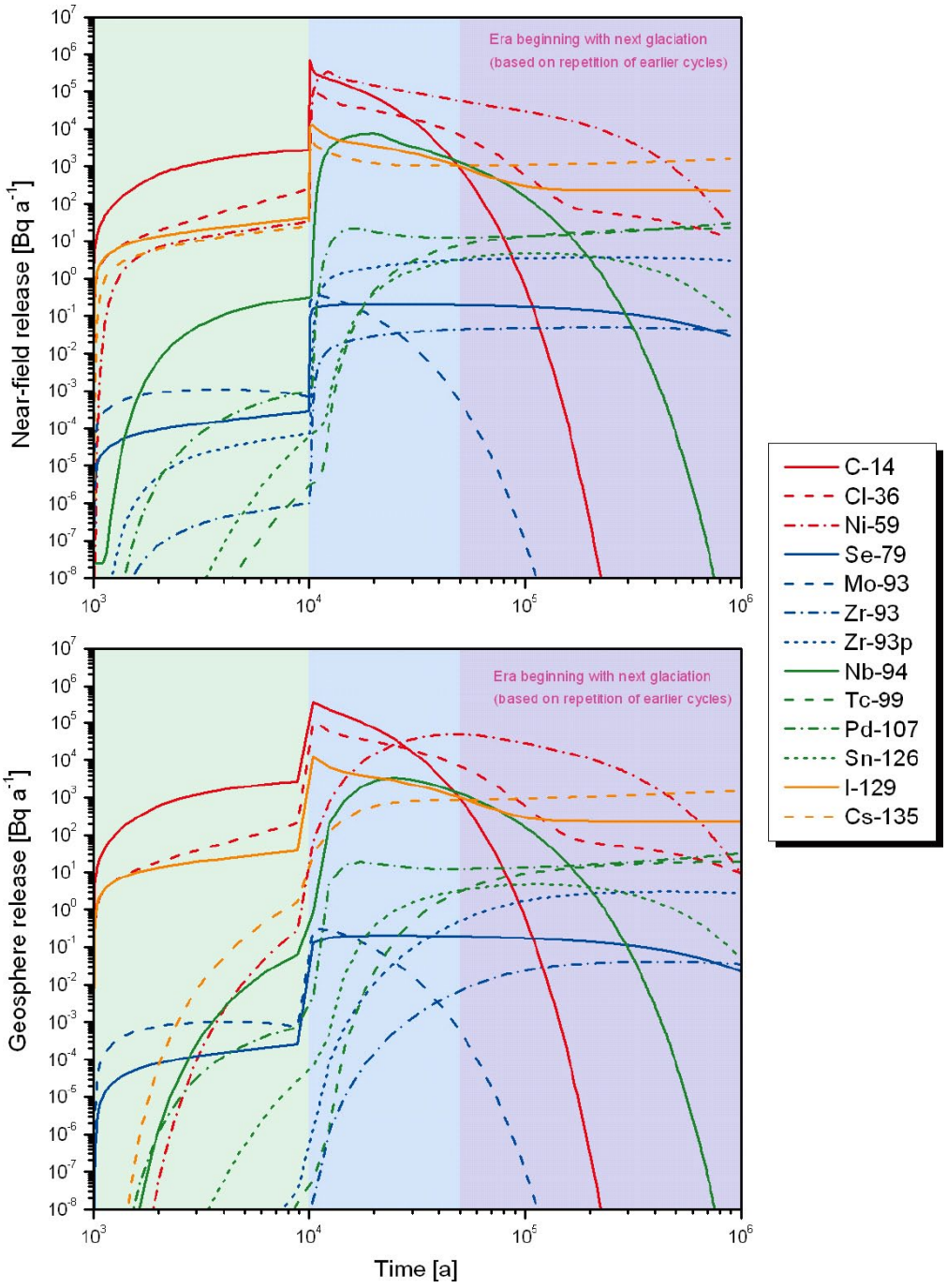

Figure G-45. *Release rates of activation and fission products from the near field (upper figure) and geosphere (lower figure) as functions of time in case PD-LOGEOR.*

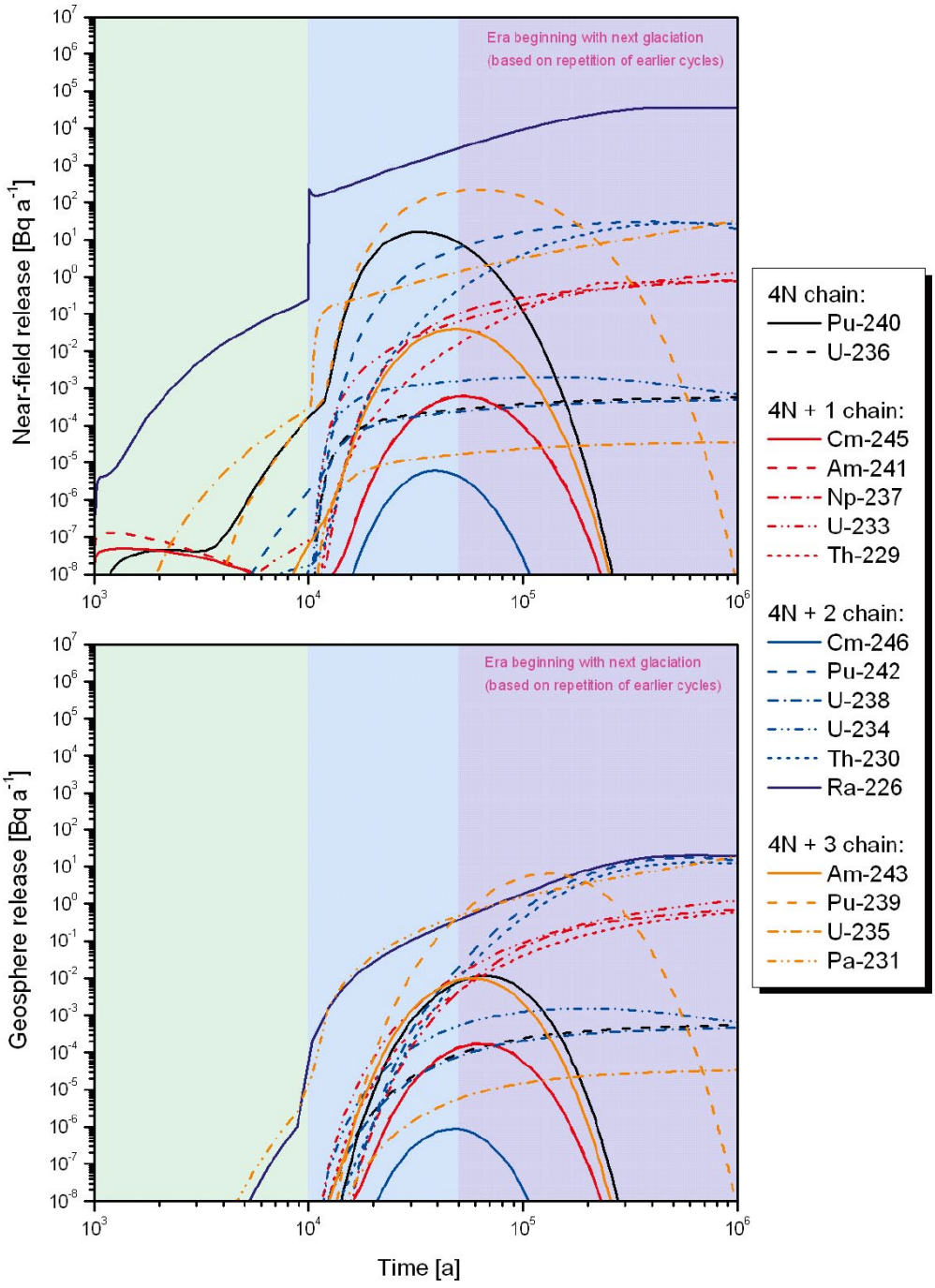

Figure G-46. *Release rates of actinide chain members from the geosphere as functions of time in case PD-LOGEOR.*

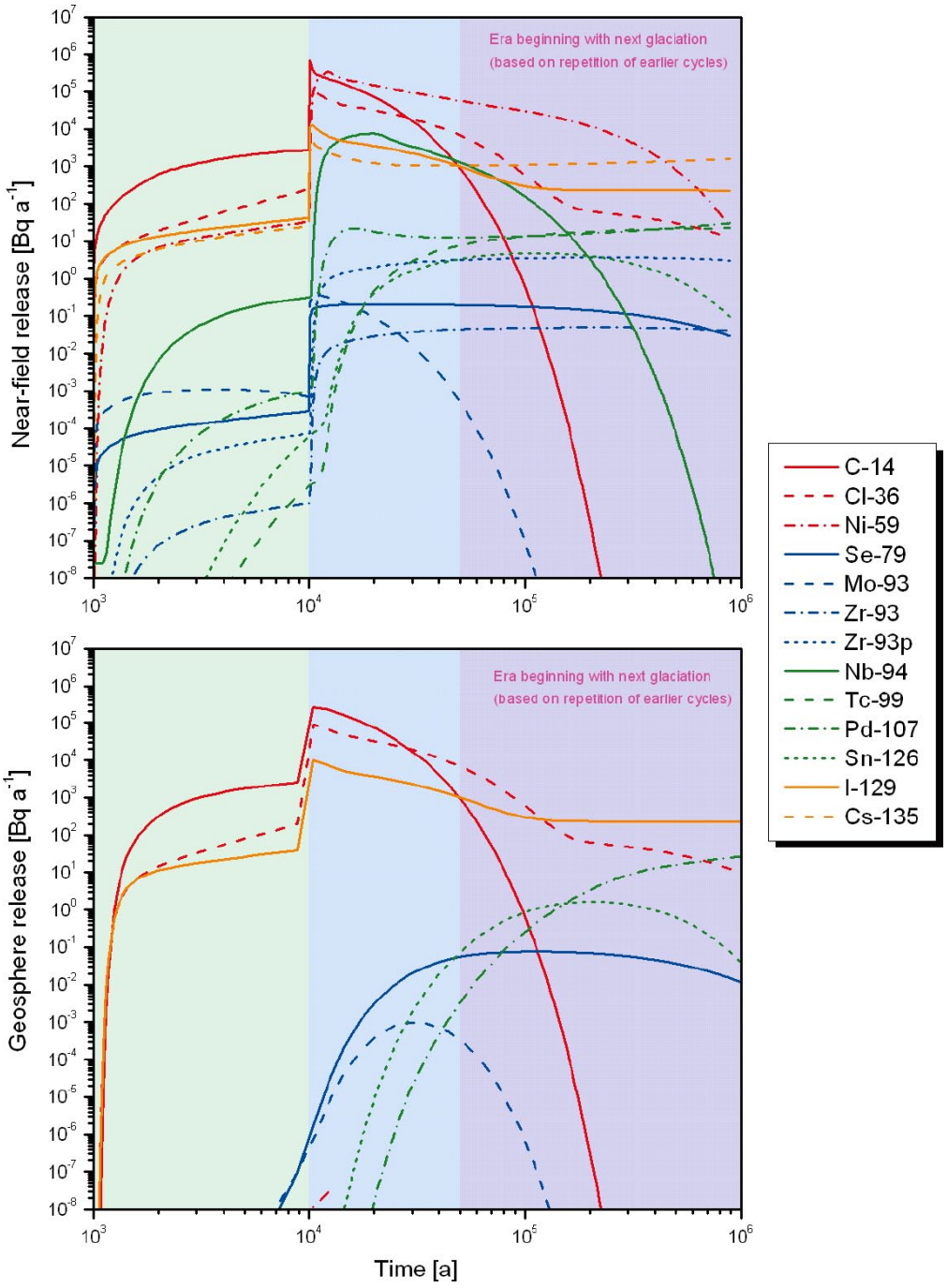

Figure G-47. *Release rates of activation and fission products from the near field (upper figure) and geosphere (lower figure) as functions of time in case PD-HIGEOR.*

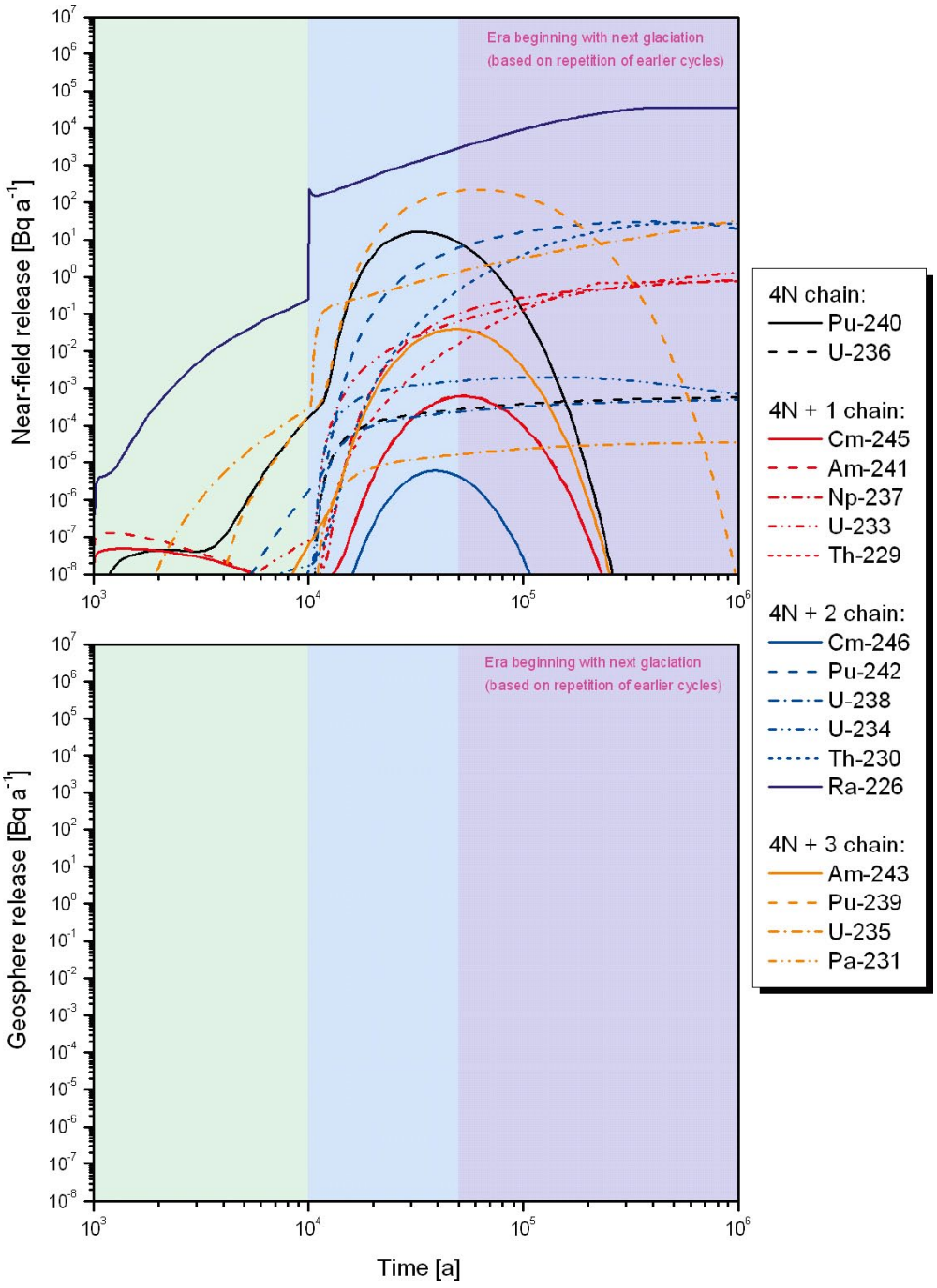

Figure G-48. *Release rates of actinide chain members from the geosphere as functions of time in case PD-HIGEOR.*

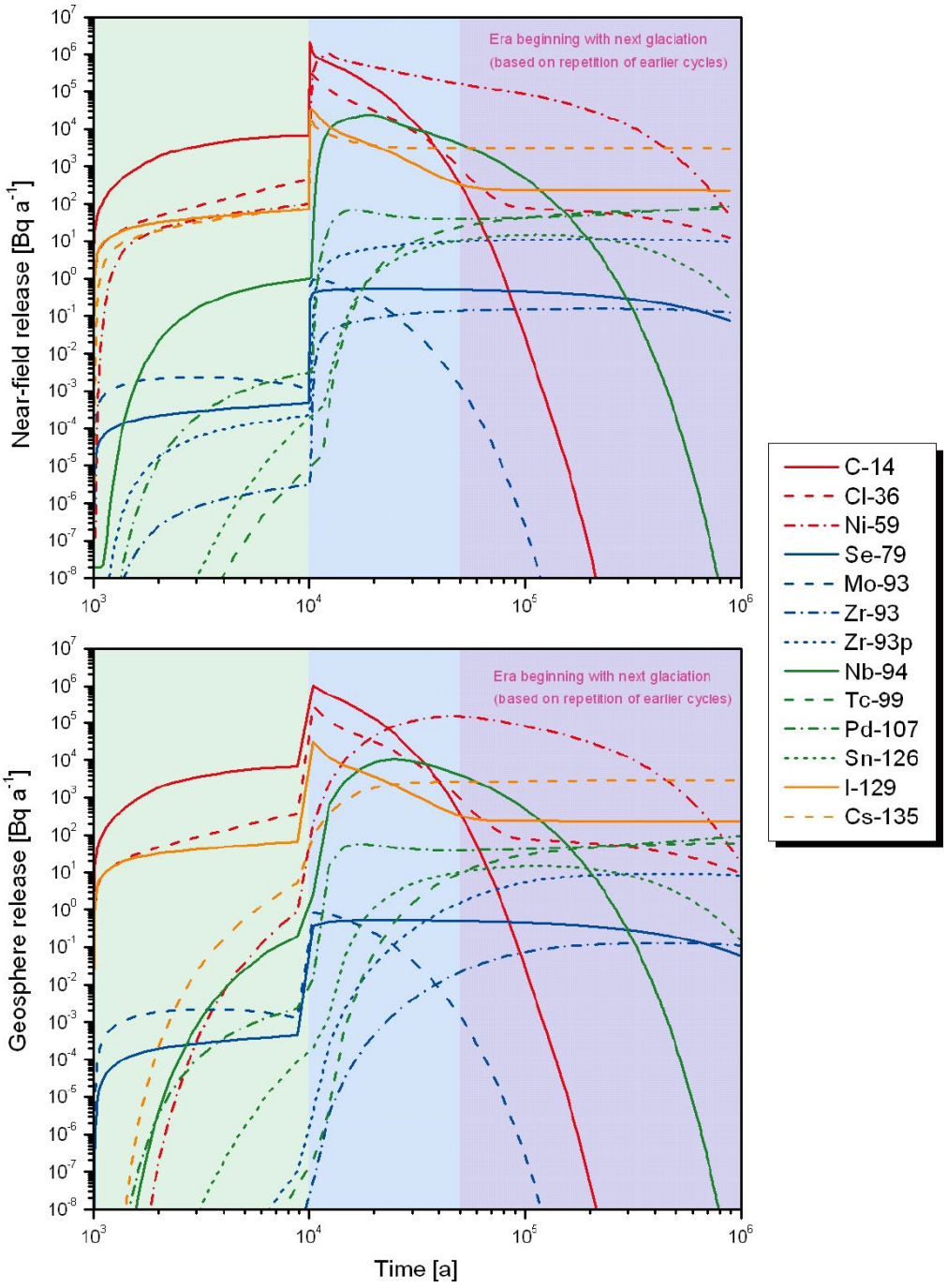

Figure G-49. *Release rates of activation and fission products from the near field (upper figure) and geosphere (lower figure) as functions of time in case PD-HIFLOWR.*

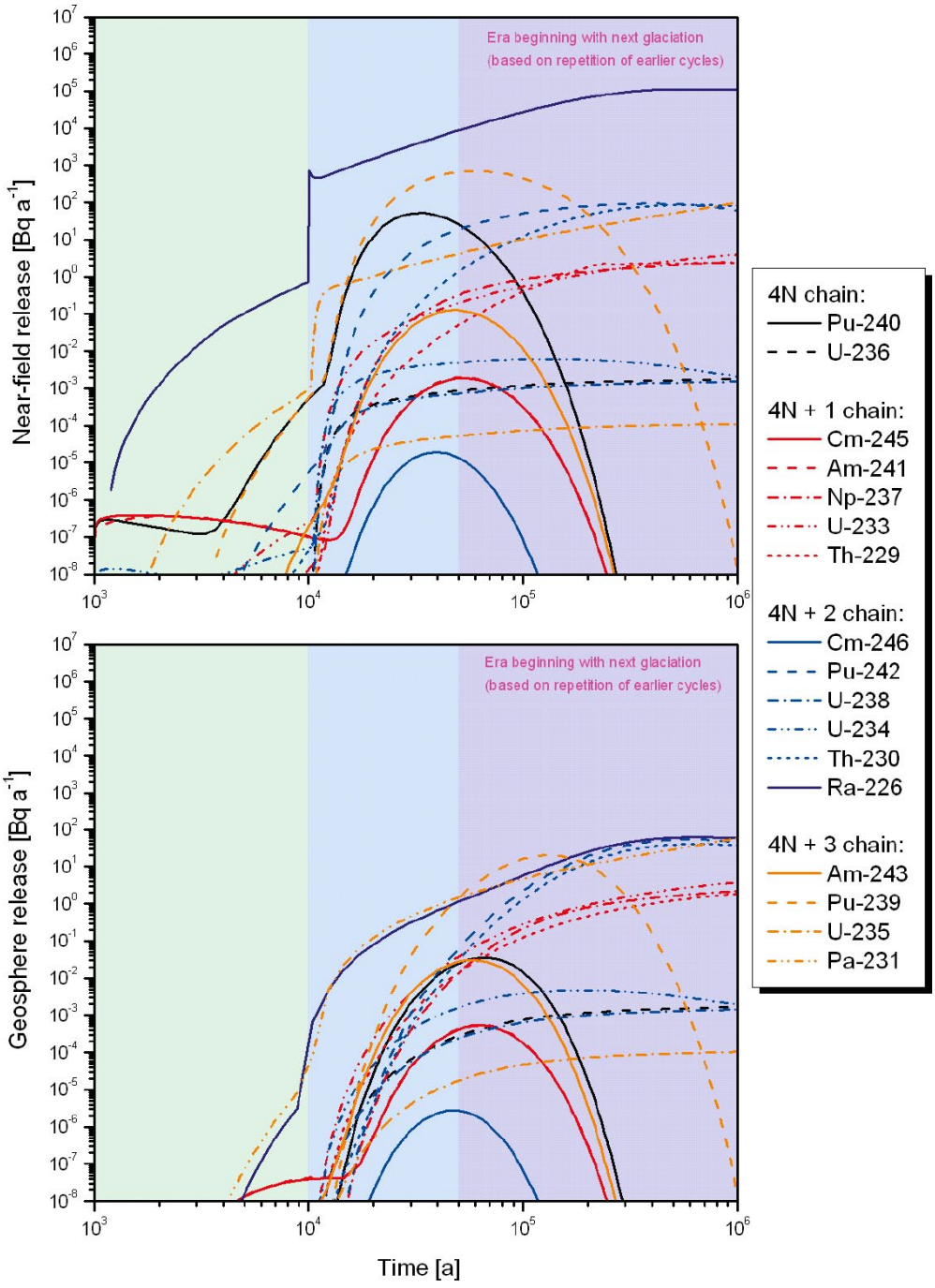

Figure G-50. *Release rates of actinide chain members from the geosphere as functions of time in case PD-HIFLOWR.*

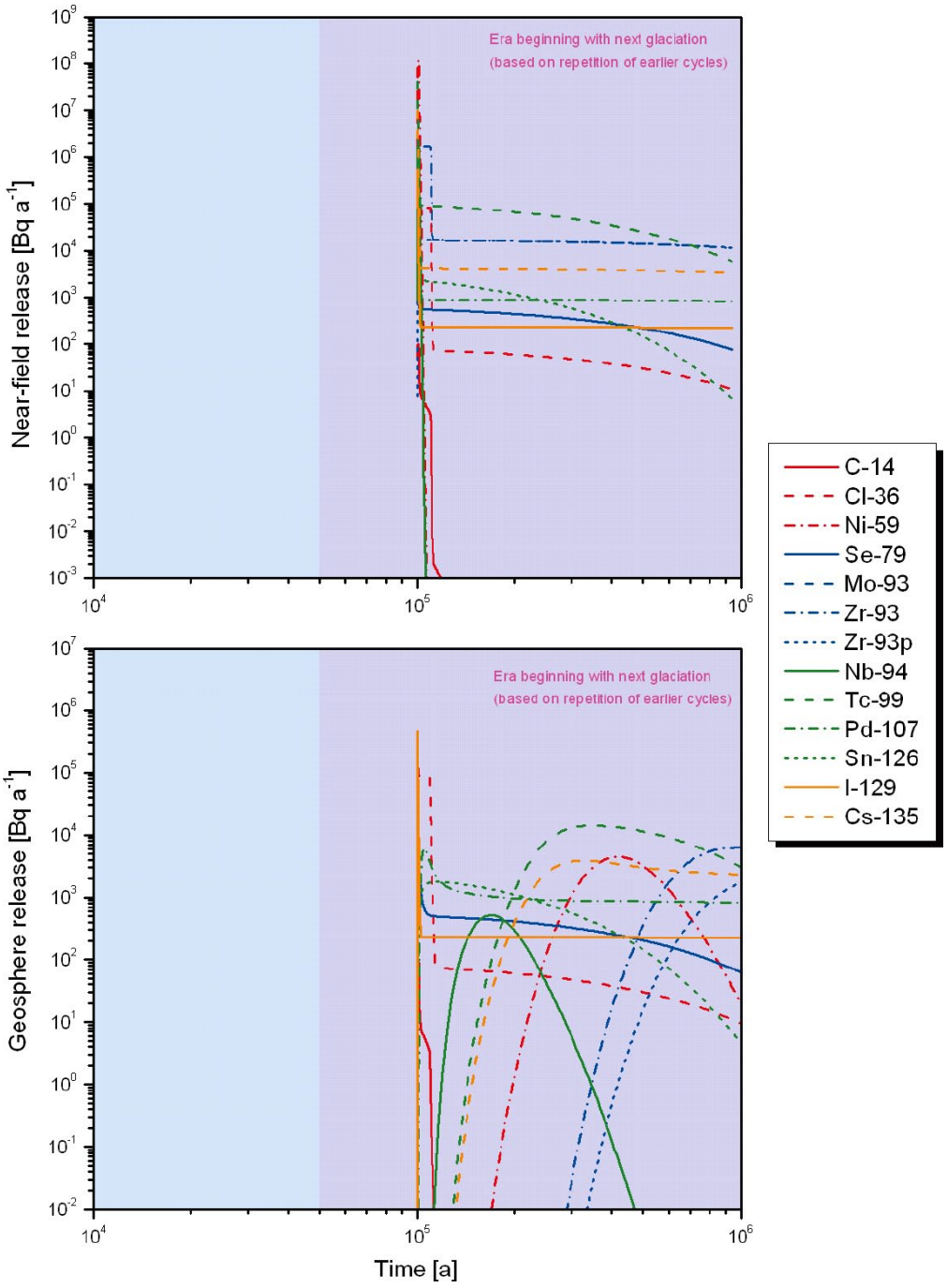

Figure G-51. *Release rates of activation and fission products from the near field (upper figure) and geosphere (lower figure) as functions of time in case CC-BC.*

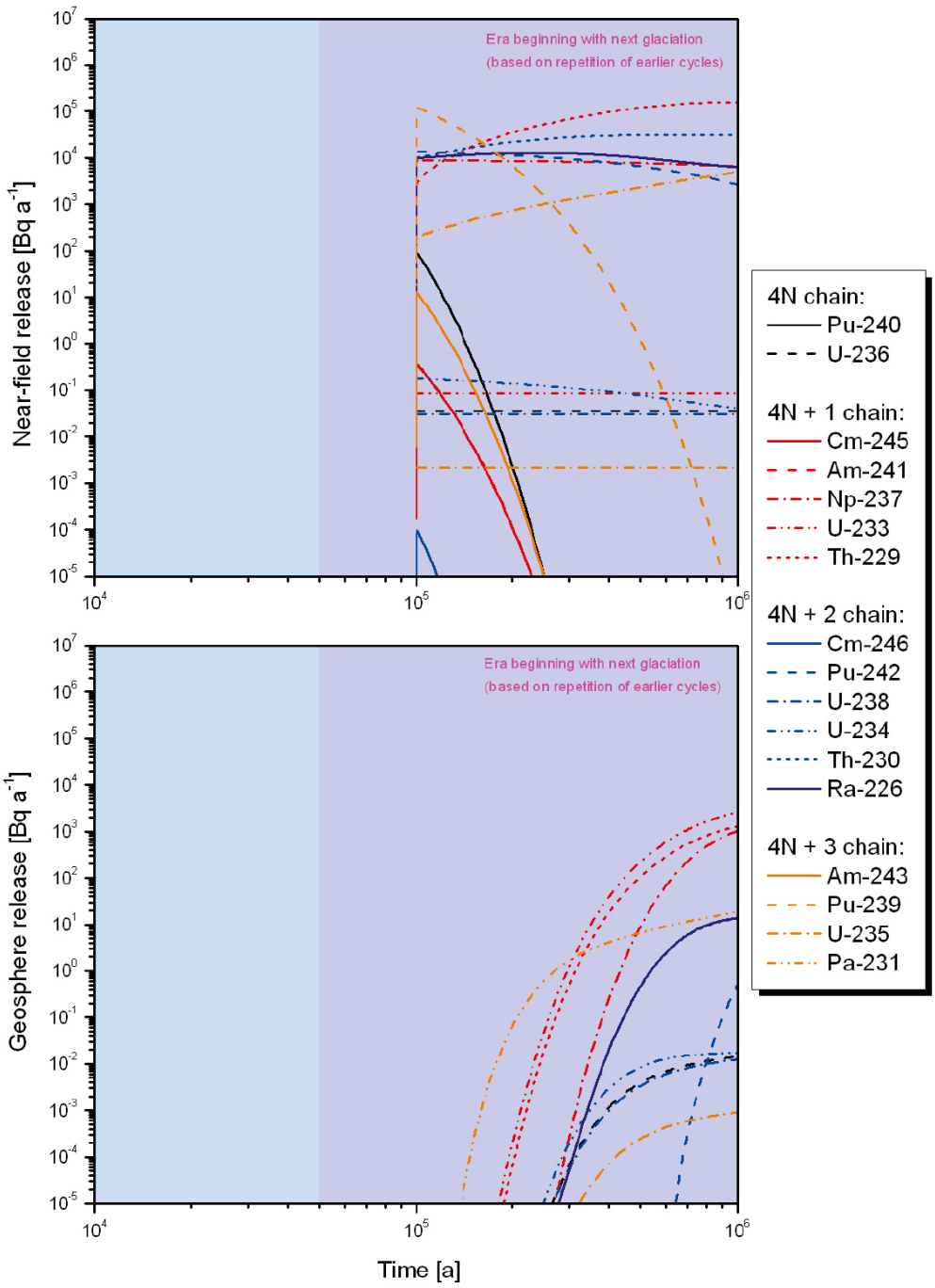

Figure G-52. *Release rates of actinide chain members from the geosphere as functions of time in case CC-BC.*

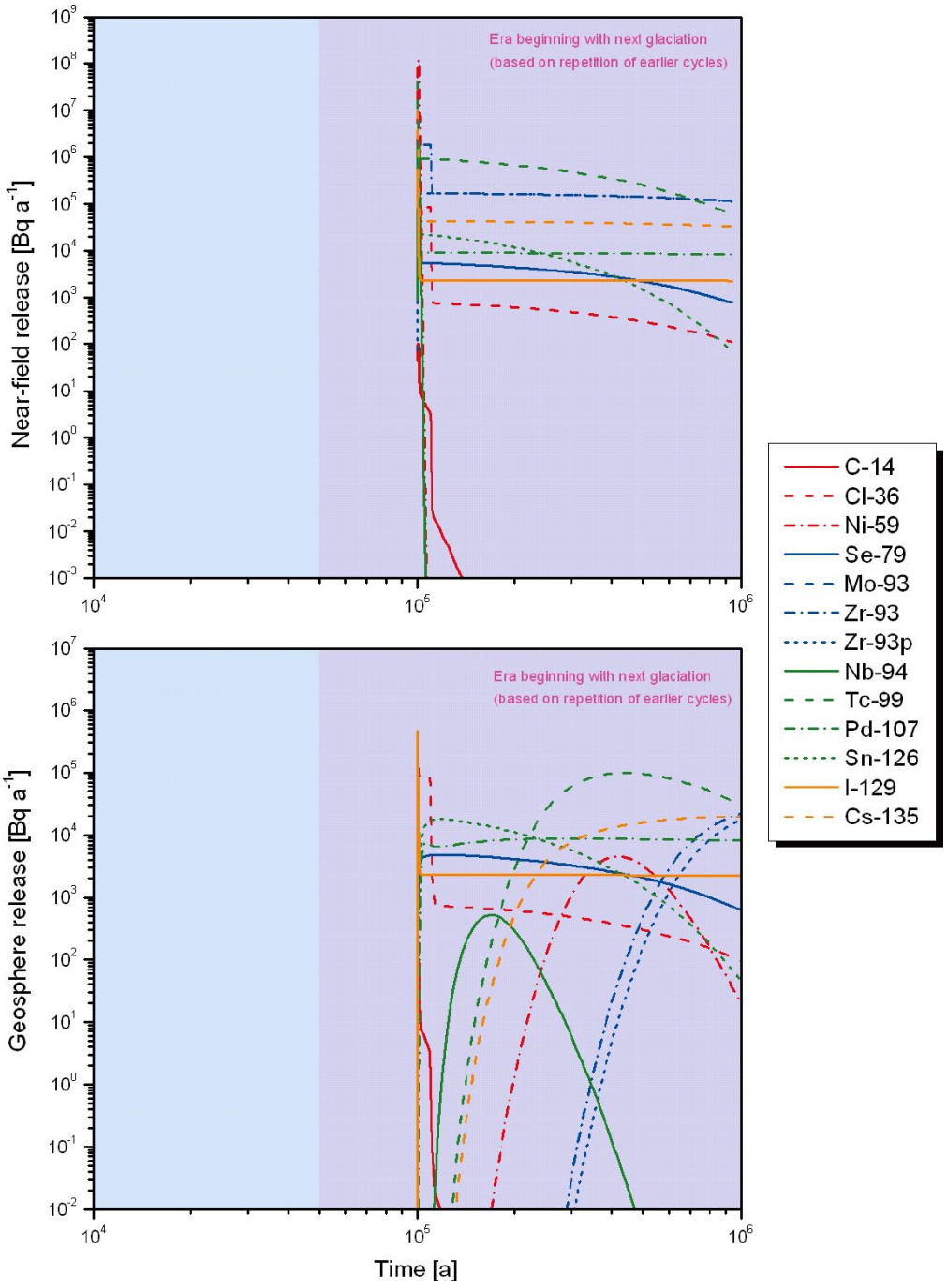

Figure G-53. *Release rates of activation and fission products from the near field (upper figure) and geosphere (lower figure) as functions of time in case CC-HIFDR.*

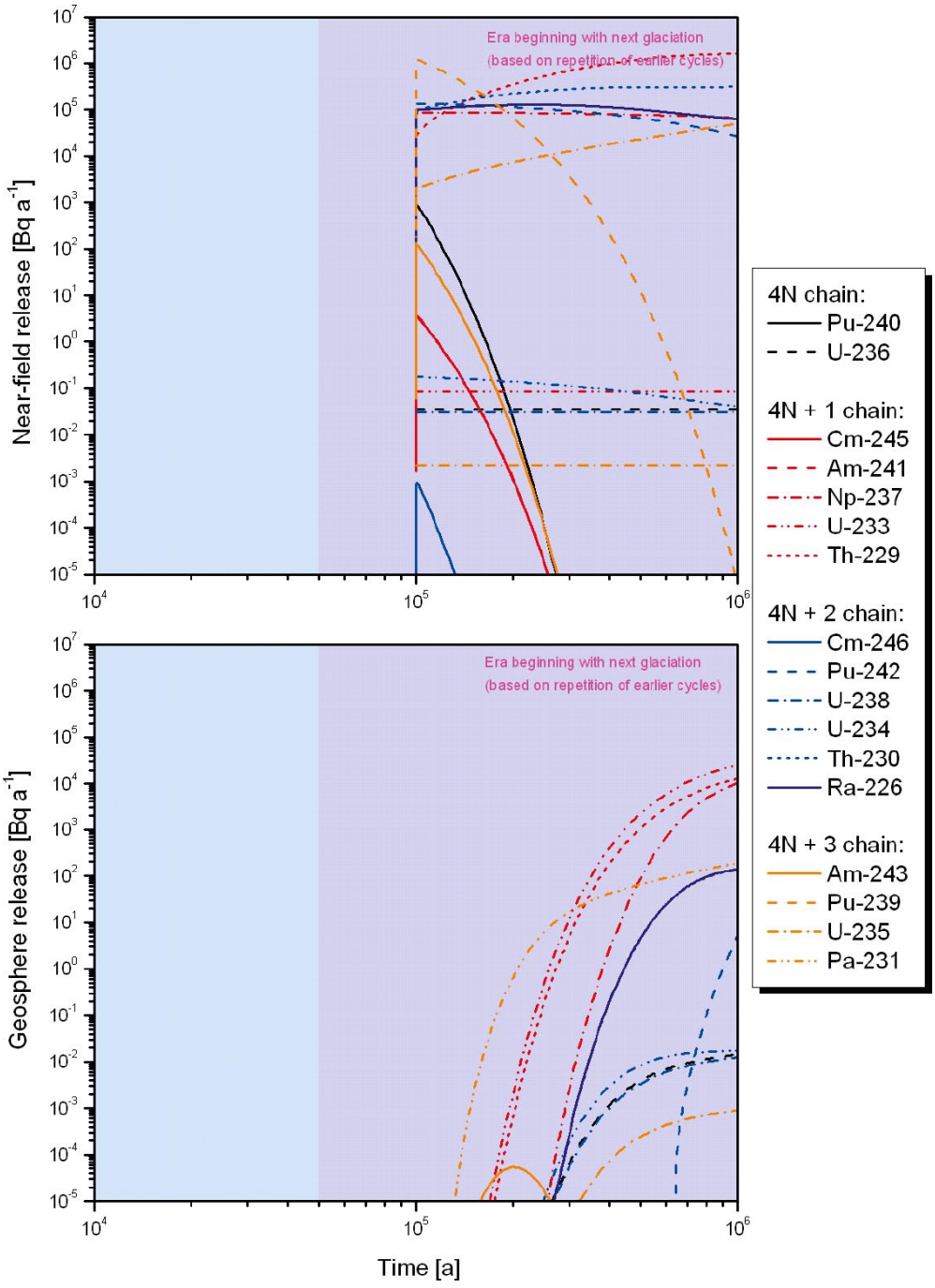

Figure G-54. *Release rates of actinide chain members from the geosphere as functions of time in case CC-HIFDR.*

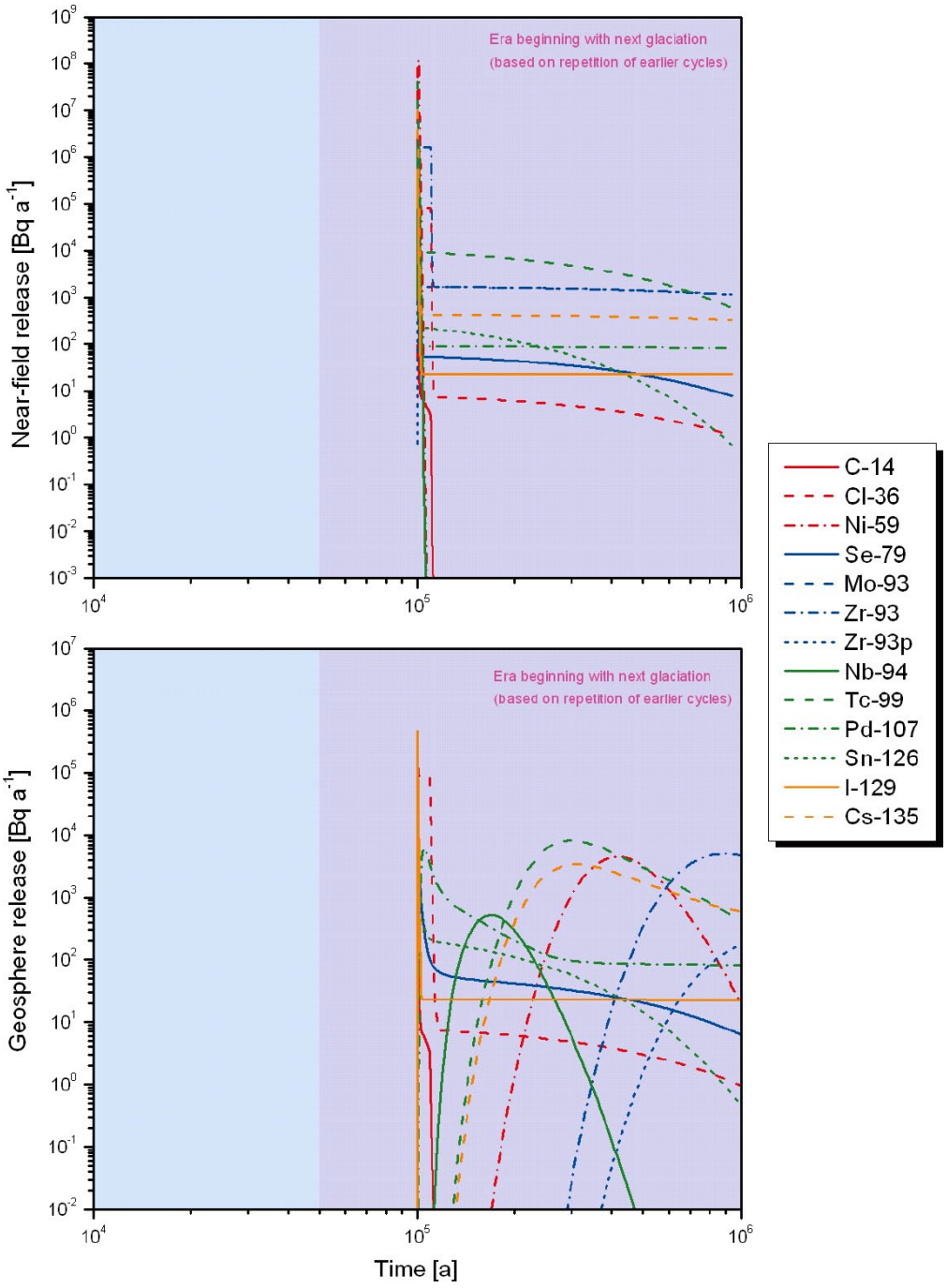

Figure G-55. *Release rates of activation and fission products from the near field (upper figure) and geosphere (lower figure) as functions of time in case CC-LOFDR.*

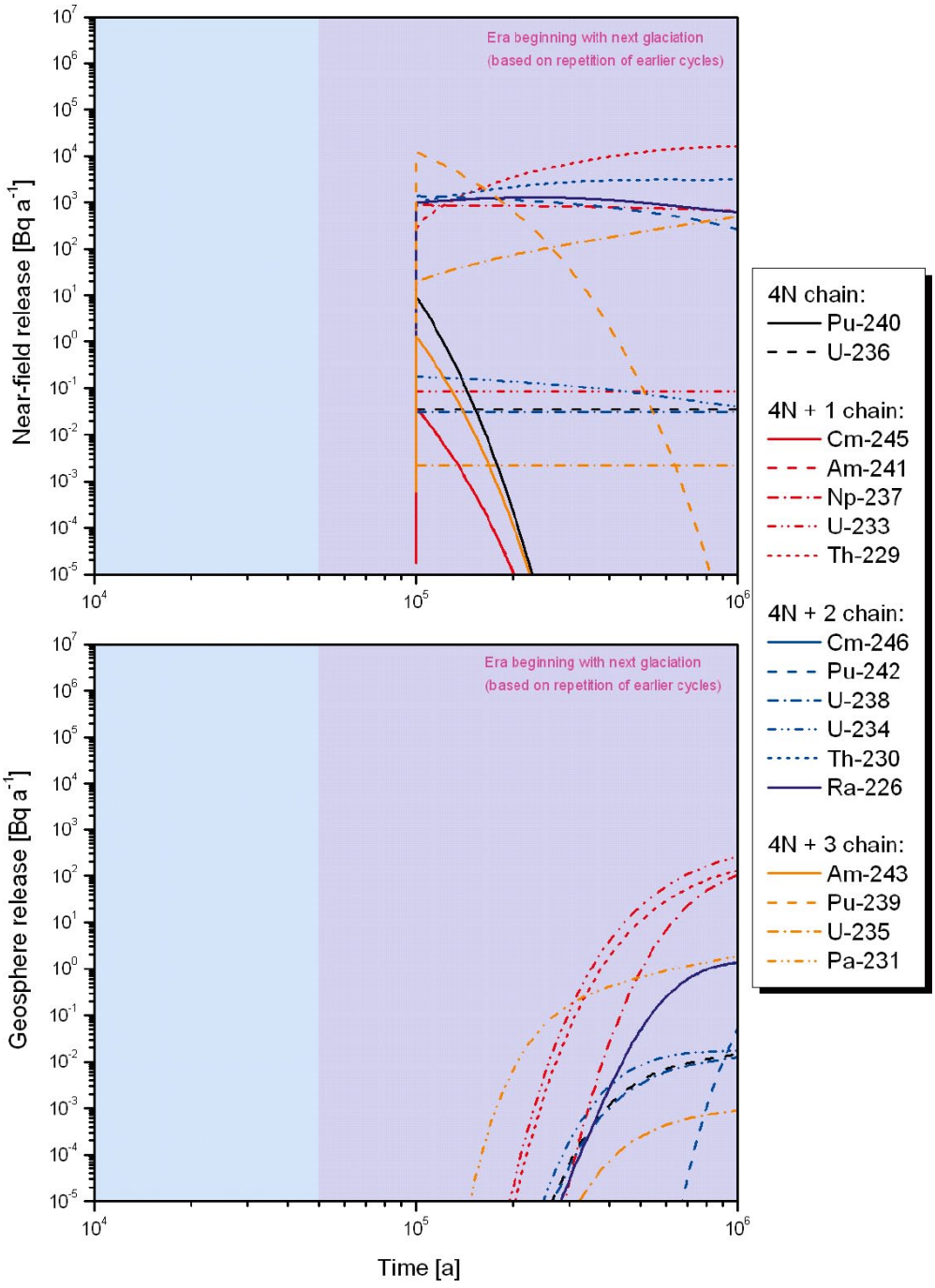

Figure G-56. *Release rates of actinide chain members from the geosphere as functions of time in case CC-LOFDR.*

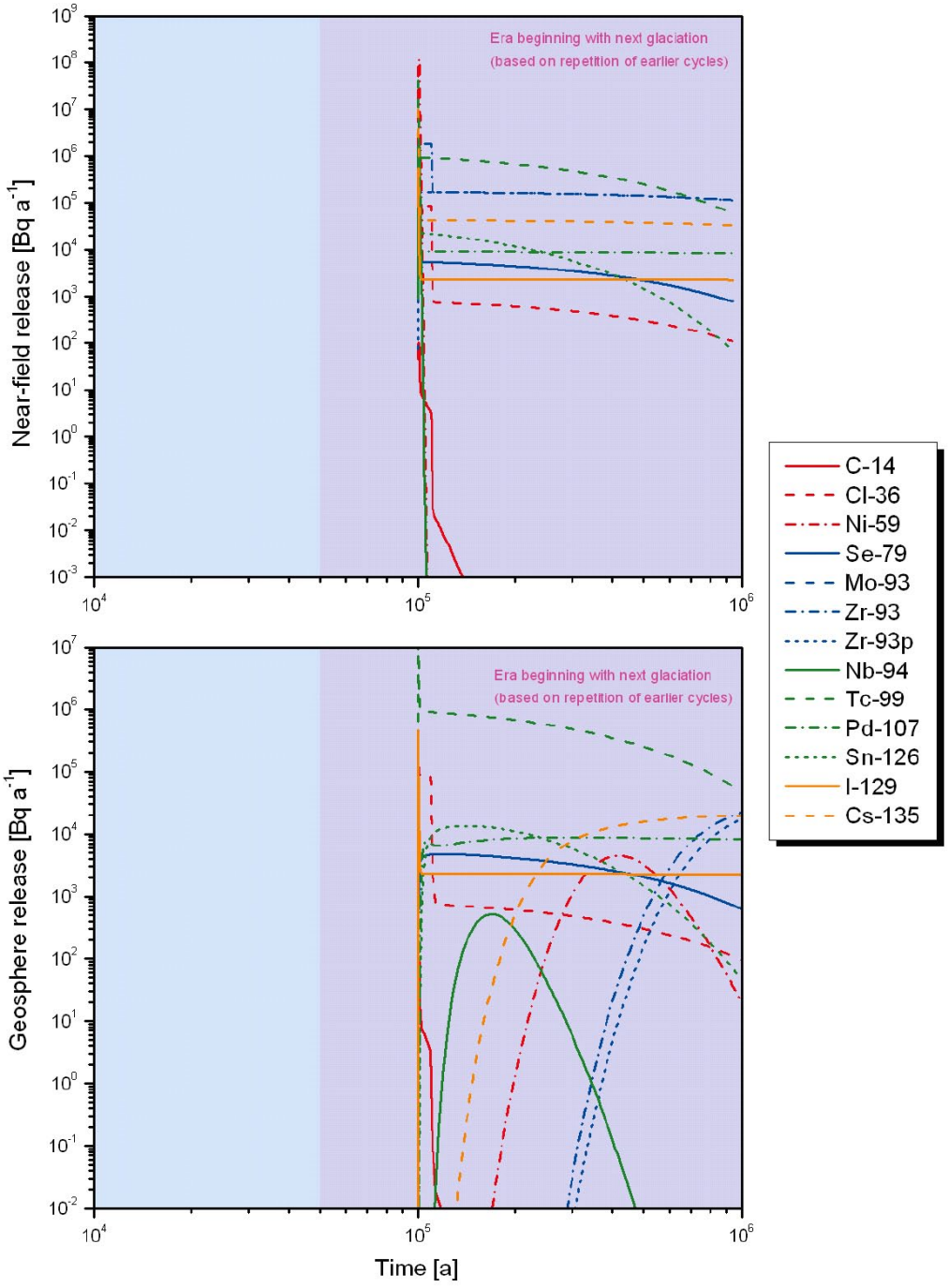

Figure G-57. *Release rates of activation and fission products from the near field (upper figure) and geosphere (lower figure) as functions of time in case CC-GMW.*

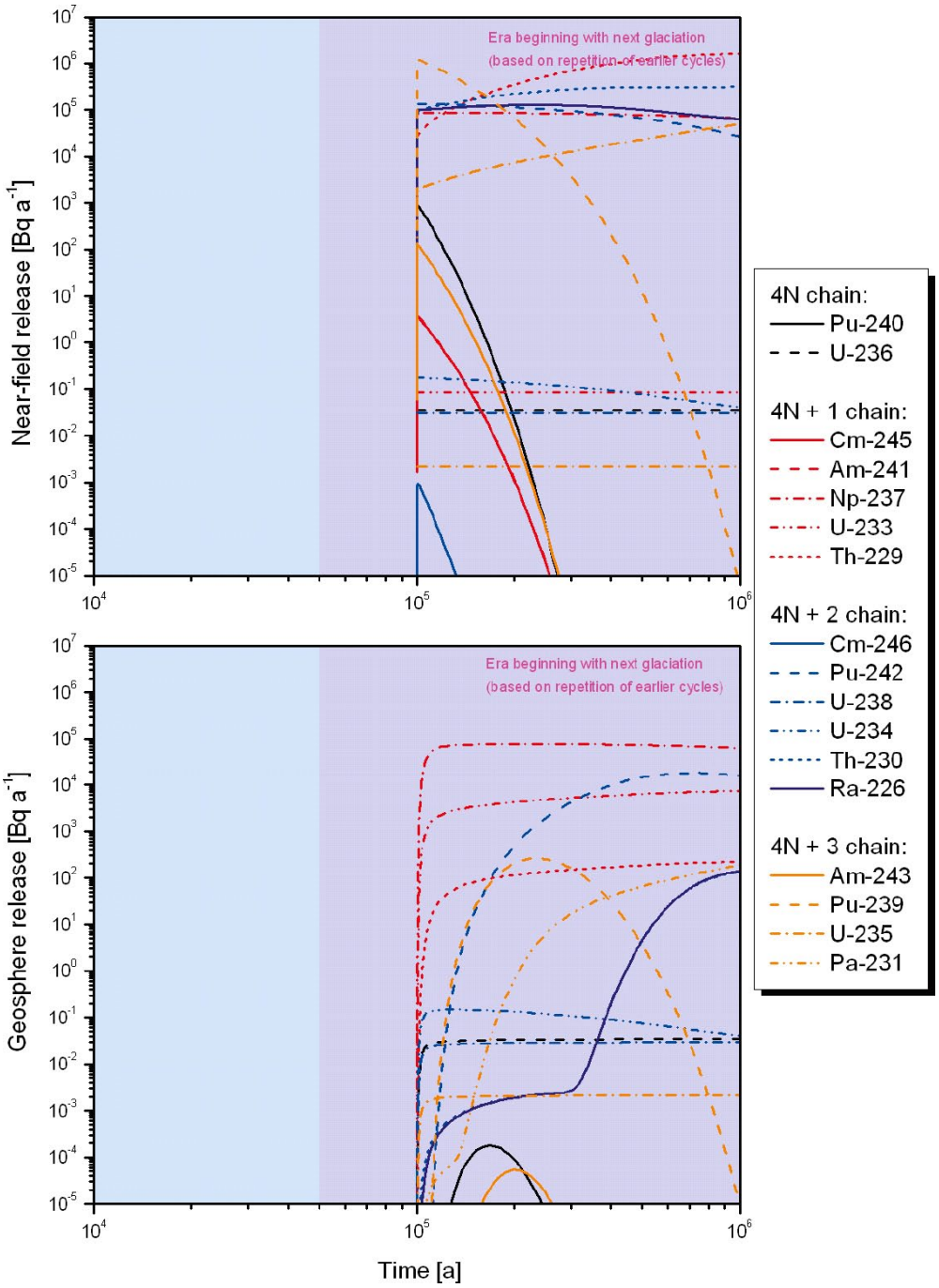

Figure G-58. *Release rates of actinide chain members from the geosphere as functions of time in case CC-GMW.*

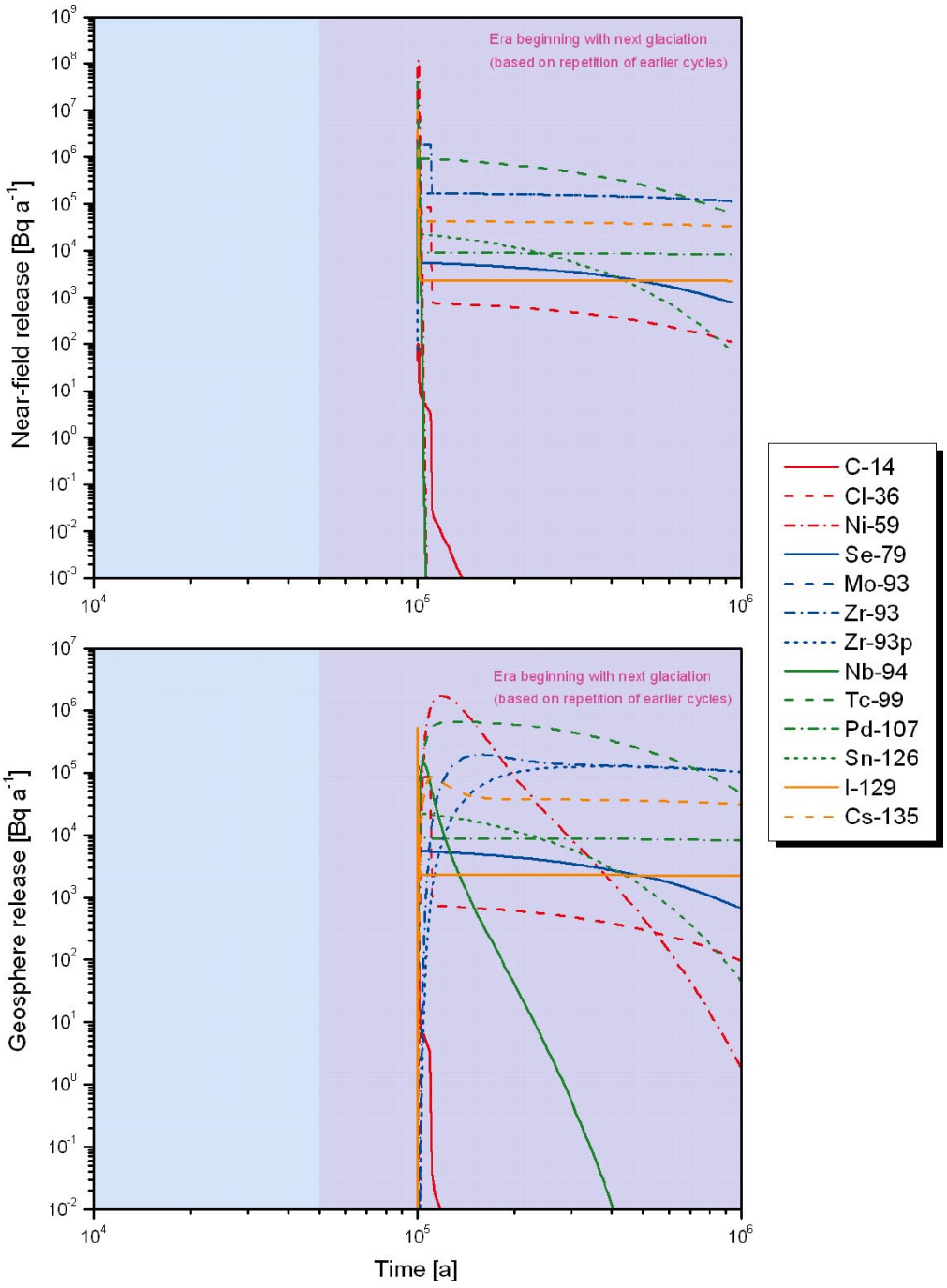

Figure G-59. *Release rates of activation and fission products from the near field (upper figure) and geosphere (lower figure) as functions of time in case CC-LOGEOR.*

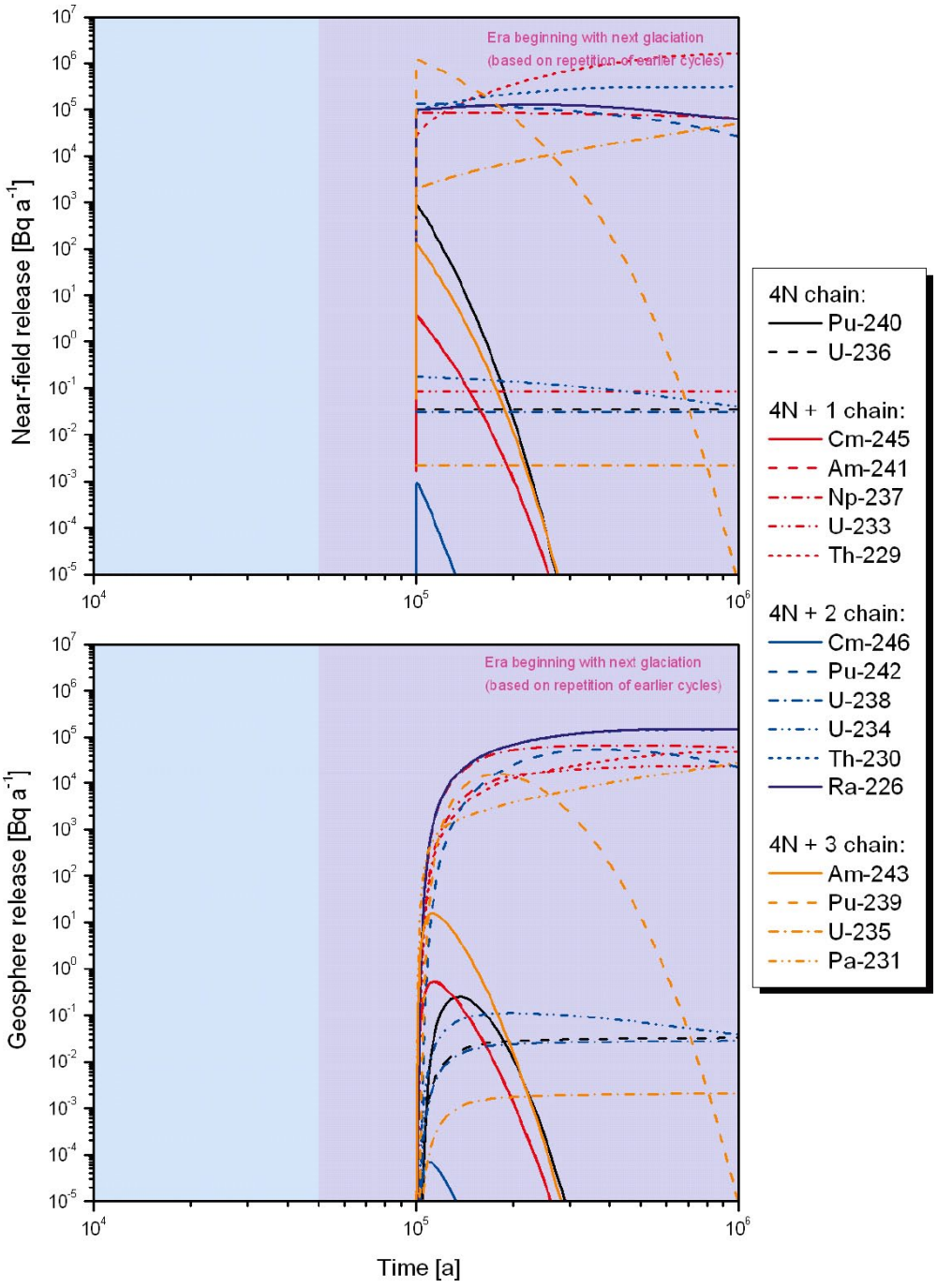

Figure G-60. *Release rates of actinide chain members from the geosphere as functions of time in case CC-LOGEOR.*

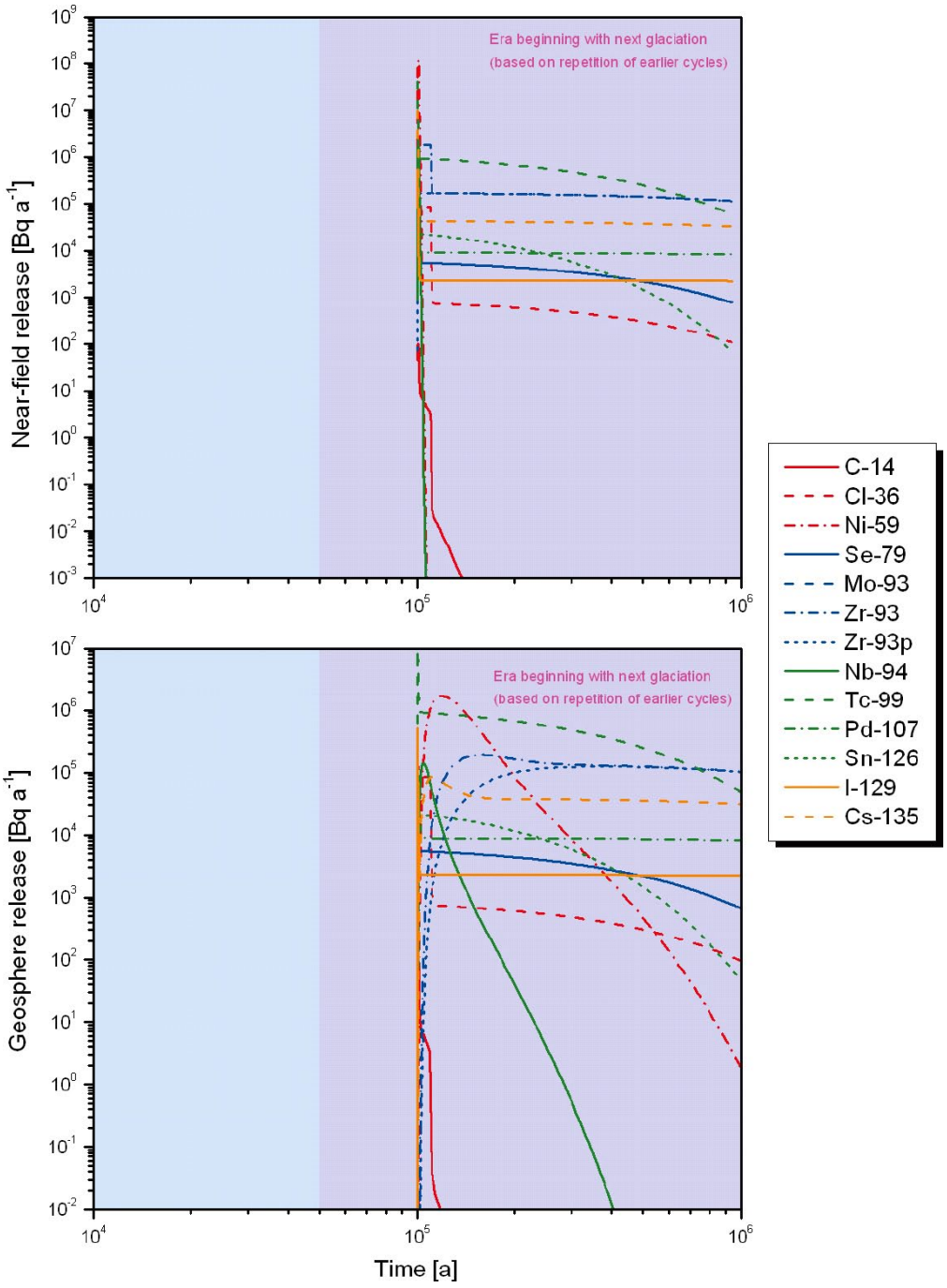

Figure G-61. *Release rates of activation and fission products from the near field (upper figure) and geosphere (lower figure) as functions of time in case CC-LOGERORG.*

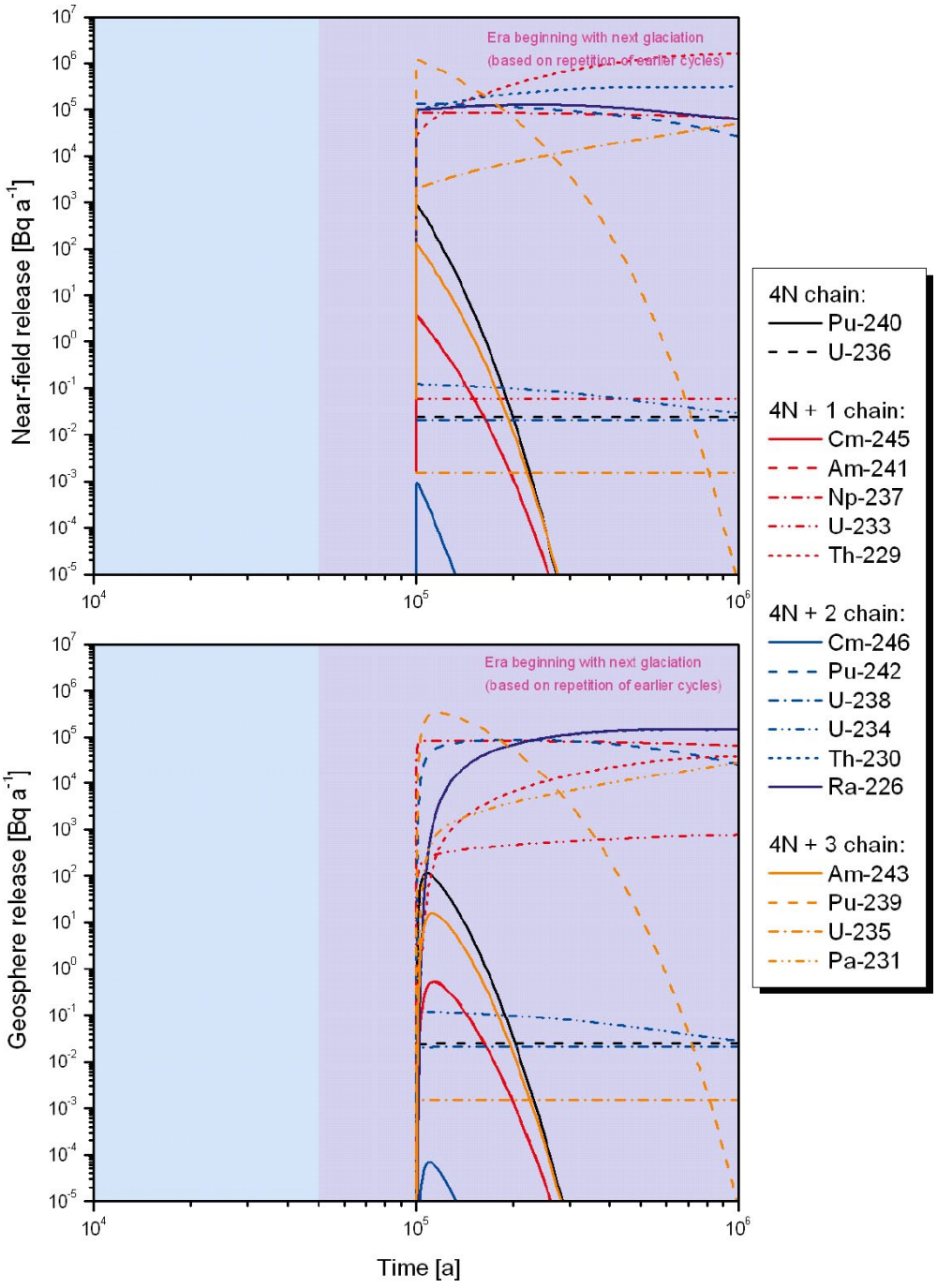

Figure G-62. *Release rates of actinide chain members from the geosphere as functions of time in case CC-LOGEORG.*

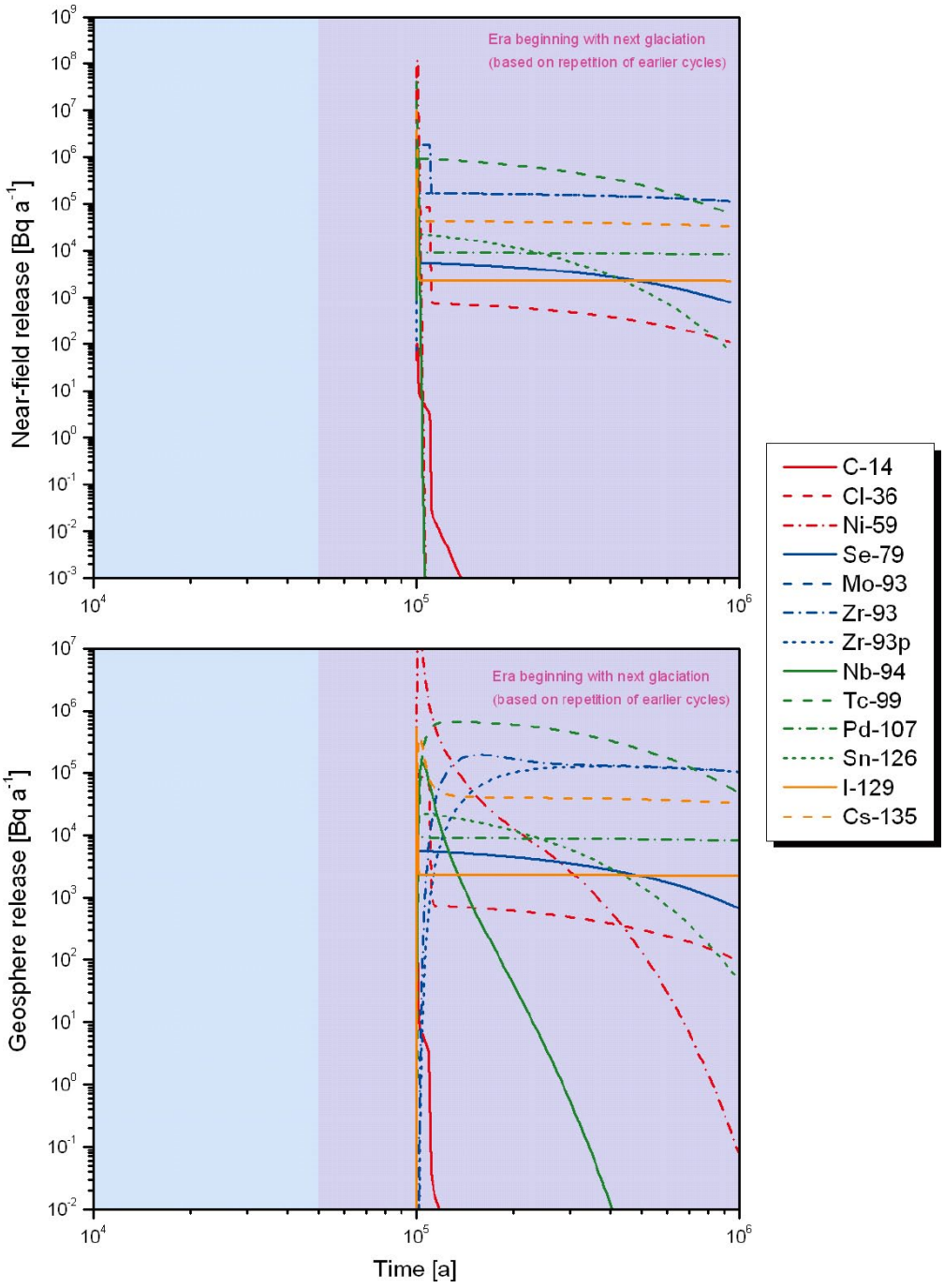

Figure G-63. *Release rates of activation and fission products from the near field (upper figure) and geosphere (lower figure) as functions of time in case CC-LOGERORS.*

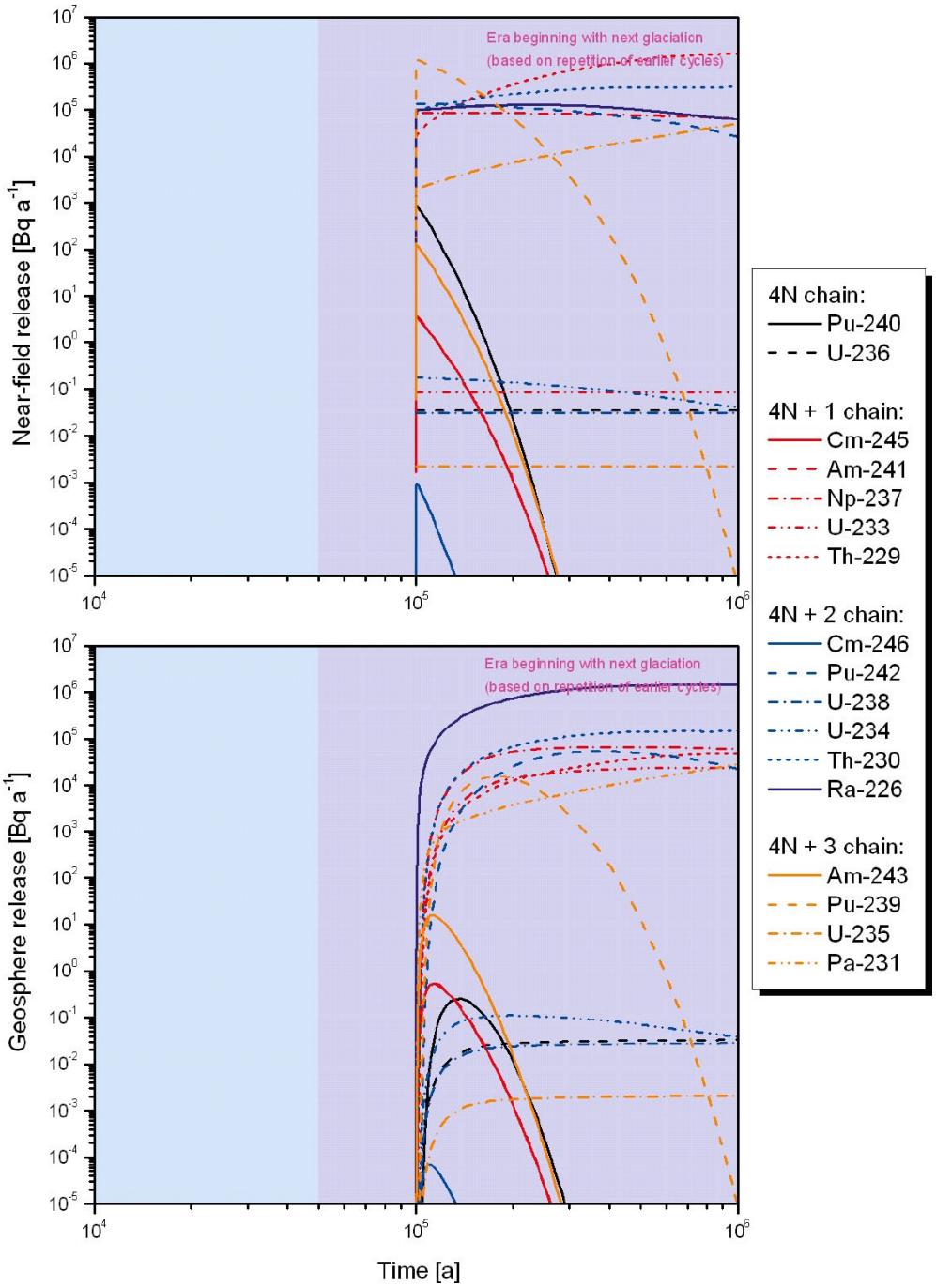

Figure G-64. *Release rates of actinide chain members from the geosphere as functions of time in case CC-LOGEORS.*

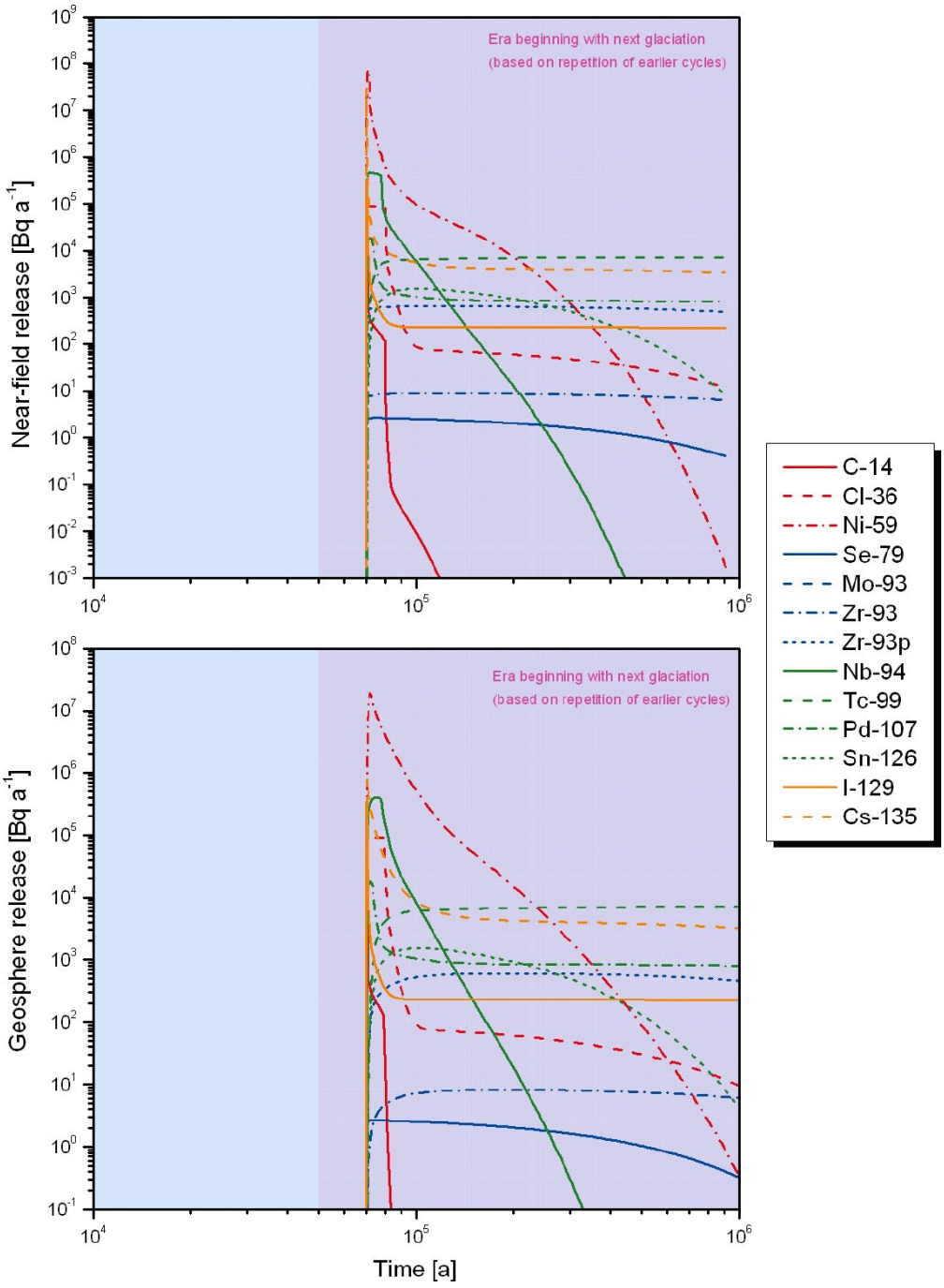

Figure G-65. *Release rates of activation and fission products from the near field (upper figure) and geosphere (lower figure) as functions of time in case RS-BC.*

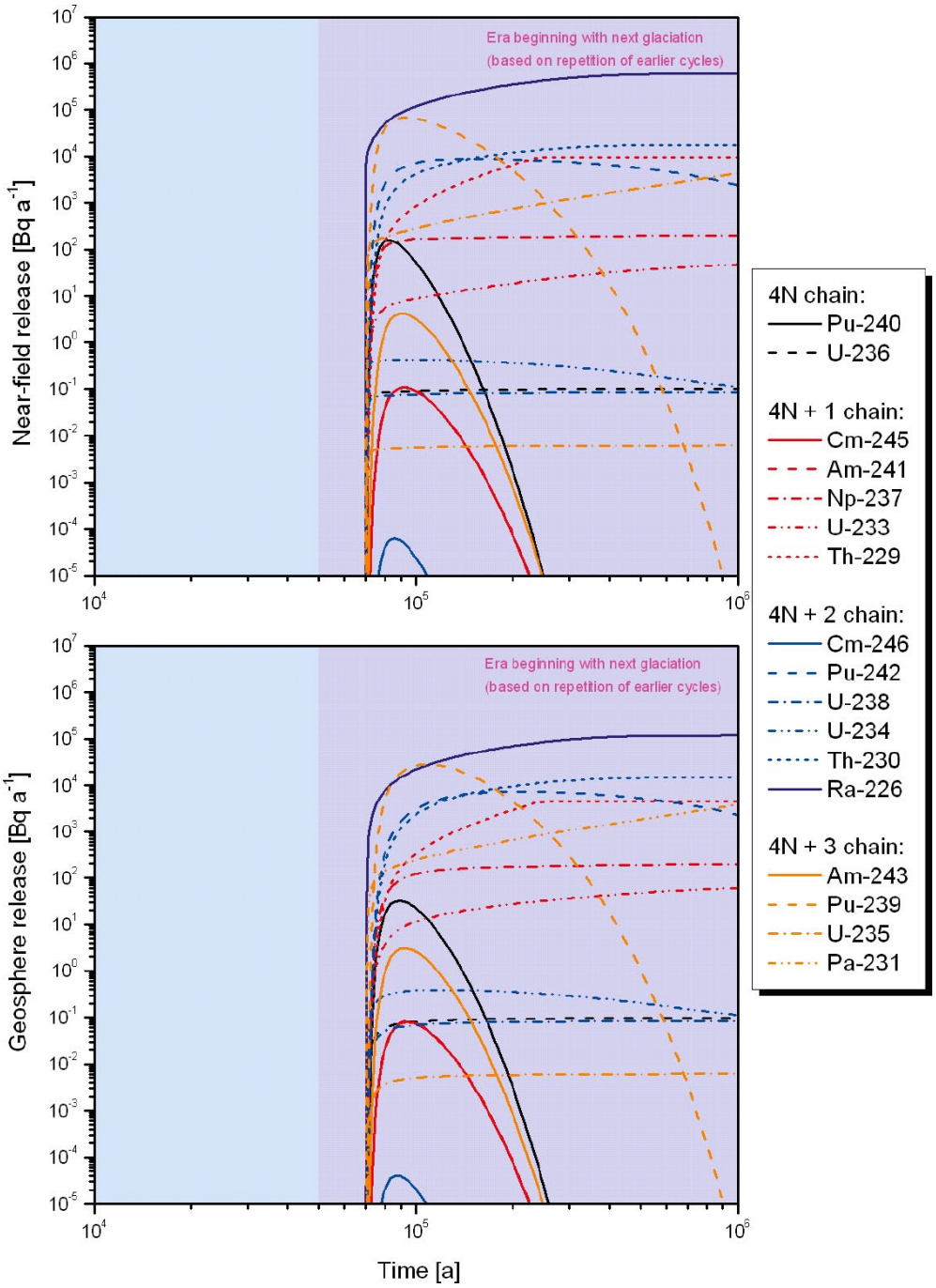

Figure G-66. *Release rates of actinide chain members from the geosphere as functions of time in case RS-BC.*

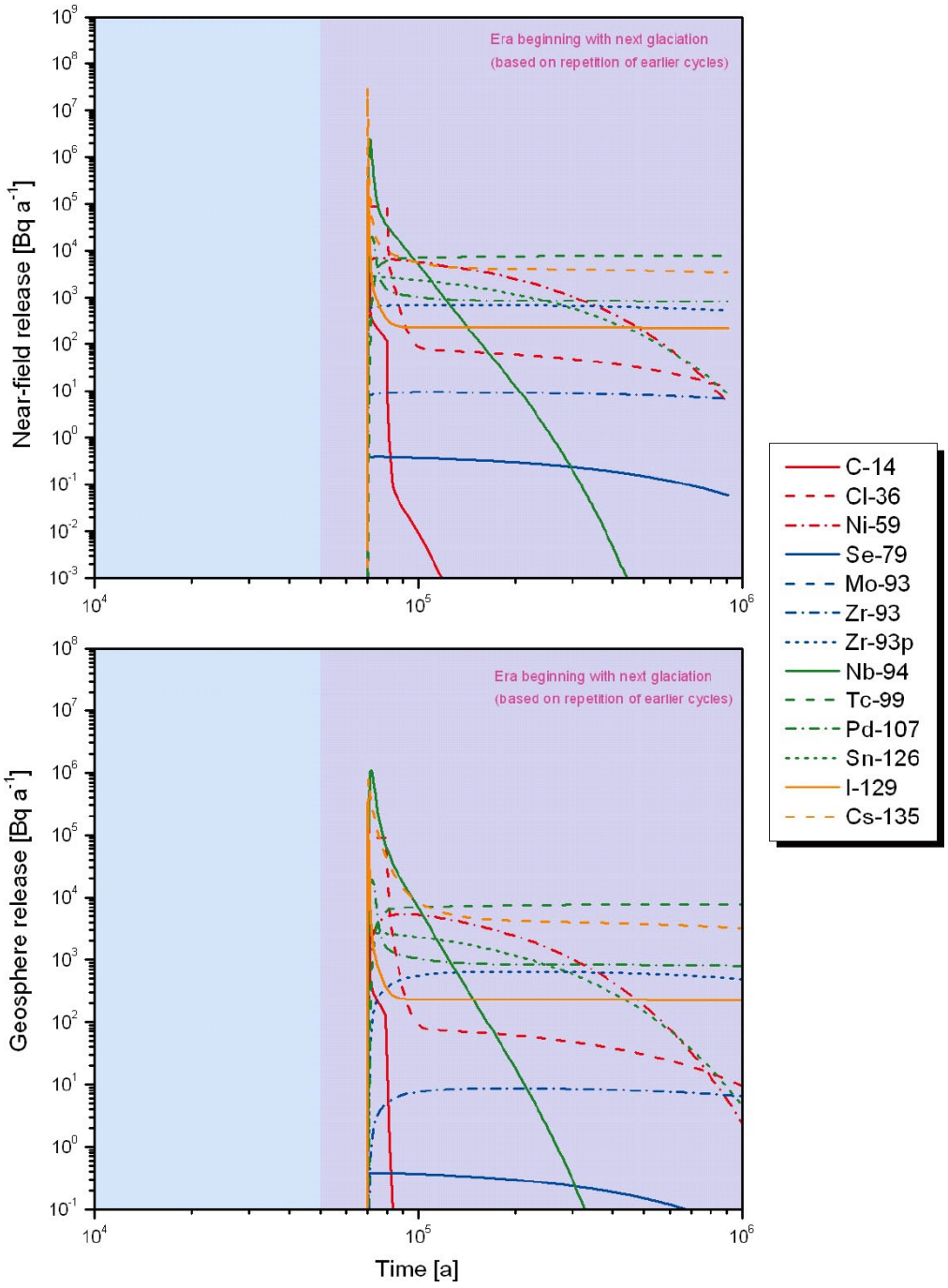

Figure G-67. *Release rates of activation and fission products from the near field (upper figure) and geosphere (lower figure) as functions of time in case RS-GMW.*

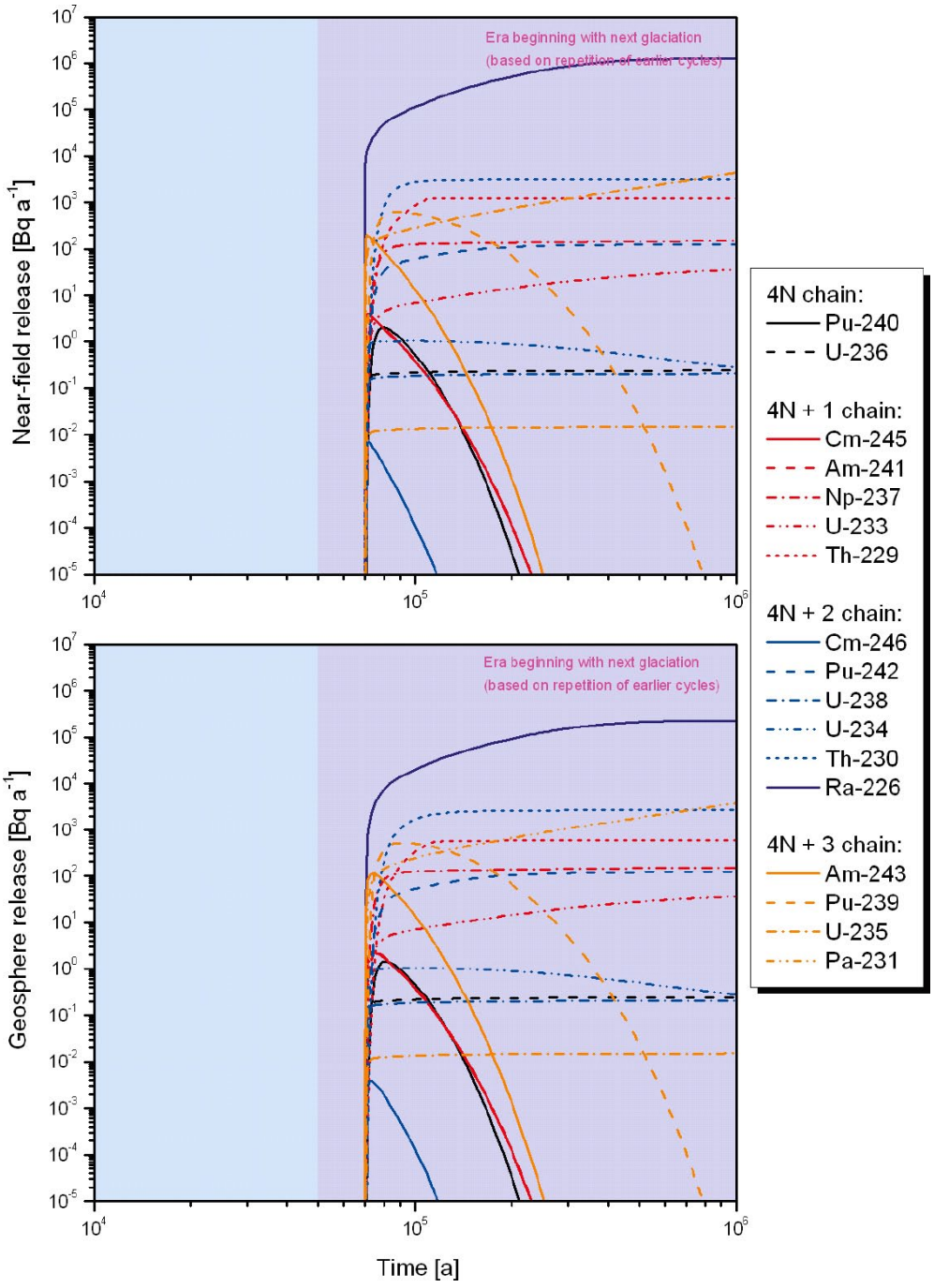

Figure G-68. *Release rates of actinide chain members from the geosphere as functions of time in case RS-GWM.*